EMERGING INFECTIOUS DISEASES®

CDC
Centers for Disease Control and Prevention

Unexpected Hazards

August 2023

Alexis Rockman (1962–), *Ark*, 2014. Oil and alkyd on wood, 44 in x 56 in/112 cm x 142 cm.

EMERGING INFECTIOUS DISEASES®

Emerging Infectious Diseases is published monthly by the Centers for Disease Control and Prevention, 1600 Clifton Rd NE, Mailstop H16-2, Atlanta, GA 30329-4027, USA. Telephone 404-639-1960; email, eideditor@cdc.gov

EMERGING INFECTIOUS DISEASES®

Unexpected Hazards **August 2023**

On the Cover

Alexis Rockman (1962–), *Ark*, 2014. Oil and alkyd on wood, 44 in x 56 in/112 cm x 142 cm. © 2023 Alexis Rockman / Artists Rights Society (ARS), New York, New York, United States.

About the Cover p. 1714

Synopses

Research

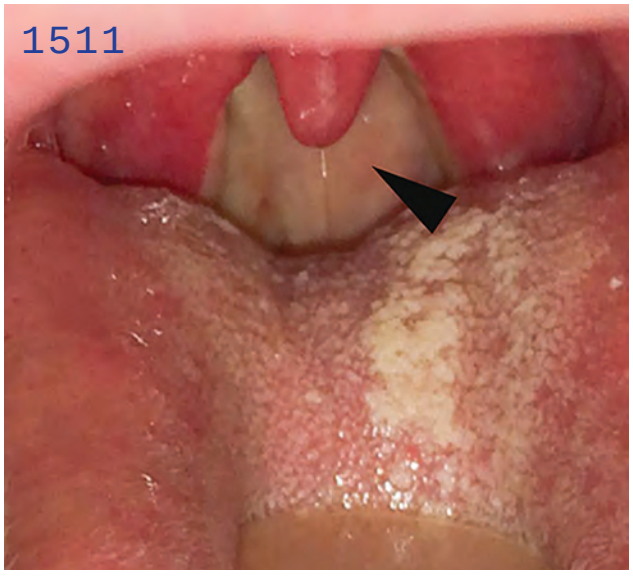

Dispatches

EMERGING INFECTIOUS DISEASES®
August 2023

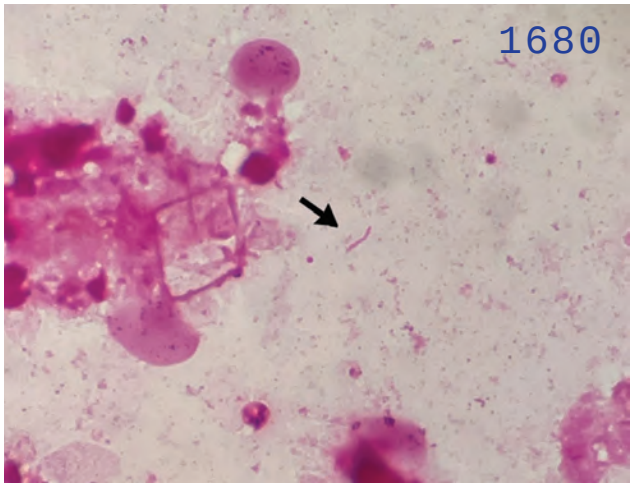

EMERGING INFECTIOUS DISEASES®
August 2023

Research Letters

About the Cover

Etymologia

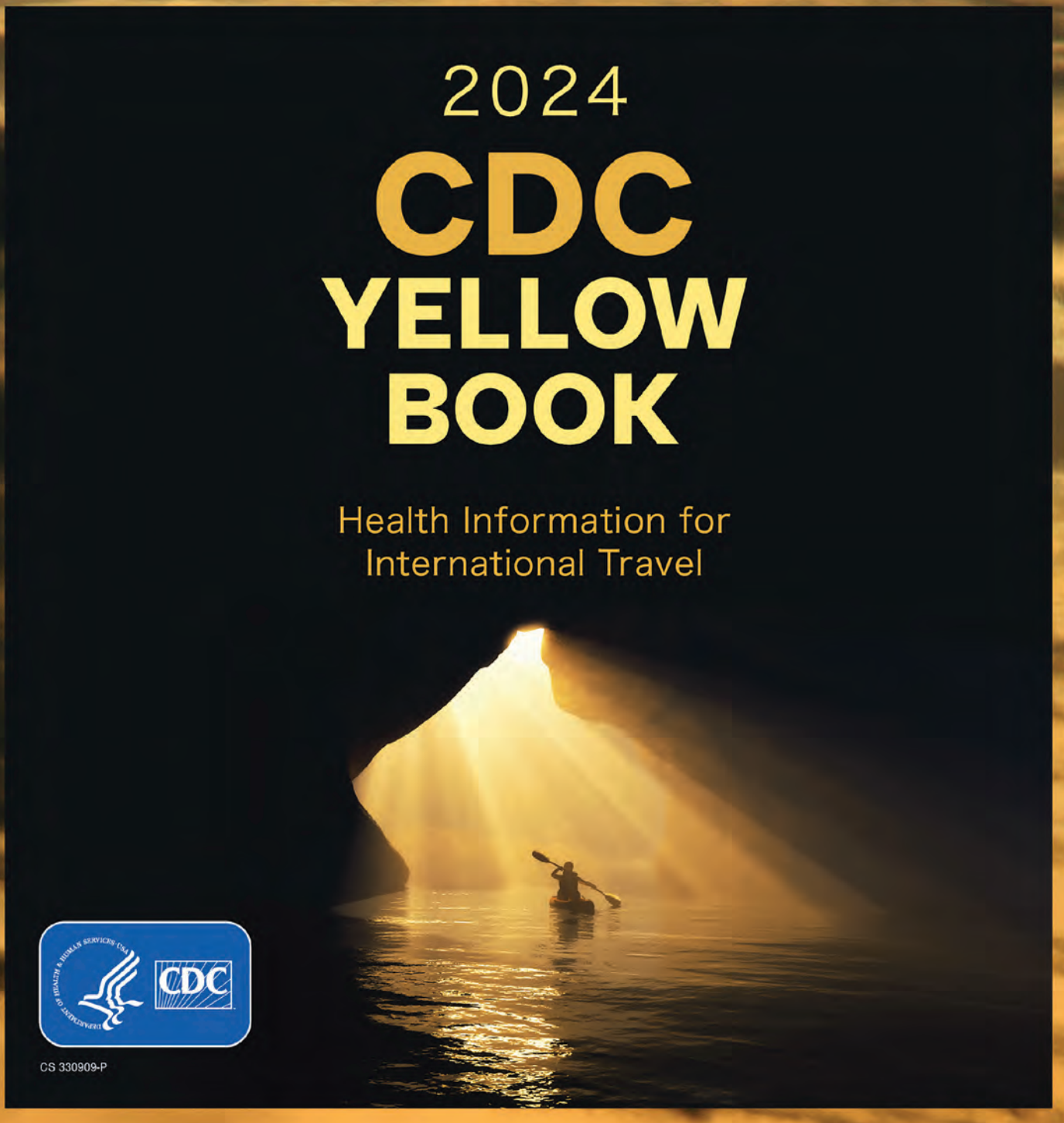

Launch of CDC Yellow Book 2024 – A Trusted Travel Medicine Resource

CDC is pleased to announce the launch of the CDC Yellow Book 2024. The CDC Yellow Book is a source of the U.S. Government's recommendations on travel medicine and has been a trusted resource among the travel medicine community for over 50 years. Healthcare professionals can use the print and digital versions to find the most up-to-date travel medicine information to better serve their patients' healthcare needs.

The CDC Yellow Book is available in print through Oxford University Press and online at www.cdc.gov/yellowbook.

Clinical Characteristics of *Corynebacterium ulcerans* Infection, Japan

Akihiko Yamamoto, Toru Hifumi, Manabu Ato, Masaaki Iwaki, Mitsutoshi Senoh, Akio Hatanaka, Shinichi Nureki, Yoshihiro Noguchi, Tomoko Hirose, Yukihiro Yoshimura, Takaaki Urakawa, Shiro Hori, Hiroto Nakada, Tomomasa Terada, Tomoko Ishifuji, Hisayo Matsuyama, Takahiro Kinebuchi, Atsuhito Fukushima, Koji Wake, Ken Otsuji, Takeru Endo, Hirokazu Toyoshima, Ikkoh Yasuda, Takeshi Tanaka, Naoki Takahashi, Kensaku Okada, Toshimasa Hayashi, Taizo Kusano, Minami Koriyama, Norio Otani, Motohide Takahashi

Medscape CME Activity

In support of improving patient care, this activity has been planned and implemented by Medscape, LLC and Emerging Infectious Diseases. Medscape, LLC is jointly accredited with commendation by the Accreditation Council for Continuing Medical Education (ACCME), the Accreditation Council for Pharmacy Education (ACPE), and the American Nurses Credentialing Center (ANCC), to provide continuing education for the healthcare team.

Medscape, LLC designates this Journal-based CME activity for a maximum of 1.00 ***AMA PRA Category 1 Credit(s)™***. Physicians should claim only the credit commensurate with the extent of their participation in the activity.

Successful completion of this CME activity, which includes participation in the evaluation component, enables the participant to earn up to 1.0 MOC points in the American Board of Internal Medicine's (ABIM) Maintenance of Certification (MOC) program. Participants will earn MOC points equivalent to the amount of CME credits claimed for the activity. It is the CME activity provider's responsibility to submit participant completion information to ACCME for the purpose of granting ABIM MOC credit.

All other clinicians completing this activity will be issued a certificate of participation. To participate in this journal CME activity: (1) review the learning objectives and author disclosures; (2) study the education content; (3) take the post-test with a 75% minimum passing score and complete the evaluation at http://www.medscape.org/journal/eid; and (4) view/print certificate. For CME questions, see page XXX.

NOTE: It is Medscape's policy to avoid the use of Brand names in accredited activities. However, in an effort to be as clear as possible, the use of brand names should not be viewed as a promotion of any brand or as an endorsement by Medscape of specific products.

Release date: July 21, 2023; Expiration date: July 21, 2024

Learning Objectives

Upon completion of this activity, participants will be able to:

- Assess the demographic and clinical characteristics of patients with *Corynebacterium ulcerans* infection, based on a case series of 34 patients in Japan from 2001 to 2020
- Compare clinical characteristics between patients with respiratory and nonrespiratory symptoms of *Corynebacterium ulcerans* infection and among 3 severity subgroups of patients with respiratory symptoms, based on a case series of 34 patients in Japan from 2001 to 2020
- Determine the clinical and treatment implications of clinical characteristics, treatment-related factors, and outcomes of *Corynebacterium ulcerans* infection, based on a case series of 34 patients in Japan from 2001 to 2020

CME Editor

Jude Rutledge, BA, Technical Writer/Editor, Emerging Infectious Diseases. *Disclosure: Jude Rutledge, BA, has no relevant financial relationships.*

CME Author

Laurie Barclay, MD, freelance writer and reviewer, Medscape, LLC. *Disclosure: Laurie Barclay, MD, has no relevant financial relationships.*

Authors

Akihiko Yamamoto, DVM, PhD; Toru Hifumi, MD, PhD; Manabu Ato, MD, PhD; Masaaki Iwaki, PhD; Mitsutoshi Senoh, PhD; Akio Hatanaka, MD, PhD; Shinichi Nureki, MD, PhD; Yoshihiro Noguchi, MD, PhD; Tomoko Hirose, MD, PhD; Yukihiro Yoshimura, MD, PhD; Takaaki Urakawa, MD, PhD; Shiro Hori, MD, PhD; Hiroto Nakada, MD, PhD; Tomomasa Terada, MD, PhD; Tomoko Ishifuji, MD, PhD; Hisayo Matsuyama, MD, PhD; Takahiro Kinebuchi, BS; Atsuhito Fukushima, MD, PhD; Koji Wake, MD, PhD; Ken Otsuji, MD, PhD; Takeru Endo, MD, PhD; Hirokazu Toyoshima, MD, PhD; Ikkoh Yasuda, MD, PhD; Takeshi Tanaka, MD, PhD; Naoki Takahashi, MD, PhD; Kensaku Okada, MD, PhD; Akihiko Yamamoto, DVM, PhD; Toru Hifumi, MD, PhD; Manabu Ato, MD, PhD; Masaaki Iwaki, PhD; Mitsutoshi Senoh, PhD; Akio Hatanaka, MD, PhD; Shinichi Nureki, MD, PhD; Yoshihiro Noguchi, MD, PhD; Tomoko Hirose, MD, PhD; Yukihiro Yoshimura, MD, PhD; Takaaki Urakawa, MD, PhD; Shiro Hori, MD, PhD; Hiroto Nakada, MD, PhD; Tomomasa Terada, MD, PhD; Tomoko Ishifuji, MD, PhD; Hisayo Matsuyama, MD, PhD; Takahiro Kinebuchi, BS; Atsuhito Fukushima, MD, PhD; Koji Wake, MD, PhD; Ken Otsuji, MD, PhD; Takeru Endo, MD, PhD; Hirokazu Toyoshima, MD, PhD; Ikkoh Yasuda, MD, PhD; Takeshi Tanaka, MD, PhD; Naoki Takahashi, MD, PhD; Kensaku Okada, MD, PhD; Toshimasa Hayashi, MD; Taizo Kusano, MD, PhD; Minami Koriyama, MD, PhD; Norio Otani, MD, PhD; and ***Motohide Takahashi, DVM, PhD.***

Corynebacterium ulcerans is a closely related bacterium to the diphtheria bacterium *C. diphtheriae*, and some *C. ulcerans* strains produce toxins that are similar to diphtheria toxin. *C. ulcerans* is widely distributed in the environment and is considered one of the most harmful pathogens to livestock and wildlife. Infection with *C. ulcerans* can cause respiratory or nonrespiratory symptoms in patients. Recently, the microorganism has been increasingly recognized as an emerging zoonotic agent of diphtheria-like illness in Japan. To clarify the overall clinical characteristics, treatment-related factors, and outcomes of *C. ulcerans* infection, we analyzed 34 cases of *C. ulcerans* that occurred in Japan during 2001–2020. During 2010–2020, the incidence rate of *C. ulcerans* infection increased markedly, and the overall mortality rate was 5.9%. It is recommended that adults be vaccinated with diphtheria toxoid vaccine to prevent the spread of this infection.

Diphtheria is an upper respiratory tract illness caused by toxin-producing *Corynebacterium diphtheriae* bacteria, and it is characterized by sore throat, fever, and formation of a pseudomembrane on the tonsils, pharynx, or both, along with nasal discharge. *C. diphtheriae* can also infect the skin, causing open sores or ulcers. However, diphtheria skin infections rarely result in any other severe disease (*1*). *C. ulcerans* is a closely related bacterium to *C. diphtheriae*, and some strains produce toxins that are very similar to diphtheria toxin (*2*,*3*). *C. ulcerans* is widely distributed in the environment and is considered one of the most harmful pathogens to livestock and wildlife. This bacterium can cause cutaneous inflammation, including mastitis, in dairy cows (*4*–*6*). *C. ulcerans* has been increasingly recognized as an emerging zoonotic agent of diphtheria-like illness in the world (*7*–*18*).

Infections caused by these 2 bacteria are difficult to distinguish clinically, and the World Health Organization (WHO) treats infections caused by toxin-producing *C. ulcerans* as part of the diphtheria case definition (*19*). *C. diphtheriae* is thought to be transmitted only among humans, but *C. ulcerans* can be transmitted to humans by nonhuman mammals and thus should be treated as a zoonosis (*7*–*18*). Dogs and cats as companion animals are considered the major causes of transmission to humans. Although there have been several reports of individual cases of *C. ulcerans* infection (*20*–*24*), information on clinical features, treatment-related factors, and outcomes is limited. In this study we elucidate the clinical features, treatment-related factors, and outcomes of *C. ulcerans* infection cases in Japan during 2001–2020.

Methods

This study was a retrospective, observational, national survey of *C. ulcerans* infections in Japan since the first reported case of this infection (*25*). The data acquisition period was 20 years, from February 2001 through December 2020. The institutional review board of St. Luke's International Hospital (Tokyo, Japan) approved this cross-sectional, survey-based study (approval no. 19-R055).

Patients and Setting

The National Institute of Infectious Disease (NIID) has comprehensively organized research and controlled clinical practice in *C. ulcerans* infectious diseases in Japan. However, in Japan, *C. ulcerans* infection is not included in the diphtheria case definition, nor is it required to be reported in all cases, so there is no obligation to report. However, because *C. ulcerans* produces diphtheria toxin, it has clinical manifestations similar to those caused by *C. diphtheriae*, for which all cases must be reported in Japan (*19*). Therefore, Japan's Ministry of Health, Labour and

Author affiliations: National Institute of Infectious Diseases, Tokyo, Japan (A. Yamamoto, M. Ato, M. Iwaki, M. Senoh); St. Luke's International Hospital, Tokyo (T. Hifumi, N. Otani); Ageo Central General Hospital, Saitama, Japan (A. Hatanaka); Oita University Faculty of Medicine, Oita, Japan (S. Nureki); International University of Health and Welfare School of Medicine, Chiba, Japan (Y. Noguchi); Japanese Red Cross Otsu Hospital, Shiga, Japan (T. Hirose); Yokohama Municipal Citizen's Hospital, Kanagawa, Japan (Y. Yoshimura); Tsuruoka Municipal Shonai Hospital, Yamagata, Japan (T. Urakawa); Japan Community Healthcare Organization Ritsurin Hospital, Kagawa, Japan (S. Hori); Holon Toriizaka Clinic, Tokyo (H. Nakada); Tokushima Prefectural Central Hospital, Tokushima, Japan (T. Terada); Itabashi Medical System Tokyo–Katsushika General Hospital, Katsushika, Tokyo (T. Ishifuji); Kawakita General Hospital, Suginami, Tokyo (H. Matsuyama); Furano Hospital, Hokkaido, Japan (T. Kinebuchi); Dokkyo Medical University, Tochigi, Japan (A. Fukushima, K. Wake); Hospital of University of Occupational and Environmental Health, Fukuoka, Japan (K. Otsuji, T. Endo); Japanese Red Cross Ise Hospital, Mie, Japan (H. Toyoshima); Fukushima Medical University, Fukushima, Japan (I. Yasuda); Nagasaki University Hospital, Nagasaki, Japan (T. Tanaka); Kimitsu Chuo Hospital, Chiba (N. Tanaka); Tottori University Hospital, Tottori, Japan (K. Okada); Maebashi Red Cross Hospital, Gunma, Japan (T. Hayashi); Chiba Children's Hospital, Chiba (T. Kusano); Chiba Rousai Hospital, Chiba (M. Koriyama); Kumamoto Health Science University, Kumamoto, Japan (M. Takahashi)

DOI: https://doi.org/10.3201/eid2908.220058

Welfare (MHLW) urged health management departments and hospitals throughout the country to call attention to the need to identify the causative bacterium in patients showing clinical symptoms similar to diphtheria. MHLW has also published diagnostic criteria for *C. ulcerans* to assist clinicians in classifying *C. diphtheriae* and *C. ulcerans* (*26*). Under those circumstances, information from doctors who treated patients with suspected diphtheria symptoms and requests for pathogen diagnosis were sent to NIID. Therefore, the data included in this analysis came from attending physicians who, at the time of care, chose to investigate and report cases as *C. ulcerans* infections.

Data Collection

The following parameters were recorded: age; sex; date of infection; location of patient's origin; whether there was a companion animal; whether there was any interaction with animals, such as breeding livestock animals, or whether the patient had lived in an environment involving contact with animals; presence or absence of bacterial isolation from patients and related animals; and clinical symptoms (throat pain, nasal discharge, pseudomembrane, fever, headache, dyspnea, hoarseness, and abscess). In addition, we collected data on vital signs (heart rate, systolic blood pressure, temperature, and respiratory rate), laboratory data (leukocyte counts, platelet counts, creatinine kinase levels, C-reactive protein [CRP] levels), types of antibiotics administered, presence or absence of administration of diphtheria antitoxin, and outcomes (days of hospitalization, days of mechanical ventilation, and survival or death).

Diagnosis of *C. ulcerans* Infection

The diagnostic criteria for the cases collected in this study used the *C. ulcerans* diagnostic criteria of MHLW (*26*). Accordingly, several conditions must be met: the infection manifests the same clinical symptoms as respiratory diphtheria with intractable pharyngeal pseudomembrane formation, and gram-positive rods are isolated from local areas, such as the pharynx and nasal cavity, and identified as *C. ulcerans*; the isolated bacterium is *C. ulcerans* alone, or *C. ulcerans* is the main component; detection of the diphtheria toxin gene and its toxin activity have been confirmed from this isolated strain by a functional test (i.e., an Elek test or equivalent test) (*1*,*26*); and cutaneous signs and symptoms are present and *C. ulcerans* is identified as the causative agent of local lymphadenopathy and abscesses (*27*,*28*).

Definitions of Symptoms

C. ulcerans infections are classified into respiratory and nonrespiratory manifestations. We defined respiratory symptoms as dyspnea, hoarseness, sore throat, cough, fever, and (occasionally) white pseudomembrane of the nasopharynx and laryngeal vestibule. Nonrespiratory symptoms were defined as skin infections and abscesses, or symptoms in patients who did not show respiratory symptoms. We further classified both types of symptoms as mild (resolving on outpatient visits), moderate (requiring hospitalization), or severe (requiring hospitalization and further ventilator support). The definitions of all cases included in this study were those we described previously as consistent with diagnosis of *C. ulcerans* infection.

Treatment of *C. ulcerans* Infection

For treatment of *C. ulcerans* infection, administration of antibiotics to which *C. ulcerans* is susceptible, such as macrolides and penicillins, is effective. In severe cases, symptomatic treatment for diphtheria pneumonia and administration of diphtheria antitoxin are effective for ventilated patients. The antitoxin used for *C. ulcerans* infection and for diseases caused by *C. diphtheriae* is delivered from the nearest national stockpile. However, depending on the distance, sometimes immediate delivery cannot be achieved.

Primary Data Analysis

We compared patients' characteristics, treatment-related factors, and outcomes between the respiratory symptoms group and nonrespiratory symptoms group by using the Mann–Whitney U test or Fisher exact test, as appropriate. We used quantitative properties in the calculation basically as they are and quantified qualitative properties by scoring and then analyzed them. In the respiratory symptoms group, we compared mild, moderate, and severe cases. Regarding the collection of clinical data, we did not impute missing data. We performed statistical analysis by using JMP Pro statistical software version 14 (SAS Institute). We considered 2-sided p values <0.05 to be statistically significant.

Results

Demographic and Clinical Characteristics of Patients

A total of 34 patients from 34 hospitals were identified during the 20-year study period (Appendix Table, https://wwwnc.cdc.gov/EID/article/29/8/22-0058-App1.pdf). The reports of *C. ulcerans* infections came from a wide range of areas, and there was no regional bias (Figure 1). Furthermore, when we

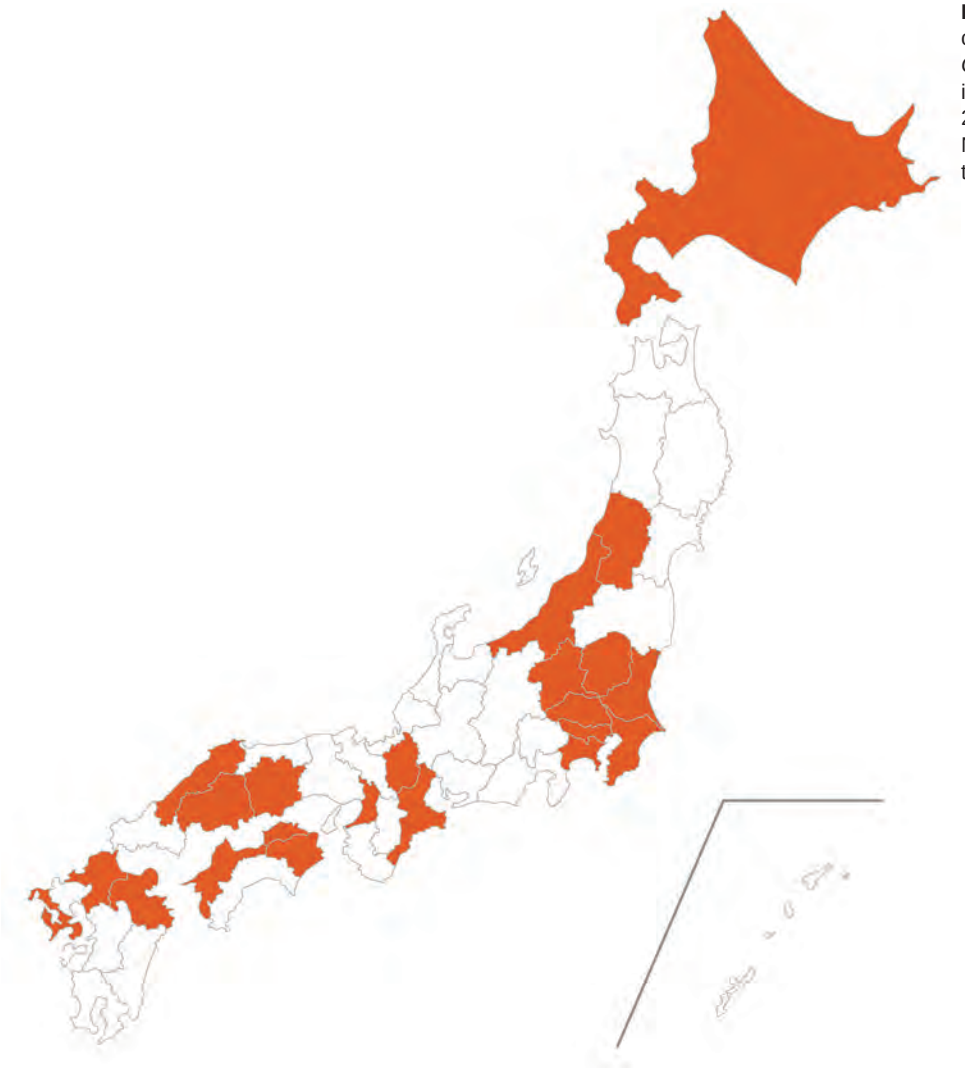

Figure 1. Prefectures containing outbreak areas of *Corynebacterium ulcerans* infection (orange), Japan, 2001–2020. Inset map shows the Nansei Islands, an archipelago in the southwestern part of Japan.

compared the number of *C. ulcerans* cases every 5 years, we found the number of cases during 2001–2010 was stable (4 total cases), but the number of cases during 2011–2015 was 7 and during 2016–2020 was 19. Therefore, compared with the number of cases during 2001–2010, the number during 2011–2015 was 1.75 times higher and during 2016–2020 was 4.75 times higher (Figure 2).

The symptoms of *C. ulcerans* infection were respiratory in 23 (67.7%) patients and nonrespiratory in 11 (32.3%) (Table 1). The median age of patients was 58 years, and 61.3% of patients were women. Almost all patients (97.1%) had contact with animals. The mortality rate was 5.9%.

Details of *C. ulcerans* Infection Cases

We divided the clinical characteristics of *C. ulcerans* patients into respiratory and nonrespiratory groups. The characteristics of respiratory symptoms include formation of pseudomembrane in addition to dyspnea, hoarseness, sore throat, and fever. In general, among the patients evaluated in our study, the pseudomembrane was often attached to the nasopharynx (Figure 3, panels A, B; Figure 4). Moreover, in severe cases, bronchoscopy showed a pseudomembranous material obstructing the bronchi (Figure 3, panel C).

Patients with pseudomembranes with bronchial obstruction were characterized by atelectasis (i.e., when part or all of the lung was devoid of air and collapses) on radiographs (Figure 4, panel A). A common cause of atelectasis was bronchial obstruction. Atelectasis spreads throughout the lungs as symptoms worsen (Figure 4, panels B, C). As lung function declines, ventilators and extracorporeal membrane oxygen therapy are required to save the patient's life. Complications after *C. ulcerans* treatment have been reported (*29*); in that particular case, the patient reported dyspnea, and a thick pseudomembrane was

found in the larynx. *C. ulcerans* producing diphtheria toxin was detected in the pseudomembranes. Antibiotic treatment improved airway symptoms, but sudden cardiac arrest occurred, followed by dyspnea and seizures. Afterward, the patient's general condition stabilized, but she remained unconscious.

In contrast, nonrespiratory *C. ulcerans* patients evaluated in our study had local lymph node abscesses near the trauma, parotid abscesses, axillary abscesses, cervical lymph node abscesses, plantar skin ulcers, subcutaneous abscesses, and mandibular abscesses. Symptoms such as abscess, thigh abscess, and purulent lymphadenitis in the right neck were observed (Appendix). MRI images of a patient's elbow showed abscesses in the axillary and parotid lymph nodes (Figures 4, panels E–F).

Comparing Clinical Characteristics between Respiratory and Nonrespiratory Symptoms Groups

Patients in the respiratory symptoms group were significantly older than patients in the nonrespiratory group (64 [interquartile range (IQR) 54–72] years vs. 38 [IQR 21–61] years; p = 0.03). When we compared the 3 severity classifications for respiratory and nonrespiratory symptoms, we found the group with respiratory symptoms had 6 patients with mild, 7 patients with moderate, and 10 patients with severe symptoms. In contrast, in the nonrespiratory symptom group, there were 5 mild cases, 6 moderate cases, and 0 severe cases. The differences in the number of mild, moderate, and severe cases of symptom severity in the 2 groups were significant (p<0.01) (Table 1). Leukocyte counts and CRP levels were relatively higher in the respiratory group than in the nonrespiratory group (p = 0.07 for both) (Table 1).

Comparing Clinical Characteristics among the 3 Severity Groups

Within the group showing respiratory symptoms, we compared clinical characteristics for the mild, moderate, and severe subgroups (Table 2). Among the respiratory group patients with pseudomembrane, 5 had mild cases, 6 had moderate cases, and 10 had severe cases. Among cases with respiratory symptoms, pseudomembrane-positive patients accounted for 83.3% of mild cases, 85.7% of moderate cases, and 100% of severe cases. Laboratory data showed a significant difference among the 3 subgroups in CRP levels (4.7 mg/dL [IQR 0.9–6.1 mg/dL] in mild, 7.7 mg/dL [IQR 1.8–12.6 mg/dL] in moderate, and 21 mg/dL [IQR 11.7–25.4 mg/dL] in severe cases; p = 0.02). Macrolide antibiotics, which are effective for *C. ulcerans*, were mainly used for mild cases. As the severity increased, many additional antibiotics, such as penicillin, cephalosporin antibiotics, and quinolone, were used. Regarding the length of hospital stay, we observed a significant difference between moderate cases (7 [IQR 7–10] days) and severe cases (29 [IQR 20–56] days; p<0.01). Diphtheria antitoxin was administered only to 4 severe case-patients (cases 5, 24, 29, and 33).

Two deaths from *C. ulcerans* infection occurred among the severe case-patients (20%; cases 5 and 18). Case-patient 5 was administered 5,000 IU of diphtheria antitoxin on her second day of hospitalization. *C. ulcerans*, which had been detected in the pseudomembrane, became negative in culture 1 week later, but the patient died on the 21st day of hospitalization without improvement in her severe pneumonia. Case-patient 18 was not administered antitoxin. She was administered antibiotics but died on the third day of her hospitalization from severe dyspnea caused by a pseudomembrane obstructing her airway (*30*).

Discussion

To compare our findings to those from other countries, we reviewed reports on diphtheria from the United Kingdom (*31*,*32*) and Belgium (*33*). Because of the history of the diphtheria pandemic in Eastern Europe in the late 1980s, surveillance of reports of *C. diphtheriae* infection are still underway in Europe, and cases continue to be identified. Therefore, the literature cases from this region during that period also contain reports of disease caused by the diphtheria toxin–producing *C. diphtheriae* and *C. ulcerans* (*31*). In Japan, the most recent case report of *C. diphtheriae* infection was in 2000 (*34*), and since then, the number of *C. ulcerans* infections have been increasing,

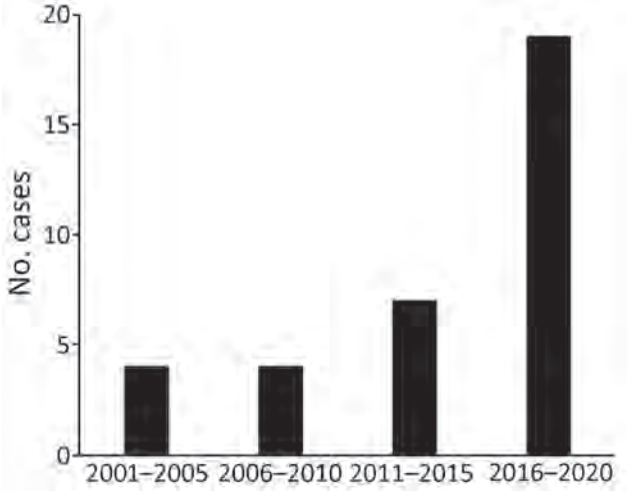

Figure 2. Increase in the number of *Corynebacterium ulcerans* infection cases, by 5-year period, Japan, 2001–2020.

Table 1. Characteristics of patients with *Corynebacterium ulcerans* infection, Japan, 2001–2020*

Characteristic	All cases, N = 34†	Respiratory cases, n = 23‡	Nonrespiratory cases, n = 11§	p value
Median age, y	58 (50–71)	64 (54–72)	38 (21–61)	0.03
Sex				
M	12 (38.7)	7 (31.8)	5 (55.6)	0.25
F	19 (61.3)	15 (68.2)	4 (44.4)	0.19
Relationship with animals¶	33 (97.1)	22 (95.7)	11 (100)	1.00
Vital signs on admission				
Heart rate, beats/min	100 (88–112)	101 (97–114)	85 (85–85)	0.13
Systolic blood pressure, mm Hg	125 (107–146)	130 (108–147)	107 (107–107)	0.32
Body temperature, °C	38 (37.4–38.5)	38 (37.4–38.4)	38.4 (35.5–38.5)	0.94
Respiratory rate, breaths/min	20 (16–26)	18 (16–28)	21 (21–21)	0.61
Laboratory data				
Leukocytes, cells/mm^3	13,800 (9,325–18,900)	14,800 (10,850–21,700)	10,500 (7,775–12,700)	0.07
Platelets, $\times 10^4$/mm^3	26.3 (22.1–27.2)	25.1 (19.9–34.1)	26.6 (26.3–26.8)	0.51
Creatine, mg/dL	0.75 (0.66–1.16)	0.75 (0.67–1.24)	0.59 (0.38–0.80)	0.34
C-reactive protein, mg/dL	6.1 (3.7–16.8)	10.8 (4.7–21)	3.9 (2.3–5.7)	0.07
Treatment antibiotic (no. cases)				
Penicillins	Penicillin G (2), sulbactam/ampicillin (9), piperacillin (5)	Penicillin G (1), sulbactam/ampicillin (8), piperacillin (4)	Penicillin G (1), sulbactam/ampicillin (1), piperacillin (1)	
Macrolides	Erythromycin (9), clarithromycin (6), azithromycin (6), clindamycin (1)	Erythromycin (6), clarithromycin (5), azithromycin (5), clindamycin (1)	Erythromycin (3), azithromycin (1), clarithromycin (1)	
Cephalosporins	Cephepime (1), cefazolin (1), ceftriaxone (1)	Cephepime (1), ceftriaxone (1)	Cefazolin (1)	
Quinolones	Levofloxacin (3)	Levofloxacin (2)	Levofloxacin (1)	
Other	Meropenem (3), faropenem (1), minocycline (1)	Meropenem (3)	Faropenem (1), minocycline (1)	
Diphtheria antitoxin	4 (11.8)	4 (17.4)	0	0.28
Classification of respiratory symptoms				
Mild	8	6	2	
Moderate	16	7	9	
Severe	10	10	0	
Outcome				
Hospital days	10 (3–30)	13 (4–31)	9 (0–26)	0.41
Ventilator days	0 (0–6)	2 (0–12)	0	0.04
Deaths#	2 (5.9)	2 (8.7)	0	1.00

*Data are medians (interquartile range) for continuous variables and no. (%) for categorical variables.
†Missing data for all cases: age (n = 3), sex (n = 3), heart rate (n = 27), systolic blood pressure (n = 27), body temperature (n = 19), respiratory rate (n = 27), leukocytes (n = 17), platelets (n = 26), creatine (n = 23), C-reactive protein (n = 17), treatment (n = 10), hospital days (n = 8), ventilator days (n = 9).
‡Missing data for respiratory cases: age (n = 1), sex (n = 1), heart rate (n = 17), systolic blood pressure (n = 17), body temperature (n = 11), respiratory rate (n = 17), pseudomembrane (n = 1), leukocyte (n = 10), platelets (n = 17), T-bilirubin (n = 17), creatine (n = 14), C-reactive protein (n = 10), treatment (n = 5), hospital days (n = 3), ventilator days (n = 4).
§Missing data for nonrespiratory cases: age (n = 2), sex (n = 2), heart rate (n = 10), systolic blood pressure (n = 10), body temperature (n = 8), respiratory rate (n = 10), leukocytes (n = 7), platelets (n = 10), T-bilirubin (n = 11), creatine (n = 9), C-reactive protein (n = 7), treatment (n = 5), hospital days (n = 5), ventilator days (n = 5).
¶Indicates the presence of animals in the patient's living environment.
#All deaths were in cases for which respiratory symptoms were classified as severe.

as shown in our study (Figure 2). The annual trend in the number of cases of *C. ulcerans* infection in the United Kingdom has also increased over the past few decades (*31*,*32*). In contrast, in Belgium, the number of cases reported during 2010–2017 hardly increased (*33*) and has remained fairly constant.

When we compared the age of patients with *C. ulcerans* infection, we found that in the United Kingdom, 60% of those affected are <15 years of age, whereas in Belgium, 90% of those affected are >45 years of age. In Japan, as in Belgium, 80% of those infected are >45 years of age. The sex ratio of patients showed similar trends in all countries; women accounted for 75% of infections in the United Kingdom, 77% in Belgium, and 67% in Japan. Martini et al. (*33*) argued that women are more likely to be patients because they tend to have more contact with companion animals than men.

When we compared transmission routes of *C. ulcerans*, we found that in the past in the United Kingdom, infections were mainly caused by cattle and poorly sterilized dairy products, but in recent years,

infections have been mainly caused by companion animals such as cats and dogs. The same trends occurred in Belgium and Japan. The change over time in the source of *C. ulcerans* infection in the United Kingdom indicates that this infection is not limited to persons involved in livestock farming and that the general public can become infected (*32*). We speculate that this change contributed to the recent increase in *C. ulcerans* infections in the United Kingdom. Because *C. ulcerans* infections in countries such as the United Kingdom, Belgium, and Japan are suspected to be transmitted from companion animals, not only physicians but also veterinarians who examine companion animals should be informed about *C. ulcerans* infection (*8*,*11*,*16*).

Regarding the prognosis of *C. ulcerans* infection, mortality rates were 6% in the United Kingdom during 1986–2017 (*31*,*32*) and 5.9% in Japan during 2001–2020. No deaths from *C. ulcerans* infections were reported in Belgium during 2010–2017 (*33*). Further details of the course of fatal cases of *C. ulcerans* infection in the United Kingdom show that all of the fatal cases were in women ≥70 years of age who had respiratory symptoms, the death of nearly one third of patients overall was possibly associated with delayed administration of antitoxin, and the death of nearly two thirds of patients overall may have been associated with delayed diagnosis of diphtheria (*31*,*32*). By comparison, 2 fatal cases in Japan occurred in women 57 and 66 years of age who had respiratory symptoms; 1 death may have been attributable to delay in administration of antitoxin, and the other death may have been because the patient was diagnosed with *C. ulcerans* infection too late.

When we compared cases of *C. ulcerans* infection in the United Kingdom and Japan in terms of deaths, we observed a similar course of death in both countries. Administration of antitoxin is the primary treatment for diphtheria, but because diphtheria antitoxin is a preparation made from horse serum immunized with diphtheria toxin, its administration may be accompanied by adverse events, such as serum sickness. The decision requires judgment in considering the risks and benefits of antitoxin administration. In the United Kingdom and Japan, 94% of patients with *C. ulcerans* infection survive. In both cases, administration of macrolide antibiotics is the main treatment method, whereas diphtheria antitoxin is administered to severely ill patients (*31*,*32*)

When we compared the symptoms caused by *C. ulcerans* infection, we found that ≈80% of patients in the United Kingdom had respiratory symptoms and ≈20% had nonrespiratory symptoms. We noted the same tendency in cases in Japan (respiratory symptoms in 66% of patients and nonrespiratory symptoms in 34%). In Belgium, on the contrary, prevalence of nonrespiratory symptoms were as high as 64%, and respiratory symptoms were observed in 36% of cases (*31*–*33*). The different proportions of respiratory and nonrespiratory symptoms of *C. ulcerans* infection in the 3 countries may be related to the immunologic status of patients with respect to diphtheria toxin. In our study, the patients with respiratory symptoms were mostly elderly and severely ill, whereas the patients with nonrespiratory symptoms were relatively young, and few were severely ill (Table 1). In Japan, young persons have high levels of antibody titers against diphtheria toxin, but this antibody titer declines with age (*35*). Patients with high antibody titers who have *C. ulcerans* may show nonrespiratory symptoms without exacerbation of respiratory symptoms. Different diphtheria toxoid vaccination schedules in the United Kingdom and Belgium may also influence symptoms after *C. ulcerans* infection (*37*,*38*).

We also considered the status of vaccination for *C. ulcerans* infections. The diphtheria vaccine in Japan became available in 1948, and after several changes in the inoculation content, the formulation now in use was implemented in 1995. The current vaccination schedule in Japan is to inoculate 3 times

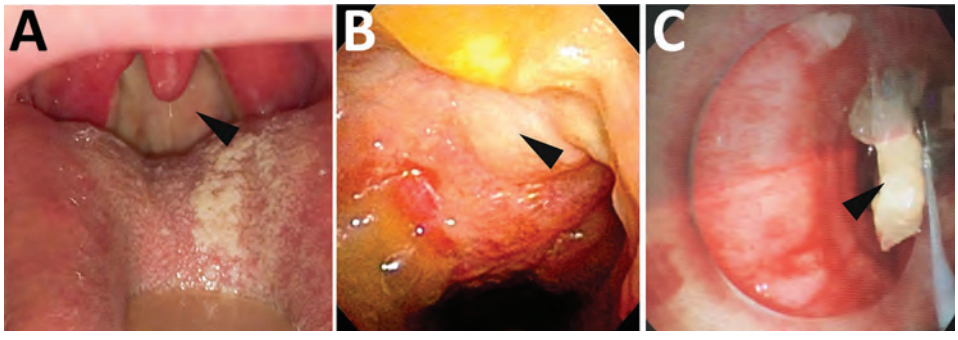

Figure 3. Endoscopic images of the pharynx and bronchi of patients with *Corynebacterium ulcerans* infection, Japan, 2001–2020. A, B) Posterior wall of the pharynx has a yellowish white pseudomembrane. Arrows indicate the white pseudomembrane attached to the pharynx (case no. 21, from Dr. Toyoshima, Japanese Red Cross Ise Hospital, Mie, Japan). C) Pseudomembrane on the bronchi. Arrows indicate the pseudomembrane attached to the bronchi (case no. 29, from Dr. Hayashi, Maebashi Red Cross Hospital, Gunma, Japan).

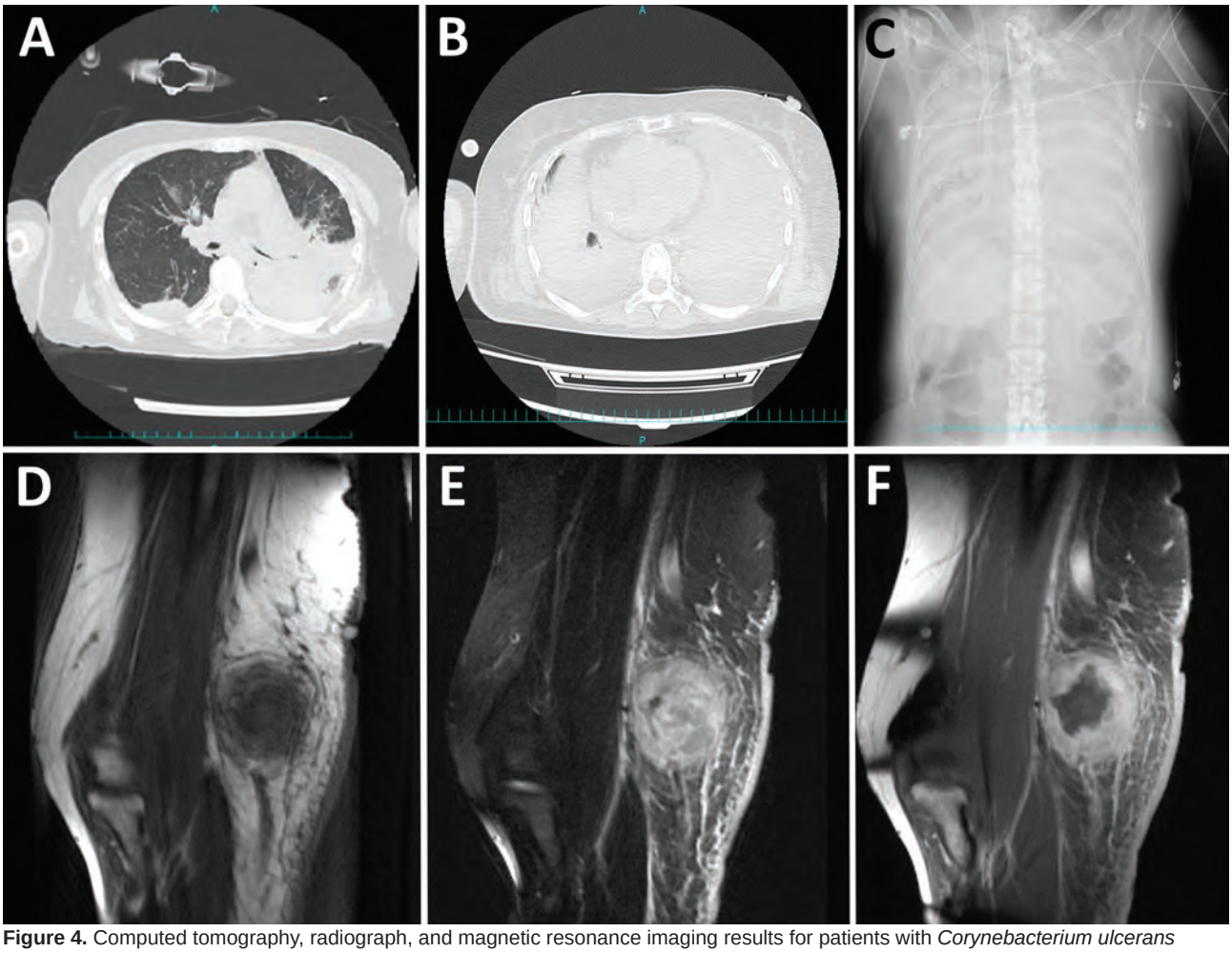

Figure 4. Computed tomography, radiograph, and magnetic resonance imaging results for patients with *Corynebacterium ulcerans* infection, Japan, 2001–2020. A–C) Chest computed tomography images and radiograph of patients with severe respiratory symptoms. Atelectasis noted at admission (A, top) and after exacerbation of symptoms (B, bottom) (case no. 29, from Dr. Hayashi, Maebashi Red Cross Hospital, Gunma, Japan). Spread of atelectasis noted on chest radiograph taken at the time of exacerbation of symptoms (C) (case no. 29, also from Dr. Hayashi, Maebashi Red Cross Hospital). D–F) Magnetic resonance imaging of an elbow abscess. Magnetic resonance imaging T1-weighted images show equal brightness to the muscles (D), fat-suppressed T2-weighted image by short-tau inversion recovery method show unevenly high brightness (E), and contrast-enhanced T1-weighted images show a mass whose margins are contrast-enhanced (F) (case no. 10, from Dr. Urakawa, Tsuruoka Municipal Shonai Hospital, Yamagata, Japan).

at intervals of 3–8 weeks starting at 3 months of age and to give the fourth inoculation 1 year after the third inoculation. At 11 years of age, children receive a fifth boost and are not vaccinated after that point (*35*). In Japan, to understand the state of immunity to diphtheria toxoid, a certain number of persons are randomly selected from prefectures nationwide and their antibody titers are measured every 4–5 years. That survey is commissioned by the government of Japan and is conducted by NIID and local health authorities. According to those survey data, the proportion of persons in their 50s who still had antibody titers at a level protective against diphtheria decreased to ≈10% (*36*). When we interviewed patients in our study and asked about their vaccination status, most of the patients >60 years of age, except for the 20-year-old patient in case 13 and the 6-year-old patient in case 14, so vaccination status was usually unknown. In addition, the average age of patients in our study with severe respiratory symptoms was 67 years (Table 2), and patients born before 1948 had not been vaccinated. We hypothesize that persons in the older age group are inadequately vaccinated or unvaccinated against diphtheria toxin and that the characteristics of *C. ulcerans* infection are related to the vaccination system in Japan.

According to reports on *C. ulcerans* infection in the United Kingdom and Belgium, many patients, especially those who died or were severely ill, were unvaccinated or inadequately vaccinated (*31*–*33*).

The vaccination schedule in the United Kingdom is to inoculate 4 times until 5 years of age; at the age of 14, persons receive a fifth booster and are not vaccinated after that point (*37*). The vaccination schedule in Belgium is to inoculate 6 times until at the age of 14–16 years. Adults in Belgium are recommended to be vaccinated with a diphtheria toxoid–containing vaccine every 10 years (*38*). When we compared the diphtheria toxoid vaccination schedule in the United Kingdom and Belgium with Japan, we found that the United Kingdom schedule is very similar to that of Japan, but the Belgium schedule is similar to the WHO-recommended schedule and the US Advisory Committee on Immunization Practices schedule and includes vaccination for adults. This difference may explain why the number of patients with *C. ulcerans* infection in Belgium has remained constant over the past decade or so (*38*).

In light of those findings, it appears that *C. ulcerans* infections tend to affect generations with reduced levels of diphtheria antitoxin antibodies. Moreover, because the risk for severe disease from *C. ulcerans* infections increases with age, we recommend that adults be vaccinated with diphtheria toxoid vaccine to prevent the spread of this infection. In fact, the European Union (which includes Belgium), the US Centers for Disease Control and Prevention, and WHO recommend that adults be vaccinated with a diphtheria toxoid–containing vaccine every 10 years after completing the initial vaccination series in childhood (*1*,*19*,*35*,*38*).

Among the limitations of this research, we summarized clinical data on 34 cases of *C. ulcerans* infection reported in Japan over a 20-year period, and we reported the clinical features, treatments performed, and prognoses of these cases. However, not all cases were captured, and some data on the reported cases may have been incomplete, which may affect the reliability of our findings. Therefore, it is necessary to verify our findings with more case information in the future.

In Japan, diphtheria caused by diphtheria toxin–producing *C. diphtheriae* occurred in ≈100,000 patients around 1945, and ≈10% of them died. This form of diphtheria was significantly reduced by regular vaccination with the diphtheria toxoid vaccine, and the last such case was reported in 2000 (*34*). Meanwhile, *C. ulcerans* infections have been increasing over the past 20 years and have replaced disease

Table 2. Comparison of the subgroups of patients with *Corynebacterium ulcerans* infection with mild, moderate, and severe respiratory symptoms, Japan, 2001–2020*

Characteristic	Mild symptoms, n = 6†	Moderate symptoms, n = 7‡	Severe symptoms, n = 10§	p value
Age, y	54 (28–61)	62 (51–76)	67 (62–72)	0.07
Sex				
M	3 (60.0)	3 (42.9)	1 (10.0)	0.11
F	2 (40.0)	4 (57.1)	9 (90.0)	0.29
Vital signs on admission				
Body temperature, °C	37 (36.6–37.4)	38 (37.6–38.8)	38 (37.5–38.7)	0.14
Pseudomembrane	5 (100)	6 (85.7)	10 (100)	0.33
Laboratory data				
Leukocytes, cells/mm^3	9,500 (6,700–14,800)	14,350 (10,363–23,550)	18,900 (13,400–22,600)	0.26
C-reactive protein, mg/dL	4.7 (0.9–6.1)	7.7 (1.8–12.6)	21 (11.7–25.4)	0.02
Treatment antibiotic (no. cases)				
Penicillins	None	Penicillin G (1), sulbactam/ampicillin (2), piperacillin (2)	Sulbactam/ampicillin (6), piperacillin (2)	
Macrolides	Erythromycin (1), clarithromycin (2)	Erythromycin (3), clarithromycin (3), azithromycin (2)	Erythromycin (2), azithromycin (3), clindamycin (1)	
Cephalosporins		Ceftriaxone (1)		
Quinolones		Levofloxacin (2)		
Other			Meropenem (3)	
Diphtheria antitoxin	0	0	4 (40.0)	0.04
Outcome				
Hospital days	0	7 (7–10)	29 (20–56)	<0.01
Ventilator days	0	0	12 (5–42)	<0.01
Deaths	0	0	2 (20.0)	0.24

*Data are medians (interquartile range) for continuous variables and no. (%) for categorical variables.
†Missing data for mild cases: age (n = 1), sex (n = 1), heart rate (n = 6), systolic blood pressure (n = 6), body temperature (n = 4), respiratory rate (n = 6), pseudomembrane (n = 1), leukocytes (n = 3), platelets (n = 6), C-reactive protein (n = 3), treatment (n = 3), hospital days (n = 3), ventilator days (n = 3).
‡Missing data for moderate: heart rate (n = 5), systolic blood pressure (n = 5), body temperature (n = 3), respiratory rate (n = 5), leukocytes (n = 3), platelets (n = 5), T-bilirubin (n = 5), creatine (n = 4), C-reactive protein (n = 3), treatment (n = 1).
§Missing data for severe: heart rate (n = 6), systolic blood pressure (n = 6), body temperature (n = 4), respiratory rate (n = 6), leukocytes (n = 4), platelets (n = 6), T-bilirubin (n = 6), creatine (n = 5), C-reactive protein (n = 4), treatment (n = 1), ventilator days (n = 1).

cases caused by *C. diphtheriae*. Clinicians and various local hygiene agencies have been alerted to this kind of infection. However, the law does not require all cases to be reported. Given the increased number of cases revealed in our study and the WHO position of considering *C. ulcerans* infections to be diphtheria, we suggest that all *C. ulcerans* cases should be included with the infections that currently must be reported immediately.

Acknowledgments

We thank Shouji Asakura, Tetsu Aizawa, Teruyuki Ishii, and Takehiko Morioka for their contributions to this article.

This research was conducted as one of the antitoxin research projects under Japan's Agency for Medical Research and Development 2019–2021 Research Development of Innovative Drugs for Emerging and Reemerging Infectious Diseases Promotion research project (project no. 21fk0108101j0003).

About the Author

Dr. Yamamoto is an infectious diseases specialist at the Management Department of Biosafety and Laboratory Animal at Japan's National Institute of Infectious Diseases. Dr. Hifumi is a physician at the Emergency and Critical Care Medicine Department at St. Luke's International Hospital. Their research interests are infectious diseases control.

References

1. Centers for Disease Control and Prevention. Diphtheria [cited 2021 Oct 20]. https://www.cdc.gov/diphtheria/index.html
2. Wong TP, Groman N. Production of diphtheria toxin by selected isolates of *Corynebacterium ulcerans* and *Corynebacterium pseudotuberculosis*. Infect Immun. 1984;43:1114–6. https://doi.org/10.1128/iai.43.3.1114-1116.1984
3. Sing A, Bierschenk S, Heesemann J. Classical diphtheria caused by *Corynebacterium ulcerans* in Germany: amino acid sequence differences between diphtheria toxins from *Corynebacterium diphtheriae* and *C. ulcerans*. Clin Infect Dis. 2005;40:325–6. https://doi.org/10.1086/426687
4. Hommez J, Devriese LA, Vaneechoutte M, Riegel P, Butaye P, Haesebrouck F. Identification of nonlipophilic corynebacteria isolated from dairy cows with mastitis. J Clin Microbiol. 1999;37:954–7. https://doi.org/10.1128/JCM.37.4.954-957.1999
5. Hart RJ. *Corynebacterium ulcerans* in humans and cattle in North Devon. J Hyg (Lond). 1984;92:161–4. https://doi.org/10.1017/S0022172400064172
6. Higgs TM, Smith A, Cleverly LM, Neave FK. *Corynebacterium ulcerans* infections in a dairy herd. Vet Rec. 1967;81:34–5. https://doi.org/10.1136/vr.81.2.34
7. Aaron L, Heurtebise F, Bachelier MN, Guimard Y. Pseudomembranous diphtheria caused by *Corynebacterium ulcerans* [in French]. Rev Med Interne. 2006;27:333–5. https://doi.org/10.1016/j.revmed.2005.12.011
8. Lartigue M-F, Monnet X, Le Flèche A, Grimont PAD, Benet JJ, Durrbach A, et al. *Corynebacterium ulcerans* in an immunocompromised patient with diphtheria and her dog. J Clin Microbiol. 2005;43:999–1001. https://doi.org/10.1128/JCM.43.2.999-1001.2005
9. Morris WE, Uzal FA, Cipolla AL. Pyogranulomatous meningoencephalitis in a goat due to *Corynebacterium ulcerans*. Vet Rec. 2005;156:317–8. https://doi.org/10.1136/vr.156.10.317
10. Foster G, Patterson T, Howie F, Simpson V, Davison N, Efstratiou A, et al. *Corynebacterium ulcerans* in free-ranging otters. Vet Rec. 2002;150:524.
11. Taylor DJ, Efstratiou A, Reilly WJ. Diphtheria toxin production by *Corynebacterium ulcerans* from cats. Vet Rec. 2002;150:355.
12. Tejedor MT, Martin JL, Lupiola P, Gutierrez C. Caseous lymphadenitis caused by *Corynebacterium ulcerans* in the dromedary camel. Can Vet J. 2000;41:126–7.
13. Bergin IL, Chien CC, Marini RP, Fox JG. Isolation and characterization of *Corynebacterium ulcerans* from cephalic implants in macaques. Comp Med. 2000;50:530–5.
14. Olson ME, Goemans I, Bolingbroke D, Lundberg S. Gangrenous dermatitis caused by *Corynebacterium ulcerans* in Richardson ground squirrels. J Am Vet Med Assoc. 1988;193:367–8.
15. Stănică E, Maximesco P, Stoian C, Pop A, Oprişan R, Potorac E. Level of antitoxic immunity and carriage of diphtheria bacilli in horses under present circumstances of dimunition of morbidity of diphtheria [in French]. Arch Roum Pathol Exp Microbiol. 1968;27:552–62.
16. Panaitescu M, Maximescu P, Michel J, Potorac E. Respiratory pathogens in non-human primates with special reference to *Corynebacterium ulcerans*. Lab Anim. 1977;11:155–7. https://doi.org/10.1258/002367777780936657
17. Fox JG, Frost WW. *Corynebacterium ulcerans* mastitis in a bonnet macaque (*Macaca radiata*). Lab Anim Sci. 1974;24:820–2.
18. May BD. *Corynebacterium ulcerans* infections in monkeys. Lab Anim Sci. 1972;22:509–13.
19. World Health Organization. Diphtheria: vaccine preventable diseases surveillance standards [cited 2021 Nov 17]. https://cdn.who.int/media/docs/default-source/immunization/vpd_surveillance/vpd-surveillance-standards-publication/who-surveillancevaccinepreventable-04-diphtheria-r2.pdf
20. Lartigue MF, Monnet X, Le Flèche A, Grimont PA, Benet JJ, Durrbach A, et al. *Corynebacterium ulcerans* in an immunocompromised patient with diphtheria and her dog. J Clin Microbiol. 2005;43:999–1001. https://doi.org/10.1128/JCM.43.2.999-1001.2005
21. Vandentorren S, Guiso N, Badell E, Boisrenoult P, Micaelo M, Troché G, et al. Toxigenic *Corynebacterium ulcerans* in a fatal human case and her feline contacts, France, March 2014. Euro Surveill. 2014;19:1–3. https://doi.org/10.2807/1560-7917.ES2014.19.38.20910
22. Mattos-Guaraldi AL, Sampaio JL, Santos CS, Pimenta FP, Pereira GA, Pacheco LG, et al. First detection of *Corynebacterium ulcerans* producing a diphtheria-like toxin in a case of human with pulmonary infection in the Rio de Janeiro metropolitan area, Brazil. Mem Inst Oswaldo Cruz. 2008;103:396–400. https://doi.org/10.1590/S0074-02762008000400014
23. Patil SM, Beck PP, Nelson TB, Acevedo AB, Roland W. Prepatellar bursitis with abscess due to *Corynebacterium ulcerans*. Case Rep Orthop. 2021;2021:3507672. https://doi.org/10.1155/2021/3507672

24. Meinel DM, Konrad R, Berger A, König C, Schmidt-Wieland T, Hogardt M, et al. Zoonotic transmission of toxigenic *Corynebacterium ulcerans* strain, Germany, 2012. Emerg Infect Dis. 2015;21:356–8. https://doi.org/10.3201/eid2102.141160
25. Hatanaka A, Tsunoda A, Okamoto M, Ooe K, Nakamura A, Miyakoshi M, et al. *Corynebacterium ulcerans* diphtheria in Japan. Emerg Infect Dis. 2003;9:752–3. https://doi.org/10.3201/eid0906.020645
26. Ministry of Health, Labour and Welfare of Japan. Q&A about *Corynebacterium ulcerans* [cited 2021 Dec 15]. https://www.mhlw.go.jp/bunya/kenkou/kekkaku-kansenshou18/corynebacterium_02.html
27. Moore LSP, Leslie A, Meltzer M, Sandison A, Efstratiou A, Sriskandan S. *Corynebacterium ulcerans* cutaneous diphtheria. Lancet Infect Dis. 2015;15:1100–7. https://doi.org/10.1016/S1473-3099 (15)00225-X
28. Wagner J, Ignatius R, Voss S, Höpfner V, Ehlers S, Funke G, et al. Infection of the skin caused by *Corynebacterium ulcerans* and mimicking classical cutaneous diphtheria. Clin Infect Dis. 2001;33:1598–600. https://doi.org/10.1086/322969
29. Ohno T, Sakamoto M, Koyama Y, Hatanaka A. A case of pseudomembranous laryngitis caused by *Corynebacterium ulcerans* with severe systemic complications. Nippon Jibiinkoka Tokeibugeka Gakkai Kaiho. 2021;124:1413–8. https://doi.org/10.3950/jibiinkotokeibu.124.10_1413
30. Yasuda I, Matsuyama H, Ishifuji T, Yamashita Y, Takaki M, Morimoto K, et al. Severe pneumonia caused by toxigenic *Corynebacterium ulcerans* infection, Japan. Emerg Infect Dis. 2018;24:588–91. https://doi.org/10.3201/eid2403.171837
31. Wagner KS, White JM, Crowcroft NS, De Martin S, Mann G, Efstratiou A. Diphtheria in the United Kingdom, 1986–2008: the increasing role of *Corynebacterium ulcerans*. Epidemiol Infect. 2010;138:1519–30. https://doi.org/10.1017/S0950268810001895
32. Gower CM, Scobie A, Fry NK, Litt DJ, Cameron JC, Chand MA, et al. The changing epidemiology of diphtheria in the United Kingdom, 2009 to 2017. Euro Surveill. 2020;25:1900462. https://doi.org/10.2807/1560-7917.ES.2020.25.11.1900462
33. Martini H, Soetens O, Litt D, Fry NK, Detemmerman L, Wybo I, et al. Diphtheria in Belgium: 2010–2017. J Med Microbiol. 2019;68:1517–25. https://doi.org/10.1099/jmm.0.001039
34. National Institute of Infectious Diseases (Japan). Diphtheriae [in Japanese] [cited 2022 Nov 17]. http://idsc.nih.go.jp/iasr/19/224/tpc224-j.html
35. National Institute of Infectious Diseases (Japan). Vaccination schedule for children in Japan [in Japanese] [cited 2022 Nov 17]. http://idsc.nih.go.jp/vaccine/dschedule.html
36. National Institute of Infectious Diseases (Japan). Infectious disease epidemic prediction survey report [in Japanese] [cited 2022 Nov 17]. https://www.niid.go.jp/niid/ja/y-reports/669-yosoku-report.html
37. Public Health England. The complete routine immunisation schedule 2013 to 2014 [cited 2022 Nov 17]. https://www.gov.uk/government/publications/the-complete-routine-immunisation-schedule-201314
38. European Centre for Disease Prevention and Control. Vaccine scheduler [cited 2022 Nov 17]. https://vaccine-schedule.ecdc.europa.eu

Address for correspondence: Akihiko Yamamoto, Management Department of Biosafety and Laboratory Animal, National Institute of Infectious Diseases, Tokyo, 2080011, Japan; email: yama-aki@nih.go.jp

Healthcare-Associated Infections Caused by *Mycolicibacterium neoaurum*

Kate Shapiro, Shane J. Cross, Ted H. Morton, Hiroto Inaba, Ashley Holland, Francisca R. Fasipe, Elisabeth E. Adderson

In support of improving patient care, this activity has been planned and implemented by Medscape, LLC and Emerging Infectious Diseases. Medscape, LLC is jointly accredited with commendation by the Accreditation Council for Continuing Medical Education (ACCME), the Accreditation Council for Pharmacy Education (ACPE), and the American Nurses Credentialing Center (ANCC), to provide continuing education for the healthcare team.

Medscape, LLC designates this Journal-based CME activity for a maximum of 1.00 ***AMA PRA Category 1 Credit(s)™***. Physicians should claim only the credit commensurate with the extent of their participation in the activity.

Successful completion of this CME activity, which includes participation in the evaluation component, enables the participant to earn up to 1.0 MOC points in the American Board of Internal Medicine's (ABIM) Maintenance of Certification (MOC) program. Participants will earn MOC points equivalent to the amount of CME credits claimed for the activity. It is the CME activity provider's responsibility to submit participant completion information to ACCME for the purpose of granting ABIM MOC credit.

All other clinicians completing this activity will be issued a certificate of participation. To participate in this journal CME activity: (1) review the learning objectives and author disclosures; (2) study the education content; (3) take the post-test with a 75% minimum passing score and complete the evaluation at http://www.medscape.org/journal/eid; and (4) view/print certificate. For CME questions, see page XXX.

NOTE: It is Medscape's policy to avoid the use of Brand names in accredited activities. However, in an effort to be as clear as possible, the use of brand names should not be viewed as a promotion of any brand or as an endorsement by Medscape of specific products.

Release date: July 14, 2023; Expiration date: July 14, 2024

Learning Objectives

Upon completion of this activity, participants will be able to:

- Assess the demographic and clinical characteristics of *Mycolicibacterium neoaurum* infection, based on a case report of a child with leukemia and catheter-related bloodstream infection and a case series of 36 previously reported episodes of *M. neoaurum* infection
- Evaluate the diagnosis and management of *Mycolicibacterium neoaurum* infection, based on a case report of a child with leukemia and catheter-related bloodstream infection and a case series of 36 previously reported episodes of *M. neoaurum* infection
- Determine the clinical implications of demographic and clinical characteristics, diagnosis, and management of *Mycolicibacterium neoaurum* infection, based on a case report of a child with leukemia and catheter-related bloodstream infection and a case series of 36 previously reported episodes of *M. neoaurum* infection

CME Editor

Susan Zunino, PhD, Technical Writer/Editor, Emerging Infectious Diseases. *Disclosure: Susan Zunino, PhD, has no relevant financial relationships.*

CME Author

Laurie Barclay, MD, freelance writer and reviewer, Medscape, LLC. *Disclosure: Laurie Barclay, MD, has no relevant financial relationships.*

Authors

Kate Shapiro, MD; Shane J. Cross, PharmD; Ted H. Morton, PharmD; Hiroto Inaba, PhD; Ashley Holland, MSN; Francisca R. Fasipe, MD; and ***Elisabeth E. Adderson, MD.***

Author affiliations: St. Jude Children's Research Hospital, Memphis, Tennessee, USA (K. Shapiro, S.J. Cross, T.H. Morton, H. Inaba, A. Holland, E.E. Adderson); University of Tennessee Health Sciences Center, Memphis (S.J. Cross, T.H. Morton, H. Inaba, E.E. Adderson); Mercy Children's Hospital, Springfield, Missouri, USA (F.R. Fasipe)

DOI: https://doi.org/10.3201/eid2908.230007

Mycolicibacterium neoaurum is a rapidly growing mycobacterium and an emerging cause of human infections. *M. neoaurum* infections are uncommon but likely underreported, and our understanding of the disease spectrum and optimum management is incomplete. We summarize demographic and clinical characteristics of a case of catheter-related *M. neoaurum* bacteremia in a child with leukemia and those of 36 previously reported episodes of *M. neoaurum* infection. Most infections occurred in young to middle-aged adults with serious underlying medical conditions and commonly involved medical devices. Overall, infections were not associated with severe illness or death. In contrast to other mycobacteria species, *M. neoaurum* was generally susceptible to multiple antimicrobial drugs and responded promptly to treatment, and infections were associated with good outcomes after relatively short therapy duration and device removal. Delays in identification and susceptibility testing were common. We recommend using combination antimicrobial drug therapy and removal of infected devices to eradicate infection.

Comprehensive phylogenetic and genomic studies support the division of the genus *Mycobacterium* into 5 main clades: the emended genus *Mycobacterium*, *Mycolicibacter* gen. nov, *Mycolicibacillus* gen. nov., *Mycolicibacterium* gen. nov., and *Mycobacteroides* gen. nov (*1*). *Mycolicibacterium* spp. include rapidly growing mycobacteria (RGM) that are not part of the *Mycobacterium abscessus* complex (i.e., *Mycobacteroides* gen. nov., which includes *M. abscessus, M. chelonae*, *M. franklinii*, *M. immunogenum*, and *M. saopaulense*).

Mycolicibacterium spp. are considered to have low pathogenicity, but some are associated with human infection. *Mycolicibacterium neoaurum*, originally described by Tsukamura in 1972, is derived from the Greek word for new gold because of distinctive yellow-orange colonies (*2*). Since its identification, increasing numbers of case reports and small case series of invasive *M. neoaurum* infections have been described. Infections are likely underrecognized because many laboratories do not identify all mycobacteria at the species level. Bacteremia might also be missed or isolates inappropriately dismissed as contaminants because mycobacteria might require longer culture incubation than conventional bacterial pathogens, and they are ubiquitous in the environment.

Although best practices for treating infections caused by more commonly reported RGM species are now recognized, our understanding of disease spectra and best infection management strategies for rarer RGM species, such as *M. neoaurum*, remains incomplete. Therefore, to improve clinical awareness of *M. neoaurum*, we summarized demographic and clinical characteristics of 36 previously reported episodes and report an additional case of *M. neoaurum* infection.

Methods

We obtained demographic and clinical characteristics of the patient in the reported case from health information records. We searched PubMed and Embase (https://www.embase.com) databases by using the terms neoaurum, *Mycobacterium neoaurum*, and *Mycolicibacterium neoaurum*. We cited cases that reported individual clinical data and were published in any year or language. Patient characteristics were summarized by using descriptive statistics. Analyses were performed by using Stata version 16.1 software (StataCorp LLC).

Results

Case Report

A 21-month-old boy with low-risk B cell acute lymphoblastic leukemia (ALL) in remission was treated by using the St. Jude Children's Research Hospital TOTAL Therapy Study 17 protocol (ClinicalTrials.gov identifier NCT03117751), which is similar to the low-risk arm of the TOTAL Therapy Study 16 protocol (identifier NCT00549848) (*3*). In brief, remission induction consists of prednisone, vincristine, daunorubicin, and pegylated asparaginase, then cyclophosphamide, cytarabine, and mercaptopurine. Consolidation therapy consists of 4 courses of high-dose methotrexate and mercaptopurine. Continuation therapy consists of 120 weeks of mercaptopurine, dexamethasone, vincristine, and methotrexate interrupted by 2 reinduction cycles with dexamethasone, vincristine, and pegylated asparaginase. Triple intrathecal therapy with methotrexate, dexamethasone, and cytarabine was provided to control leukemia in the central nervous system.

During week 13 of continuation therapy, the patient had a fever of 103°F, cough, coryza, anorexia, and diarrhea and was hospitalized 1 day after onset of those signs and symptoms. His medical history was remarkable because of episodes of mucositis associated with chemotherapy, a recent respiratory syncytial virus upper respiratory tract infection, and distant placement of a subcutaneous port (SCP) for intravenous access. He received trimethoprim/sulfamethoxazole (TMP/SMX) for *Pneumocystis* pneumonia prophylaxis. He lived with his family in an urban area, and no history of difficulties accessing his SCP or erythema, discharge, or tenderness at the SCP insertion site had been observed. His physical

examination was unremarkable except for mild pallor. His blood leukocyte count was 10.9 × 10^3 cells/μL (reference range 6.0–17.0 × 10^3 cells/μL), consisting of 77% neutrophils, 9% lymphocytes (absolute lymphocyte count 0.97 × 10^3 cells/μL [reference range 1.20–4.00 × 10^3 cells/μL]), and 13% monocytes. He was mildly anemic; hemaglobin level was 10.7 g/dL (reference range 11.3–12.3 g/dL). Serum C-reactive protein was elevated at 10.7 mg/L (reference range <5.0 mg/dL), aspartate aminotransferase level was 136 U/L (reference range 10–50 U/L), and alanine aminotransferase level was 520 U/L (reference range ≤50 U/L). Serum bilirubin was within reference range. A respiratory PCR panel was positive for respiratory syncytial virus.

The patient's symptoms resolved overnight, and he was discharged. One bacteria species was isolated after a 5-day incubation of blood cultures obtained from the patient's SCP at hospital admission by using the BacT/ALERT automated microbial detection system (bioMérieux). The organism was initially reported as a gram-positive coccobacillus but stained weakly, prompting acid-fast bacillus (AFB) staining, which gave positive results. *M. neoaurum* was identified initially by matrix-assisted laser desorption/ionization time-of-flight mass spectrometry and confirmed by 16S rRNA sequencing; both of those analyses were performed at the Mayo Clinic Laboratories (Rochester, MN, USA). The Mayo Clinic Laboratories also performed antimicrobial drug susceptibility testing by using the broth microtiter dilution method. Results were reported as MICs (in μg/mL) and interpreted according to Clinical and Laboratory Standards Institute guidelines (*4*).

The patient was readmitted for further bacteremia evaluation 9 days after initial blood cultures were obtained. *M. neoaurum* was again isolated from blood drawn from the SCP and catheter tip, but blood cultures obtained from a peripheral vein were sterile. Results of chest radiograph were unremarkable. We initiated empirical therapy with intravenous imipenem/cilastatin, oral azithromycin, and oral ciprofloxacin. We removed the SCP on hospital day 3, and 3 blood cultures obtained after port removal were sterile. We inserted a central catheter line peripherally on hospital day 6. Antimicrobial drug susceptibility tests showed that the *M. neoaurum* isolate was susceptible to cefoxitin, imipenem, ciprofloxacin, moxifloxacin, amikacin, tobramycin, doxycycline, TMP/SMX, and linezolid and resistant to clarithromycin. The MIC for tigecycline was 0.12 μg/mL. We ultimately treated the patient with imipenem/cilastatin, azithromycin, and ciprofloxacin for 16 days, then with TMP/SMX and ciprofloxacin for 26 days, and he remained well 15 months later.

Literature Review

We found 238 articles in the literature and included 31 reports describing 36 cases in this review (Appendix Table, https://wwwnc.cdc.gov/EID/article/29/8/23-0007-App1.pdf). Including the case report we described, the median age of patients was 46 (interquartile range [IQR] 25–59) years, and 19 (51%) were female. All but 1 patient had serious underlying chronic medical conditions: malignancy (n = 13, 35%), cardiovascular disease (n = 9, 24%), chronic renal insufficiency (n = 6, 16%), diabetes (n = 6, 16%), and gastrointestinal disorders (n = 4, 11%). Some patients had indwelling central venous catheters (CVCs) (n = 19, 51%) or other foreign bodies, such as prosthetic valves (n = 3), pacemakers (n = 2), peritoneal dialysis catheters (n = 2), hemodialysis catheter (n = 1), and an orthopedic external fixation device (n = 1).

The most common manifestation of infection was bacteremia (n = 22, 59%); a total of 11 patients had central line-associated bacteremia, 8 had CVC-related bacteremia, 1 had bacteremia associated with a pacemaker lead infection, and 1 had bacteremia from a hemodialysis fistula (*5*). Bacteremia occurred in 1 patient without a CVC who had undergone liver transplantation. Pneumonia occurred in 4 patients, 3 of whom had underlying pulmonary disease. Skin and soft tissue infections were reported in 3 patients, and postsurgical infections were found in 2 patients (a pacemaker pocket infection and infection at a pin exit site). Both patients with endocarditis had histories of intravenous drug abuse and had undergone previous mitral valve replacement. Both patients with peritonitis had indwelling peritoneal dialysis catheters. Other infections included single episodes of granulomatous meningitis and urinary tract infection.

Delays in identifying *M. neoaurum* were common. The median time to reporting positive cultures was 4.5 (IQR 1–10) days. Most isolates were identified as gram-positive or gram-variable coccobacilli or bacilli. In 1 case, AFB staining was delayed, leading to preliminary identification of the isolate as *Rhodococcus* sp. (*6*). In 24 cases for which the method of definitive identification was reported, investigators used chromatography (n = 6); matrix-assisted laser desorption/ionization time-of-flight mass spectrometry (n = 4); or sequencing of 16S rRNA (n = 15), the β subunit of RNA polymerase *ropB* gene (n = 1), or 65-kDa heat shock protein gene *hsp65* (n = 8). In 2 cases, a specific mycobacterial PCR was used for identification.

Of 21 isolates tested, all were susceptible to doxycycline, linezolid, and moxifloxacin according to the published report or Clinical and Laboratory Standards Institute broth microdilution interpretive criteria for RGM. Most isolates were susceptible to amikacin (17 of 18 isolates), cefoxitin (12 of 13), ciprofloxacin (15 of 16), imipenem (14 of 15), and meropenem (3 of 3) (Table) (*6*–*23*). Isolates were less reliably susceptible to TMP/SMX (10 of 15 isolates) and clarithromycin (7 of 15). Patients were treated with a variety of antimicrobial agents and regimens for a median duration of 6 (IQR 5–13) weeks; 3 patients received no antimicrobial drug therapy, and treatment details were not reported for 1 case. Combination antimicrobial drug therapy was used initially in 25 (74%) and, ultimately, 26 (76%) patients. Most (16 of 19) patients with CVC-associated bacteremia had their CVC removed. Infection management involving other medical devices often included device removal. However, several infections were treated only with antimicrobial drugs, including 1 of 2 cases of endocarditis, 1 of 2 infections associated with peritoneal dialysis catheters, 1 pacemaker pocket infection, and 1 pin tract infection. The patient with meningitis died; the long-term outcome of another patient with a urinary tract infection was not reported. Otherwise, infections in all patients were cured. One patient with CVC-related bacteremia who was treated medically had a relapse that was successfully treated by CVC removal and a second course of antimicrobial drugs. The relative risk for relapse among patients with CVC-associated infections who had their CVC removed was 0.083 (95% CI 0.0041–1.6860; p = 0.105); the number needed to treat for 1 patient to benefit was 2.9.

Other Reports

In addition to the individual cases in this review, a case series of 4 patients with *M. neoaurum* bacteremia has been reported (*24*). Their median age was 54 years, and 3 were male. All 4 patients were immunocompromised (3 with hematologic malignancies, 1 with a solid tumor) but not neutropenic. Three patients were treated by catheter removal and a combination of antimicrobial drugs. In 1 case, the isolate

Table. Methods of determination and antimicrobial drug susceptibilities of isolates from the current case and published reports of healthcare-associated infections caused by *Mycolicibacterium neoaurum**

Reference	Method	Antimicrobial drug susceptibility†
Case report	Broth microdilution	Amikacin, ≤1, S; cefoxitin, 4, S; ciprofloxacin, ≤0.12, S; clarithromycin, 8, R; doxycycline, ≤0.12, S; imipenem, 0.12, S; linezolid, ≤1, S; moxifloxacin, 0.06, S; tigecycline, 0.12, no interpretation; TMP/SMX, 2/38, S
(*6*)	Agar dilution	Amikacin, 0.5, S; ciprofloxacin, 0.016, S; clarithromycin, 4, I; doxycycline, 0.064, S; linezolid, 0.25, S; meropenem, 0.25, S; moxifloxacin, 0.008, S; TMP/SMX, 0.25, S
(*7*)	Etest	Amikacin, S; clarithromycin, S; TMP/SMX, S
(*8*)	Disk diffusion	Amikacin, S; cefoxitin, S; doxycycline, S; imipenem, S; TMP/SMX, S
(*9*)	Etest	Amikacin, S; cefoxitin, S; ciprofloxacin, S; clarithromycin, S; imipenem, S; linezolid, S; TMP/SMX, R
(*10*)	Broth microdilution	Amikacin, S; cefoxitin, S; ciprofloxacin, S; clarithromycin, R; doxycycline, S; imipenem, S; linezolid, S; moxifloxacin, S; TMP/SMX, S
(*11*)	Disk diffusion	Amikacin, S; cefoxitin, S; ciprofloxacin, S; clarithromycin, R; imipenem, S; TMP/SMX, R
(*12*)	Broth microdilution	Amikacin, ≤8, S; cefoxitin, ≤16, S; ciprofloxacin, ≤1, S; doxycycline, ≤1, S; imipenem, ≤2, S; linezolid, ≤1, S; moxifloxacin, ≤0.5, S; TMP/SMX, 1/19, S
(*13*)	Not reported	Amikacin, R; ciprofloxacin, R; imipenem, R; TMP/SMX, R
(*14*)	Not reported	Amikacin, ≤1, S; cefoxitin, 8, S; ciprofloxacin, ≤0.12, S; clarithromycin, >4, R; doxycycline, ≤0.25, S
(*14*)	Not reported	Amikacin, 8, S; doxycycline, 0.5, S; linezolid, 1, S
(*14*)	Broth microdilution	Amikacin, 1, S; cefoxitin, 8, S; ciprofloxacin, 0.25, S; clarithromycin, 0.25, S; imipenem, 1, S; linezolid, 2, S
(*15*)	Not reported	Amikacin, ≤1, S; cefoxitin, 8, S; ciprofloxacin, 0.25, S; clarithromycin, >16, R; doxycycline, 1, S; imipenem, ≤2, S; linezolid, 4, S; moxifloxacin, ≤0.25, S; TMP/SMX, 0.5/9.5, S
(*16*)	Disk diffusion	Amikacin, S; ciprofloxacin, S; doxycycline, S; imipenem, S; meropenem, S; TMP/SMX, S
(*17*)	Etest	Ciprofloxacin, S; clarithromycin, R; doxycycline, S; imipenem, S
(*18*)	Broth microdilution	Amikacin, ≤1.0, S; cefoxitin, 32, I; ciprofloxacin, ≤0.125, S; clarithromycin, 2, S; doxycycline, ≤0.125, S; imipenem, 2, S; linezolid, <2, S; moxifloxacin, ≤0.125, S; TMP/SMX, 16/304, R
(*19*)	Not reported	Amikacin, ≤8, S; cefoxitin, ≤16, S; ciprofloxacin, ≤1, S; clarithromycin, 1, S; doxycycline, ≤1, S; imipenem, ≤2, S; linezolid, ≤1, S; moxifloxacin, ≤0.5, S; TMP/SMX, <0.5/9.5, S
(*20*)	Etest	Cefoxitin, 2, S; ciprofloxacin, 0.6, S; clarithromycin, 0.125, S; imipenem, 0.19, S; linezolid, 1.5, S; moxifloxacin, 0.2, S; TMP/SMX, 32, R
(*21*)	Broth microdilution	Amikacin, <1, S; cefoxitin, 8, S; clarithromycin, 2, S; imipenem, <2, S; linezolid, 2, S; meropenem, 2, S; moxifloxacin, ≤0.25, S; TMP/SMX, 1/19, S
(*22*)	Disk diffusion	Amikacin, S; clarithromycin, R; ciprofloxacin, S; doxycycline, S
(*23*)	Etest	Imipenem, 0.12, S

*Values for each antimicrobial drug are MICs in μg/mL. Etest, bioMérieux. I, intermediate; S, sensitive; R, resistant; TMP/SMX, trimethoprim/sulfamethoxazole.
†MICs were interpreted according to broth microdilution criteria in the Clinical and Laboratory Standards Institute guidelines for rapidly growing mycobacteria (*4*).

was considered a contaminant and not treated. All infections were cured. In another report, 2 of 28 patients (both children) with cancer had bacteremia attributed to *M. neoaurum* (*25*).

Discussion

Previous reports have described *M. neoaurum* infections as primarily affecting immunocompromised persons. However, infections that we described in our case report and literature review might be more appropriately considered healthcare-associated infections, because most patients were not immunocompromised but had medical devices or had undergone invasive procedures before infections developed. In our study, 3 patients with pulmonary infections had conditions that predisposed them to anatomic lung abnormalities and infections caused by other mycobacteria species (*26*). Furthermore, 1 patient with a skin and soft tissue infection had a history of penetrating trauma, but 2 others with this condition did not report trauma. However, injury might not have been recalled, or *M. neoaurum* inoculation might have occurred through an unrecognized skin break. In a single-center study of cutaneous nontuberculous mycobacteria infections, histories of trauma, surgical procedure, or environmental exposure to mycobacteria were common among patients; *M. neoaurum* caused 2 of 78 infections (*27*). As the population of persons with chronic medical conditions increases, more *M. neoaurum* infections will likely be recognized.

We found that 1 infection in our case series occurred in a previously healthy, 25-year-old woman who showed signs of pulmonary disease that was AFB smear positive; the infecting organism was confirmed as *M. neoaurum* by 16S rRNA sequencing (*18*). Although this finding suggests that *M. neoaurum* might cause occasional disease in healthy persons, the patient might have had an unrecognized risk factor for mycobacterial infection, such as interferon gamma receptor 1 deficiency, which would only become apparent over time (*28*). The patient responded to antimicrobial drug therapy, but her long-term outcome was not reported.

One patient in our review who had several serious medical comorbidities had rapidly progressive dementia and diagnostic imaging studies suggestive of recurrent ischemic stroke (*29*); an autopsy revealed granulomatous meningitis. Results of conventional diagnostic microbiology were uninformative, but broad-range bacterial rDNA PCR amplified a product that was 99% homologous to *M. neoaurum* DNA. However, histopathologic stains did not reveal AFB, cultures were sterile, and the patient met criteria for an alternative diagnosis of probable Creutzfeldt-Jacob disease, suggesting that PCR might have been falsely positive (*29*,*30*). Except for this case, all patients in our review were promptly cured of their infections, and no patient required intensive care or died. Thus, in contrast to other RGM species, *M. neoaurum* appears to have low virulence and is associated with limited illness and death (*26*).

M. neoaurum has been isolated from soil, tap water, fish, domesticated animals, and animal products (*31*–*33*). Infections are presumed to result from exposure of susceptible hosts to organisms in the environment (*34*). Nosocomial infections caused by RGM are not uncommon and are often related to contamination of medical devices, wounds, or aqueous solutions. An outbreak of *Mycobacterium mucogenicum* and *M. neoaurum* bacteremia among patients with hematologic malignancies has been reported (*7*). *M. mucogenicum* and other nontuberculous mycobacteria, but not *M. neoaurum*, were isolated from the hospital water system (water tanks, showers, wash basins). Environmental measures, such as cleaning or replacing fixtures, general cleaning, chlorinating the water supply, and minimizing stagnation, reduced but did not eliminate water contamination. After changes were made to protocols for the care of CVCs, however, no further cases were reported. Environmental samples from the hospital and home environment of a patient with pulmonary *M. neoaurum* infection were similarly analyzed (*35*). Again, other mycobacteria were isolated from these sources, but *M. neoaurum* was not identified. Therefore, additional studies will be needed to elucidate the pathogenesis and risk factors for *M. neoaurum* infection.

Delays in identifying *M. neoaurum* and obtaining susceptibility test results pose challenges to microbiologists and clinicians. The median time to initial culture positivity in this series was >4 days and as high as 10 days, which might exceed the usual incubation duration for blood cultures, leading to premature no growth determinations (*6*,*36*). Many hospital laboratories no longer routinely speciate bacteria or perform susceptibility testing, and delays in appropriate treatment might be compounded by the need to send isolates to a reference laboratory. In this case series, empirical therapy was often directed at more common RGM. In some cases, susceptibility testing was not performed, and therapy success was judged by the patient's clinical response. The quality of care for patients with RGM infections might be improved by educating laboratory personnel regarding characteristics of less commonly identified RGM, developing protocols that promote rapid identification, and

sending isolates to laboratories with specialized expertise in identification and susceptibility testing.

The optimal type and duration of antimicrobial drug therapy for *M. neoaurum* infections has not been established. *M. neoaurum* bacteria are resistant to most antituberculosis medications. In 1 study, all 46 *M. neoaurum* isolates tested were susceptible to amikacin, cefoxitin, ciprofloxacin, doxycycline, imipenem, linezolid, moxifloxacin, and TMP/SMX, but only 8% were susceptible to clarithromycin (*37*). Isolates in our case series were also susceptible to most tested antimicrobial drugs but less consistently than previously described (*37*). Of note, most reports included in our study did not describe the methodology used for testing susceptibilities or used methods that were not recommended. In particular, macrolide susceptibility might have been overestimated if prolonged incubation was not used to detect inducible macrolide resistance (*38*). Furthermore, whereas most *M. neoaurum* infections have responded well to therapy, a formal correlation between antimicrobial drug susceptibility and clinical outcomes has not been made. As in our case report, other clinicians have frequently used a combination of agents that often include a macrolide, a fluoroquinolone, or both. Although initial combination therapy might be desirable, ≈25% of patients in our case series received monotherapy or were treated by device removal alone, and 1 patient with bacteremia recovered without treatment.

The ability of RGM to cause medical device infections and subsequent need for device removal to eradicate infection has been attributed in part to RGM biofilm formation (*39*). Not all RGM produce biofilms, however, and biofilm formation by *M. neoaurum* has not been specifically investigated (*40*–*42*). Failure to remove CVCs in patients with catheter-associated bacteremia was associated with treatment failure in our case series; however, the small number of cases precludes a precise estimate of risk. Good outcomes were reported in some cases when it was not feasible to remove devices. The ideal duration of antimicrobial drug therapy is also uncertain; ≥4 weeks has been recommended for patients with other RGM infections (*39*). For *M. neoaurum* infections described in this report, patients with bacteremia treated with antimicrobial drugs for ≤4 weeks had outcomes equivalent to those receiving a longer course.

RGM treatment for patients with underlying medical disorders might be challenging because of antimicrobial drug resistance, relatively high rates of adverse events, and some medications having multiple and serious drug interactions. In our case report, the patient required ongoing treatment for ALL that included mercaptopurine, methotrexate, dexamethasone, and vincristine. The availability of a relatively large number of antimicrobial drugs to which his isolate was susceptible permitted us to continue his chemotherapy without substantial disruption. Imipenem and cilastatin do not have notable interactions with those chemotherapeutic agents. Although TMP/SMX might theoretically exacerbate myelosuppression by mercaptopurine, the combination is commonly used during ALL treatment, and we felt this treatment would be manageable. However, clarithromycin (a strong cytochrome P450 3A4 inhibitor) has potentially severe interactions with vincristine and dexamethasone and is withheld typically for a specified period before and after administration of vincristine. Ciprofloxacin used in combination with dexamethasone might increase the risk for tendinitis or tendon rupture. During ALL induction therapy, patients are usually prescribed concurrent levofloxacin (for antibacterial prophylaxis) and corticosteroids for several weeks, and we have not observed frequent or severe adverse effects (*43*). We believe that, with careful observation, benefits of this regimen exceeded risks in our patient.

In conclusion, we established that infections caused by the emerging RGM pathogen *M. neoaurum* occurred in patients with diverse demographic characteristics, but almost all cases were healthcare associated. In contrast to isolates of other RGM species, *M. neoaurum* isolates were generally susceptible to tested antimicrobial drugs; a notable exception was clarithromycin. We recommend using combination antimicrobial drug therapy and removal of infected devices, although a shorter treatment duration than is generally recommended for RGM might be effective for *M. neoaurum* infections. We found that delays in identification of isolates and susceptibility testing occurred, but outcomes of most infections were good.

Acknowledgments

We thank Vani Shanker for her critical review of the manuscript.

This work was supported by the American Lebanese Syrian Associated Charities.

About the Author

Dr. Shapiro earned her medical degree from the Renaissance School of Medicine at Stony Brook University in 2018 and completed pediatric residency training at Stony Brook Children's Hospital in 2021. She currently works as a clinical postdoctoral fellow at St. Jude Children's Research Hospital and Le Bonheur Children's Hospital.

References

1. Gupta RS, Lo B, Son J. Phylogenomics and comparative genomic studies robustly support division of the genus *Mycobacterium* into an emended genus *Mycobacterium* and four novel genera. Front Microbiol. 2018;9:67. https://doi.org/10.3389/fmicb.2018.00067
2. Tsukamura M. A new species of rapidly growing, scotochromogenic mycobacteria, *Mycobacterium neoaurum Tsukamura* n. sp. [in Japanese]. Med Biol. 1972;85:229–33.
3. Jeha S, Pei D, Choi J, Cheng C, Sandlund JT, Coustan-Smith E, et al. Improved CNS control of childhood acute lymphoblastic leukemia without cranial irradiation: St Jude Total Therapy Study 16. J Clin Oncol. 2019;37:3377–91. https://doi.org/10.1200/JCO.19.01692
4. Clinical and Laboratory Standards Institute. Susceptibility testing of mycobacteria, *Nocardia* spp., and other aerobic actinomycetes, 3rd edition (M24-3E). Wayne (PA): The Institute; 2018.
5. Mermel LA, Allon M, Bouza E, Craven DE, Flynn P, O'Grady NP, et al. Clinical practice guidelines for the diagnosis and management of intravascular catheter-related infection: 2009 update by the Infectious Diseases Society of America. Clin Infect Dis. 2009;49:1–45. https://doi.org/10.1086/599376
6. Hayton ER, Koch O, Scarborough M, Sabharwal N, Drobniewski F, Bowler ICJW. Rapidly growing mycobacteria as emerging pathogens in bloodstream and device-related infection: a case of pacemaker infection with *Mycobacterium neoaurum*. JMM Case Rep. 2015;2:1–3. https://doi.org/10.1099/jmmcr.0.000054
7. Baird SF, Taori SK, Dave J, Willocks LJ, Roddie H, Hanson M. Cluster of nontuberculous mycobacteraemia associated with water supply in a haemato-oncology unit. J Hosp Infect. 2011;79:339–43. https://doi.org/10.1016/j.jhin.2011.07.006
8. Davison MB, McCormack JG, Blacklock ZM, Dawson DJ, Tilse MH, Crimmins FB. Bacteremia caused by *Mycobacterium neoaurum*. J Clin Microbiol. 1988;26:762–4. https://doi.org/10.1128/jcm.26.4.762-764.1988
9. Rubia MF, Chozas N, García-Martos P, Reyes F. *Mycobacterium neoaurum* bacteremia in an immunodepressed patient [in Spanish]. Enferm Infecc Microbiol Clin. 2009;27:58–9. https://doi.org/10.1016/j.eimc.2008.02.003
10. Hawkins C, Qi C, Warren J, Stosor V. Catheter-related bloodstream infections caused by rapidly growing nontuberculous mycobacteria: a case series including rare species. Diagn Microbiol Infect Dis. 2008;61:187–91. https://doi.org/10.1016/j.diagmicrobio.2008.01.004
11. Holland DJ, Chen SC, Chew WW, Gilbert GL. *Mycobacterium neoaurum* infection of a Hickman catheter in an immunosuppressed patient. Clin Infect Dis. 1994;18:1002–3. https://doi.org/10.1093/clinids/18.6.1002
12. Moseley JE Jr, Thind SK. *Mycobacterium neoaurum* bloodstream infection associated with a totally implanted subclavian port in an adult with diabetes and history of colon cancer. Case Rep Infect Dis. 2020;2020:8878069. https://doi.org/10.1155/2020/8878069
13. Pang L, Chen Z, Xu D, Cheng W. Case report: *Mycobacterium neoaurum* infection during ICI therapy in a hepatocellular carcinoma patient with psoriasis. Front Immunol. 2022;13:972302. https://doi.org/10.3389/fimmu.2022.972302
14. van Duin D, Goldfarb J, Schmitt SK, Tomford JW, Tuohy MJ, Hall GS. Nontuberculous mycobacterial blood stream and cardiac infections in patients without HIV infection. Diagn Microbiol Infect Dis. 2010;67:286–90. https://doi.org/10.1016/j.diagmicrobio.2010.02.006
15. Walayat S, Awwal T, Roy M, Ahmad S. *Mycobacterium neoaurum* line-related bacteremia with pulmonary involvement: case report and review of literature. IDCases. 2018;11:88–90. https://doi.org/10.1016/j.idcr.2018.01.004
16. Woo PC, Tsoi HW, Leung KW, Lum PN, Leung AS, Ma CH, et al. Identification of *Mycobacterium neoaurum* isolated from a neutropenic patient with catheter-related bacteremia by 16S rRNA sequencing. J Clin Microbiol. 2000;38:3515–7. https://doi.org/10.1128/JCM.38.9.3515-3517.2000
17. Becker ML, Suchak AA, Wolfe JN, Zarychanski R, Kabani A, Nicolle LE. *Mycobacterium neoaurum* bacteremia in a hemodialysis patient. Can J Infect Dis. 2003;14:45–8. https://doi.org/10.1155/2003/840103
18. Kim CK, Choi SI, Jeon BR, Lee YW, Lee YK, Shin HB. Pulmonary infection caused by *Mycobacterium neoaurum*: the first case in Korea. Ann Lab Med. 2014;34:243–6. https://doi.org/10.3343/alm.2014.34.3.243
19. Morimoto Y, Chan ED, Heifets L, Routes JM. Pulmonary infection with *Mycobacterium neoaurum* identified by 16S ribosomal DNA sequence. J Infect. 2007;54:e227–31. https://doi.org/10.1016/j.jinf.2006.12.010
20. Bastón-Paz N, Bolaños-Rivero M, Hernández-Cabrera M, Martín-Sánchez AM. Pacemaker infection with *Mycobacterium neoaurum* [in Spanish]. Rev Esp Quimioter. 2018;31:379–82.
21. Kusano T, Fukasawa C, Yamamoto S, Shiratori E, Murata S, Takaki A, et al. Pin tract infection caused by *Mycobacterium neoaurum* in a 14-year-old child: a case report. J Infect Chemother. 2021;27:1244–7. https://doi.org/10.1016/j.jiac.2021.03.005
22. McNally CF, Mangino JE. *Mycobacterium neoaurum*: a case report and review of the literature. Infect Dis Clin Pract. 2000;9:273–5. https://doi.org/10.1097/00019048-200009060-00013
23. Zanetti S, Faedda R, Fadda G, Dupré I, Molicotti P, Ortu S, et al. Isolation and identification of *Mycobacterium neoaurum* from a patient with urinary infection. New Microbiol. 2001;24:189–92.
24. Pérez-Cortés Villalobos A, Rotstein C. *Mycobacterium mucogenicum* and *Mycobacterium neoaurum* bacteremia in immunocompomised hosts. J Assoc Med Microbiol Infect Dis Can. 2021;6:55–62. PubMed https://doi.org/10.3138/jammi-2020-0025
25. Redelman-Sidi G, Sepkowitz KA. Rapidly growing mycobacteria infection in patients with cancer. Clin Infect Dis. 2010;51:422–34. https://doi.org/10.1086/655140
26. Daley CL, Iaccarino JM, Lange C, Cambau E, Wallace RJ, Andrejak C, et al. Treatment of nontuberculous mycobacterial pulmonary disease: an official ATS/ERS/ESCMID/IDSA clinical practice guideline. Clin Infect Dis. 2020;71:905–13. https://doi.org/10.1093/cid/ciaa1125
27. Philips RC, Hoyer PE, White SM, Tinkey KT, Loeffelholz M, Andersen CR, et al. Cutaneous nontuberculous mycobacteria infections: a retrospective case series of 78 patients from the Texas Gulf Coast region. J Am Acad Dermatol. 2019;81:730–9. https://doi.org/10.1016/j.jaad.2019.04.022
28. Dorman SE, Picard C, Lammas D, Heyne K, van Dissel JT, Baretto R, et al. Clinical features of dominant and recessive interferon gamma receptor 1 deficiencies. Lancet. 2004;364:2113–21. https://doi.org/10.1016/S0140-6736(04)17552-1
29. Heckman GA, Hawkins C, Morris A, Burrows LL, Bergeron C. Rapidly progressive dementia due to *Mycobacterium neoaurum* meningoencephalitis. Emerg Infect Dis. 2004;10:924–7. https://doi.org/10.3201/eid1005.030711

30. Han XY. *Mycobacterium neoaurum* contamination. Emerg Infect Dis. 2005;11:1316–7. https://doi.org/10.3201/eid1108.040861
31. Padya L, Chin'ombe N, Magwenzi M, Mbanga J, Ruhanya V, Nziramasanga P. Molecular identification of *Mycobacterium* species of public health importance in cattle in Zimbabwe by 16S rRNA gene sequencing. Open Microbiol J. 2015;9:38–42. https://doi.org/10.2174/1874285801509010038
32. Puk K, Guz L. Occurrence of *Mycobacterium* spp. in ornamental fish. Ann Agric Environ Med. 2020;27:535–9. https://doi.org/10.26444/aaem/114913
33. Sevilla IA, Molina E, Tello M, Elguezabal N, Juste RA, Garrido JM. Detection of mycobacteria by culture and DNA-based methods in animal-derived food products purchased at Spanish supermarkets. Front Microbiol. 2017;8:1030. https://doi.org/10.3389/fmicb.2017.01030
34. Desai AN, Hurtado RM. Infections and outbreaks of nontuberculous mycobacteria in hospital settings. Curr Treat Options Infect Dis. 2018;10:169–81. https://doi.org/10.1007/s40506-018-0165-9
35. Kaevska M, Sterba J, Svobodova J, Pavlik I. *Mycobacterium avium* subsp. *avium* and *Mycobacterium neoaurum* detection in an immunocompromised patient. Epidemiol Infect. 2014;142:882–5. https://doi.org/10.1017/S0950268813001660
36. Ransom EM, Alipour Z, Wallace MA, Burnham CA. Evaluation of optimal blood culture incubation time to maximize clinically relevant results from a contemporary blood culture instrument and media system. J Clin Microbiol. 2021;59:e02459-20. https://doi.org/10.1128/JCM.02459-20
37. Brown-Elliott BA, Woods GL. Antimycobacterial susceptibility testing of nontuberculous mycobacteria. J Clin Microbiol. 2019;57:e00834-19. https://doi.org/10.1128/JCM.00834-19
38. Huang WC, Yu MC, Huang YW. Identification and drug susceptibility testing for nontuberculous mycobacteria. J Formos Med Assoc. 2020;119:S32–41. https://doi.org/10.1016/j.jfma.2020.05.002
39. El Helou G, Viola GM, Hachem R, Han XY, Raad II. Rapidly growing mycobacterial bloodstream infections. Lancet Infect Dis. 2013;13:166–74. https://doi.org/10.1016/S1473-3099(12)70316-X
40. Martín-de-Hijas NZ, García-Almeida D, Ayala G, Fernández-Roblas R, Gadea I, Celdrán A, et al. Biofilm development by clinical strains of non-pigmented rapidly growing mycobacteria. Clin Microbiol Infect. 2009;15:931–6. https://doi.org/10.1111/j.1469-0691.2009.02882.x
41. Brown-Elliott BA, Wallace RJ Jr, Petti CA, Mann LB, McGlasson M, Chihara S, et al. *Mycobacterium neoaurum* and *Mycobacterium bacteremicum* sp. nov. as causes of mycobacteremia. J Clin Microbiol. 2010;48:4377–85. https://doi.org/10.1128/JCM.00853-10
42. Ilinov A, Nishiyama A, Namba H, Fukushima Y, Takihara H, Nakajima C, et al. Extracellular DNA of slow growers of mycobacteria and its contribution to biofilm formation and drug tolerance. Sci Rep. 2021;11:10953. https://doi.org/10.1038/s41598-021-90156-z
43. Karol SE, Sun Y, Tang L, Pui CH, Ferrolino J, Allison KJ, et al. Fluoroquinolone prophylaxis does not increase risk of neuropathy in children with acute lymphoblastic leukemia. Cancer Med. 2020;9:6550–5. https://doi.org/10.1002/cam4.3249

Address for correspondence: Elisabeth Adderson, St. Jude Children's Research Hospital, 262 Danny Thomas Pl, Mailstop 320, Memphis, TN 38120, USA; email: elisabeth.adderson@stjude.org

Response to Vaccine-Derived Polioviruses Detected through Environmental Surveillance, Guatemala, 2019

Rodrigo Rodríguez,[1] Elisa Juárez,[1] Concepción F. Estívariz, Coralia Cajas, Gloria Rey-Benito, María Olga Bautista Amézquita, Stacey Jeffries Miles, Oscar Orantes, María Cecilia Freire, Ana-Elena Chévez, Leticia Castillo Signor, Leanna Sayyad, Claudia Jarquin, Emilia Cain, Andrea Patricia Villalobos Rodríguez, Linda Mendoza, Carlos A. Ovando, Haroldo de Jesús Barillas Mayorga, Ericka Gaitán, Antonio Paredes, Hanen Belgasmi-Allen, Lorena Gobern, Marc Rondy

Guatemala implemented wastewater-based poliovirus surveillance in 2018, and three genetically unrelated vaccine-derived polioviruses (VDPVs) were detected in 2019. The Ministry of Health (MoH) response included event investigation through institutional and community retrospective case searches for acute flaccid paralysis (AFP) during 2018–2020 and a bivalent oral polio/measles, mumps, and rubella vaccination campaign in September 2019. This response was reviewed by an international expert team in July 2021. During the campaign, 93% of children 6 months to <7 years of age received a polio-containing vaccine dose. No AFP cases were detected in the community search; institutional retrospective searches found 37% of unreported AFP cases in 2018–2020. No additional VDPV was isolated from wastewater. No evidence of circulating VDPV was found; the 3 isolated VDPVs were classified as ambiguous VDPVs by the international team of experts. These detections highlight risk for poliomyelitis reemergence in countries with low polio vaccine coverage.

Poliomyelitis is a highly infectious disease, caused by poliovirus serotypes 1, 2, and 3, that primarily affects children <5 years of age. The main risk factors for poliovirus transmission are low immunization coverage, poor sanitation, and high population density (*1*). Since the worldwide launch of the Global Polio Eradication Initiative (GPEI) in 1988, polio cases have declined by >99% (*2*). Strategies to reduce the number of polio cases globally have focused on achieving high polio vaccination coverage and implementing robust acute flaccid paralysis (AFP) surveillance (*3*).

Administration of the injectable inactivated poliovirus vaccine (IPV) or live attenuated oral poliovirus vaccine (OPV, Sabin-strain virus types) can prevent poliomyelitis. IPV induces humoral protection, whereas OPV induces humoral and mucosal immunity and limits viral shedding, reducing person-to-person transmission (*4*). However, in areas with low vaccination coverage and poor sanitation, using OPV may exceptionally result in the emergence of vaccine-derived polioviruses (VDPVs) (*3*,*5*,*6*). VDPVs are classified as cVDPV (circulating VDPV, when there is evidence of community transmission), iVDPV (immunodeficiency-associated VDPV, isolated from persons with primary immunodeficiencies), or aVDPV (ambiguous VDPV, isolated from persons without immunodeficiency or from wastewater samples without evidence of transmission). aVDPVs are generally considered to

Author affiliations: Pan American Health Organization, Washington, DC, USA (R. Rodríguez, G. Rey-Benito, M.C. Freire, A.-E. Chévez, E. Cain, A.P. Villalobos Rodríguez); Ministry of Public Health and Social Assistance, Guatemala City, Guatemala (E. Juárez, M.O. Bautista Amézquita, L. Castillo Signor, L. Mendoza, C.A. Ovando, H. de J. Barillas Mayorga, E. Gaitán, A. Paredes, L. Gobern); US Centers for Disease Control and Prevention, Atlanta, Georgia, USA (C.F. Estívariz, S.J. Miles, L. Sayyad, H. Belgasmi-Allen), Pan American Health Organization, Guatemala City (C. Cajas, O. Orantes, C. Jarquin, M. Rondy); Poliovirus Regional Reference Laboratory, Malbrán Institute, Buenos Aires, Argentina (M.C. Freire); National Health Laboratory, Guatemala City (L. Mendoza)

DOI: http://doi.org/10.3201/eid2908.230236

[1]These first authors contributed equally to this article.

be of low public health significance; however, they can still be an indicator of low vaccination coverage and poor sanitation, which can create the conditions for the emergence and circulation of potentially more dangerous cVDPVs. In the past decade, cVDPV outbreaks have caused >2,700 poliomyelitis cases globally (*7*–*10*).

In Guatemala, the last case of clinical poliomyelitis was detected in 1990 (*11*); the country routinely vaccinates children against poliomyelitis with trivalent IPV and bivalent (serotypes 1 and 3) OPV (bOPV) (*12*). Because of low vaccination coverage (<90% with third dose of polio-containing vaccine in 2017) and poor AFP surveillance indicators, the Regional Certification Commission (RCC) classified Guatemala as a high-risk country for polio reemergence in 2018. To complement AFP surveillance, the Pan American Health Organization's (PAHO) Technical Advisory Group recommended implementing wastewater-based environmental surveillance in high-risk settings in the Americas in 2016 (*13*). After that recommendation was published, the Guatemala Ministry of Health (MoH) implemented poliovirus environmental surveillance in 2 urban municipalities in Guatemala in November 2018 (*14*).

The detection of 3 VDPVs from wastewater sampled in January, March, and December 2019 led the Guatemala MoH to implement a series of activities to classify these events and minimize the risk for transmission in the population (Figure). In July 2021, a team of international experts evaluated that response, according to the Global Polio Eradication Initiative's (GPEI) Poliovirus Outbreak Response Assessment (OBRA) guidelines (*15*). We present the results of the investigation conducted by the MoH and the OBRA evaluation of their response.

Methodology

Environmental Surveillance, VDPV Detection, and Genomic Sequencing

Guatemala MoH implemented monthly collection of wastewater samples in November 2018. Three sampling sites in 2 municipalities were selected for logistical and financial reasons. The selected municipalities, Villa Nueva (VNA) and San Juan Sacatepéquez (SJS), were of high risk for poliovirus transmission (*16*): high population density (1,573 inhabitants/km^2 in VNA and 943 inhabitants/km^2 in SJS), OPV coverage <90% in 2014–2017, underperforming AFP surveillance indicators (<1 case/100,000 children <15 years of age), and poor sanitation conditions. In each municipality, the MoH revised wastewater networks to define 3 sampling points that would lead to a maximum population size unaffected by polluting industrial plants.

During November 2018–July 2021, trained MoH staff monthly collected a 1 L wastewater sample from each site and transported them in cold chain (2°C–8°C) the same day to the National Health Laboratory. Samples were stored at −80°C, then shipped at −20°C to the US Centers for Disease Control and Prevention (CDC) reference laboratory for polioviruses to be processed and tested for the presence of poliovirus (*16*–*18*). All poliovirus isolates underwent genomic sequencing and analysis of the region coding the viral protein 1 surface protein for nucleotide substitutions compared with the parent Sabin strains.

Event Investigation

To classify the isolated VDPVs, the MoH relied on preexisting national protocols. Within 72 hours of receiving the notification of VDPV detection in wastewater samples, MoH personnel conducted health facility and community-based AFP case search in the areas surrounding the sampling sites. In each site, after obtaining verbal consent from parents, they also collected and tested stool samples for poliovirus from 20 healthy children <5 years of age without a history of OPV vaccination in the previous 30 days.

MoH epidemiologists retrospectively reviewed medical records from all 42 national hospitals for patients admitted during January 2018–December 2020 who had diagnoses compatible with polio or AFP, identified by codes from the International Classification of Diseases, 10th Revision (ICD-10). The retrospective record search was conducted in 2 phases during July 2019–December 2020. Finally, MoH epidemiologists revised hospital-based information systems to identify reported cases of primary immunodeficiency in 2018–2019 in patients residing in the affected municipalities.

Routine AFP Surveillance

During 2017–2020, a total of 42 reporting hospitals conducted AFP surveillance in Guatemala. The surveillance system was classified as good quality if it reported ≥1 AFP case/100,000 children <15 years of age/year. Of reported AFP cases, ≥80% should have adequate sample collection and 80% should include an investigation conducted within 48 hours (*19*).

Assessment of Polio Immunization Coverage and Supplementary Immunization Activities

Since 2016, Guatemala routinely vaccinates children with 1 IPV dose at 2 months of age, 2 bOPV doses at 4 and 6 months of age, and 2 bOPV booster doses at 18 months and 4 years of age (*12*). A nationwide catch-up vaccination campaign for bOPV

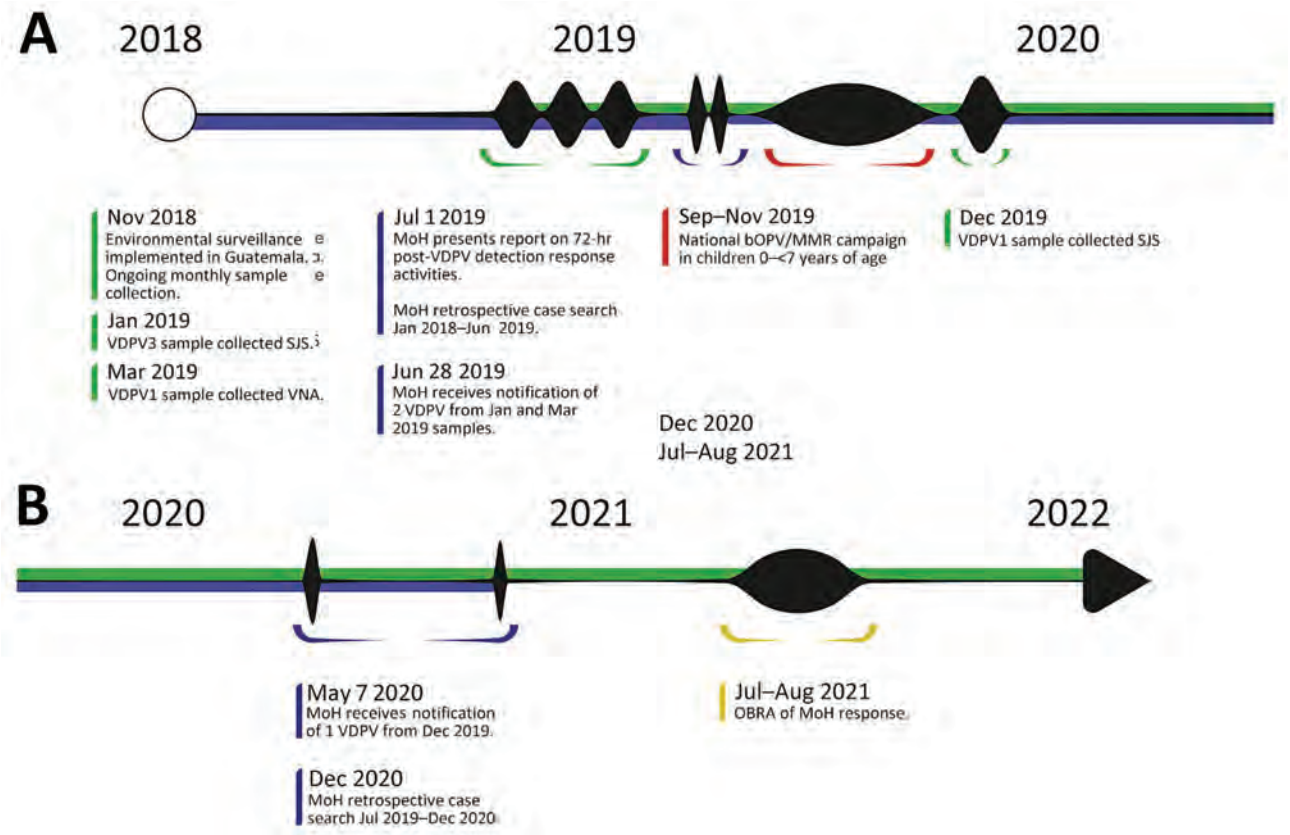

Figure. Timeline of MoH VDPV detection response activities and OBRA evaluation, Guatemala, 2018–2022. 1 Green represents environmental surveillance-related activities. Blue represents MoH response activities. Red represents supplementary immunization campaign. Yellow represents OBRA. MoH, Guatemala Ministry of Health; OBRA, Poliovirus Outbreak Response Assessment; VDPV, vaccine-derived polioviruses.

and measles, mumps, rubella (MMR) was already planned for September–October 2019 for children 1–6 years of age. The detection of VDPVs led officials to lower the eligibility age to 6 months for bOPV and mobilize additional funding to support vaccination activities, a nationwide communication campaign, and technical support at the national and local level.

We calculated routine vaccination coverage during 2017–2020 using the number of third doses of bOPV registered in the national electronic immunization system (individual personal data) as numerator. This national system is exclusively used by MoH vaccination centers and may include social security institute centers on some occasions (based on personal willingness to share data). We calculated the bOPV vaccination campaign coverage using the number of doses registered in an electronic immunization system designed for the vaccination campaign (aggregated data). We estimated population denominators using national census-based projections.

OBRA Implementation

In July 2021, an OBRA team virtually evaluated the MoH's response to 3 VDPV detections in 4 key components: response planning and coordination, AFP surveillance sensitivity, vaccination, and health promotion and social mobilization. The team consisted of vaccination, epidemiologic surveillance, and laboratory experts from PAHO and CDC, as well as a national facilitator from the National Polio Elimination Certification Committee (NCC). The assessment involved reviewing technical documentation such as AFP and environmental surveillance protocols and vaccination reports; conducting interviews with national and local authorities, health personnel, and the National Polio Eradication Commission; and participating in work sessions with the OBRA team to discuss the data and provide recommendations. The assessment results were communicated to the MoH and local public health authorities through a virtual debriefing in August 2021 and a written report in September 2021.

Ethics Considerations

The Guatemala MOH determined that the community survey, including collection of stool specimens, did not constitute human subjects research. We obtained verbal consent from household members who participated in the community survey and from parents of children <5 years of age who provided a specimen. The information obtained would be used to guide the public health response to a potential outbreak and did not involve risk to participants' health.

Results

Environmental Surveillance, VDPV Detection, and Genomic Sequencing

During November 2018–July 2021, we collected 192 wastewater samples in SJS and VNA. We detected ≥1 enterovirus in 97% of samples collected in SJS and in 96% of samples collected in VNA. We isolated Sabin-like vaccine poliovirus in 83 samples (43%), Sabin type 1 poliovirus in 20% of samples and type 3 in 33%.

We detected 3 genetically unrelated VDPVs in 2019 (Appendix Figure, https://wwwnc.cdc.gov/EID/article/29/8/23-0236-App1.pdf). We identified a VDPV3 with 11 nt changes from Sabin type 3 in a January 2019 sample from Aldea Cruz Blanca, SJS, and a VDPV1 with 11 nt changes from Sabin type 1 in a March 2019 sample from Platanitos. We reported detecting those 2 VDPVs to the Guatemalan MoH on July 1, 2019. We isolated a VDPV1 with 10 nt changes from Sabin type 1 in a sample collected in December 2019 in Aldea Cruz Blanca, SJS, and reported it to the MoH in May 2020. The VDPVs were not genetically linked to any previously sequenced VDPV1 or VDPV3 worldwide. As of July 2021, no other VDPVs have been detected.

Event Investigation

We identified no cases of AFP from community case searches in which 1,580 children were screened. We isolated no VDPVs from stool samples collected among 61 healthy children sampled (20 children each for the first 2 VDPV detections and 21 children for the third detection).

We conducted a retrospective case review during January 1, 2018–August 31, 2020, in 2 phases after the VDPV notifications in July 2019 and May 2020; we reviewed 3,342,166 records from 42 national hospitals. The reviewers identified 7,318 (0.2%) persons with paralysis diagnoses, of whom 150 (2.1%) met the case definition for AFP. Of those, 56 (37%) cases had not been reported to the AFP surveillance system. No potential cases of primary immunodeficiency from the affected municipalities were found from national hospital-based information systems.

Routine AFP Surveillance

During 2017–2020, AFP yearly incidence met the target of 1 case/100,000 children in 2019. In 2017, 2018, and 2020, AFP incidence rate was 0.6–0.9 cases/100,000 children. Overall, 164 (76%) of 214 cases reported in 2017–2020 had an adequate sample collected, and 87 (41%) were investigated within 48 hours of being reported (Table 1).

Vaccination Coverage and OPV/MMR Supplementary Immunization Campaign

During 2017–2020, the percentage of children <1 year of age who received 3 doses of polio vaccine as 2 doses of IPV and 1 dose of bOPV was 84.8%–89.8% at the national level (Table 2). Vaccination coverage for that vaccination series in the health areas where VDPVs were isolated was 62.1%–75.3% during the same period.

During the national bOPV/MMR vaccination campaign conducted in September–November 2019 in response to the VDPV detections, 93.0% of children 6 months to <7 years of age received 1 dose of bOPV. The campaign coverage reached 94.8% among children 6 months to <7 years of age in VNA and 91.2% in SJS.

OBRA Results

The 2021 OBRA conducted in Guatemala found no evidence of circulating VDPVs in Guatemala and that the MoH response planning and coordination after VDPV identification in 2019 environmental surveillance samples was appropriate. The 3 VDPVs detected in wastewater samples were classified as aVDPVs.

Discussion

In Guatemala, the environmental surveillance of poliovirus in wastewater detected 3 genetically unrelated

Table 1. Surveillance indicators for acute flaccid paralysis, Guatemala, 2017–2020*

Year	No. reported AFP cases	Incidence rate per 100,000 children <15 y	Adequate sample collected, no. (%)	Investigation within 48 h, no. (%)
Expected value	55	1.0	≥80%	≥80%
2017	46	0.7	29 (63)	NA
2018	59	0.9	50 (85)	11 (19)
2019	72	1.1	55 (77)	49 (68)
2020	37	0.6	30 (81)	27 (73)

*Information not systematically collected before 2018. Source: Department of Epidemiology, Guatemalan Ministry of Health. NA, not available.

Table 2. Polio vaccination coverage in children <1 y of age, Guatemala, 2017–2020*

		Villa Nueva		San Juan Sacatepequez		National	
Year	Dose	Population	No. (%) vaccinated	Population	No. (%) vaccinated	Population	No. (%) vaccinated
2017	Polio 3	8,339	6,282 (75.3)	6,159	3,824 (62.1)	381,396	342,437 (89.8)
2018	Polio 3	8,296	6,055 (73.0)	6,141	3,942 (64.2)	382,841	324,761 (84.8)
2019	Polio 3	7,252	5,495 (75.8)	5,856	4,056 (69.3)	366,448	320,963 (87.6)
2020	Polio 3	6,671	5,570 (83.5)	5,513	4,252 (77.1)	340,876	304,898 (89.4)
2019	bOPV	57,979	54,942 (94.8)	41,639	37,969 (91.2)	2,649,334	2,463,881 (93.0)

*The 2019 nationwide bOPV campaign targeted children 6 mo to >7 y of age. Polio 3 indicates a third dose of oral or injectable polio-containing vaccine. bOPV, bivalent oral poliovirus vaccine. Source: National Immunization Program, Guatemala Ministry of Health.

VDPVs in 1 year. After careful revision of the MoH response and investigation, an international team of experts classified those 3 events as aVDPVs.

Although the Americas region was declared free from polio in 1994, recent events remind us that sustaining this status is a continuous challenge. In June 2022, a VDPV2 was isolated in an unvaccinated person in New York, New York, USA, and classified as cVPDV2 after being isolated from wastewater (*8*). This virus, genetically linked to other VDPV2 viruses identified in Israel and the United Kingdom (*20*), demonstrates the global threat that importation of poliovirus from anywhere in the world represents. In March 2023, a case of VDPV1 was detected in an unvaccinated child from a community with low vaccination coverage in Peru (*21*). The virus presented 31 nt changes compared with the type 1 Sabin virus and was not genetically linked to any VDPV1 identified in the world. This case is an example of the imminent risk for reemergence of poliomyelitis through VDPVs emerging in communities with low OPV vaccination coverage.

The OBRA team concluded that there was enough evidence to consider that none of the 3 VDPVs isolated in Guatemala had given rise to a clinical case of poliomyelitis in the country; however, those findings highlight the need to improve vaccination coverage and AFP surveillance to prevent or timely detect poliovirus reemergence. Through repeated workshops using the OBRA report structure (AFP surveillance, environmental surveillance, immunizations, and community mobilization), the Guatemala MoH translated results and recommendations from the evaluation into a roadmap to mitigate the risk for polio reemergence.

In Guatemala, 1 of 3 AFP cases detected through retrospective hospital-based case search had not been identified through routine surveillance. Such an underperforming surveillance system could place the country at risk of failing to detect clinical poliomyelitis in a timely manner. To improve AFP surveillance, the MoH implemented a daily zero-notification process, in which hospitals daily ascertain the absence of AFP cases in their admitted patients. After the OBRA evaluation, MoH strengthened the national surveillance team through increased staff and interinstitutional (national laboratory, epidemiology department and national immunizations program) training supported by national and international experts. MoH and non-MoH hospitals made efforts to improve AFP notification; AFP notifications increased to 0.9 cases/100,000 children in 2021 and 1.2 cases/100,000 children in 2022. Environmental surveillance continued through monthly wastewater sample collection in the same sampling sites; as of December 2022, no further VDPV or WPV had been detected.

National vaccination coverage with 3 doses of polio vaccine was 85% in 2018, the year before the VDPV isolations; at that time, coverage was 73% in VNA and 64% in SJS. Vaccination coverage in areas with poor access to clean water allowed for VPDVs to emerge and be detected in wastewaters. The first two VDPVs were notified in July 2019, which was 2 months before the launch of a planned national catch-up bOPV/MMR vaccination campaign. Notification of the VDPVs in accordance with international health regulations led to international awareness as well as technical and financial assistance from PAHO, the United Nations Children's Fund, and GPEI for the MoH to successfully implement its vaccination campaign, reaching 93% of children 6 months to <7 years of age vaccinated with a dose of bOPV. In accordance with GPEI guidelines for polio outbreak response, vaccination campaigns should be organized after VDPV is classified as cVDPV (*22*). After the isolation of the third VDPV and its notification in May 2020, case investigation led to its classification as aVDPV; no further vaccination campaign was organized. Since the OBRA evaluation, declining polio vaccination coverage during the COVID-19 pandemic (*7*,*23*,*24*) has built a pool of susceptible children representing a risk for polio reemergence (*25*,*26*). National vaccination coverage for 3 doses of polio-containing vaccine in Guatemala has declined from 89% in 2020 to 76% in 2022 (27). Routine immunization programs in Guatemala must be intensified through outreach strategies and a better understanding of local issues contributing

to low vaccination coverage. Since November 2022, MoH has implemented local workshops to identify reasons for low performance of vaccine preventable disease surveillance and immunization programs. During those 2-day workshops, participants from local and central MoH, municipalities, community leaders, and health service users have jointly developed mitigation plans using a problem tree analysis methodology.

Because of an elevated risk for polio reemergence, adequate response preparedness is essential for timely response to poliovirus detection. The OBRA team concluded that the outbreak response planning and implementation of activities in Guatemala were adequate according to international standards defined by GPEI. Existing, regularly updated guidelines and periodic outbreak preparedness training were key elements that enabled the Guatemala MoH to respond adequately to these events.

In conclusion, the detection of 3 unrelated VDPVs in Guatemala confirmed the strong risk for poliomyelitis emergence in sites with low vaccination coverage. Although no evidence of a circulating VDPV was found, improving polio vaccination coverage is critical to prevent new VDPV emergences and spread. Strengthening AFP surveillance for timely detection of clinical cases is essential for a rapid response to be implemented in all areas of the country. In high-risk countries, complementing AFP surveillance with risk-assessed environmental surveillance is of great value for early detection of reverted vaccine virus before they generate poliomyelitis cases or can circulate widely in the community.

Acknowledgments

We thank Aideé Ramirez, José C. Rodriguez, Judith Cifuentes, and Jane Iber; Chen Qi, who assisted with VDPV sample sequencing; Kimberly Wong for site selection visit, sample processing, and data analysis; and Everardo Vega for conception and leadership of the collaboration during 2018–2021, for their expertise, contributions, and assistance with implementation of activities described in this report.

Financial support for this content was provided by PAHO and the Guatemala Ministry of Health.

About the Author

Dr. Rodríguez is the post-VDPV detection team coordinator for Poliovirus Outbreak Response Assessment in Guatemala, where he was previously PAHO/WHO advisor. His research interests include vaccine preventable diseases, program evaluation, community surveillance for health risks, and vital statistics analysis. Dr. Juárez is an epidemiologist at Hospital de Amatitlán in Amatitlán, Guatemala, and member of the Guatemalan National Polio Eradication Certification Committee Secretariat, 2013–2021. Her primary research interests are public health and immunization.

References

1. Odoom JK, Obodai E, Boateng G, Diamenu S, Attiku K, Avevor P, et al. Detection of vaccine-derived poliovirus circulation by environmental surveillance in the absence of clinical cases. Hum Vaccin Immunother. 2021;17:2117–24. https://doi.org/10.1080/21645515.2020.1852009
2. Lee SE, Greene SA, Burns CC, Tallis G, Wassilak SGF, Bolu O. Progress toward poliomyelitis eradication—worldwide, January 2021–March 2023. [cited 2023 May 15]. MMWR Morb Mortal Wkly Rep. 2023;72:517–22. https://doi.org/10.15585/mmwr.mm7219a3
3. Coulliette-Salmond AD, Alleman MM, Wilnique P, Rey-Benito G, Wright HB, Hecker JW, et al. Haiti poliovirus environmental surveillance. Am J Trop Med Hyg. 2019;101:1240–8. https://doi.org/10.4269/ajtmh.19-0469
4. Sutter RW, Kew OM, Cochi SL. Poliovirus vaccine—live. In: Plotkin SA, Orenstein WA, Offit PA, editors. Vaccines. 5th ed. Philadelphia: W.B. Saunders Company; 2008. p. 631–85.
5. Burns CC, Diop OM, Sutter RW, Kew OM. Vaccine-derived polioviruses. J Infect Dis. 2014;210(Suppl 1):S283–93. https://doi.org/10.1093/infdis/jiu295
6. Global Polio Eradication Initiative. Vaccine-derived polioviruses [cited 2023 May 4]. https://polioeradication.org/polio-today/polio-prevention/the-virus/vaccine-derived-polio-viruses
7. Bigouette JP, Henderson E, Traoré MA, Wassilak SGF, Jorba J, Mahoney F, et al. Update on vaccine-derived poliovirus outbreaks—worldwide, January 2021–December 2022. MMWR Morb Mortal Wkly Rep. 2023;72:366–71. https://doi.org/10.15585/mmwr.mm7214a3
8. Link-Gelles R, Lutterloh E, Schnabel Ruppert P, Backenson PB, St George K, Rosenberg ES, et al.; 2022 U.S. Poliovirus Response Team. Public health response to a case of paralytic poliomyelitis in an unvaccinated person and detection of poliovirus in wastewater—New York, June–August 2022. MMWR Morb Mortal Wkly Rep. 2022;71:1065–8. https://doi.org/10.15585/mmwr.mm7133e2
9. World Health Organization. Circulating vaccine-derived poliovirus type 3—Israel. Disease Outbreak News. 2022 [cited 2022 Aug 4]. https://www.who.int/emergencies/disease-outbreak-news/item/2022-DON366
10. World Health Organization. Circulating vaccine-derived poliovirus type 2—global update. Disease Outbreak News. 2021 [cited 2022 Aug 4]. https://www.who.int/emergencies/disease-outbreak-news/item/circulating-vaccine-derived-poliovirus-type-2-global-update
11. Global Polio Eradication Initiative. Polio-free countries [cited 2023 Apr 14]. https://polioeradication.org/where-we-work/polio-free-countries
12. Pan American Health Organization. National vaccination schedule, Guatemala, 2018 [in Spanish]. 2018 [cited 2023 Apr 14]. https://www3.paho.org/gut/index.php?option=com_docman&view=download&slug=esquema-de-vacunacion-2018&Itemid=
13. Regional Certification Commission for Polio Eradication. 8th meeting of the Regional Certification Commission for the Polio Endgame in the Region of the Americas—final

report. 2017 [cited 2023 Apr 14]. https://www.paho.org/en/file/52076/download?token=Krrnz_bs
14. Ministerio de Salud Pública y Asistencia Social. Protocol for environmental surveillance of poliovirus in Guatemala, 2018–2019 [in Spanish]. 2018.
15. World Health Organization. Poliovirus outbreak response assessment (OBRA). 2019 [cited 2021 Nov 4]. https://apps.who.int/iris/handle/10665/330311
16. World Health Organization. Guidelines for environmental surveillance of poliovirus circulation. 2003 [cited 2022 Jun 2]. https://polioeradication.org/wp-content/uploads/2016/07/WHO_V-B_03.03_eng.pdf
17. World Health Organization Department of Immunizations. Vaccines and biologicals. Polio laboratory manual. 2004 [cited 2022 Jun 2]. https://polioeradication.org/wp-content/uploads/2017/05/Polio_Lab_Manual04.pdf
18. Belgasmi H, Miles SJ, Sayyad L, Wong K, Harrington C, Gerloff N, et al. CaFÉ: a sensitive, low-cost filtration method for detecting polioviruses and other enteroviruses in residual waters. Front Environ Sci. 2022;10:914387. https://doi.org/10.3389/fenvs.2022.914387
19. Global Polio Eradication Initiative. Surveillance indicators. 2023 [cited 2023 Apr 17]. https://polioeradication.org/polio-today/polio-now/surveillance-indicators/
20. World Health Organization. Detection of circulating vaccine derived polio virus 2 (cVDPV2) in environmental samples—the United Kingdom of Great Britain and Northern Ireland and the United States of America. 2022 Sep [cited 2023 Apr 14]. https://www.who.int/emergencies/disease-outbreak-news/item/2022-DON408
21. Pan American Health Organization. Epidemiological update: poliomyelitis in the region of the Americas. 2023 Mar [cited 2023 Mar 28]. https://www.paho.org/en/file/125018/download?token=OmjJp1Bz
22. Word Health Organization. Standard operating procedures: responding to a poliovirus event or outbreak. 2022 [cited 2023 May 4]. https://polioeradication.org/wp-content/uploads/2022/09/Standard-Operating-Procedures-For-Responding-to-a-Poliovirus-Event-Or-Outbreak-20220905-V4-EN.pdf
23. Rachlin A, Patel JC, Burns CC, Jorba J, Tallis G, O'Leary A, et al. Progress toward polio eradication—worldwide, January 2020–April 2022. MMWR Morb Mortal Wkly Rep. 2022;71:650–5. https://doi.org/10.15585/mmwr.mm7119a2
24. Rachlin A, Danovaro-Holliday MC, Murphy P, Sodha SV, Wallace AS. Routine vaccination coverage—worldwide, 2021. MMWR Morb Mortal Wkly Rep. 2022;71:1396–400. https://doi.org/10.15585/mmwr.mm7144a2
25. Grassly NC. The final stages of the global eradication of poliomyelitis. Philos Trans R Soc Lond B Biol Sci. 2013;368:20120140. https://doi.org/10.1098/rstb.2012.0140
26. Global Polio Eradication Initiative. Polio environmental surveillance expansion plan: eradication and endgame strategic plan 2013–2018 [cited 2022 Jun 3]. https://polioeradication.org/who-we-are/strategic-plan-2013-2018
27. Pan American Health Organization, Ministerio de Salud Pública y Asistencia Social de Guatemala. Routine vaccination coverage dashboard, Guatemala [in Spanish]. 2023 [cited 2023 Apr 26]. https://tableros.mspas.gob.gt/vacunacionesquemaregular/

Address for correspondence: Marc Rondy, Diagonal 6, 10-50, Edificio Interaméricas, Torre Norte, 4to nivel, Guatemala City, Guatemala; email: rondymar@paho.org

Outbreak of NDM-1– and OXA-181–Producing *Klebsiella pneumoniae* Bloodstream Infections in a Neonatal Unit, South Africa

Rindidzani E. Magobo, Husna Ismail, Michelle Lowe, Wilhelmina Strasheim, Ruth Mogokotleng, Olga Perovic, Stanford Kwenda, Arshad Ismail, Manala Makua, Abram Bore, Rose Phayane, Harishia Naidoo, Tanya Dennis, Makhosazane Ngobese, Wim Wijnant, Nelesh P. Govender, for Baby GERMS-SA[1]

After an increase in carbapenem-resistant *Klebsiella pneumoniae* (CRKP) bloodstream infections and associated deaths in the neonatal unit of a South Africa hospital, we conducted an outbreak investigation during October 2019–February 2020 and cross-sectional follow-up during March 2020–May 2021. We used genomic and epidemiologic data to reconstruct transmission networks of outbreak-related clones. We documented 31 cases of culture-confirmed CRKP infection and 14 deaths. Two outbreak-related clones (bla_{NDM-1} sequence type [ST] 152 [n = 16] and $bla_{OXA-181}$ ST307 [n = 6]) cocirculated. The major clone bla_{NDM-1} ST152 accounted for 9/14 (64%) deaths. Transmission network analysis identified possible index cases of $bla_{OXA-181}$ ST307 in October 2019 and bla_{NDM-1} ST152 in November 2019. During the follow-up period, 11 new cases of CRKP infection were diagnosed; we did not perform genomic analysis. Sustained infection prevention and control measures, adequate staffing, adhering to bed occupancy limits, and antimicrobial stewardship are key interventions to control such outbreaks.

Author affiliations: National Institute for Communicable Diseases, a Division of the National Health Laboratory Service, Johannesburg, South Africa (R.E. Magobo, H. Ismail, M. Lowe, W. Strasheim, R. Mogokotleng, O. Perovic, S. Kwenda, A. Ismail, N.P. Govender); University of the Witwatersrand, Johannesburg (O. Perovic, N.P. Govender); National Department of Health, Pretoria (M. Makua); Gauteng Provincial Department of Health, Johannesburg (A. Bore); Tembisa Provincial Hospital, Johannesburg (R. Phayane, H. Naidoo, T. Dennis, M. Ngobese, W. Wijnant); University of Cape Town, Cape Town, South Africa (N.P. Govender); University of Exeter, Exeter, UK (N.P. Govender).

DOI: https://doi.org/10.3201/eid2908.230484

Carbapenem-resistant Enterobacterales (CRE) are classified as critical priority bacterial pathogens by the World Health Organization (*1*). *Klebsiella pneumoniae* is a major cause of neonatal infections in low- and middle-income countries (*2*,*3*). In a national population-level analysis, *K. pneumoniae* accounted for 26% of invasive neonatal infections in South Africa during 2014–2019 (*4*). Resistance mechanisms to carbapenems include enzymatic inactivation, changes to outer-membrane permeability, and efflux pump upregulation (*5*). Several outbreaks of *K. pneumoniae* infection in neonatal units have been investigated in South Africa since 1992 (*6*–*11*). Some of those studies used molecular typing methods, such as multilocus sequence typing and pulsed-field gel electrophoresis (PFGE), that lack sufficient resolution to distinguish between clonal strains (*8*–*12*). Whole-genome sequencing (WGS) is a powerful tool to investigate healthcare-associated pathogens such as *K. pneumoniae* and has been widely used in combination with epidemiologic information to track outbreaks and transmission routes of pathogens (*13*–*17*).

In December 2019, the National Institute for Communicable Diseases (NICD) in South Africa was notified of 8 cases of culture-confirmed carbapenem-resistant *K. pneumoniae* (CRKP) bloodstream infections in a neonatal unit at a provincial tertiary hospital. The outbreak began with 4 cases reported in October 2019. The objectives of this investigation were to verify the existence of an outbreak; describe the antimicrobial susceptibility profiles, resistance mechanisms, and transmission dynamics of CRKP clones in circulation; and monitor the incidence of

[1]Members of Baby GERMS-SA are listed at the end of this article.

CRKP infections within 1 year of instituting outbreak interventions.

Materials and Methods

Hospital Setting and Surveillance

Tembisa Provincial Tertiary Hospital is located in the Tembisa township in Gauteng Province, South Africa; the township has a population size of 2.5 million. The hospital also serves the communities of Midrand and Diepsloot and as a referral site for 20 clinics in the surrounding area, spanning 3 municipalities (the cities of Johannesburg, Ekurhuleni, and Tshwane). Annually, the hospital sees >280,000 patients. The hospital facility has 840 beds in total, 704 for adults, 71 for newborn babies, and 64 for pediatric patients; the average daily admission is 150 patients. The hospital's neonatal unit consists of wards A and B. Neonates are assigned to a section within a ward depending on age and the acuity of their condition at admission. Ward A has high-care (A1), low-care (A2), and isolation rooms; the approved bed capacity is 40. Ward B consists of a kangaroo mother care section (designed to increase skin-to-skin contact between mother and infant for preterm or low birthweight infants), a neonatal intensive care unit, a low-care unit, and a pediatric intensive care unit that is separated from the other rooms by a door. Ward B has a total of 31 beds. The intended medical staff complement during a day shift in ward A was 8 doctors, with an intended bed-to-doctor ratio of 5:1 and an intended bed-to-nurse ratio of 3:1. One medical officer was usually on night call for all the neonatal wards. Ward B had 3 doctors and 4 nurses, with an overall bed-to-staff ratio of 4.4:1.

Coincidentally, enhanced surveillance for neonatal infections as part of the Baby GERMS-SA study was conducted at this hospital during October 1, 2019–September 30, 2020 (*18*). In brief, neonates with culture-confirmed bloodstream infections or meningitis were enrolled into the surveillance program if they met the case definition (i.e., a neonate <28 days of age from whom a pathogen was isolated from blood or cerebrospinal fluid). The diagnostic laboratory submitted the corresponding bacterial and fungal isolates to the NICD for further characterization. Demographic, clinical, and outcome data were retrospectively abstracted from their imaged medical records. In addition, admissions and patient bed-days were recorded by month for the neonatal unit.

Outbreak Investigation

A multidisciplinary investigation team consisting of members of the NICD, Infection Control Service Laboratory (National Health Laboratory Service), the Gauteng Provincial Department of Health, and the National Department of Health was assembled in January 2020. To estimate baseline rates of bloodstream infections, we obtained a line list from the NICD surveillance data warehouse for infants ≤6 months of age admitted to Tembisa Provincial Tertiary Hospital with blood cultures positive for any bacterial or fungal organism during January 2017–September 2019. We excluded organisms considered commensals by the US Centers for Disease Control and Prevention National Healthcare Safety Network (*19*). We regarded blood cultures with the same organism isolated within 21 days of the first positive culture as duplicates and excluded those. We defined an outbreak as an increase of ≥100% in the number of observed cases of CRKP infection in a month above the expected (average) number in the preceding 2 months. On March 11, 2020, before the initial investigation closeout, the World Health Organization declared the global COVID-19 pandemic (*20*). We calculated monthly bloodstream infection rates during the follow-up period, March 2020–May 2021, using the same methods used in the initial outbreak investigation.

External Infection Prevention and Control Audit Process

During the initial investigation, we conducted an external infection prevention and control (IPC) audit in January 2020 using the National Department of Health standardized Infection Control Assessment Tool (*21*). We compiled recommendations for immediate, mid-term, and long-term interventions. A similar internal audit by the hospital response team was conducted in August 2020 to monitor improvements in adherence to IPC measures. Specific IPC measures had been implemented early after the observed increase in the number of cases. For instance, all colonized and infected babies were cohorted or isolated in separate sections of the ward. Additional cleaning of the unit was conducted several times beginning in November 2019. Hand hygiene was monitored for both staff and parents entering the unit. When the neonatal unit reached 100% bed capacity, maternity cases were rerouted to other facilities, although this intervention could not be sustained during the COVID-19 pandemic.

Cases and Isolates

We defined a case as culture-confirmed bloodstream infection caused by *K. pneumoniae* resistant to any carbapenem (i.e., meropenem, imipenem, doripenem, or ertapenem) in an infant ≤6 months of age. The case

definition was not restricted to neonates <28 days of age because babies who stayed in hospital beyond the neonatal period remained at risk for infection. We analyzed all isolates submitted to NICD from this hospital during October 1, 2019–February 29, 2020, including those submitted for Baby GERMS-SA surveillance. The hospital provided monthly infection reports to NICD, listing cases of CRKP infection with dates of birth, birthweights, dates of specimen collection, and outcome information. We conducted the follow-up analysis in May 2021, 18 months after the outbreak started in October 2019.

Microbiological Analysis

We confirmed species-level identification using matrix-assisted laser desorption/ionization time-of-flight mass spectrometry (Bruker Daltonics, https://www.bruker.com) and performed antimicrobial susceptibility testing using the MicroScan WalkAway 96-plus system with the NM44 card (Siemens Healthineers, https://www.siemens-healthineers.com). We interpreted MICs for the tested antimicrobial agents according to Clinical and Laboratory Standards Institute guidelines and defined multidrug-resistant isolates as those with nonsusceptibility to ≥1 agent in ≥3 antimicrobial classes (22). We screened for carbapenemase genes and strain relatedness using real-time multiplex PCR and PFGE and performed WGS to determine sequence types, identify acquired antimicrobial resistance genes, and confirm presence of plasmid replicons, O antigen locus types, and K locus types. We compared core genome single-nucleotide polymorphism (SNP) distances and epidemiologic information to investigate the transmission events of CRKP in the neonatal unit (Appendix, https://wwwnc.cdc.gov/EID/article/29/8/23-0484-App1.pdf).

Results

Baseline, Outbreak, and Follow-Up Periods

During January 2017–September 2019, a total of 1,771 positive blood cultures were reported from infants ≤6 months of age at the hospital. Of those, 864 (49%) blood cultures yielded probable pathogenic organisms; 724 were in neonatal wards A and B. We excluded 144 duplicates from the analysis. Of the remaining 580 isolates, 428 were from patients with single-isolate bloodstream infection episodes and were included in the analysis. *K. pneumoniae* accounted for 29% (122/428) of cases, *Staphylococcus aureus* 36% (153/428), and *Acinetobacter baumannii* 27% (116/428). Of the 122 cases of *K. pneumoniae* isolated during the January 2017–September 2019 baseline period, 8% (10/122) were CRKP; 5 of those cases were diagnosed in January 2019 (Figure 1).

The number of CRKP bloodstream infection cases increased during October 1, 2019–February 29, 2020; a total of 31 cases and 15 deaths were reported. Most cases (n = 14) were reported in December 2019; in the preceding 2 months only 3 non-CRKP cases were diagnosed (average 1.5 cases/month) (Figure 2).

During the follow-up period (March 2020–May 2021), 299 positive blood cultures with probable pathogenic organisms were obtained from infants admitted to the neonatal unit (wards A and B). *K. pneumoniae* accounted for 38 of those episodes (13%); of those, 29% (n = 11) isolates were carbapenem-resistant (Appendix).

External IPC Audit Findings and Internal Follow-Up Audit

The initial external IPC auditors found that neonatal unit ward A exceeded the approved bed capacity by 60% (64 admissions in a ward with 40 approved

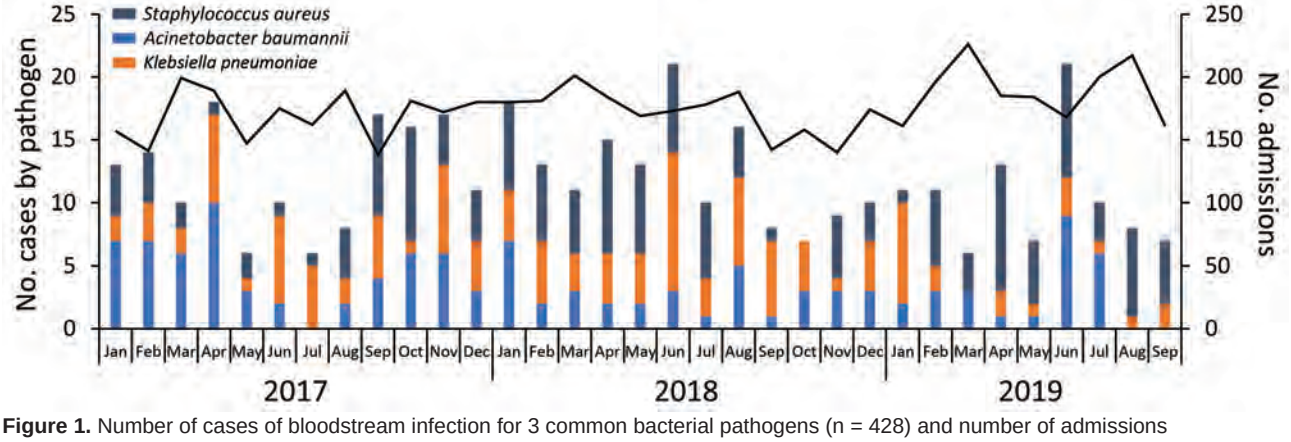

Figure 1. Number of cases of bloodstream infection for 3 common bacterial pathogens (n = 428) and number of admissions (n = 5,796) in the neonatal unit during baseline period, South Africa, January 2017–September 2019. Black data line indicates number of admissions. Scales for the y-axes differ substantially to underscore patterns but do not permit direct comparisons.

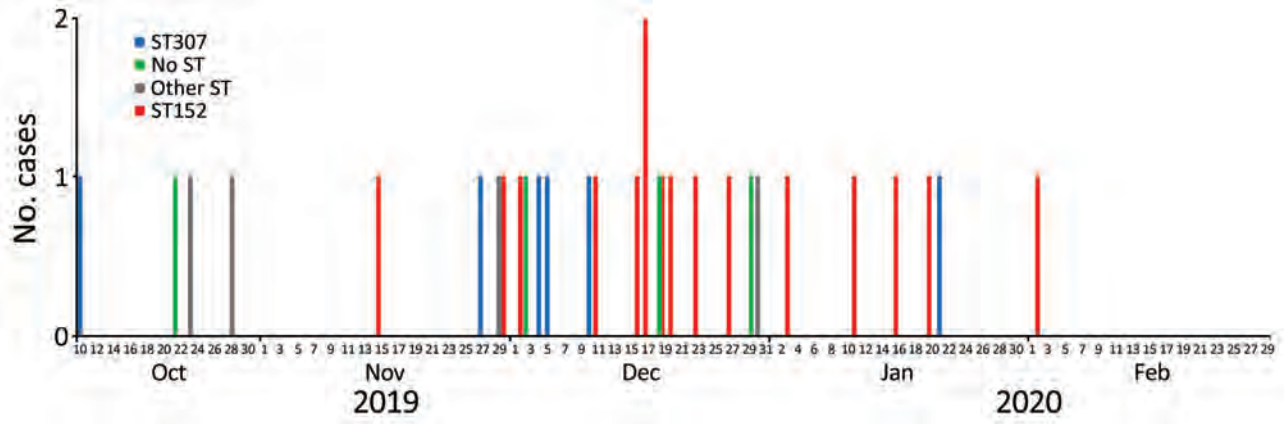

Figure 2. Epidemic curve of 31 cases of carbapenem-resistant *Klebsiella pneumoniae* bloodstream infection by date of specimen collection and ST of isolate during outbreak period, South Africa, October 2019–February 2020. ST, sequence type.

beds); ward A had 13 nurses per shift and a bed-to-nurse ratio of 5:1. Occupancy increased to 180% above the approved capacity during the internal audit in August 2020. Attrition occurred at a rate of 16 nurses and 13 clinical staff over a period of 7 months. Adherence to hand hygiene was 95% during the external audit and 100% during the follow-up internal audit. Hand hygiene adherence remained at >96% a year later in May 2021, maintained through a peer-monitoring system. Liquid hand soap with an antimicrobial agent, alcohol-based antiseptic, and hand lotions (aqueous cream) were initially not available for staff, but availability improved on follow-up. Alcohol-based antiseptic dispensers were available at each bed during the follow-up audit. Handwashing supplies were ordered, and stock levels were monitored. Elbow-operated taps were installed to improve quality of hand hygiene practices. Unannounced IPC audits were performed, but no direct observations were reported. The overall score for sterilizing and disinfecting instruments improved from 27% to 47% in August 2020. Policies or standard operating procedures (SOPs) were subsequently developed, and staff members signed to demonstrate their understanding of SOPs. The unit had no designated area for mixing standard intravenous fluids because of infrastructural challenges, single-dose vials were not used, and no SOP for multidose vials was in place in the ward (Appendix Table). Most external audit recommendations were implemented. For example, an integrated IPC and occupational health and safety team was established to maximize human resource capacity and budget allocations and to strengthen infection surveillance. However, some crucial initial IPC audit recommendations could not be sustained because of COVID-19 demands (e.g., diverting patients to neighboring hospitals when ward capacity was reached and converting the milk room into a kangaroo mother care unit). Although an antimicrobial stewardship committee was established, implementing its recommendations was delayed because attention and resources were diverted to the COVID-19 response.

Isolates and Cases

During October 2019–February 2020, a total of 31 laboratory-confirmed cases of CRKP bloodstream infections were reported in the neonatal unit. Of those, we did not have isolates for 2 cases (Figure 3), but laboratory reports indicated that these isolates were resistant to ertapenem, imipenem, and meropenem. The NICD reference laboratory received 34 isolates for the remaining 29 cases. Of those, 2 cases had 3 isolates each and 1 case had 2 isolates. The first isolate (i.e., the isolate with earliest specimen collection date) per case from 29 cases was selected for molecular characterization. Twenty-seven isolates were confirmed as *K. pneumoniae* subspecies *pneumoniae*; antimicrobial susceptibility profiling and genomic characterization was performed. We excluded 2 isolates identified as *Pseudomonas aeruginosa* that were likely contaminated during shipping.

Antimicrobial Susceptibility

All isolates were multidrug-resistant. In total, 89% (24/27) of the isolates were resistant to ertapenem and 81% (22/27) were resistant to meropenem (Figure 3).

Genomic Characterization

We identified 3 clonal clusters consisting of 6 sequence types from 27 isolates by using core genome maximum-likelihood phylogeny (Appendix Figure 1). Sequence type (ST) 152 accounted for 59% (16/27)

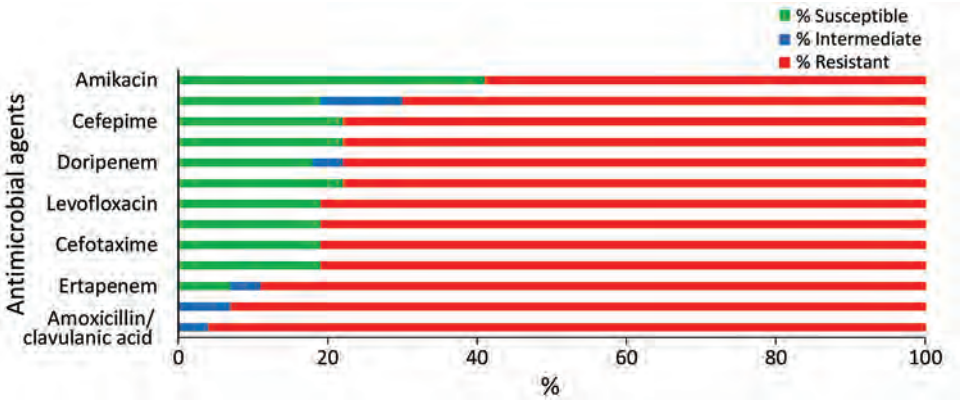

Figure 3. Reference laboratory antimicrobial susceptibility profiles of 27 viable *Klebsiella pneumoniae* isolates from cases of bloodstream infection during a neonatal unit outbreak, South Africa, October 2019–February 2020.

of the cases, followed by ST307 (6/27; 22%) and ST17 (2/27; 7%); ST25, ST45, and ST297 each accounted for a single case (1/27; 4%). We found that 94% (26/27) of the isolates carried carbapenemase genes. All isolates within ST152 clone harbored the bla_{NDM-1} gene and contained ColRNAI, *Inc*FIB(K), *Inc*FIB(pB171), and *Inc*FII(Yp) plasmid incompatibility groups. Further analysis revealed that the bla_{NDM-1} gene was carried on the *Escherichia coli* B171 plasmid pB171 (accession no. AB024946). Phenotypic resistance to third and fourth generation cephalosporins was confirmed by the presence of extended-spectrum β-lactamases, such as $bla_{CTX-M-15}$ and other β-lactamase genes (bla_{TEM-1} and bla_{SHV-1}) (Appendix Figure 1).

Table. Clinical characteristics of WGS-confirmed cases of carbapenem-resistant *Klebsiella pneumoniae* bloodstream infection in newborns admitted to the neonatal unit of a tertiary care hospital, South Africa, October 2019–February 2020*

Pt no.	Age, d/sex	Weight at birth, g	Gestational age, wks	Ward†	Other pathogens	Outcome	Isolate	Collection date	ST	K type	O type
Pt 1	13/F	1,300	32	A		Transferred	BG32	2019 Oct 10	307	KL102	O2afg
Pt 2	31/M	1,000	28	A		Discharged	BG113	2019 Oct 23	17	KL25	O5
Pt 3	0/M	3,200	42	A		Discharged	BG265	2019 Oct 28	17	KL25	O5
Pt 4	7/M	1,000	28	A1, B	*Acinetobacter baumannii*	Died	BG314	2019 Nov 15	152	KL149	O4
Pt 5	20/F	890	28	A		Discharged	BG315	2019 Nov 27	307	KL102	O2afg
Pt 6	10/F	1,360	27	A1, A2, B	*Enterobacter cloacae*	Died	BG313	2019 Nov 29	297	KL158	O1
Pt 7	2/M	1,000	NR	A	*Acinetobacter baumannii*	Died	BG263	2019 Nov 30	152	KL149	O4
Pt 8	5/F	1,700	34	A		Died	BG264	2019 Dec 2	152	KL149	O4
Pt 9	17/M	1,100	NR	B		Died	BG259	2019 Dec 4	307	KL102	O2afg
Pt 10	9/M	2,690	38	A		Died	BG258	2019 Dec 5	307	KL102	O2afg
Pt 11	23/M	1,100	28	B		Died	BG254	2019 Dec 10	307	KL102	O2afg
Pt 12	7/M	840	26	A1, isolation		Discharged	BG255	2019 Dec 11	152	KL149	O4
Pt 13	1/M	NR	NR	A		Discharged	BG222	2019 Dec 16	152	KL149	O4
Pt 14	21/M	1,570	34	A		Discharged	BG218	2019 Dec 17	152	KL149	O4
Pt 15	4/F	3,050	39	A		Died	BG213	2019 Dec 17	152	KL149	O4
Pt 16	19/F	970	NR	A	*Enterobacter cloacae*	Died	BG223	2019 Dec 19	152	KL149	O4
Pt 17	7/F	800	29	A		Died	BG219	2019 Dec 20	152	KL149	O4
Pt 18	3/M	1,300	29	A1		Died	BG215	2019 Dec 23	152	KL149	O4
Pt 19	3/F	1,700	34	A		Discharged	BG214	2019 Dec 27	152	KL149	O4
Pt 20	6/M	810	29	A2		Died	BG442	2019 Dec 30	25	KL2	O1
Pt 21	0/F	1,670	33	A		Discharged	BG272	2020 Jan 3	152	KL149	O4
Pt 22	0/M	1,100	30	A1, isolation		Discharged	BG271	2020 Jan 11	152	KL149	O4
Pt 23	8/M	970	30	A1, isolation, B		Discharged	BG460	2020 Jan 16	152	KL149	O4
Pt 24	12/M	1,240	28	A1, A2, B		Died	BG316	2020 Jan 20	152	KL149	O4
Pt 25	13/M	1,010	27	A1, isolation, B		Discharged	BG317	2020 Jan 21	307	KL102	O2afg
Pt 26	6/M	925	29	A1, B		Died	BG449	2020 Feb 2	152	KL149	O4

*The specimen type used for all patients was blood culture. NR, not recorded; Pt, patient; ST, sequence type; WGS, whole-genome sequencing.
†Wards A1, A2, and Isolation are sections (cubicles) within ward A with a total approved bed capacity of 40.

The gene $bla_{OXA-181}$ was present in all isolates belonging to ST307. Three isolates carrying the $bla_{OXA-181}$ gene coharbored the bla_{OXA-48} gene. All isolates within $bla_{OXA-181}$ ST307 clone shared ColKP3, IncFIB(Mar), and IncX3 plasmid incompatibility groups. Plasmid analysis showed that $bla_{OXA-181}$ gene in ST307 clone isolates was carried on *K. pneumoniae* KP3 plasmid KP3-A (accession no. JN205800) (Appendix Figure 1).

Clinical Characteristics of 26 WGS-Confirmed Cases of CRKP

Of the 26 WGS-confirmed cases of CRKP, 67% (18/26) of the infants were boys; median age was 7 days (interquartile range 3–17 days). Birthweights ranged from 760 to 3,200 g; the median weight was 1,100 g (interquartile range 970–1595 g). Four of the 26 infants required resuscitation at birth. Invasive devices were inserted in all infants. Two infants had a record of underlying abnormalities (congenital anemia and neonatal seizures). Just over half (54% [14/26]) of infants died in hospital. Of these, 64% (9/14) had cultured isolates belonging to the ST152 clone (Table).

Genomic and Epidemiologic Links among Outbreak-Associated Isolates

The first case (Pt1) of CRKP BSI $bla_{OXA-181}$ ST307 clone was confirmed on October 10, 2019 in ward A. The $bla_{OXA-181}$ ST307 was responsible for 4 more cases (2 each in wards A and B) in late November and during the first week of December 2019. The last case belonging to $bla_{OXA-181}$ ST307 clone was identified in January 2020. The transmission network revealed that Pt1 was a possible index case. Although this patient was later transferred to an academic hospital for further treatment, this clone continued to disseminate within the neonatal unit. Five more cases were detected with the transmission stemming from the intermediate host with SNP differences of <10 among the clonal isolates (Figure 4, panel A).

The first case-patient (Pt4) of the major outbreak-related bla_{NDM-1} ST152 clone was diagnosed on November 15, 2019, in ward A of the neonatal unit, followed by another case (Pt7) 15 days later in ward A. During December 11, 2019–February 2, 2020, a total of 14 more cases were isolated in the neonatal unit. Isolates from Pt14 and Pt17 were not considered part of the outbreak because they had >30 SNPs compared to other isolates. No further cases caused by the bla_{NDM-1} ST152 clone were diagnosed after February 2020. Transmission network analysis identified Pt4 as the index case for the ST152 clone outbreak. However, Pt4 died on November 16, 2019, ten days before Pt7 was admitted, suggesting the role of an intermediate host or environmental source in the dissemination of bla_{NDM-1} ST152 clone in the neonatal unit. Pt8's infection was diagnosed 2 days after the diagnosis of Pt7. Pt8 died a day after diagnosis. No further transmission from Pt7 or Pt8 to other patients could be established. Nine patients (Pt12–Pt19 and Pt22) in whom transmission stemmed directly from Pt4 were potentially infected through an intermediate source. Further dissemination of the ST152 clone was observed between Pt21, Pt23, and Pt26 in January 2020. These patients were admitted to ward A but moved between ward A and ward B. The transmission network revealed 2 possible events: first, from Pt21 to Pt24, who died a day after diagnosis; and second, that transmission occurred from Pt21 to Pt23, then from Pt23 to Pt26. However, Pt26 was admitted to ward A, 15 days after Pt23 was discharged from the hospital, suggesting the role of

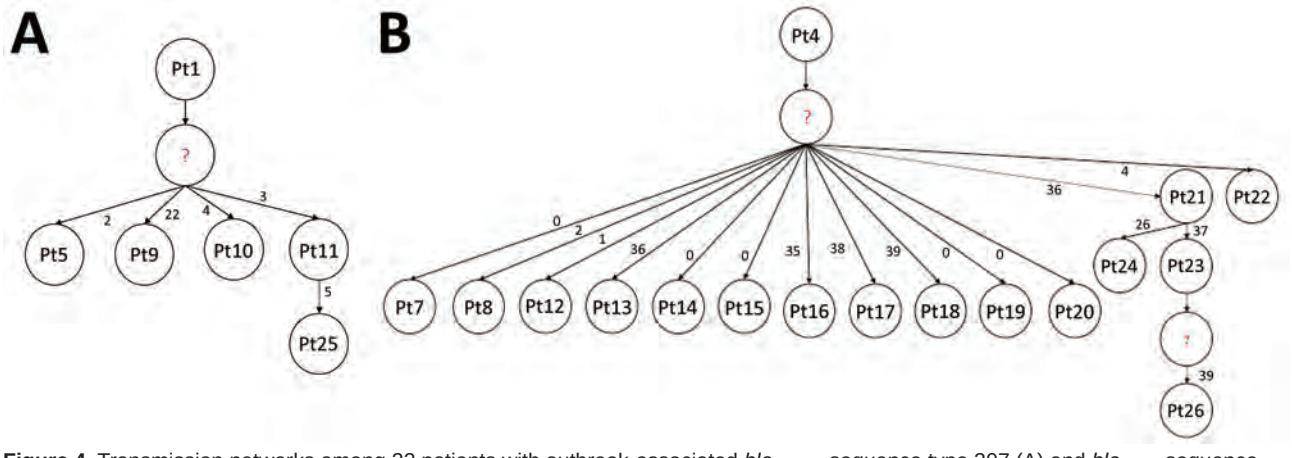

Figure 4. Transmission networks among 22 patients with outbreak-associated $bla_{OXA-181}$ sequence type 307 (A) and bla_{NDM-1} sequence type 152 (B) clones of *Klebsiella pneumoniae* isolated from a neonatal unit during outbreak, South Africa, October 2019–February 2020. Question marks denote missing isolates; numbers along branches indicate number of single-nucleotide polymorphisms between index isolate and other isolates.

an intermediate in the spread of bla_{NDM-1} ST152 clone (Figure 4, panel B).

Discussion

We describe the successful integration of genomic and epidemiologic data in tracking an outbreak of CRKP infections in the neonatal unit of a South Africa hospital. The number of CRKP bloodstream infections increased substantially in the neonatal unit beginning in October 2019. Two outbreak-related clones (bla_{NDM-1} ST152 and $bla_{OXA-181}$ ST307) cocirculated. The major outbreak clone bla_{NDM-1} ST152 accounted for >60% of deaths. Fine transmission networks identified possible index cases of $bla_{OXA-181}$ ST307 and bla_{NDM-1} ST152 clones. The spread and dissemination of these clones from patient to patient might have been enabled by healthcare workers or environmental or fomite contamination, resulting from breaches in IPC measures.

Reports of CRE infections in Africa have increased markedly; the most commonly reported carbapenemases are bla_{NDM-1} and bla_{OXA-48} and variants (*23*–*27*). In this study, *K. pneumoniae* carrying bla_{NDM-1}, bla_{OXA-48}, and $bla_{OXA-181}$ were dominant in the neonatal unit, which was consistent with previous reports (*23*–*27*). The bla_{NDM} gene was first described in South Africa in an *Enterobacter cloacae* strain in 2011 (*28*). Recent data from South Africa sentinel surveillance of CRE bloodstream infections have shown a change in the distribution of carbapenemase genes (*29*). Previously, bla_{NDM} was the most commonly detected gene in Enterobacterales, followed by bla_{OXA-48} (*25*). However, beginning in 2016, bla_{OXA-48} and variants began to dominate, followed by bla_{NDM} (*29*). This change is worrisome because bla_{OXA-48} and variants are more difficult to identify using phenotypic laboratory methods. Most outbreaks reported in South Africa are also associated with bla_{OXA-48} and variants (*30*–*32*). The emergence of bla_{NDM-1} *K. pneumoniae* as a cause of outbreaks is concerning because once inserted into drug-resistant plasmids, virulence determinants render these strains highly resistant, virulent, and easily transmissible regardless of the clone (*33*).

The first laboratory-confirmed outbreak of $bla_{OXA-181}$ *K. pneumoniae* in South Africa was described in 2015 from a hematology unit in Cape Town (*30*). After that, Strydom et al. (*31*) identified *K. pneumoniae* superclone ST307 carrying $bla_{OXA-181}$ on a self-transmissible plasmid IncX3 (p72_X3_OXA181) as the source of a CRKP outbreak that spread across multiple wards in a Pretoria hospital during September 2015–December 2016. Furthermore, $bla_{OXA-181}$ was endemic among patients colonized with *K. pneumoniae* in a KwaZulu-Natal hospital intensive care unit, and the spread was enabled by plasmid replicon *E. coli* p010-B-OXA181 (*32*). A combination of genomic and epidemiologic data was used either to track outbreaks or reconstruct transmission events that occurred during an outbreak (*14*,*16*,*34*–*36*). In our study, bla_{NDM-1} and $bla_{OXA-181}$ *K. pneumoniae* strains were responsible for outbreaks that occurred simultaneously in the neonatal unit. The resistant genes were spread by transmissible plasmids *E. coli* B171 plasmid pB171 (bla_{NDM-1}) and *K. pneumoniae* KP3 plasmid KP3-A ($bla_{OXA-181}$). A recent report describing an outbreak of CRKP bloodstream infections in a neonatal unit in another South Africa hospital showed that bla_{OXA-48} and variants *K. pneumoniae* were responsible for the outbreak (*11*). Although the main objectives of the outbreak investigation by Essel et al. (*11*) were to confirm the outbreak and assess the IPC program, the molecular typing technique used has low discriminatory power to distinguish genetically related isolates. Lowe et al. (*37*) documented the rapid spread of ST307 clone carrying $bla_{OXA-181}$ in >40 hospitals across 3 provinces in South Africa, highlighting the critical need for more enhanced genomic surveillance of *K. pneumoniae* ST307 super clone in healthcare settings.

Given the rapid transfer and acquisition of endemic carbapenemase genes, IPC measures are critical to preventing and managing outbreaks. Both IPC audits flagged <50% adherence to instrument sterilization and disinfection procedures. Therefore, breaches in aseptic techniques during invasive medical device insertion or maintenance practices might have been involved in the causal pathway to neonatal bacteremia. Inadequate staffing, exceeded bed capacity, aging and undermaintained hospital infrastructure, and general lack of institutional support for IPC and antimicrobial stewardship initiatives also contribute to the spread of healthcare-associated infections (*38*). Dramowski et al. presented a framework for prevention of healthcare-associated infections in neonates and children, which highlighted the need for a nationally endorsed prevention strategy to ensure that children in South Africa receive safe and high-quality care (*39*).

The strength of this study was involvement of multiple stakeholders who enabled different segments of the outbreak investigation. Genomic and epidemiologic data were used to confirm the existence of the outbreak, identify the sources of the outbreak, and reconstruct probable transmission events. The first limitation of our study is that we conducted a search for cases of bloodstream infection among infants <6 months of age through a laboratory audit, but we did not extend this search to the rest of the hospital.

Second, not all isolates from laboratory-confirmed CRKP cases were available for molecular characterization. Finally, genetic links among isolates from infected neonates and contaminated environment, fomites, or colonized healthcare workers could not be established because we did not perform contemporary environmental sampling or a colonization survey.

In conclusion, a combination of high-resolution WGS and epidemiologic data enabled a detailed description of this healthcare-associated infection outbreak in a neonatal unit and established transmission links. Continued monitoring of pathogens carrying endemic carbapenemases is necessary to prevent further reemergence of outbreaks. IPC measures complemented with adequate staffing levels, adherence to bed occupancy limits, improved neonatal unit infrastructure, and antimicrobial stewardship are key to sustainably reducing neonatal healthcare-associated infections.

Members of Baby GERMS-SA: Nelesh P. Govender (principal investigator), Susan T. Meiring, Olga Perovic, Vanessa C. Quan, Anne von Gottberg, Linda de Gouveia, Cheryl Cohen, Angela Dramowski, Juliet Paxton, Danie Erwee, Camira Pillay, Rudzani C. Mashau, Rindidzani Magobo, Ntombi Dube, Relebohile Ramatsa, Melissa Ngubane, Bernard Motsetse, Lousia Phalatse, Tebogo Modiba, Dianette Pearce, Lesley Ingle, Zikhona Gabazana, Naseema Bulbulia, Patrick Pitjeng, Rosah Mabokachaba, Rotondwa Mudau, Rubeina Badat, Ruth Mogokotleng, Sabelle Jallow, Serisha Naicker, Siphiwe Kutta, Sydney Mogokotleng, Tsidiso Maphanga, Wilhelmina Strasheim (NICD, Johannesburg); site investigators: Cheryl Mackay (Dora Nginza Hospital, Eastern Cape), Mphekwa T. Mailula (Mankweng Hospital, Limpopo), Rose Phayane (Tembisa Hospital, Gauteng), Constance Kapongo (Queen Nandi Regional Hospital, Kwa-Zulu-Natal), Omphile Mekgoe (Tshepong Hospital, North West), M. Terry (Rob Ferreira hospital, Mpumalanga).

This work was partly funded by the Bill and Melinda Gates Foundation (grant no. INV008112) (principal investigator N.P.G.).

About the Author

Dr. Magobo is a medical scientist with experience in genomic epidemiology of bacterial and fungal pathogens causing healthcare-associated infections.

References

1. Tacconelli E, Carrara E, Savoldi A, Harbarth S, Mendelson M, Monnet DL, et al.; WHO Pathogens Priority List Working Group. Discovery, research, and development of new antibiotics: the WHO priority list of antibiotic-resistant bacteria and tuberculosis. Lancet Infect Dis. 2018;18:318–27. https://doi.org/10.1016/S1473-3099(17)30753-3
2. Okomo U, Akpalu ENK, Le Doare K, Roca A, Cousens S, Jarde A, et al. Aetiology of invasive bacterial infection and antimicrobial resistance in neonates in sub-Saharan Africa: a systematic review and meta-analysis in line with the STROBE-NI reporting guidelines. Lancet Infect Dis. 2019; 19:1219–34. https://doi.org/10.1016/S1473-3099(19)30414-1
3. Sands K, Carvalho MJ, Portal E, Thomson K, Dyer C, Akpulu C, et al.; BARNARDS Group. Characterization of antimicrobial-resistant Gram-negative bacteria that cause neonatal sepsis in seven low- and middle-income countries. Nat Microbiol. 2021;6:512–23. https://doi.org/10.1038/s41564-021-00870-7
4. Mashau RC, Meiring ST, Dramowski A, Magobo RE, Quan VC, Perovic O, et al.; Baby GERMS-SA. Culture-confirmed neonatal bloodstream infections and meningitis in South Africa, 2014–19: a cross-sectional study. Lancet Glob Health. 2022;10:e1170–8. https://doi.org/10.1016/S2214-109X(22)00246-7
5. Queenan AM, Bush K. Carbapenemases: the versatile β-lactamases. Clin Microbiol Rev. 2007;20:440–58. https://doi.org/10.1128/CMR.00001-07
6. Coovadia YM, Johnson AP, Bhana RH, Hutchinson GR, George RC, Hafferjee IE. Multiresistant *Klebsiella pneumoniae* in a neonatal nursery: the importance of maintenance of infection control policies and procedures in the prevention of outbreaks. J Hosp Infect. 1992;22:197–205. https://doi.org/10.1016/0195-6701(92)90044-M
7. Pillay T, Pillay DG, Adhikari M, Sturm AW. Piperacillin/tazobactam in the treatment of Klebsiella pneumoniae infections in neonates. Am J Perinatol. 1998;15:47–51. https://doi.org/10.1055/s-2007-993898
8. Gregersen N, Van Nierop W, Von Gottberg A, Duse A, Davies V, Cooper P. *Klebsiella pneumoniae* with extended spectrum beta-lactamase activity associated with a necrotizing enterocolitis outbreak. Pediatr Infect Dis J. 1999;18:963–7. https://doi.org/10.1097/00006454-199911000-00005
9. Cotton MF, Wasserman E, Pieper CH, Theron DC, van Tubbergh D, Campbell G, et al. Invasive disease due to extended spectrum beta-lactamase-producing *Klebsiella pneumoniae* in a neonatal unit: the possible role of cockroaches. J Hosp Infect. 2000;44:13–7. https://doi.org/10.1053/jhin.1999.0650
10. Marais E, Moodley A, Govender N, Kularatne R, Thomas J, Duse A. Clusters of *Klebsiella pneumoniae* infection in neonatal intensive care units in Gauteng. S Afr Med J. 2006;96:813.
11. Essel V, Tshabalala K, Ntshoe G, Mphaphuli E, Feller G, Shonhiwa AM, et al. A multisectoral investigation of a neonatal unit outbreak of *Klebsiella pneumoniae* bacteraemia at a regional hospital in Gauteng Province, South Africa. S Afr Med J. 2020;110:783–90. https://doi.org/10.7196/SAMJ.2020.v110i8.14471
12. Sabat AJ, Budimir A, Nashev D, Sá-Leão R, van Dijl J, Laurent F, et al.; ESCMID Study Group of Epidemiological Markers (ESGEM). Overview of molecular typing methods for outbreak detection and epidemiological surveillance. Euro Surveill. 2013;18:20380. https://doi.org/10.2807/ese.18.04.20380-en
13. Smit PW, Stoesser N, Pol S, van Kleef E, Oonsivilai M, Tan P, et al. Transmission dynamics of hyper-endemic multi-drug resistant *Klebsiella pneumoniae* in a Southeast Asian neonatal unit: a longitudinal study with whole genome sequencing. Front Microbiol. 2018;9:1197. https://doi.org/10.3389/fmicb.2018.01197

14. Sui W, Zhou H, Du P, Wang L, Qin T, Wang M, et al. Whole genome sequence revealed the fine transmission map of carbapenem-resistant *Klebsiella pneumonia* isolates within a nosocomial outbreak. Antimicrob Resist Infect Control. 2018;7:70. https://doi.org/10.1186/s13756-018-0363-8
15. Chen D, Hu X, Chen F, Li H, Wang D, Li X, et al. Co-outbreak of multidrug resistance and a novel ST3006 *Klebsiella pneumoniae* in a neonatal intensive care unit: a retrospective study. Medicine (Baltimore). 2019;98:e14285.
16. Wang Y, Luo C, Du P, Hu J, Zhao X, Mo D, et al. Genomic epidemiology of an outbreak of *Klebsiella pneumoniae* st471 producing extended-spectrum β-lactamases in a neonatal intensive care unit. Infect Drug Resist. 2020;13:1081–90. https://doi.org/10.2147/IDR.S236212
17. Labi AK, Nielsen KL, Marvig RL, Bjerrum S, Enweronu-Laryea C, Bennedbæk M, et al. Oxacillinase-181 carbapenemase-producing *Klebsiella pneumoniae* in neonatal intensive care unit, Ghana, 2017–2019. Emerg Infect Dis. 2020;26:2235–8. https://doi.org/10.3201/eid2609.200562
18. Meiring S, Mashau R, Magobo R, Perovic O, Quan V, Cohen C, et al. Study protocol for a population-based observational surveillance study of culture-confirmed neonatal bloodstream infections and meningitis in South Africa: Baby GERMS-SA. BMJ Open. 2022;12:e049070. https://doi.org/10.1136/bmjopen-2021-049070
19. Dudeck MA, Horan TC, Peterson KD, Allen-Bridson K, Morrell G, Anttila A, et al. National Healthcare Safety Network Report, data summary for 2011, device-associated module. 2013;41:286–300.
20. World Health Organization. WHO Director-General's opening remarks at the media briefing on COVID-19—11 March 2020 [cited 2021 Jun 30]. https://www.who.int/director-general/speeches/detail/who-director-general-s-opening-remarks-at-the-media-briefing-on-covid-19---11-march-2020
21. National Department of Health. Infection control assessment tool—September 2013. Pretoria: Government of South Africa.
22. Magiorakos AP, Srinivasan A, Carey RB, Carmeli Y, Falagas ME, Giske CG, et al. Multidrug-resistant, extensively drug-resistant and pandrug-resistant bacteria: an international expert proposal for interim standard definitions for acquired resistance. Clin Microbiol Infect. 2012;18:268–81. https://doi.org/10.1111/j.1469-0691.2011.03570.x
23. Nordmann P, Poirel L. The difficult-to-control spread of carbapenemase producers among Enterobacteriaceae worldwide. Clin Microbiol Infect. 2014;20:821–30. https://doi.org/10.1111/1469-0691.12719
24. Kieffer N, Nordmann P, Aires-de-Sousa M, Poirel L. High prevalence of carbapenemase-producing *Enterobacteriaceae* among hospitalized children in Luanda, Angola. Antimicrob Agents Chemother. 2016;60:6189–92. https://doi.org/10.1128/AAC.01201-16
25. Singh-Moodley A, Perovic O. Antimicrobial susceptibility testing in predicting the presence of carbapenemase genes in Enterobacteriaceae in South Africa. BMC Infect Dis. 2016;16:536. https://doi.org/10.1186/s12879-016-1858-7
26. Sangare SA, Rondinaud E, Maataoui N, Maiga AI, Guindo I, Maiga A, et al. Very high prevalence of extended-spectrum beta-lactamase-producing *Enterobacteriaceae* in bacteriemic patients hospitalized in teaching hospitals in Bamako, Mali. PLoS One. 2017;12:e0172652. https://doi.org/10.1371/journal.pone.0172652
27. Abderrahim A, Djahmi N, Pujol C, Nedjai S, Bentakouk MC, Kirane-Gacemi D, et al. First case of NDM-1-producing *Klebsiella pneumoniae* in Annaba University Hospital, Algeria. Microb Drug Resist. 2017;23:895–900. https://doi.org/10.1089/mdr.2016.0213
28. Lowman W, Sriruttan C, Nana T, Bosman N, Duse A, Venturas J, et al. NDM-1 has arrived: first report of a carbapenem resistance mechanism in South Africa. S Afr Med J. 2011;101:873–5.
29. Perovic O, Ismail H, Van Schalkwyk E, Lowman W, Prentice E, Senekal M, et al. Antimicrobial resistance surveillance in the South African private sector report for 2016. S Afr J Infect Dis. 2018;33:114–7. https://doi.org/10.1080/23120053.2018.1482646
30. Jacobson RK, Manesen MR, Moodley C, Smith M, Williams SG, Nicol MP, et al. Molecular characterisation and epidemiological investigation of an outbreak of $bla_{OXA-181}$ carbapenemase-producing isolates of *Klebsiella pneumoniae* in South Africa. S Afr Med J. 2015;105:1030–5. https://doi.org/10.7196/SAMJ.2015.v105i12.9926
31. Strydom KA, Chen L, Kock MM, Stoltz AC, Peirano G, Nobrega DB, et al. *Klebsiella pneumoniae* ST307 with OXA-181: threat of a high-risk clone and promiscuous plasmid in a resource-constrained healthcare setting. J Antimicrob Chemother. 2020;75:896–902. https://doi.org/10.1093/jac/dkz550
32. Madni O, Amoako DG, Abia ALK, Rout J, Essack SY. Genomic investigation of carbapenem-resistant *Klebsiella pneumoniae* colonization in an intensive care unit in South Africa. Genes (Basel). 2021;12:951. https://doi.org/10.3390/genes12070951
33. Shankar C, Nabarro LEB, Muthuirulandi Sethuvel DP, Raj A, Devanga Ragupathi NK, Doss GP, et al. Draft genome of a hypervirulent *Klebsiella quasipneumoniae* subsp. *similipneumoniae* with novel sequence type ST2320 isolated from a chronic liver disease patient. J Glob Antimicrob Resist. 2017;9:30–1. https://doi.org/10.1016/j.jgar.2017.01.004
34. Onori R, Gaiarsa S, Comandatore F, Pongolini S, Brisse S, Colombo A, et al. Tracking nosocomial *Klebsiella pneumoniae* infections and outbreaks by whole-genome analysis: small-scale Italian scenario within a single hospital. J Clin Microbiol. 2015;53:2861–8. https://doi.org/10.1128/JCM.00545-15
35. Snitkin ES, Zelazny AM, Thomas PJ, Stock F, Henderson DK, Palmore TN, et al.; NISC Comparative Sequencing Program Group. Tracking a hospital outbreak of carbapenem-resistant *Klebsiella pneumoniae* with whole-genome sequencing. Sci Transl Med. 2012;4:148ra116. https://doi.org/10.1126/scitranslmed.3004129
36. Yang Y, Yang Y, Chen G, Lin M, Chen Y, He R, et al. Molecular characterization of carbapenem-resistant and virulent plasmids in *Klebsiella pneumoniae* from patients with bloodstream infections in China. Emerg Microbes Infect. 2021;10:700–9. https://doi.org/10.1080/22221751.2021.1906163
37. Lowe M, Kock MM, Coetzee J, Hoosien E, Peirano G, Strydom KA, et al. *Klebsiella pneumoniae* ST307 with $bla_{OXA-181}$, South Africa, 2014–2016. Emerg Infect Dis. 2019;25:739–47. https://doi.org/10.3201/eid2504.181482
38. Gill CJ, Mantaring JBV, Macleod WB, Mendoza M, Mendoza S, Huskins WC, et al. Impact of enhanced infection control at 2 neonatal intensive care units in the Philippines. Clin Infect Dis. 2009;48:13–21. https://doi.org/10.1086/594120
39. Dramowski A, Cotton MF, Whitelaw A. A framework for preventing healthcare-associated infection in neonates and children in South Africa. S Afr Med J. 2017;107:192–5. https://doi.org/10.7196/SAMJ.2017.v107i3.12035

Address for correspondence: Nelesh P. Govender, National Institute for Communicable Diseases, Centre for Healthcare-Associated Infections, Antimicrobial Resistance and Mycoses, Private Bag X4, Sandringham, 2132, South Africa; email: neleshg@nicd.ac.za

Spatial Epidemiologic Analysis and Risk Factors for Nontuberculous Mycobacteria Infections, Missouri, USA, 2008–2019

Carlos Mejia-Chew, Miguel A. Chavez, Min Lian, Angela McKee, Leighton Garrett, Thomas C. Bailey, Andrej Spec, Mansi Agarwal, George Turabelidze

Nontuberculous mycobacteria (NTM) infections are caused by environmental exposure. We describe spatial distribution of NTM infections and associations with sociodemographic factors and flooding in Missouri, USA. Our retrospective analysis of mycobacterial cultures reported to the Missouri Department of Health and Social Services surveillance system during January 1, 2008–December 31, 2019, detected geographic clusters of infection. Multilevel Poisson regression quantified small-area geographic variations and identified characteristics associated with risk for infection. Median county-level NTM infection rate was 66.33 (interquartile range 51–91)/100,000 persons. Risk of clustering was significantly higher in rural areas (rate ratio 2.82, 95% CI 1.90–4.19) and in counties with >5 floodings per year versus no flooding (rate ratio 1.38, 95% CI 1.26–1.52). Higher risk for NTM infection was associated with older age, rurality, and more flooding. Clinicians and public health professionals should be aware of increased risk for NTM infections, especially in similar environments.

Nontuberculous mycobacteria (NTM) are ubiquitous, environmental, opportunistic microorganisms. Most NTM infections are acquired by inhalation, microaspiration, or direct inoculation (*1*). A recent meta-analysis using data from cultured samples found the global rate of change in NTM disease showed an increase of 4.1% per 100,000 persons per year (*2*). In the United States, 2 recent studies using medical claims data reported an increase in incidence of NTM disease by 7.5% per year (*3*,*4*). One study found the lowest prevalence of NTM pulmonary disease (NTM-PD) among Medicare beneficiaries in the US Midwest and classified the region at low risk for NTM-PD clustering (*4*). However, another study examined 5 US states, including Missouri, a state located in the midwestern United States with an estimated population of 6 million (*5*), reported an annual increase of 9.9% over a 6-year study period. Missouri showed the most yearly variability in NTM prevalence rates; some rates were almost 3 times lower than in the other states studied (*6*).

Geographic differences in distribution of NTM species likely related to local climate factors or population density variations have been observed worldwide (*2*,*7*–*9*). One study identified specific watersheds near densely populated areas in Colorado, USA, associated with increased risk for clustering of slow-growing NTM infections (*10*). A study in Queensland, Australia, found higher risk for *Mycobacterium intracellulare* infection associated with shallower soil depth and *M. kansasii* with higher soil density (*11*). Another study in Queensland examined the effects of climatic factors on infection trends and found slow-growing NTM incidence increased after a lag period of several months after heavy rainfall, possibly because of the time required for rain to disperse and transport bioaerosols (*12*). However, a prolonged lag period between exposure and disease manifestation is thought to be the norm in NTM disease, so quantifying the effects of individual climatic events is difficult.

Furthermore, extreme weather events such as heavy rainfall, flooding, and drought likely influence the prevalence of additional environmental

Author affiliations: Washington University School of Medicine, St. Louis, Missouri, USA (C. Mejia-Chew, M.A. Chavez, M. Lian, T.C. Bailey, A. Spec, M. Agarwal); Missouri Department of Health and Senior Services. Jefferson City, Missouri, USA (A. McKee, L. Garrett); Missouri Department of Health and Senior Services. St. Louis (G. Turabelidze)

DOI: http://doi.org/10.3201/eid2908.230378

organisms (*13*). One study reported increased cases of NTM infections associated with higher numbers of hurricanes affecting the state of Florida (*14*). The proportion of dry to wet areas in Missouri is similar to those of other states considered highly burdened with NTM-PD (*4*). Also, similar to other midwestern states, natural disasters such as tornadoes and floods are common, and earthquakes occur periodically (*15*). Flooding is one of the deadliest severe weather hazards in Missouri because the state is traversed by the Mississippi, Missouri, and White Rivers and their basins (*15*). Using Missouri Department of Health and Senior Services (MDHSS) NTM surveillance data, we aimed to identify spatial clusters of NTM infections and correlate them with sociodemographic factors and seasonal flooding patterns to identify factors associated with higher rates of infection. Washington University (St. Louis, MO, USA) and MDHSS institutional review boards approved this study.

Methods

Patient Population

NTM infection is a reportable condition in Missouri. The surveillance database contains patient sex assigned at birth, date of birth, residential address or postal (ZIP) code, specimen source of the culture, collection date, NTM species isolated, and date on which positive result was reported. We extracted all reports of NTM infections from the MDHSS communicable disease surveillance database collected during January 1, 2008–December 31, 2019.

Definitions

To be included, cases needed to have ≥1 mycobacterial culture positive for an NTM species and residential address or postal code for the sample donor. We excluded duplicate cultures and those positive for *M. gordonae*, given its low pathogenicity (*16*). We defined extrapulmonary NTM infection as a positive culture from a nonrespiratory specimen. For NTM-PD, we applied the microbiologic diagnostic criteria recommended by current guidelines developed by leading international respiratory medicine and infectious diseases societies for defining a case: 2 positive sputum cultures with the same NTM species or a single positive culture obtained through bronchoscopy (*17*). For subanalyses, we grouped NTM into slow-growing and rapid-growing species (*18*). We based annual incidence rates on the number of persons in a calendar year positive for an NTM isolate (infection rate) or fulfilling disease criteria (pulmonary and extrapulmonary disease rates) divided by the population of Missouri in the year of sampling, according to 2010–2019 US Census data (*5*). We calculated index rates using only the first NTM-positive culture from each individual participant.

Descriptive Analysis

For categorical variables, we summarized descriptive statistics for persons with NTM cultures using sample proportions. For continuous variables, we used sample medians and interquartile ranges (IQRs).

Spatial Statistical and Multilevel Analyses

Using spatial and space-time scan statistics (*19*,*20*) based on census tract–level coordinates and counts (i.e., centroids of census tracts, NTM cases, background population sizes), we applied a Poisson model to detect geographic hotspots of higher-than-expected NTM infections. We defined hotspots as areas in which NTM infection rates were significantly higher than the statewide average and elsewhere in Missouri. To infer the statistical significance of each potential cluster, we applied a circular window with a varied radius (≤50% of the total at-risk population in the study area) to scan the study area and generate 999 Monte Carlo permutation datasets for computing the statistics.

Because we considered the general population at risk, a multilevel framework (individual patients nested in their residential counties) was necessary to control bias from potential correlations of patients residing in the same county. We performed multilevel Poisson regression analysis to generate the predicted county-level incidence rates of NTM infection, quantify the small-area geographic variation in NTM infections, and identify neighborhood characteristics associated with NTM infections. The terms small-area and neighborhood refer to census tracts in cluster analyses and counties in multivariate multilevel Poisson regression. To remove potential bias from small populations in some counties when estimating county-level NTM infection rates, we used multilevel modeling–based prediction (adjusting for age, sex, and race and ethnicity) instead of observed values to report the smoothed rate. For multilevel Poisson regression analysis of predicted county-level incidence rates, we adjusted the model for demographics only to generate smoothed small-area incidence rates. To quantify small-area geographic variations in NTM infections and identify neighborhood characteristics associated with NTM infections, we fit multilevel Poisson regression to a

single multivariate model to estimate county-level variation in NTM incidence (random effect measured by median rate ratio [MRR]) and potential associations of county-level factors (fixed effects measured by rate ratio [RR]).

We further integrated the NTM county-population dataset with neighborhood contextual measures, including dates of flooding events in specific counties during 2008–2019, rural–urban context (defined as rural, urban, or metropolitan using the rural–urban continuum area code from the US Department of Agriculture; https://www.ers.usda.gov/data-products/rural-urban-continuum-codes), county-level percentage of population below federal poverty line, and county-level percentage of non-Hispanic Black population. We did not include other minorities, which represented <5% of the state population, in the analyses (*5*). We also used an adjusted multivariate multilevel model for individual-level demographics (age, sex, and race and ethnicity). We reported MRR, a measure of geographic heterogeneity with a value ≥1 (*21*), because it reflects the average difference between a pair of counties randomly selected from the study area, with a higher value indicating more small-area variation.

We analyzed geographic clusters by using SaTScan software version 9.7 (https://www.satscan.org) and managed datasets and performed multilevel modeling in SAS version 9.4 (SAS Institute Inc., https://www.sas.com). We visualized identified census tracts included in the significant clusters and predicted/smoothed county-level incidence rates by using the ArcGIS software package version 10.6.1 (ESRI https://www.esri.com).

Results

Cohort Characteristics

We identified 14,203 mycobacterial cultures reported to MDHSS during the study period, of which 10,996 met the inclusion criteria. After excluding 77 duplicates and 1,450 *M. gordonae* isolates, we included 9,469 culture-positive samples from 5,288 persons in the analyses. Median age of persons with NTM infection was 67 years (IQR 54–76 years); 52.1% were White and 52.7% female. A total of 3,292 (62%) persons provided respiratory cultures and 481 (9.1%) extrapulmonary cultures; culture source was unknown for 1,515 (28.6%). Smoothed median rate of NTM infection was 68.04 (IQR 59.65–81.12)/100,000 persons for the study period, and compared with the 2008 baseline, yearly rate of infections had increased 5.7% by 2010 and 12.2% by 2019.

The 5 most frequently isolated NTM species were *M. avium* (60.1%), *M. fortuitum* (8.3%), *M. abscessus* (6.5%), *M. chelonae* (5.6%), and *M. kansasii* (3.8%). Among isolates, 72% were slow-growing NTM; median time to positivity from culture collection was 20 days (IQR 13–30 days) (Table 1). The proportion of new isolates per NTM species remained stable during 2008–2019, except for *M. avium*, which exhibited a positive but not statistically significant increase (19.6%, p = 0.067) (Appendix Figure, https://wwwnc.cdc.gov/EID/article/29/8/23-0378-App1.pdf).

Using the standardized population of Missouri, we estimated an age-adjusted rate of NMT infection of 84.80/100,000 persons (82.28 for men, 87.09 for women) and 29.87/100,000 persons for NTM-PD (25.68 for men, 33.85 for women). By type of NTM, age-adjusted rates were 24.04/100,000 persons for rapid-growing infections and 60.76/100,000 persons for slow-growing infections (Appendix Table 1).

Pulmonary and Extrapulmonary Nontuberculous Mycobacterial Disease

Among all NTMs detected in respiratory specimens, 1,875 (56.9%) fulfilled the microbiologic diagnostic criteria for NTM-PD. Patients with NTM-PD were more commonly female (58% vs. 43.5%; p <0.001), older (median age 70 vs. 59 years; p <0.001), and infected with slow-growing NTM (83.9% vs. 48.6%) compared with those with extrapulmonary disease (Appendix Table 2). Among the 669 (35.7%) patients with NTM-PD who provided >1 respiratory sample with the same NTM species isolated, the predominant NTM species was *M. avium* (81.2%), followed by *M. kansasii* (4.19%) and *M. abscessus* (3.9%). Among the 481 (9.1%) patients with extrapulmonary infection, the most commonly isolated NTM species were *M. avium* (37.9%), *M. fortuitum* (17.2%), *M. chelonae* (14.9%), and *M. abscessus* (8.1%).

Geographic Variation and Clustering of NTM Infections

We excluded data from the 4.95% of geocoded locations outside the state of Missouri from further analyses. During the study period, the counties with the highest incidence were all rural: Buchanan (171.46/100,000 persons), Cape Girardeau (134.81/100,000 persons), and Sullivan (121.1/100,000 persons); those findings were mainly driven by high NTM-PD incidence rates in Cape Girardeau (90.45/100,000 persons) and Buchanan County (58.9/100,000 persons). By comparison, incidence of NTM infections in the 2 most populous metropolitan areas were 111.1/100,000 persons for St. Louis County, in which St. Louis is located, and

95.91/100,000 persons for Jackson County, in which Kansas City is located. The 3 counties with the highest incidence rates of extrapulmonary NTM cases were Sullivan (12.8/100,000 persons), McDonald (11.8/100,000 persons), and Jackson (10.6/100,000 persons) (Figure 1). Using spatial and space-time scan statistics across the state, we identified hotspots of significantly higher-than-expected NTM infection, NTM-PD, and extrapulmonary disease (Figure 2). Persons living in Cape Girardeau County were 3.62 times more likely to have any NTM infection and 4.52 times more likely to have slow-growing NTM infection than persons living elsewhere in Missouri.

Multilevel Analysis of Contextual and Individual Characteristics of NTM Infections

Multilevel Poisson analysis (Table 2) showed substantial small-area geographic variation in NTM infections across counties (variance 0.32, MRR 1.73; p<0.001). Risk for NTM infections was significantly higher in counties with >5 floods per year than in those with no flooding (RR 1.38, 95% CI 1.26–1.52) but not in counties with the highest poverty rates (highest vs. lowest quartile incomes, RR 0.78, 95% CI 0.54–1.13) or highest percentages of non-Hispanic Black population (highest vs. lowest quartiles, RR 0.84, 95% CI 0.58–1.21). Compared with metropolitan counties, both rural (RR 2.82, 95% CI 1.90–4.19) and urban (RR 2.08, 95% CI 1.53–2.82) counties had higher risks for NTM infection. Compared with persons ≤20 years of age, risk for NTM infection was significantly higher among persons 20–49 years of age (RR 7.23, 95% CI 5.11–10.2) and 50–64 years of age (RR 26.7, 95% CI 18.9–37.7), and even more so among persons ≥65 years of age (RR 76.8, 95% CI 54.6–108.2). Of note, risk of NTM infection was lower among women than men (RR 0.94, 95% CI 0.89–0.99) but higher among non-Hispanic Black persons than among non-Hispanic White persons (RR 2.62, 95% CI 2.31–2.98).

Table 1. Characteristics of 5,288 patients with NTM infections, Missouri, USA, 2008–2019*

Characteristics	Value†
Demographics	
Median age, y (IQR)	67 (54–76)
Sex‡	
F	2,785 (52.7)
M	2,498 (47.2)
Not recorded	5 (0.1)
Race/ethnicity	
Non-Hispanic White	2,753 (52.1)
Non-Hispanic Black	459 (8.7)
Asian	91 (1.7)
Other/unknown	1,985 (37.5)
NTM characteristics	
Median NTM rate (IQR)†	68.04 (59.65–81.12)
Slow-growing mycobacteria	3,806 (72.0)
Mycobacterium avium	4,752 (60.13)
M. kansasii	305 (3.86)
Rapid-growing mycobacteria	1,482 (28.0)
M. fortuitum	660 (8.35)
M. chelonae	230 (6.69)
M. abscessus	196 (5.7)
Median time to culture positivity, d (IQR), n = 4,956	20 (13–30)

*Values are no. (%) patients except as indicated. NTM, nontuberculous mycobacteria; IQR, interquartile range.
†Over study period, per 100,000 population.

Discussion

We identified clusters of NTM infections in Missouri associated with sociodemographic factors and flooding. In counties where NTM infection rates were 3–4 times those for the rest of the counties, higher-than-expected rates were associated with older age, rurality, non-Hispanic Black race, male sex, and higher numbers of annual floods. Of note, overall average NTM incidence rate in Missouri was higher in our study than previously reported in large national datasets (*3*,*22*). This discrepancy might be related to differing sources of NTM reporting, because previous studies relied on International Classification of Disease (ICD) codes, which have low sensitivity, to identify NTM cases, not the mandatory laboratory reporting that our study used (*23*).

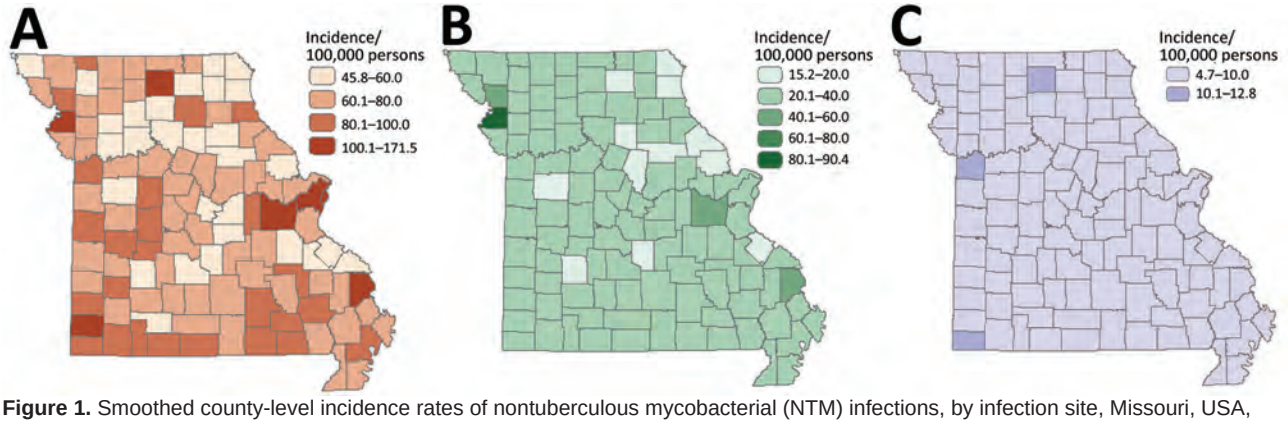

Figure 1. Smoothed county-level incidence rates of nontuberculous mycobacterial (NTM) infections, by infection site, Missouri, USA, 2008–2019. A) All NTM; B) pulmonary NTM; C) extrapulmonary NTM.

In keeping with the known epidemiology of NTM infections, most cultures in our study came from respiratory sources (*17*). NTM-PD rates approximated those previously described in epidemiologic studies from large administrative healthcare sources (*3*,*4*,*6*). More than half the persons in our study were ≥65 years of age and female, both factors significantly associated with NTM-PD. Of note, on the basis of the multilevel Poisson analysis, women had a slightly lower risk of NTM infection than men. Like increased NTM infections reported worldwide (*2*), *M. avium* was the most common NTM species in both pulmonary and extrapulmonary infections and the only NTM species that exhibited an increasing incidence over time. Reasons for this reported increase are likely multifactorial and include better mycobacterial diagnostic tools, increased NTM disease awareness, and extreme weather events disrupting the NTM ecologic niche (*13*). However, unlike in other locations worldwide, the number of *M. abscessus* infections reported in Missouri during the study period remained stable.

We found that counties in Missouri with >5 flooding events per year had a 38% higher rate of NTM infections than those without flooding. A study conducted in Florida found higher numbers of hurricanes, which can lead to flooding, associated with higher numbers of NTM infections (*14*). Those findings support the hypothesis that trends in flooding events may correlate with NTM infection rates, possibly because disruptions in the ecosystem of environmental mycobacteria from extreme weather events could increase human exposure and risk for potential infection.

Our study was limited by its retrospective design and use of mandatory laboratory reporting data. Lack of clinical data did not enable us to differentiate between disease and colonization; for this reason, we used the term NTM infection throughout the text and used NTM-PD only when patients fulfilled microbiologic diagnostic criteria for NTM disease. In addition, the MDHSS NTM surveillance database was not routinely queried for inconsistencies; hence, incomplete data on key variables could have introduced bias. However, except for 37% missing or unknown entries for race, missingness was <5% for key variables and unlikely to have biased analyses. Furthermore, other environmental factors identified in previous studies (*11*,*12*) could have influenced NTM infection rates, but we focused on a factor, flooding, that had not been studied before.

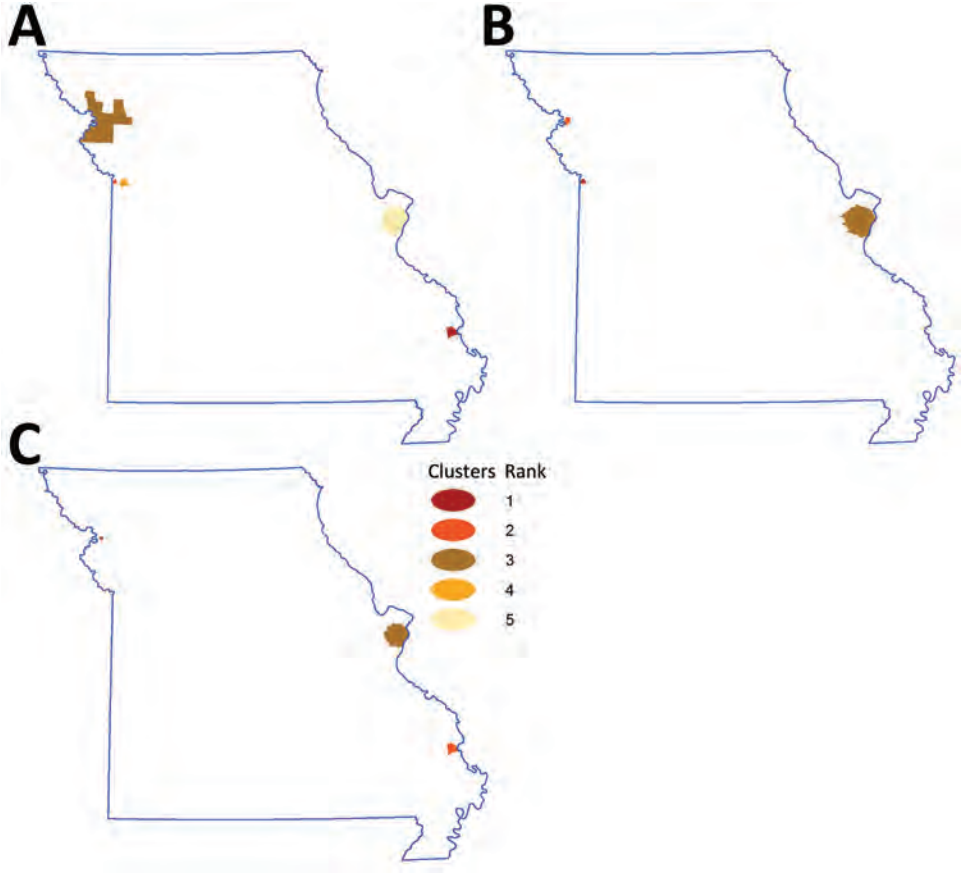

Figure 2. Geographic hotspots of nontuberculous mycobacteria (NTM) infection, by NTM type, Missouri, USA, 2008–2019. Colors indicate rank order, based on relative risk point estimates. A) For all NTM infections, relative risk was 3.62 for rank 1, 2.45 for rank 2, 2.19 for rank 3, 1.66 for rank 4, and 1.53 for rank 5. B) For rapid-growing NTM, relative risk was 3.84 for rank 1, 2.69 for rank 2, and 1.99 for rank 3. C) For slow-growing NTM, relative risk was 5.42 for rank 1, 4.52 for rank 2, and 1.42 for rank 3.

Table 2. Results of multilevel Poisson regression analyses of risk for nontuberculous mycobacterial infection, Missouri, USA, 2008–2019

Variable	Rate ratio (95% CI)
Fixed effects	
County-level flooding	
No flooding	Referent
1–3 times	1.19 (1.11–1.29)
4–5 times	1.29 (1.17–1.43)
>5 times	1.38 (1.26–1.52)
County rural–urban context	
Rural	2.82 (1.90–4.19)
Urban	2.08 (1.53–2.82)
Metro	Referent
County-level poverty levels	
1st quartile (lowest)	Referent
2nd quartile	0.88 (0.62–1.25)
3rd quartile	0.71 (0.49–1.03)
4th quartile (highest)	0.78 (0.54–1.13)
County-level ratio non-Hispanic Black	
1st quartile (lowest)	Referent
2nd quartile	1.17 (0.81–1.69)
3rd quartile	1.09 (0.76–1.56)
4th quartile (highest)	0.84 (0.58–1.21)
Patient age group, y	
<20	Referent
20–49	7.23 (5.11–10.2)
50–64	26.7 (18.9–37.7)
≥65	76.8 (54.6–108.2)
Sex	
M	Referent
F	0.94 (0.89–0.99)
Race/ethnicity	
Non-Hispanic White	Referent
Non-Hispanic Black	2.62 (2.31–2.98)
Others*	32.2 (30.3–34.2)
Random effect	
Variance 0.32, p<0.001	1.73

*Asian (91; 1.72%), native American (9; 0.17%), unknown race (1,976; 37%).

In conclusion, we identified increasing rates of NTM infection over time. NTM infection clustering in Missouri was associated with older age, rurality, and higher rates of annual flooding events. Further investigation is warranted to determine the degree to which extreme weather events contribute to the increasing incidence and prevalence of NTM-PD worldwide. In addition, clinicians and public health professionals should be aware of the increased risk for NTM infections, especially in locations with environments similar to those described here.

This study was financially sponsored by Insmed Incorporated.

C.M.-C. reports a Centers for Disease Control and Prevention subaward, a vendor/individual agreement with Wayne State University, and serves as associate editor for Open Forum Infectious Diseases, outside the submitted work. C.M.-C. also reports research grants from the Centers for Disease Control and Prevention and Insmed Incorporated.

Author contributions: study concept and design, C.M.-C. and G.T.; acquisition, analysis, or interpretation of data, C.M.-C., M.A.C., M.L., M.A., G.T., T.C.B., A.S.; drafting of the manuscript, C.M.-C. All authors take responsibility for the accuracy of the data presented.

About the Author

Dr. Mejia-Chew is an assistant professor in the Division of Infectious Disease at Washington University in St. Louis, MO. His research interest is in mycobacterial infections, particularly nontuberculous mycobacteria.

References

1. Falkinham JO III. Environmental sources of nontuberculous mycobacteria. Clin Chest Med. 2015;36:35–41. https://doi.org/10.1016/j.ccm.2014.10.003
2. Dahl VN, Mølhave M, Fløe A, van Ingen J, Schön T, Lillebaek T, et al. Global trends of pulmonary infections with nontuberculous mycobacteria: a systematic review. Int J Infect Dis. 2022;125:120–31. https://doi.org/10.1016/j.ijid.2022.10.013
3. Winthrop KL, Marras TK, Adjemian J, Zhang H, Wang P, Zhang Q. Incidence and prevalence of nontuberculous mycobacterial lung disease in a large US managed care health plan, 2008–2015. Ann Am Thorac Soc. 2020;17:178–85. https://doi.org/10.1513/AnnalsATS.201804-236OC
4. Adjemian J, Olivier KN, Seitz AE, Holland SM, Prevots DR. Prevalence of nontuberculous mycobacterial lung disease in US Medicare beneficiaries. Am J Respir Crit Care Med. 2012;185:881–6. https://doi.org/10.1164/rccm.201111-2016OC
5. Missouri Census Data Center. Geocorr 22: geographic correspondence engine, version 1.8 [cited 2022 Nov 11]. https://mcdc.missouri.edu/applications/geocorr2022.html
6. Donohue MJ, Wymer L. Increasing prevalence rate of nontuberculous mycobacteria infections in five states, 2008–2013. Ann Am Thorac Soc. 2016;13:2143–50. https://doi.org/10.1513/AnnalsATS.201605-353OC
7. Adjemian J, Olivier KN, Seitz AE, Falkinham JO III, Holland SM, Prevots DR. Spatial clusters of nontuberculous mycobacterial lung disease in the United States. Am J Respir Crit Care Med. 2012;186:553–8. https://doi.org/10.1164/rccm.201205-0913OC
8. Honda JR, Virdi R, Chan ED. Global environmental nontuberculous mycobacteria and their contemporaneous man-made and natural niches. Front Microbiol. 2018;9:2029. https://doi.org/10.3389/fmicb.2018.02029
9. Hoefsloot W, van Ingen J, Andrejak C, Angeby K, Bauriaud R, Bemer P, et al.; Nontuberculous Mycobacteria Network European Trials Group. The geographic diversity of nontuberculous mycobacteria isolated from pulmonary samples: an NTM-NET collaborative study. Eur Respir J. 2013;42:1604–13. https://doi.org/10.1183/09031936.00149212
10. Lipner EM, Knox D, French J, Rudman J, Strong M, Crooks JL. A geospatial epidemiologic analysis of nontuberculous mycobacterial infection: an ecological study in Colorado. Ann Am Thorac Soc. 2017;14:1523–32. https://doi.org/10.1513/AnnalsATS.201701-081OC
11. Chou MP, Clements AC, Thomson RM. A spatial epidemiological analysis of nontuberculous mycobacterial

infections in Queensland, Australia. BMC Infect Dis. 2014;14:279. https://doi.org/10.1186/1471-2334-14-279
12. Thomson RM, Furuya-Kanamori L, Coffey C, Bell SC, Knibbs LD, Lau CL. Influence of climate variables on the rising incidence of nontuberculous mycobacterial (NTM) infections in Queensland, Australia 2001–2016. Sci Total Environ. 2020;740:139796. https://doi.org/10.1016/j.scitotenv.2020.139796
13. Honda JR, Bernhard JN, Chan ED. Natural disasters and nontuberculous mycobacteria: a recipe for increased disease? Chest. 2015;147:304–8. https://doi.org/10.1378/chest.14-0974
14. Kambali S, Quinonez E, Sharifi A, Shahraki AH, Kumar N, Dushyantha J, et al. Pulmonary nontuberculous mycobacterial disease in Florida and association with large-scale natural disasters. BMC Public Health. 2021;21:2058. https://doi.org/10.1186/s12889-021-12115-7
15. Missouri Department of Public Safety: State Emergency Management Agency. Flooding [cited 2023 Jan 4]. https://sema.dps.mo.gov/plan_and_prepare/flooding.php#:~:text=Flooding%20is%20the%20deadliest%20severe,who%20had%20been%20in%20vehicles
16. van Ingen J, Bendien SA, de Lange WC, Hoefsloot W, Dekhuijzen PN, Boeree MJ, et al. Clinical relevance of non-tuberculous mycobacteria isolated in the Nijmegen-Arnhem region, the Netherlands. Thorax. 2009;64:502–6. https://doi.org/10.1136/thx.2008.110957
17. Daley CL, Iaccarino JM, Lange C, Cambau E, Wallace RJ Jr, Andrejak C, et al. Treatment of nontuberculous mycobacterial pulmonary disease: an official ATS/ERS/ESCMID/IDSA clinical practice guideline. Eur Respir J. 2020;56:2000535. https://doi.org/10.1183/13993003.00535-2020
18. Runyon EH. Anonymous mycobacteria in pulmonary disease. Med Clin North Am. 1959;43:273–90. https://doi.org/10.1016/S0025-7125(16)34193-1
19. Kulldorff M, Huang L, Pickle L, Duczmal L. An elliptic spatial scan statistic. Stat Med. 2006;25:3929–43. https://doi.org/10.1002/sim.2490
20. Schootman M, Jeffe DB, Lian M, Gillanders WE, Aft R. The role of poverty rate and racial distribution in the geographic clustering of breast cancer survival among older women: a geographic and multilevel analysis. Am J Epidemiol. 2009;169:554–61. https://doi.org/10.1093/aje/kwn369
21. Lian M, Struthers J, Liu Y. Statistical assessment of neighborhood socioeconomic deprivation environment in spatial epidemiologic studies. Open J Stat. 2016;6:436–42. https://doi.org/10.4236/ojs.2016.63039
22. Park SC, Kang MJ, Han CH, Lee SM, Kim CJ, Lee JM, et al. Prevalence, incidence, and mortality of nontuberculous mycobacterial infection in Korea: a nationwide population-based study. BMC Pulm Med. 2019;19:140. https://doi.org/10.1186/s12890-019-0901-z
23. Mejia-Chew C, Yaeger L, Montes K, Bailey TC, Olsen MA. Diagnostic accuracy of health care administrative diagnosis codes to identify nontuberculous mycobacteria disease: a systematic review. Open Forum Infect Dis. 2021;8:ofab035. https://doi.org/10.1093/ofid/ofab035

Address for correspondence: Carlos Mejia-Chew, Infectious Diseases, Washington University School of Medicine, 4523 Clayton Ave, Campus Box 8051, St. Louis, MO 63110-0193, USA; email: carlosmejia@wustl.edu

Reproduction Number [ˈr̥e-prə-ˈdak-shən ˈnəm-bər]

Vijay Sharma, Rajnish Sharma, Balbir B. Singh

The basic reproduction number (R_0, pronounced R naught) is derived from demography terminology used to estimate the overall population reproduction rate. R_0 is an essential metric in the study of epidemics. This value measures the estimated number of new cases of an infection caused by an infectious person in a population of disease-susceptible person.

The effective reproduction number (R_t) is similar to R_0, but R_t measures the number of persons infected by infectious person when some portion of the population has already been infected. This idea can be traced back to the work performed by Richard Bockh, Alfred Lotka and others.

A modern application of R_0 in epidemiology was reported in 1952 when George Macdonald constructed population models about the spread of malaria. Macdonald used the notation Z_0 instead of R_0 to differentiate it from the preceding demography terminology. The notation R_0 was adopted instead of Z_0 during the Dahlem conference in 1982 (Figure).

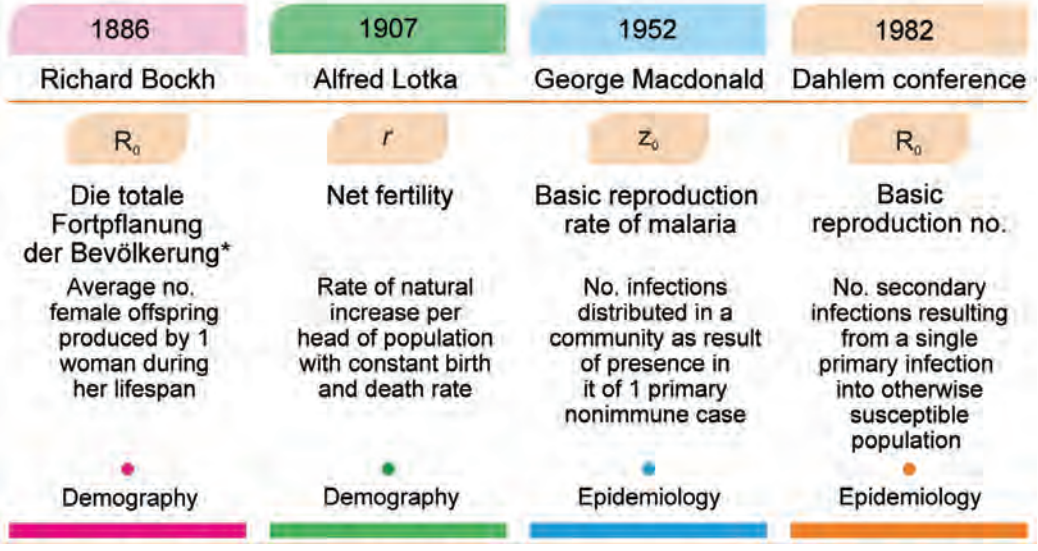

Figure. History and concept of basic reproduction number (R_0). *The total reproduction of the population.

Sources

1. Anderson RM. Transmission dynamics and control of infectious disease agents. In: Anderson RM, May RM, editors. Population biology of infectious diseases: life sciences report 25, Dahlem// conference. Berlin: Springer-Verlag; 1982. p. 149–76.
2. Delamater PL, Street EJ, Leslie TF, Yang YT, Jacobsen KH. Complexity of basic reproduction number (R_0). Emerg Infect Dis. 2019;25:1–4. https://doi.org/10.3201/eid2501.171901
3. Heesterbeek JA. A brief history of R_0 and a recipe for its calculation. Acta Biotheor. 2002;50:189–204. https://doi.org/10.1023/A:1016599411804
4. Macdonald G. The analysis of equilibrium in malaria. Trop Dis Bull. 1952;49:813–29.
5. Smith DL, Battle KE, Hay SI, Barker CM, Scott TW, McKenzie FE. Ross, Macdonald, and a theory for the dynamics and control of mosquito-transmitted pathogens. PLoS Pathog. 2012;8:e1002588. https://doi.org/10.1371/journal.ppat.1002588

Author affiliation: Guru Angad Dev Veterinary and Animal Sciences University, Punjab, India

DOI: https://doi.org/10.3201/eid2908.221445

Address for correspondence: Balbir B. Singh, Centre for One Health, Guru Angad Dev Veterinary and Animal Sciences University, Ludhiana, Punjab 141004, India; email: bbsdhaliwal@gmail.com

Waterborne Infectious Diseases Associated with Exposure to Tropical Cyclonic Storms, United States, 1996–2018

Victoria D. Lynch, Jeffrey Shaman

In the United States, tropical cyclones cause destructive flooding that can lead to adverse health outcomes. Storm-driven flooding contaminates environmental, recreational, and drinking water sources, but few studies have examined effects on specific infections over time. We used 23 years of exposure and case data to assess the effects of tropical cyclones on 6 waterborne diseases in a conditional quasi-Poisson model. We separately defined storm exposure for windspeed, rainfall, and proximity to the storm track. Exposure to storm-related rainfall was associated with a 48% (95% CI 27%–69%) increase in Shiga toxin–producing *Escherichia coli* infections 1 week after storms and a 42% (95% CI 22%–62%) increase Legionnaires' disease 2 weeks after storms. Cryptosporidiosis cases increased 52% (95% CI 42%–62%) during storm weeks but declined over ensuing weeks. Cyclones are a risk to public health that will likely become more serious with climate change and aging water infrastructure systems.

Tropical cyclones are a seasonal occurrence in the Eastern United States, where they cause widespread destruction and endanger public health (*1*–*3*). Among many storm-related hazards, extreme flooding is a concern because it can lead to the contamination of recreational, irrigation, and drinking water sources (*4*–*6*) and might increase risks for transmission of waterborne infectious diseases (*7*). Elevated case counts and outbreaks have been attributed to individual storms (*8*), but the effect of tropical cyclones on specific waterborne infections has not been evaluated over multiple storm seasons. Understanding waterborne pathogen transmission is a pressing public health challenge because the burden of disease will likely increase in conjunction with an aging population (*9*), deteriorating drinking and wastewater treatment systems (*10*), and increased storm-related flooding due to climate change (*11*).

Bacterial, parasitic, and viral pathogens cause ≈7.15 million cases of waterborne disease annually in the United States (*12*). Infections are typically mild but can lead to life-threatening enteric or respiratory illness for immunocompromised, young, or elderly persons (*13*,*14*). Cyclonic storms drive transmission because floodwater mobilizes pathogens in the environment and inundates water system infrastructure, which causes further contamination through ineffective treatment or sewage overflows (*15*,*16*). After cyclonic storms, high pathogen loads frequently are detected in floodwater (*17*,*18*) and in environmental and drinking water sources (*19*–*21*). Floods also can contaminate irrigation water used on crops (*22*); therefore, flood-driven contamination can influence transmission of pathogens that are predominantly foodborne.

However, contamination does not necessarily lead to transmission; although extreme weather events have been associated with gastrointestinal illness or specific outbreaks (*23*–*25*), some storms have been found to have no effect on incidence of cases (*26*). Those inconsistent associations reflect the relevance of pathogen-specific factors, particularly pathogen biology and primary reservoirs, in determining the effects of storms on transmission.

Pathogens that form oocysts or are members of biofilm communities persist in environmental waters for weeks, which can increase the likelihood of transmission (*27*,*28*), whereas pathogens that do not persist in the environment might be flushed from waterways by flooding (*29*). Pathogen biology also affects the efficacy of water treatment; in particular,

Author affiliation: Columbia University, New York, New York, USA

DOI: https://doi.org/10.3201/eid2908.221906

Cryptosporidium and *Legionella* are resistant to common decontamination methods (*30*,*31*), whereas *Giardia* is readily removed from water (*32*).

Cyclonic storms can also lead to different types of contamination depending on the land use and drinking water or sanitation infrastructure of affected regions. Cattle and poultry are the primary reservoirs for several gastrointestinal pathogens, and flooding near livestock production can contaminate drinking water sources with animal waste (*33*). Flooding near livestock production is of particular concern in rural agricultural regions where many persons rely on private wells that are untreated and vulnerable to inundation (*34*). On the other hand, storms in densely populated areas often lead to floodwater contaminated with human sewage (*35*). Urban flooding also can damage water treatment or distribution systems that serve entire cities, leading to large outbreaks (*36*).

The effect of cyclonic storms on waterborne disease also might depend on storm characteristics that determine the extent of flooding and destruction. Storms are generally defined by windspeed and rainfall, factors that are often weakly correlated with each other upon landfall (*37*) and lead to different conditions in affected areas. Slow-moving storms tend to cause greater accumulation of rain and more severe flooding, whereas tropical cyclones with high windspeeds might bring less rain but cause wind-related property or infrastructure destruction (*1*,*38*). Storm type also could dictate disaster management decisions and individual-level responses, such as the ability to comply with evacuation orders. In addition, storm severity influences healthcare-seeking behavior and healthcare infrastructure. Storm-related disruptions might dissuade persons with mild or moderate conditions from seeking care (*39*), whereas catastrophic storms can prevent persons with urgent needs from accessing healthcare systems (*40*).

Storm severity is projected to increase with atmospheric warming, so developing a thorough understanding of storm effects on waterborne diseases could aid climate change adaptation and public health policies. Previous research has largely focused on specific storms and outbreaks or on nonspecific gastrointestinal illness; however, associations over multiple storm seasons have not been thoroughly examined. In this study, we examined the effects of tropical cyclones on waterborne infectious diseases over more than a decade and determined whether those associations varied by pathogen or type of storm exposure.

Methods

Data

Case data

We used surveillance data from the National Notifiable Diseases Surveillance System (NNDSS; https://www.cdc.gov/nndss) to identify weekly cases of cryptosporidiosis, giardiasis, Legionnaires' disease, *Escherichia coli* infections, salmonellosis, and shigellosis during 1996–2018 for each US state. Those infections are caused by parasitic (*Cryptosporidium* and *Giardia*), biofilm-forming bacterial (*Legionella*), and enteric bacterial (*E. coli*, *Salmonella*, *Shigella)* pathogens that can lead to severe gastrointestinal or respiratory illness. Of the 6 *E. coli* strains, NNDSS only tracks Shiga toxin–producing *E. coli* (STEC) infections.

The data consist of laboratory-confirmed cases from hospitalizations, emergency department visits, and primary care visits that are reported to local health departments and compiled by state health departments to submit to the Centers for Disease Control and Prevention (CDC), which manages the NNDSS and case definitions (Appendix Table 1, https://wwwnc.cdc.gov/EID/article/29/8/22-1906-App1.pdf). We restricted our analyses to the 30 states and Washington, DC, that experienced ≥1 tropical cyclone during the study period and to June–November, the months of the Atlantic storm season. We also used US Census data (*9*) to determine county and state populations during the study period.

Storm Data

We obtained storm track, windspeed, and rainfall data for tropical cyclones that made landfall in the United States during 1996–2018 from the hurricaneexposure version 0.1.1 and hurricaneexposuredata version 0.1.0 packages in R (R Foundation for Statistical Computing, https://www.r-project.org). For each county, we defined the primary exposure day as the day with the shortest distance between the county center and the storm track. We used storm track and surface windspeed data from the National Hurricane Center's HURDAT-2 dataset (https://www.nhc.noaa.gov/data) and included maximum and sustained windspeeds on the primary exposure day. We used rainfall data from the North American Land Data Assimilation System 2 (https://ldas.gsfc.nasa.gov/nldas) and included in our dataset the total daily rainfall in each exposed county from 5 days before to 3 days after the primary exposure day. To inform the selection of exposure variables used in the analysis, we assessed correlations among

distance, wind, and rainfall variables, including total and daily maximum rainfall.

Storm Exposure Definition

Informed by the correlation analysis of storm variables, we defined county-level exposure to storms according to total rainfall, maximum sustained windspeed, and distance from the storm track. In the primary analysis, we defined exposure separately for each variable and repeated the analyses using several exposure thresholds. We considered counties exposed when they experienced 50, 75, or 100 mm of total rainfall associated with the storm or were within 500, 250, or 150 km of the storm track. The National Oceanic and Atmospheric Administration categorizes cyclones as tropical storms or hurricanes on the basis of windspeed (https://www.nhc.noaa.gov/climo); consistent with those definitions, we considered counties exposed to tropical storms when maximum sustained windspeeds were ≥34 knots but <64 knots (gale-force wind on the Beaufort scale) and exposed to hurricanes when maximum sustained windspeeds were ≥64 knots. We assessed correlations among the exposure thresholds. To determine state-level exposure, we calculated the percent of the state population in exposed counties during storm weeks and classified the state as exposed if 75%, 50%, 25%, 5%, or any (>0%) of the population was exposed; we repeated the analysis for each of those population thresholds.

In the secondary analysis, we combined storm exposure variables to describe categories of cyclonic storms. We categorized storms as high rain–high wind if total rainfall was ≥100 mm and windspeed was ≥64 knots; as high rain–low wind if total rainfall was ≥100 mm and windspeed was ≥34 but <64 knots; and as low rain–low wind if total rainfall was <100 mm and windspeeds were ≥34 but <64 knots. We did not include a low rain–high wind category because no storms met that definition. We considered counties exposed to a specific storm type if the storm met both the rainfall and windspeed criteria. Hurricane-force winds are rare and usually affect a small proportion of a state's population (Appendix Table 2); therefore, we defined state population exposure thresholds only by rainfall exposure, as in the primary analysis. We considered a state exposed to a given storm type if it met the rainfall-based population exposure threshold (e.g., for a 25% population-exposure threshold, ≥25% of the state's population had to be exposed to storm-related rainfall) and any of the counties were exposed to the given storm type.

Statistical Analysis

We modeled the association between exposure to tropical cyclones and case rates by using a conditional quasi-Poisson model (Appendix), which accounted for overdispersion in the case data (*41*). We compared case rates in weeks with and without storms across matched strata based on state and week of the year. That structure addressed potential confounding due to variation among states (i.e., different state policies regarding storm preparedness or case reporting) and controlled for seasonality. We modeled cyclonic storm occurrence as a binary exposure variable and lagged from 0 to 3 weeks to account for the incubation periods of the pathogens and the potential for delays in seeking healthcare after destructive storms. The model included a flexibly adjusted term for year to control for long-term trends that could affect storm exposure or waterborne infectious disease transmission. We used annual state population as an offset to obtain the rate of cases and we modeled case rates for each pathogen separately. We repeated the analysis for all exposure definitions and population exposure thresholds. We used the Bonferroni-Holmes method to adjust 95% CIs for multiple comparisons. Finally, we repeated the method with counties stratified by drinking water source or for rural or urban location (Appendix).

Results

The number of cases reported to NNDSS varied by pathogen, and most infections involved enteric bacteria (Table 1). Most infections peaked in the late summer or early fall, but the amplitude of seasonality differed among pathogens and by geographic region (Figure 1). Cryptosporidiosis exhibited the strongest and most consistent seasonality; cases peaked in September in all geographic regions. In most states, Legionnaires' disease and parasitic infections displayed only a moderate increase during summer months (Appendix Figure 1). Enteric bacterial infections were more common across all states, and salmonellosis showed a strong summer seasonality in most states (Appendix Figure 2). During 1996–2018, Legionnaires' disease and cryptosporidiosis cases increased, and giardiasis decreased, in all geographic regions; the other infections were relatively consistent over time (Appendix Figure 3). The burden of disease also varied by geographic region; salmonellosis and shigellosis cases were more common in the Southeast, but Legionnaires' disease was concentrated in the Mid-Atlantic region (Appendix Figure 4). *E. coli* infections, cryptosporidiosis, and giardiasis were all more common in the Upper Midwest and New England states than in other geographic regions (Appendix Figure 4).

Table 1. Description of pathogens included in analysis of waterborne infectious diseases associated with exposure to tropical cyclonic storms, United States, 1996–2018*

Pathogen	No. (%) cases in NNDSS	Pathogen type	Incubation period, d (range)†	Estimated cases attributed to waterborne transmission, %‡	Years reported in NNDSS
Legionella	77,765 (3.8)	Biofilm-forming bacteria	5–6 (2–10)	97	1996–2018
Cryptosporidium	151,573 (7.4)	Parasite	7 (2–12)	43	1998–2018
Giardia	297,379 (14.6)	Parasite	7 (1–14)	44	2002–2018
STEC	128,332 (6.3)	Enteric bacteria	0.5–4 (0.5–10)	5	1996–2018
Salmonella	964,293 (47.3)	Enteric bacteria	0.5–2 (0.5–16)	6	1998–2016
Shigella	421,369 (20.4)	Enteric bacteria	1–3 (0.5–7)	4	1998–2018

*NNDSS, National Notifiable Disease Surveillance System (https://www.cdc.gov/nndss); STEC, Shiga toxin–producing *Escherichia coli*.
†According to D.W.K. Acheson (*42*).
‡According to S.A. Collier et al. (*12*).

Wind, rainfall, and distance variables were not highly correlated, but different measures of the same variable, such as maximum rainfall and total rainfall, were correlated (Appendix Figure 4). Among the storm variable thresholds used to determine county-level exposure, hurricane- and gale-force wind exposure were not highly correlated ($r = 0.21$), but ≥50-mm, ≥75-mm, and ≥100-mm rainfall exposure thresholds were highly correlated ($r = 0.50–0.72$) (Appendix Figure 5). Using the most inclusive storm exposure threshold, gale-force wind, 134 cyclonic storms occurred during the study period (Table 2). Those storms affected 2,363 counties in 30 states and Washington, DC, over 177 weeks. Counties with the greatest number of weeks of gale-force wind exposure storms were concentrated along the coast, particularly in North and South Carolina (Figure 2). Exposure to ≥75 mm of rainfall was most common in South Florida but was overall more

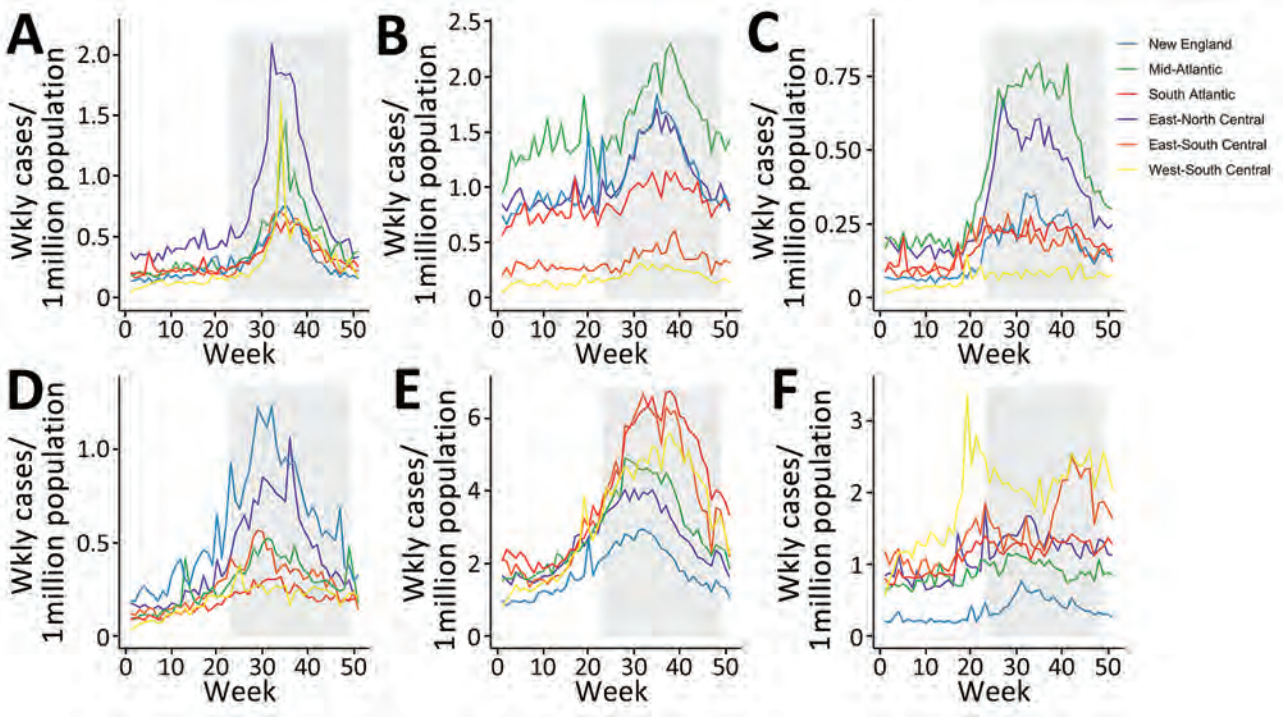

Figure 1. Average weekly cases by geographic region in a study of waterborne infectious diseases associated with exposure to tropical cyclonic storms, United States, 1996–2018. Graphs indicate weekly number of cases per 1,000,000 populations for the following waterborne diseases: A) cryptosporidiosis; B) giardiasis; C) Legionnaires' disease; D) *Escherichia coli* infection; E) salmonellosis; and F) shigellosis. Not all infections were reported for the entire study period (Table 1). The shaded region represents the weeks encompassed in the annual Atlantic storm season, June 1–November 30. The geographic regions reflect the reporting areas used for infectious disease surveillance in the National Notifiable Diseases Surveillance System (https://www.cdc.gov/nndss). The New England region comprises the states of Connecticut, Maine, Massachusetts, New Hampshire, Rhode Island, and Vermont; the Mid-Atlantic Region comprises New Jersey, New York, and Pennsylvania; the South-Atlantic Region comprises Delaware, Florida, Georgia, Maryland, North Carolina, South Carolina, Virginia, West Virginia, and Washington, DC; the East-North Central Region comprises Illinois, Indiana, Michigan, Ohio, and Wisconsin; the East-South Central Region comprises Alabama, Kentucky, Mississippi, and Tennessee; and the West-South Central Region comprises Arkansas, Louisiana, Oklahoma, and Texas.

Table 2. Cyclonic storm exposure definitions used to assess waterborne infectious diseases associated with exposure to tropical cyclonic storms, United States, 1996–2018

Storm exposure variables, definition	No. storms	No. counties affected
Total rainfall, mm		
50	98	2,165
75	96	2,041
100	87	1,732
Sustained wind gusts*		
Gale-force winds	134	1,025
Hurricane-force winds	31	136
Distance from storm track, km		
500	134	2,363
250	134	2,179
150	117	2,072

*National Oceanic and Atmospheric Administration (https://www.noaa.gov) designates tropical storms as those with gale-force winds, defined as ≥34 knots to <64 knots, and hurricane-force winds as ≥64 knots.

widespread and uniform than the wind and distance metrics (Figure 2). We noted no long-term trend in the number of cyclonic storms during the study period (Appendix Figure 6).

Cryptosporidiosis case rates greatly increased during storm weeks at low population exposure thresholds; storms that brought ≥75 mm of rainfall were associated with a 40% increase in case rates when any of the state's population was exposed and a 52% increase when ≥5% of the population was exposed (Figure 3). Similar associations persisted across lagged exposures, but the effects were weaker, ranging from 12%–20% increases in the poststorm weeks (Appendix Table 3). Legionnaires' disease case rates were also highly associated with storm exposure, but the effect was strongest 2 and 3 weeks after a storm and at higher population exposure thresholds (Figure 3). When 75% of the state population was exposed to a storm, case rates increased by 31% in lag week 1, 42% in lag week 2, and 39% in lag week 3 (Appendix Table 3). *E. coli* case rates exhibited a clearer peak and decline associated with lagged storm events. After an initial decrease during the storm week, case rates increased 48% in week 1 and 33% in week 2 post storm when 75% of the state's population was exposed (Figure 3). Salmonellosis and giardiasis were not greatly associated with storm exposure, and shigellosis case rates slightly decreased during storm weeks (Figure 3).

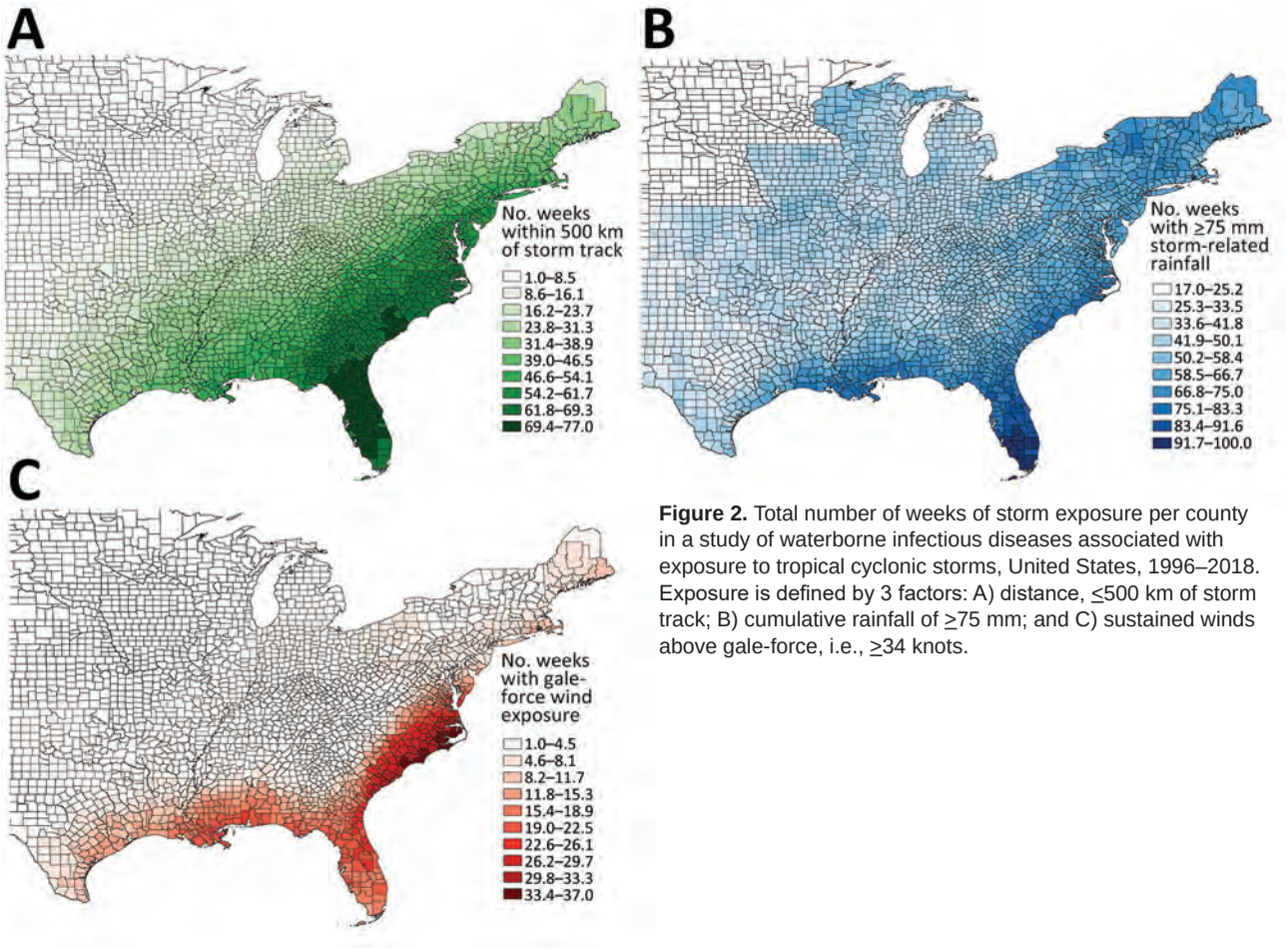

Figure 2. Total number of weeks of storm exposure per county in a study of waterborne infectious diseases associated with exposure to tropical cyclonic storms, United States, 1996–2018. Exposure is defined by 3 factors: A) distance, ≤500 km of storm track; B) cumulative rainfall of ≥75 mm; and C) sustained winds above gale-force, i.e., ≥34 knots.

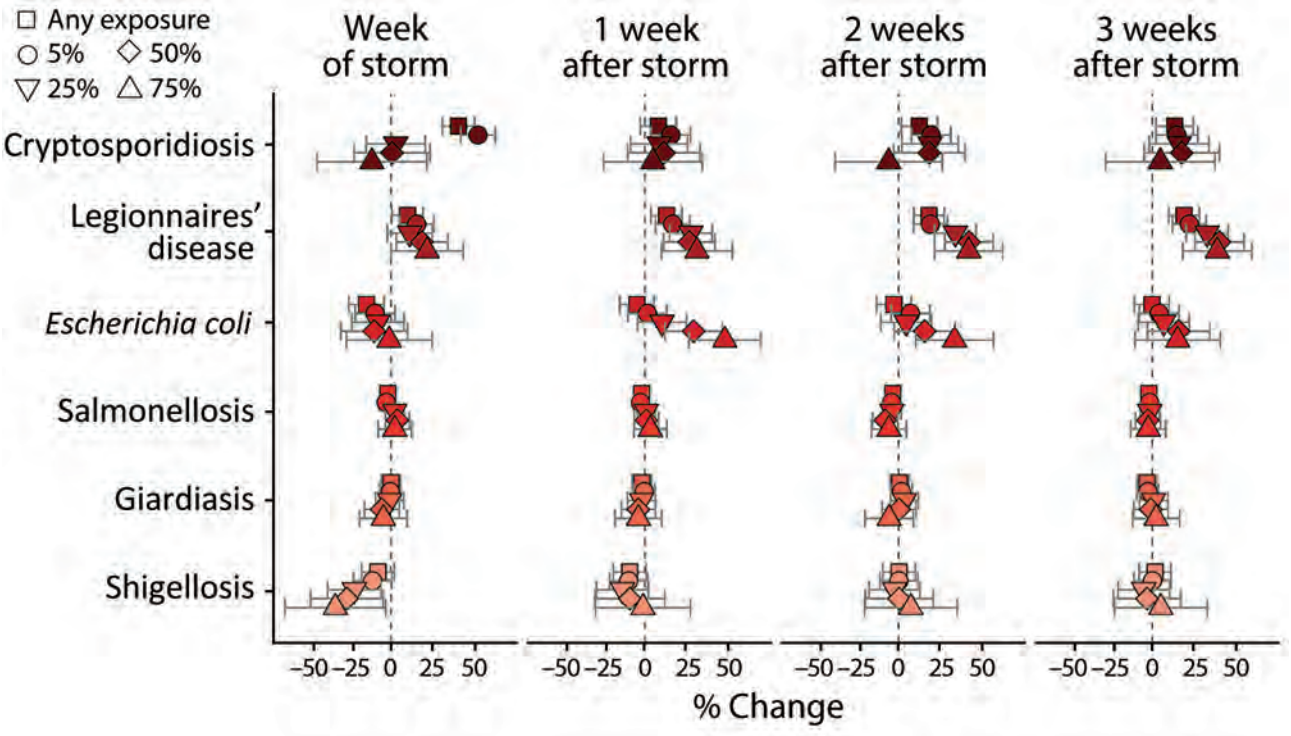

Figure 3. Average percent change in weekly case rates in a study of waterborne infectious diseases associated with exposure to tropical cyclonic storms, United States, 1966–2018. Estimated percentage change (shapes) and Bonferroni-corrected 95% CI (bars) are reported for each infectious disease and population-exposure threshold. Estimates are reported for week of the storm (week 0) and 1–3 weeks after the storm and are associated with exposure to ≥75 mm of storm-related rainfall.

The associations between storm-related rainfall and cryptosporidiosis, Legionnaires' disease, and *E. coli* case rates were consistent across different exposure definitions (Figure 4). Storms with less (≥50 mm) or more (≥100 mm) rainfall were associated with substantial initial increases in cryptosporidiosis cases that attenuated over lag weeks 1–3. The strength of the association between Legionnaires' disease case rates and storm exposure increased in conjunction with population exposure threshold and amount of rainfall (Figure 4). Similarly, the lagged increase in *E. coli* rates was more pronounced in storms with ≥100 mm of rainfall. The associations between case rates and storm exposure were similar when exposure was defined by distance from the storm track instead of rainfall (Appendix Figure 7). Stratifying exposure by drinking water source or rural or urban location also yielded similar results; the lagged effect on *E. coli* and Legionnaires' disease rates was slightly more pronounced when restricted to rural or groundwater-reliant counties, but associations were otherwise consistent (Appendix).

Storm exposure defined by hurricane-force winds was associated with increased cryptosporidiosis case rates 2 and 3 weeks after storms, but otherwise had no effect on rates (Appendix Figure 8). Conversely, gale-force wind exposure was associated with decreased cryptosporidiosis and giardiasis rates during the storm week and had no effect in the lagged weeks after storms (Appendix Figure 8).

Combining wind and rainfall exposure in storm type categories supported the findings of the wind exposure analysis. High rain–high wind, high rain–low wind, and low rain–low wind storms were all associated with decreased giardiasis case rates during the storm week before returning to baseline 1 week poststorm (Figure 5). Consistent with the rainfall analysis, high rain–low wind storms were positively associated with cryptosporidiosis rates up to 2 weeks poststorm, but unlike for rainfall alone, cases also increased 3 weeks after high rain–high wind and low rain–low wind storms: a 58% increase in cryptosporidiosis rates when ≥5% of the population was exposed to high wind–high rain storms and a 17% increase after low rain–low wind storms (Figure 5).

Discussion

In this analysis, we found tropical cyclones were associated with waterborne diseases, although the effect magnitude varied by exposure. The associations also

differed among the specific pathogens; Legionnaires' disease, *E. coli*, and cryptosporidiosis rates increased with rainfall, whereas salmonellosis, shigellosis, and giardiasis rates were unaffected, or decreased, during storm weeks. Those divergent associations likely reflect factors that mediate the relationship between storms and disease, including pathogen biology, transmission routes, and severity of infection.

Legionnaires' disease and *E. coli* case rates consistently increased with rainfall and population exposure thresholds, but the timing of the effects differed between these infections. *E. coli* rates peaked 1 week after storms and returned to baseline by week 3, whereas Legionnaires' disease rates were highest 3 weeks after storms. Those findings support microbiological studies that have analyzed bacterial counts in streams and water systems after specific hurricanes (*43*,*44*); elevated *E. coli* loads were reported 12–24 hours after a storm started, whereas *Legionella* increased 4–5 days later (*43*). *Legionella* are natural inhabitants of aquatic environments and replicate in water, typically in biofilm communities that colonize household plumbing and water infrastructure systems (*13*,*45*). Thus, the *Legionella* load can increase over time, whereas other bacterial pathogens that do not replicate in the environment typically have bacterial loads that peak after the initial contamination event and dissipate over time (*46*).

Cryptosporidiosis case rates also increased with storm-related rainfall but only at low population thresholds and concurrent with the storm week. Cryptosporidiosis cases were most common in the north-central Midwest, a region that infrequently experiences tropical storms or hurricanes severe enough to affect >25% of the population. The substantial increase in cases concurrent with storm weeks might be driven by several widespread outbreaks attributed to specific storm events that damaged water treatment facilities (*47*). *Cryptosporidium* is resistant to standard chemical disinfectants and is small enough to pass through sand filtration systems common in water treatment plants (*29*); thus, when the parasite contaminates water distribution systems that serve large populations, massive outbreaks can occur (*8*).

County-level exposure to heavy rainfall and cyclonic windspeed often were uncorrelated, which is characteristic of tropical cyclones (*37*), and the effect of extreme wind on cases differed from that of rainfall

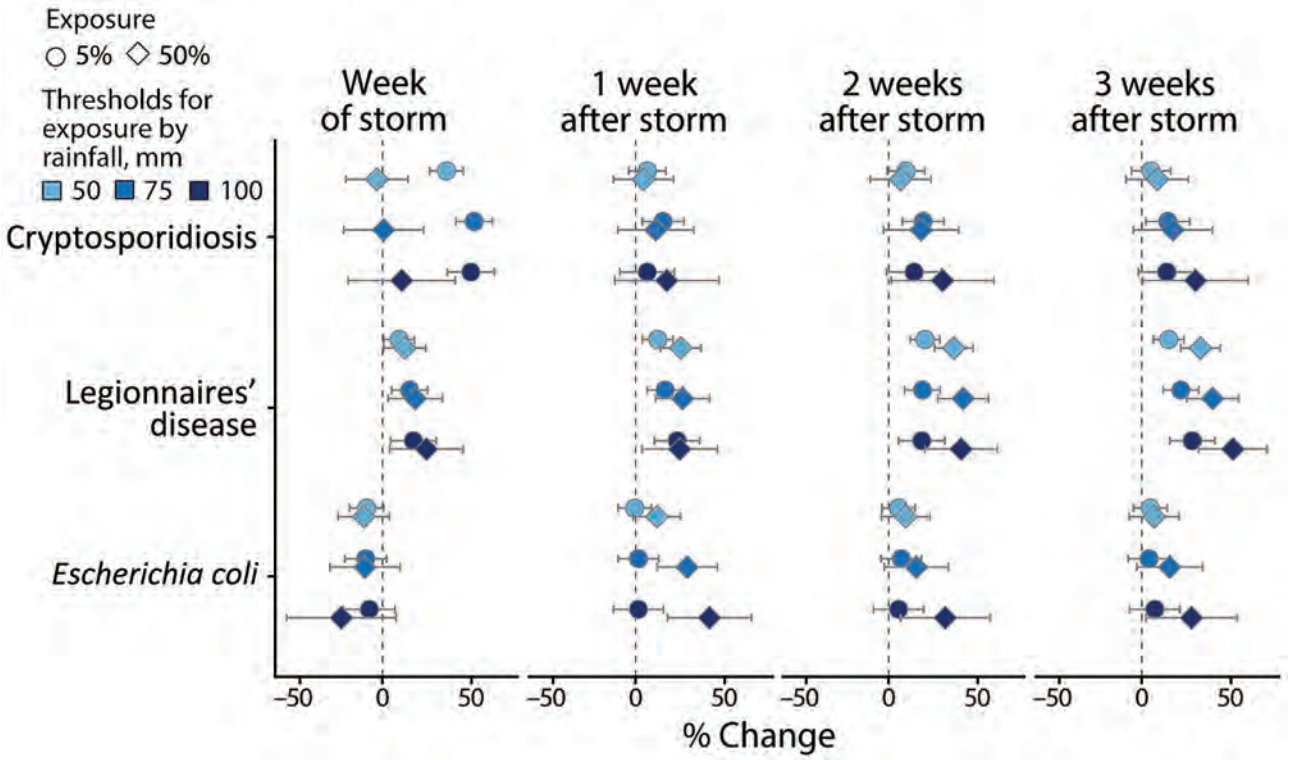

Figure 4. Average percent change in weekly case rates associated with exposure to storm-related rainfall in a study of waterborne infectious diseases associated with exposure to tropical cyclonic storms, United States, 1996–2018. Exposure is defined by 3 cumulative rainfall thresholds, ≥50 mm, ≥75 mm, or ≥100 mm; and for 2 population-exposure thresholds, 5% or 50% exposed. Estimates (shapes) and Bonferroni-corrected 95% CIs (bars) are reported for cryptosporidiosis, Legionnaires' disease, and *Escherichia coli* infections for the week of the storm (week 0) and 1–3 weeks after the storm.

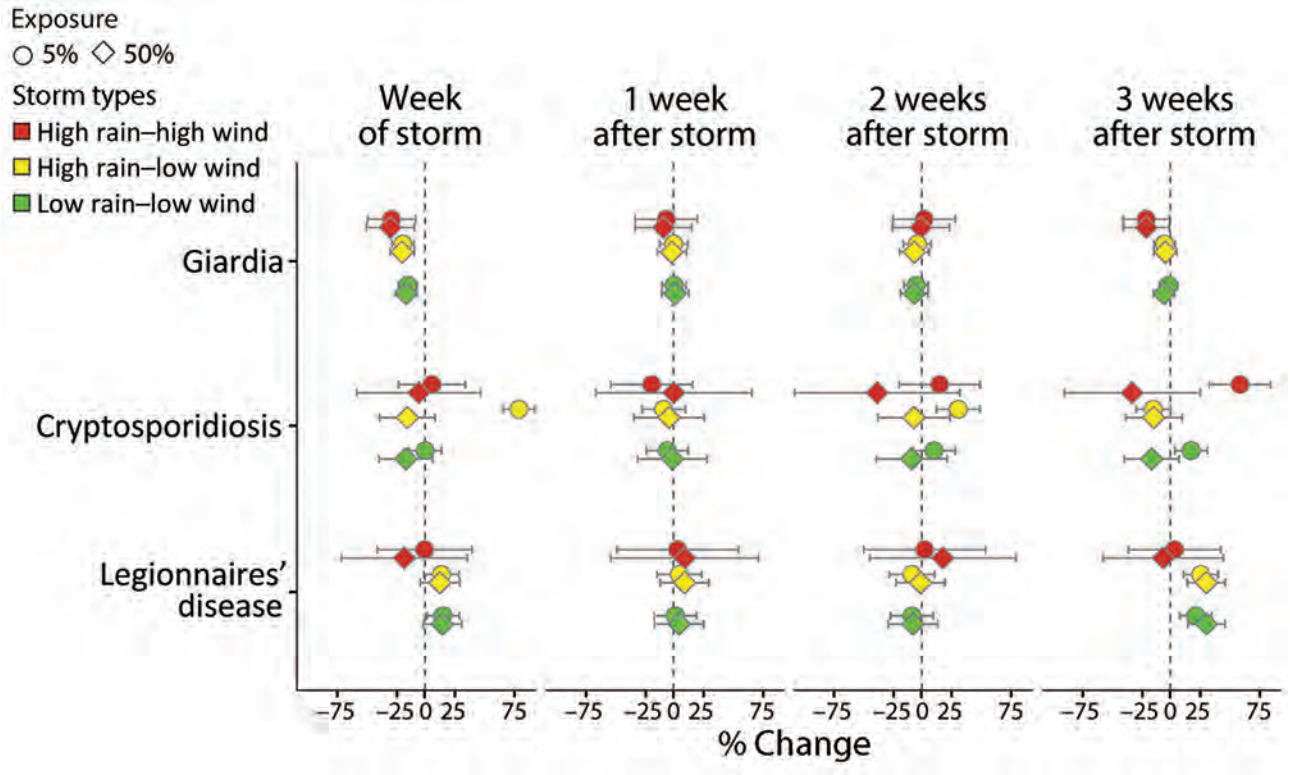

Figure 5. Average percent change in weekly waterborne infectious disease case rates associated with exposure to tropical cyclonic storm types, United States, 1996–2018. Exposure is defined by 3 categories according to rainfall and wind thresholds: high rain–high wind (red); high rain–low wind (yellow); and low rain–low wind (green). Estimates (shapes) and Bonferroni-corrected 95% CIs (bars) are reported for giardiasis, cryptosporidiosis, and Legionnaires' disease at 2 population-exposure thresholds (shape) for the week of the storm (week 0) and 1–3 weeks after the storm. The population-exposure thresholds refer to the percentage of the state population exposed to storm-related rainfall only; no hurricane-force winds affected >25% of the state population.

for several infections. Gale-force wind was associated with a lagged increase in Legionnaire' disease, but the effect on *E. coli* and cryptosporidiosis was minimal; hurricane-force wind was only associated with increased cryptosporidiosis rates 3 weeks after storms. Such attenuated effects could reflect the intricate, and possibly opposing, factors that influence transmission. High windspeeds are typically associated with destructive storms that can damage sanitation infrastructure, increasing the probability of transmission (*18*), but also could lead to population displacement (*48*), reducing the likelihood that persons will have contact with contaminated water. Extreme storms can also disrupt healthcare systems or alter healthcare-seeking behavior, which can lead to a reduction in detecting or reporting cases (*49*).

For areas that experienced both rainfall and cyclonic wind, we combined exposures into storm-type categories; the results underscored the necessity for pathogen-specific analyses and the limitations inherent in studying events that rarely occur. The high rain–high wind category encompassed the most devastating storms that occurred during the study period, including Hurricanes Katrina and Ivan, but represented a small fraction of all storms. Those events were associated with a substantial decrease in giardiasis but had no effect on Legionnaires' disease. *Giardia* transmission often occurs in recreational waters, such as swimming pools and rivers, and might be thwarted during storm weeks, when the population is less likely to engage in recreational activities. On the other hand, the burden of Legionnaires' disease was highest in regions that infrequently experience hurricane-force winds. High rain–high wind storms were associated with a substantial increase in cryptosporidiosis cases 3 weeks after storms, but the effect might have been driven by a 2-month span in 2008 when Texas experienced 2 hurricanes and a third tropical cyclone in succession and reported extremely high cryptosporidiosis case counts for an extended period.

Unlike the other infections, salmonellosis was unaffected by cyclonic storms at all population thresholds. *Salmonella* transmission is predominantly foodborne, and outbreaks attributed to contaminated

food are common, particularly during the summer (*42*). The high frequency of salmonellosis outbreaks makes it difficult to detect elevated case counts associated with storms because comparison weeks for storms coincide with those for foodborne outbreaks. Storm-related rainfall was associated with a slight decrease in shigellosis at high population thresholds during storm weeks. Shigellosis is typically mild, and the negative association might reflect a reduction in seeking healthcare for minor illnesses after disruptive storm events.

Except for shigellosis, other disease cases studied exhibited a summer seasonality that coincided with the cyclonic storm season in the United States. However, the inconsistent associations between storms and specific pathogens demonstrated that the effects were not simply driven by overlapping seasonal patterns. Salmonellosis and *E. coli* cases peaked during the same weeks in most regions, but storm-related rainfall had no effect on salmonellosis and a strong positive effect on *E. coli*. This study demonstrated the need for more pathogen-specific analyses that combine microbiological water quality data from multiple sources with epidemiologic data.

One limitation of this study is the spatial mismatch between cases and storm data. Aggregating from county- to state-level storm exposure introduced the possibility of misclassification bias because state-level exposure might be inconsistent with the conditions experienced by cases. We aimed to address this limitation by repeating the analysis at several population thresholds to define exposure and by assessing the consistency of the associations. That type of nondifferential misclassification would also be biased toward the null and underestimate the associations (*50*). Another limitation resulted from the spatial resolution, which only enabled us to perform a rough estimate of the effect of storms stratified by drinking water source or rural or urban location using county-level averages. Highly resolved water source and location data could provide insight into the mechanisms underlying the associations between storms and some waterborne diseases.

In summary, we found that tropical cyclones represent a risk to public health in the United States, although findings for individual pathogens varied. The US sanitation infrastructure is aging (*10*), and the country will likely experience more severe storm-related flooding as a result of climate change (*11*). Thus, identifying the drivers of pathogen transmission, and opportunities for intervention, will be crucial to reducing disease burden after cyclonic storm events.

V.L. was supported by a training grant from the National Institutes of Health (NIH; grant no. T32ES023770); both authors were supported by NIH grant no. R01AI163023. This study had no funding for its design, data analysis or interpretation, or writing.

J.S. and Columbia University disclose partial ownership of SK Analytics. J.S. discloses consulting for Business Network International (BNI).

About the Authors

Dr. Lynch is a postdoctoral researcher in the Environmental Health Sciences Department at Columbia University Mailman School of Public Health, New York, NY, USA. Her research interests include infectious disease epidemiology and extreme climatic events, particularly their effect on exacerbating health disparities. Dr. Shaman is professor of environmental health sciences at Columbia Mailman School of Public Health, and a professor and associate dean at Columbia Climate School, New York. His primary research interests include the use of mathematical and statistical models to describe, understand, and forecast the transmission dynamics of infectious diseases, and to investigate the broader effects of climate and weather on human health.

References

1. Rappaport EN. Fatalities in the United States from Atlantic tropical cyclones: new data and interpretation. Bull Am Meteorol Soc. 2014;95:341–6. https://doi.org/10.1175/BAMS-D-12-00074.1
2. Parks RM, Anderson GB, Nethery RC, Navas-Acien A, Dominici F, Kioumourtzoglou MA. Tropical cyclone exposure is associated with increased hospitalization rates in older adults. Nat Commun. 2021;12:1545. https://doi.org/10.1038/s41467-021-21777-1
3. Erickson TB, Brooks J, Nilles EJ, Pham PN, Vinck P. Environmental health effects attributed to toxic and infectious agents following hurricanes, cyclones, flash floods and major hydrometeorological events. J Toxicol Environ Health B Crit Rev. 2019;22:157–71. https://doi.org/10.1080/10937404.2019.1654422
4. Young I, Smith BA, Fazil A. A systematic review and meta-analysis of the effects of extreme weather events and other weather-related variables on *Cryptosporidium* and *Giardia* in fresh surface waters. J Water Health. 2015;13:1–17. https://doi.org/10.2166/wh.2014.079
5. Andrade L, O'Dwyer J, O'Neill E, Hynds P. Surface water flooding, groundwater contamination, and enteric disease in developed countries: A scoping review of connections and consequences. Environ Pollut. 2018;236:540–9. https://doi.org/10.1016/j.envpol.2018.01.104
6. Weller D, Brassill N, Rock C, Ivanek R, Mudrak E, Roof S, et al. Complex interactions between weather, and microbial and physicochemical water quality impact the likelihood of detecting foodborne pathogens in agricultural water. Front Microbiol. 2020;11:134. https://doi.org/10.3389/fmicb.2020.00134

7. Craun GF, Brunkard JM, Yoder JS, Roberts VA, Carpenter J, Wade T, et al. Causes of outbreaks associated with drinking water in the United States from 1971 to 2006. Clin Microbiol Rev. 2010;23:507–28. https://doi.org/10.1128/CMR.00077-09
8. Cann KF, Thomas DR, Salmon RL, Wyn-Jones AP, Kay D. Extreme water-related weather events and waterborne disease. Epidemiol Infect. 2013;141:671–86. https://doi.org/10.1017/S0950268812001653
9. US Census Bureau. Demographic turning points for the United States: population projections for 2020 to 2060 [cited 2022 Jul 11]. https://www.census.gov/content/dam/Census/library/publications/2020/demo/p25-1144.pdf
10. Allaire M, Wu H, Lall U. National trends in drinking water quality violations. Proc Natl Acad Sci U S A. 2018;115:2078–83. https://doi.org/10.1073/pnas.1719805115
11. Woodruff JD, Irish JL, Camargo SJ. Coastal flooding by tropical cyclones and sea-level rise. Nature. 2013;504:44–52. https://doi.org/10.1038/nature12855
12. Collier SA, Deng L, Adam EA, Benedict KM, Beshearse EM, Blackstock AJ, et al. Estimate of burden and direct healthcare cost of infectious waterborne disease in the United States. Emerg Infect Dis. 2021;27:140–9. https://doi.org/10.3201/eid2701.190676
13. Cunha BA, Burillo A, Bouza E. Legionnaires' disease. Lancet. 2016;387:376–85. https://doi.org/10.1016/S0140-6736(15)60078-2
14. Fletcher SM, Stark D, Harkness J, Ellis J. Enteric protozoa in the developed world: a public health perspective. Clin Microbiol Rev. 2012;25:420–49. https://doi.org/10.1128/CMR.05038-11
15. Jagai JS, DeFlorio-Barker S, Lin CJ, Hilborn ED, Wade TJ. Sanitary sewer overflows and emergency room visits for gastrointestinal illness: analysis of Massachusetts data, 2006–2007. Environ Health Perspect. 2017;125:117007. https://doi.org/10.1289/EHP2048
16. Sauer EP, Vandewalle JL, Bootsma MJ, McLellan SL. Detection of the human specific Bacteroides genetic marker provides evidence of widespread sewage contamination of stormwater in the urban environment. Water Res. 2011;45:4081–91. https://doi.org/10.1016/j.watres.2011.04.049
17. Wade TJ, Sandhu SK, Levy D, Lee S, LeChevallier MW, Katz L, et al. Did a severe flood in the Midwest cause an increase in the incidence of gastrointestinal symptoms? Am J Epidemiol. 2004;159:398–405. https://doi.org/10.1093/aje/kwh050
18. Amaral-Zettler LA, Rocca JD, Lamontagne MG, Dennett MR, Gast RJ. Changes in microbial community structure in the wake of Hurricanes Katrina and Rita. Environ Sci Technol. 2008;42:9072–8. https://doi.org/10.1021/es801904z
19. Cho S, Hiott LM, Barrett JB, McMillan EA, House SL, Humayoun SB, et al. Prevalence and characterization of *Escherichia coli* isolated from the Upper Oconee Watershed in Northeast Georgia. PLoS One. 2018;13:e0197005. https://doi.org/10.1371/journal.pone.0197005
20. Beaudeau P, Schwartz J, Levin R. Drinking water quality and hospital admissions of elderly people for gastrointestinal illness in Eastern Massachusetts, 1998–2008. Water Res. 2014;52:188–98. https://doi.org/10.1016/j.watres.2014.01.005
21. Den Boer JW, Coutinho RA, Yzerman EP, van der Sande MA. Use of surface water in drinking water production associated with municipal Legionnaires' disease incidence. J Epidemiol Community Health. 2008;62:e1. https://doi.org/10.1136/jech.2007.061598
22. Holvoet K, Sampers I, Seynnaeve M, Uyttendaele M. Relationships among hygiene indicators and enteric pathogens in irrigation water, soil and lettuce and the impact of climatic conditions on contamination in the lettuce primary production. Int J Food Microbiol. 2014;171:21–31. https://doi.org/10.1016/j.ijfoodmicro.2013.11.009
23. Wade TJ, Lin CJ, Jagai JS, Hilborn ED. Flooding and emergency room visits for gastrointestinal illness in Massachusetts: a case-crossover study. PLoS One. 2014;9:e110474. https://doi.org/10.1371/journal.pone.0110474
24. Rangel JM, Sparling PH, Crowe C, Griffin PM, Swerdlow DL. Epidemiology of *Escherichia coli* O157:H7 outbreaks, United States, 1982–2002. Emerg Infect Dis. 2005;11:603–9. https://doi.org/10.3201/eid1104.040739
25. Hrudey SE, Payment P, Huck PM, Gillham RW, Hrudey EJ. A fatal waterborne disease epidemic in Walkerton, Ontario: comparison with other waterborne outbreaks in the developed world. Water Sci Technol. 2003;47:7–14. https://doi.org/10.2166/wst.2003.0146
26. Bloom MS, Palumbo J, Saiyed N, Lauper U, Lin S. Food and waterborne disease in the greater New York City area following Hurricane Sandy in 2012. Disaster Med Public Health Prep. 2016;10:503–11. https://doi.org/10.1017/dmp.2016.85
27. Lefebvre M, Razakandrainibe R, Villena I, Favennec L, Costa D. *Cryptosporidium*-biofilm interactions: a review. Appl Environ Microbiol. 2021;87:e02483-20. https://doi.org/10.1128/AEM.02483-20
28. Berendt RF. Survival of *Legionella pneumophila* in aerosols: effect of relative humidity. J Infect Dis. 1980;141:689. https://doi.org/10.1093/infdis/141.5.689
29. Karanis P, Kourenti C, Smith H. Waterborne transmission of protozoan parasites: a worldwide review of outbreaks and lessons learnt. J Water Health. 2007;5:1–38. https://doi.org/10.2166/wh.2006.002
30. Kitajima M, Haramoto E, Iker BC, Gerba CP. Occurrence of *Cryptosporidium*, *Giardia*, and *Cyclospora* in influent and effluent water at wastewater treatment plants in Arizona. Sci Total Environ. 2014;484:129–36. https://doi.org/10.1016/j.scitotenv.2014.03.036
31. Breiman RF, Butler JC. Legionnaires' disease: clinical, epidemiological, and public health perspectives. Semin Respir Infect. 1998;13:84–9.
32. Adam RD. Biology of *Giardia lamblia*. Clin Microbiol Rev. 2001;14:447–75. https://doi.org/10.1128/CMR.14.3.447-475.2001
33. Lake IR, Bentham G, Kovats RS, Nichols GL. Effects of weather and river flow on cryptosporidiosis. J Water Health. 2005;3:469–74. https://doi.org/10.2166/wh.2005.048
34. Reynolds KA, Mena KD, Gerba CP. Risk of waterborne illness via drinking water in the United States. Rev Environ Contam Toxicol. 2008;192:117–58.
35. Sidhu JP, Hodgers L, Ahmed W, Chong MN, Toze S. Prevalence of human pathogens and indicators in stormwater runoff in Brisbane, Australia. Water Res. 2012;46:6652–60. https://doi.org/10.1016/j.watres.2012.03.012
36. Collinet-Adler S, Ward HD. Cryptosporidiosis: environmental, therapeutic, and preventive challenges. Eur J Clin Microbiol Infect Dis. 2010;29:927–35. https://doi.org/10.1007/s10096-010-0960-9
37. Anderson GB, Ferreri J, Al-Hamdan M, Crosson W, Schumacher A, Guikema S, et al. Assessing United States county-level exposure for research on tropical cyclones and human health. Environ Health Perspect. 2020;128:107009. https://doi.org/10.1289/EHP6976
38. Kruk MC, Gibney EJ, Levinson DH, Squires M. A climatology of inland winds from tropical cyclones for the Eastern United States. J Appl Meteorol Climatol. 2010;49:1538–47. https://doi.org/10.1175/2010JAMC2389.1

39. Radcliff TA, Chu K, Der-Martirosian C, Dobalian A. A model for measuring ambulatory access to care recovery after disasters. J Am Board Fam Med. 2018;31:252–9. https://doi.org/10.3122/jabfm.2018.02.170219
40. Noe RS, Schnall AH, Wolkin AF, Podgornik MN, Wood AD, Spears J, et al. Disaster-related injuries and illnesses treated by American Red Cross disaster health services during Hurricanes Gustav and Ike. South Med J. 2013;106:102–8. https://doi.org/10.1097/SMJ.0b013e31827c9e1f
41. Armstrong BG, Gasparrini A, Tobias A. Conditional Poisson models: a flexible alternative to conditional logistic case cross-over analysis. BMC Med Res Methodol. 2014;14:122. https://doi.org/10.1186/1471-2288-14-122
42. Acheson DWK. Food and waterborne illnesses. In: Schaechter M, ed. Encyclopedia of microbiology, 3rd edition. New York: Academic Press; 2009. p. 365–81.
43. Ulrich N, Rosenberger A, Brislawn C, Wright J, Kessler C, Toole D, et al. Restructuring of the aquatic bacterial community by hydric dynamics associated with Superstorm Sandy. Appl Environ Microbiol. 2016;82:3525–36. https://doi.org/10.1128/AEM.00520-16
44. Brigmon RL, Turick CE, Knox AS, Burckhalter CE. The impact of storms on *Legionella pneumophila* in cooling tower water, implications for human health. Front Microbiol. 2020;11:543589. https://doi.org/10.3389/fmicb.2020.543589
45. Falkinham JO III, Hilborn ED, Arduino MJ, Pruden A, Edwards MA. Epidemiology and ecology of opportunistic premise plumbing pathogens: *Legionella pneumophila*, *Mycobacterium avium*, and *Pseudomonas aeruginosa*. Environ Health Perspect. 2015;123:749–58. https://doi.org/10.1289/ehp.1408692
46. Winfield MD, Groisman EA. Role of nonhost environments in the lifestyles of *Salmonella* and *Escherichia coli*. Appl Environ Microbiol. 2003;69:3687–94. https://doi.org/10.1128/AEM.69.7.3687-3694.2003
47. Wilkerson W, Archer WR. Epidemiology in Texas 1998 annual report. Austin: Texas Department of Health; 1999.
48. Saulnier DD, Brolin Ribacke K, von Schreeb J. No calm after the storm: a systematic review of human health following flood and storm disasters. Prehosp Disaster Med. 2017;32:568–79. https://doi.org/10.1017/S1049023X17006574
49. Lane K, Charles-Guzman K, Wheeler K, Abid Z, Graber N, Matte T. Health effects of coastal storms and flooding in urban areas: a review and vulnerability assessment. J Environ Public Health. 2013;2013:913064. https://doi.org/10.1155/2013/913064
50. Carroll RJ, Ruppert D, Stefanski LA, Crainiceanu CM. Measurement error in nonlinear models: a modern perspective, second edition. New York: Chapman and Hall/CRC; 2006.

Address for correspondence: Victoria D. Lynch, Mailman School of Public Health, 722 W 168th St, Fl 11, New York, NY 10032, USA; email: vdl2103@cumc.columbia.edu

etymologia revisited

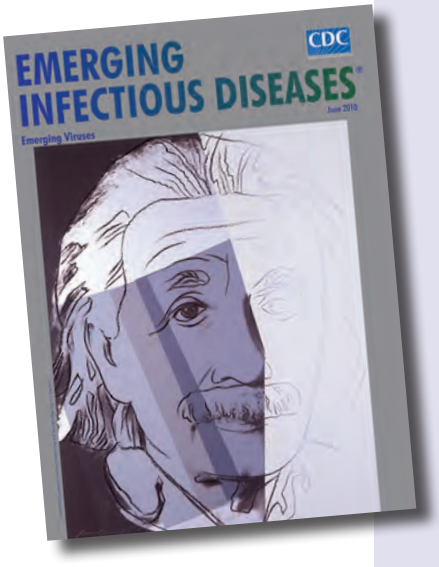

Originally published in June 2010

Lassa Virus

[lah sə] virus

This virus was named after the town of Lassa at the southern end of Lake Chad in northeastern Nigeria, where the first known patient, a nurse in a mission hospital, had lived and worked when she contracted this infection in 1969. The virus was discovered as part of a plan to identify unknown viruses from Africa by collecting serum specimens from patients with fevers of unknown origin. Lassa virus, transmitted by field rats, is endemic in West Africa, where it causes up to 300,000 infections and 5,000 deaths each year.

References:

1 Frame JD, Baldwin JM Jr, Gocke DJ, Troup JM. Lassa fever, a new virus disease of man from West Africa. I. Clinical description and pathological findings. Am J Trop Med Hyg. 1970;19:670–6
2. Mahy BW. The dictionary of virology, 4th ed. Burlington (MA): Elsevier; 2009.

https://wwwnc.cdc.gov/eid/article/16/6/et-1606_article

Elimination of *Dirofilaria immitis* Infection in Dogs, Linosa Island, Italy, 2020–2022

Emanuele Brianti, Ettore Napoli, Giovanni De Benedetto, Luigi Venco, Jairo Alfonso Mendoza-Roldan, Angelo Basile, Marcos Antônio Bezerra-Santos, Jason Drake, Roland Schaper, Domenico Otranto

On Linosa Island, Italy, *Dirofilaria immitis* infection has been hyperendemic in dogs and seroprevalent among islanders. In 2020, we implemented a heartworm disease elimination program on Linosa Island. Of 54 dogs tested for *D. immitis* antigen and microfilariae, 28 had positive results and received treatment with oral doxycycline twice daily for 4 weeks plus topical imidacloprid/moxidectin monthly for 12 months. The 26 dogs with negative results received monthly topical imidacloprid/moxidectin as preventive. During month 1, the number of microfilaremic dogs was reduced by 76.5%. From month 2 on, all animals were microfilariae negative, and during months 3 to 9, the number of antigen-positive dogs decreased progressively. Treatment of positive dogs coupled with chemoprophylaxis for noninfected dogs was effective, protecting them from new infections. The elimination program reduced the risk for human infection, representing a One Health paradigm. Monitoring and chemoprophylaxis are advocated to maintain the status of heartworm disease–free area.

Dirofilaria immitis and *D. repens* (Spirurida, Onchocercidae) nematodes are among the most common species of filariae that cause diseases in dogs and other animals; both species infect humans (*1*,*2*). In dogs, *D. immitis* filariae cause the severe illness heartworm disease (HWD), whereas *D. repens* infection is less severe. Both *Dirofilaria* species are transmitted by mosquitoes; in Europe, the competent vectors are *Culex pipiens* and *Aedes albopictus* mosquitoes (*3*). However, the involvement of flying insects other than mosquitos has been recently hypothesized, including black flies belonging to the *Simulium turgaicum* complex (*4*) and *Culicoides paolae* biting midges (*5*).

Unlike *D. repens* filariae, which are more widely distributed in Europe, including the Italian Peninsula (*1*,*6*–*8*), *D. immitis* worms are more frequently recorded in central Europe (*9*), including regions in northern Italy (*10*,*11*). Nevertheless, autochthonous cases of HWD in dogs from central and southern Italy have been retrospectively reported from 2009 (*1*) through 2019 (*12*); highly endemic foci in southern regions of Italy have been described (*13*,*14*). That new epidemiologic scenario developed after the arrival of a new invasive mosquito species (i.e., *Ae. albopictus*) and the increased movement of animals throughout the country combined with lack of chemoprophylactic strategies for dogs from non–HWD-endemic regions (*9*,*12*,*13*). The island of Linosa, Italy, represents a paradigm of that scenario. A highly endemic focus of *D. immitis* filariae was recently described on the small and remote island located in the middle of the Mediterranean Basin, where 58.9% of dogs tested positive for HWD by modified Knott and SNAP 4Dx Plus tests (*14*). In the same epidemiologic context, 7.9% of human islanders tested positive for *D. immitis* antibodies (*15*), which emphasizes the role of *D. immitis*–infected dogs as a source for human infections in specifically isolated environments, thus advocating for treating infected animals in the context of One Health.

Traditionally, HWD is treated with melarsomine dihydrochloride, the sole registered heartworm adulticide drug (*16*,*17*). However, an alternative therapeutic approach, known as the slow-kill protocol, that combines macrocyclic lactones with doxycycline, targeting the bacterial endosymbiont *Wolbachia*, has been used successfully in experimentally and naturally infected dogs, (*18*–*20*). That protocol was recently recognized by the American Heartworm Society and the European Society of Dirofilariosis and Angiostrongylosis

Author affiliations: University of Messina, Messina, Italy (E. Brianti, E. Napoli, G. De Benedetto, A. Basile); Ospedale Veterinario Città di Pavia, Pavia, Italy (L. Venco); University of Bari, Valenzano, Italy (J.A. Mendoza-Roldan, M.A. Bezerra-Santos, D. Otranto); Bu-Ali Sina University, Hamedan, Iran (D. Otranto); Elanco Animal Health, Monheim, Germany (J. Drake); RS Consultancy, Monheim (R. Schaper)

DOI: https://doi.org/10.3201/eid2908.221910

as an alternative strategy when treatment with melarsomine is either unavailable or contraindicated. Compared with the melarsomine treatment, doxycycline (10 mg/kg 2×/d) for 4 weeks combined with monthly administration of a topical formulation of 10% wt/vol imidacloprid and 2.5% wt/vol moxidectin for 9 months proved to be safe and effective for treating HWD in naturally infected dogs and for clearing dogs of circulating microfilariae (*20*).

Because of its geographic and epidemiologic peculiarities, Linosa Island offered an exceptional opportunity to use this elimination program for HWD. The program involved therapeutically and prophylactically administering the alternative protocol to all infected dogs and administering monthly preventive of 10% wt/vol imidacloprid plus 2.5% wt/vol moxidectin to all remaining uninfected dogs on the island. The study was complemented by an entomologic survey to assess mosquito vectors within this unique epidemiologic context.

The study was approved by the ethics committee of animal experiments of the Department of Veterinary Medicine, University of Bari, Italy (approval number 01/2021). It was conducted according to the VICH GL9 principles of Good Clinical Practice (*21*).

Methods

Animal Sampling and Diagnosis

In October 2020 (T0), we physically examined all 58 dogs on Linosa Island and recorded signalment and history (e.g., age, sex, breed, clinical signs, and treatments) in individual files. At T0, we collected blood samples from each dog and stored them in two 1-mL K_3EDTA tubes and in one 5-mL tube with clot activator. We used the Knott test (*22*) to detect and identify circulating microfilariae in whole-blood samples and a duplex real-time quantitative PCR (qPCR) to differentiate *Dirofilaria* species (*23*).

We analyzed serum samples for the presence of *D. immitis*–specific antigens by using the SNAP 4Dx Plus rapid ELISA (IDEXX, https://www.idexx.com). We considered dogs that were positive for *D. immitis*, either microscopically, serologically, or molecularly, to be infected and assigned them to the treatment group (G1); we assigned dogs that were negative to the prevention group (G2). Before the beginning of treatment, we performed cardiac ultrasonography for all *D. immitis*–infected dogs to detect adult parasites in the pulmonary arteries. We used an echocardiographic unit (Vivid-iQ; GE Healthcare, https://www.gehealthcare.com) equipped with dedicated multifrequency phased array transducers (6s-RS and M5-RS). In brief, we used the right parasternal long-axis view optimized for the right pulmonary vein and artery (standard view 1) and the right parasternal short-axis view optimized for the right pulmonary artery (standard view 2) to detect worms (*24*). We did not perform thoracic radiography because no facility was available on the island.

Treatment and Follow-up

D. immitis–infected dogs (G1) received doxycycline (Ronaxan; Boehringer Ingelheim, https://www.boehringer-ingelheim.com) (10 mg/kg orally 2×/d) for 4 weeks plus a monthly application of a spot-on formulation containing 10% wt/vol imidacloprid and 2.5% wt/vol moxidectin (Advocate; Elanco Animal Health, www.elanco.com) for 12 months. Dogs in the G2 group underwent monthly chemoprophylactic treatment with the same spot-on product used for the G1 dogs.

G1 dogs underwent follow-up examination at 1, 2, 3, 6, 9, 12 and 18 months (designated as T1, T2, T3, T6, T9, T12, and T18) after enrollment (Figure 1).

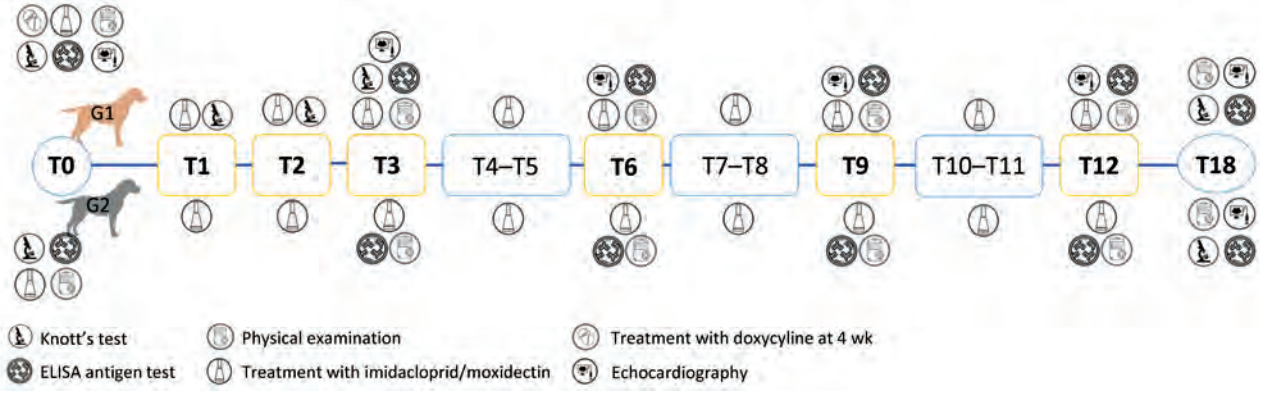

Figure 1. Schematic design of study of elimination of *Dirofilaria immitis* infection in dogs, Linosa Island, Italy, 2020, and follow-up examinations. G1, infected group; G2, noninfected group; T, time after start of elimination program, in months. Boldface indicates follow-up visits.

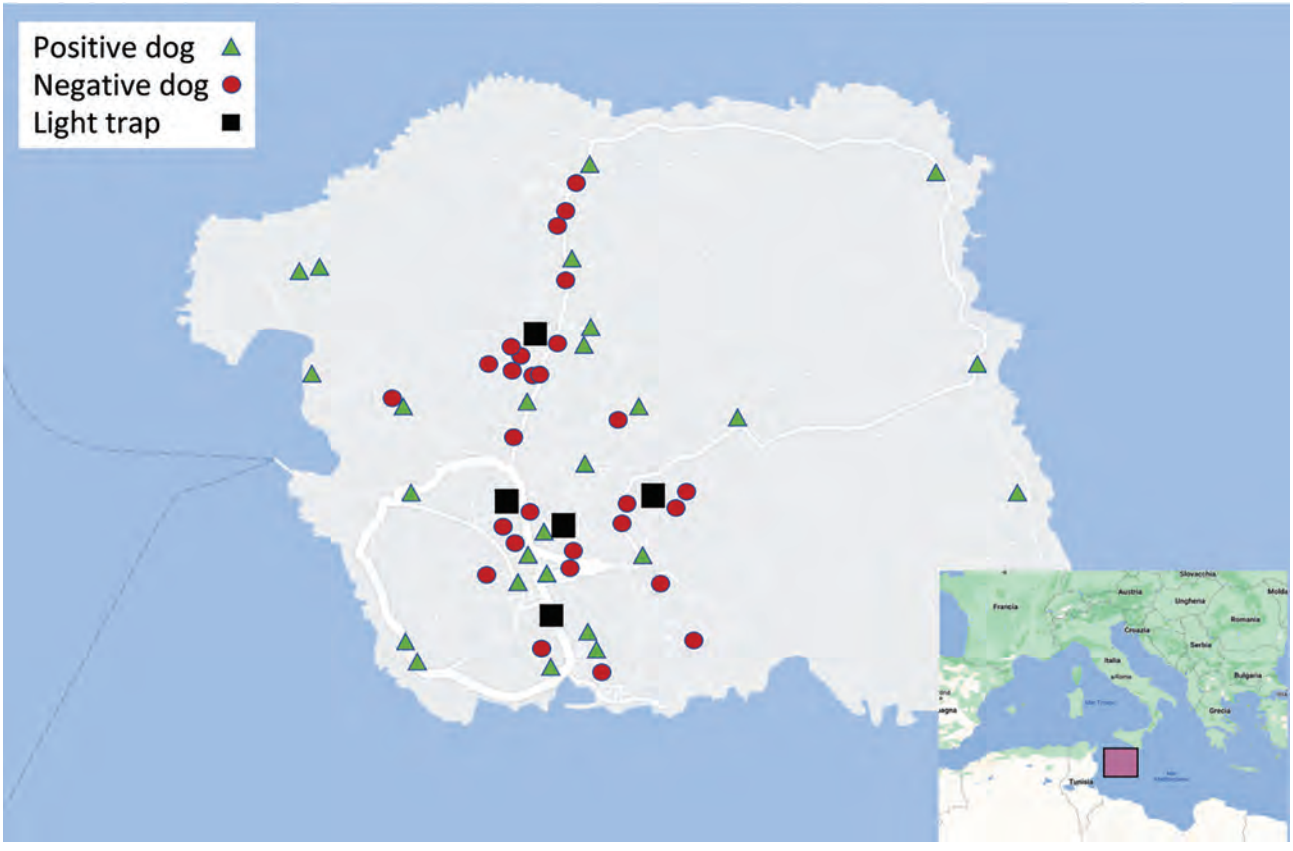

Figure 2. Linosa Island (Sicily, Italy) indicating the positions of infected dogs, noninfected dogs, and light traps used to capture mosquitoes. Inset shows location of Linosa Island.

At each follow-up visit, we clinically examined dogs and collected blood samples that we analyzed by Knott test (at T1, T2, and T18) or by SNAP 4Dx Plus test (at T1, T2, T3, T6, T9, T12 and T18). We repeated cardiac ultrasonography for G1 dogs at T3, T6, T9, T12, and T18. G2 dogs underwent clinical examination monthly, and we tested them for parasite antigenemia (by SNAP 4Dx Plus test) at T3, T6, T9, T12, and T18 (Figure 1).

Of the 58 dogs examined at T0, we included only 54 in the study because 2 dogs were going to be on the island for only a few weeks/months and the owners of the other 2 dogs did not consent to their study participation. For dogs that were permanently introduced onto the island after the beginning of the study, we performed clinical examination and specific testing (i.e., Knott test and testing for *D. immitis* circulating antigens) with owner consent and allocated them to G1 or G2 according to the test results. We advised owners to immediately report any clinical signs (i.e., cough, hemoptysis, syncope) that might appear during the study and to reduce physical activity for all infected dogs, regardless of symptoms, as much as possible.

Mosquito Collection

We collected mosquitos from 5 locations where cases of *D. immitis* infection in dogs were detected (Figure 2). We trapped mosquitoes daily during October 2020–November 2021, 5:30 P.M.–9:00 A.M., by using 1 light trap per site, set ≈50 cm above the ground. We replaced net bags daily and stored insects in the net bags at −20°C according to collection site/day. After morphologically identifying mosquitoes to the species level (*25*), we further analyzed female mosquitoes with qPCR to detect and differentiate *Dirofilaria* spp.

Molecular Diagnosis

We extracted genomic DNA from samples of dog blood by using the commercial QIAamp DNA Micro Kit (QIAGEN GmbH, https://www.qiagen.com) and samples of mosquito abdomen and thorax by using an in-house method (*26*). We tested all DNA samples with qPCR by using 2 species-specific primer sets targeting partial cytochrome *c* oxidase subunit 1 for *D. immitis* DNA and the second internal transcribed spacer-2 of nuclear ribosomal DNA for *D. repens* DNA, as previously described (*23*). We tested all

DNA samples in duplicate and included positive and negative controls in each qPCR run.

Results

We detected *D. immitis* infection in 28 (51.9%) of 54 (33 male, 21 female) enrolled dogs (Appendix, https://wwwnc.cdc.gov/EID/article/29/8/22-1910-App1.pdf). We found circulating microfilariae in 17 (60.7%) infected dogs and specific *D. immitis* antigens in 27 (96.4%). All microfilaremic animals except 1 had positive ELISA antigen test results (Appendix). Microfilariae were morphologically and molecularly identified as *D. immitis*.

At the time of enrollment (T0), we conducted echocardiography on 23 of 28 infected dogs and found *D. immitis* adults within the pulmonary arteries of 20 (Appendix). On T0, we allocated 28 dogs to G1 and 26 to G2. A total of 4 dogs (3 in G1 and 1 in G2) were unavailable for follow-up analysis because of events not associated with treatment (e.g., low owner compliance or neoplastic disease). During the study period, 5 new dogs were permanently introduced onto the island (3 in January 2021 and 2 in March 2021); they tested negative for *D. immitis* infection and were included in group G2.

At T1, the number of microfilaremic dogs was reduced by 76.5%; only 4 of 17 dogs were positive by Knott test. From T2 until the end of the study, no microfilariae were found in G1 dogs. By T1, 3 infected dogs had become antigen negative (no antigen detected) according to ELISA test (Appendix). From T3 on, the number of antigen-positive dogs decreased progressively (20 at T3, 10 at T6, and 2 at T9) (Appendix). All dogs in G1 were negative for *D. immitis* circulating antigens at the 1-year follow-up visit (T12, October 2021).

Cardiac ultrasonography showed filarial parasites in the pulmonary arteries in 14 dogs at T3, 9 dogs at T6, 6 dogs at T9, and 3 dogs at T12 (Appendix). At T18, all G1 dogs scored negative by Knott test and ELISA antigen test, and no parasites were detected by echocardiography. Group 2 dogs tested negative for *D. immitis* antigens at all scheduled follow-up visits.

In this study, treatment with doxycycline and 10% wt/vol imidacloprid plus 2.5% wt/vol moxidectin seemed to be safe, and no adverse events were observed. However, in 1 dog from the G1 group, a thromboembolic-like disorder with hindlimb paralysis and pain was observed a few days after the beginning of treatment. Doxycycline treatment was temporarily suspended, and fluid therapy was promptly administered in association with unfractionated heparin (200 U/kg subcutaneously every 8 h for 3 d) and prednisone (1 mg/kg 2×/d in gradually decreasing doses for 15 d), resulting in full recovery of that G1 animal after 5 days.

Another dog that was apparently healthy at T0 exhibited ascites and diffuse edema of the hindlimbs at the clinical examination conducted on T3. Ultrasonography revealed a high parasite burden within the pulmonary arteries, associated with posthepatic portal hypertension. Treatment with sildenafil (2 mg/kg 3×/d for ≥6 mo) was administered. At the T6 follow-up visit, the dog had improved clinically, although pulmonary hypertension was still present, but pulmonary hypertension was absent at the next follow-up visits.

During this study, we collected 359 mosquitoes (169 male and 190 female) belonging to 6 species, the most abundant of which was *C. pipiens* (Table). Of the 190 females collected, 53 were engorged, and none of the analyzed specimens scored positive to *Dirofilaria* spp. DNA.

Discussion

In a short time, *D. immitis* parasites were eliminated from Linosa Island after we combined an alternative adulticide protocol for infected dogs with administration of preventives to noninfected animals. The peculiar epidemiologic context of the island (i.e., geographically confined area, limited number of dogs, and absence of wild reservoirs) aided the campaign. After the HWD focus in southernmost Europe was described (*14*), we planned and successfully implemented our project. In contrast to programs targeting other mosquitoborne diseases, such as malaria,

Table. Number and species of mosquitoes captured with light traps on Linosa Island, Italy, October 2020–November 2021

Mosquito species	No. (%) specimens	No. female	No. male
Culex pipiens	114 (31.8)	57	57
Culiseta annulata	69 (19.2)	38	31
Aedes mariae complex	55 (15.3)	37	18
Culex laticinctus	53 (14.8)	27	26
Culex spp.*	41 (11.4)	16	25
Aedes albopictus	16 (4.5)	8	8
Culiseta langereolata	6 (1.7)	5	1
Aedes spp.*	5 (1.4)	2	3
Total	359 (100)	190	169

*Ruined mosquito specimens were morphologically identified to genus level only.

this elimination campaign did not target the vector (*27*) and instead targeted the parasite specifically by eliminating the circulating juvenile forms and adult parasites in infected dogs while simultaneously protecting noninfected animals with chemoprophylaxis.

Treatment with doxycycline and imidacloprid/moxidectin was effective and safe for all of the dogs; side effects were observed in only 2 dogs, probably resulting from thromboembolism after worm death, which is a side effect associated with any adulticide protocol. Nevertheless, the risk for thromboembolism is also linked to patients' excessive physical activity after treatment, which cannot be ruled out (*28*). Furthermore, protocols that cause the progressive, slow death of adult parasites expand the temporal window of thromboembolic risk compared with conventional treatment (*24*). A retrospective study suggests that the risk for thromboembolic events is higher 3 months after the start of the alternative treatment protocol than after start of the melarsomine protocol and that exercise restriction for treated animals is advisable for longer periods or until antigen test results are negative (*28*,*29*). Regardless, the alternative protocol has proven to be effective (*20*,*24*,*30*) and may result in fewer adverse events than those resulting from melarsomine alone (*31*,*32*) if exercise restriction and other precautions are adequately implemented.

For this study, we chose the combined doxycycline/moxidectin protocol over the conventional adulticide therapy, considering the potential adverse events associated with the sudden death of adult worms causing pulmonary thrombosis (*32*) and the lack of veterinary services available on the island. On the other hand, the adulticide effects of doxycycline on developing and adult stages of the parasite are slow (*33*), and macrocyclic lactones are effective against *D. immitis* L3 and L4 and kill only adult parasites after prolonged use (*2*). Whether the 2 drugs work better together to eliminate *D. immitis* parasites in a short time because of a cumulative or synergistic effect is not known.

Eliminating circulating microfilariae in infected dogs after the beginning of the study (T2) drastically reduced the number of dogs acting as reservoirs on the island and therefore the risk for *D. immitis* infection of mosquitoes. All of the actions contributed to breaking the life cycle of the parasite, a finding that was supported by the fact that none of the examined mosquitoes scored positive for *Dirofilaria* spp. DNA up to November 2021, unlike before the study had started a few months earlier (*14*).

The protocol that we used led to progressive reduction of detectable antigens in treated animals from T3 to T9 and to dogs testing negative at T12. This finding is similar or even better than what was recorded in previous studies that used the same protocol (*20*,*34*,*35*). Also, the conversion to the antigen-negative status observed was faster than that recorded with ivermectin alone (*24*,*36*) or with ivermectin (every 2 weeks for 6 months) and doxycycline (10 mg/kg/d orally for 30 d) in which only 73% or 80% of treated dogs reached antigen-negative status (*30*,*31*).

The use of macrocyclic lactones as adulticides has been discouraged by several authors because it may take many months for adult worms to die, enabling the disease to progress and allowing for the potential selection of macrocyclic lactone–resistant strains (*37*). Moreover, potential interference with antigen test results has also been suggested (*37*). Several studies have reported false-negative antigen test results in dogs and cats treated with macrocyclic lactones, presumably resulting from formation of immune complexes and the consequent binding of the antigens (*37*–*39*). To overcome this problem, 2 consecutive negative antigen test results 6 months apart have been suggested as a valid criterion for considering a dog cleared of infection (*34*). Therefore, in this elimination program, all dogs were probably cured of infection because in no dog was antigen detected at T12 or 6 months after (T18). This finding is also strongly supported by ultrasonography in which no adult heartworms were observed at the T18 follow-up visit. Our data may also be useful in where *D. immitis* parasites are endemic and melarsomine is not commercially available (e.g., Brazil, eastern Europe).

Despite the presence of domestic and feral cats on Linosa Island (*40*), our study did not include those hosts because of lack of owner compliance and the difficulty of sampling these animals in a remote environment. However, considering the occurrence and possible role of cats as reservoirs of *D. immitis* parasites (*41*), further studies evaluating the prevalence of this parasite in cat populations on Linosa Island are warranted.

Considering the zoonotic potential of *D. immitis* worms, elimination of HWD in dogs is pivotal for reducing the risk for human infection. Indeed, in previous surveys conducted on the human population from Linosa Island, up to 7.9% of islanders were positive for circulating *D. immitis* antibodies (*15*), which represented one of the highest percentages of human exposure ever reported. Therefore, results from our study suggest that adulticide treatment of all infected dogs, coupled with prevention for noninfected dogs, not only protects animals from HWD but may also potentially reduce the risk for human infection. Such an

approach represents a paradigm for the One Health concept. Continuous monitoring and chemoprophylaxis of the canine population on the island and of all newly introduced dogs are highly recommended to maintain the status of HWD-free area.

Acknowledgments

We thank Laura Helen Kramer for her critical revision of the manuscript and acknowledge Elanco Animal Health for financial support of this study.

The study was conducted under the frame of the Project PE-13, INF-ACT, which is part of the National Recovery and Resilience Plan.

About the Author

Dr. Brianti is full professor at Department of Veterinary Sciences, University of Messina, Italy. His main research activity is focused on parasitic diseases of veterinary and public health concern.

References

1. Otranto D, Capelli G, Genchi C. Changing distribution patterns of canine vector borne diseases in Italy: leishmaniosis vs. dirofilariosis. Parasit Vectors. 2009;26:1–S2. https://doi.org/10.1186/1756-3305-2-S1-S2
2. McCall JW, Genchi C, Kramer LH, Guerrero J, Venco L. Heartworm disease in animals and humans. Adv Parasitol. 2008; 66:193–285. https://doi.org/10.1016/S0065-308X(08)00204-2
3. Eldridge BF, Edman JDI. Introduction to medical entomology. In: Eldridge BF, Edman JD, editors. Medical Entomology. Berlin: Springer; 2000. p. 1–13.
4. Khanzadeh F, Khaghaninia S, Maleki-Ravasan N, Koosha M, Oshaghi MA. Molecular detection of *Dirofilaria* spp. and host blood-meal identification in the *Simulium turgaicum* complex (Diptera: Simuliidae) in the Aras River Basin, northwestern Iran. Parasit Vectors. 2020;13:548. https://doi.org/10.1186/s13071-020-04432-4
5. Napoli E, Panarese R, La Russa F, Cambera I, Mendoza-Roldan JA, Otranto D, et al. Detection of *Dirofilaria* DNA and host blood-meal identification in *Culicoides paolae* biting-midges. Parasitology. 2022;149:948–72. https://doi.org/10.1017/S0031182022000440
6. Capelli G, Genchi C, Baneth G, Bourdeau P, Brianti E, Cardoso L, et al. Recent advances on *Dirofilaria repens* in dogs and humans in Europe. Parasit Vectors. 2018;11:663. https://doi.org/10.1186/s13071-018-3205-x
7. Fioretti DP, Diaferia M, Grelloni V, Maresca C. Canine filariosis in Umbria: an update of the occurrence one year after the first observation of autochthonous foci. Parassitologia. 2003;45:79–83.
8. Scaramozzino P, Gabrielli S, Di Paolo M, Sala M, Scholl F, Cancrini G. Dog filariosis in the Lazio region (central Italy): first report on the presence of *Dirofilaria repens*. BMC Infect Dis. 2005;5:75. https://doi.org/10.1186/1471-2334-5-75
9. Genchi C, Kramer LH. The prevalence of *Dirofilaria immitis* and *D. repens* in the Old World. Vet Parasitol. 2020; 280:108995. https://doi.org/10.1016/j.vetpar.2019.108995
10. Genchi C, Rinaldi L, Cascone C, Mortarino M, Cringoli G. Is heartworm disease really spreading in Europe? Vet Parasitol. 2005;133:137–48. https://doi.org/10.1016/j.vetpar.2005.04.009
11. Genchi C, Rinaldi L, Mortarino M, Genchi M, Cringoli G. Climate and *Dirofilaria* infection in Europe. Vet Parasitol. 2009;163:286–92. https://doi.org/10.1016/j.vetpar.2009.03.026
12. Mendoza-Roldan J, Benelli G, Panarese R, Iatta R, Furlanello T, Beugnet F, et al. *Leishmania infantum* and *Dirofilaria immitis* infections in Italy, 2009–2019: changing distribution patterns. Parasit Vectors. 2020;13:193. https://doi.org/10.1186/s13071-020-04063-9
13. Panarese R, Iatta R, Mendoza-Roldan JA, Szlosek D, Braff J, Liu J, et al. Comparison of diagnostic tools for the detection of *Dirofilaria immitis* infection in dogs. Pathogens. 2020;9:499. https://doi.org/10.3390/pathogens9060499
14. Brianti E, Panarese R, Napoli E, De Benedetto G, Gaglio G, Bezerra-Santos MA, et al. *Dirofilaria immitis* infection in the Pelagie archipelago: the southernmost hyperendemic focus in Europe. Transbound Emerg Dis. 2022;69:1274–80. https://doi.org/10.1111/tbed.14089
15. Mendoza-Roldan JA, Gabrielli S, Cascio A, Manoj RRS, Bezerra-Santos MA, Benelli G, et al. Zoonotic *Dirofilaria immitis* and *Dirofilaria repens* infection in humans and an integrative approach to the diagnosis. Acta Trop. 2021;223: 106083. https://doi.org/10.1016/j.actatropica.2021.106083
16. Keister DM, Dzimianski MT, McTier TL, McCall JW, Brown J. Dose selection and confirmation of RM 340, a new filaricide for the treatment of dogs with immature and mature *Dirofilaria immitis*. In: Sol MD, editor. Proceedings of the Heartworm Symposium '92; Austin, Texas, USA; March 7–29, 1992. p. 225–9.
17. Vezzoni A, Genchi C, Raynaud JP. Adulticide efficacy of RM340 in dogs with mild and severe natural infections. In: Proceedings of the Heartworm Symposium '92; Austin, Texas, USA; March 7–29, 1992. p. 231–240.
18. Bazzocchi C, Mortarino M, Grandi G, Kramer LH, Genchi C, Bandi C, et al. Combined ivermectin and doxycycline treatment has microfilaricidal and adulticidal activity against *Dirofilaria immitis* in experimentally infected dogs. Int J Parasitol. 2008;38:1401–10. https://doi.org/10.1016/j.ijpara.2008.03.002
19. Manoj RRS, Latrofa MS, Mendoza-Roldan JA, Otranto D. Molecular detection of *Wolbachia* endosymbiont in reptiles and their ectoparasites. Parasitol Res. 2021;120:3255–61. https://doi.org/10.1007/s00436-021-07237-1
20. Genchi M, Vismarra A, Lucchetti C, Viglietti A, Crosara S, Gnudi G, et al. Efficacy of imidacloprid 10%/moxidectin 2.5% spot on (Advocate®, Advantage Multi®) and doxycycline for the treatment of natural *Dirofilaria immitis* infections in dogs. Vet Parasitol. 2019;273:11–6. https://doi.org/10.1016/j.vetpar.2019.07.011
21. European Medicines Agency/Committee for Veterinary Medicinal Products. VICH GL9 principles of good clinical practice [cited 2023 Jun 9]. https://www.ema.europa.eu/en/documents/scientific-guideline/vich-gl9-good-clinical-practices-step-7_en.pdf
22. Genchi M, Ciuca L, Vismarra A, Ciccone E, Cringoli G, Kramer L, et al. Evaluation of alternative reagents on the performance of the modified Knott's test. Vet Parasitol. 2021;298:109555. https://doi.org/10.1016/ j.vetpar.2021.109555
23. Latrofa MS, Annoscia G, Dantas-Torres F, Traversa D, Otranto D. Towards a rapid molecular identification of the common phlebotomine sand flies in the Mediterranean region. Vet Parasitol. 2012;184:267–70. https://doi.org/10.1016/j.vetpar.2011.08.031

24. Venco L, Mihaylova L, Boon JA. Right Pulmonary Artery Distensibility Index (RPAD Index). A field study of an echocardiographic method to detect early development of pulmonary hypertension and its severity even in the absence of regurgitant jets for Doppler evaluation in heartworm-infected dogs. Vet Parasitol. 2014;206:60–6. https://doi.org/10.1016/j.vetpar.2014.08.016
25. Severini F, Toma L, Di Luca M, Romi R. Le zanzare italiane: generalità e identificazione e gli adulti (Diptera, Culicidae). Fragm Entomol. 2009;41:213–372. https://doi.org/10.4081/fe.2009.92
26. Latrofa MS, Angelou A, Giannelli A, Annoscia G, Ravagnan S, Dantas-Torres F, et al. Ticks and associated pathogens in dogs from Greece. Parasit Vectors. 2017;10:301. https://doi.org/10.1186/s13071-017-2225-2
27. Kumar A. Some considerable issues concerning malaria elimination in India. J Vector Borne Dis. 2019;56:25–31. https://doi.org/10.4103/0972-9062.257770
28. Ames MK, VanVranken P, Evans C, Atkins CE. Non-arsenical heartworm adulticidal therapy using topical moxidectin-imidacloprid and doxycycline: a prospective case series. Vet Parasitol. 2020;282:109099. https://doi.org/10.1016/j.vetpar.2020.109099
29. Ames MK, Atkins CE. Treatment of dogs with severe heartworm disease. Vet Parasitol. 2020;283:109131. https://doi.org/10.1016/j.vetpar.2020.109131
30. Grandi G, Quintavalla C, Mavropoulou A, Genchi M, Gnudi G, Bertoni G, et al. A combination of doxycycline and ivermectin is adulticidal in dogs with naturally acquired heartworm disease (*Dirofilaria immitis*). Vet Parasitol. 2010; 169:347–51. https://doi.org/10.1016/j.vetpar.2010.01.025
31. Mavropoulou A, Gnudi G, Grandi G, Volta A, Kramer LH, Quintavalla C. Clinical assessment of post-adulticide complications in *Dirofilaria immitis*-naturally infected dogs treated with doxycycline and ivermectin. Vet Parasitol. 2014;205:211–5. https://doi.org/10.1016/j.vetpar.2014.06.014
32. Kramer L, Grandi G, Passeri B, Gianelli P, Genchi M, Dzimianski MT, et al. Evaluation of lung pathology in *Dirofilaria immitis*-experimentally infected dogs treated with doxycycline or a combination of doxycycline and ivermectin before administration of melarsomine dihydrochloride. Vet Parasitol. 2011;176:357–60. https://doi.org/10.1016/j.vetpar.2011.01.021
33. McCall JW. The safety-net story about macrocyclic lactone heartworm preventives: a review, an update, and recommendations. Vet Parasitol. 2005;133:197–206. https://doi.org/10.1016/j.vetpar.2005.04.005
34. Bendas AJR, Mendes-de-Almeida F, Von Simson C, Labarthe N. Heat pretreatment of canine samples to evaluate efficacy of imidacloprid + moxidectin and doxycycline in heartworm treatment. Parasit Vectors. 2017;10:246. https://doi.org/10.1186/s13071-017-2189-2
35. Savadelis MD, Ohmes CM, Hostetler JA, Settje TL, Zolynas R, Dzimianski MT, et al. Assessment of parasitological findings in heartworm-infected beagles treated with Advantage Multi® for dogs (10% imidacloprid + 2.5% moxidectin) and doxycycline. Parasit Vectors. 2017;10:245. https://doi.org/10.1186/s13071-017-2190-9
36. McCall JW, Guerrero J, Roberts RE, Supakorndej N, Mansour AE, Dzimianski MT, et al. Further evidence of clinical prophylactic, retroactive (reach back), and adulticidal activity of monthly administration of ivermectin (Heartgard Plus™) in dogs experimentally infected with heartworms. In: Proceedings of the Heartworm Symposium '01; San Antonio, Texas, USA; April 20–22, 2001. p. 189–200.
37. Drake J, Gruntmeir J, Merritt H, Allen L, Little SE. False negative antigen tests in dogs infected with heartworm and placed on macrocyclic lactone preventives. Parasit Vectors. 2015;8:68–73. https://doi.org/10.1186/s13071-015-0698-4
38. Velasquez L, Blagburn BL, Duncan-Decoq R, Johnson EM, Allen KE, Meinkoth J, et al. Increased prevalence of *Dirofilaria immitis* antigen in canine samples after heat treatment. Vet Parasitol. 2014;206:67–70. https://doi.org/10.1016/j.vetpar.2014.03.021
39. Little SE, Munzing C, Heise SR, Allen KE, Starkey LA, Johnson EM, et al. Pre-treatment with heat facilitates detection of antigen of *Dirofilaria immitis* in canine samples. Vet Parasitol. 203:250–2. https://doi.org/10.1016/j.vetpar.2014.01.007
40. Ozella L, Cecchetti M, Pessani D. Diet of feral cats during the Scopoli's shearwater breeding season on Linosa Island, Mediterranean Sea. Ital J Zool (Modena). 2016;83:589–99. https://doi.org/10.1080/11250003.2016.1237562
41. Panarese R, Iatta R, Lia RP, Passantino G, Ciccarelli S, Gernone F, et al. Dirofilarioses in two cats in southern Italy. Parasitol Res. 2021;120:4247–51. https://doi.org/10.1007/s00436-021-07127-6

Address for correspondence: Emanuele Brianti, University of Messina, Viale Giovanni Palatucci, 98168 Messina, Italy; ebrianti@unime.it or Domenico Otranto, University of Bari Aldo Moro, strada provinciale per Casamassima km3, 70010 Valenzano, Italy; domenico.otranto@uniba.it

Prospecting for Zoonotic Pathogens by Using Targeted DNA Enrichment

Egie E. Enabulele, Winka Le Clec'h, Emma K. Roberts, Cody W. Thompson, Molly M. McDonough, Adam W. Ferguson, Robert D. Bradley, Timothy J. C. Anderson, Roy N. Platt II

More than 60 zoonoses are linked to small mammals, including some of the most devastating pathogens in human history. Millions of museum-archived tissues are available to understand natural history of those pathogens. Our goal was to maximize the value of museum collections for pathogen-based research by using targeted sequence capture. We generated a probe panel that includes 39,916 80-bp RNA probes targeting 32 pathogen groups, including bacteria, helminths, fungi, and protozoans. Laboratory-generated, mock-control samples showed that we are capable of enriching targeted loci from pathogen DNA 2,882–6,746-fold. We identified bacterial species in museum-archived samples, including *Bartonella*, a known human zoonosis. These results showed that probe-based enrichment of pathogens is a highly customizable and efficient method for identifying pathogens from museum-archived tissues.

Many serious human pathogens result from zoonotic transmission, including 61% of known human pathogens and 75% of emerging human pathogens (*1*). For example, rabies virus is transmitted by saliva of infected animals (*2*). The plague bacteria (*Yersina pestis*), the causative agent of the largest documented pandemic in human history that reduced the population of Europe by 30%–50%, was transmitted from rats to humans by fleas (*3*). Other zoonoses include Ebola virus (*4*), tularemia (*Francisella tularensis*) (*5*), and tuberculosis (*6*). The SARS-CoV-2 pandemic, thought to have a bat reservoir, has stimulated renewed emphasis on zoonotic pathogen surveillance (*7*,*8*).

Natural history museums are repositories of biologic information in the form of voucher specimens that represent a major, underused resource for studying zoonotic pathogens (*9*–*13*). Originally, specimens were archived as dried skin and skeletal vouchers or preserved in fluids (ethanol) after fixation with formalin or formaldehyde. Now, best practices include preserving specimens and associated soft tissues in liquid nitrogen (−190°C) or mechanical freezers (−80°C) from the time they are collected (*14*). Those advances in preservation make it possible to extract high-quality DNA and RNA that can be used for pathogen surveillance. For example, retroactive sampling of archived tissues from the US Southwest found that Sin Nombre virus, a New World hantavirus, was circulating in wild rodent populations almost 20 years before the first human cases were reported (*15*).

It is critical to develop a range of tools for extracting pathogen information from museum-archived samples. Targeted sequencing using probe enrichment has become the tool of choice for medical genomics (*16*), population genetics (*17*), phylogenetics (*18*), and ancient DNA (*19*,*20*). Those methods are designed to enrich small amounts of DNA target from a background of contaminating DNA. Probe-based, targeted sequencing has been used to enrich pathogens from complex host–pathogen DNA mixtures (*21*). For example, Keller et al. used probes to capture and sequence complete *Y. pestis* genomes from burial sites >1,500 years old (*22*). Enrichment is frequently achieved by designing a panel of probes to specifically target a handful of pathogens of interest (*23*,*24*). Similarly, commercial probe sets are available for many types of viruses and human pathogens (*23*–*25*). However, many of these probe sets are limited to specific pathogens that might not infect other host species.

Our goal was to develop a panel of biotinylated baits, or probes, to identify the eukaryotic and bacterial pathogens responsible for 32 major zoonoses (Table 1). We aimed to capture both known and related pathogens, using the fact that probes can capture sequences that are ≤10% divergent. To perform this

Author affiliations: Texas Biomedical Research Institute, San Antonio, Texas, USA (E.E. Enabulele, W. Le Clec'h, T.J.C. Anderson, R.N. Platt II); Texas Tech University, Lubbock, Texas, USA (E.K. Roberts, R.D. Bradley); University of Michigan, Ann Arbor, Michigan, USA (C.W. Thompson); Chicago State University, Chicago, Illinois, USA (M.M. McDonough); Field Museum of Natural History, Chicago (A.W. Ferguson)

DOI: https://doi.org/10.3201/eid2908.221818

capture, we used a modified version of the ultraconserved element (UCE) targeted sequencing technique (*26*,*27*) to specifically enrich pathogen DNA. Biotinylated baits are designed to target conserved genomic regions among diverse groups of pathogens (Figure 1). The baits are hybridized to a library potentially containing pathogen DNA. Bait-bound DNA fragments are enriched during a magnetic bead purification step before sequencing (Figure 2). The final library contains hundreds or thousands of orthologous loci with single-nucleotide variants or indels from the targeted pathogen groups that can then be used for population or phylogenetic analyses.

Methods

We have compiled a detailed description of the methods used (Appendix 1, https://wwwnc.cdc.gov/EID/article/29/8/22-1818-App1.pdf; https://doi.org/10.17504/ protocols.io.5jyl8jnzrg2w/v1). Code is available on GitHub (https://www.github.com/nealplatt/pathogen_probes; https://doi.org/10.5281/zenodo.7319915). Raw sequence data are available from the National Center for Biotechnology Information (BioProject PRJNA901509; Appendix 2, https://wwwnc.cdc.gov/EID/article/29/8/22-1818-App2.xlsx). A summary of our methods follows.

Panel Development

We developed a panel of baits for targeted sequencing of 32 zoonotic pathogens. To develop this panel, we used the Phyluce version 1.7.1 (*26*,*27*) protocol to design baits for conserved loci within each pathogen group. First, we simulated and mapped reads from each species within a pathogen group to a focal genome assembly (Table 1; Figure 1, panel A). We used the mapped reads to identify putative orthologous loci that were >80% similar across the group and generated in silico baits from the focal genome (Figure 1, panel B). These baits were mapped back to each member (Figure 1, panel C) to identify single-copy orthologs within the group. Next, we designed 2 overlapping 80-bp baits from loci in each member of the group (Figure 1, panel D) and removed baits with >95% sequence similarity (Figure 1, panel E). We repeated those steps for each pathogen group (Figure 1, panel F). We compared the remaining baits with mammalian genomes and replaced them to minimize

Table 1. Zoonotic pathogens targeted for DNA enrichment in study of prospecting for zoonotic pathogens by using targeted DNA enrichment

Pathogen group	Taxonomic level	Focal pathogen	Zoonoses
Anaplasma	Genus	*Anaplasma phagocytophilum*	Anaplasmosis
Apicomplexa	Phylum	*Plasmodium falciparum*	Malaria
Bacillus cereus group*	Species group	*Bacillus anthracis*	Anthrax
Bartonella	Genus	*Bartonella bacilliformis*	Cat-scratch fever
Borrelia	Genus	*Borrelia burgdorferi*	Lyme disease
Burkholderia	Genus	*Burkholderia mallei*	Glanders
Campylobacter	Genus	*Campylobacter jejuni*	Campylobacteriosis
Cestoda	Class	*Taenia multiceps*	Taeniasis
Chlamydia	Genus	*Chlamydia trachomatis*	Chlamydia
Coxiella	Genus	*Coxiella burnetii*	Q fever
Ehrlichia	Genus	*Ehrlichia canis*	Ehrlichiosis
Eurotiales	Order	*Talaromyces marneffei*	Talaromycosis
Francisella	Genus	*Francisella tularensis*	Tularemia
Hexamitidae	Family	*Giardia intestinalis*	Giardiasis
Kinetoplastea	Class	*Leishmania major*	Leishmaniasis
Leptospira	Genus	*Leptospira interrogans*	Leptospirosis
Listeria	Genus	*Listeria monocytogenes*	Listeriaosis
Mycobacterium	Genus	*Mycobacterium tuberculosis*	Tuberculosis
Nematodes (clade I)	Phylum (clade)	*Trichinella spiralis*	Trichinosis
Nematodes (clade III)	Phylum (clade)	*Brugia malayi*	Filariasis
Nematodes (clade IVa)	Phylum (clade)	*Strongyloides stercoralis*	Strongyloidiasis
Nematodes (clade IVb)	Phylum (clade)	*Steinernema carpocapsae*	None
Nematodes (clade V)	Phylum (clade)	*Haemonchus contortus*	None
Onygenales	Order	*Histoplasma capsulatum*	Histoplasmosis
Pasteurella	Genus	*Pasteurella multocida*	Pasteurellosis
Rickettsia	Genus	*Rickettsia rickettsii*	Typhus
Salmonella	Genus	*Salmonella enterica*	Salmonellosis
Streptobacillus	Genus	*Streptobacillus moniliformis*	Rat-bite fever
Trematoda	Class	*Schistosoma mansoni*	Schistosomiasis
Tremellales	Order	*Cryptococcus neoformans*	Cryptococcosis
*Trypanosoma**	Genus	*Trypanosoma cruzi*	Sleeping sickness
Yersinia	Genus	*Yersinia pestis*	Plague

*Supplemented with additional probes/baits.

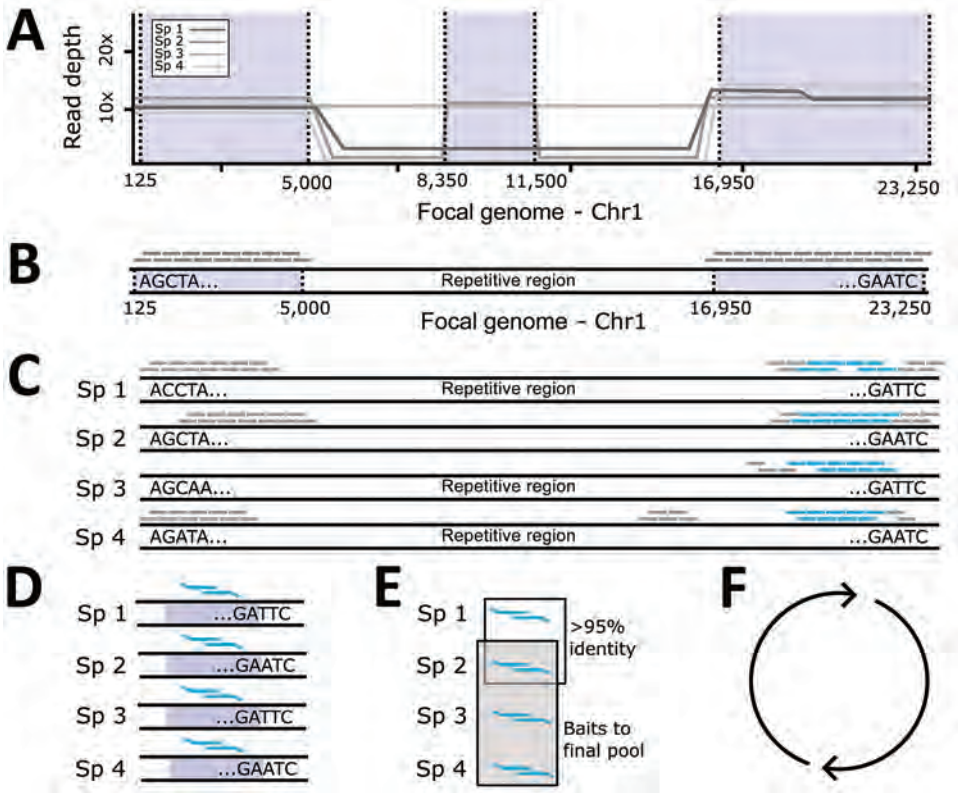

Figure 1. Probe panel design for study of prospecting for zoonotic pathogens by using targeted DNA enrichment. A) Simulated reads from each pathogen within a group were mapped back to a single focal genome. B) We identified regions with consistent coverage from each member of the pathogen group to identify putative, orthologous loci and generated a set of in silico probes from the focal genome. C) Those in silico probes were then mapped back to the genomes of each member in the pathogen group to find single copy, orthologous regions, present in most members. D, E) We designed 2 overlapping 80-bp baits to target the loci in each member of the pathogen group (D) and compared them with each another to remove highly similar probes (E). One probe was retained from each group of probes with high sequence similarity (>95%). F) We identified the probes necessary to capture 49 loci in that pathogen group. This process was repeated for the next pathogen group. Finally, all probes were combined together into a single panel. Chr, chromosome; Sp, specimen.

cross-reactivity with the host. Finally, we combined baits to capture 49 loci from each pathogen group into a panel that was synthesized by Daicel Arbor Biosciences (https://arborbiosci.com).

Museum-Archived and Control Samples

We extracted DNA from 38 museum samples by using the DNeasy Kit (QIAGEN, https://www.qiagen.com) (Table 2). We generated control samples

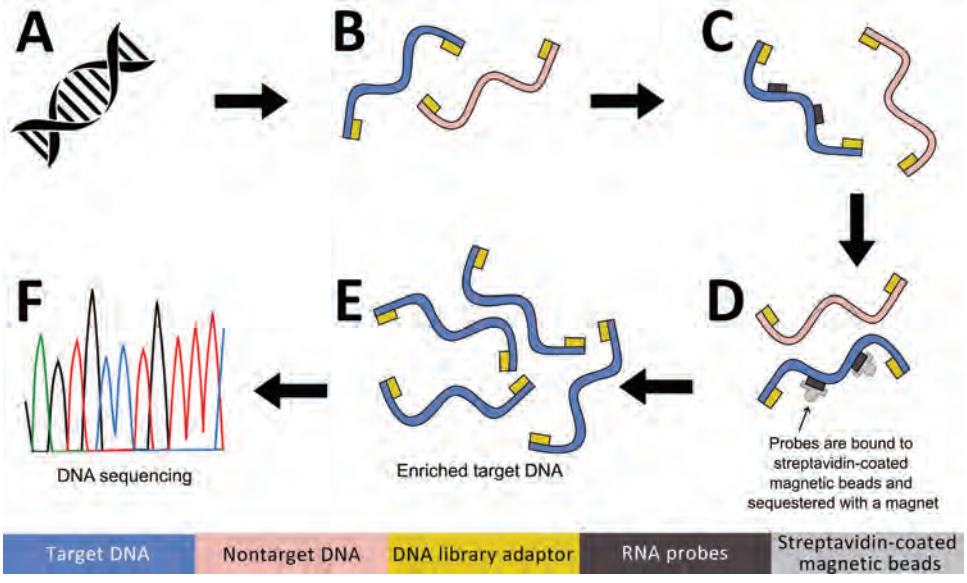

Figure 2. Targeted DNA enrichment workflow for study of prospecting for zoonotic pathogens by using targeted DNA enrichment. A) Genomic DNA extracted using the DNeasy Kit (QIAGEN, https://www.qiagen.com). B) Next-generation sequencing libraries prepared using KAPA Hyperplus Kit (https://www.biocompare.com) and barcoding each library with IDT xGen Stubby Adaptor-UDI Primers (https://www.idtdna.com). C) RNA probes hybridization using the high sensitivity protocol of myBaits version 5. (https://arborbiosci.com). D) Probes bound to streptavidin-coated magnetic beads and sequestered with a magnet (E) 15 cycles PCR amplification of enriched libraries. F) Libraries sequenced on an Illumina Hi-Seq 2500 platform (https://www.illumina.com).

by spiking naive mouse DNA with 1% microorganism DNA from *Mycobacterium bovis*, *M. tuberculosis*, *Plasmodium vivax*, *P. falciparum*, and *Schistosoma mansoni*. We then further diluted an aliquot of this 1% pathogen mixture into mouse DNA to create a 0.001% host–pathogen mixture. This range was designed to test the lower limits of detection but also represent a reasonable host–pathogen proportion. For example, *Theileria parva*, a tick-transmitted apicomplexan, is present in samples from 0.9% through 3% (*28*), and 1.5% of DNA sequence reads in clinical blood samples is from *P. vivax* (*29*).

Library Preparation

We generated standard DNA sequencing libraries from 500 ng of DNA per sample. We combined

Table 2. Specimens examined using targeted sequencing in study of prospecting for zoonotic pathogens by using targeted DNA enrichment*

Museum accession no.	Source species (common name)	Locality, country: state, county	Date	SRA ID
TK48533	*Myotis volans* (long-legged myotis)	Mexico: Durango, Arroyo El Triguero	1995 May 18	SAMN31718202
TK49668	*Didelphis virginiana* (Virginia opossum)	United States: Texas, Kerr	1996 May 14	SAMN31718203
TK49674	*Peromyscus attwateri* (Texas mouse)	United States: Texas, Kerr	1996 May 14	SAMN31718204
TK49686	*Peromyscus laceianus* (deer mouse)	United States: Texas, Kerr	1996 May 14	SAMN31718205
TK49712	*Dasypus novemcinctus* (nine-banded armadillo)	United States: Texas, Kerr	1996 May 16	SAMN31718206
TK49732	*Lasiurus borealis* (eastern red bat)	United States: Texas, Kerr	1996 May 17	SAMN31718207
TK49733	*Myotis velifer* (vesper bat)	United States: Texas, Kerr	1996 May 16	SAMN31718208
TK57832	*P. attwateri*	United States: Texas, Kerr	1997 May 14	SAMN31718209
TK70836	*Desmodus rotundus* (common vampire bat)	Mexico: Durango, San Juan de Camarones	1997 Jun 27	SAMN31718210
TK90542	*Sigmodon hirsutus* (southern cotton rat)	Mexico: Chiapas, Comitán	1999 Jul 9	SAMN31718211
TK93223	*Peromyscus melanophrys* (plateau mouse)	Mexico: Oaxaca, Las Minas	2000 Jul 13	SAMN31718212
TK93289	*Carollia subrufa* (gray short-tailed bat)	Mexico: Chiapas, Ocozocoautla	2000 Jul 16	SAMN31718213
TK93402	*Chaetodipus eremicus* (Chihuahan pocket mouse)	Mexico: Coahuila	2000 Jul 22	SAMN31718214
TK101275	*Glossophaga commissarisi* (Commissaris' long-tongued bat)	Honduras: Comayagua, Playitas	2001 Jul 10	SAMN31718215
TK136205	*Heteromys desmarestianus* (Desrmarest's spiny pocket mouse)	Honduras: Atlantida, Jardin Botanico Lancetilla	2004 Jul 16	SAMN31718216
TK136222	*Peromyscus mexicanus* (Mexican deer mouse)	Honduras: Colon, Trujillo	2004 Jul 17	SAMN31718217
TK136228	*H. desmarestianus*	Honduras: Colon, Trujillo	2004 Jul 17	SAMN31718218
TK136240	*Glossophaga soricine* (Pallas's long-tongued bat)	Honduras: Colon, Trujillo	2004 Jul 16	SAMN31718219
TK136756	*Eptesicus furinalis* (Argentine brown bat)	Honduras: Colon, Trujillo	2004 Jul 17	SAMN31718220
TK136783	*Glossophaga leachii* (gray long-tongued bat)	Honduras: Colon, Trujillo	2004 Jul 17	SAMN31718221
TK148935	*Rhogeessa tumida* (back-winged little yellow bat)	Mexico: Tamaulipas, Soto la Marina	2008 Jul 27	SAMN31718222
TK148943	*M. velifer*	Mexico: Tamaulipas, Soto la Marina	2008 Jul 27	SAMN31718223
TK150290	*Balantiopteryx plicata* (gray sac-winged bat)	Mexico: Michoacan, El Marqués	2006 Jul 22	SAMN31718224
TK154677	*Gerbilliscus leucogaster* (bushveld gerbil)	Botswana: Ngamiland, Koanaka Hills	2008 Jun 29	SAMN31718225
TK154685	*G. leucogaster*	Botswana: Ngamiland, Koanaka Hills	2008 Jun 29	SAMN31718226
TK154687	*G. leucogaster*	Botswana: Ngamiland, Koanaka Hills	2008 Jun 29	SAMN31718227
TK164683	*Mastomys natalensis* (Natal multimammate mouse)	Botswana: Ngamiland, Koanaka Hills	2009 Jul 18	SAMN31718228
TK164686	*M. natalensis*	Botswana: Ngamiland, Koanaka Hills	2009 Jul 18	SAMN31718229
TK164689	*M. natalensis*	Botswana: Ngamiland, Koanaka Hills	2009 Jul 18	SAMN31718230
TK164690	*M. natalensis*	Botswana: Ngamiland, Koanaka Hills	2009 Jul 18	SAMN31718231
TK164702	*M. natalensis*	Botswana: Ngamiland, Koanaka Hills	2009 Jul 19	SAMN31718232
TK164714	*M. natalensis*	Botswana: Ngamiland, Koanaka Hills	2009 Jul 19	SAMN31718233
TK164728	*M. natalensis*	Botswana: Ngamiland, Koanaka Hills	2009 Jul 19	SAMN31718234
TK166246	*P. attwateri*	United States: Texas, Kerr	2010 May 17	SAMN31718235
TK179690	*P. attwateri*	United States: Texas, Kerr	2013 May 20	SAMN31718236
TK185677	*P. attwateri*	United States: Texas, Kerr	2018 May 21	SAMN31718237
TK197046	*P. attwateri*	United States: Texas, Kerr	2016 May 26	SAMN31718238
TK199855	*P. attwateri*	United States: Texas, Kerr	2019 May 21	SAMN31718239

*ID, identification; SRA, National Center for Biotechnology Information Sequence Read Archive.

individual libraries with similar DNA concentrations into pools of 4 samples and used the myBaits version 5 (Daicel Arbor Biosciences) high sensitivity protocol to enrich target loci. We used 2 rounds of enrichment (24 h at 65°C), washed away unbound DNA, and amplified the remainder for 15 cycles before pooling for sequencing.

Classifying Reads

First, we generated a dataset of target loci by mapping the probes to representative and reference genomes in RefSeq v212 with BBMap v38.96 (*30*). For each probe, we kept the 10 best sites that mapped with ≥85% sequence identity along with 1,000 bp upstream and downstream. These sequences were combined into a database to classify reads by using Kraken2 version 2.1.1 (*31*) (Figure 3, panel A). Next, we extracted pathogen reads with KrakenTools version 1.2 (https://github.com/jenniferlu717/KrakenTools). We assembled those reads (Figure 3, panel B) with the SPAdes genome assembler version 3.14.1 (*32*) and filtered them to remove low quality contigs (<100 bp and <10× median coverage). We removed samples that had <2 contigs from downstream analyses. During this time, we extracted target loci in available reference genomes (Figure 3, panel C). Next, we identified (Figure 3, panel D), aligned and trimmed (Figure 3, panel E) orthologs before concatenating them into a single alignment (Figure 3, panel F). Finally, we generated and bootstrapped a phylogenetic tree (Figure 3, panel G) by using RaxML-NG version 1.0.1 (*33*). We repeated those steps for each pathogen group (Figure 3, panel H).

Host Identification

There were sufficient mtDNA sequences from most samples to verify museum identifications by comparing reads to a Kraken2 version 2.1.2 (*31*) database of mammalian mitochondrial genomes. We filtered the classifications by removing samples with <50 classified reads and single-read, generic classifications.

Results

Panel Development

We used the ultraconserved element protocol developed by Faircloth et al. (*26*,*27*) to develop a set of 39,893 biotinylated baits that target 32 pathogen groups responsible for 32 zoonoses. Each pathogen group is targeted at 49 loci with a few diverse taxa, *Bacillus cereus* and *Trypanosoma* species, targeted at 98 loci. We complied information on pathogen groups, focal taxa, genome accessions, and number of baits (Table 3).

Control Samples

We tested the efficacy of our bait set on laboratory-made host–pathogen mixtures containing DNA from

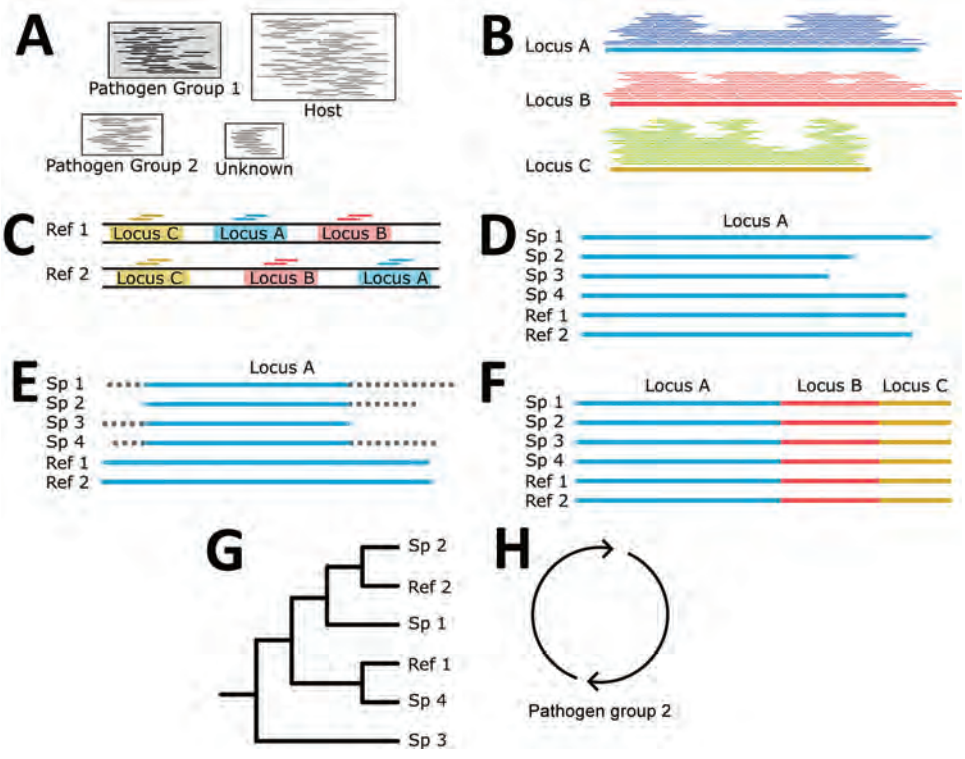

Figure 3. Building phylogenies from parasite reads for study of prospecting for zoonotic pathogens by using targeted DNA enrichment. A) After read classification, we extracted all the reads associated with a pathogen group. B) Those reads were assembled into contigs with a genome assembler. C) Simultaneously, we identified and extracted the target loci from all members of the pathogen group with available reference genomes to ensure that our final phylogeny has representatives from as many members of the pathogen group as possible. D, E) For each targeted locus, we combined the assembled contigs (D) and genome extracted loci for (E) multiple sequence alignment and trimming. F, G) Each aligned and trimmed locus is concatenated together (F) for phylogenetic analyses (G). H) If necessary, those steps are repeated for reads classified in other pathogen groups. Ref, reference; Sp, specimen.

Table 3. Summary of probes developed for targeted capture of pathogen DNA in study of prospecting for zoonotic pathogens by using targeted DNA enrichment

Pathogen group	Type	Probe count	Locus count	RefSeq genome count	Focal pathogen	GenBank accession no.
Anaplasma	Bacteria	368	49	57	*Anaplasma phagocytophilum*	GCF000013125
Apicomplexa	Eukaryote	3,219	49	64	*Plasmodium falciparum*	GCA000002765
Bacillus cereus group*	Bacteria	833	98	134	*Bacillus anthracis*	GCF000008165
Bartonella	Bacteria	1,812	49	31	*Bartonella bacilliformis*	GCF000015445
Borrelia	Bacteria	688	49	16	*Borreliella burgdorferi*	GCF000502155
Burkholderia	Bacteria	683	49	39	*Burkholderia mallei*	GCF000011705
Campylobacter	Bacteria	2,194	49	33	*Campylobacter jejuni*	GCF000009085
Cestoda	Eukaryote	907	49	18	*Taenia multiceps*	GCA001923025
Chlamydia	Bacteria	830	49	15	*Chlamydia trachomatis*	GCF000008725
Coxiella	Bacteria	144	49	70	*Coxiella burnetii*	GCF000007765
Ehrlichia	Bacteria	235	49	7	*Ehrlichia canis*	GCF000012565
Eurotiales	Eukaryote	4,097	49	158	*Talaromyces marneffei*	GCF000001985
Francisella	Bacteria	470	49	14	*Francisella tularensis*	GCF000008985
Hexamitidae	Eukaryote	782	49	19	*Giardia intestinalis*	GCA000002435
Kinetoplastea	Eukaryote	2,917	49	49	*Leishmania major*	GCF000002725
Leptospira	Bacteria	2,517	49	69	*Leptospira interrogans*	GCF000092565
Listeria	Bacteria	765	49	23	*Listeria monocytogenes*	GCF000196035
Mycobacterium	Bacteria	2,463	49	86	*Mycobacterium tuberculosis*	GCF000195955
Nematodes, clade I	Eukaryote	357	49	13	*Trichinella spiralis*	GCA000181795
Nematodes, clade III	Eukaryote	1,494	49	25	*Brugia malayi*	GCA000002995
Nematodes, clade IVa	Eukaryote	252	49	7	*Strongyloides stercoralis*	GCA000947215
Nematodes, clade IVb	Eukaryote	1,487	43	34	*Steinernema carpocapsae*	GCA000757645
Nematodes, clade V	Eukaryote	3,242	48	47	*Haemonchus contortus*	GCA007637855
Onygenales	Eukaryote	1,973	49	38	*Histoplasma capsulatum*	GCF000149585
Pasteurella	Bacteria	615	49	11	*Pasteurella multocida*	GCF000754275
Rickettsia	Bacteria	394	49	37	*Rickettsia rickettsii*	GCF001951015
Salmonella	Bacteria	145	49	35	*Salmonella enterica*	GCF001159405
Streptobacillus	Bacteria	245	49	7	*Streptobacillus moniliformis*	GCF000024565
Trematoda	Eukaryote	924	49	18	*Schistosoma mansoni*	GCA000237925
Tremellales	Eukaryote	1,999	49	26	*Cryptococcus neoformans*	GCF000091045
Trypanosoma*	Eukaryote	617	97	10	*Trypanosoma cruzi*	GCF000209065
Yersinia	Bacteria	225	49	22	*Yersinia pestis*	GCF000009065

*Supplemented.

Mus musculus, *Mycobacterium tuberculosis*, *Plasmodium falciparum*, *P. vivax*, and *Schistosoma mansoni*. We generated 4 control samples containing either 1% or 0.001% pathogen DNA that was enriched or not enriched. We classified reads against the database of target loci and found that 42.7% of all reads (*Mycobacterium* = 13.1%, *Plasmodium* = 28.1%, *Schistosoma* = 1.5%) were from control pathogens in the 1% enriched control sample. However, only 0.03% of the corresponding 1% unenriched control was from target loci. Aside from the raw percentages, we compared the coverage of each probed region in the 1% enriched and unenriched control samples (Figure 4, panels B–D) to understand how enrichment effected coverage at each locus. Mean coverage per *Mycobacterium* locus increased from 0.14× to 944.5× (6,746-fold enrichment), 0.53× to 1,527.4× for *Plasmodium* loci (2,882-fold enrichment), and 0.02× to 117.9× (5,895-fold enrichment) for schistosome loci. Because the sequencing library from the 0.001% unenriched sample did not work during the sequencing reaction, we do not have a baseline to examine enrichment in the 0.001% samples.

We extracted reads assigned to each pathogen group and assembled and aligned them with target loci extracted from reference genomes of closely related species by using tools from Phyluce version 1.7.1 (*26*,*27*). We were able to assemble 0–23 target loci per pathogen group in the control samples (Table 4). Assembled loci varied in size from 109 to 1,991 bp (median 636.5 bp). For each sample/group with >2 loci captured, we generated a phylogenetic tree along with other members of the taxonomic group (Figure 5). In each case, pathogen loci from the control samples were sister groups to the appropriate reference genome with strong bootstrap support. For example, the *Schistosoma* loci assembled from the 1% enriched control sample were sister to the *S. mansoni* genome (GCA000237925) in 100% of bootstrap replicates.

Museum Samples

Next, we tested our bait set on museum-archived tissues. We generated 649.3 million reads across all 38 samples (mean 17.1 million reads/sample). An initial classification showed that, on average, 4.3% of reads

were assignable to loci in the database. Those reads were designated to 93 genera. However, 78 of those genera were at low frequency (≤1,000 reads/sample) (Figure 4). Many of the low frequency hits are likely the result of bioinformatic noise. *Bartonella* and *Plasmodium* species were the most common genera; each was present in 36 of 38 museum samples. The distribution of *Bartonella* reads was strongly bimodal

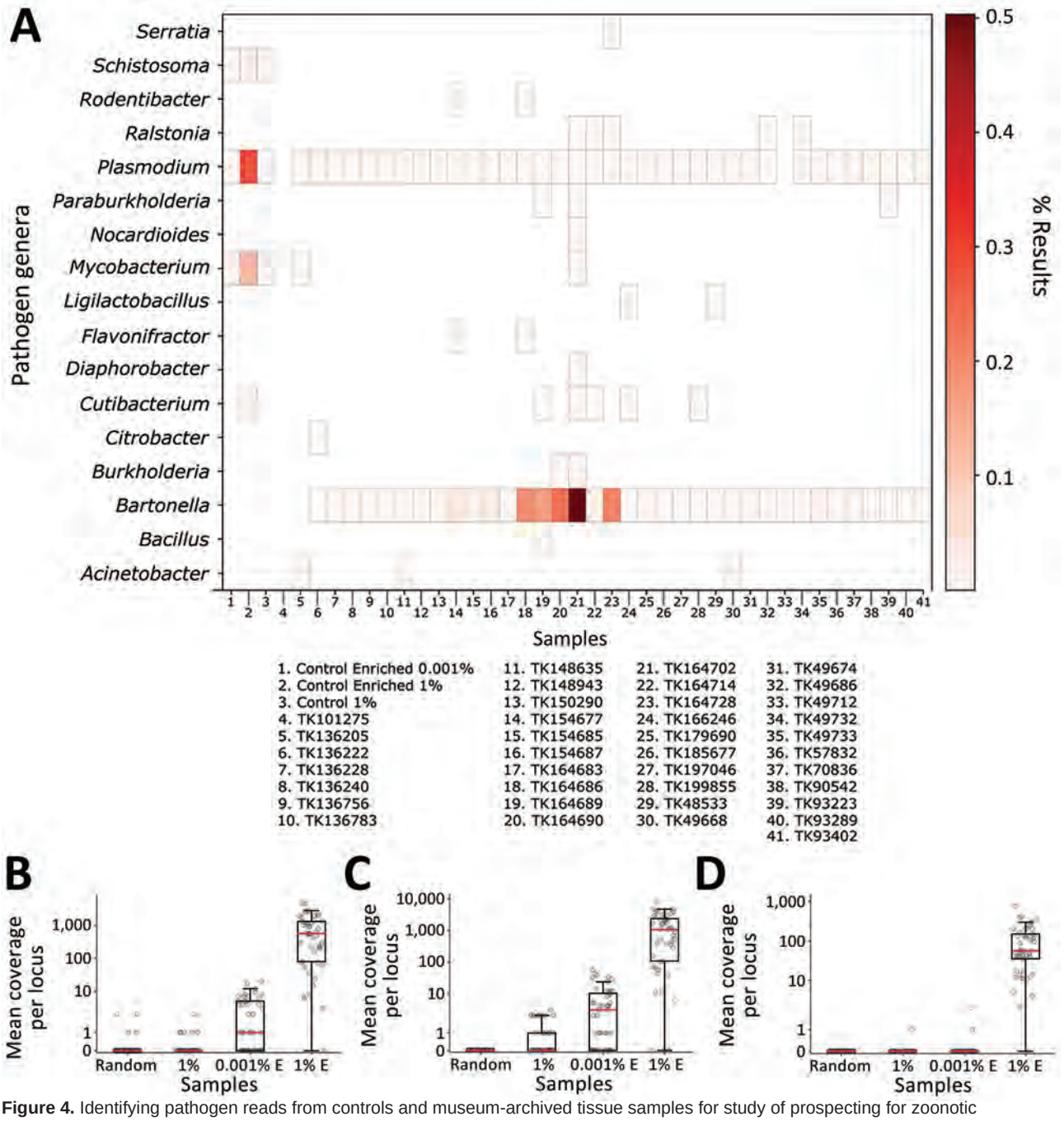

Figure 4. Identifying pathogen reads from controls and museum-archived tissue samples for study of prospecting for zoonotic pathogens by using targeted DNA enrichment. Control reads are indicated by the percentage of pathogen DNA 1% or 0.001%. A) Reads were compared with a database of target loci and assigned a taxonomic classification based on these results. Reads were assigned to 93 genera; of those, 17 (shown) were present in >1 sample, including controls, with ≥1,000 reads. A heatmap of those results shows the relative proportion of reads assigned to each genus. Details of samples are provided in Table 2. B–D) Coverage at each probed locus is shown across all control samples for Mycobacterium (B), Plasmodium (C), and Schistosoma (D). Each point in the chart is coverage calculated at a single target locus. Horizontal lines within boxes indicate medians, box tops and bottoms indicate lower and upper quartiles, and whiskers represent minimum and maximum values, excluding outliers. Each sample is indicated with a circle. E, enriched.

Table 4. Parasite reads identified in and loci assembled from control samples

Enriched	Pathogen concentration, %	Total reads	*Schistosoma*		*Plasmodium*		*Mycobacterium*	
			Reads	Loci	Reads	Loci	Reads	Loci
True	0.001	509,672	3	0	168	7	556	0
True	1	398,469	5,879	23	52,274	8	112,141	23
False	1	375,786	15	0	17	0	83	0

such that 18 samples had <12 reads and 18 samples had >1,000 reads (median 552 reads/sample). In 5 samples, the percentage of *Bartonella* reads was exceedingly high (>10%). In comparison, the median number of *Plasmodium* reads never exceeded 0.04% of reads from a single museum sample (mean 158.5 reads/sample).

We used phylogenetic analyses and rules of monophyly to identify putative pathogens to species or strain for each of the 15 genera with ≥1,000 reads (Figure 4, panel A). We were unable to assemble >1 target locus for any specimen in 13 genera. We were able to assemble 3–20 loci (mean 8 loci/sample) from 16 samples containing *Bartonella* (Figure 6), 3 loci from a sample containing *Paraburkholderia* reads (Figure 7), and 8 loci from a sample containing *Ralstonia* reads (Figure 8).

Host Identification

We compared reads from each sample to a database of mitochondrial genomes to identify the host. In general, reads from the mitochondria comprised a small proportion (≤1%, mean 0.04%) of each sample (Figure 9). Despite the low number of mitochondrial reads, generic classifications from the mitochondrial database coincided with the museum identifications after filtering samples with ≤50 mitochondrial reads. For the remaining samples, the correct genus was identified by >85% (mean 98%) of reads from that sample. Classifying reads less than the generic level is limited by mitochondrial genome availability, but where possible, we were able to confirm museum identifications at the species level.

Discussion

We developed a set of 39,893 biotinylated baits for targeted sequencing of >32 zoonotic pathogens, and their relatives, from host DNA samples. To test the efficacy of the bait panel, we used 4 control samples that contained either 1% or 0.001% pathogen DNA and further subdivided into pools that were enriched and unenriched. Our results (Figure 4) showed a

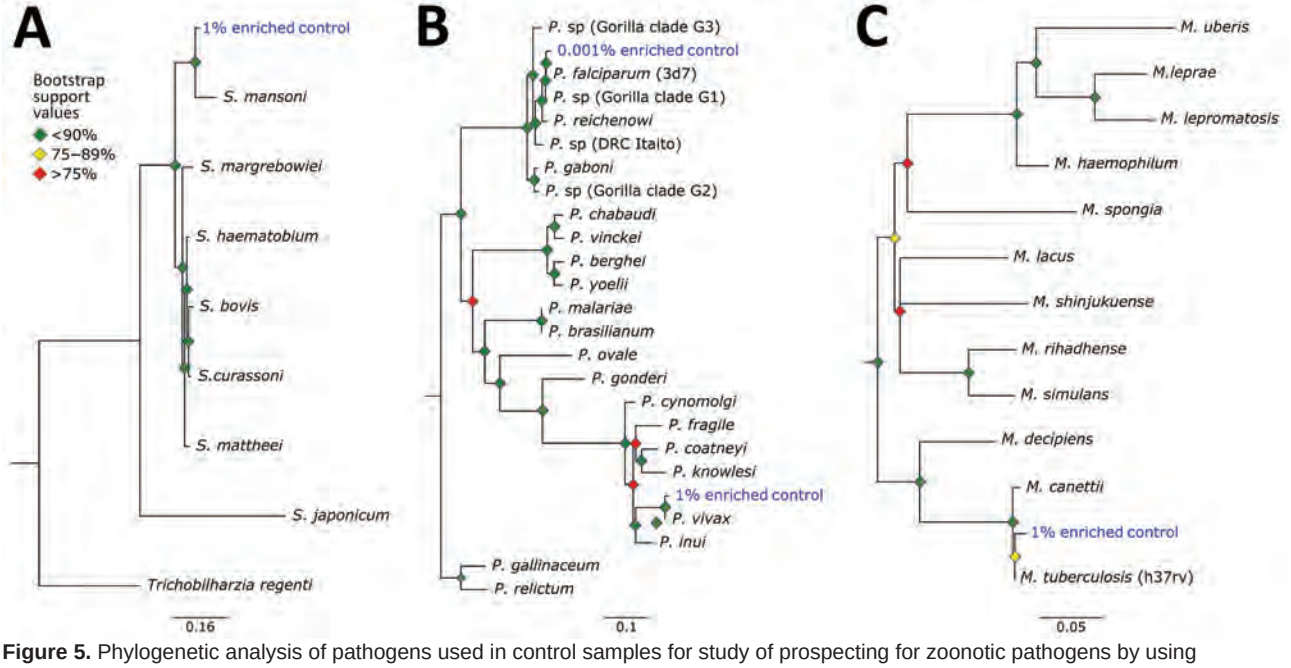

Figure 5. Phylogenetic analysis of pathogens used in control samples for study of prospecting for zoonotic pathogens by using targeted DNA enrichment. A) *Schistosoma*; B) *Plasmodium*; C) *Mycobacterium*. Reads from each control pathogen (*M. tuberculosis*, *P. falciparum*, *P. vivax*, and *S. mansoni*) were extracted, assembled, aligned, and trimmed for maximum-likelihood phylogenetic analyses. The phylogenies were used to identify the species or strain of pathogen used in the controls. Blue indicates control samples. Bootstrap support values are indicated by colored diamonds at each available node. Branches with <50% bootstrap support were collapsed. Nodal support is indicated by color coded diamonds. Scale bars indicate nucleotide substitutions per site. Assembly accession numbers (e.g., GCA902374465) and tree files are available from https://doi.org/10.5281/zenodo.8014941.

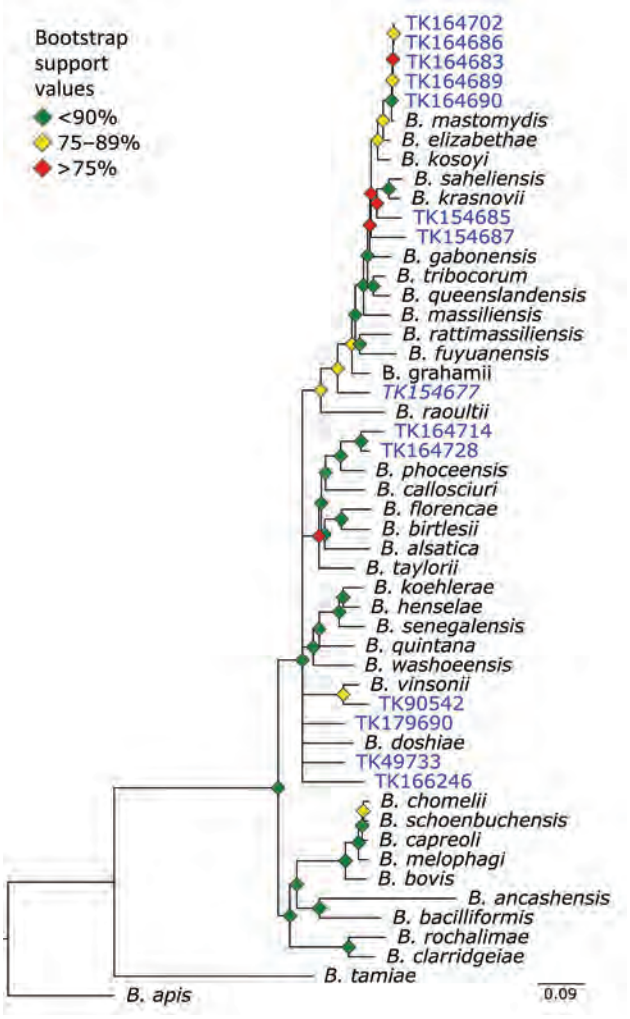

Figure 6. Phylogenetic analysis of *Bartonella* using museum archived samples in study of prospecting for zoonotic pathogens by using targeted DNA enrichment. Blue indicates museum archived samples; museum accession numbers are given (Table 1). Branches with <50% bootstrap support were collapsed. Nodal support is indicated by color coded diamonds. Scale bar indicates nucleotide substitutions per site. Assembly accession numbers (e.g., CA902374465) and tree files are available from https://doi.org/10.5281/zenodo.8014941.

large increase of pathogen DNA in the 1% enriched sample when compared with its unenriched counterpart. Specifically, enrichment increased the amount of pathogen DNA from 0.03% to 42.1%.

We were able to generate phylogenetically informative loci from *Plasmodium*, *Mycobacterium*, and *Schistosoma* species in the 1% enriched control sample. On the basis of genome size, we estimate genome copies as 91,611 for *Plasmodium*, 261,030 for *Mycobacterium*, and 3,159 for *Schistosoma* in the control sample. This finding indicates that the probe set is able to detect these pathogens from even a few thousand genome copies per sample (*Schistosoma* species). In contrast, we were only able to generate phylogenetically informative loci from *P. falciparum* in 0.001% enriched sample, which would hypothetically contain ≈39 genome copies. This finding implies that the bait set might be capable of identifying pathogens present in samples with only a few hundred genome copies. However, there are limitations to *Plasmodium* detection that should be considered.

In each sample, reads were detected from only a few loci rather than from the entire genome. For example, in the 1% enriched sample, 5,879 of the 398,469 reads came from 32 loci totaling 19.6 kb. Had the unenriched sample contained the same number of reads, randomly distributed across the genome, it would have amounted to 1 read every 62 kb. We found that enrichment increased coverage at probed loci from 0.23× to 863.3×, a 3,732.3-fold increase when averaged across all pathogens/loci (Figure 4). Those results show that although large amounts of host DNA might remain in a sample, the targeted loci are greatly enriched.

We tested the panel of baits on 38, museum-archived, small mammal samples without previous knowledge of infection history. Reads from these samples were initially designated to 93 different genera, but most of these genera contained a limited number of reads. For example, almost half of the 93 genera (n = 43) were identified on the basis of a single read across all 38 samples, most likely a bioinformatic artifact. We identified 15 genera in which 1 sample had ≥1,000 reads. For each of these 15 genera, we extracted any reads classified within the same family (e.g., genus *Bartonella*, family Bartonellaceae) and assembled, aligned, and trimmed them for phylogenetic analyses. In most cases, the reads failed the assembly step (n = 6), were filtered on the basis of locus size or coverage (n = 5), or assembled into multiple loci that were not targeted by our bait set (n = 2); we did not pursue those reads any further. However, we were able to generate phylogenies for specimens positive for *Bartonella*, *Ralstonia*, and *Paraburkholderia* species.

Bartonella is a bacterial genus responsible for cat-scratch disease, Carrión's disease, and trench fever (*34*). Transmission often occurs between humans and their pets or from infected fleas ticks, or other arthropod vectors (*35*). We were able to recover target loci for 14 of 36 specimens. A phylogeny of *Bartonella* species placed the museum samples in multiple clades (Figure 6). For example, 5 specimens formed a monophyletic clade sister to *B. mastomydis*. *B. mastomydis* recently was described from *Mastomys erythroleucus* mice collected in Senegal (*36*). Appropriately, the

samples we tested were collected from *M. natalensis* mice from Botswana (Table 2). Another clade contained *B. vinsonii* and a *Sigmodon* rat (TK90542) collected in Mexico. Zoonotic transmission of *B. vinsonii* has been implicated in neurologic disorders (*37*). Other museum samples probably contain novel *Bartonella* species/strains or at least represent species/strains without genomic references.

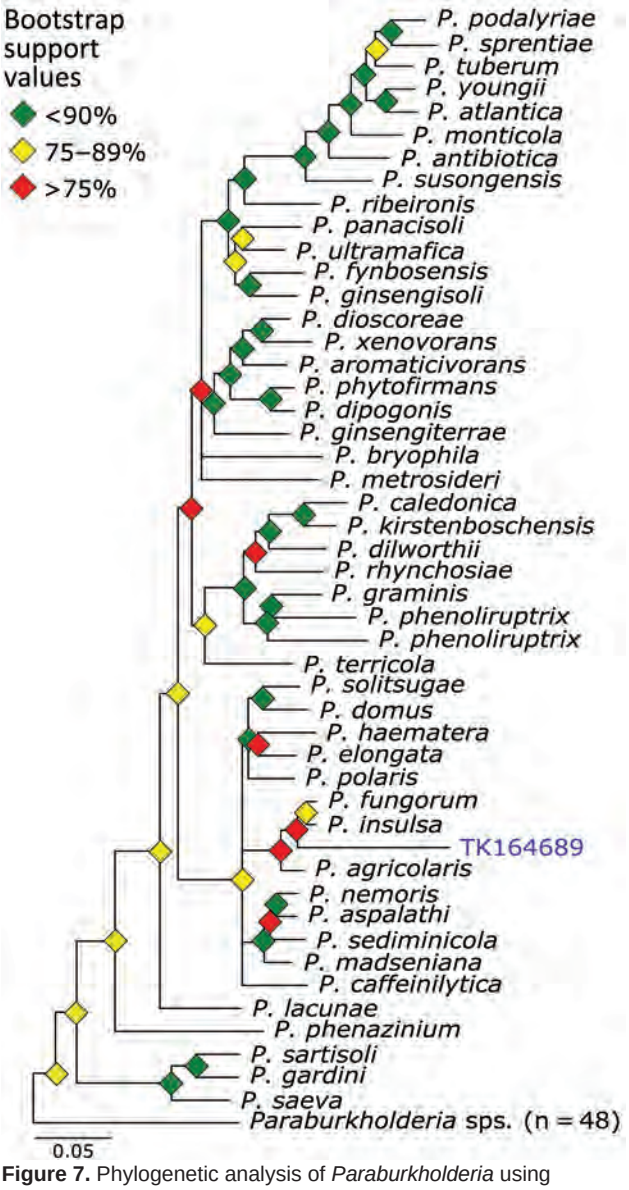

Figure 7. Phylogenetic analysis of *Paraburkholderia* using museum archived samples in study of prospecting for zoonotic pathogens by using targeted DNA enrichment. Blue indicates museum archived samples; museum accession numbers are given (Table 1). Branches with <50% bootstrap support were collapsed. Nodal support is indicated by color coded diamonds. Scale bar indicates nucleotide substitutions per site. Assembly accession numbers (e.g., GCA90237446) and tree files are available from https://doi.org/10.5281/zenodo.8014941.

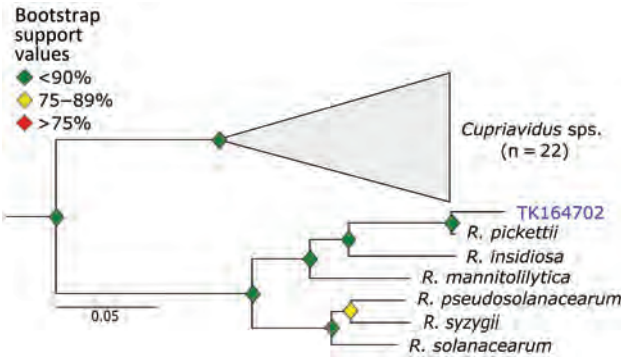

Figure 8. Phylogenetic analysis of Ralstonia using museum archived samples in study of prospecting for zoonotic pathogens by using targeted DNA enrichment. Blue indicates museum archived samples; museum accession numbers are given (Table 1). Branches with <50% bootstrap support were collapsed. Nodal support is indicated by color coded diamonds. Scale bar indicates nucleotide substitutions per site. Assembly accession numbers (e.g., GCA90237446) and tree files are available from https://doi.org/10.5281/zenodo.8014941.

Paraburkholderia is a genus of bacteria commonly associated with soil microbiomes and plant tissues. We identified *Paraburkholderia* reads in 3 specimens and were able to place 1 of those in a phylogeny sister to a clade containing *P. fungorum* and *P. insulsa*. Because bootstrap values across the phylogeny were moderate in general, and weak in this particular region (Figure 7), placement of this sample is tenuous. *P. fungorum* is the sole member of *Paraburkholderia* believed to be capable of infecting humans, but it is only a rare, opportunistic, human pathogen (*38*–*40*).

Ralstonia is a bacteria genus closely related to the genus *Pseudomonas*. We identified *Ralstonia* reads in 5 samples and were able to place a specimen on a phylogeny. This sample is closely affiliated with *R. pickettiii* (Figure 8). We are unaware of any examples of zoonotic transmission of *R. pickettii*. Rather, *R. pickettii* has been identified as a common contaminant in laboratory reagents (*41*), and outbreaks have been caused by contaminated medical supplies (*42*). We failed to identify nucleic acids in any of our negative controls during library preparation. Furthermore, if there were systemic contamination, we would expect to find *Ralstonia* species in all of our samples, rather than the 5 of 36 observed. Thus, because we cannot rule out reagent contamination, the presence of *Ralstonia* species in the museum samples should be interpreted with caution.

We were able to capture, sequence, and assemble loci from taxa that were not represented in the databases used to design the bait panel. This ability was possible for 2 reasons. First, the bait panel is highly redundant. The baits are sticky and able to capture

nucleic acid fragments that are ≤10%–12% divergent (*43*). We designed the panel with ≤5% sequence divergence between any pair of baits at a particular locus (Figure 10). Second, sampled loci within each pathogen group spanned a range of divergences. Conserved loci were more likely to catch more divergent species that might not have been present in our initial dataset. For example, we recovered multiple species of *Bartonella* that were not present in our probe set, for which related genomes were available. However, for *Ralstonia* and *Paraburkholderia* species, we identified these samples from reads targeted by probes for the genus *Burkholderia*, a pathogenic taxon in the same family (Burkholderacea). The ability to identify taxa at these distances is because of the more conserved loci targeted by the bait panel.

During the initial read classification stage, we identified low levels of *Plasmodium* species in all but 2 museum samples, which was unexpected. Museum samples contained ≤3,221 *Plasmodium* reads/sample (mean 428.3 reads/sample), but we were unable to assemble them into loci for phylogenetic analyses. This limitation effectively removed those samples from downstream analyses. The *P. falciparum* genome is extremely AT rich (82%, 44), which might result in bioinformatic false-positive results. We suspect that AT-rich, low-complexity regions of the host genome are misclassified as parasite reads. To test this hypothesis, we used fqtrim 0.9.7 (https://ccb.jhu.edu/software/fqtrim) to identify and remove low-complexity sequences within those reads. This filter by itself reduced the number of *Plasmodium* reads in the museum samples by 75.5% (maximum 298 reads, mean 57.2 reads). In comparison, only 8.2% of reads from 0.001% enriched control samples and 0.2% of reads from 1% enriched control samples were removed.

Several technical issues still need to be addressed. First, enrichment increases the targeted

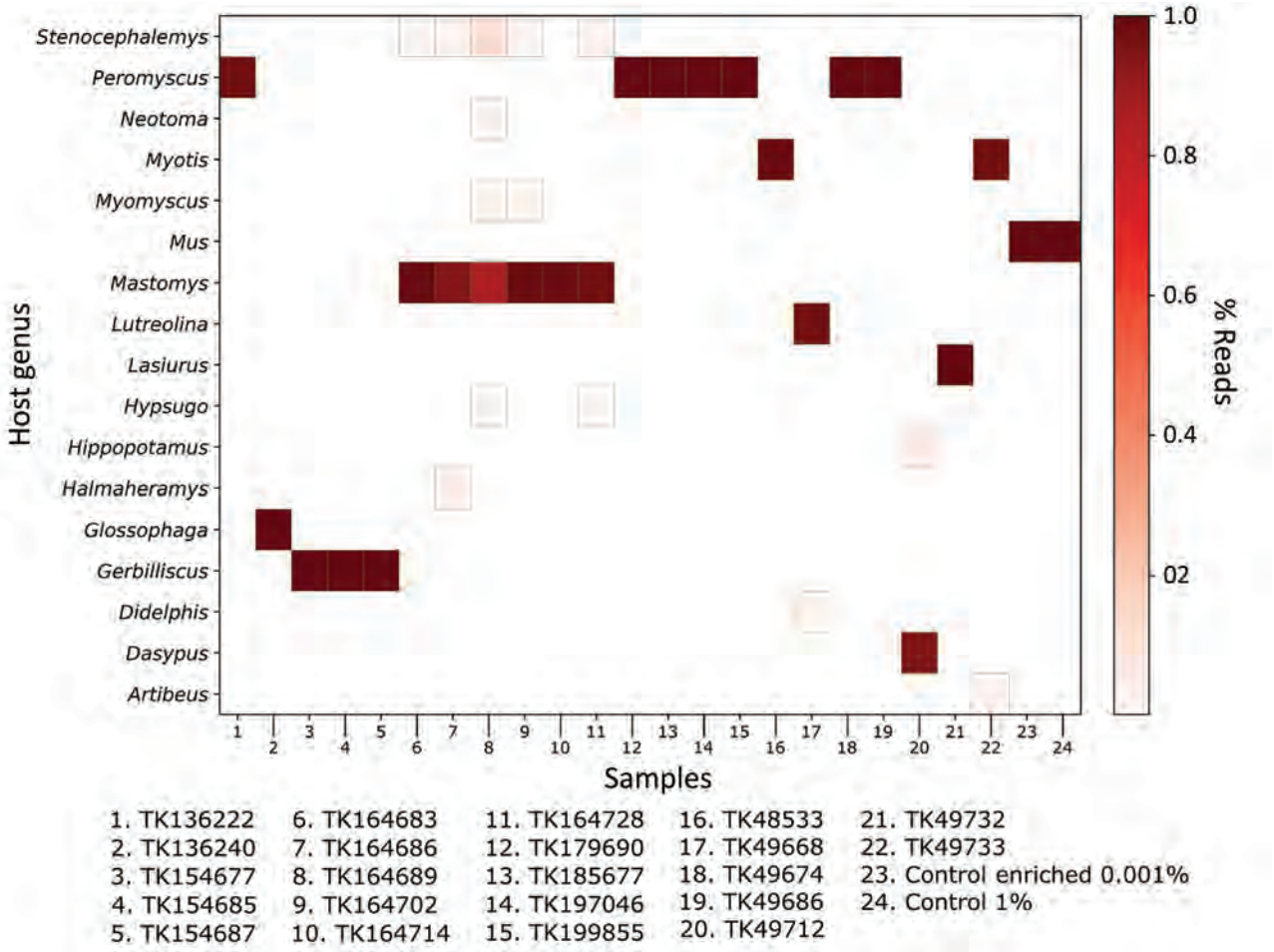

Figure 9. Genetic identification of mammal host from unenriched, mitochondrial reads in study of prospecting for zoonotic pathogens by using targeted DNA enrichment. Reads were compared with a database of mammalian mitochondria and assigned a taxonomic classification based on these results. A heatmap of the results shows the relative proportion of classified reads assigned to mammalian genera. Samples with <50 mitochondrial reads and single-read genera are not shown.

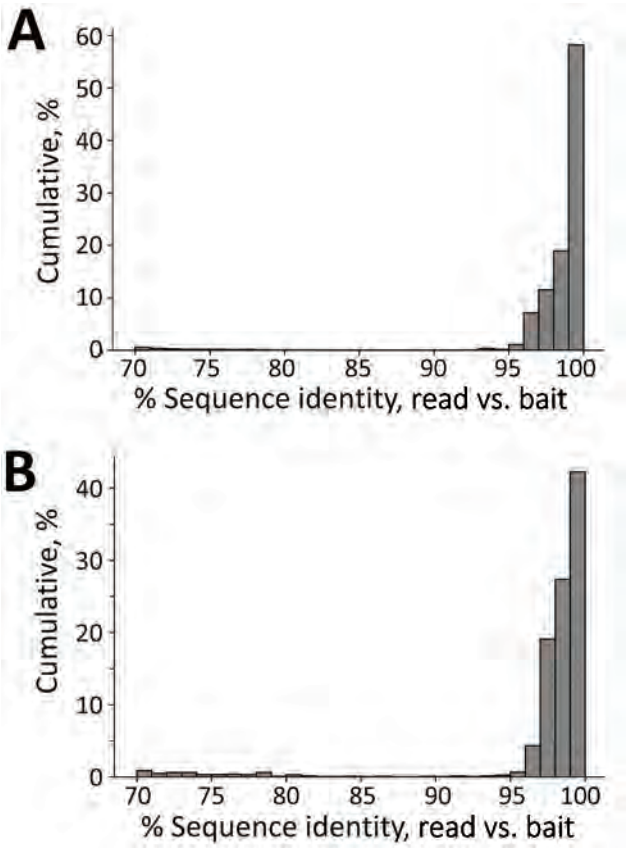

Figure 10. Sequence identity between enriched reads and baits in the probe panel used for targeting zoonotic pathogens in study of prospecting for zoonotic pathogens by using targeted DNA enrichment. Reads from each sample were classified against a database of target loci. Sequence identity between pathogen-derived reads and the most similar bait in the bait panel for all pathogens excluding Bartonella species (A) and for only Bartonella species (B). Bartonella was the most common pathogen in our samples, and the number of reads was biased toward a few individuals.

loci coverage by 3 orders of magnitude. However, the amount of host DNA remaining in each sample is still high. Ideally, host DNA would be rare or absent. Second, the bait panel requires relatively large up-front costs. Third, although the bait panel is developed to target a wide range of taxa, it is not possible to know which species are missed. The best way to circumvent that issue is to use controls spiked with various pathogens of interest, similar to how mock communities are used in other metagenomic studies (*45*). Those mock controls are commercially available for bacterial communities (e.g., ZymoBIOMICS Microbial Community Standards; Zymo Research, http://www.zymoresearch.com), but we have been unable to find similar products that contain eukaryotic pathogens. Solutions to those problems will make targeted sequencing with bait panels a viable tool for pathogen surveillance. Fourth, the sensitivity of the probes will depend on the sequence divergence between the probes and pathogen DNA. The more diverged the 2 are, the less efficient the capture will be. This limitation indicates that pathogen groups that have biased or limited genomic data will be less likely to capture off-target species once divergence increases by >5%–10%. Finally, the current probe panel is capable of capturing and identifying pathogens if there are ≥3,000 genome copies in the sample. Sensitivity needs to be improved in future iterations of the panel. One method could be to target pathogen-specific, repetitive sequences (*46*). Because those sequences are already present in the genome hundreds to thousands of times, it should be possible to greatly increase the sensitivity of the probe panel.

Although further effort is required to resolve these issues, we believe that enrichment of pathogen DNA from museum tissue samples is a viable tool worth further development. In its current form, enrichment represents a coarse tool that can be used to scan for various pathogens from archived tissues. More refined tests, such as quantitative PCR and targeted sequencing, can be used to answer taxon-specific questions. Target enrichment will be necessary for maximizing the pathogen data that are available from the hundreds of thousands of museum-archived tissues and will play a critical role in understanding our susceptibility to future zoonotic outbreaks.

Acknowledgments

We thank Sandy Smith, John Heaner, Larry Schlesinger, Ian Cheeseman, and Frederic Chevalier for providing computational and laboratory support and Kathy McDonald, Heath Garner, and Caleb Phillips for providing small mammal tissues.

This study was supported by the Texas Biomedical Research Forum (grant 19-04773).

About the Author

Dr. Enabulele is a postdoctoral research associate at the Texas Biomedical Research Institute, San Antonio, TX. His primary research interests are public health parasitology, neglected tropical diseases, and pathogen genomics.

References

1. Plowright RK, Parrish CR, McCallum H, Hudson PJ, Ko AI, Graham AL, et al. Pathways to zoonotic spillover. Nat Rev Microbiol. 2017;15:502–10. https://doi.org/10.1038/nrmicro.2017.45

2. Dean DJ, Evans WM, McClure RC. Pathogenesis of rabies. Bull World Health Organ. 1963;29:803–11.
3. Perry RD, Fetherston JD. Yersinia pestis—etiologic agent of plague. Clin Microbiol Rev. 1997;10:35–66. https://doi.org/10.1128/CMR.10.1.35
4. Leroy EM, Epelboin A, Mondonge V, Pourrut X, Gonzalez J-P, Muyembe-Tamfum J-J, et al. Human Ebola outbreak resulting from direct exposure to fruit bats in Luebo, Democratic Republic of Congo, 2007. Vector Borne Zoonotic Dis. 2009;9:723–8. https://doi.org/10.1089/vbz.2008.0167
5. Petersen JM, Schriefer ME. Tularemia: emergence/re-emergence. Vet Res. 2005;36:455–67. https://doi.org/10.1051/vetres:2005006
6. Müller B, Dürr S, Alonso S, Hattendorf J, Laisse CJ, Parsons SD, et al. Zoonotic *Mycobacterium bovis*–induced tuberculosis in humans. Emerg Infect Dis. 2013;19:899–908. https://doi.org/10.3201/eid1906.120543
7. Jo WK, de Oliveira-Filho EF, Rasche A, Greenwood AD, Osterrieder K, Drexler JF. Potential zoonotic sources of SARS-CoV-2 infections. Transbound Emerg Dis. 2021;68:1824–34. https://doi.org/10.1111/tbed.13872
8. van Aart AE, Velkers FC, Fischer EA, Broens EM, Egberink H, Zhao S, et al. SARS-CoV-2 infection in cats and dogs in infected mink farms. Transbound Emerg Dis. 20221; 69:3001–7. https://doi.org/10.1111/tbed.14173
9. Colella JP, Bates J, Burneo SF, Camacho MA, Carrion Bonilla C, Constable I, et al. Leveraging natural history biorepositories as a global, decentralized, pathogen surveillance network. PLoS Pathog. 2021;17:e1009583. https://doi.org/10.1371/journal.ppat.1009583
10. McLean BS, Bell KC, Dunnum JL, Abrahamson B, Colella JP, Deardorff ER, et al. Natural history collections-based research: progress, promise, and best practices. J Mammal. 2016;97:287–97. https://doi.org/10.1093/jmammal/gyv178
11. Cook JA, Arai S, Armién B, Bates J, Bonilla CA, Cortez MB, et al. Integrating biodiversity infrastructure into pathogen discovery and mitigation of emerging infectious diseases. Bioscience. 2020;70:531–4. https://doi.org/10.1093/biosci/biaa064
12. Dunnum JL, Yanagihara R, Johnson KM, Armien B, Batsaikhan N, Morgan L, et al. Biospecimen repositories and integrated databases as critical infrastructure for pathogen discovery and pathobiology research. PLoS Negl Trop Dis. 2017;11:e0005133. https://doi.org/10.1371/journal.pntd.0005133
13. Thompson CW, Phelps KL, Allard MW, Cook JA, Dunnum JL, Ferguson AW, et al. Preserve a voucher specimen! The critical need for integrating natural history collections in infectious disease studies. MBio. 2021;12:e02698–20. https://doi.org/10.1128/mBio.02698-20
14. Soniat TJ, Sihaloho HF, Stevens RD, Little TD, Phillips CD, Bradley RD. Temporal-dependent effects of DNA degradation on frozen tissues archived at −80°C. J Mammal. 2021;102:375–83. https://doi.org/10.1093/jmammal/gyab009
15. Yates TL, Mills JN, Parmenter CA, Ksiazek TG, Parmenter RR, Vande Castle JR, et al. The ecology and evolutionary history of an emergent disease: hantavirus pulmonary syndrome. Evidence from two El Niño episodes in the American southwest suggests that El Niño–driven precipitation, the initial catalyst of a trophic cascade that results in a delayed density-dependent rodent response, is sufficient to predict heightened risk for human contraction of hantavirus pulmonary syndrome. Bioscience. 2002;52:989–98. https://doi.org/10.1641/0006-3568(2002)052[0989:TEAEHO]2.0.CO;2
16. Choi M, Scholl UI, Ji W, Liu T, Tikhonova IR, Zumbo P, et al. Genetic diagnosis by whole exome capture and massively parallel DNA sequencing. Proc Natl Acad Sci U S A. 2009; 106:19096–101. https://doi.org/10.1073/pnas.0910672106
17. Yi X, Liang Y, Huerta-Sanchez E, Jin X, Cuo ZX, Pool JE, et al. Sequencing of 50 human exomes reveals adaptation to high altitude. Science. 2010;329:75–8. https://doi.org/10.1126/science.1190371
18. McCormack JE, Hird SM, Zellmer AJ, Carstens BC, Brumfield RT. Applications of next-generation sequencing to phylogeography and phylogenetics. Mol Phylogenet Evol. 2013;66:526–38. https://doi.org/10.1016/j.ympev.2011.12.007
19. Vernot B, Zavala EI, Gómez-Olivencia A, Jacobs Z, Slon V, Mafessoni F, et al. Unearthing Neanderthal population history using nuclear and mitochondrial DNA from cave sediments. Science. 2021;372:eabf1667. https://doi.org/10.1126/science.abf1667
20. Fu Q, Hajdinjak M, Moldovan OT, Constantin S, Mallick S, Skoglund P, et al. An early modern human from Romania with a recent Neanderthal ancestor. Nature. 2015;524:216–9. https://doi.org/10.1038/nature14558
21. Gaudin M, Desnues C. Hybrid capture-based next generation sequencing and its application to human infectious diseases. Front Microbiol. 2018;9:2924. https://doi.org/10.3389/fmicb.2018.02924
22. Keller M, Spyrou MA, Scheib CL, Neumann GU, Kröpelin A, Haas-Gebhard B, et al. Ancient *Yersinia pestis* genomes from across Western Europe reveal early diversification during the First Pandemic (541–750). Proc Natl Acad Sci U S A. 2019;116:12363–72. https://doi.org/10.1073/pnas.1820447116
23. Lee JS, Mackie RS, Harrison T, Shariat B, Kind T, Kehl T, et al. Targeted enrichment for pathogen detection and characterization in three felid species. J Clin Microbiol. 2017;55:1658–70. https://doi.org/10.1128/JCM.01463-16
24. Wylie TN, Wylie KM, Herter BN, Storch GA. Enhanced virome sequencing using targeted sequence capture. Genome Res. 2015;25:1910–20. https://doi.org/10.1101/gr.191049.115
25. O'Flaherty BM, Li Y, Tao Y, Paden CR, Queen K, Zhang J, et al. Comprehensive viral enrichment enables sensitive respiratory virus genomic identification and analysis by next generation sequencing. Genome Res. 2018;28:869–77. https://doi.org/10.1101/gr.226316.117
26. Faircloth BC, McCormack JE, Crawford NG, Harvey MG, Brumfield RT, Glenn TC. Ultraconserved elements anchor thousands of genetic markers spanning multiple evolutionary timescales. Syst Biol. 2012;61:717–26. https://doi.org/10.1093/sysbio/sys004
27. Faircloth BC. Identifying conserved genomic elements and designing universal bait sets to enrich them. Methods Ecol Evol. 2017;8:1103–12. https://doi.org/10.1111/2041-210X.12754
28. Gotia HT, Munro JB, Knowles DP, Daubenberger CA, Bishop RP, Silva JC. Absolute quantification of the host-to-parasite DNA ratio in *Theileria parva*–infected lymphocyte cell lines. PLoS One. 2016;11:e0150401. https://doi.org/10.1371/journal.pone.0150401
29. Cowell AN, Loy DE, Sundararaman SA, Valdivia H, Fisch K, Lescano AG, et al. Selective whole-genome amplification is a robust method that enables scalable whole-genome sequencing of from unprocessed clinical samples. MBio. 2017;8:e02257-16. https://doi.org/10.1128/mBio.02257-16
30. Bushnell B. BBMap: a fast, accurate, splice-aware aligner. Berkeley (CA): Lawrence Berkeley National Laboratory; 2014.

31. Wood DE, Lu J, Langmead B. Improved metagenomic analysis with Kraken 2. Genome Biol. 2019;20:257. https://doi.org/10.1186/s13059-019-1891-0
32. Bankevich A, Nurk S, Antipov D, Gurevich AA, Dvorkin M, Kulikov AS, et al. SPAdes: a new genome assembly algorithm and its applications to single-cell sequencing. J Comput Biol. 2012;19:455–77. https://doi.org/10.1089/cmb.2012.0021
33. Kozlov AM, Darriba D, Flouri T, Morel B, Stamatakis A. RAxML-NG: a fast, scalable and user-friendly tool for maximum likelihood phylogenetic inference. Bioinformatics. 2019;35:4453–5. https://doi.org/10.1093/bioinformatics/btz305
34. Jacomo V, Kelly PJ, Raoult D. Natural history of *Bartonella* infections (an exception to Koch's postulate). Clin Diagn Lab Immunol. 2002;9:8–18.
35. Chomel BB, Boulouis HJ, Maruyama S, Breitschwerdt EB. *Bartonella* spp. in pets and effect on human health. Emerg Infect Dis. 2006;12:389–94. https://doi.org/10.3201/eid1203.050931
36. Dahmani M, Diatta G, Labas N, Diop A, Bassene H, Raoult D, et al. Noncontiguous finished genome sequence and description of *Bartonella mastomydis* sp. nov. New Microbes New Infect. 2018;25:60–70. https://doi.org/10.1016/j.nmni.2018.03.005
37. Briese T, Kapoor A, Mishra N, Jain K, Kumar A, Jabado OJ, et al. Virome capture sequencing enables sensitive viral diagnosis and comprehensive virome analysis. MBio. 2015;6:e01491–15. https://doi.org/10.1128/mBio.01491-15
38. Gerrits GP, Klaassen C, Coenye T, Vandamme P, Meis JF. *Burkholderia fungorum* septicemia. Emerg Infect Dis. 2005;11:1115–7. https://doi.org/10.3201/eid1107.041290
39. Vandamme P, Peeters C. Time to revisit polyphasic taxonomy. Antonie van Leeuwenhoek. 2014;106:57–65. https://doi.org/10.1007/s10482-014-0148-x
40. Angus AA, Agapakis CM, Fong S, Yerrapragada S, Estrada-de los Santos P, Yang P, et al. Plant-associated symbiotic *Burkholderia* species lack hallmark strategies required in mammalian pathogenesis. PLoS One. 2014;9:e83779. https://doi.org/10.1371/journal.pone.0083779
41. Salter SJ, Cox MJ, Turek EM, Calus ST, Cookson WO, Moffatt MF, et al. Reagent and laboratory contamination can critically impact sequence-based microbiome analyses. BMC Biol. 2014;12:87. https://doi.org/10.1186/s12915-014-0087-z
42. Chen YY, Huang WT, Chen CP, Sun SM, Kuo FM, Chan YJ, et al. An outbreak of *Ralstonia pickettii* bloodstream infection associated with an intrinsically contaminated normal saline solution. Infect Control Hosp Epidemiol. 2017;38:444–8. https://doi.org/10.1017/ice.2016.327
43. Bi K, Vanderpool D, Singhal S, Linderoth T, Moritz C, Good JM. Transcriptome-based exon capture enables highly cost-effective comparative genomic data collection at moderate evolutionary scales. BMC Genomics. 2012;13:403. https://doi.org/10.1186/1471-2164-13-403
44. Weber JL. Analysis of sequences from the extremely A + T-rich genome of *Plasmodium falciparum*. Gene. 1987;52:103–9. https://doi.org/10.1016/0378-1119(87)90399-4
45. Tourlousse DM, Narita K, Miura T, Ohashi A, Matsuda M, Ohyama Y, et al. Characterization and demonstration of mock communities as control reagents for accurate human microbiome community measurements. Microbiol Spectr. 2022;10:e0191521. https://doi.org/10.1128/spectrum.01915-21
46. Bennuru S, O'Connell EM, Drame PM, Nutman TB. Mining filarial genomes for diagnostic and therapeutic targets. Trends Parasitol. 2018;34:80–90. https://doi.org/10.1016/j.pt.2017.09.003

Address for correspondence: Roy N. Platt, Texas Biomedical Research Institute, 8715 W Military Dr, San Antonio, TX 78245-0549, USA; email: rplatt@txbiomed.org

Omicron COVID-19 Case Estimates Based on Previous SARS-CoV-2 Wastewater Load, Regional Municipality of Peel, Ontario, Canada

Lydia Cheng,[1] Hadi A. Dhiyebi,[1] Monali Varia, Kyle Atanas, Nivetha Srikanthan, Samina Hayat, Heather Ikert, Meghan Fuzzen, Carly Sing-Judge, Yash Badlani, Eli Zeeb, Leslie M. Bragg, Robert Delatolla, John P. Giesy, Elaine Gilliland, Mark R. Servos

We determined correlations between SARS-CoV-2 load in untreated water and COVID-19 cases and patient hospitalizations before the Omicron variant (September 2020–November 2021) at 2 wastewater treatment plants in the Regional Municipality of Peel, Ontario, Canada. Using pre-Omicron correlations, we estimated incident COVID-19 cases during Omicron outbreaks (November 2021–June 2022). The strongest correlation between wastewater SARS-CoV-2 load and COVID-19 cases occurred 1 day after sampling (r = 0.911). The strongest correlation between wastewater load and COVID-19 patient hospitalizations occurred 4 days after sampling (r = 0.819). At the peak of the Omicron BA.2 outbreak in April 2022, reported COVID-19 cases were underestimated 19-fold because of changes in clinical testing. Wastewater data provided information for local decision-making and are a useful component of COVID-19 surveillance systems.

Public health surveillance of COVID-19 activity has expanded from monitoring of persons with laboratory-confirmed SARS-CoV-2 infection to including wastewater surveillance. Studies conducted in early 2020 provided proof of concept that wastewater surveillance of SARS-CoV-2 can be used to determine prevalence of COVID-19 in several countries (*1*–*3*). Other studies have since shown the viability of that surveillance indicator (*4*–*7*) with varying success when biomarkers such as pepper mild mottle virus (PMMoV) and crAssphage were used to normalize the measurements of SARS-CoV-2 in fecal matter in samples (*4*,*8*,*9*). Wastewater surveillance indicators become especially relevant when PCR testing eligibility changed or when clinical testing capacity was overwhelmed, resulting in an incomplete picture of local COVID-19 activity.

The Regional Municipality of Peel in Ontario, Canada (hereafter referred to as Peel) serves 1.5 million residents of the cities/towns of Brampton, Caledon, and Mississauga in Ontario, Canada (*10*). As of July 16, 2022, the COVID-19 incidence rate in Peel was one of the highest in Ontario; cumulative incidence was 12,098 laboratory-confirmed COVID-19 cases per 100,000 Peel residents, compared with 9,164/100,000 Ontario residents (*11*). Since April 2020, Peel has sampled untreated wastewater from its 2 wastewater treatment plants (WWTPs) and tested it for SARS-CoV-2. Peel's WWTPs, serving ≈96% of the region's residential postal codes, are Clarkson (population served 643,331) and G.E. Booth (population served 1,089,738).

On December 30, 2021, as the Omicron BA.1 variant surged in Ontario, the province restricted clinical PCR testing (which had previously been available to any symptomatic person or close contact of a COVID-19 case-patient) to groups at greatest risk, including hospitalized patients, patient-facing health-

Author affiliations: Regional Municipality of Peel, Mississauga, Ontario, Canada (L. Cheng, M. Varia, K. Atanas, E. Gilliland) University of Waterloo, Waterloo, Ontario, Canada (H.A. Dhiyebi, N. Srikanthan, S. Hayat, H. Ikert, M. Fuzzen, C. Sing-Judge, Y. Badlani, E. Zeeb, L.M. Bragg, M.R. Servos) University of Ottawa, Ottawa, Ontario, Canada (R. Delatolla) University of Saskatchewan, Saskatoon, Saskatchewan, Canada (J.P. Giesy); Baylor University, Waco, Texas, USA (J.P. Giesy)

DOI: https://doi.org/10.3201/eid2908.221580

[1]These first authors contributed equally to this article.

care workers, and staff and residents in hospitals and congregate living settings (*12*). This policy change, the only one to substantially affect the number of completed tests during our study period, resulted in a shift in Peel's COVID-19 surveillance strategy. Wastewater surveillance of SARS-CoV-2 became a requisite tool for monitoring community-level COVID-19 activity and was used as a key indicator to provide information for local public health decision-making and communication (*13*).

We report correlations between clinical COVID-19 indicators (reported cases and hospitalizations) and SARS-CoV-2 load in untreated wastewater at various lags across COVID-19 pandemic waves 2–6 in Peel during August 2020–June 2022. We also estimated the number of incident COVID-19 cases in Peel, on the basis of SARS-CoV-2 load in wastewater before the clinical PCR testing policy change, during the Omicron outbreaks when PCR testing was restricted. Last, we assessed the usefulness of normalizing SARS-CoV-2 concentrations to PMMoV.

Methods

Wastewater Sampling and SARS-CoV-2 RNA Measurement

We sampled wastewater from G.E. Booth and Clarkson WWTPs, located in Mississauga, 3–5 weekdays per week, according to the needs of Peel Public Health and the recommendations of the US Centers for Disease Control and Prevention (*14*) (Appendix Table 1, https://wwwnc.cdc.gov/EID/article/29/8/22-1580-App1.pdf). We obtained daily flow rates (m^3/day) for each WWTP. In total, we included 356 samples from G.E. Booth and 359 samples from Clarkson in this study.

We collected 24-hour composite samples of untreated wastewater influent, before any screening or grit removal, by using Hach model AS950 automatic samplers (https://www.hach.com) and stored them in high-density polyethylene containers. We kept containers at 4°C and transported them to the University of Waterloo (Waterloo, ON, Canada) for extraction and quantification of SARS-CoV-2 RNA. Sample analysis and reporting occurred within 2 weeks of collection; most samples were analyzed within the same week.

We used a polyethylene glycol precipitation method (*2*) for each wastewater sample as follows: we added 40 mL of sample to a 50-mL centrifuge tube with polyethylene glycol (4 g) and NaCl (0.9 g) and spiked a surrogate (e.g., human coronavirus 229E or murine hepatitis virus) into the sample. The sample was shaken on ice for 2 h and left to settle at 4°C overnight. We then centrifuged the sample at 12,000 × *g* for 1.5 h to concentrate the virus into the solids with the supernatant discarded. We extracted SARS-CoV-2 RNA and purified it from the solids by using either TRIzol reagent (Invitrogen, https://www.thermofisher.com) or Power Microbiome Kit (QIAGEN, https://www.qiagen.com), following the manufacturer's protocol, with up to 250 mg (wet weight) of the pellet resuspended in either TriZOL or TriZOL/PM1 solution. We eluted the RNA in 100 µL nuclease-free water. Extracted RNA then underwent 1-step quantitative reverse transcription PCR for SARS-CoV-2 (N1, N2 gene targets [*15*]) and PMMoV (*16*) (Appendix).

COVID-19 Case-Patient, Hospitalization, and Testing Data

We extracted nonnominal data for patients who met the provincial case definition of having confirmed or probable COVID-19 (*17*). Data fields included residential postal code and episode date (earliest date of symptom onset, specimen collection, or date reported). Case-patient data were restricted to persons who had a permanent residential address in Peel at the time of COVID-19 diagnosis and who experienced episodes from August 30, 2020, through June 18, 2022 (n = 185,895). We classified case-patients by sewershed—G.E. Booth, Clarkson, septic system, or unknown—on the basis of residential postal code matched to the 2019 Postal Code Conversion File (https://www.canadapost-postescanada.ca/cpc/doc/en/marketing/postal-code-conversion-file-reference-guide.pdf), which we spatially joined with the Peel sewershed geographic boundary file. We validated postal codes that did not match with the Postal Code Conversion File by using the Canada Post Find a Postal Code web tool (https://www.canadapost-postescanada.ca/info/mc/personal/postalcode/fpc.jsf). We then aggregated case-patients by episode date and sewershed. Among 185,895 COVID-19 case-patients, 1.5% were not matched to either WWTP sewershed, 0.9% were associated with septic systems, and 0.6% were unable to be matched to the geographic boundary file.

Patient hospitalization information, obtained from COVID-19 case follow-up, is underreported in the Ontario Ministry of Health's COVID-19 case registry, Case and Contact Management Solution. Therefore, we acquired aggregate COVID-19 patient hospitalization data from the Ontario Ministry of Health's Daily Bed Census, for August 30, 2020, through June

18, 2022 (https://data.ontario.ca/dataset/bed-census-summary-bcs). We extracted the daily number of acute care admissions among laboratory-confirmed COVID-19 patients, regardless of patient residence or reason for admission, to the 3 acute hospitals located in Peel (Trillium Health Partners [Credit Valley Hospital and Mississauga Hospital] and William Osler Health System [Brampton Civic Hospital]). To describe SARS-CoV-2 clinical testing trends during the study period, we extracted completed PCR tests for Peel residents from the Ontario Ministry of Health Ontario Laboratory Information System, by week of specimen collection.

Data Processing

We categorized data from August 30, 2020, through June 18, 2022, by epidemic wave, each characterized by the dominance of the wild-type or a variant of SARS-CoV-2. We reported SARS-CoV-2 N-gene values as the mean concentration (copies/mL) of the N1 and N2 gene targets for each sampling date and WWTP. We retained in the dataset mean concentration values below the limit of detection (0.5 copies/mL) or limit of quantification (3.5 copies/mL) as reported from the quantitative reverse transcription PCR analysis. Normalized data were presented as the mean concentration of N1 and N2 divided by the concentration of PMMoV. We calculated daily load per WWTP by multiplying the flow rate by the mean N-gene concentration or PMMoV-normalized data.

To visualize trends at each sewershed, we plotted daily wastewater loads and COVID-19 cases. We assessed wastewater load and case data for normality by visually inspecting quantile-quantile plots and histograms after applying various data transformations. The natural log transformation, after adding a constant of 1 (ln[x + 1]), resulted in approximately normally distributed data in both datasets (Appendix Figure 1). To assess the strength of linear associations between log-transformed SARS-CoV-2 loads in wastewater and log-transformed COVID-19 cases, we computed Pearson correlation coefficients (r) by using lags of 0–5 days between sampling date and case episode date. We repeated that analysis by using PMMoV-normalized, log-transformed wastewater load data. We considered correlation coefficients to be significant at $p<0.05$.

Because the number of COVID-19 patient hospitalizations at Peel hospitals were not specific to sewersheds, we summed the daily wastewater loads at both WWTPs, applied the ln(x + 1) transformation because it resulted in more normally distributed data, and calculated r between log-transformed total N-gene load and log-transformed hospitalizations. We computed correlation coefficients per wave at lags of 1–14 days between wastewater sampling date and hospitalization date. We repeated that analysis by using log-transformed PMMoV-normalized wastewater data.

Wastewater-to-Case Ratios, Linear Regression, and Case Estimations

After observing the strongest linear association between SARS-CoV-2 load in wastewater and reported COVID-19 cases at a 1-day lag, we computed the median daily wastewater-to-case ratio per wave. We compared these median wastewater-to-case ratios per wave by using the Kruskal-Wallis test, followed

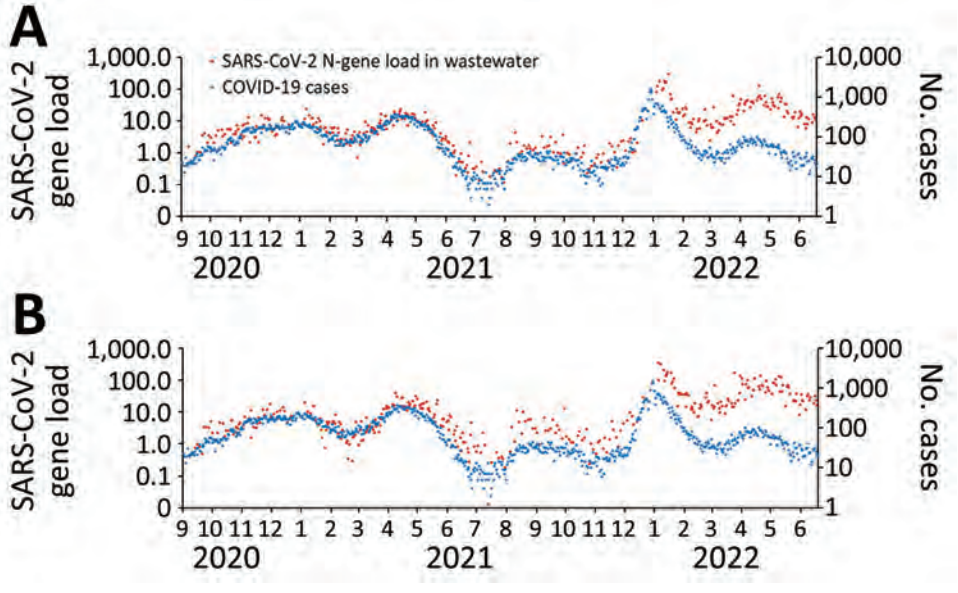

Figure 1. Mean SARS-CoV-2 N-gene load (10^{12} copies/d) in untreated wastewater at Clarkson Wastewater Treatment Plant and reported COVID-19 case-patients residing in the Clarkson sewershed, Regional Municipality of Peel, Ontario, Canada, September 1, 2020–June 18, 2022. A) Nonnormalized; B) pepper mild mottle virus normalized. Data are plotted on the logarithmic scale.

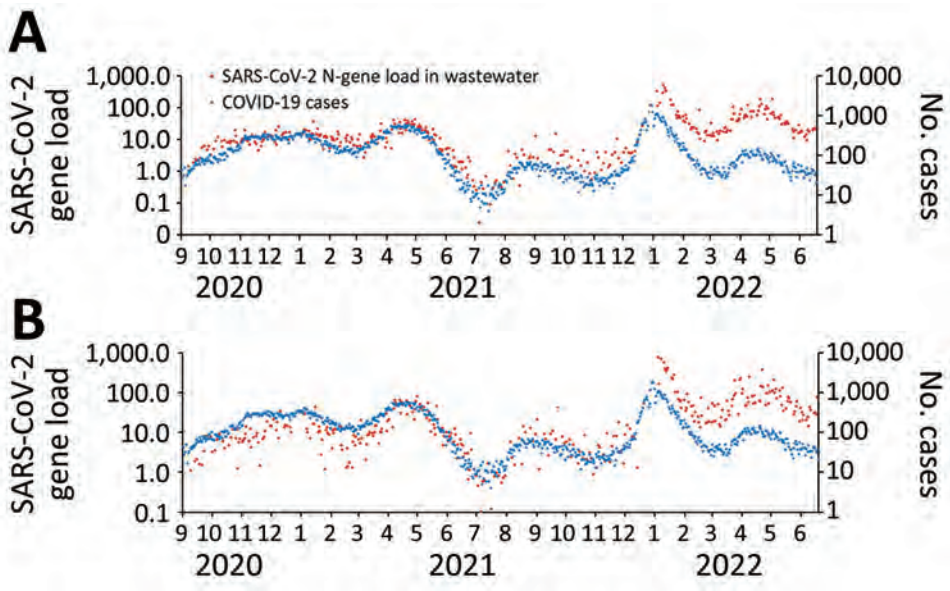

Figure 2. Mean SARS-CoV-2 N-gene load (10^{12} copies/d) in untreated wastewater at G.E. Booth Wastewater Treatment Plant and reported COVID-19 case-patients residing in the G.E. Booth sewershed, Regional Municipality of Peel, Ontario, Canada, September 1, 2020–June 18, 2022. A) Nonnormalized; B) pepper mild mottle virus normalized. Data are plotted on the logarithmic scale.

by the Dunn test for pairwise comparisons (*18*). Because clinical PCR testing eligibility was limited as of December 30, 2021, we hypothesized that laboratory-confirmed COVID-19 cases during the Omicron waves were underestimated. We therefore used wastewater load and reported case data in the pre-Omicron waves to fit a model to estimate reported case incidence during Omicron waves. We created a simple linear regression model by using the sum of the daily transformed N-gene load in wastewater at the 2 WWTPs and daily transformed COVID-19 case counts at the 2 WWTPs at a 1-day lag during the pre-Omicron waves (2–4), and we estimated the number of cases, with corresponding 95% prediction intervals, for the Omicron waves (5 and 6), on the basis of the measured wastewater SARS-CoV-2 load. For statistical analyses, we used Stata version MP17.0 (StataCorp LLC, https://www.stata.com).

Results

Trends in Wastewater SARS-CoV-2 Load and COVID-19 Clinical Indicators

During waves 2–4 (August 30, 2020–November 28, 2021, before Omicron emerged), the trends and magnitude of reported COVID-19 cases were temporally associated with both the non-normalized SARS-CoV-2 load and PMMoV-normalized load in wastewater (Figures 1, 2). The median daily SARS-CoV-2 load at G.E. Booth was double that of Clarkson, corresponding to the larger size of the G.E. Booth sewershed (Table 1). During waves 2 and 3, the numbers of average weekly clinical PCR tests conducted and overall percent positivity were similar (Table 1; Appendix Figure 1). Furthermore, trends in COVID-19 hospitalizations visually correlated with trends in wastewater load (Figure 3; Appendix Figure 3). During wave 4, dominated by the Delta variant, COVID-19 cases, hospitalizations, and clinical PCR tests were fewer; test positivity was lower; median N-gene loads in wastewater were less; and the proportion of wastewater samples with N-gene concentrations less than the limit of quantification was high (36%).

By December 2021, when Omicron BA.1 emerged (wave 5), the magnitude of reported cases no longer aligned with the magnitude of wastewater SARS-CoV-2 load (Figures 1, 2). SARS-CoV-2 load at both WWTPs reached a historic peak in January 2022. Of note, the largest number of daily COVID-19 case-patients ever reported in Peel, for both sewersheds, was on December 29, 2021. COVID-19 patient admissions at Peel hospitals also increased during wave 5; daily median was 12 and maximum was 63 admissions. Clinical PCR tests completed among Peel residents increased sharply in late December 2021 and dropped steeply in January 2022 after the change in PCR testing eligibility (Appendix Figure 1). Test positivity peaked at 31.4% during the week ending January 8, 2022.

COVID-19 wave 6, which occurred in Peel in spring 2022, was driven by Omicron BA.2. Daily median SARS-CoV-2 loads in wastewater were greater than in previous waves; however, loads did not exceed maximum daily values observed during the preceding Omicron BA.1 wave. Median daily COVID-19 patient hospitalizations remained similar to those in the previous

Table 1. Summary of wastewater and COVID-19 clinical data, by wastewater treatment plant and epidemic wave, Regional Municipality of Peel, Ontario, Canada, August 30, 2020–June 18, 2022*

Characteristic	Epidemic wave				
	2, 2020 Aug 30–2021 Feb 20	3, 2021 Feb 21–2021 Jul 17	4, 2021 Jul 18–2021 Nov 27	5, 2021 Nov 28–2022 Mar 12	6, 2022 Mar 13–2022 Jun 18
Predominant COVID-19 variant	Original	Alpha	Delta	Omicron BA.1	Omicron BA.2
No. wastewater sample days					
Clarkson WWTP	89	94	53	56	67
G.E. Booth WWTP	89	95	50	55	67
Median daily load of SARS-CoV-2 in wastewater, N-gene copies × 10^{12} (range)					
Clarkson WWTP	5.2 (0.5–23.8)	4.4 (<0.01–22.8)	1.0 (0.1–4.3)	10.6 (1.1–299.0)	22.8 (6.0–128.5)
G.E. Booth WWTP	10.1 (1.4–37.3)	9.8 (0.02−48.9)	2.6 (0.3−15.0)	24.1 (1.9–537.6)	42.1 (9.6–186.5)
Median PMMoV-normalized daily load of SARS-CoV-2 in wastewater, N-gene copies × 10^{2} (range)					
Clarkson WWTP	4.6 (0.3–20.4)	5.4 (0.01–39.9)	1.7 (0.2–13.4)	20.4 (3.9–357.3)	39.4 (8.1–173.9)
G.E. Booth WWTP	7.9 (1.1–44.4)	10.4 (0.1–83.9)	4.6 (0.5–43.3)	41.8 (1.3–793.6)	60.1 (14.7–389.6)
No. (%) wastewater samples with concentrations below limit of quantification†					
Clarkson WWTP	1 (1.1)	17 (18.1)‡	19 (35.8)	0 (0.0)	0 (0.0)
G.E. Booth WWTP	1 (1.1)	14 (14.7)§	18 (36.0)	0 (0.0)	0 (0.0)
Median daily no. of reported COVID-19 cases (range)					
Clarkson WWTP	109 (13–246)	100 (2–365)	24 (5–44)	83 (19–1,518)	45 (12–101)
G.E. Booth WWTP	189 (17–421)	165 (4–579)	31 (8–69)	136 (26–1,877)	64 (21–150)
Median daily no. acute care admissions of COVID-19 patients at Peel hospitals (range)	5 (0–19)	6 (0–28)	2 (0–10)	12 (0–63)	12 (3–30)
Mean weekly no. clinical SARS-CoV-2 PCR tests in Peel	21,237	21,050	14,125	18,696	8,513
Clinical PCR tests positive for SARS-CoV-2 in Peel, %	8.3	10.2	2.7	16.7	9.0

*WWTP, wastewater treatment plant.
†Limit of quantification: 3.5 SARS-CoV-2 N-gene copies per mL.
‡1 sample had N-gene concentration below the limit of detection (0.5 copies/mL).
§2 samples had N-gene concentration below the limit of detection (0.5 copies/mL).

wave. Weekly clinical SARS-CoV-2 PCR tests dropped by nearly 60% in wave 6, compared with waves 2–3.

Association between SARS-CoV-2 Concentrations in Wastewater and Clinical Indicators

For waves 2–6 combined, the strongest correlation between nonnormalized SARS-CoV-2 load in wastewater and reported COVID-19 cases occurred on the same day of sampling (G.E. Booth, r = 0.6030; Clarkson, r = 0.6273; both WWTPs, r = 0.6296; Table 2). Before Omicron, the strongest correlations occurred on the same day as sampling at G.E. Booth (r = 0.8698) and 1 day after sampling at Clarkson (r = 0.8864) and when load data were combined for both WWTPs (r = 0.9106). By wave, the strongest correlations occurred during the Alpha-dominant wave 3. Correlation coefficients were poorer as more time passed between the wastewater sample date and incident cases. PMMoV normalization, compared with no normalization, resulted in weaker correlations for both WWTPs before the Omicron waves and for G.E. Booth during the Omicron waves (Appendix Table 2).

Pearson correlation coefficients assessing the relationship between total wastewater SARS-CoV-2 load at the 2 WWTPs and total COVID-19 patient hospitalizations were highest during the Alpha-dominant wave 3 (Table 3; r = 0.8679 at a 4-day lag) and the Omicron BA.1-dominant wave 5 (r = 0.9161 at a 7-day lag). In the Delta-dominant wave 4, associations were weak and some were not

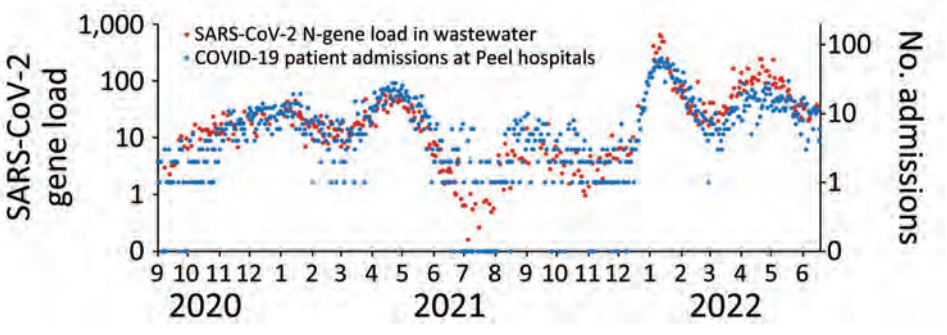

Figure 3. Mean combined SARS-CoV-2 N-gene loads (10^{12} copies/d) in untreated wastewater at Clarkson and G.E. Booth Wastewater Treatment Plants and acute-care admissions of confirmed COVID-19 patients at Peel hospitals, Regional Municipality of Peel, Ontario, Canada, September 1, 2020–June 18, 2022. Data are plotted on the logarithmic scale. For data visualization purposes, daily hospitalization values of zero were converted to 0.1 and are shown along the x-axis.

Table 2. Pearson correlation coefficients (*r*) between ln(x + 1) transformed daily wastewater SARS-CoV-2 load and ln(x + 1) transformed incident COVID-19 cases, by wastewater treatment plant and epidemic wave, at various lags, Regional Municipality of Peel, Ontario, Canada*

WWTP, lag, d	Epidemic waves							
	2	3	4	5	6	2–6	2–4, pre-Omicron	5–6, Omicron
Clarkson								
0	0.7078	0.8809	0.5747	0.7203	0.6655†	0.6273†	0.8677	0.5469†
1	0.7144†	0.8966	0.6661†	0.7248†	0.5933	0.6220	0.8864†	0.5384
2	0.6935	0.8901	0.5041	0.6607	0.5712	0.5849	0.8705	0.4743
3	0.6678	0.9089†	0.5321	0.6155	0.5480	0.5863	0.8788	0.4497
4	0.6653	0.9037	0.4539	0.5791	0.5468	0.5771	0.8727	0.4236
5	0.6550	0.8906	0.5550	0.5298	0.5762	0.5737	0.8699	0.4023
G.E. Booth								
0	0.7173†	0.8993	0.5774†	0.7922†	0.7572†	0.6030†	0.8698†	0.6828†
1	0.6935	0.9068†	0.5167	0.7601	0.7227	0.5932	0.8696	0.6535
2	0.6714	0.8722	0.4735	0.7076	0.7251	0.5529	0.8452	0.6165
3	0.6466	0.8889	0.4923	0.6767	0.7314	0.5650	0.8559	0.5974
4	0.6575	0.8808	0.4425	0.6347	0.7144	0.5592	0.8492	0.5658
5	0.6499	0.8641	0.4998	0.5953	0.7095	0.5467	0.8417	0.5502
Clarkson and G.E. Booth								
0	0.7647†	0.9422	0.6447†	0.7908†	0.7910†	0.6296†	0.9101	0.6601†
1	0.7431	0.9438†	0.6266	0.7655	0.7357	0.6150	0.9106†	0.6341
2	0.7290	0.9246	0.5295	0.7025	0.7276	0.5774	0.8921	0.5830
3	0.7087	0.9326	0.5505	0.6675	0.7186	0.5820	0.8972	0.5616
4	0.7121	0.9292	0.5051	0.6223	0.7017	0.5756	0.8931	0.5282
5	0.7057	0.9163	0.5706	0.5814	0.7111	0.5678	0.8887	0.5115

*Colors indicate strength of association: gray, weak ($r<0.4$); yellow, moderate ($0.4 \leq r < 0.7$); green, strong ($r \geq 0.7$). WWTP, wastewater treatment plant.
†Largest *r* per wave.

statistically significant. Overall, across the study period, the greatest correlation occurred between wastewater load and hospitalizations 4 days after sampling (r = 0.8189). PMMoV normalization resulted in weaker correlation coefficients, and the greatest coefficient occurred 1 day after sampling (r = 0.7883; Appendix Table 3).

Estimation of COVID-19 Cases in Peel during the Omicron BA.1 and BA.2 Outbreaks

At each WWTP, the median wastewater-to-case ratios did not statistically differ from each other for waves 2–4. However, the ratios were significantly greater ($p<0.05$) during waves 5 and 6 (Appendix Table 4, Figure 4). Thus, starting in wave 5, each unit of SARS-CoV-2 load in wastewater was associated with fewer reported COVID-19 cases, as expected, resulting from reduced eligibility for clinical PCR testing.

To estimate the number of COVID-19 cases that would have been reported in waves 5 and 6 had testing eligibility not changed, we created a simple linear regression model by using the summed transformed wastewater load at both WWTPs and summed

Table 3. Pearson correlation coefficients (*r*) between ln(x + 1) transformed daily SARS-CoV-2 load in wastewater and ln(x + 1) transformed hospitalizations among COVID-19 patients, by epidemic wave, at various lags, Peel region Regional Municipality of Peel, Ontario, Canada*

Lag, d	Epidemic waves					
	2	3	4	5	6	2–6
1	0.6294	0.7920	0.5681†	0.8841	0.4827	0.8110
2	0.5772	0.7617	NS	0.8968	0.5602	0.7967
3	0.6388	0.7608	0.3798	0.8613	0.5009	0.7889
4	0.5600	0.8679†	NS	0.8781	0.5117	0.8189†
5	0.5666	0.7513	NS	0.8618	0.5008	0.7621
6	0.6121	0.8024	NS	0.8913	0.4187	0.8062
7	0.6531†	0.7860	NS	0.9161†	0.5695	0.8120
8	0.6163	0.7625	0.4292	0.8711	0.5767†	0.8009
9	0.6254	0.8036	0.3733	0.8649	0.4673	0.8163
10	0.5249	0.7694	0.3894	0.8498	0.4713	0.7804
11	0.5955	0.8015	0.1440	0.7630	0.4292	0.7853
12	0.5333	0.7351	0.2552	0.7957	0.4124	0.7608
13	0.6369	0.7758	0.2907	0.7420	0.3114	0.7770
14	0.5650	0.7605	0.1717	0.7474	0.3976	0.7525

*Colors indicate strength of association: gray, weak ($r<0.4$); yellow, moderate ($0.4 \leq r < 0.7$); green, strong ($r \geq 0.7$). NS, not significant ($p \geq 0.05$).
†Largest *r* per wave.

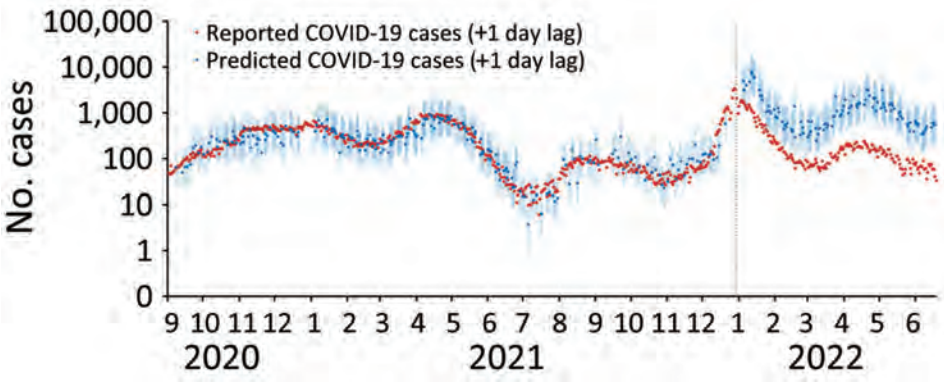

Figure 4. Predicted number of Peel COVID-19 cases (+ 1 day of wastewater sampling date) based on linear regression model using data before wave 5, Regional Municipality of Peel, Ontario, Canada, September 1, 2020–June 18, 2022. Data are plotted on the logarithmic scale. Light blue shaded area represents 95% prediction intervals. Vertical dotted line marks the date when clinical PCR testing for SARS-CoV-2 was restricted to high-risk populations, December 30, 2021.

COVID-19 case data, at a 1-day lag, from waves 2–4 (Figure 4). At the peak measured wastewater load of wave 5 on January 11, 2022, there were 1,160 reported COVID-19 cases, compared with a prediction of 7,515 cases (95% prediction interval 2,871–19,672), representing a 6.5-fold difference. At the peak of wave 6 (greatest measured wastewater load on April 21, 2022), there was an 18.7-fold difference between the estimated number of cases and reported COVID-19 cases (3,170 [95% prediction interval 1,224–8,211] vs. 170 reported cases).

Discussion

In December 2021, after the emergence of the Omicron variant, to conserve testing capacity the Ontario provincial government implemented changes to PCR test eligibility. As a result, we observed a rapid decrease in completed clinical PCR tests, high percentage positivity, and an increased wastewater-to-case ratio in Peel, indicating an underestimation of reported cases. Similar changes in wastewater-to-case ratios have been reported, resulting from changes in clinical testing strategies in other Canada municipalities (*19*). On the basis of the observed linear association between cases and SARS-CoV-2 load in wastewater in Peel, we estimated that the number of predicted cases was ≈6.5-fold greater than the number of reported cases at the peak of wave 5 (characterized by Omicron BA.1) and ≈18.7-fold greater than reported cases at the peak of wave 6 (Omicron BA.2). In January 2022 (wave 5), Peel Public Health provided near real-time incident case estimations based on wastewater concentrations to Peel hospitals that were experiencing considerable pressures for beds. Those data were, in turn, used to validate the hospitals' short-term scenario planning and to predict further challenges to hospital occupancy and staffing.

This simple method of case estimation can be easily replicated; however, it relies on linear regression, frequent sampling, and a historical baseline. The linear associations observed in Peel might have been applicable because of sewage collection system characteristics specific to the region. For example, Peel's storm water and sanitary sewage systems are separated. Furthermore, most of Peel's wastewater comes from residential sources; during August 2020–June 2022, the source of 72% of wastewater effluent was residential and the sources of 28% were industrial, commercial, or institutional. Last, Peel's 2 WWTPs serve >95% of Peel's residents, representing high population-level coverage.

Our study used calculations of load, which require daily measurements of total flow. In earlier analyses, we found similar linear associations between SARS-CoV-2 N-gene concentrations (copies/mL) at the 2 Peel WWTPs and the COVID-19 cases and hospitalizations (data not shown). However, to provide information about Peel as a whole, we found it beneficial to calculate total load to combine data from 2 WWTPs.

Although reported COVID-19 cases during the Omicron waves were known to be an underestimation of true cases, overall trends in reported cases still correlated with trends of SARS-CoV-2 load in wastewater. This association was also observed between SARS-CoV-2 loads in wastewater and hospitalizations of COVID-19 patients during wave 5, which was dominated by Omicron BA.1. This finding might indicate that, within Peel, SARS-CoV-2 load in wastewater might be predictive of hospitalizations for COVID-19, independent of changes in testing uptake, although the optimal lags were variant dependent. The findings of wastewater signal being an indicator of community disease burden were also reported from another Ontario study (*20*). However, because of many complex factors, such as differing virulence of new variants, advancements in treatment, vaccine effectiveness, waning immunity, and outbreaks in hospitals, hospitalizations associated with COVID-19 can vary. Those factors may have explained the poor linear relationship

between wastewater concentrations and hospitalizations in the Omicron BA.2–dominant wave 6.

In many wastewater surveillance systems, including the one for Peel, concentrations of SARS-CoV-2 in wastewater are normalized to concentrations of PMMoV, a fecal marker. In our study, PMMoV normalization generally did not improve the correlation between wastewater load and COVID-19 case counts, similar to findings in other studies (*8*,*9*,*21*), or COVID-19 patient hospitalizations, when compared with use of nonnormalized data. This lack of improved correlation might result from the low amount of inflow and infiltration as well as the source of wastewater being mainly residential (72%). Although normalization through PMMoV did not result in improved correlations in Peel, it might be useful in other systems (*4*). Furthermore, monitoring of fecal biomarkers may be used to assess sample quality (e.g., determining whether PMMoV concentrations are within an expected range for a given site).

Our results demonstrate the value of using population-based wastewater surveillance to detect increasing local COVID-19 activity and confirm declining case trends. Among the study limitations, data for numbers of COVID-19 cases included Peel residents and did not include patients who resided in neighboring jurisdictions but who would have contributed to SARS-CoV-2 in the G.E. Booth sewershed. However, we estimated that this contribution was relatively small, considering the large geographic area of the sewershed. Second, the COVID-19 hospitalization data used in our study were aggregated, and we were thus unable to discern whether patients were Peel residents. Third, our application of a historical, pre-Omicron, linear relationship to estimate COVID-19 cases during the Omicron waves was based on the assumption that fecal shedding patterns of SARS-CoV-2 remained the same regardless of SARS-CoV-2 variant, previous infection, and vaccination status. It has been reported that the amount of Omicron BA.2 on nasopharyngeal swabs was double that of Omicron BA.1 (*22*); but we are unaware of recent studies specific to virus in feces. If more fecal virus shedding is produced by Omicron than by other variants, our estimates of case underreporting would be overestimated. Fourth, we are unable to verify the number of true infections without population-level seroprevalence studies. Last, although linear regression is easily understood and accessible, interpretability of our case estimation results is limited as a result of autocorrelation. We found that residuals of the linear regression model exhibited positive autocorrelation, which may have resulted in less precise coefficient estimates and underestimated SEs and 95% prediction intervals. Further work is needed to determine modeling methods that might be more appropriate for analysis of wastewater time-series data (e.g., the SEIR [*23*] and PRESENS [*24*] models) and might also be easily implemented and interpretable by public health authorities. Despite this limitation, there was still value in using a simple method to approximate COVID-19 cases by using wastewater data. Furthermore, our predictions agreed with other estimates projected by hospital partners.

In summary, in the Regional Municipality of Peel, Canada, on the basis of strong historical linear associations between SARS-CoV-2 N-gene load in wastewater and reported COVID-19 cases, we estimated that reported COVID-19 cases were underestimated 19-fold at the peak of the Omicron BA.2 wave in April 2022. As a result of identifying SARS-CoV-2 wastewater load and population-level COVID-19 clinical outcomes, the monitoring of wastewater in Peel has provided critical information about community transmission of COVID-19 that is independent of clinical testing availability and uptake. Wastewater surveillance data can provide information for local decision-making and be a key metric in addition to traditional public health surveillance indicators, particularly for outcomes that are limited by availability of testing information and require triangulation of multiple data sources.

Acknowledgments

We gratefully acknowledge the University of Waterloo COVID-19 research team, Trillium Health Partners and William Osler Health System, members of the Ontario Wastewater Consortium, and Region of Peel Public Works and Public Health colleagues, including Matthew Badran, Erin Darling, Dave Brasher, Terrence Brouse, Bernardo Carrillo-Villaran, Alexandre Nunes, Alyssa Accardo, David Guillette, and Gregory Kujbida.

This work was funded by the Regional Municipality of Peel and the Ontario Ministry of the Environment, Conservation and Parks' Wastewater Surveillance Initiative. This research was undertaken thanks in part to funding from the Canada First Research Excellence Fund under the Global Water Futures Program; an NSERC Discovery Grant (M.R.S.); the Canada Research Chairs program (M.R.S., J.P.G.); and the Distinguished Visiting Professorship in the Department of Environmental Sciences, Baylor University (J.P.G.).

The datasets (wastewater and clinical cases) are available from the corresponding author on reasonable request.

About the Author

Ms. Cheng is an epidemiologist at Peel Public Health, where she supports public health surveillance of communicable and infectious diseases.

References

1. Medema G, Heijnen L, Elsinga G, Italiaander R, Brouwer A. Presence of SARS-coronavirus-2 RNA in sewage and correlation with reported COVID-19 prevalence in the early stage of the epidemic in the Netherlands. Environ Sci Technol Lett. 2020;7:511–6. https://doi.org/10.1021/acs.estlett.0c00357
2. Wu F, Zhang J, Xiao A, Gu X, Lee WL, Armas F, et al. SARS-CoV-2 titers in wastewater are higher than expected from clinically confirmed cases. mSystems. 2020;5:e00614–20. https://doi.org/10.1128/mSystems.00614-20
3. Ahmed W, Angel N, Edson J, Bibby K, Bivins A, O'Brien JW, et al. First confirmed detection of SARS-CoV-2 in untreated wastewater in Australia: a proof of concept for the wastewater surveillance of COVID-19 in the community. Sci Total Environ. 2020;728:138764. https://doi.org/10.1016/j.scitotenv.2020.138764
4. D'Aoust PM, Mercier E, Montpetit D, Jia JJ, Alexandrov I, Neault N, et al. Quantitative analysis of SARS-CoV-2 RNA from wastewater solids in communities with low COVID-19 incidence and prevalence. Water Res. 2021;188:116560. https://doi.org/10.1016/j.watres.2020.116560
5. La Rosa G, Iaconelli M, Mancini P, Bonanno Ferraro G, Veneri C, Bonadonna L, et al. First detection of SARS-CoV-2 in untreated wastewaters in Italy. Sci Total Environ. 2020;736:139652. https://doi.org/10.1016/j.scitotenv.2020.139652
6. Randazzo W, Truchado P, Cuevas-Ferrando E, Simón P, Allende A, Sánchez G. SARS-CoV-2 RNA in wastewater anticipated COVID-19 occurrence in a low prevalence area. Water Res. 2020;181:115942. https://doi.org/10.1016/j.watres.2020.115942
7. Wurtzer S, Marechal V, Mouchel JM, Maday Y, Teyssou R, Richard E, et al. Evaluation of lockdown effect on SARS-CoV-2 dynamics through viral genome quantification in wastewater, Greater Paris, France, 5 March to 23 April 2020. Euro Surveill. 2020;25:2000776. https://doi.org/10.2807/1560-7917.ES.2020.25.50.2000776
8. Feng S, Roguet A, McClary-Gutierrez JS, Newton RJ, Kloczko N, Meiman JG, et al. Evaluation of sampling, analysis, and normalization methods for SARS-CoV-2 concentrations in wastewater to assess COVID-19 burdens in Wisconsin communities. ACS EST Water. 2021;1:1955–65. https://doi.org/10.1021/acsestwater.1c00160
9. Xie Y, Challis JK, Oloye FF, Asadi M, Cantin J, Brinkmann M, et al. RNA in municipal wastewater reveals magnitudes of COVID-19 outbreaks across four waves driven by SARS-CoV-2 Variants of Concern. ACS EST Water. 2022;2:1852–62. https://doi.org/10.1021/acsestwater.1c00349
10. Statistics Canada. Population and dwelling counts: Canada, and census divisions (municipalities), Table 98–10–0002–03 [cited 2022 Jun 14]. https://doi.org/10.25318/9810000201-eng
11. Public Health Ontario. Ontario COVID-19 Data Tool. Cumulative counts and rates of COVID-19 in Ontario. 2022 Jul 16 [cited 2022 Jul 22]. https://www.publichealthontario.ca/en/data-and-analysis/infectious-disease/covid-19-data-surveillance/covid-19-data-tool?tab=maps
12. Ontario Ministry of Health. Updated eligibility for PCR testing and case and contact management guidance in Ontario. 2021 Dec 30 [cited 2022 Jul 22]. https://news.ontario.ca/en/backgrounder/1001387/updated-eligibility-for-pcr-testing-and-case-and-contact-management-guidance-in-ontario
13. Region of Peel - Public Health. Peel COVID-19 and respiratory illness reporting. 2022 Jan 21 [cited 2022 Jul 22]. https://www.peelregion.ca/coronavirus/case-status
14. Centers for Disease Control and Prevention National Wastewater Surveillance System. Developing a wastewater surveillance sampling strategy. 2022 Dec 9 [cited 2022 Jan 20]. https://www.cdc.gov/nwss/sampling/index.html
15. Centers for Disease Control and Prevention. CDC's influenza SARS-CoV-2 multiplex assay [cited 2022 Jul 22]. https://stacks.cdc.gov/view/cdc/88834
16. Zhang T, Breitbart M, Lee WH, Run JQ, Wei CL, Soh SWL, et al. RNA viral community in human feces: prevalence of plant pathogenic viruses. PLoS Biology. 2006;4:0108–0118. https://doi.org/10.1371/journal.pbio.0040003
17. Ontario Ministry of Health. Ontario Public Health Standards: Requirements for programs, services and accountability. Infectious Diseases Protocol. Appendix 1: Case definitions and disease-specific information [cited 2023 Jan 20]. https://www.health.gov.on.ca/en/pro/programs/publichealth/coronavirus/docs/2019_case_definition.pdf
18. Dinno A. Nonparametric pairwise multiple comparisons in independent groups using Dunn's test. Stata J. 2015;15:292–300. https://doi.org/10.1177/1536867X1501500117
19. D'Aoust PM, Tian X, Towhid ST, Xiao A, Mercier E, Hegazy N, et al. Wastewater to clinical case (WC) ratio of COVID-19 identifies insufficient clinical testing, onset of new variants of concern and population immunity in urban communities. Sci Total Environ. 2022;853:158547. https://doi.org/10.1016/j.scitotenv.2022.158547
20. Hegazy N, Cowan A, D'Aoust PM, Mercier É, Towhid ST, Jia J-J, et al. Understanding the dynamic relation between wastewater SARS-CoV-2 signal and clinical metrics throughout the pandemic. Sci Total Environ. 2022;853:158458. https://doi.org/10.1016/j.scitotenv.2022.158458
21. Maal-Bared R, Qiu Y, Li Q, Gao T, Hrudey SE, Bhavanam S, et al. Does normalization of SARS-CoV-2 concentrations by pepper mild mottle virus improve correlations and lead time between wastewater surveillance and clinical data in Alberta (Canada): comparing twelve SARS-CoV-2 normalization approaches. Sci Total Environ. 2023;856:158964. https://doi.org/10.1016/j.scitotenv.2022.158964
22. Lentini A, Pereira A, Winqvist O, Reinius B. Monitoring of the SARS-CoV-2 Omicron BA.1/BA.2 lineage transition in the Swedish population reveals increased viral RNA levels in BA.2 cases. Med. 2022;3:636–643.e4. https://doi.org/10.1016/j.medj.2022.07.007
23. McMahan CS, Self S, Rennert L, Kalbaugh C, Kriebel D, Graves D, et al. COVID-19 wastewater epidemiology: a model to estimate infected populations. Lancet Planet Health. 2021;5:e874–81. https://doi.org/10.1016/S2542-5196(21)00230-8
24. Ando H, Murakami M, Ahmed W, Iwamoto R, Okabe S, Kitajima M. Wastewater-based prediction of COVID-19 cases using a highly sensitive SARS-CoV-2 RNA detection method combined with mathematical modeling. Environ Int. 2023;173:107743. https://doi.org/10.1016/j.envint.2023.107743

Address for correspondence: Monali Varia, Regional Municipality of Peel, 7120 Hurontario St., PO Box 630, RPO Streetsville, Mississauga, ON L5M 2C1, Canada; email: monali.varia@peelregion.caw

Predicting COVID-19 Incidence Using Wastewater Surveillance Data, Denmark, October 2021–June 2022

Oliver McManus, Lasse Engbo Christiansen, Maarten Nauta, Lene Wulff Krogsgaard, Naja Stolberg Bahrenscheer, Lene von Kappelgaard, Tobias Christiansen, Mikkel Hansen, Nicco Claudio Hansen, Jonas Kähler, Anders Rasmussen, Stine Raith Richter, Lasse Dam Rasmussen, Kristina Træholt Franck, Steen Ethelberg

Analysis of wastewater is used in many settings for surveillance of SARS-CoV-2, but it remains unclear how well wastewater testing results reflect incidence. Denmark has had an extensive wastewater analysis system that conducts 3 weekly tests in ≈200 sites and has 85% population coverage; the country also offers free SARS-CoV-2 PCR tests to all residents. Using time series analysis for modeling, we found that wastewater data, combined with information on circulating variants and the number of human tests performed, closely fitted the incidence curve of persons testing positive. The results were consistent at a regional level and among a subpopulation of frequently tested healthcare personnel. We used wastewater analysis data to estimate incidence after testing was reduced to a minimum after March 2022. These results imply that data from a large-scale wastewater surveillance system can serve as a good proxy for COVID-19 incidence and for epidemic control.

The COVID-19 pandemic has shown the need for accurate surveillance data. Incidence rate data, commonly collected as part of human surveillance, can only be interpreted with the understanding that local testing strategies vary over time. COVID-19 surveillance using wastewater testing, in which SARS-CoV-2 RNA fragments shed in the feces of infected persons are quantified, has been implemented in many countries (*1*–*5*). Wastewater data have been suggested as a complement to or even a substitute for human surveillance data, particularly in times of low human testing activity. The association between wastewater concentrations and incidence has been demonstrated in multiple settings, but few studies have succeeded in predicting incidence through wastewater surveillance, and the direct value of wastewater testing for epidemic control remains debatable (*1*).

In response to the pandemic, Denmark set up an extensive wastewater surveillance system, which was implemented in July 2021 and fully rolled out in October 2021. During the study period, the system included 201 wastewater treatment plant (WWTP) inlets, which were sampled 3 times a week and covered 85% of the population. Denmark has also had exceptionally high COVID-19 testing capacity, offering unlimited, free reverse transcription PCR (RT-PCR) testing through public testing stations (*6*,*7*; M.A. Gram et al., unpub. data, http://medrxiv.org/lookup/doi/10.1101/2023.02.06.23285556). The per capita testing rate has been among the highest in the world during some periods of the pandemic; the country tested up to 27% of the population per week in December 2021 and was capturing an estimated 70% of active COVID-19 cases at the start of 2022 (M.A. Gram et al., unpub. data). However, testing activity was scaled down in early 2022, to <1% per week by June 2022 (*8*,*9*).

Given the variation in testing rates, wastewater concentrations should not be directly compared with observed incidence. Instead, models should include information on changing testing rates over time.

Author affiliations: European Centre for Disease Prevention and Control, Solna, Sweden (O. McManus); Statens Serum Institut, Copenhagen, Denmark (O. McManus, L.E. Christiansen, M. Nauta, L.W. Krogsgaard, N.S. Bahrenscheer, L. von Kappelgaard, T. Christiansen, M. Hansen, N.C. Hansen, J. Kähler, A. Rasmussen, S.R. Richter, L.D. Rasmussen, K.T. Franck, S. Ethelberg); University of Copenhagen, Copenhagen, Denmark (S. Ethelberg)

DOI: https://doi.org/10.3201/eid2908.221634

Another strategy is to look at a subgroup of regularly tested persons, where the effect of fluctuations in testing patterns should be less pronounced. Such a subgroup exists in Denmark, where recommendations were made for regular screening tests for certain care personnel (*10*).

The association between wastewater data and incidence might be affected by the SARS-CoV-2 variants in circulation, because those variants could have different fecal shedding patterns. Viral load for oropharyngeal samples has been shown to be higher for Delta than previous variants (B. Li et al., unpub. data, https://www.medrxiv.org/content/10.1101/2021.07.07.21260122v2), but how fecal shedding differs among variants is not known (*11*). Other variables, such as temperature and traveling time of SARS-CoV-2 in sewers, dilution by precipitation or wastewater from industry, and inhibitors of laboratory analyses, might affect viral quantification, (*12*,*13*).

We used the results of wastewater surveillance to predict the observed incidence of SARS-CoV-2 infections in Denmark. We performed the analysis at the national and regional level and among a subgroup of healthcare personnel.

Methods

Overview

We conducted a time-series analysis, constructing a model to explain observed incidence by wastewater concentrations. Besides the main national-level analysis, we also tested the model at a regional level and on a subpopulation of healthcare personnel. We used the human testing rate as a covariate in our model and considered interactions between wastewater concentrations and the proportion of circulating Omicron versus Delta variants and between wastewater concentrations and wastewater temperature. The study period was September 27, 2021–June 26, 2022.

Data Sources

Wastewater

Throughout the study period, 24-hour composite samples were taken 3 times a week from 202 WWTP inlets across Denmark. Sampling started on Mondays, Tuesdays, and Thursdays. Where possible, the samples were flow-proportional, which enabled sampling of more water at times of heavy flow, providing a more representative sample of the 24-hour water flow. Otherwise, samples were time-proportional, sampling a fixed amount of water at fixed time intervals.

Samples were purified and analyzed using quantitative real-time RT-PCR at Eurofins Miljø, a central commercial laboratory in Vejen, Denmark. We measured cycle threshold (Ct) values for 2 SARS-CoV-2 genes (the N2 region of the nucleocapsid gene and the RNA-dependent RNA polymerase [RdRp]) and converted them to concentrations (copies/L). We calculated limits of detection (LOD) and limits of quantification (LOQ) for each gene in each sample. We imputed values <LOD as LOD/2, and <LOQ as (LOD + LOQ)/2. Starting in 2022, we also measured the concentrations of 2 indicators of fecal concentration: crAssphage and pepper mild mottle virus (*14*,*15*). For consistency with 2021 data, we used those measurements as data quality indicators but not to normalize SARS-CoV-2 concentrations.

For each sample, utility companies reported the volume of wastewater that entered WWTPs over the 24-hour sampling window and the temperature of wastewater upon entry. Utility companies also provided geographic information, which we used to calculate the resident population of each catchment area by linking to the Danish Civil Registration System (*16*).

Incidence

In-person PCR COVID-19 testing was available for free to all residents throughout our study period; results were collected centrally in the Danish Microbiology Database (*17*). Testing recommendations changed throughout the study period; the most substantial change occurred on March 10, 2022. After that date, tests for the general population were recommended only for symptomatic persons in groups at high risk (*9*). We extracted data on daily incidence of PCR-confirmed COVID-19 cases and weekly PCR testing rate from Denmark's official COVID-19 statistics (*18*) for its 5 administrative regions.

Care Personnel

We used data on healthcare personnel, consisting of care home staff and in-home caretakers, for a secondary analysis. During September 4, 2021–April 28, 2022, weekly PCR tests were recommended for healthcare personnel for screening purposes. After this time and until the end of the study period, the recommendation was 1 test every 2 weeks (*10*). Because of those recommendations, we believed incidence in this group might be less affected by testing patterns and therefore a better measure of actual community incidence than observed incidence among the general population. Information on this group came from Denmark's centrally collected data on COVID-19

tests and results, linked to employment information through the Civil Registration System (*16*,*19*).

Variants

Denmark had extensive whole-genome sequencing to monitor SARS-CoV-2 variants, sequencing up to 15,000 samples/week (*20*,*21*). We calculated the weekly proportion of sequences belonging to the Delta and Omicron variants through the start of June 2022, excluding other variants that were present in negligible amounts.

Data Processing

Our wastewater measure for each sample is expressed as the average number of SARS-CoV-2 RNA copies shed per person living in the WWTP catchment area during a 24-hour sampling period. We calculated this value using the equation

$$X = \frac{C \times V}{P}$$

where C is the geometric mean of the N2 and RdRp gene concentrations (in copies/L) and is log-normally distributed, V is the volume of wastewater (in liters) that entered the WWTP in a 24-hour measurement period, and P is the population size of the catchment area. We removed outliers of wastewater volume measurements, defined as being >1.5 times the interquartile range from the 25th or 75th percentile, and then truncated values at 1.96 SDs from the mean on the log scale.

We aggregated all data into weekly observations: incidence was weekly cases per 100,000 population; testing rate was weekly tests per 1,000 population; wastewater concentrations were the weekly weighted median of all average copies per person measurements (≈600 values of *X* per week), using the $\log_{10}$-transformed population size of each WWTP catchment area as the weights (the choice of weight being a compromise between equal weighting because of the uncertainty of individual measurements and weighting according to population size); wastewater temperature was similarly the weekly weighted median. Wastewater concentrations were log-normally distributed, and the variance of incidence and testing rates increases with the values, so we used $\log_{10}$-transformed versions of those variables in our models, using the same transformation for all to ease interpretation.

Exclusions

Because great fluctuations in the fecal load of wastewater are not expected, finding such a fluctuation in measurements of the fecal indicators pepper mild mottle virus and crAssphage indicated a likely failure in sampling or laboratory analysis. We therefore excluded samples with missing or extreme concentrations of these fecal indicators, defined as concentrations ≥3 SDs from the mean for each WWTP, on the log scale. We also excluded samples that the laboratory received on unexpected days of the week. Such samples might not have been comparable to others because more time had passed in which RNA content could have degraded during transit. Furthermore, we excluded samples with missing values for the volume of wastewater entering the WWTP over a 24-hour sampling period. Finally, we excluded samples from WWTPs where we had no geographic information defining the catchment area, which we needed to define the population served by each WWTP. We also discarded wastewater temperature data reported as <1°C or >30°C, but we did not exclude other data for those samples from the analysis.

Statistical Analysis

First, we plotted the national incidence and wastewater concentrations to compare patterns visually. Second, we fitted a model to see whether wastewater results were a predictor of national incidence. We split the data into a training and testing set. We used training data from before June 9, 2022, to select and estimate our models. We reserved data from June 9, 2022, onward (7 weekly datapoints) as an out-of-sample test dataset for model validation. We constructed an ARIMAX (autoregressive integrated moving average with exogenous variables) model, using incidence as the dependent variable and wastewater concentrations and testing rate as the explanatory variables. We tested including the interaction between wastewater concentrations and the circulating variant (expressed as proportion of Delta sequences) and the interaction between wastewater concentration and wastewater temperature. We only included temperature as an interaction with the wastewater concentration to restrict it to describe degradation of RNA and not the overall seasonal effect on incidence. Likewise, the proportion of Delta was included as an interaction with the wastewater concentration to adjust for different shedding patterns for the different variants. We selected which covariates to include based on the Akaike information criterion. For consistency, we used the terms selected for the national model in the secondary models as well. Third, we also estimated the model allowing for a time delay between wastewater results and incidence. We examined lag times of 0, 1, and 2 weeks in each direction, comparing the resulting models by

the Akaike information criterion. Fourth, we validated the model on the out-of-sample dataset not used in the model estimation, using the root mean squared error. Fifth, we repeated the modeling steps in 2 secondary analyses: reestimating the main model independently for each region and for the subpopulation of care personnel only. For the care personnel model, we used both incidence and testing rate specific to care personnel. Sixth, we used the national model to predict the incidence that would have been observed had the testing rate remained stable throughout the study period by generating model predictions where we fixed the testing rate at a constant value. We used the highest recorded testing rate in the study period for this. We used R version 4.1.3 (The R Project for Statistical Computing, https://cran.r-project.org) for statistical analyses (Appendix, https://wwwnc.cdc.gov/EID/article/29/8/22-1634-App1.pdf).

Results

Description of Data

We included 18,737 wastewater samples from 202 WWTPs in the study (Appendix Table 1). Our initial dataset consisted of 21,069 samples, but we excluded 2,361 samples (29 for extreme concentrations of fecal indicators, 301 from WWTPs with unknown populations, 81 that arrived on unexpected days of the week, 919 missing data on wastewater flow in the sampling period, and 1,031 with sampling method not listed as flow-proportional or time-proportional). Of the included samples, 15,801 were flow-proportional and 2,764 were time-proportional. After aggregating by week at national level, we had 39 wastewater data points. We included a median of 515 (interquartile range 480.5–532.5) weekly samples.

Wastewater concentrations and incidence followed similar patterns, increasing until early 2022, decreasing until late May, and then increasing again (Figure 1). Testing rates remained fairly stable during November 2021–February 2022, after which they decreased to low levels. Per person, on average 2.6 times as many weekly tests occurred among healthcare personnel as occurred among the general population.

Incidence followed a similar pattern in all regions (Appendix Figure 1), although slightly offset in time. Numbers throughout 2021 were slightly higher in the Capital region and neighboring Zealand region than in the other 3 regions. The pattern of testing rate over time also did not differ greatly by region (Appendix Figure 2).

Until late November 2021, nearly all human isolates sequenced were the Delta variant. Omicron quickly took over in December, reaching ≈50% halfway through the month and >95% in the first week of January 2022. After that, nearly all samples were Omicron (Appendix Figure 3).

Model Results

Our final models were based on wastewater concentration, testing rate, and the interaction of wastewater concentration with circulating variants (percentage Delta). They did not include the interaction between wastewater results and wastewater temperature, because it did not improve the model (Appendix). The model performed best with no lead or lag time between wastewater results and incidence.

The pattern of the model fit and validation estimates follows the pattern of observed incidence well (Figure 2; Appendix Figure 4). However, only 43% of validation points were covered by the 95% prediction intervals in the national model (Appendix Table 3).

The coefficients for wastewater results were generally 0.4–0.5 during Omicron; coefficients were lower during Delta by ≈0.15–0.20 (Table). The coefficient for wastewater was higher in the care personnel model

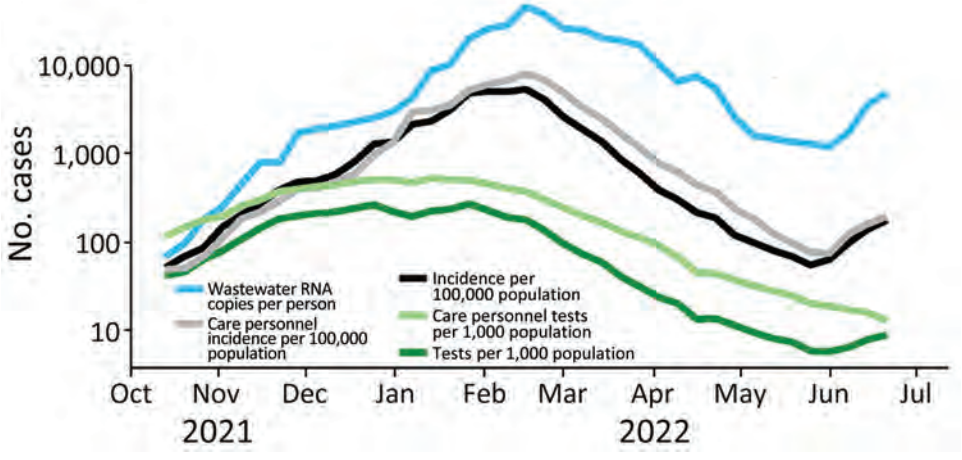

Figure 1. Comparison of results of COVID-19 wastewater surveillance with incidence and testing rate (both national and for care personnel) over time, Denmark, illustrating the agreement between wastewater concentrations and incidence. Wastewater concentrations are based on 18,565 individual samples. Testing rates were high during November 2021–February 2022 and decreased after that time.

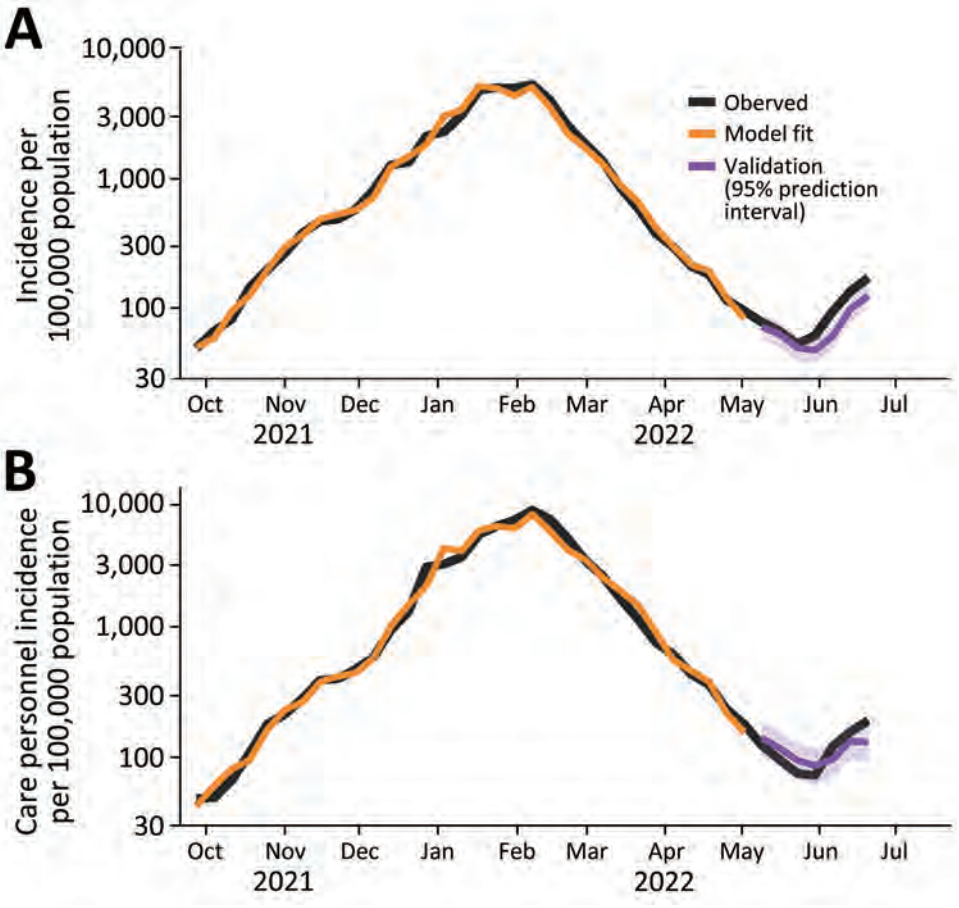

Figure 2. Model fit and forecasts for the national model (A) and the care personnel model (B) used in study of predicting COVID-19 incidence using wastewater surveillance data, Denmark. The fitted values (orange) are seen to follow the observed incidence (black) during the training period. The forecasts in the test period (purple) are also shown against the observed incidence (black).

(0.52 [95% CI 0.46–0.59] during Omicron) than in the main national model (0.40 [95% CI 0.34–0.46]). At a regional level, the wastewater coefficient was lower for the Capital region than other regions (0.31 [95% CI 0.24–0.38] during Omicron).

Predicted Incidence at Stable Testing

We used the national model to estimate the COVID-19 incidence that would have been observed if the testing rate had remained constant (Figure 3). We used the highest testing rate in our study period (270 weekly tests/1,000 persons, as in the week of January 17, 2022). The difference between the model predictions and the observed incidence can be used as a measure of underreporting. Given the estimate from serologic studies that 70% of actual cases were captured in early 2022, we estimate that ≈15% of actual cases were captured by the national PCR testing system from April 2022 on.

Discussion

We constructed a model to explain the observed incidence of COVID-19 in Denmark using wastewater data, information on the circulating variants, and the number of human tests performed as predictors. We found that we could accurately reconstruct the observed incidence curve. Results were consistent at a regional level and among the subgroup of frequently tested care personnel. Using data from a country with extensive wastewater and human testing systems, we demonstrated that predicting incidence based on wastewater surveillance is possible. We used these results to predict the incidence that could have been observed in Denmark if testing activity had remained high. In Denmark, after mass-testing programs were rolled back in the spring of 2022, wastewater analysis became a key source of information for the healthcare system in its handling of the COVID-19 pandemic.

The steeper association between wastewater and incidence during the Omicron period than in the Delta period might indicate that shedding dynamics differ between variants. However, the transition from Delta to Omicron coincided with the peak of rollout of vaccine booster doses (22). Information is lacking on how vaccination affects fecal shedding, but nasopharyngeal viral loads appear lower among vaccinated persons (2). Further studies are needed on how

fecal shedding is affected by SARS-CoV-2 variants and vaccination status.

The model fit at the regional level was generally very similar to that for national results, although wastewater concentrations had less effect in the model for the Capital region. A likely factor is that the Capital region is dominated by 4 very large catchment areas, and correlations between wastewater concentration and incidence are poorer in larger catchment areas (*1*). Commuting across catchment areas, which is typical for the densely populated Capital region, might also have played a role.

We performed a subanalysis of healthcare personnel, who were consistently tested at a higher rate than the general population for screening purposes. We reasoned that the incidence of healthcare personnel would be less dependent on testing rates than the observed incidence in the general population. In fact, testing among this group followed a similar pattern over time to that of the general population and gave similar model results, possibly because the overall testing rate in Denmark was so high.

We used the national model to estimate what observed incidence would have been if the testing rate had remained at its maximum. We estimated that the proportion of actual cases identified had fallen to ≈15% by April 2022. However, if tests became more targeted over time as recommendations for regular screening tests were relaxed, the percentage of cases identified could be higher.

SARS-CoV-2 is known to decay faster at higher temperatures (*12*,*13*), but including an interaction term between wastewater results and temperature did not improve our model fit. The effect of temperature might have been outweighed by other unmeasured factors that affect SARS-CoV-2 decay, such as retention time in the sewage system or other chemical components of wastewater.

Unlike other studies (*1*), we did not find wastewater results to be a leading indicator of incidence. That

Table. Estimated coefficients from the national model, care personnel model, and regional model in study using wastewater surveillance data to predict COVID-19 incidence, Denmark, October 2021–June 2022*

Model	Term	Estimate (95% CI)	p value
National	AR (1)	0.46 (0.16–0.76)	0.004
	Wastewater concentration	0.4 (0.34–0.46)	<0.001
	Testing rate	0.87 (0.81–0.94)	<0.001
	Wastewater concentration × Delta (%)	−0.15 (−0.19 to −0.11)	<0.001
	Intercept	−0.14 (−0.32 to 0.04)	0.12
Care personnel	AR (1)	0.32 (−0.06 to 0.70)	0.1
	Wastewater concentration	0.52 (0.46–0.59)	<0.001
	Testing rate (care personnel)	0.84 (0.73–0.94)	<0.001
	Wastewater concentration × Delta (%)	−0.17 (−0.21 to −0.13)	<0.001
	Intercept	−2.45 (−2.83 to −2.07)	<0.001
Regional			
Capital Region	AR (1)	0.31 (−0.07 to 0.70)	0.12
	Wastewater concentration	0.31 (0.24–0.38)	<0.001
	Testing rate	1.03 (0.94–1.11)	<0.001
	Wastewater concentration × Delta (%)	−0.15 (−0.19 to −0.12)	<0.001
	Intercept	−0.11 (−0.34 to 0.12)	0.3
Central Denmark	AR (1)	−0.19 (−0.56 to 0.18)	0.3
	Wastewater concentration	0.48 (0.45–0.52)	<0.001
	Testing rate	0.88 (0.84–0.92)	<0.001
	Wastewater concentration × Delta (%)	−0.14 (−0.16 to −0.12)	<0.001
	Intercept	−0.48 (−0.60 to −0.36)	<0.001
North Denmark	AR (1)	−0.09 (−0.46 to 0.28)	0.6
	Wastewater concentration	0.47 (0.43–0.51)	<0.001
	Testing rate	0.91 (0.86–0.96)	<0.001
	Wastewater concentration × Delta (%)	−0.16 (−0.19 to −0.13)	<0.001
	Intercept	−0.49 (−0.64 to −0.33)	<0.001
Southern Denmark	AR (1)	0.16 (−0.19 to 0.51)	0.4
	Wastewater concentration	0.48 (0.44–0.52)	<0.001
	Testing rate	0.83 (0.78–0.88)	<0.001
	Wastewater concentration × Delta (%)	−0.15 (−0.17 to −0.12)	<0.001
	Intercept	−0.39 (−0.52 to −0.26)	<0.001
Zealand	AR (1)	0.07 (−0.34 to 0.47)	0.7
	Wastewater concentration	0.42 (0.37–0.48)	<0.001
	Testing rate	0.8 (0.73–0.86)	<0.001
	Wastewater concentration × Delta (%)	−0.14 (−0.17 to −0.11)	<0.001
	Intercept	−0.11 (−0.26 to 0.04)	0.2

*The response variable incidence, wastewater concentration, and testing rate are included after $\log_{10}$-transformation. AR (1) denotes the first-order autoregressive term.

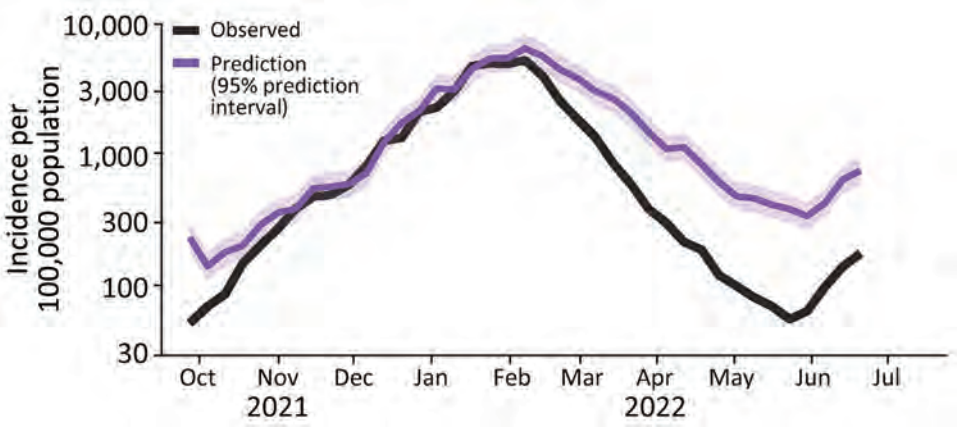

Figure 3. Predicted COVID-19 incidence at a constant testing rate (purple) based on the national model, compared with observed incidence (black), in study of wastewater surveillance data as a predictor of COVID-19 incidence, Denmark. The prediction is an estimate of the true incidence. The proportion of estimated true cases captured decreased from >80% to ≈20% during 2022.

difference might be because our analysis was based on weekly data, so we could only assess lag times in 7-day intervals. However, a lag of <1 week would likely have limited effects on public health action in practice. In addition, extensive human testing occurred during most of the study period, so infections might have been detected earlier than in other settings.

In our models, the coefficient for wastewater concentrations was <1. This result might seem surprising, because it means that a doubling in wastewater concentrations is not associated with a doubling in incidence (after adjusting for testing rate). Several explanations exist for this finding. First, the variability in the number of viral copies shed is best described by a log-normal distribution (*23*,*24*). The cumulative number of copies shed by a population will therefore follow a highly skewed distribution (*24*,*25*), which in itself is expected to lead to a coefficient <1, as seen in simulation models generating the relationship between the number of infected persons in the population and concentration of RNA in sewage (*26*). Second, observed incidence depends on the testing pattern; specifically, the probability that an infected person will be tested and have a positive result. The testing rate that we included in our models is an imperfect measure of this probability. Third, testing rate itself is influenced by incidence. Testing rates were highest, on average, when incidence was high. This factor might have increased the predictive power of testing rate in our models and therefore disadvantaged wastewater as a predictor. This interpretation is supported by the fact that the coefficient for testing rate in the national model (0.87 [95% CI 0.81–0.94]) is higher than the 0.7 that was found in Denmark's method for estimating the reproduction number in the fall of 2020 (*27*). The secondary analysis of healthcare personnel provides further support. We expected observed incidence in this population to be a closer reflection of actual incidence (compared to national observed incidence numbers) because the testing rate was more stable. That expectation is consistent with our results: a larger coefficient for wastewater concentrations and marginally smaller (though with overlapping 95% CIs) coefficient for testing rate.

The first limitation of our model is that testing rate is influenced by incidence and changes in recommendations. However, this effect was likely smaller in our setting than in most others because there were high numbers of screening tests for asymptomatic people for much of the study period. Another limitation is that the performance of the model on the validation data was mixed. Validation model estimates clearly followed the same pattern as the observed incidence, but they were lower than the observed data; most of the 95% prediction intervals did not include the observed data. This discrepancy is likely because of the changes in recommendations in the first half of 2022, in which a gradual shift occurred toward less testing for screening purposes and a larger share of diagnostic testing of symptomatic persons. Finally, we could not incorporate the unknown effect of immunity (through vaccination or previous infection) on fecal shedding.

This study benefited from copious wastewater testing data because of the extensive surveillance system in Denmark. One remaining question is how well wastewater data perform in less developed surveillance systems. Denmark's surveillance was scaled down after this study period to incorporate fewer WWTPs and fewer weekly samples. Repeating this analysis once enough data has been collected under the new system might help answer that question.

In conclusion, we performed a large-scale study of the association between wastewater results and observed incidence of COVID-19. Our relatively simple model makes it easy to specifically examine the

association between wastewater results and incidence. We found that wastewater testing results can be used to accurately model the observed incidence of COVID-19, in combination with data on human tests. This finding implies that wastewater testing can serve as a proxy for incidence in the context of little to no human testing. The link between wastewater concentrations and incidence has been stronger since Omicron has been dominant. We found no effect of temperature on the association. For a wastewater surveillance system as extensive as that of Denmark, we believe wastewater results are a trustworthy indicator of actual incidence, especially in a situation in which human testing rates continue to decline.

Acknowledgments

We gratefully thank our partners at the utility companies who collected the wastewater samples. We also thank our partners at Eurofins Miljø for performing the laboratory analyses.

Funding came from a Danish governmental grant as part of epidemic control measures.

Data used for this study are available at https://github.com/oloverm/ww-incidence and https://zenodo.org/record/8060977.

About the Author

Mr. McManus is an epidemiologist at Denmark's national public health institute, Statens Serum Institut, and a fellow of the European Programme for Intervention Epidemiology Training. His primary research interest is wastewater surveillance of COVID-19.

References

1. Li X, Zhang S, Sherchan S, Orive G, Lertxundi U, Haramoto E, et al. Correlation between SARS-CoV-2 RNA concentration in wastewater and COVID-19 cases in community: a systematic review and meta-analysis. J Hazard Mater. 2023;441:129848.
2. Morvan M, Jacomo AL, Souque C, Wade MJ, Hoffmann T, Pouwels K, et al. An analysis of 45 large-scale wastewater sites in England to estimate SARS-CoV-2 community prevalence. Nat Commun. 2022;13:4313. https://doi.org/10.1038/s41467-022-31753-y
3. RIVM. Coronavirus monitoring in sewage research. 2022 [cited 2022 Sep 5]. https://www.rivm.nl/en/covid-19/sewage
4. Cluzel N, Courbariaux M, Wang S, Moulin L, Wurtzer S, Bertrand I, et al.; Obépine consortium. A nationwide indicator to smooth and normalize heterogeneous SARS-CoV-2 RNA data in wastewater. Environ Int. 2022;158:106998. https://doi.org/10.1016/j.envint.2021.106998
5. Tiwari A, Lipponen A, Hokajärvi AM, Luomala O, Sarekoski A, Rytkönen A, et al. Detection and quantification of SARS-CoV-2 RNA in wastewater influent in relation to reported COVID-19 incidence in Finland. Water Res. 2022;215:118220. https://doi.org/10.1016/j.watres.2022.118220
6. Michlmayr D, Hansen CH, Gubbels SM, Valentiner-Branth P, Bager PM, Obel N, et al. Observed protection against SARS-CoV-2 reinfection following a primary infection: a Danish cohort study among unvaccinated using two years of nationwide PCR-test data. Lancet Reg Health Eur. 2022;20:100452. https://doi.org/10.1016/j.lanepe.2022.100452
7. Gram MA, Emborg HD, Schelde AB, Friis NU, Nielsen KF, Moustsen-Helms IR, et al. Vaccine effectiveness against SARS-CoV-2 infection or COVID-19 hospitalization with the Alpha, Delta, or Omicron SARS-CoV-2 variant: a nationwide Danish cohort study. Beeson JG, editor. PLOS Med. 2022;19:e1003992.
8. Hasell J, Mathieu E, Beltekian D, Macdonald B, Giattino C, Ortiz-Ospina E, et al. A cross-country database of COVID-19 testing. Sci Data. 2020;7:345. https://doi.org/10.1038/s41597-020-00688-8
9. Statens Serum Institut. When COVID-19 struck the world and Denmark—see the timeline here [in Danish]. 2022 [cited 2023 Jun 23]. https://www.ssi.dk/aktuelt/nyheder/2022/da-covid-19-ramte-verden-og-danmark-se-tidslinjen-her
10. Danish Health Authority. Guidance about prevention of infection with new coronavirus in care homes, residential facilities, etc. and in home care [in Danish]. 2022 [cited 2022 Jul 14]. https://www.sst.dk/da/Udgivelser/2022/Vejledning-om-forebyggelse-af-smitte-med-ny-coronavirus-paa-plejehjem-mv-og-i-hjemmeplejen
11. Bertels X, Demeyer P, Van den Bogaert S, Boogaerts T, van Nuijs ALN, Delputte P, et al. Factors influencing SARS-CoV-2 RNA concentrations in wastewater up to the sampling stage: a systematic review. Sci Total Environ. 2022;820:153290. https://doi.org/10.1016/j.scitotenv.2022.153290
12. Li X, Zhang S, Shi J, Luby SP, Jiang G. Uncertainties in estimating SARS-CoV-2 prevalence by wastewater-based epidemiology. Chem Eng J. 2021;415:129039. https://doi.org/10.1016/j.cej.2021.129039
13. Bivins A, Greaves J, Fischer R, Yinda KC, Ahmed W, Kitajima M, et al. Persistence of SARS-CoV-2 in water and wastewater. Environ Sci Technol Lett. 2020;7:937–42. https://doi.org/10.1021/acs.estlett.0c00730
14. Wilder ML, Middleton F, Larsen DA, Du Q, Fenty A, Zeng T, et al. Co-quantification of crAssphage increases confidence in wastewater-based epidemiology for SARS-CoV-2 in low prevalence areas. Water Res X. 2021;11:100100. https://doi.org/10.1016/j.wroa.2021.100100
15. Kitajima M, Sassi HP, Torrey JR. Pepper mild mottle virus as a water quality indicator. Npj Clean Water. 2018;1:19. https://doi.org/10.1038/s41545-018-0019-5
16. Schmidt M, Pedersen L, Sørensen HT. The Danish Civil Registration System as a tool in epidemiology. Eur J Epidemiol. 2014;29:541–9. https://doi.org/10.1007/s10654-014-9930-3
17. Voldstedlund M, Haarh M, Mølbak K; MiBa Board of Representatives. The Danish Microbiology Database (MiBa) 2010 to 2013. Euro Surveill. 2014;19:20667. https://doi.org/10.2807/1560-7917.ES2014.19.1.20667
18. Statens Serum Institut. COVID-19 inventories [in Danish]. 2021 [cited 2022 Aug 1]. https://covid19.ssi.dk/overvagningsdata/download-fil-med-overvaagningdata
19. States Serum Institut. Weekly trends: COVID-19 and other respiratory infections, week 28, 2022 [cited 2022 Sep 30]. https://www.ssi.dk/-/media/cdn/files/covid19/

tendensrapport/rapport/ugentlige-tendenser-covid19-andre-luftvejs-uge28-2022_fdj1.pdf
20. Danish Covid-19 Genome Consortium. Genomic overview of SARS-CoV-2 in Denmark. 2022 [cited 2022 Sep 9]. https://www.covid19genomics.dk/statistics
21. Espenhain L, Funk T, Overvad M, Edslev SM, Fonager J, Ingham AC, et al. Epidemiological characterisation of the first 785 SARS-CoV-2 Omicron variant cases in Denmark, December 2021. Euro Surveill. 2021;26:2101146. https://doi.org/10.2807/1560-7917.ES.2021.26.50.2101146
22. Mathieu E, Ritchie H, Ortiz-Ospina E, Roser M, Hasell J, Appel C, et al. A global database of COVID-19 vaccinations. Nat Hum Behav. 2021;5:947–53. https://doi.org/10.1038/s41562-021-01122-8
23 McMahan CS, Self S, Rennert L, Kalbaugh C, Kriebel D, Graves D, et al. COVID-19 wastewater epidemiology: a model to estimate infected populations. Lancet Planet Health. 2021;5:e874–81. https://doi.org/10.1016/S2542-5196(21)00230-8
24. Nauta M, McManus O, Træholt Franck K, Lindberg Marving E, Dam Rasmussen L, Raith Richter S, et al. Early detection of local SARS-CoV-2 outbreaks by wastewater surveillance: a feasibility study. Epidemiol Infect. 2023;151:e28. https://doi.org/10.1017/S0950268823000146
25. Fenton L. The sum of log-normal probability distributions in scatter transmission systems. IEEE Trans Commun. 1960;8:57–67. https://doi.org/10.1109/TCOM.1960.1097606
26. Medema G, Been F, Heijnen L, Petterson S. Implementation of environmental surveillance for SARS-CoV-2 virus to support public health decisions: opportunities and challenges. Curr Opin Environ Sci Health. 2020;17:49–71. https://doi.org/10.1016/j.coesh.2020.09.006
27. Statens Serum Institut. Expert report October 23, 2020 - Incidence and projection of COVID-19 cases [in Danish]. 2020 [cited 2022 Sep 30]. https://covid19.ssi.dk/-/media/ssi-files/ekspertrapport-af-den-23-oktober-2020-incidens-og-fremskrivning-af-covid19-tilflde.pdf

Address for correspondence: Steen Ethelberg, Department of Infectious Disease Epidemiology and Prevention, Statens Serum Institut, Artillerivej 5, 2300 Copenhagen, Denmark; e-mail: set@ssi.dk

Multidrug-Resistant Bacterial Colonization and Infections in Large Retrospective Cohort of Mechanically Ventilated COVID-19 Patients[1]

Davide Mangioni, Liliane Chatenoud, Jacopo Colombo, Emanuele Palomba, Fernando A. Guerrero, Matteo Bolis, Nicola Bottino, Giuseppe Breda, Maria V. Chiaruttini, Gabriele Fior, Manuela Marotta, Giovanni Massobrio, Caterina Matinato, Antonio Muscatello, Paola Previtali, Sara Santambrogio, Francesca Tardini, Gianluca Zuglian, Giacomo Grasselli, Roberto Fumagalli, Andrea Gori, Nino Stocchetti, Gianpaola Monti,[2] Alessandra Bandera,[2] and the MDR in FIERA Study Group[3]

Few data are available on incidence of multidrug-resistant organism (MDRO) colonization and infections in mechanically ventilated patients, particularly during the COVID-19 pandemic. We retrospectively evaluated all patients admitted to the COVID-19 intensive care unit (ICU) of Hub Hospital in Milan, Italy, during October 2020–May 2021. Microbiologic surveillance was standardized with active screening at admission and weekly during ICU stay. Of 435 patients, 88 (20.2%) had MDROs isolated ≤48 h after admission. Of the remaining patients, MDRO colonization was diagnosed in 173 (51.2%), MDRO infections in 95 (28.1%), and non-MDRO infections in 212 (62.7%). Non-MDRO infections occurred earlier than MDRO infections (6 days vs. 10 days; p<0.001). Previous exposure to antimicrobial drugs within the ICU was higher in MDRO patients than in non-MDRO patients (116/197 [58.9%] vs. 18/140 [12.9%]; p<0.001). Our findings might serve as warnings for future respiratory viral pandemics and call for increased measures of antimicrobial stewardship and infection control.

Bacterial superinfections represent a major threat for patients in intensive care units (ICUs), severely affecting clinical course and length of hospital stay. The COVID-19 pandemic caused an unprecedented rate of ICU admissions and drastically changed ICU care itself, in terms of infection control measures and therapeutic usage of steroids and immunomodulating drugs. The percentages of hospital-acquired infections (HAIs) in COVID-19 patients vary widely, ranging from 7% to 13% in nonintensive hospital wards and up to 45% in ICUs (*1*–*3*).

Several studies have assessed the burden of multidrug-resistant organisms (MDROs) in COVID-19 patients admitted to ICUs, reporting heterogeneous results with prevalence ranging from 11% to 50% and incidence rate from 4.5 cases/1,000 patient-days to 30 cases/1,000 patient-days (*4*–*21*). However, studies published so far have relevant limitations, often not clearly discriminating between colonization and infection (*8*,*9*,*11*,*12*), and either including small

Author affiliations: Foundation IRCCS Ca' Granda Ospedale Maggiore Policlinico di Milano, Milan, Italy (D. Mangioni, E. Palomba, M. Bolis, N. Bottino, G. Breda, G. Massobrio, C. Matinato, A. Muscatello, G. Zuglian, G. Grasselli, A. Gori, N. Stocchetti, A. Bandera); University of Milan, Milan (D. Mangioni, E. Palomba, G. Grasselli, A. Gori, N. Stocchetti, A, Bandera); Istituto di Ricerche Farmacologiche Mario Negri IRCCS, Milan (L. Chatenoud, M.V. Chiaruttini); Harvard Medical School, Boston, Massachusetts, USA (J. Colombo); ASST Grande Ospedale Metropolitano Niguarda, Milan (J. Colombo, F.A. Guerrero, G. Fior, M. Marotta, P. Previtali, S. Santambrogio, F. Tardini, R. Fumagalli, G. Monti); ULSS 3 Serenissima, Venice, Italy (G. Zuglian); University of Milano-Bicocca, Milan (R. Fumagalli)

DOI: https://doi.org/10.3201/eid2908.230115

[1]Preliminary results were presented at the European Congress of Clinical Microbiology and Infectious Diseases, 2022, Lisbon, Portugal, April 23–26, 2022 (abstract no. 02641).

[2]These senior authors contributed equally to this article.

[3]Study group members are listed at the end of this article.

populations or showing heterogeneity in clinical settings and microbiologic surveillance procedures when describing larger pool of persons, such as in multicentric studies (*18*–*20*).

Our study was conducted to address the need for further evidence on incidence and etiology of MDRO colonization and infections in mechanically ventilated COVID-19 patients. We analyzed clinical and microbiologic data systematically collected in a large ICU in northern Italy.

Methods

Study Design and Setting

We conducted a retrospective cohort study on routinely collected data of COVID-19 patients admitted to the Milano Fiera ICU during October 23, 2020–May 31, 2021. This ICU was a large COVID-19 ICU developed in Milan, Italy, to face the effect of the pandemic. It admitted patients who had SARS-CoV-2 infection requiring mechanical ventilation from different healthcare settings: emergency department, nonintensive hospital wards, and other ICUs. This ICU could accommodate up to 100 patients divided into distinct units (modules) managed by ICU staff from different hospitals. Microbiologic surveillance was standardized and consisted of perineal and nasal swab specimens for MDROs and endotracheal aspirate cultures obtained at ICU admission and then once (perineal and nasal swab specimens) or twice (endotracheal aspirate) a week. All modules referred to the IRCCS Ca' Granda Ospedale Maggiore Policlinico Foundation for laboratory and microbiologic analyses and for infectious diseases specialist consultation.

Study Participants and Data Collection

All consecutive patients who had laboratory-confirmed SARS-CoV-2 infection and were admitted to the ICU were considered for inclusion. Exclusion criteria were age <18 years, length of mechanical ventilation <48 h, and lack of comprehensive clinical documentation. We collected demographic, clinical, laboratory, and outcome data from clinical records and microbiologic and therapeutic data from dedicated hospital databases (Appendix, https://wwwnc.cdc.gov/EID/article/29/8/23-0115-App1.pdf). The study was registered by the Milan Area 2 Ethical Committee (#701_2021) and was conducted in accordance with standards of the Helsinki Declaration. Written informed consent was waived because of the retrospective nature of the analysis. The study was retrospectively registered at clinicaltrials.gov on March 24, 2022 (identifier: NCT05293418).

Microbiologic Data Processing

For each patient, we retrieved bacterial isolates from a microbiology database, which were independently reviewed by dedicated intensivists and infectious disease specialists and classified as contamination, colonization, or infection, according to international guidelines (Appendix) (*22*,*23*). In brief, infections were defined by the presence of a major bacterial load associated with clinical manifestations within the infection window period (±3 days from specimen collection) (*22*,*23*), Isolates were classified as colonization when no adverse clinical signs or symptoms were documented. We defined contamination as all microbiologic isolates that did not meet the criteria of infection or colonization and that were listed in the US Centers for Disease Control and Prevention National Healthcare Safety Network (https://www.cdc.gov/nhsn/index.html) list of common commensals. We retained only the first species-specific MDRO colonization of each patient for further analysis.

We distinguished new infectious episodes from persistent infections according to the European Centre for Disease Prevention and Control definitions (*23*). We stratified infection episodes as infection without sepsis, sepsis or septic shock according to Sepsis-3 criteria (*24*). We defined secondary bloodstream infections (BSIs) by using the secondary BSI attribution period according to the Centers for Diseases Control and Prevention National Healthcare Safety Network (*22*). We also defined isolates as MDROs when they were nonsusceptible to ≥1 agents in ≥3 antimicrobial drug categories (*25*) or when harboring specific antimicrobial drug resistance mechanisms (e.g., methicillin-resistant *Staphylococcus* spp., vancomycin-resistant *Enterococcus* spp., extended-spectrum β-lactamase/AmpC/carbapenemases–producing Enterobacterales) by using rapid detection methods (*4*).

Statistical Analysis

We reported patient characteristics overall and for selected groups of interest, such as MDROs acquired before/after ICU admittance and MDRO infection/colonization. Medians (interquartile range [IQRs]) are reported for continuous variables and numbers (percentages) for categorical variables. We calculated crude incidence rates (IRs) per 1,000 patient-days and relative 95% CIs, considering for each patient any first species-specific MDRO colonization or each new MDRO/non-MDRO HAI (*26*). We used SAS version 9.4 software (SAS Institute, https://www.sas.com) for statistical analysis (Appendix).

Results

Population Description

A total of 451 patients from 46 different hospitals were admitted to ICUs during October 2020–May 2021. Of those, 435 were included in the analysis. We provide details of the patient selection process (Figure 1) and trends of patient admission by referring hospital per month (Appendix Figure 1).

Only 12/435 patients (2.7%) were reported to have MDRO colonization/infection before ICU admission. In 88/435 patients (20.2%), MDRO were isolated within 48 h upon entry to the ICU ($MDR_{\leq 48h}$), and those patients were similarly distributed between referring hospitals (Appendix Figure 2). This group was composed of 78 colonizations and 10 infections; 35/78 (44.9%) colonized patients subsequently had MDRO infections develop. Compared with the 347 patients who had no evidence of MDRO during the first 48 hours of ICU stay (no-MDR+$MDR_{>48h}$), the $MDR_{\leq 48h}$ group was characterized by higher admittance from other ICUs and lower admittances from emergency departments (ICU 31/88 [35.2%] in $MDR_{\leq 48h}$ vs. 86/347 [24.8%]) in no-MDR+$MDR_{>48h}$;

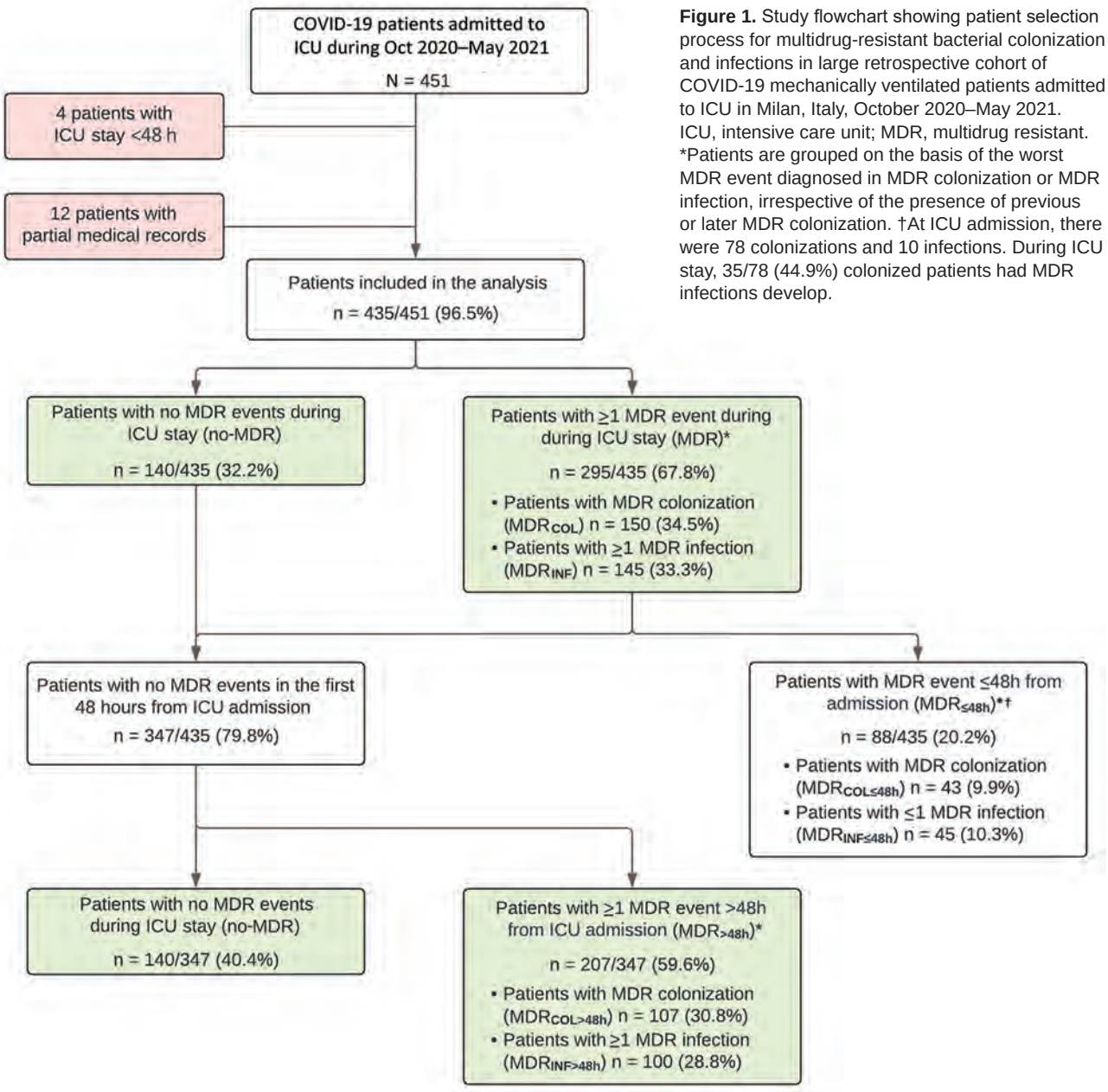

Figure 1. Study flowchart showing patient selection process for multidrug-resistant bacterial colonization and infections in large retrospective cohort of COVID-19 mechanically ventilated patients admitted to ICU in Milan, Italy, October 2020–May 2021. ICU, intensive care unit; MDR, multidrug resistant. *Patients are grouped on the basis of the worst MDR event diagnosed in MDR colonization or MDR infection, irrespective of the presence of previous or later MDR colonization. †At ICU admission, there were 78 colonizations and 10 infections. During ICU stay, 35/78 (44.9%) colonized patients had MDR infections develop.

emergency department 15/88 [17.1%] in $MDR_{\leq 48h}$ vs. 102/347 [29.4%] in no-MDR+$MDR_{>48h}$). The $MDR_{\leq 48h}$ group showed slightly longer (although not significantly) length of stay in the ICU of origin than patients who developed MDRO events later during their stay and to no-MDR patients (medians 11.5, 9, and 7 days, respectively; p = 0.09). The $MDR_{\leq 48h}$ group was also characterized by a larger amount of antimicrobial drug intake before ICU admission (no antimicrobial drug in 25/88 [28%] of $MDR_{\leq 48h}$ vs. 126/327 [36.3%] of no-MDR+$MDR_{>48h}$; ≥3 classes of antimicrobial drugs in 12/88 [13.6%] of $MDR_{\leq 48h}$ vs. 23/347 [6.6%] of no-MDR+$MDR_{>48h}$). We compiled demographic and clinical characteristics by groups (Appendix Table 1) and duration between hospitalization and transfer to the ICU on the basis of patients' setting of provenance (Appendix Table 2).

Of the 347 patients who had no MDRO isolates within the first 48 hours from ICU admission, 207 (67.5%) had ≥1 MDRO event ($MDR_{>48h}$); 107 (30.8%) patients had MDRO colonization only ($MDR_{COL>48h}$) and 100 (28.8%) had ≥1 MDRO infection ($MDR_{INF>48h}$) (Figure 1). We compiled patient characteristics and outcomes (Table 1, https://wwwnc.cdc.gov/EID/article/29/8/23-0115-T1.htm) overall and for no-MDR and $MDR_{>48h}$ patients, further stratified as $MDR_{COL>48h}$ and $MDR_{INF>48h}$. Median age was 65 years (IQR 59–71 years); 95/347 (27.4%) patients were female. More than 80% of patients had ≥1 concurrent condition, and hypertension was the most common (181/347, 52.2%). Patients who had ever smoked were more frequent in the $MDR_{INF>48h}$ group (26/100, 26%) than in the $MDR_{COL>48h}$ group (11/107, 10.3%; p = 0.003). Transfer to the ICU occurred mostly from nonintensive hospital wards (159/347, 45.8%), but relevant proportions were transferred directly from the emergency department (102/347, 29.4%) or from other ICUs (86/347, 24.8%). Patients were transferred to ICU early during hospitalization, a median time of 5 days from first hospital admittance.

Groups did not differ for steroid use or antimicrobial drug therapies received before ICU admission. According to clinical practice, steroids had been administered for SARS-CoV-2 infection management in 252/347 (72.6%) patients, mostly (228/347, 65.7%) with only a standard dose (dexamethasone 6 mg/d). Most patients (221/347, 63.7%) had previously received antimicrobial drugs before ICU admission. MDRO events before ICU admission were reported in only 4 patients (1.2%). During ICU stay, 118 patients (34%) died, but there were no significant differences between groups. When compared with no-MDR patients, we found that $MDR_{>48h}$ patients had a longer duration of mechanical ventilation (median 18 vs. 14 days; p = 0.001) and of ICU stay (median 25 vs. 15.5 days; p = 0.001). Those differences were largely caused by the $MDR_{INF>48h}$ group (Table 1).

Bacterial Isolate Description and Incidence

Complete microbiologic reports were available for 426/435 patients, including 338/347 patients (97.4%) with no MDRO isolates within the first 48 hours of ICU admission. We describe the selection process conducted to assess incidences of HAIs and of MDRO events distinguishing between colonization and infection (Figure 2). We identified 801 bacterial isolates from 271 patients that correspond to first MDRO colonization (255 isolates in 173/338 patients, 51.2%) and new episodes of bacterial superinfections, either by MDRO (130 isolates in 95/338 patients, 28.1%) or antimicrobial drug–susceptible bacteria (non-MDRO, 416 isolates in 212/338 patients, 62.7%). A total of 73 (21.6%) patients had both MDRO colonization and MDRO infection develop during ICU stay, and infections were caused by the same colonizing bacterial species in nearly one third of them (24/73, 32.9%) (Appendix Table 3). Clinical interpretation of bacterial isolates as colonization/infection by attending physicians at the time of arrival of microbiologic results was found to be highly concordant with the retrospective evaluation conducted according to international guidelines (κ coefficient 0.902, 95% CI 0.890–0.913) (Appendix Table 4).

Overall, 546 bacterial HAIs were recorded, 130 (23.8%) caused by MDRO. Gram-negative bacteria accounted for 59.7% (326/546) of all HAIs and for 60% (78/130) of infections caused by MDROs. Bacterial species responsible for HAIs varied by infection site and severity of infection (Appendix Tables 5, 6). Ventilator-associated lower respiratory tract infections (VALRTIs) represented most infectious episodes (359/546, 65.7%), followed by BSI (141, 25.8%) and urinary tract infections (40, 7.3%). Among BSIs, 31/141 (22%) were associated with a central line, 43 (30.5%) were secondary to VALRTI or urinary tract infections, and the remaining 67 (47.5%) were classified as primary BSI without a known bacteremic focus (Appendix Figure 3).

Among MDRO colonization, *Enterococcus faecium* (112/255 isolates, 43.9%) was the most frequent isolate, followed by *Klebsiella* spp. (34, 13.3%), *Escherichia coli* (26, 10.2%), *Staphylococcus aureus* (25, 9.8%), *Pseudomonas aeruginosa* (15, 5.9%) and *Acinetobacter baumannii* (13, 5.1%). We compiled the percentages of MDRO colonization, MDRO HAIs, and non-MDRO

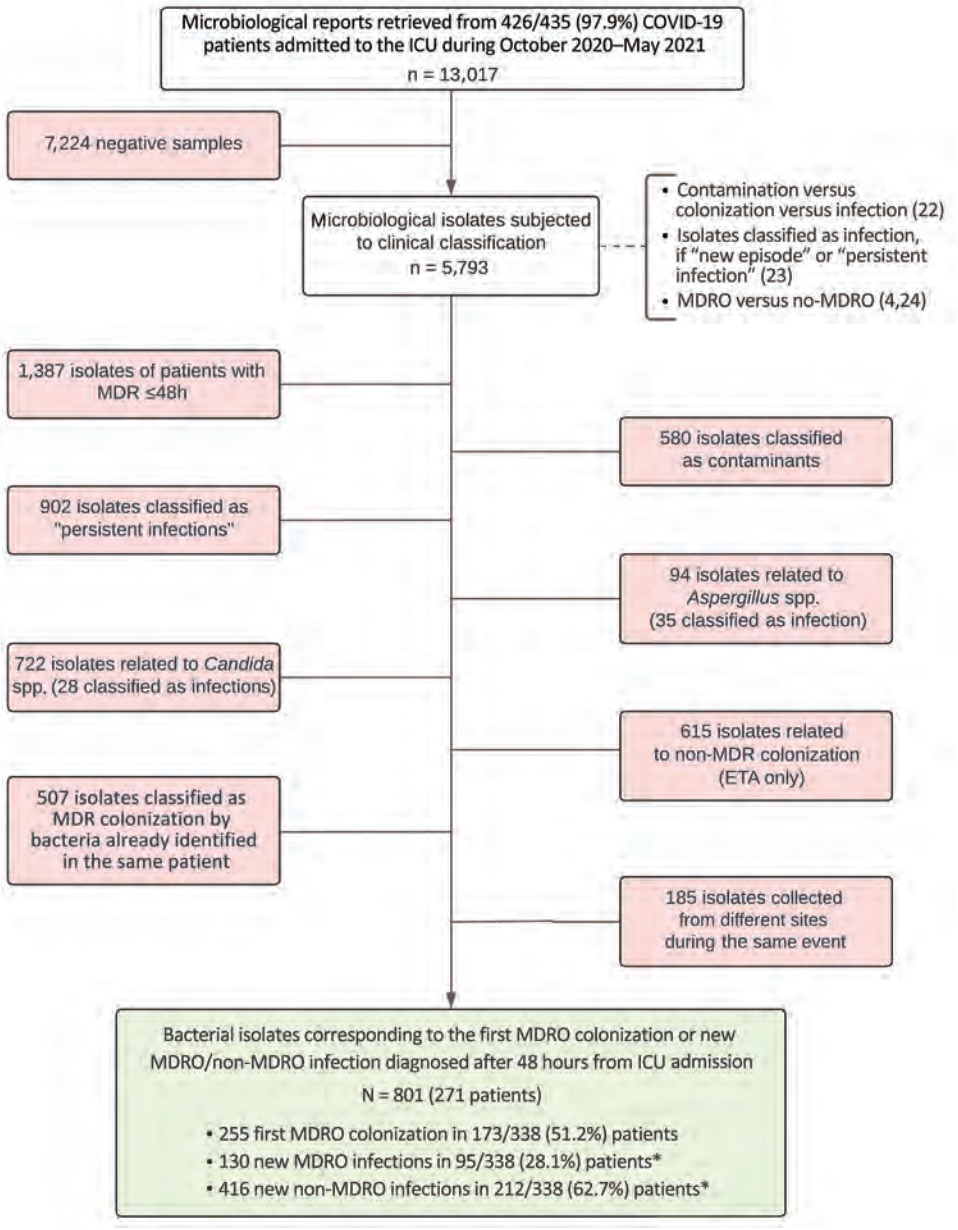

Figure 2. Study flowchart showing microbial isolates selection process for multidrug-resistant bacterial colonization and infections in large retrospective cohort of COVID-19 mechanically ventilated patients admitted to ICU in Milan, Italy, October 2020–May 2021. ETA, emergency treatment area; ICU, intensive care unit; MDR, multidrug resistant; MDRO, MDR organism. *Of 338 patients, 159 (47.0%) had either MDRO or non-MDRO infections; 74/338 (21.9%) had both MDRO and non-MDRO infections.

HAIs for the most frequently isolated bacteria of the World Health Organization priority pathogens list (*27*) (Appendix Figure 4).

First MDRO colonization occurred at a median time of 13 (IQR 8–12) days after ICU admission. HAIs caused by antimicrobial drug–susceptible bacteria occurred earlier than in those caused by MDROs at 6 (IQR 3–10) and 10 (IQR 6–17) days from admission ($p<0.001$) (Figure 3). The incidence rates for MDRO colonization was 29.97 cases/1,000 patient-days (95% CI 26.34–34.10), for MDRO infection was 14.99 cases/1,000 patient-days (95% CI 12.36–18.19), and for non-MDRO infection, was 50.12 cases/1,000 patient-days (95% CI 44.59–56.32). Infection rates varied substantially by infection site (Table 2).

Association of Antimicrobial Drugs and Steroids to MDRO Events

We investigated possible associations between MDRO events and previous steroid and antimicrobial drug therapies (Appendix Tables 7, 8). Because steroids were included in the management of COVID-19 pneumonia from the early stage of the disease, we evaluated their intake before and during ICU stay. Almost the entire population had received steroid therapy (313/338, 92.6%), without major differences

between no-MDR (132/140, 94.3%), $MDR_{COL>48h}$ (98/103, 95.1%) and $MDR_{INF>48h}$ (83/95, 87.4%) (Appendix Table 7).

To assess possible association between MDRO events and previous antimicrobial drug use, we focused on therapies administered during the first 10 days of ICU stay. This timeline was set to balance observation time between no-MDR and $MDR_{>48h}$ groups because three fourths of MDRO events occurred within this timeframe. Also, three fourths of patients in no-MDR group stayed in ICU ≥10 days (Appendix Table 8). Previous exposure to antimicrobial drugs was notably higher in patients who developed MDRO events than in patients who did not (116/197 [58.9%] in $MDR_{>48h}$ vs 18/140 [12.9%] in no-MDR; p<0.001) (Appendix Table 8).

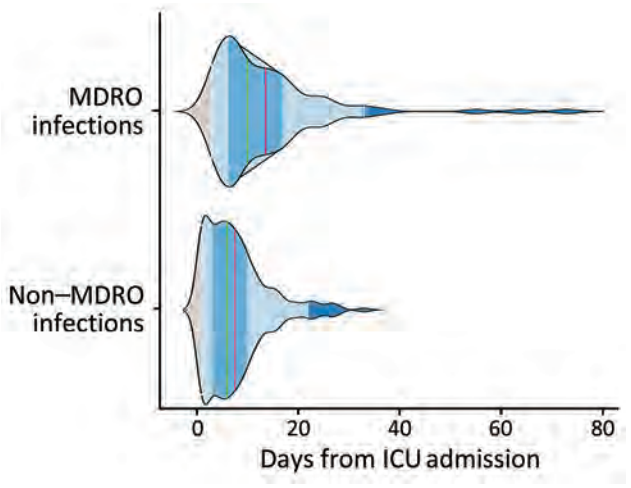

Figure 3. Multidrug-resistant bacterial colonization and infections in large retrospective cohort of COVID-19 mechanically ventilated patients admitted to ICU in Milan, Italy, October 2020–May 2021. Kernel density plot (violin plot) shows healthcare-associated infections by onset time comparing MDRO with non-MDRO. Red lines indicate mean and green lines median onset times; medium blue shading indicates interquartile ranges, and the light blue shading indicates 95% CIs of the mean (p<0.001 by Wilcoxon rank-sum test). ICU, intensive care unit; MDRO, multidrug-resistant organism.

Discussion

We describe incidences and clinical characteristics of HAIs and MDRO events, distinguishing between colonization and infection, in a large cohort of ICU COVID-19 patients from a country with high prevalence of MDRO (*28*). Despite being composed of patients admitted from >45 different hospitals, our cohort is homogeneous for concurrent conditions and risk factors for MDRO acquisition, clinical severity of COVID-19, management of antimicrobial drug therapy, and infection prevention and control strategies within the ICU, including surveillance sampling.

Antimicrobial drug resistance represents a major challenge in the ICU. Its occurrence is the result of the influx of previously colonized patients and acquisition of MDROs during ICU stay, as a consequence of antimicrobial drug overexposure and interpatient transmission, as well as contact with colonized healthcare workers, fomites, or the environment. The incidence of MDROs is strongly influenced by pandemic periods, such as during COVID-19, when unprecedented patient loads in ICUs resulted in breaches in IPC, such as gaps in microbiologic surveillance, lack of communication between clinicians, and reduced attention to environmental measures and contact precautions among healthcare workers (*29*). In addition, ICU admissions caused by viral pandemics place a strain on ICU resources, requiring the reallocation of non-ICU beds, along with the use of non-ICU staff to meet the urgent demand. In this setting, strengthening measures, such as active surveillance with prompt recognition of outbreaks, staff training, increased environmental disinfection and cohorting, become essential to reducing MDRO circulation (*30*).

In the pre–COVID-19 pandemic era, the prevalence of infections caused by MDROs in ICU patients varied from a reported rate of 14.1% in VALRTIs acquired in ICUs in North America (*31*) to an average

Table 2. Incidence rate of MDRO events, overall and divided by infection site, of COVID-19 patients admitted to ICU in Milan, Italy, October 2020–May 2021, who had no MDRO isolates within the first 48 h of admission*

Characteristic	Infections			
	VALRTIs	BSIs	UTIs	Total
MDRO events, first colonization plus new infections	NA	NA	NA	41.68 (36.98–46.99)
First MDRO colonization	NA	NA	NA	29.97 (26.34–34.1)
New MDRO infection	9.44 (7.58–11.74)	4.89 (3.55–6.75)	0.47 (0.14–1.08)	14.99 (12.36–18.19)
New non-MDRO infection	33.25 (29.04–38.07)	11.62 (9.23–14.64)	4.19 (2.97–5.72)	50.12 (44.59–56.32)
Overall new infections, MDRO plus non-MDRO	42.41 (37.81–47.58)	16.57 (13.51–20.31)	5.15 (3.36–6.26)	65.13 (58.76–72.2)

*Values are IR/1,000 person-days (95% CIs). The time considered for IRs was set from ICU admission to discharge, except for VALRTI, where total intubation time was considered. BSIs, bloodstream infections; ICU, intensive care unit; IR, incidence rate; MDRO, multidrug-resistant organism; NA, not applicable (MDRO colonization refers to patients and not infection sites); UTIs, urinary tract infections; VALRTIs, ventilator-associated lower respiratory tract infections.

of >40% in 2 large multicentric worldwide studies of nosocomial BSIs (*32*,*33*). Variability exists between participating countries, ranging from 8% (Australia) to >75%–80% in Asia, eastern Europe, and southern Europe. Carbapenem resistance was present in more than one third of gram-negative bacteria, and 36% of all gram-positive bacteria were MDR (*32*,*33*).

Several studies have been published on MDRO incidence, etiology and source of HAIs in ICU COVID-19 patients (*4*–*21*) (Table 3, https://wwwnc.cdc.gov/EID/article/29/8/23-0115-T3.htm). Most of those studies evaluated overall MDRO infections or specific HAIs, such as BSI or VALRTIs (*7*,*15*–*17*,*19*,*21*), whereas colonization events were assessed in only a few studies (*8*–*12*,*14*). Incidence measures of MDRO events varied widely; cumulative incidence of the first MDRO event was 5%–57% (*7*,*17*) and incidence rate 2.6–31.48 cases/1,000 patient-days (*11*,*16*). The percentage of MDRO was 27%–100% for all recorded events (*15*,*17*). Compared with the amount of literature evaluating MDRO events during ICU stay, we found that few data are available on MDRO proportions among COVID-19 patients at ICU admission. In recent work of the multicenter HAI-ICU surveillance network in France, the percentage of MDR gram-negative bacteria among >4,000 COVID-19 patients admitted was 11.7% (*34*).

In our cohort, 20% of patients had MDRO isolation within the first 48 hours, indicating acquisition before ICU admittance. We found that patients who had MDROs isolated during the first 48 hours were more frequently transferred from other ICUs and exposed to a higher number of antimicrobial drugs before ICU admission. Both of those factors are well known to be associated with development of infections by antimicrobial drug–resistant pathogens (*6*). Only 2.7% of our cohort had MDRO colonization/infection before ICU admission. The marked difference between expected and observed MDRO prevalence at ICU admission probably reflects the major issues in IPC during the emergency situation of the pandemic mentioned beforehand.

Considering patients without MDRO isolation within the first 48 hours, we observed no differences in demographic characteristics or in clinical severity at admission between patients who showed or not showed development of MDRO events during ICU stay, underlying consistency between groups at ICU admission. In our cohort, we did not find direct association between MDRO infection and in-ICU deaths. However, length of ICU stay and duration of mechanical ventilation were longer for patients with MDRO events and, among them, longer for patients who had infections than for colonized patients. No causative effect can be drawn from these results because occurrence of MDRO events could be either responsible for longer ICU stay or its direct consequence because of longer exposure time (*35*,*36*).

Active surveillance screening coupled with the evaluation of all microbial isolates enabled us to precisely identify patients who had with MDRO events. Two thirds of the cohort showed development of MDRO colonization or infection during ICU stay. Half of our patients were given diagnoses of MDRO colonization during ICU stay, compared with 21% observed in a recent study analyzing a smaller population (*10*). Our results can be, in part, explained by strict routine microbiologic surveillance, which enabled prompt and precise recognition of such cases. Data from previous studies on bacterial superinfections in COVID-19 ICU patients are heterogenous and describe MDRO HAIs in 11%–250% of the population (*6*,*13*). Our results confirm the substantial risk for mechanically ventilated COVID-19 patients to have MDRO infections develop; such infections affected almost 30% of our cohort during ICU stays. Also, more than twice as many patients had antimicrobial drug–susceptible HAIs.

We found high concordance between clinical diagnosis and retrospective evaluation of HAIs according to literature criteria. We believe this result well demonstrates how implementation of structured antimicrobial stewardship and IPC measures, with collaboration of infectious disease consultants and intensivists, can strongly effect management of critically ill patients, favoring accurate diagnosis and therapeutic choices, according to international guidelines.

Patients who had MDRO events had greater exposure to antimicrobial drugs the first 10 days of ICU stay than patients who had no MDRO findings. This observation is consistent with results of recent studies conducted on large population of patients, which showed major associations between exposure to specific antimicrobial drug classes and drug resistance, and a decreasing pattern over time (*37*,*38*). However, accurate analysis of the association between antimicrobial drug exposure and MDRO events was beyond the scope of this study because other variables, such as average intake time of each antimicrobial drug class and infections with antimicrobial drug–susceptible bacteria during the observation time, should be considered.

The first limitation of this study is that it was a retrospective monocentric cohort and, therefore, had intrinsic risks of limited accuracy and generalizability. However, interpretation of all microbiologic findings has been conducted ex post on the basis of standardized literature criteria and independent from the

physicians' view. Also, even though the study was monocentric, patients were admitted from >45 hospitals and assisted by different hospital staff. Advantages to this study design derive from the standardized microbiologic surveillance, both in terms of timing and laboratory method, as well as from homogeneous antimicrobial stewardship and IPC strategies among ICU modules. This factor enabled us to provide precise and consistent data in terms of incidence of HAIs and MDRO events, not only infections but also colonization.

Second, this study was not conducted for evaluation of the effect of antimicrobial drugs on development of MDRO or the effect of MDRO events on ICU deaths and length of stay; the sample size was probably inadequate for these issues. Therefore, our findings on this issue should be interpreted with caution.

Third, patients' data before ICU admission were retrieved from information registered at ICU entry and not from hospital databases of the single referring centers. Accuracy of previous MDRO events and steroids and antimicrobial drug treatments might be limited, although these factors play a major role in routine management of ICU patients, and we do not expect major gaps in data acquisition.

In conclusion, our in-depth analysis of incidence measures of HAIs and MDRO events contributes to increase knowledge of MDRO colonization and infections in ICU COVID-19 patients. These findings should be a priority in contributing toward IPC and antimicrobial stewardship policies for ensuring the best clinical care.

MDR in FIERA study group: Valeria Pastore, Mara Tomasello, Lisa Cariani, Anna Grancini, Anna Maraschini (Foundation IRCCS Ca' Granda Ospedale Maggiore Policlinico, Milan, Italy); Teresio Arazzi (Rho Hospital, Rho, Italy); Alessandro Protti (Humanitas Clinical and Research Center IRCCS, Rozzano, Milan, Italy); Virginia Porta (Legnano Hospital, Legnano, Italy); Marco Dei Poli (San Donato Hospital, Milano, Italy); Paolo Severgnini (Varese Hospital, Varese, Italy); Egle Rondelli (San Gerardo Hospital, Monza, Italy).

This study was partially supported by the Italian Ministry of Health and projects STOP-COVID and PREP-COVID.

Deidentified patient data used for the results reported in this article, including data in text, tables, figures, and appendixes, will be available to researchers who provide a methodologically sound proposal to achieve their aims. Proposals should be addressed to andrea.gori@unimi.it and davide.mangioni@policlinico.mi.it. To gain access, data applicants will need to sign a data access agreement.

D.M., J.C., G.Ma., and A.B. designed the study; L.C. and M.C.V. performed methods and formal analysis; D.M., J.C., E.P., F.A.G., M.B., B.B., M.C., G.F., M.M., G.Mo, P.P., S.S., F.T., and G.Z. performed investigations; D.M. and E.P. wrote the original draft of the paper, wrote, reviewed, and edited the paper, and performed a literature review; L.C., J.C., F.A.G., M.B., N.B., B.B., M.C., G.F., M.M., G.Ma., C.M., A.M., P.P., S.S., F.T., G.Z., G.G., R.F., A.G., N.S., G.Mo., and A.B. wrote, reviewed, and edited the paper; and N.B., N,S., G.Ma., and A.B. supervised the study. All authors have read and agreed to the published version of the manuscript.

About the Author

Dr. Mangioni is an assistant professor at the University of Milan and Consultant in Infectious Diseases at the Foundation IRCCS Ca' Granda Ospedale Maggiore Policlinico di Milano, Milan, Italy. His primary research interests are infections in critically ill patients and infections caused by multidrug-resistant organisms.

References

1. Lansbury L, Lim B, Baskaran V, Lim WS. Co-infections in people with COVID-19: a systematic review and meta-analysis. J Infect. 2020;81:266–75. https://doi.org/10.1016/j.jinf.2020.05.046
2. Pasero D, Cossu AP, Terragni P. Multi-drug resistance bacterial infections in critically ill patients admitted with COVID-19. Microorganisms. 2021;9:1773. https://doi.org/10.3390/microorganisms9081773
3. Russell CD, Fairfield CJ, Drake TM, Turtle L, Seaton RA, Wootton DG, et al.; ISARIC4C investigators. Co-infections, secondary infections, and antimicrobial use in patients hospitalised with COVID-19 during the first pandemic wave from the ISARIC WHO CCP-UK study: a multicentre, prospective cohort study. Lancet Microbe. 2021;2:e354–65. https://doi.org/10.1016/S2666-5247(21)00090-2
4. Grasselli G, Scaravilli V, Mangioni D, Scudeller L, Alagna L, Bartoletti M, et al. Hospital-acquired infections in critically ill patients with COVID-19. Chest. 2021;160:454–65. https://doi.org/10.1016/j.chest.2021.04.002
5. Ramos R, de la Villa S, García-Ramos S, Padilla B, García-Olivares P, Piñero P, et al. COVID-19 associated infections in the ICU setting: a retrospective analysis in a tertiary-care hospital. Enferm Infecc Microbiol Clin. 2021.
6. Karruli A, Boccia F, Gagliardi M, Patauner F, Ursi MP, Sommese P, et al. Multidrug-resistant infections and outcome of critically ill patients with coronavirus disease 2019: a single center experience. Microb Drug Resist. 2021;27:1167–75. https://doi.org/10.1089/mdr.2020.0489
7. Palanisamy N, Vihari N, Meena DS, Kumar D, Midha N, Tak V, et al. Clinical profile of bloodstream infections in COVID-19 patients: a retrospective cohort study. BMC Infect Dis. 2021;21:933. https://doi.org/10.1186/s12879-021-06647-x
8. Baiou A, Elbuzidi AA, Bakdach D, Zaqout A, Alarbi KM, Bintaher AA, et al. Clinical characteristics and risk factors for the isolation of multi-drug-resistant Gram-negative bacteria from critically ill patients with COVID-19. J Hosp

Infect. 2021;110:165–71. https://doi.org/10.1016/j.jhin.2021.01.027
9. Bogossian EG, Taccone FS, Izzi A, Yin N, Garufi A, Hublet S, et al. The acquisition of multidrug-resistant bacteria in patients admitted to COVID-19 intensive care units: a monocentric retrospective case–control study. Microorganisms. 2020;8:1–11. https://doi.org/10.3390/microorganisms8111821
10. Fernández P, Moreno L, Yagüe G, Andreu E, Jara R, Segovia M. Colonization by multidrug-resistant microorganisms in ICU patients during the COVID-19 pandemic. Med Intensiva [English Ed]. 2021;45:313–5.
11. Pascale R, Bussini L, Gaibani P, Bovo F, Fornaro G, Lombardo D, et al. Carbapenem-resistant bacteria in an intensive care unit during the coronavirus disease 2019 (COVID-19) pandemic: a multicenter before-and-after cross-sectional study. Infect Control Hosp Epidemiol. 2022;43:461–6. https://doi.org/10.1017/ice.2021.144
12. Temperoni C, Caiazzo L, Barchiesi F. High prevalence of antibiotic resistance among opportunistic pathogens isolated from patients with COVID-19 under mechanical ventilation: results of a single-center study. Antibiotics (Basel). 2021;10:1080. https://doi.org/10.3390/antibiotics10091080
13. Pourajam S, Kalantari E, Talebzadeh H, Mellali H, Sami R, Soltaninejad F, et al. Secondary bacterial infection and clinical characteristics in patients with COVID-19 admitted to two intensive care units of an academic hospital in Iran during the first wave of the pandemic. Front Cell Infect Microbiol. 2022;12:784130. https://doi.org/10.3389/fcimb.2022.784130
14. Sathitakorn O, Jantarathaneewat K, Weber DJ, Warren DK, Nanthapisal S, Rutjanawech S, et al. The feasibility of procalcitonin and CPIS score to reduce inappropriate antibiotics use among severe-critically ill COVID-19 pneumonia patients: a pilot study. Am J Infect Control. 2022;50:581–4. https://doi.org/10.1016/j.ajic.2022.01.030
15. Bonazzetti C, Morena V, Giacomelli A, Oreni L, Casalini G, Galimberti LR, et al. Unexpectedly high frequency of enterococcal bloodstream infections in coronavirus disease 2019 patients admitted to an Italian ICU: an observational study. Crit Care Med. 2021;49:e31–40. https://doi.org/10.1097/CCM.0000000000004748
16. Scaravilli V, Guzzardella A, Madotto F, Beltrama V, Muscatello A, Bellani G, et al. Impact of dexamethasone on the incidence of ventilator-associated pneumonia in mechanically ventilated COVID-19 patients: a propensity-matched cohort study. Crit Care. 2022;26:176. https://doi.org/10.1186/s13054-022-04049-2
17. Mantzarlis K, Deskata K, Papaspyrou D, Leontopoulou V, Tsolaki V, Zakynthinos E, et al. Incidence and risk factors for blood stream infection in mechanically ventilated COVID-19 patients. Antibiotics (Basel). 2022;11:1053. https://doi.org/10.3390/antibiotics11081053
18. Falcone M, Suardi LR, Tiseo G, Galfo V, Occhineri S, Verdenelli S, et al. Superinfections caused by carbapenem-resistant Enterobacterales in hospitalized patient with COVID-19: a multicentre observational study from Italy (CREVID study). JAC Antimicrobial Resist. 2022;4:dlac064.
19. Yohannes S, Ahmed Z, Schelling R, Perinkulam Sathyanarayanan S, Pratt A, Schreiber MP. Incidence and impact of ventilator associated multidrug resistant pneumonia in patients with SARS-COV2. Crit Care Res Pract. 2022;2022:9730895. https://doi.org/10.1155/2022/9730895
20. Menekşe Ş, Deniz S. Secondary infections in COVID-19 patients: A two-centre retrospective observational study. J Infect Dev Ctries. 2022;16:1294–301. https://doi.org/10.3855/jidc.15637
21. Bansal S, Kalpakam H, Kumar A, Varsha A, Thorbole A, Mehta RM. Lower respiratory tract sampling in COVID-19 acute respiratory distress syndrome: a focus on microbiology, cellular morphology, cytology, and management impact. Lung India. 2022;39:139–44. https://doi.org/10.4103/lungindia.lungindia_532_21
22. Centers for Disease Control and Prevention. National Healthcare Safety Network (NHSN) Patient safety component manual; 2021.
23. European Centre for Disease Prevention and Control. Surveillance of healthcare-associated infections and prevention indicators in European intensive care units; 2017.
24. Singer M, Deutschman CS, Seymour CW, Shankar-Hari M, Annane D, Bauer M, et al. The third international consensus definitions for sepsis and septic shock (Sepsis-3). JAMA. 2016;315:801–10. https://doi.org/10.1001/jama.2016.0287
25. Magiorakos AP, Srinivasan A, Carey RB, Carmeli Y, Falagas ME, Giske CG, et al. Multidrug-resistant, extensively drug-resistant and pandrug-resistant bacteria: an international expert proposal for interim standard definitions for acquired resistance. Clin Microbiol Infect. 2012;18:268–81. https://doi.org/10.1111/j.1469-0691.2011.03570.x
26. Glynn RJ, Buring JE. Ways of measuring rates of recurrent events. BMJ. 1996;312:364–7. https://doi.org/10.1136/bmj.312.7027.364
27. World Health Organization. WHO publishes list of bacteria for which new antibiotics are urgently needed. 2017 [cited 2023 Jun 21]. https://www.who.int/news/item/27-02-2017-who-publishes-list-of-bacteria-for-which-new-antibiotics-are-urgently-needed
28. European Centre for Disease Prevention and Control. Antimicrobial resistance in the EU/EEA (EARS-Net). Annual epidemiological report 2020. Solna (Sweden): The Centre; 2022.
29. Witt LS, Howard-Anderson JR, Jacob JT, Gottlieb LB. The impact of COVID-19 on multidrug-resistant organisms causing healthcare-associated infections: a narrative review. JAC Antimicrob Resist. 2022;5:2dlac130.
30. Mangioni D, Fox V, Chatenoud L, Bolis M, Bottino N, Cariani L, et al. Genomic characterization of carbapenem-resistant *Acinetobacter baumannii* (CRAB) in mechanically ventilated COVID-19 patients and impact of infection control measures on reducing CRAB circulation during the second wave of the SARS-CoV-2 pandemic in Milan, Italy. Microbiol Spectr. 2023;11:e0020923. https://doi.org/10.1128/spectrum.00209-23
31. Lat I, Daley MJ, Shewale A, Pangrazzi MH, Hammond D, Olsen KM, et al.; DEFINE study group and the Discovery Research Network. A multicenter, prospective, observational study to determine predictive factors for multidrug-resistant pneumonia in critically ill adults: the DEFINEsStudy. Pharmacotherapy. 2019;39:253–60. https://doi.org/10.1002/phar.2171
32. Tabah A, Koulenti D, Laupland K, Misset B, Valles J, Bruzzi de Carvalho F, et al. Characteristics and determinants of outcome of hospital-acquired bloodstream infections in intensive care units: the EUROBACT International Cohort Study. Intensive Care Med. 2012;38:1930–45. https://doi.org/10.1007/s00134-012-2695-9
33. Tabah A, Buetti N, Staiquly Q, Ruckly S, Akova M, Aslan AT, et al.; EUROBACT-2 Study Group, ESICM, ESCMID ESGCIP and the OUTCOMEREA Network. Epidemiology and outcomes of hospital-acquired

bloodstream infections in intensive care unit patients: the EUROBACT-2 international cohort study. Intensive Care Med. 2023;49:178–90. https://doi.org/10.1007/s00134-022-06944-2
34. Lepape A, Machut A, Bretonniere C, Friggeri A, Vacheron CH, Savey A, et al. Effect of COVID-19 infection and pandemic period on healthcare-associated infections acquired in intensive care units. Clin Microbiol Infect. 2023;29:530–6. https://doi.org/10.1016/j.cmi.2022.10.023
35. Martin-Loeches I, Torres A, Rinaudo M, Terraneo S, de Rosa F, Ramirez P, et al. Resistance patterns and outcomes in intensive care unit (ICU)-acquired pneumonia. Validation of European Centre for Disease Prevention and Control (ECDC) and the Centers for Disease Control and Prevention (CDC) classification of multidrug resistant organisms. J Infect. 2015;70:213–22. https://doi.org/10.1016/j.jinf.2014.10.004
36. Liu P, Li X, Luo M, Xu X, Su K, Chen S, et al. Risk factors for carbapenem-resistant *Klebsiella pneumoniae* infection: a meta-analysis. Microb Drug Resist. 2018;24:190–8. https://doi.org/10.1089/mdr.2017.0061
37. Baraz A, Chowers M, Nevo D, Obolski U. The time-varying association between previous antibiotic use and antibiotic resistance. Clin Microbiol Infect. 2022;0.
38. Tacconelli E, Górska A, De Angelis G, Lammens C, Restuccia G, Schrenzel J, et al. Estimating the association between antibiotic exposure and colonization with extended-spectrum β-lactamase-producing Gram-negative bacteria using machine learning methods: a multicentre, prospective cohort study. Clin Microbiol Infect. 2020;26:87–94. https://doi.org/10.1016/j.cmi.2019.05.013

Address for correspondence: Andrea Gori, School of Medicine and Surgery, Department of Pathophysiology and Transplantation, University of Milan Infectious Diseases Unit, IRCCS Ca' Granda Ospedale Maggiore Policlinico Foundation, Via Francesco Sforza 35, Milan 20122, Italy; email: andrea.gori@unimi.

Economic Evaluation of Wastewater Surveillance Combined with Clinical COVID-19 Screening Tests, Japan

Byung-Kwang Yoo, Ryo Iwamoto, Ungil Chung, Tomoko Sasaki, Masaaki Kitajima

The COVID-19 pandemic has imposed substantial burdens on the global society. To find an optimal combination of wastewater surveillance and clinical testing for tracking COVID-19, we evaluated the economic efficiency of hypothetical screening options at a single facility in Japan. To conduct cost-benefit analyses, we developed standard decision models in which we assumed model parameters from literature and primary data, such as screening policies used at the Tokyo Olympic and Paralympic Village in 2021. We compared hypothetical 2-step screening options that used clinical PCR to diagnose COVID-19 after a positive result from primary screening using antigen tests (option 1) or wastewater surveillance (option 2). Our simulation results indicated that option 2 likely would be economically more justifiable than option 1, particularly at lower incidence levels. Our findings could help justify and promote the use of wastewater surveillance as a primary screening at a facility level for COVID-19 and other infectious diseases.

COVID-19, caused by SARS-CoV-2, has imposed substantial disease and social burdens on the global society; ≈6.85 million deaths were confirmed worldwide by February 2023 (*1*). To reduce disease burden, both clinical screening tests and epidemic surveillance systems are required and need to be efficiently implemented under tight budget constraints.

Although clinical PCR and antigen tests are essential for detecting individual cases, those tests have multiple limitations, such as testing avoidance behaviors, low detection rates among asymptomatic persons, and challenges when high demand for testing during epidemic peaks exceeds laboratory capacity. An additional limitation is the relatively high cost at a population level, which hinders frequent implementation even among high-risk subpopulations and essential workers. Because of those limitations, an epidemic surveillance system based on clinical tests tends to underestimate prevalence and have reduced representation because of insufficient sample sizes.

Wastewater surveillance is expected to address limitations of clinical tests (*2*). A sample of wastewater can be highly representative for all residents at a specific facility or for hundreds of thousands of residents in an area covered by a single wastewater treatment plant. Although wastewater surveillance is a risk measure of a community and not an individual resident, when compared as separate options, a simple cost comparison favors wastewater surveillance over clinical tests (*3*).

The appropriate sampling site can differ depending on the population level targeted by wastewater surveillance. When a large population is targeted, such as all residents within a citywide sewershed, sampling of influent wastewater at a wastewater treatment plant is most effective (*4*). When neighborhood-scale sewersheds are targeted, wastewater should be sampled from manholes or pumping stations (*5*). Finally, when a single facility is targeted, wastewater samples must be collected immediately after being discharged from the facility; in most cases, such samples can be collected from a manhole (*6*).

We aimed to find an optimal combination of wastewater surveillance and clinical testing that complement, rather than substitute for, each other. Therefore, we performed an economic evaluation to

Author affiliations: Waseda University, Saitama, Japan (B.-K. Yoo); Kanagawa University of Human Services, Kanagawa, Japan (B.-K. Yoo, U. Chung); Shionogi & Co. Ltd. and AdvanSentinal Inc., Osaka, Japan (R. Iwamoto); The University of Tokyo, Tokyo, Japan (U. Chung); Independent consultant, Shiga, Japan (T. Sasaki); Hokkaido University, Hokkaido, Japan (M. Kitajima)

DOI: https://doi.org/10.3201/eid2908.221775

estimate the return on investment (ROI) of hypothetical screening options at a single facility in Japan.

Methods

We conducted a cost-benefit analysis to estimate the economic efficiency of various hypothetical screening options for confirming SARS-CoV-2 infections among asymptomatic or presymptomatic persons at a single residential facility, as measured by ROI, an equivalent to benefit-to-cost ratio. If 1 option is cost-saving compared with its comparator, that option's ROI is estimated to be >1. For example, an estimated ROI of 1.50 indicates that a $100 investment in 1 option will produce a net savings of $50. Our cost-benefit analyses adopted a societal perspective with a 1-month timeframe.

We compared 2 hypothetical 2-step screening options that used clinical PCR tests to diagnose individual COVID-19 cases after a positive result from a primary screening with antigen tests (option 1) or wastewater surveillance (option 2). Those screening options partly followed those used in the Tokyo Olympic and Paralympic Village in 2021 (*6*,*7*). We assumed antigen test results would be available in ≤1 hour, PCR test results would be available on the same day, and wastewater surveillance results would be available by the day after sampling.

More specifically, under option 1, the residents at a facility would all undergo antigen testing daily for 4 days as a primary screening. Any resident who tests positive would receive secondary screening on the same day with 2 PCR tests to confirm the diagnosis. Option 2 was to conduct wastewater surveillance at a facility as a primary screening for days 1–3. If a previous day's wastewater surveillance indicated a positive result, all persons at the facility would undergo secondary screening with 2 consecutive PCR tests to clinically diagnose an infected case during days 2–4.

Option 1 and option 2 are substitutes only in terms of their primary screening, either antigen tests or facility-based wastewater surveillance. For both options, the primary screening (antigen tests or facility-based wastewater surveillance) and secondary screening (PCR for clinical diagnosis) are complementary.

We assumed model parameters on the basis of available literature and primary data and developed a standard decision model (Table 1; Appendix Figure 1, https://wwwnc.cdc.gov/EID/article/29/8/22-1775-App1.pdf). Our base-case analysis with a deterministic model assumed a point estimate for each parameter. To address the uncertainties of model parameters, we also implemented a probabilistic analysis with Monte Carlo simulations by assigning distributions (Table 1). For instance, we assumed a triangular distribution for the parameter sensitivity of wastewater surveillance using a mode of 66% (range 46%–84%). That parameter sensitivity could be affected by various factors, including variability in viral shedding over the course of an infection and between different infected persons, dilution and decay of virus in the sewer, and analytical sensitivity of the method used for virus detection in wastewater. Monte Carlo simulations provided the mean and the 95% probabilistic confidence interval (PCI) values of the ROI estimates. We used TreeAge software (https://treeage.com) to perform analyses for decision models.

Because economic efficiency is highly sensitive to the disease incidence, our base-case analysis included the 3 scenarios: 10, 100, or 1,000 newly reported clinically positive cases per million residents per day (PMPD) in the area around the facility. In other words, our study did not assign a certain distribution for the incidence because of a very wide range of feasible values.

The 10 PMPD incidence value corresponds to the minimum level at which wastewater surveillance sampled at a wastewater treatment plant can detect SARS-CoV-2 (*4*). Our 1-way sensitivity analyses all assumed the incidence value of 100 PMPD, above which a correlation was observed in our primary data between SARS-CoV-2 RNA load in wastewater sampled at a wastewater treatment plant and the incidence based on clinical PCR tests in the area (*21*).

The 1,000 PMPD incidence value is equal to the ratio of 1 newly infected case among 1,000 residents in a hypothetical facility, and 1,000 was close to the smallest population of the sampling area in the Tokyo Olympic and Paralympic Village in 2021 (*6*). Our base-case analyses all assumed the facility had 100 residents, which we based on the average number of beds in long-term care facilities (LTCFs) in Japan (*22*).

Hypothetical study populations in our base-case analyses all were 100 residents at a LTCF who were expected to receive greater benefits from screening tests in terms of preventing COVID-19–related illness and death compared with the general population. For instance, LTCF residents in Japan have an average age of ≈86 years (*29*) and were estimated to be 19 times as likely to die after a clinical COVID-19 diagnosis than the general population in Japan (*23*).

Our study estimated the benefit of confirming 1 infected case by PCR under each screening option by using 2 components: the benefit of reducing hospitalization and death for a confirmed case, and

Table 1. Decision model parameters in an economic evaluation of wastewater surveillance combined with clinical COVID-19 screening tests, Japan*

Parameters†	Point estimate (range)	Reference
Test characteristics		
Sensitivity		
Wastewater surveillance	0.66 (0.46–0.84)	M. Kitajima, unpub. data
PCR‡	0.74 (0.64–0.83)	(*8*,*9*)
Ratio of antigen test against PCR test	0.76 (0.54–0.97)	(*8*–*10*)
PCR test after positive antigen test	0.99 (0.64–0.999)	(*8*,*9*)
Specificity		
PCR	0.974 (0.96–0.995)	(*9*,*10*)
Antigen test	0.99 (0.97–0.995)	(*10*)
Ratio of wastewater surveillance against PCR test	0.99	
Cost		
Laboratory cost of wastewater surveillance per facility per day	$379 ($189–$758)	(*11*,*12*)
Labor cost to sample at a facility per facility per day	$1,136 ($152–$2,045)	(*13*)
Antigen test§	$16 ($10–$23)	(*14*,*15*)
Clinical PCR§	$38 ($20–$53)	(*14*,*15*)
Isolation per test-positive case	$758 ($379–$1,515)	(*16*)
Hospitalization per case¶	$19,394 ($16,212–$25,227)	(*17*–*19*)
Value of QALY saved per case	$37,879	(*20*)
Other		
Incidence per day per 1 million residents	100 (10–10,000)	(*4*,*21*)
No. residents at a facility	100 (50–200)	(*6*,*22*)
Mortality rate among persons who test positive#	0.0035 (0.0018–0.0104)	(*23*)
Ratio of mortality rate among persons ≥80 years of age vs. general population	19 (15–22)	(*23*)
Life-years saved by avoiding COVID-19	11.4 (11.1–11.7)	(*24*,*25*)
Ratio to convert life-years saved to QALYs saved	0.68 (0.64–0.71)	(*24*,*26*)
Hospitalization rate among persons who test positive	0.18 (0.04–0.40)	(*17*)
Proportion of severe cases among hospitalized cases	0.1 (0.05–0.19)	(*17*)
Effective reproduction number of infected cases	1.3 (0.9–2.0)	(*27*)
Screening effectiveness in reducing hospitalization and mortality rates because of an earlier diagnosis	0.54 (0.23–0.62)	(*28*)
Ratio of loss value of missing an infected case compared with benefit value of finding an infected case	1 (0–2.0)	

*All monetary values are expressed in 2022 US dollars. QALY, quality-adjusted life-years.
†All parameters with a minimum and a maximum value in this table are defined as a triangular distribution in the probabilistic analysis, detailed in the Appendix (https://wwwnc.cdc.gov/EID/article/29/8/22-1775-App1.pdf).
‡Because the second clinical PCR test was conducted immediately after the first clinical PCR test, the sensitivity of the second clinical PCR was assumed to be equal to the specificity of the PCR test in this table.
§Test cost plus labor cost for sampling; 30 min multiplied by minimum wage of $7 USD per hour (*15*).
¶Hospitalization cost was assumed as $16,212 + $64,394 x (proportion of severe cases among hospitalized cases – 0.05).
#The range was defined to range from the rate before the vaccination period to the rate after the vaccination period (Appendix).

the benefit of preventing secondary infection. Because scant literature addressed the effectiveness of screening in reducing hospitalization and mortality rates among persons who test positive, we assumed effectiveness was equivalent to the clinical efficacy of antiviral agents among patients with COVID-19 at its early stage (e.g., ≤7 days after the onset of signs or symptoms), who are not hospitalized yet but could be subsequently hospitalized or die (*28*). We reduced the clinical efficacy by 30%, because 30% of infected persons never develop symptoms (*30*). Consequently, our screening effectiveness had a triangular distribution with a mode of 0.54 (range 0.23–0.62). We estimated the benefit of preventing secondary infection to be 0.57 under our base-case analyses, which was dependent on a reproduction number of 1.3 (*27*), an infectious period of 8.03 days (*31*), and other factors (*30*). In addition, our model accounted for the loss of missing an infected case that produced a second-generation infected case every day (Appendix).

To assign benefit values for reducing hospitalization and mortality rates, we estimated the related monetary value for 3 outcomes among confirmed cases: isolation (*14*–*16*), hospitalization (*17*–*19*), and death (*20*,*24*–*26*). All monetary values are expressed in 2022 US dollars (USD). We assigned a value for death by applying the monetary value of $37,879 for each quality-adjusted life-year (QALY) saved or lost under the cost-effectiveness analysis set by the Ministry of Health, Labour and Welfare of Japan (*20*). To estimate QALYs lost due to COVID-19, we first calculated life years lost based on age at death (*24*) and life expectancy among a certain age and sex (*25*). To convert life years lost to QALYs lost, we applied the ratios estimated among the population of the Netherlands (*26*), because the relevant data were not available for Japan.

Results

When COVID-19 incidence was 10 PMPD, our deterministic base-case analysis indicated that option 1 alone, compared with doing nothing (comparator do-nothing), was not economically justifiable because its cost ($67.04) exceeded its benefit ($1.39) and the ROI of 0.021 ($1.39/$67.04) was ≤1.0 (Table 2). Although option 2 alone compared with do-nothing was not justifiable because of the low ROI (0.021), option 2 became justifiable when its comparator was changed from do-nothing to option 1. That is, compared with option 1, option 2 saved $13.44, which could be interpreted as relative benefit, and had a $0.25 lower benefit, which could be interpreted as relative cost. Thus, compared with option 1, the relative value of option 2 was a high ROI of 54 ($13.44/$0.25) (Table 2).

When COVID-19 incidence was 1,000 PMPD under our base-case analysis, we estimated the ROI of option 1 to be 2.10 and of option 2 to be 2.23 (Table 2). One-way sensitivity analysis of the deterministic model showed the threshold incidence values, above or below which an option's ROI is >1. Those threshold values were 480 PMPD for option 1 alone, 450 PMPD for option 2 alone, and 630 PMPD for the relative value of option 2 (Table 3). One-way sensitivity analysis also showed that when incidence increased, the ROI of options 1 and 2 increased and that the relative value of option 2 declined (Figure).

Additional 1-way sensitivity analyses of the base-case analysis showed that within the feasible range of parameters, all 3 types of ROI estimates were sensitive to incidence and had values above and below 1.0. The ROI estimates of options 1 and 2 alone, compared with do-nothing, were robust to all parameters except incidence. The ROI estimates of options 1 and 2 alone had a negative association with test costs and a positive association with test sensitivity and specificity (Table 4).

The estimated range of the ROI for the relative value of option 2 includes negative values (Table 4). For the ratio of sensitivity of antigen tests against PCR, option 2 was always preferred over option 1; option 2 dominated option 1 when the ROI estimates were negative for that ratio. In other words, a simple linear relationship did not occur between the ratio of sensitivity of antigen tests against PCR and the ROI for the relative value of option 2. For instance, when that ratio increased from 0.64 to 0.97, the ROI estimate for the relative value of option 2 was always >1 (Appendix Table 8). When the ratio was 0.638, option 2's benefit became equal to option 1's benefit, which did not mathematically enable estimation of the ROI for the relative value of option 2. When the ratio increased from 0.54 to 0.63, option 2's benefit exceeded option 1's benefit; thus, option 2 dominated option 1.

The ROI estimates regarding the relative value of option 2 were sensitive to 3 cost-related parameters. In other words, an estimated threshold point existed, below or above which a preferred option changed. For instance, option 2 was preferred only when the labor cost to sample a facility was lower than the threshold point of $1,512. When labor cost exceeded that threshold point, option 1 was preferred. Likewise, when the cost of the antigen test was lower than the threshold point of $13.18, option 1 was preferred, but when it was greater than that threshold point, option 2 was preferred. Because the cost of wastewater surveillance per facility was fixed, the cost per facility resident could be substantially reduced by a larger number of facility residents. Therefore, when the number of residents was lower than the threshold point of 81, option 1 was preferred, but when it was greater than that threshold, option 2 was preferred.

The probabilistic analyses showed that the base-case analyses with a deterministic model were robust, particularly for cost, benefit, and ROI estimates for option 1 alone or option 2 alone (Table 5). Although the estimated PCIs included a large negative value as a lower bound, option 2 was mostly preferred to option 1 when the incidence was 10 or 100

Table 2. Base-case analysis with a deterministic model in an economic evaluation of wastewater surveillance combined with clinical COVID-19 screening tests, Japan*

	Option 1			Option 2			Relative value of option 2		
Incidence†	Cost	Benefit	ROI‡	Cost	Benefit	ROI‡	Incremental cost§	Incremental benefit¶	Relative ROI#
10	$67.04	$1.39	0.021	$53.60	$1.14	0.021	–$13.44	–$0.25	54
100	$67.05	$14.09	0.21	$53.61	$11.94	0.22	–$13.43	–$2.15	6.25
1,000	$67.12	$141.11	2.10	$53.75	$119.94	2.23	–$13.37	–$21.16	0.63

*Option 1 is clinical testing only; option 2 is wastewater surveillance and clinical testing. If one option is cost-saving compared with its comparator, the option's ROI is estimated to exceed 1. The comparator of options 1 and 2 is do-nothing. All monetary values are expressed in 2022 US dollars (USD). ROI, return on investment.
†Disease incidence per day per 1 million residents in the area.
‡ROI is benefit divided by cost for each option.
§Incremental cost is the cost of option 2 minus cost of option 1. A negative value of incremental cost indicates that option 2 has a lower cost or is cost-saving, compared with option 1. This could be interpreted as option 2's relative benefit.
¶Incremental benefit is the benefit of option 2 minus benefit of option 1. A negative value of incremental benefit indicates that option 2 has a lower benefit compared with option 1, which could be interpreted as option 2's relative cost.
#Relative ROI is incremental cost divided by incremental benefit.

Table 3. One-way sensitivity analyses of the base-case analysis of the incidence parameter in an economic evaluation of wastewater surveillance combined with clinical COVID-19 screening tests, Japan*

	Option 1			Option 2			Relative value of option 2		
Incidence†	Cost	Benefit	ROI‡	Cost	Benefit	ROI‡	Incremental cost§	Incremental benefit¶	Relative ROI#
10	$67.04	$1.39	0.02	$53.60	$1.14	0.02	–$13.44	–$0.25	54
50	$67.04	$7.03	0.10	$53.61	$5.94	0.11	–$13.44	–$1.09	12
100	$67.05	$14.09	0.21	$53.61	$11.94	0.22	–$13.43	–$2.15	6
400	$67.07	$56.43	0.84	$53.66	$47.94	0.89	–$13.41	–$8.49	1.58
445	$67.08	$62.78	0.94	$53.67	$53.34	0.99	–$13.41	–$9.44	1.42
450	$67.08	$63.49	0.95	$53.67	$53.94	1.01	–$13.41	–$9.54	1.40
475	$67.08	$67.01	0.999	$53.67	$56.94	1.06	–$13.41	–$10.07	1.33
480	$67.08	$67.72	1.010	$53.67	$57.54	1.07	–$13.41	–$10.18	1.32
500	$67.08	$70.54	1.05	$53.68	$59.94	1.12	–$13.40	–$10.60	1.26
600	$67.09	$84.65	1.26	$53.69	$71.94	1.34	–$13.40	–$12.71	1.05
630	$67.09	$88.89	1.32	$53.70	$75.54	1.41	–$13.39	–$13.35	1.004
635	$67.09	$89.59	1.34	$53.70	$76.14	1.42	–$13.39	–$13.45	0.996
700	$67.10	$98.77	1.47	$53.71	$83.94	1.56	–$13.39	–$14.83	0.90
1,000	$67.12	$141.11	2	$53.75	$119.94	2	–$13.37	–$21.16	0.63
2,000	$67.20	$282.23	4	$53.91	$239.95	4	–$13.29	–$42.29	0.31
5,000	$67.45	$705.62	10	$54.37	$599.96	11	–$13.07	–$105.66	0.12
10,000	$67.85	$1,411.26	21	$55.14	$1,199.97	22	–$12.71	–$211.29	0.06

*Option 1 is clinical tests only; option 2 is wastewater surveillance and clinical tests. If an option is cost-saving compared with its comparator, the option's ROI is estimated to exceed 1. The comparator of options 1 and 2 is do-nothing. All monetary values were expressed in 2022 US dollars. ROI, return on investment.
†Disease incidence per day per 1 million residents in the area.
‡ROI is benefit divided by cost for each option.
§Incremental cost is the cost of option 2 minus cost of option 1. A negative value of incremental cost indicates that option 2 has a lower cost or is cost-saving, compared with option 1. This could be interpreted as option 2's relative benefit.
¶Incremental benefit is the benefit of option 2 minus benefit of option 1. A negative value of incremental benefit indicates that option 2 has a lower benefit compared with option 1, which could be interpreted as option 2's relative cost.
#Relative ROI is incremental cost divided by incremental benefit.

PMPD. More specifically, over 1,000 iterations, when incidence was 10 PMPD, option 2 was preferred in 84.7% of the time; when incidence was 100 PMPD, option 2 was preferred 80.8% of the time; and when incidence was 1,000 PMPD, option 2 was preferred 25.2% of the time. Thus, qualitative conclusions of probabilistic analyses were similar to those of deterministic analyses.

Discussion

Our simulation results indicate that a primary screening with wastewater surveillance (option 2) at a single facility was highly likely to be economically more justifiable than a primary screening with antigen tests (option 1), particularly at lower incidence levels (<630 PMPD). Option 2 tended to have a much lower cost (interpreted as relative benefit) and a slightly lower benefit (interpreted as relative cost) compared with option 1. Of note, when the comparator was do-nothing, option 1 alone and option 2 alone had low economic efficiency when the disease incidence was low; option 1 alone was economically justifiable only when the incidence was >480 PMPD and option 2 alone was economically justifiable only when the incidence was >450 PMPD. At incidence levels >1,000 PMPD, option 2 is economically less efficient than option 1 because clinical tests would not be implemented on day 1 under option 2, which would lead to more secondary infections and more costs for isolation or hospitalization. Our results appeared generally robust to the feasible range of model parameters, although some results were sensitive to parameters related to the disease incidence and cost of tests.

Our analytical models are expected to have high generalizability to and be robust for SARS-CoV-2 variants, unlike vaccination effectiveness, which can potentially be reduced by variants. In addition, our analytic approach would be readily applicable to other emerging infectious diseases.

The negative ROI estimates regarding the relative value of option 2 should be interpreted with caution because 2 opposite interpretations are possible. One interpretation prefers option 2, such as when option 2 detected many more infected cases than option 1 at a facility with <77 residents. On the contrary, the other interpretation prefers option 1, such as when fewer COVID-19 cases were missed by option 1 than option 2 and when the antigen test cost was <$12.64.

We expected the face validity of our simulation results to be achieved to some extent, partly because the assumptions of our hypothetical screening options mainly followed the screening policies used in the Tokyo Olympic and Paralympic Village (*6*,*7*). Also, the assumed range of the laboratory cost for wastewater surveillance ($189–$758) appeared reasonable, compared with costs reported by other studies (*11*,*12*,*32*).

In addition, we used conservative assumptions in our base-case analysis, such as relatively high costs for additional labor to sample wastewater at a facility for surveillance (*13*). Another set of conservative assumptions that reduced the benefit of confirming 1 infected case were the exclusion of COVID-19–related medical expenditure for outpatient care and the possible financial loss related to shutdown of a LTCF. We excluded those items from our analyses because cost-related data were absent in the literature.

One weakness of this study is the limited generalizability to other settings. We assumed the monetary value of finding 1 COVID-19 case at a facility depended partly on related medical expenditure and QALY saved. QALY varies in different countries; in Japan, the value is $37,879/QALY (*20*). Also, the monetary value of finding 1 case consisted of mortality rate in the population, hospitalization rate in the population, and medical expenditures per hospitalized case, all of which could vary substantially at the population level because of viral variants occurring over time and across regions within a country. In addition, mortality and hospitalization rates vary markedly among subpopulations defined by age and high-risk chronic conditions. Such uncertainties indicate the need to frequently update the simulation model to correspond to regional epidemics and target populations.

Because of the absence of literature, the validity of our ROI estimates was difficult to compare with estimates from previous studies. Although 1 study compared wastewater surveillance at a treatment plant and clinical PCR tests in its costs, that study compared cost per population screened without accounting for clinically confirmed cases after wastewater surveillance (*3*). Therefore, the estimates in that study were not appropriate comparisons for our ROI estimates. When the goal of screening is to identify and isolate an infected case, wastewater surveillance should be used as a primary screening, after which secondary screening should be performed by using clinical tests.

Major policy implications derived from this study's findings are exemplified by the threshold levels to start or suspend a specific screening option. Compared with do-nothing, threshold incidence levels were 480 PMPD for option 1 alone and 450 PMPD for option 2 alone, but those thresholds are <1,000 PMPD. The 1,000 PMPD incidence is equivalent to 1 newly infected case at a single large facility with 1,000 residents. That is, before finding the first newly infected case at a single facility, options 1 and 2 should be started, ideally triggered when the incidence of the area around the facility, such as the city, town, or neighborhood, reaches the threshold levels we reported for each option.

The ROI estimates for the relative value of option 2 compared with option 1 tended to be high at a very low incidence, when the absolute benefit of option 2 is small compared with do-nothing. One practical incidence level to trigger option 2 is 10 PMPD, above which wastewater surveillance conducted by using a recently developed method can detect SARS-CoV-2 RNA at a treatment plant (*4*). Another trigger incidence is 100 PMPD, above which conventional wastewater surveillance methods can detect SARS-CoV-2 RNA (*4*). Regularly monitoring data from wastewater surveillance at a treatment plant could enable efficient triggers for option 1 and option 2 at a specific facility in the same area.

Because wastewater surveillance at a treatment plant covers a city-scale population, the additional cost per resident would be very small, even when

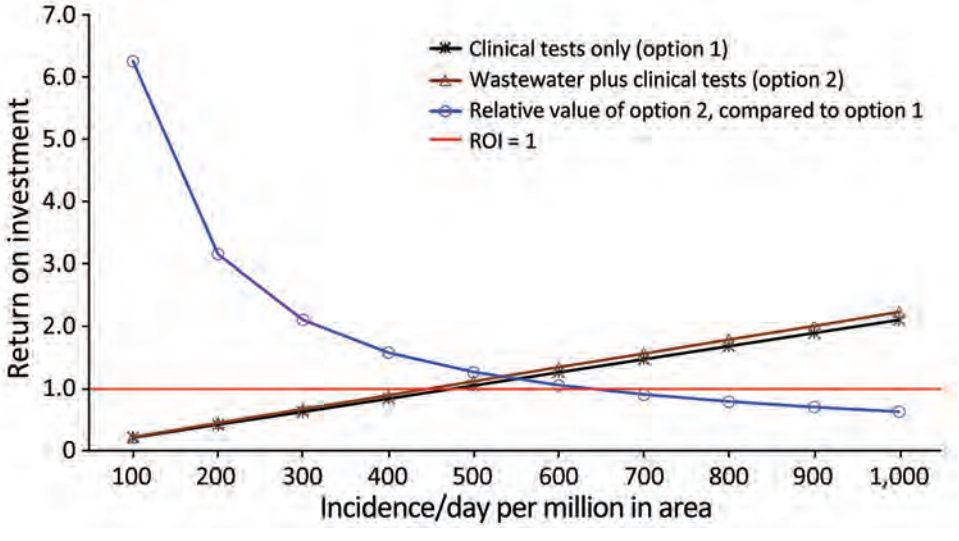

Figure. ROI comparison of 2 options used in an economic evaluation of wastewater surveillance combined with clinical COVID-19 screening tests, Japan. ROIs for the relative value of option 2 are expressed as $\log_{10}$ and determined by 1-way sensitivity analyses of the base-case analysis (Table 3). Red horizontal line indicates ROI = 1. ROI, return on investment.

focusing on an institutionalized population; for instance, increasing the per resident cost in our model by <1%. Although the central government of Japan implemented pilot projects of wastewater surveillance at both city and facility levels during fiscal year 2022 (*33*), government officials did not expand the scale of those projects, partly because of a lack of evidence regarding economic efficiency. Thus, our findings could help the central government of Japan justify the expansion of these projects.

Table 4. One-way sensitivity analyses of the base-case analysis in an economic evaluation of wastewater surveillance combined with clinical COVID-19 screening tests, Japan*

Parameters	Parameter values	Return on investment†		Relative ROI‡
		Option 1	Option 2	
Test characteristics				
Sensitivity				
Wastewater surveillance	0.46	0.21	0.12	2
	0.84	0.21	0.26	80
PCR	0.64	0.18	0.22	32
	0.83	0.23	0.22	4
Ratio of antigen test against PCR test	0.54	0.14	0.22	−5.43
	0.97	0.24	0.22	3
PCR test after positive antigen test	0.64	0.12	0.10	5
	0.999	0.21	0.22	6
Specificity				
PCR	0.96	0.21	0.21	5
	0.995	0.21	0.25	9
Antigen test	0.97	0.19	0.22	9
	0.995	0.22	0.22	6
Cost				
Wastewater surveillance cost per day per facility				
Laboratory cost	$189	0.21	0.25	9
	$758	0.21	0.18	0.96
Labor cost to sample	$152	0.21	0.50	20
	$2,045	0.21	0.15	−6.43
Antigen test¶	$10	0.33	0.22	−4.91
	$23	0.15	0.22	19
Clinical PCR¶	$20	0.215	0.24	7
	$53	0.207	0.21	5
Isolation per test-positive case	$379	0.209	0.222	6.33
	$1,515	0.212	0.224	6.09
Hospitalization per case#	$16,212	0.18	0.19	7
	$25,227	0.26	0.27	5
Other				
Incidence per day per 1 million population	10	0.02	0.02	54
	10,000	21	22	0.06
No. residents at a facility	50	0.21	0.12	−14.89
	1,000	0.21	0.94	25
Mortality rate among persons who test positive	0.0018	0.19	0.20	7
	0.0104	0.30	0.32	4
Ratio of mortality rate among persons ≥80 years of age vs. the general population	0.5	0.004	0.004	161
	22	0.24	0.26	5
Life-years saved by avoiding COVID-19	11.1	0.209	0.221	6.28
	11.7	0.211	0.224	6.21
Ratio to convert life-years saved to QALYs saved	0.64	0.207	0.220	6.33
	0.71	0.212	0.225	6.19
Hospitalization rate among persons who test positive	0.04	0.08	0.08	14
	0.40	0.42	0.46	4
Proportion of severe cases among hospitalized cases	0.05	0.18	0.19	7
	0.19	0.26	0.28	5
Effective reproduction number of infected cases	0.9	0.28	0.31	7
	2.0	0.17	0.16	5
Effectiveness of screening in reducing hospitalization and mortality rates because of an earlier diagnosis	0.23	0.09	0.10	14
	0.62	0.24	0.26	5
Ratio of loss value of missing and infected cases compared with benefit value of finding an infected case	0.0	0.25	0.31	148
	2.0	0.17	0.13	3

*The lower and upper bounds of each parameter are shown to illustration the association between a parameter and its ROI. Incidence was assumed to be 100 persons per day per 1 million residents in the area. All monetary values are expressed in 2022 US dollars. QALY, quality-adjusted life-years; ROI, return on investment.
†Option 1 is clinical tests only; option 2 is wastewater surveillance and clinical tests.
‡Relative ROI of option 2 compared with option 1.

Table 5. Base-case analysis using a deterministic model and a probabilistic model in an economic evaluation of wastewater surveillance combined with clinical COVID-19 screening tests, Japan*

	Option 1			Option 2			Relative value of option 2		
Incidence†	Cost	Benefit	ROI 1‡	Cost	Benefit	ROI 2‡	Inc. cost§	Inc. benefit¶	Rel. ROI#
10									
DA	$67.04	$1.39	0.021	$53.60	$1.14	0.021	–$13.44	–$0.25	54
Mean PA	$70.03	$1.43	0.021	$50.68	$0.97	0.021	–$19.35	–$0.46	45
(95% PCI)	($49.85–$90.25)	($0.42–$2.85)	(0.006–0.043)	($25.27–$90.23)	($0.19–$2.04)	(0.004–0.051)	(–$54.48 to $24.31)	(–$1.20 to $0.08)	(−194 to 387)
100									
DA	$67.05	$14.09	0.21	$53.61	$11.94	0.22	–$13.43	–$2.15	6.25
Mean PA	$68.54	$14.75	0.22	$50.86	$10.37	0.23	–$17.68	–$4.38	5.74
(95% PCI)	($48.77–$88.86)	($5.11–$28.35)	(0.07–0.45)	($24.95–$92.14)	($3.03–$20.71)	(0.05–0.60)	(–$52.33 to $23.34)	(–$11.35 to $1.31)	(−24 to 37)
1,000									
DA	$67.12	$141.11	2.10	$53.75	$119.94	2.23	–$13.37	–$21.16	0.63
Mean PA	$69.50	$147.29	2.17	$50.61	$104.58	2.29	–$18.89	–$42.71	0.34
(95% PCI)	($48.76–$89.54)	($52.37–$279.00)	(0.73–4.57)	($24.56–$89.89)	($30.91–$215.00)	(0.55–5.59)	(–$52.28 to $23.15)	(–$110 to $8.65)	(−2.14 to 3.71)

*A probabilistic model to compare clinical tests only (option 1) to wastewater surveillance combined with clinical tests (option 2). If one option is cost-saving compared with its comparator, the option's ROI is estimated to exceed 1. The comparator of options 1 and 2 is do-nothing. DA, deterministic model analysis; inc., incremental; PA, probabilistic model analysis with Monte Carlo simulations; PCI, probabilistic confidence interval; rel., relative; ROI, return on investment.
†Disease incidence per day per 1 million residents in the area.
‡ROI is benefit divided by cost for each option.
§Incremental cost is the cost of option 2 minus cost of option 1. A negative value of incremental cost indicates that option 2 has a lower cost or is cost-saving, compared with option 1. This could be interpreted as option 2's relative benefit.
¶Incremental benefit is the benefit of option 2 minus benefit of option 1. A negative value of incremental benefit indicates that option 2 has a lower benefit compared with option 1, which could be interpreted as option 2's relative cost.
#Relative ROI is incremental cost divided by incremental benefit.

Another major policy implication is the threshold level for the number of residents at a facility. Our base-case analyses used hypothetical study populations of 100 residents at an LTCF. Our sensitivity analyses showed that the ROIs for option 2 alone and relative value of option 2 might increase when the number of residents increased; hence, wastewater surveillance cost per resident declined. The number of residents per facility could be easily increased to >1,000, the upper bound of our 1-way sensitivity analyses, if a facility, such as a large apartment complex, included younger residents. However, a lower mortality rate for younger residents would reduce the general screening benefit, thus reducing the ROI. An estimated minimum (threshold) number of 81 residents at an LTCF appears to help set a public guideline for wastewater surveillance.

Additional policy implications would help set goals for related industry. Because option 1 and option 2 differ in a primary screening, the difference in sensitivity between antigen tests and wastewater surveillance affected the economic efficiency for the relative value of option 2. Improved sensitivity of antigen tests is feasible but requires a longer time to diagnose a case, which reduces the benefit of antigen tests by postponing the diagnosis timing compared with 1-hour diagnosis time assumed under our base-case analysis. In other words, shortening the time to diagnosis for a screening test result would generally improve the test's economic efficiency, a goal for related industry.

Future research could further explore the monetary values of time needed for screening, such as time required by caregivers who collect samples from LTC residents or young children. If those time costs are much larger in a certain setting, like a kindergarten, the relative economic efficiency of wastewater surveillance against clinical tests would increase.

Although one of the general advantages of wastewater surveillance is fewer privacy and stigmatization concerns than possible with clinical surveillance (*34*), ethical issues could arise in 2 cases. First, targeting a specific facility or a small catchment could lead to social harm and financial burdens to the targeted population (*34*). Second, regardless of the target population size, ethical issues might arise when the wastewater surveillance is used for applying restrictive measures, such as group quarantine or business closure in the target area or facility (*35*). Researchers, policymakers, and regulators need to collaborate to account for ethical issues in implementing wastewater surveillance (*36*), which could enable wastewater surveillance to represent a new frontier in surveillance, monitoring, and screening.

In conclusion, our findings could help justify and promote the use of wastewater surveillance as a primary screening at a single facility when a set of quantified conditions estimated in our simulation are met.

Of note, regular wastewater surveillance at a treatment plant will help trigger the start of any screening tests at a specific facility. Because few economic evaluations of wastewater surveillance have yet been conducted, our findings can contribute to related academic fields and policy making.

This article was preprinted at https://dx.doi.org/10.2139/ssrn.4214533.

About the Author

Dr. Yoo is a professor in the Faculty of Human Sciences, School of Human Sciences, Waseda University, Saitama, Japan, and a professor in the School of Health Innovation, Kanagawa University of Human Services, Kanagawa, Japan. He is a health economist with the long-term research experiences in disease prevention and promoting health policy, particularly infectious diseases.

References

1. World Health Organization. Coronavirus disease (COVID-19) pandemic [cited 2023 Feb 23]. https://www.who.int/emergencies/diseases/novel-coronavirus-2019
2. Kitajima M, Ahmed W, Bibby K, Carducci A, Gerba CP, Hamilton KA, et al. SARS-CoV-2 in wastewater: state of the knowledge and research needs. Sci Total Environ. 2020;739:139076. https://doi.org/10.1016/j.scitotenv.2020.139076
3. Hart OE, Halden RU. Computational analysis of SARS-CoV-2/COVID-19 surveillance by wastewater-based epidemiology locally and globally: feasibility, economy, opportunities and challenges. Sci Total Environ. 2020;730:138875. https://doi.org/10.1016/j.scitotenv.2020.138875
4. Ando H, Murakami M, Ahmed W, Iwamoto R, Okabe S, Kitajima M. Wastewater-based prediction of COVID-19 cases using a highly sensitive SARS-CoV-2 RNA detection method combined with mathematical modeling. Environ Int. 2023;173:107743. https://doi.org/10.1016/j.envint.2023.107743
5. Oh C, Zhou A, O'Brien K, Jamal Y, Wennerdahl H, Schmidt AR, et al. Application of neighborhood-scale wastewater-based epidemiology in low COVID-19 incidence situations. Sci Total Environ. 2022;852:158448. https://doi.org/10.1016/j.scitotenv.2022.158448
6. Kitajima M, Murakami M, Kadoya SS, Ando H, Kuroita T, Katayama H, et al. Association of SARS-CoV-2 load in wastewater with reported COVID-19 cases in the Tokyo 2020 Olympic and Paralympic Village from July to September 2021. JAMA Netw Open. 2022;5:e2226822. https://doi.org/10.1001/jamanetworkopen.2022.26822
7. Kitajima M, Murakami M, Iwamoto R, Katayama H, Imoto S. COVID-19 wastewater surveillance implemented in the Tokyo 2020 Olympic and Paralympic Village. J Travel Med. 2022;29:taac004. https://doi.org/10.1093/jtm/taac004
8. Marando M, Tamburello A, Gianella P, Taylor R, Bernasconi E, Fusi-Schmidhauser T. Diagnostic sensitivity of RT-PCR assays on nasopharyngeal specimens for detection of SARS-CoV-2 infection: a systematic review and meta-analysis. Caspian J Intern Med. 2022;13(Suppl 3):139–47.
9. Tsang NNY, So HC, Ng KY, Cowling BJ, Leung GM, Ip DKM. Diagnostic performance of different sampling approaches for SARS-CoV-2 RT-PCR testing: a systematic review and meta-analysis. Lancet Infect Dis. 2021;21:1233–45. https://doi.org/10.1016/S1473-3099(21)00146-8
10. Tapari A, Braliou GG, Papaefthimiou M, Mavriki H, Kontou PI, Nikolopoulos GK, et al. Performance of antigen detection tests for SARS-CoV-2: a systematic review and meta-analysis. Diagnostics (Basel). 2022;12:1388. https://doi.org/10.3390/diagnostics12061388
11. Kantor RS, Greenwald HD, Kennedy LC, Hinkle A, Harris-Lovett S, Metzger M, et al. Operationalizing a routine wastewater monitoring laboratory for SARS-CoV-2. PLOS Water. 2022;1:e0000007. https://doi.org/10.1371/journal.pwat.0000007
12. Safford HR, Shapiro K, Bischel HN. Opinion: wastewater analysis can be a powerful public health tool—if it's done sensibly. Proc Natl Acad Sci U S A. 2022;119:e2119600119. https://doi.org/10.1073/pnas.2119600119
13. Ministry of Land Infrastructure, Transport and Tourism. Engineer unit price for a design outsourcing for fiscal year 2021 [in Japanese] [cited 2022 Aug 23]. https://www.mlit.go.jp/tec/content/001387446.pdf
14. Ministry of Health Labour and Welfare. Approval information for in-vitro diagnostic reagents (test kits) for COVID-19 [in Japanese] [cited 2022 Aug 22]. https://www.mhlw.go.jp/stf/newpage_11331.html
15. Ministry of Health Labour and Welfare. Current status of minimum wage amendments by regions for FY 2021 [in Japanese] [cited 2022 Aug 4]. https://www.mhlw.go.jp/stf/seisakunitsuite/bunya/koyou_roudou/roudoukijun/minimumichiran
16. Ministry of Health Labour and Welfare. Handling of the emergency comprehensive support program (for medical care) for COVID-19 in FY 2022 [in Japanese] [cited 2022 Aug 31]. https://www.mhlw.go.jp/content/000968054.pdf
17 Ministry of Health Labour and Welfare. Survey on medical treatment and number of inpatient beds [in Japanese] [cited 2021 Sep 14]. https://www.mhlw.go.jp/stf/seisakunitsuite/newpage_00023.html
18. Global Health Consulting. The unit price of a COVID-19 patient—54,000 yen for mild cases, 80,000 yen for moderate cases, and 142,000 yen for severe cases–is not worth the investment cost, according to the president of Japan Municipal Hospital Association (JMHA) [in Japanese] [cited 2021 Nov 24]. https://gemmed.ghc-j.com/?p=38100
19. Ministry of Health Labour and Welfare. Amendments for the rules on "major medical institutions for COVID-19 and cooperative medical institutions accepting suspected COVID-19 patients" [in Japanese] [cited 2022 Aug 31]. https://www.mhlw.go.jp/content/000764832.pdf
20. Central Social Insurance Medical Council, Ministry of Health, Labour and Welfare (MHLW). Examination of scientific matters for cost-effectiveness evaluation (part 4) [in Japanese] [cited 2022 Aug 31]. https://www.mhlw.go.jp/content/12404000/000380564.pdf
21. Kanagawa Prefectural Government. Wastewater surveillance reports at the wastewater treatment plants in Kanagawa prefecture, Japan [cited 2022 Sep 2]. https://www.pref.kanagawa.jp/docs/ga4/covid19/simulation.html
22. Ministry of Health Labour and Welfare. Overview of survey of institutions and establishments for long-term care for FY 2020 [in Japanese] [cited 2022 Aug 23]. https://www.mhlw.go.jp/toukei/saikin/hw/kaigo/service20/dl/kekka-gaiyou_1.pdf
23. Ministry of Health Labour and Welfare. Visualizing the data: information on COVID-19 infections [in Japanese]

[cited 2022 Jul 26]. https://covid19.mhlw.go.jp/extensions/public/index.html
24. National Institute of Population and Social Security Research (IPSS). Data on COVID-19 [cited 2022 Aug 31]. www.ipss.go.jp/projects/j/Choju/covid19/index-en.asp
25. Ministry of Health, Labour and Welfare. Abridged life tables for Japan 2020 [cited 2022 Aug 25]. https://www.mhlw.go.jp/english/database/db-hw/lifetb20/dl/lifetb20-06.pdf
26. Wouterse B, Ram F, van Baal P. Quality-adjusted life-years lost due to COVID-19 mortality: methods and application for The Netherlands. Value Health. 2022;25:731–5. https://doi.org/10.1016/j.jval.2021.12.008
27. Neilan AM, Losina E, Bangs AC, Flanagan C, Panella C, Eskibozkurt GE, et al. Clinical impact, costs, and cost-effectiveness of expanded severe acute respiratory syndrome coronavirus 2 testing in Massachusetts. Clin Infect Dis. 2021;73:e2908–17. https://doi.org/10.1093/cid/ciaa1418
28. Lai CC, Wang YH, Chen KH, Chen CH, Wang CY. The clinical efficacy and safety of anti-viral agents for non-hospitalized patients with COVID-19: a systematic review and network meta-analysis of randomized controlled trials. Viruses. 2022;14:1706. https://doi.org/10.3390/v14081706
29. e-Stat. Survey of institutions and establishments for long-term care—result detail for FY 2019 [in Japanese] [cited 2022 Jun 16]. https://www.e-stat.go.jp/stat-search/files?&stat_infid=000032069585
30. Johansson MA, Quandelacy TM, Kada S, Prasad PV, Steele M, Brooks JT, et al. SARS-CoV-2 transmission from people without COVID-19 symptoms. JAMA Netw Open. 2021;4:e2035057. https://doi.org/10.1001/jamanetworkopen.2020.35057
31. Centers for Disease Control and Prevention. Ending isolation and precautions for people with COVID-19: interim guidance [cited 2022 Aug 7]. https://www.cdc.gov/coronavirus/2019-ncov/hcp/duration-isolation.html
32. Financial Markets Department, Bank of Japan. Foreign exchange rates [cited 2022 Aug 22]. https://www.boj.or.jp/en/statistics/market/forex/fxdaily/fxlist/fx220822.pdf
33. Office for COVID-19 and Other Emerging Infectious Disease Control, Cabinet Secretariat, Government of Japan. Policies for COVID-19 emerging infectious disease control [in Japanese] [cited 2023 Feb 24]. https://corona.go.jp/surveillance
34. Honda R, Murakami M, Hata A, Ihara M. Public health benefits and ethical aspects in the collection and open sharing of wastewater-based epidemic data on COVID-19. Data Sci J. 2021;20:27. https://doi.org/10.5334/dsj-2021-027
35. Gable L, Ram N, Ram JL. Legal and ethical implications of wastewater monitoring of SARS-CoV-2 for COVID-19 surveillance. J Law Biosci. 2020;7:lsaa039. https://doi.org/10.1093/jlb/lsaa039
36. Ram N, Shuster W, Gable L, Ram JL. Ethical and legal wastewater surveillance. Science. 2023;379:652. https://doi.org/10.1126/science.adg7147

Address for correspondence: Byung-Kwang Yoo, Faculty of Human Sciences, School of Human Sciences, Waseda University, 2-579-15 Mikajima, Tokorozawa City, Saitama 359-1192, Japan; email: yoobk3@gmail.com

etymologia revisited

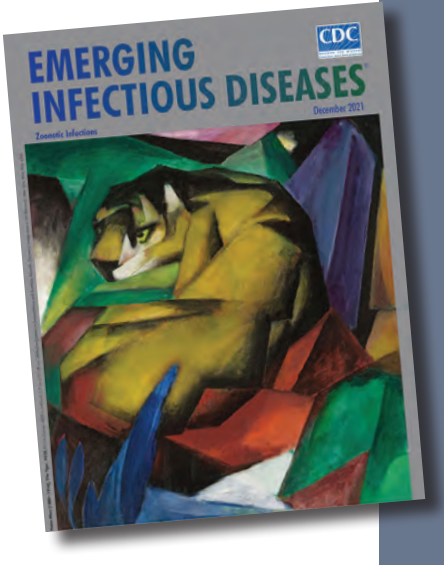

Originally published in December 2021

Trichinella spiralis

[tri kuh neh′ luh spr a′ luhs]

Trichinella is derived from the Greek words *trichos* (hair) and *ella* (diminutive); *spiralis* means spiral. In 1835, Richard Owen (1804–1892) and James Paget (1814–1899) described a spiral worm (*Trichina spiralis*)–lined sandy diaphragm of a cadaver. In 1895, Alcide Raillet (1852–1930) renamed it as *Trichinella spiralis* because *Trichina* was attributed to an insect in 1830. In 1859, Rudolf Virchow (1821–1902) described the life cycle. The genus includes many distinct species, several genotypes, and encapsulated and nonencapsulated clades based on the presence/absence of a collagen capsule.

References

1. Campbell WC. History of trichinosis: Paget, Owens and the discovery of *Trichinella spiralis*. Bull Hist Med. 1979;53:520–52.
2. Centers for Disease Control and Prevention. Trichinellosis: general information [cited 2021 May 11]. https://www.cdc.gov/parasites/trichinellosis/ gen_info/faqs.html
3. Gottstein B, Pozio E, Nöckler K. Epidemiology, diagnosis, treatment, and control of trichinellosis. Clin Microbiol Rev. 2009;22:127–45. https://doi.org/10.1128/CMR.00026-08
4. Observations on *Trichina spiralis*. Boston Med Surg J. 1860; 63:294–8. https://doi.org/10.1056/NEJM186011080631504
5. Zarlenga D, Thompson P, Pozio E. *Trichinella* species and genotypes. Res Vet Sci. 2020;133:289–96. https://doi.org/10.1016/j.rvsc.2020.08.012

https//wwwnc.cdc.gov/eid/article/27/12/et-2712_article

Genome-Based Epidemiologic Analysis of VIM/IMP Carbapenemase-Producing *Enterobacter* spp., Poland

Radosław Izdebski, Marta Biedrzycka, Paweł Urbanowicz, Dorota Żabicka, Marek Gniadkowski

We sequenced all nonduplicate 934 VIM/IMP carbapenemase-producing Enterobacterales (CPE) reported in Poland during 2006–2019 and found ≈40% of the isolates (n = 375) were *Enterobacter* spp. During the study period, incidence of those bacteria gradually grew in nearly the entire country. The major factor affecting the increase was clonal spread of several *E. hormaechei* lineages responsible for multiregional and interregional outbreaks (≈64% of all isolates), representing mainly the pandemic sequence type (ST) 90 or the internationally rare ST89 and ST121 clones. Three main VIM-encoding integron types efficiently disseminated across the clone variants (subclones) with various molecular platforms. Those variants were predominantly *Pseudomonas aeruginosa*–derived In238-like elements, present with IncHI2+HI2A, IncFII+FIA, IncFIB, or IncN3 plasmids, or chromosomal genomic islands in 30 *Enterobacter* STs. Another prevalent type, found in 34 STs, were In916-like elements, spreading in Europe recently with a lineage of IncA-like plasmids.

In the past few decades, bacterial infections with limited therapeutic options have become a serious threat for medicine. This problem is primarily caused by antimicrobial resistance (AMR), which disseminates by clonal spread of resistant organisms and horizontal transmission of mobile genetic elements with AMR genes. Several taxa have been classified as main AMR pathogens, including *Klebsiella pneumoniae* and *Enterobacter* spp. of the order Enterobacterales (*1*), and carbapenemase-producing Enterobacterales (CPE) are among the most challenging multidrug-resistant organisms (*2*). Important carbapenemase types, metallo-β-lactamases (MBLs) of the families VIM and IMP, have been recorded in enterobacteria in Europe since 2001 (*3*), often in the Mediterranean region (*4*–*10*). The $bla_{VIM/IMP}$ gene cassettes have usually been located in class 1 integrons, either assembled in *Pseudomonas* spp. and then transferred to Enterobacterales (*4*–*6*) or typical for Enterobacterales (*4*,*7*–*10*). The integrons have been carried by diverse plasmids with various replicons (*4*,*7*,*8*,*10*,*11*).

In Poland, VIM-type enzymes were originally identified in 2006 in *K. pneumoniae,* followed soon by *Enterobacter hormaechei* (*12*). Molecular analysis of all 121 VIM/IMP CPE isolates from 2006–2012 revealed high prevalence of *Enterobacter* spp. (≈53%) and relatively low contribution of *K. pneumoniae* (≈9%). *Enterobacter* spp. was dominated by *E. hormaechei* sequence type (ST) 90 and ST89, mostly with In238-like integrons of *Pseudomonas aeruginosa* origin. We describe the genomic analysis of all VIM/IMP *Enterobacter* spp. isolates in Poland during 2006–2019, in the context of all VIM/IMP CPE from that period, and international *Enterobacter* spp. genomes from public databases.

Methods

Study Design, Bacterial Isolates, Whole-Genome Sequencing, and Species Identification

The National Reference Centre for Susceptibility Testing conducts CPE surveillance in Poland, collecting isolates with basic patient, hospital ward, and isolate data. We tested the isolates by using CarbaNP (*13*) and phenotypic tests (*14*), and used PCRs for bla_{NDM}-, bla_{VIM}-, bla_{IMP}-, bla_{KPC}-, and bla_{OXA-48}-like genes (*4*). A collection of 934 isolates from 246 hospitals in 117 cities were all nonduplicate VIM/IMP CPE confirmed during 2006–2019. We sequenced all those isolates by using MiSeq (Illumina, https://www.illumina.com), with de novo assemblies as described (*15*), and subjected them to species identification on the basis of average nucleotide identities by using FastANI 1.32 with a ≥95%

Author affiliations: National Medicines Institute, Warsaw, Poland

DOI: https://doi.org/10.3201/eid2908.230199

cutoff (*16*). We further analyzed the largest group of 375 isolates of the genus *Enterobacter* from 145 hospitals in 76 towns. We also sequenced 9 selected isolates by using MinION (Oxford Nanopore Technologies, https://nanoporetech.com) (*15*). We performed hybrid assemblies by using Unicycler 0.4.8 (*17*).

Molecular Typing and Comparative Genomic Analysis

We performed multilocus sequence typing (MLST) of all 375 *Enterobacter* spp. isolates (*18*) in silico by using mlst (https://github.com/tseemann/mlst). We performed the in-sample clonality single-nucleotide polymorphism (SNP) analysis for individual sequence types (STs) by using BioNumerics 7.6.3 (Applied Maths, https://www.applied-maths.com) and using index (i.e., initial) isolates of the STs as references. For the SNP-based phylogenetic analysis in the international context, we downloaded all (nonfiltered) 3,244 *Enterobacter* spp. genomes available in RefSeq (https://www.ncbi.nlm.nih.gov/refseq) as of June 6, 2022, and subjected them to MLST. We included isolates of the major STs (Appendix Table 1, https://wwwnc.cdc.gov/EID/article/29/8/23-0199-App1.pdf) in our analysis, which we performed by using Parsnp 1.5.4 (https://github.com/marbl/parsnp). We visualized the Parsnp-generated phylotrees by using iTOL (https://itol.embl.de).

Acquired AMR Genes, Integrons, and Plasmids or Genomic Islands Carrying $bla_{VIM/IMP}$ Genes

We detected acquired AMR genes by using ABRicate and the ResFinder database with 99.5% identity criterion (*19*) and profiled replicon types with PlasmidFinder 2.1 (*20*). We performed structural analysis and annotation of MBL-encoding integrons, plasmids, and genomic islands manually in Geneious Prime 2022.0.1 (Biomatters, https://www.geneious.com) by using BLASTn (https://blast.ncbi.nlm.nih.gov/Blast.cgi). We visualized plasmid and island structures by using BRIG (http://brig.sourceforge.net) and Easyfig 2.2.5. (http://mjsull.github.io/Easyfig).

Nucleotide Sequence Accession Numbers

We submitted genomic data for the *Enterobacter* spp. isolates to the US National Center for Biotechnology Information (BioProject no. PRJNA877430). Plasmid sequences are available under the following GenBank accession numbers: p743A, OQ111274; p5955A, OQ111275; p7753A, OQ111276; p4969H, OQ111277; p5435N, OQ111278; p5713F, OQ111279; p6234F, OQ111280. Sequences of genomic islands are available under the following GenBank accession numbers: *Eh*GI3, OQ116783; *Eh*GI4, OQ116782,.

Results

Taxonomic Distribution of VIM/IMP-Type CPE in Poland

We collected 934 VIM/IMP CPE during 2006–2019 from 246 hospitals in 117 cities of all 16 regions of Poland (Appendix Figure 1, panel A). In annual numbers of cases, a gradual increase occurred, from a few cases during 2006–2008 up to 242 in 2019 (Appendix Table 2). We identified 9 genera, including *Enterobacter* (40.1%), *Klebsiella* (*K. pneumoniae* and *K. oxytoca* groups, 34.4%), *Citrobacter* (10.7%), *Escherichia* (9.2%), and *Serratia* (4.2%). The distribution of genera varied in time, including predominance of *Enterobacter* spp. and remarkable contribution of *K. oxytoca* during 2006–2013 (*12*) and still high prevalence of *Enterobacter* spp. but also a dynamic *K. pneumoniae* increase during 2014–2019 (Appendix Figure 1, panel B). Of note, annual numbers of *Enterobacter* spp. isolates grew at a roughly constant rate by the end of 2018, then escalating in 2019. VIM-type MBLs prevailed vastly (99.3%), whereas IMPs contributed marginally (0.7%). The 375 *Enterobacter* spp. isolates originated from 145 hospitals out of 76 towns and were recovered during various infections (64.3%), mainly of the urinary tract (31.5% of the infections) and wounds (28.6%), or from carriage (34.9%).

Species and Clonality of *Enterobacter* spp.

We identified 6 species among the 375 *Enterobacter* isolates, largely *E. hormaechei* (362 [96.5%]) with 5 subspecies: *steigerwaltii* (n = 244), *xiangfangensis* (n = 71), *hoffmannii* (n = 35), *oharae* (n = 11) and *hormaechei* (n = 1) (Appendix Table 2). The remaining species were *E. roggenkampii* (8 [2.2%]), *E. asburiae* (2 [0.5%]), and *E. kobei*, *E. ludwigii*, and *E. mori* (1 [0.3%] each). We distinguished 56 STs (Table, https://wwwnc.cdc.gov/EID/article/29/8/23-0199-T1.htm; Figure 1); 5 STs had >10 isolates each (258 [68.8%]): ST90 (117 [31.2%] of all *Enterobacter* spp.), ST89 (74 [19.7%]), ST121 (36 [9.6%]), ST66 (18 [4.8%]), and ST134 (13 [3.5%]). Isolates of closely related STs (single-locus variants) represented clonal groups (CGs) or clonal complexes (CCs) (Table; Figure 1).

bla_{VIM} and bla_{IMP} Genes and Their Integrons in *Enterobacter* spp.

We found 5 bla_{VIM} genes, primarily of the bla_{VIM-1} group (91.5% of all MBLs in *Enterobacter* spp.); most were bla_{VIM-4} (49.1%), bla_{VIM-1} (40.6%), and bla_{VIM-40} (1.9%) (Table). The bla_{VIM-2} group included bla_{VIM-2} (4.0%) and bla_{VIM-20} (3.4%), whereas all bla_{IMP}s were bla_{IMP-19} (1.1%).

We characterized 16 integrons, including 4 new ones (Appendix Table 3). Elements of the In238 type

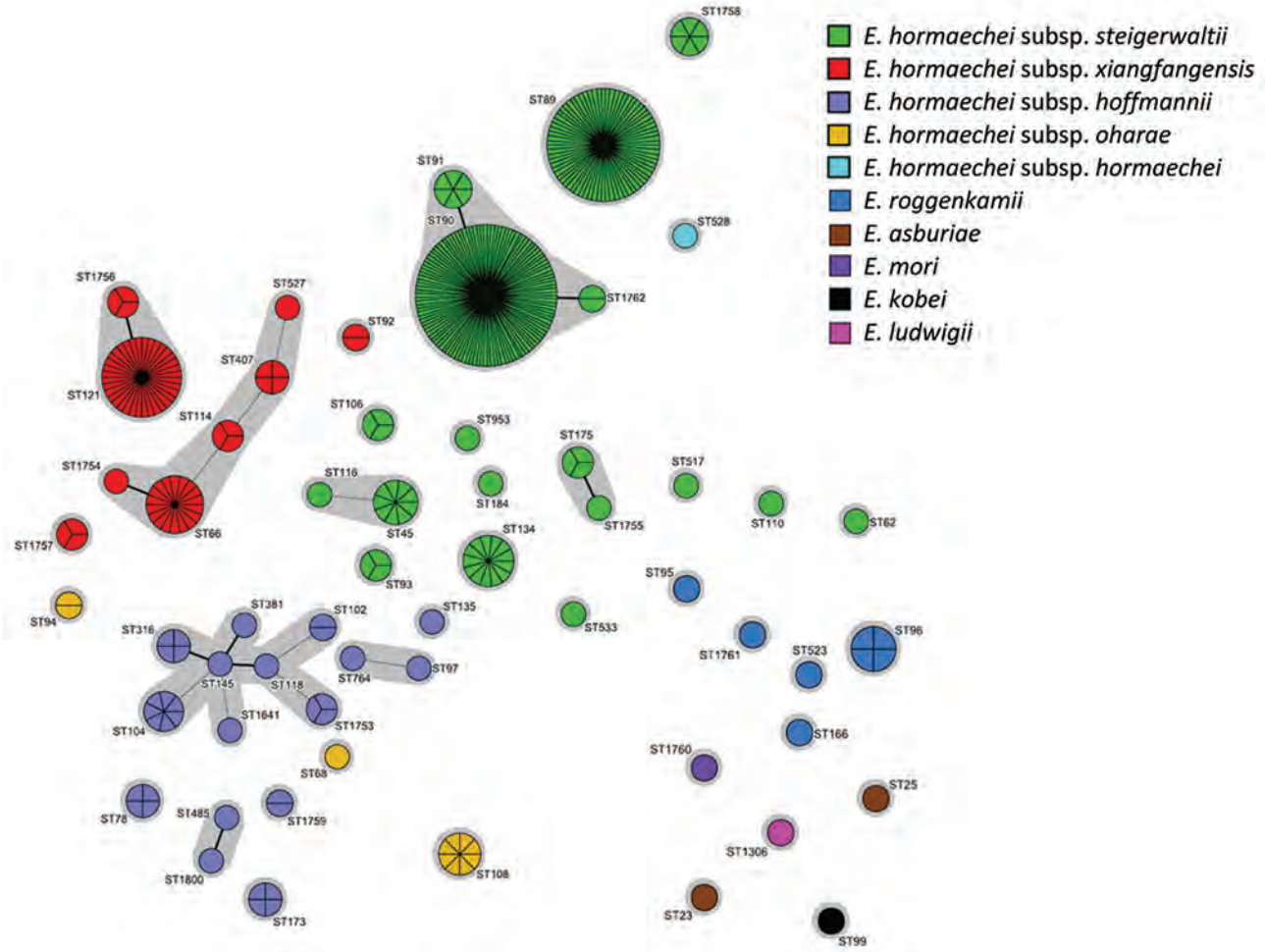

Figure 1. Population structure of *Enterobacter* spp. isolates identified in a genome-based epidemiologic analysis of VIM/IMP carbapenemase-producing *Enterobacter* spp., Poland, 2006–2019. The minimum-spanning tree was constructed on the basis of 7-loci multilocus sequence type data. Each circle represents 1 ST, and each fragment of a pie chart corresponds to 1 isolate. The size of a circle is proportional to the number of isolates of that ST. Connecting lines infer phylogenetic relatedness in terms of several allelic differences (thick solid line indicates a single-locus variant, thin solid line indicates a double-locus variant). ST, sequence type.

prevailed (190 [50.4%]; 30 STs), carrying $bla_{\text{VIM-4}}$ (In238/In238a), $bla_{\text{VIM-40}}$ (In1445), or $bla_{\text{VIM-1}}$ (In237a) genes. The second most prevalent In916 type (146 [38.7%]; 34 STs) had $bla_{\text{VIM-1}}$. The $bla_{\text{VIM-2}}$-like genes were located mostly in In1008-type integrons (26 [6.9%]; 5 STs), as $bla_{\text{VIM-2}}$ (In1008) or $bla_{\text{VIM-20}}$ (In1444). $bla_{\text{IMP-19}}$ was in a new element In2241. We noticed temporal changes in the integron distribution; the incidence of In238s grew from 2009 (n = 6) to 2014 (n = 24) and then stabilized, whereas that of In916 rapidly increased from the original identification in 2014 (n = 9) to 2019 (n = 57).

Epidemiology of Major *E. hormaechei* Clones and Multiregional and Interregional Outbreaks

The most widespread clone was *E. hormaechei* subsp. *steigerwaltii* ST90 (117 [31.2%]), recorded during 2009–2019 in 58 hospitals in 38 cities, mostly in southern regions (Figure 2; Appendix Table 4). Most of the 111 isolates with In238/In238a differed by 19–207 SNPs from the reference isolate (mean 71 SNPs) and formed a subclone (0–172 SNPs between closest relatives), likely resulting from multiregional expansion (outbreak I). We also classified 2 In238-carrying isolates of ST1762 (CC90) into this cluster (127–132 SNPs).

We observed *E. hormaechei* subsp. *steigerwaltii* ST89 (74 [19.7% of all isolates]) during 2006–2019 in 26 centers in 18 towns (Appendix Table 5, Figure 2). Most of the isolates (n = 67 [90.5% of ST89 isolates]) comprised 3 regional subclones with different integrons, representing outbreak II in Łódzkie (48 [0–75 SNPs between closest relatives]; In916), outbreak III in Wielkopolskie (12 [0–49 SNPs]; In1444), and outbreak IV in Kujawsko–Pomorskie (7 [4–12 SNPs]; In1445).

We identified *E. hormaechei* subsp. *xiangfangensis* CC121 isolates (ST121, 36 [9.6%]; ST1756, 3 [0.8%]) during 2014–2019 in 22 hospitals in 12 cities, mainly in the Mazowieckie and Łódzkie regions (Appendix Table 6, Figure 3). All those isolates were related to each other, with up to 84 SNPs with the reference (mean 46 SNPs); however, 2 outbreaks were distinguished based on the integron data: an interregional outbreak V (27 [0–46 SNPs between closest relatives]; In916) and a regional outbreak VI (6 [1–9 SNPs]; In238a).

Of the clones of lower incidence, ST66 and ST1754 (CG66; n = 19) were split into 2 genetically and geographically separated subclones (0–17 and 0–23 SNPs within the groups [404 SNPs between them]; both with In916), likely representing an interregional outbreak VII and a regional outbreak VIII (Appendix Table 7, Figure 4). ST134 (n = 13) showed variety as well, with a cluster of related organisms (9 [6–24 SNPs]; In238) arising from an apparent regional outbreak IX (Appendix Table 8, Figure 5).

Phylogeny and International Context of Major *E. hormaechei* Clones

The clonal analysis of all 3,244 *Enterobacter* spp. genomes in RefSeq (as of June 6, 2022) revealed 546 STs; 61 STs were represented by >10 records. Out of the major VIM-positive clones in Poland, only ST90 and ST66 were among the 10 most numerous STs. Otherwise, the prevalent RefSeq clones were either not present (e.g., ST171 and ST133) or marginal (e.g., ST78 and ST114). However, the RefSeq genomes were unfiltered, which could have affected some of the observations. The phylogenetic analysis of 46 international ST90 genomes revealed 2 main clades and most of the 117 isolates in Poland, including outbreak I, belonged to a branch with several carbapenemase-free isolates from the

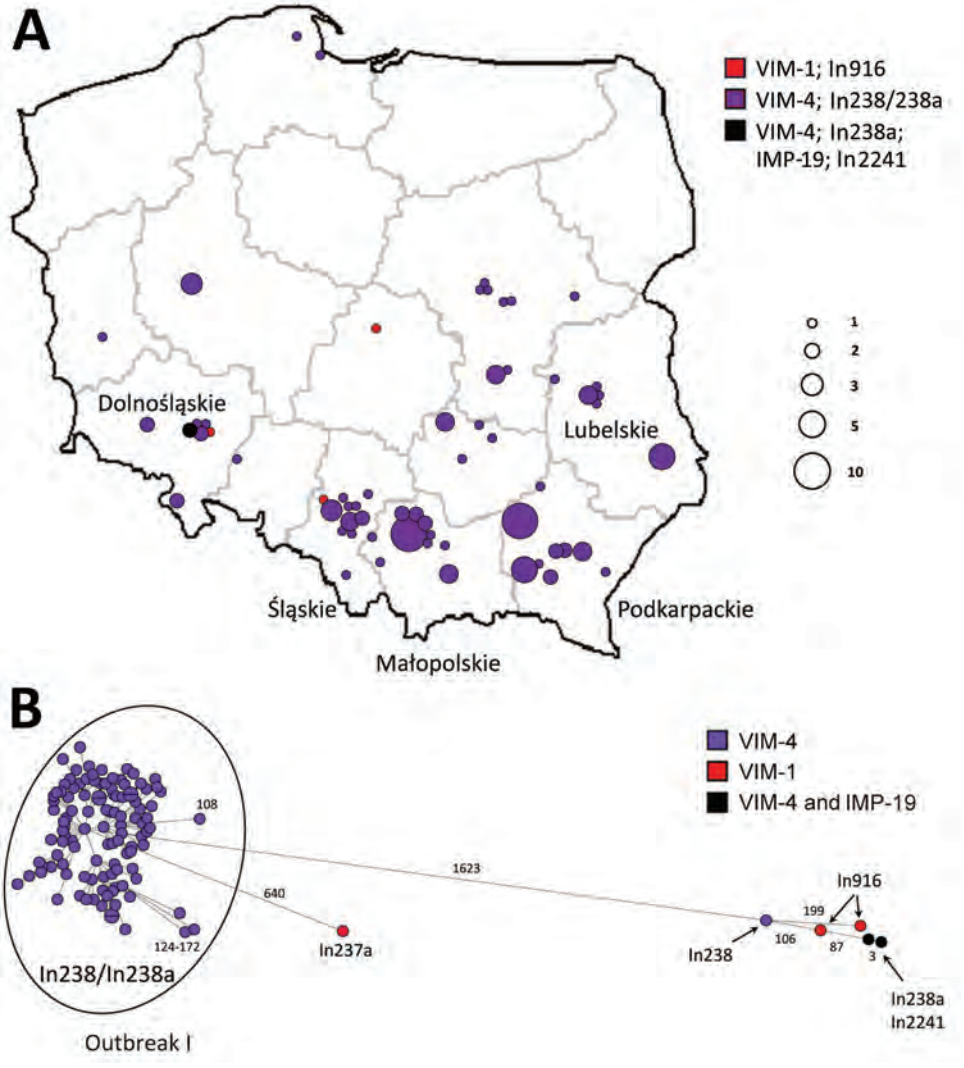

Figure 2. Geographic distribution and clonal analysis of *Enterobacter hormaechei* clonal complex 90 (ST90 and ST1762) in Poland, 2006–2019. A) Geographic distribution of the isolates; main administrative regions are labeled. Circles represent medical centers where the isolates were recorded. Sizes of the circles are proportional to numbers of cases of infection. B) SNP-based minimum-spanning tree of the isolates. Lengths of branches are related to numbers of SNPs between linked isolates. Numbers of SNPs are indicated above the branches or next to the dots. SNP, single nucleotide polymorphism; ST, sequence type.

United Kingdom, France, Portugal, and Brazil (Appendix Figure 6).

ST89 was represented in RefSeq only by 2 isolates in Germany (1 with GIM-1) and 24 NDM-1–positive isolates in Poland during 2017–2020, which we analyzed in a previous study (*21*). Therefore, the phylotree comprised 100 isolates, including 98 from Poland (Appendix Figure 7), and consisted of 2 major lineages, each split then into multiple branches, correlating with the regional distribution of the isolates, regardless of their MBL content. The first lineage contained all of the VIM outbreak II isolates in Łódzkie plus a cluster of related NDM isolates from a neighboring area. The second lineage was divided into 2 major branches, 1 of which comprised the VIM outbreak IV in Kujawsko–Pomorskie and a large NDM epidemic from the adjacent region of Mazowieckie. The other branch contained mainly isolates from western Poland, including the VIM outbreak III from Wielkopolskie. Consistently, the 2 isolates in Germany were also located on the latter branch.

Only 7 ST121 genomes were present in RefSeq; the 36 VIM isolates in Poland, including outbreaks V–VI, formed 1 of 2 main lineages together with isolates from Brazil, Uganda, Morocco, Germany, and Poland (NDM) (*21*) (Appendix Figure 8). A total of 51 international ST66 isolates formed 2 lineages; 8 isolates in Poland of the outbreak VII belonged, primarily, to the lineage with isolates from Spain, France, and Germany mainly, whereas 10 outbreak VIII isolates clustered within the second lineage of more global character (Appendix Figure 9). ST134 records were sporadic in RefSeq (n = 9), and the 13 isolates in Poland, including outbreak IX, were located within 1 lineage together with single isolates from the United States, Lebanon, and Iran (Appendix Figure 10).

Resistomes

The resistome analysis demonstrated a large number and a variety of acquired AMR genes (6–27 genes per isolate; mean 15.8) (Appendix Table 9), in addition to the natural *Enterobacter* spp. *ampC* cephalosporinase genes. Their exact numbers could be specified only for the 9 MinION-sequenced genomes because some genes were in multiple copies in individual isolates (Appendix Table 10). The diversity of resistomes (AMR gene types and numbers) was common across and within the epidemic subclones; for some of those, the only stable AMR genes (i.e., present in all isolates of a subclone) were those in the MBL integrons. For instance, the ST90 isolates of the outbreak I had 67 AMR gene profiles, and ST89 isolates of the outbreak II had 33 AMR gene profiles. Along with $bla_{VIM/IMP}$s, most of the isolates had genes coding for extended-spectrum β-lactamases (bla_{SHV} and bla_{CTX-M} types, bla_{GES-7}, and bla_{PER-2}) or acquired AmpC-like cephalosporinases (bla_{CMY-83}, bla_{DHA-1}, and bla_{FOX-20}). Along with various aminoglycoside-modifying enzyme genes, numerous isolates had the 16S rRNA methylase gene *armA*, inactivating all aminoglycosides. Different variants of fluoroquinolone-resistance genes *qnrA/B/E/S* were commonly represented; 65 isolates contained the *mcr-9.1* colistin-resistance gene.

Plasmids Harboring bla_{VIM} Genes

We identified 44 plasmid replicon types with 1–8 replicons per organism. The most frequent replicons were IncHI2 (n = 237), IncHI2A (n = 232), IncA (n = 165), IncFII (n = 140), and IncFIA (n = 116). Replicon profiles remarkably varied both between and within the subclones (Appendix Table 11). Long-read sequencing revealed the plasmid content, and the replicon and AMR gene distribution between the plasmids in 7 isolates representing the main epidemic subclones: ST90–In238 (n = 2; outbreak I), ST89–In916 (outbreak II), ST121–In916 (outbreak V), ST121–In238a (outbreak VI), ST66–In916 (outbreak VII), and ST134–In238 (outbreak IX) (Appendix Table 10). We performed the structural analysis on the plasmids with bla_{VIM}-harboring integrons.

In the 4 isolates with In238/In238a, including the 2 ST90–In238 representatives, the integrons were on 4 different plasmids. In 1 of those (isolate 4969–09), In238 was on an IncHI2+HI2A plasmid (p4969H; ≈261 kb), related to numerous others from *Enterobacterales* worldwide (91%–95% coverage; ≈100% identity), occasionally with $bla_{IMP/VIM}$ genes (Appendix Figure 11). One such plasmid from the Czech Republic, p51929_MCR_VIM (93% coverage; ≈100% identity), also contained In238 (*22*). The second ST90–In238 isolate (6234–09) had that integron on a plasmid with unique FII and FIA replicons (p6234F; ≈91 kb); FII was of some similarity to pECL_A (≈83%) (*23*) and FIA to R27 (≈84%) (*24*). The IncFII+FIA scaffold matched 9 GenBank records well (>60% coverage, >98% identity) (Appendix Figure 12). Of note, in p4969H and p6234F, the In238 integron was located in novel, almost identical Tn*21*-like transposons Tn*7536*, similar to Tn*1696* (*25*) (Appendix Figure 13).

The ST121–In238a isolate (5713–17) had In238a on an IncFIB-like plasmid (p5713F; ≈120 kb), with the replicon similar to pB171 (≈91%) (*26*), homologous to 8 bla_{VIM}-negative records (80%–90% coverage; ≈100% identity) (Appendix Figure 14). Last, in the ST134–In238 isolate (5435–13) the integron resided on an IncN3-like plasmid (p5435N; ≈46 kb), matching several records (89% coverage; ≈100% identity), including

some with $bla_{IMP/VIM}$ genes (Appendix Figure 15). The In238-type integrons in p5713F and p5435N were not located in Tn*21*-like transposons.

In the 3 isolates with In916: ST89 (7753–18), ST121 (743–14) and ST66 (5955–16), the integron resided on IncA plasmids (p7753A, ≈162 kb; p743A, ≈170 kb; and p5955A, ≈154 kb). Those isolates were highly related to each other and to 9 In916-carrying IncA plasmids (84%–96% coverage, ≈100% identity), including 5 from Italy (different *Enterobacterales*) (*7*) and 1 from Poland (*K. pneumoniae*) (*27*) (Appendix Figure 16). The plasmids varied mostly by rearrangements within the AMR region containing an IS*26*–bla_{SHV-12}–In916–IS*26* module (≈37.8-≈51.8 kb). This region in p743A was almost identical to plasmids pGB_VIM and pGA_VIM from Italy (*7*) (Appendix Figure 17).

Genomic Islands with bla_{VIM} Genes

An isolate representing the epidemic subclone ST89–In1445 (8770–11; outbreak IV) had a new genomic island *Eh*GI3 with the bla_{VIM-40} gene, and the isolate of the clone ST89–In1444 (2944–06; outbreak III) had another new genomic island with bla_{VIM-20}. *Eh*GI3 (≈94.6 kb), inserted into the $tRNA^{Gly}$ gene, was a *clc*-like integrative and conjugative element (ICE) (41% coverage and ≈87% identity with the *clc* reference [*28*]), similar to ICEs found mainly in pseudomonads (*29*) (Appendix Figure 18). *Eh*GI4 (≈71.1 kb) was a mosaic region flanked by 2 IS*26* copies with direct repeats, carrying In1444 and multiple AMR genes (e.g., *armA*).

Discussion

We describe VIM/IMP CPE in Poland, which markedly increased in recent years after a period of rather low prevalence. During 2017–2019, the annual VIM/IMP CPE numbers recorded by the National Reference Centre for Susceptibility Testing (n = 545) were comparable with KPC (n = 686) or OXA-48 (n = 383) producers but far behind NDM organisms (n>6,000 [https://www.korld.nil.gov.pl]) (*12*,*14*,*15*,*21*,*30*). Among all carbapenemase-producing *Enterobacter* spp., the organisms with VIM/IMP-like enzymes were the predominant group (59.4%). The leading position of *Enterobacter* spp. among VIM/IMP CPE was maintained for all years of the study; however, the dynamic spread of *K. pneumoniae* in more recent years has notably changed the species composition. A substantial role of *Enterobacter* spp. among VIM CPE has been observed also in other countries of Europe (*8*,*11*).

The successful dissemination of VIM-producing *Enterobacter* spp. in Poland has depended largely on several epidemic subclones of *E. hormaechei* ST90, ST89, and ST121 lineages, responsible for multiregional and interregional outbreaks I–VI (≈63% of all isolates). ST90 is a global clone, often reported with various carbapenemases (*11*). Its population in Poland has been dominated by the ST90–In238/In238a subclone, and since 2009 it has been expanding over a large territory (outbreak I). On the contrary, ST89 seems to be a local lineage, having been reported mostly in Poland with various VIMs, OXA-48, or NDM-1 so far. However, its repeated identification with GIM-1 in Germany indicates broader spread in central Europe (*21*,*31*,*32*).

The ST89 VIM-producing isolates in Poland were clustered into 3 regional subclones, ST89–In916, ST89–In1444, and ST89–In1445 (outbreaks II–IV), closely related to the previously described ST89 NDM-1 subclones from the same or neighboring areas (*21*). This finding indicates that ST89 has produced a series of regional sublineages, acquiring and then disseminating with different AMR genes. The epidemiology of ST121 has been unclear. According to RefSeq, it appears to be nonprevalent, although present broadly in the world. In Poland, it has spread extensively, acquiring several VIM integrons and causing major regional outbreaks (V-VI).

The second essential factor of the VIM-producing *Enterobacter* spp. expansion in Poland has been the horizontal transmission of 3 major VIM integron types. The In238 type with bla_{VIM-1}-like genes and In1008 type with bla_{VIM-2}-like genes formed 2 evolving families of elements, with individual variants differing by mutations in bla_{VIM} cassettes, and by 3′-termini of these in the case of In238 (specific 169bp repeats in some variants) (*12*,*33*). Both types were found originally in *P. aeruginosa* in Poland in 1998 (In238) (*33*) and 2001 (In1008) (*34*) and most likely were transmitted to Enterobacterales during 2006–2009 (*12*). However, In238 variants have been observed more broadly in central and southern Europe (*22*,*35*–*37*). The third major integron type, Enterobacterales-specific In916, has been recorded since the early 2010s in Spain, Italy, and France (*4*,*8*,*11*,*38*), and in Poland it has spread since at least 2013 (R. Izdebski and M. Gniadkowski, unpub. data). All those integron types have been acquired by *E. hormaechei* at the beginning of their dissemination in Enterobacterales in Poland with various molecular platforms.

In our previous study, the 2006–2012 predominant In238-type integrons in *E. hormaechei* ST89 and ST90 were assigned to IncHI2, PCR-nontypeable (largely), or IncM plasmids (*12*). We long-read sequenced 2 ST90–In238 isolates, representing outbreak I, in this study and found them to have In238

on the IncHI2+HI2A or IncFII+FIA (previously nontypeable) plasmids, suggesting exchange between them. Given that the integron was located within almost identical Tn*21*-like transposons (Tn*7536*) in both plasmids, those might have been responsible for the inter-plasmid transfer. However, the 2 remaining long-read sequenced ST121 and ST134 isolates with In238/In238a had these integrons on yet other plasmids, IncFIB (ST121) and IncN3 (ST134), and not in a transposonic context. This finding indicates that acquisition and circulation of the In238-like elements among 36 STs of *Enterobacter* spp. in Poland have been multifactorial and complex phenomena. Regarding acquisition, an interesting case was provided by the ST89 isolate with the In238-like integron In1445, located within the *clc*-type ICE *Eh*GI3. In238 variants have been frequent in VIM-producing *P. aeruginosa* (*39*) and *P. putida* in Poland (*40*), being usually chromosomal in those. *Eh*GI3 turned out to be almost identical to an ICE in 1 of the *P. putida* group isolates, indicating exchange of such elements between pseudomonads and Enterobacterales (P. Urbanowicz, M. Gniadkowski, unpub. data).

On the other hand, the proliferation of In916 seems to be relatively clear. In Europe, this integron has been associated with IncA, IncFII$_K$, IncHI2, IncN, or PCR-nontypeable plasmids (*4*,*7*,*8*), and in our study isolates, it has entirely correlated with the IncA plasmids. A close relatedness between the In916-carrying IncA plasmids in Poland and Italy was proved, which together with high conjugative potential (*7*) have explained their spread on a large geographic scale. As in Italy (*7*) and France (*8*), rapid dissemination of these plasmids in Poland since 2013–2014 has contributed to the increase in VIM-producing Enterobacterales and *Enterobacter* spp., making In916 the most prevalent integron in 2019 (≈63%). The In916-carrying IncA plasmids occurred in 30 *Enterobacter* STs, including ST89, CC121 and CG66 subclones of 4 regional outbreaks, revealing that both the horizontal and clonal spread contributed to their recent proliferation.

Our study has shown the epidemiology of VIM-producing *Enterobacter* spp. during 14 years of VIM CPE surveillance in Poland, substantially updating the previous report (*12*). The results enable the precise definition of several *E. hormaechei* subclones of a remarkable epidemic potential, responsible for a series of territorial outbreaks, and enable the characterization of the main molecular platforms transmitting integrons with *bla*$_{VIM}$ genes in *Enterobacter* populations. The study revealed several factors specific for Poland or central Europe, namely the prominent role of apparently rare *E. hormaechei* clones (ST89 or ST121), peculiar integrons of pseudomonadal origins (In238 and In1008 types), and unique VIM-encoding plasmids (IncFII+FIA with In238). We have also demonstrated some cosmopolitan elements, such as the global status of the epidemic ST90 clone and pan-Europe dissemination of In916-carrying IncA-like plasmids. All these observations indicate that AMR VIM-producing *E. hormaechei* and the VIM-encoding plasmids create an epidemiologic danger for hospital environments throughout Europe that clinicians and infection control specialists should be aware of.

Acknowledgments

We are very thankful to all colleagues of the National Reference Centre for Susceptibility Testing for their excellent work within the CPE surveillance program. We also cordially thank all microbiologists from clinical diagnostic laboratories who contributed to the study collection of bacterial isolates, and Mikołaj "Nick" Mogilnicki and Anatole Conrad Tompkins for checking style and expression of the manuscript.

This work was supported by the Polish National Science Centre (grant no. 2019/33/B/NZ7/01461).

About the Author

Dr. Izdebski is an associate professor at the National Medicines Institute, Warsaw, Poland. His research interests focus on population genetics of Enterobacterales, *Pseudomonas*, and *Acinetobacter*.

References

1. Boucher HW, Talbot GH, Bradley JS, Edwards JE, Gilbert D, Rice LB, et al. Bad bugs, no drugs: no ESKAPE! An update from the Infectious Diseases Society of America. Clin Infect Dis. 2009;48:1–12. https://doi.org/10.1086/595011
2. Centers for Disease Control and Prevention. Antibiotic resistance threats in the United States, 2019 [cited 2023 Apr 24]. https://www.cdc.gov/drugresistance/pdf/threats-report/2019-ar-threats-report-508.pdf
3. Cantón R, Akóva M, Carmeli Y, Giske CG, Glupczynski Y, Gniadkowski M, et al.; European Network on Carbapenemases. Rapid evolution and spread of carbapenemases among *Enterobacteriaceae* in Europe. Clin Microbiol Infect. 2012; 18:413–31. https://doi.org/10.1111/j.1469-0691.2012.03821.x
4. Papagiannitsis CC, Izdebski R, Baraniak A, Fiett J, Herda M, Hrabák J, et al.; MOSAR WP2, WP3 and WP5 study groups. Survey of metallo-β-lactamase-producing *Enterobacteriaceae* colonizing patients in European ICUs and rehabilitation units, 2008–11. J Antimicrob Chemother. 2015;70:1981–8. https://doi.org/10.1093/jac/dkv055
5. Lombardi G, Luzzaro F, Docquier JD, Riccio ML, Perilli M, Colì A, et al. Nosocomial infections caused by multidrug-resistant isolates of *Pseudomonas putida* producing VIM-1 metallo-β-lactamase. J Clin Microbiol. 2002;40:4051–5. https://doi.org/10.1128/JCM.40.11.4051-4055.2002

6. Riccio ML, Pallecchi L, Fontana R, Rossolini GM. In70 of plasmid pAX22, a bla_{VIM-1}-containing integron carrying a new aminoglycoside phosphotransferase gene cassette. Antimicrob Agents Chemother. 2001;45:1249–53. https://doi.org/10.1128/AAC.45.4.1249-1253.2001
7. Arcari G, Di Lella FM, Bibbolino G, Mengoni F, Beccaccioli M, Antonelli G, et al. A multispecies cluster of VIM-1 carbapenemase-producing *Enterobacterales* linked by a novel, highly conjugative, and broad-host-range IncA plasmid forebodes the reemergence of VIM-1. Antimicrob Agents Chemother. 2020;64:e02435-19. https://doi.org/10.1128/AAC.02435-19
8. Emeraud C, Petit C, Gauthier L, Bonnin RA, Naas T, Dortet L. Emergence of VIM-producing *Enterobacter cloacae* complex in France between 2015 and 2018. J Antimicrob Chemother. 2022;77:944–51. https://doi.org/10.1093/jac/dkab471
9. Miriagou V, Tzelepi E, Gianneli D, Tzouvelekis LS. *Escherichia coli* with a self-transferable, multiresistant plasmid coding for metallo-β-lactamase VIM-1. Antimicrob Agents Chemother. 2003;47:395–7. https://doi.org/10.1128/AAC.47.1.395-397.2003
10. Colinon C, Miriagou V, Carattoli A, Luzzaro F, Rossolini GM. Characterization of the IncA/C plasmid pCC416 encoding VIM-4 and CMY-4 β-lactamases. J Antimicrob Chemother. 2007;60:258–62. https://doi.org/10.1093/jac/dkm171
11. Peirano G, Matsumura Y, Adams MD, Bradford P, Motyl M, Chen L, et al. Genomic epidemiology of global carbapenemase-producing *Enterobacter* spp., 2008–2014. Emerg Infect Dis. 2018;24:1010–9. https://doi.org/10.3201/eid2406.171648
12. Izdebski R, Baraniak A, Żabicka D, Sękowska A, Gospodarek-Komkowska E, Hryniewicz W, et al. VIM/IMP carbapenemase-producing Enterobacteriaceae in Poland: epidemic *Enterobacter hormaechei* and *Klebsiella oxytoca* lineages. J Antimicrob Chemother. 2018;73:2675–81. https://doi.org/10.1093/jac/dky257
13. Nordmann P, Poirel L, Dortet L. Rapid detection of carbapenemase-producing *Enterobacteriaceae*. Emerg Infect Dis. 2012;18:1503–7. https://doi.org/10.3201/eid1809.120355
14. Baraniak A, Machulska M, Żabicka D, Literacka E, Izdebski R, Urbanowicz P, et al.; NDM-PL Study Group. Towards endemicity: large-scale expansion of the NDM-1-producing *Klebsiella pneumoniae* ST11 lineage in Poland, 2015–16. J Antimicrob Chemother. 2019;74:3199–204. https://doi.org/10.1093/jac/dkz315
15. Izdebski R, Sitkiewicz M, Urbanowicz P, Krawczyk M, Brisse S, Gniadkowski M. Genomic background of the *Klebsiella pneumoniae* NDM-1 outbreak in Poland, 2012–18. J Antimicrob Chemother. 2020;75:3156–62. https://doi.org/10.1093/jac/dkaa339
16. Jain C, Rodriguez-R LM, Phillippy AM, Konstantinidis KT, Aluru S. High throughput ANI analysis of 90K prokaryotic genomes reveals clear species boundaries. Nat Commun. 2018;9:5114. https://doi.org/10.1038/s41467-018-07641-9
17. Wick RR, Judd LM, Gorrie CL, Holt KE. Unicycler: Resolving bacterial genome assemblies from short and long sequencing reads. PLOS Comput Biol. 2017;13:e1005595. https://doi.org/10.1371/journal.pcbi.1005595
18. Miyoshi-Akiyama T, Hayakawa K, Ohmagari N, Shimojima M, Kirikae T. Multilocus sequence typing (MLST) for characterization of *Enterobacter cloacae*. PLoS One. 2013;8:e66358. https://doi.org/10.1371/journal.pone.0066358
19. Zankari E, Hasman H, Cosentino S, Vestergaard M, Rasmussen S, Lund O, et al. Identification of acquired antimicrobial resistance genes. J Antimicrob Chemother. 2012;67:2640–4. https://doi.org/10.1093/jac/dks261
20. Carattoli A, Zankari E, García-Fernández A, Voldby Larsen M, Lund O, Villa L, et al. In silico detection and typing of plasmids using PlasmidFinder and plasmid multilocus sequence typing. Antimicrob Agents Chemother. 2014;58:3895–903. https://doi.org/10.1128/AAC.02412-14
21. Izdebski R, Biedrzycka M, Urbanowicz P, Papierowska-Kozdój W, Dominiak M, Żabicka D, et al. Multiple secondary outbreaks of NDM-producing *Enterobacter hormaechei* in the context of endemic NDM-producing *Klebsiella pneumoniae*. J Antimicrob Chemother. 2022;77:1561–9. https://doi.org/10.1093/jac/dkac076
22. Bitar I, Papagiannitsis CC, Kraftova L, Chudejova K, Mattioni Marchetti V, Hrabak J. Detection of five *mcr-9*-carrying *Enterobacterales* isolates in four Czech hospitals. MSphere. 2020;5:e01008–20. https://doi.org/10.1128/mSphere.01008-20
23. Ren Y, Ren Y, Zhou Z, Guo X, Li Y, Feng L, et al. Complete genome sequence of *Enterobacter cloacae* subsp. *cloacae* type strain ATCC 13047. J Bacteriol. 2010;192:2463–4. https://doi.org/10.1128/JB.00067-10
24. Sherburne CK, Lawley TD, Gilmour MW, Blattner FR, Burland V, Grotbeck E, et al. The complete DNA sequence and analysis of R27, a large IncHI plasmid from *Salmonella typhi* that is temperature sensitive for transfer. Nucleic Acids Res. 2000;28:2177–86. https://doi.org/10.1093/nar/28.10.2177
25. Partridge SR, Brown HJ, Stokes HW, Hall RM. Transposons Tn*1696* and Tn*21* and their integrons In4 and In2 have independent origins. Antimicrob Agents Chemother. 2001;45:1263–70. https://doi.org/10.1128/AAC.45.4.1263-1270.2001
26. Tobe T, Hayashi T, Han CG, Schoolnik GK, Ohtsubo E, Sasakawa C. Complete DNA sequence and structural analysis of the enteropathogenic *Escherichia coli* adherence factor plasmid. Infect Immun. 1999;67:5455–62. https://doi.org/10.1128/IAI.67.10.5455-5462.1999
27. Biedrzycka M, Izdebski R, Urbanowicz P, Polańska M, Hryniewicz W, Gniadkowski M, et al. MDR carbapenemase-producing *Klebsiella pneumoniae* of the hypervirulence-associated ST23 clone in Poland, 2009–19. J Antimicrob Chemother. 2022;77:3367–75. https://doi.org/10.1093/jac/dkac326
28. Gaillard M, Vallaeys T, Vorhölter FJ, Minoia M, Werlen C, Sentchilo V, et al. The *clc* element of *Pseudomonas* sp. strain B13, a genomic island with various catabolic properties. J Bacteriol. 2006;188:1999–2013. https://doi.org/10.1128/JB.188.5.1999-2013.2006
29. Hong JS, Yoon EJ, Lee H, Jeong SH, Lee K. Clonal dissemination of *Pseudomonas aeruginosa* sequence type 235 isolates carrying bla_{IMP-6} and emergence of bla_{GES-24} and bla_{IMP-10} on novel genomic islands PAGI-15 and -16 in South Korea. Antimicrob Agents Chemother. 2016;60:7216–23. https://doi.org/10.1128/AAC.01601-16
30. Baraniak A, Izdebski R, Zabicka D, Bojarska K, Górska S, Literacka E, et al.; KPC-PL2 Study Group. Multiregional dissemination of KPC-producing *Klebsiella pneumoniae* ST258/ST512 genotypes in Poland, 2010–14. J Antimicrob Chemother. 2017;72:1610–6. https://doi.org/10.1093/jac/dkx054
31. Majewski P, Wieczorek P, Sacha PT, Frank M, Juszczyk G, Ojdana D, et al. Emergence of OXA-48 carbapenemase-producing *Enterobacter cloacae* ST89 infection in Poland. Int J Infect Dis. 2014;25:107–9. https://doi.org/10.1016/j.ijid.2014.02.024
32. Wendel AF, Meyer S, Deenen R, Köhrer K, Kolbe-Busch S, Pfeffer K, et al. Long-term, low-frequency cluster of a

German-imipenemase-1-producing *Enterobacter hormaechei* ssp. *steigerwaltii* ST89 in a tertiary care hospital in Germany. Microb Drug Resist. 2018;24:1305–15. https://doi.org/10.1089/mdr.2017.0433
33. Patzer J, Toleman MA, Deshpande LM, Kamińska W, Dzierzanowska D, Bennett PM, et al. *Pseudomonas aeruginosa* strains harbouring an unusual bla_{VIM-4} gene cassette isolated from hospitalized children in Poland (1998–2001). J Antimicrob Chemother. 2004;53:451–6. https://doi.org/10.1093/jac/dkh095
34. Fiett J, Baraniak A, Mrówka A, Fleischer M, Drulis-Kawa Z, Naumiuk Ł, et al. Molecular epidemiology of acquired-metallo-β-lactamase-producing bacteria in Poland. Antimicrob Agents Chemother. 2006;50:880–6. https://doi.org/10.1128/AAC.50.3.880-886.2006
35. Kristóf K, Tóth A, Damjanova I, Jánvári L, Konkoly-Thege M, Kocsis B, et al. Identification of a bla_{VIM-4} gene in the internationally successful *Klebsiella pneumoniae* ST11 clone and in a *Klebsiella oxytoca* strain in Hungary. J Antimicrob Chemother. 2010;65:1303–5. https://doi.org/10.1093/jac/dkq133
36. Libisch B, Muzslay M, Gacs M, Minárovits J, Knausz M, Watine J, et al. Molecular epidemiology of VIM-4 metallo-β-lactamase-producing *Pseudomonas* sp. isolates in Hungary. Antimicrob Agents Chemother. 2006;50:4220–3. https://doi.org/10.1128/AAC.00300-06
37. Scoulica EV, Neonakis IK, Gikas AI, Tselentis YJ. Spread of bla_{VIM-1}-producing *E. coli* in a university hospital in Greece. Genetic analysis of the integron carrying the bla_{VIM-1} metallo-β-lactamase gene. Diagn Microbiol Infect Dis. 2004;48:167–72. https://doi.org/10.1016/j.diagmicrobio.2003.09.012
38. Porres-Osante N, Azcona-Gutiérrez JM, Rojo-Bezares B, Undabeitia E, Torres C, Sáenz Y. Emergence of a multiresistant KPC-3 and VIM-1 carbapenemase-producing *Escherichia coli* strain in Spain. J Antimicrob Chemother. 2014;69:1792–5. https://doi.org/10.1093/jac/dku055
39. Urbanowicz P, Izdebski R, Baraniak A, Żabicka D, Hryniewicz W, Gniadkowski M. Molecular and genomic epidemiology of VIM/IMP-like metallo-β-lactamase-producing *Pseudomonas aeruginosa* genotypes in Poland. J Antimicrob Chemother. 2021;76:2273–84. https://doi.org/10.1093/jac/dkab188
40. Urbanowicz P, Izdebski R, Biedrzycka M, Literacka E, Hryniewicz W, Gniadkowski M. Genomic epidemiology of MBL-producing *Pseudomonas putida* group isolates in Poland. Infect Dis Ther. 2022;11:1725–40. https://doi.org/10.1007/s40121-022-00659-z

Address for correspondence: Radosław Izdebski, National Medicines Institute, Chełmska 30/34, 00-725 Warsaw, Poland; email: r.izdebski@nil.gov.pl

etymologia revisited

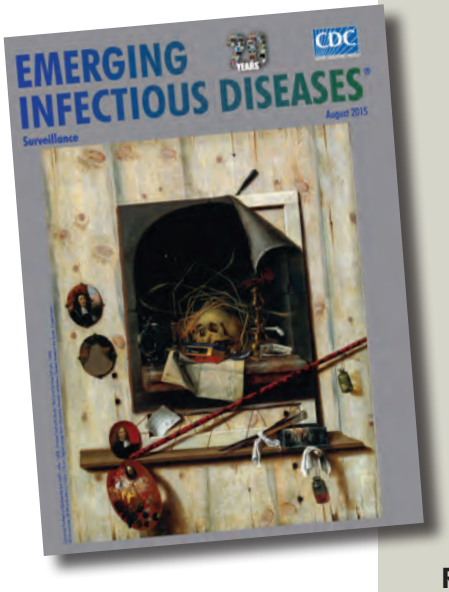

Originally published in August 2015

Escherichia coli

[esh”ə-rik’e-ə co’lī]

A gram-negative, facultatively anaerobic rod, *Escherichia coli* was named for Theodor Escherich, a German-Austrian pediatrician. Escherich isolated a variety of bacteria from infant fecal samples by using his own anaerobic culture methods and Hans Christian Gram’s new staining technique. Escherich originally named the common colon bacillus *Bacterium coli commune*. Castellani and Chalmers proposed the name *E. coli* in 1919, but it was not officially recognized until 1958.

References:

1. Oberbauer BA. Theodor Escherich—Leben und Werk. Munich: Futuramed-Verlag; 1992.
2. Shulman ST, Friedmann HC, Sims RH. Theodor Escherich: the first pediatric infectious diseases physician? Clin Infect Dis. 2007;45:1025–9 .

https://wwwnc.cdc.gov/eid/article/21/8/et-2108_article

Human Fecal Carriage of *Streptococcus agalactiae* Sequence Type 283, Thailand

Timothy Barkham, Wen Ying Tang, Yi-Chen Wang,
Paiboon Sithithaworn, Kulthida Y. Kopolrat, Chanika Worasith

Streptococcus agalactiae (group B *Streptococcus*) sequence type 283 bacteremia, found almost exclusively in Southeast Asia, is associated with consuming raw freshwater fish, but some patients deny consumption. We detected fecal carriage in 5/184 (2.7%) persons in northeast Thailand. Human carriers might contribute to transmission or be the original source of this sequence type.

The epidemiology of the *Streptococcus agalactiae* bacterium (group B *Streptococcus* [GBS]) in Southeast Asia differs from that traditionally seen in the literature. Investigations after the foodborne outbreak of GBS sepsis in 2015 in Singapore concluded that GBS sepsis is primarily a foodborne infection of adults in parts of Southeast Asia (*1*).

The Singapore outbreak was associated with consumption of raw freshwater fish (*2*,*3*). The GBS were serotype III sequence type 283 (ST283) and behaved more aggressively in adults than other GBS; adults without comorbidities made up 22% of the ST283 bacteremia cases but only 2% of non-ST283 GBS cases (*4*). Subsequent studies showed that although ST283 is almost absent from the rest of the world, ST283 disease is widespread around Southeast Asia in humans and tilapia; human data from Laos and Thailand showed ST283 accounted for 76% (Laos) and 73% (Thailand) of invasive GBS collected during 2000–2017 (*1*,*5*). Aquaculture data from Malaysia, Thailand, and Vietnam show that ST283 accounted for 12%–100% of all GBS isolated from streptococcosis in farmed tilapia during 2003–2018 (*1*,*6*). Whole-genome analysis shows ST283 from humans and tilapia are 1 clone (*1*,*7*). Because consumption of raw freshwater fish is common in affected Southeast Asia countries (T. Barkham, unpub. data), raw tilapia could plausibly be the main source of human ST283, although this theory has not been studied.

This fishborne epidemiology is reflected in a report of 2 sisters in their 50s without comorbidities who returned to Laos after visiting friends and relatives in the United States. Both sisters became ill with ST283 bacteremia a day after a meal that included Mekong fish salad, traditionally made with raw freshwater fish (*8*). However, in case–control studies in Singapore in 2015, which reported statistically strong associations between eating raw freshwater fish and ST283 bacteremia, 21/40 participants in a retrospective study (*3*) and 2/9 participants in a prospective study (*2*) denied eating raw freshwater fish. This finding could be because of poor recollection or varying definitions of raw, as in the case of dishes prepared without heat but regarded as being no longer raw (e.g., raw fish fileted or ground and mixed with lemon juice or other sauces). Nevertheless, the possibility of interhuman transmission or that other foods are a source also deserves study. In addition, when authorities investigated a surge of 18 ST283 bacteremia cases in Singapore in July 2020, no affected persons admitted eating raw freshwater fish. Selling raw freshwater fish as a ready-to-eat food was illegal at that time in Singapore, so this denial was not surprising, but it might also suggest an alternative source or vehicle.

Studies of vaginal and rectal carriage in women in Southeast Asia have not reported sequence types, because their focus has been capsular serotypes for use in developing vaccines. Two small sequencing studies failed to find ST283; 1 looked at stool samples from 82 food handlers and fishmongers in Singapore during the 2015 outbreak (*4*), and the other looked at an opportunistic collection of 38 vaginal

Author affiliations: Tan Tock Seng Hospital, Singapore (T. Barkham, W.Y. Tang); National University of Singapore, Singapore (Y.-C. Wang); Khon Kaen University, Khon Kaen, Thailand (P. Sithithaworn, K.Y. Kopolrat, C. Worasith)

DOI: https://doi.org/10.3201/eid2908.230098

GBS samples isolated from women with colpitis in Hanoi, Vietnam, in 2016 (*1*).

Clinical evidence for carriage and human-to-human transmission of this bacterial strain is provided by several cases of ST283 neonatal early onset disease in Hong Kong (*5*) and Laos (*1*); at least 2 from Laos were isolated on the infants' first day of life, which suggests maternal carriage. We sought to verify carriage. Because ST283 is known to account for 73% of invasive GBS in humans in parts of Thailand (*1*), we assessed ST283 carriage in a population in Thailand that consumes raw freshwater fish, as verified by the widespread occurrence of *Opisthorchis viverrini*, a liver fluke infection acquired by eating raw freshwater fish.

The Study

We collected samples in January 2019 from Nong Bua and Dong Mun subdistricts of Nong Kung Si District, Kalasin Province, Thailand. This area is within the Northeast region of Thailand, where the prevalence of liver fluke infection is high. Participants were a random sample of persons ≥15 years of age who had ever eaten uncooked freshwater fish, been infected by or treated for liver flukes, or knew of any family member who had had liver cancer. The study was approved by the Ethics Committee of Khon Kaen University, Thailand (approval no. HE601370). The first feces and urine samples of the morning were chilled and transported to the laboratory at Khon Kaen University. Each fecal sample was processed for parasite (fluke) examination by the formalin ethyl-acetate concentration technique, and aliquots were stored at −20°C and sent to Singapore for GBS detection. DNA was extracted with the QIA DNeasy PowerSoil Kit (QIAGEN, https://www.qiagen.com) with an additional wash step. We used PCR to detect serotype III GBS (*9*) and performed multilocus sequence typing (MLST) (*10*) on DNA extracts that were positive for serotype III. We included an internal control. We centrifuged each urine sample and kept the supernatant for *O. viverrini* antigen analysis (*11*).

We recruited 184 participants; 18 of the 184 stool samples were positive for serotype III GBS. MLST of these 18 samples found five ST283, three ST1, three ST651, one ST17, one ST862, and two with undefined profiles (with alleles 9,1,170,1,1,53,2, and 16,1,2,1,9,2,2); 3 had inadequate PCR products for sequencing. All samples were negative for PCR inhibition. Stool microscopy found fluke eggs in 4 (2.2%) samples. The *O. viverrini* urine-antigen test was positive in the same 4 samples and in 1 additional sample. We detected 1 serotype III GBS sequence type in each of those 5 stool samples: ST283, ST1, ST17, ST651, and 1 sequence without adequate PCR products for MLST.

Conclusions

This study demonstrates human carriage of GBS ST283 and establishes that humans might play a part in the transmission of ST283 or could even be the original source. Our finding supports the assumed transmission from mother to newborn described in Laos (*1*). Questions remain as to whether carriage is temporary, perhaps reflecting recent dietary exposure, or long lasting. The transmission of *Opisthorchis* flukes depends on human fecal waste being disposed of in fresh water and humans consuming raw fish from the same water, so each species consumes raw products from the other. The prevalence of those flukes in parts of Southeast Asia is a testament to the ongoing presence of these practices, which could explain the high rates of GBS ST283 in humans and tilapia in the same geographic areas. This hypothesized transmission cycle has not been studied for ST283.

The data reported here might not be representative of all the numerous different ethnic and cultural groups in and around Southeast Asia. We hope these data will stimulate and support further epidemiologic studies, including studies on patterns of consumption of raw freshwater fish in different cultural groups in Southeast Asia, as recommended in the ST283 risk profile published by the Food and Agriculture Organization of the United Nations (*12*).

In summary, we detected GBS ST283 in 2.7% of 184 stool samples collected in northeastern Thailand from a population known to consume raw freshwater fish. We remain uncertain of the dynamics of human carriage of GBS ST283 and its contribution to human-to-human transmission, human disease, and the contamination of aquaculture, but our findings indicate that human carriers might play a part in transmitting GBS ST283 or could be its original source.

This work was funded by the Department of Laboratory Medicine and the Molecular Biology Laboratory, Tan Tock Seng Hospital, Singapore; the Department of Geography, National University of Singapore; and the Department of Parasitology, Khon Kaen University, Thailand.

About the Author

Dr. Barkham studied medicine and microbiology in London, UK. He has been working in Singapore since 1999, and his interests include a mix of clinical service, research, and teaching.

References

1. Barkham T, Zadoks RN, Azmai MNA, Baker S, Bich VTN, Chalker V, et al. One hypervirulent clone, sequence type 283, accounts for a large proportion of invasive *Streptococcus agalactiae* isolated from humans and diseased tilapia in Southeast Asia. PLoS Negl Trop Dis. 2019;13:e0007421. https://doi.org/10.1371/journal.pntd.0007421
2. Rajendram P, Mar Kyaw W, Leo YS, Ho H, Chen WK, Lin R, et al. Group B *Streptococcus* sequence type 283 disease linked to consumption of raw fish, Singapore. Emerg Infect Dis. 2016;22:1974–7. https://doi.org/10.3201/eid2211.160252
3. Tan S, Lin Y, Foo K, Koh HF, Tow C, Zhang Y, et al. Group B *Streptococcus* serotype III sequence type 283 bacteremia associated with consumption of raw fish, Singapore. Emerg Infect Dis. 2016;22:1970–3. https://doi.org/10.3201/eid2211.160210
4. Kalimuddin S, Chen SL, Lim CTK, Koh TH, Tan TY, Kam M, et al.; Singapore Group B Streptococcus Consortium. 2015 epidemic of severe *Streptococcus agalactiae* sequence type 283 infections in Singapore associated with the consumption of raw freshwater fish: a detailed analysis of clinical, epidemiological, and bacterial sequencing data. Clin Infect Dis. 2017;64(suppl_2):S145–52. https://doi.org/10.1093/cid/cix021
5. Ip M, Ang I, Fung K, Liyanapathirana V, Luo MJ, Lai R. Hypervirulent clone of group B *Streptococcus* serotype III sequence type 283, Hong Kong, 1993–2012. Emerg Infect Dis. 2016;22:1800–3. https://doi.org/10.3201/eid2210.151436
6. Kayansamruaj P, Soontara C, Unajak S, Dong HT, Rodkhum C, Kondo H, et al. Comparative genomics inferred two distinct populations of piscine pathogenic *Streptococcus agalactiae*, serotype Ia ST7 and serotype III ST283, in Thailand and Vietnam. Genomics. 2019;111:1657–67. https://doi.org/10.1016/j.ygeno.2018.11.016
7. Chen SL. Genomic insights into the distribution and evolution of group B Streptococcus. Front Microbiol. 2019;10:1447. https://doi.org/10.3389/fmicb.2019.01447
8. Luangraj M, Hiestand J, Rasphone O, Chen SL, Davong V, Barkham T, et al. Invasive *Streptococcus agalactiae* ST283 infection after fish consumption in two sisters, Lao PDR. Wellcome Open Res. 2022;7:148. https://doi.org/10.12688/wellcomeopenres.17804.1
9. Breeding KM, Ragipani B, Lee KD, Malik M, Randis TM, Ratner AJ. Real-time PCR-based serotyping of *Streptococcus agalactiae*. Sci Rep. 2016;6:38523. https://doi.org/10.1038/srep38523
10. Jones N, Bohnsack JF, Takahashi S, Oliver KA, Chan MS, Kunst F, et al. Multilocus sequence typing system for group B streptococcus. J Clin Microbiol. 2003;41:2530–6. https://doi.org/10.1128/JCM.41.6.2530-2536.2003
11. Worasith C, Kamamia C, Yakovleva A, Duenngai K, Wangboon C, Sithithaworn J, et al. Advances in the diagnosis of human opisthorchiasis: development of *Opisthorchis viverrini* antigen detection in urine. PLoS Negl Trop Dis. 2015;9:e0004157. https://doi.org/10.1371/journal.pntd.0004157
12. Food and Agriculture Organization of the United Nations. Risk profile—group B Streptococcus (GBS)–*Streptococcus agalactiae* sequence type (ST) 283 in freshwater fish. 2021 [cited 2023 Jun 13]. https://www.fao.org/documents/card/en?details=CB5067EN

Address for correspondence: Timothy Barkham, Department of Laboratory Medicine, Tan Tock Seng Hospital, 308433, Singapore; email: timothy_barkham@ttsh.com.sg

Emerging *Corynebacterium diphtheriae* Species Complex Infections, Réunion Island, France, 2015–2020

Thomas Garrigos,[1] Anais Grimal,[1] Edgar Badell, Nicolas Traversier, Sandrine Picot, Anne Lignereux, Mahery Ramiandrisoa, Céline Ben Cimon, Marie-Christine Jaffar-Bandjee, Houssein Gbaguidi-Haore, Julie Toubiana, Sylvain Brisse, Guillaume Miltgen,[2] Olivier Belmonte[2]

Clinical, epidemiologic, and microbiologic analyses revealed emergence of 26 cases of *Corynebacterium diphtheriae* species complex infections on Réunion Island, France, during 2015–2020. Isolates were genetically diverse, indicating circulation and local transmission of several diphtheria sublineages. Clinicians should remain aware of the risk for diphtheria and improve diagnostic methods and patient management.

Diphtheria is a contagious, potentially fatal infection caused by toxin-producing bacteria of the *Corynebacterium diphtheriae* species complex, which includes *C. diphtheriae*, *C. ulcerans*, *C. pseudotuberculosis*, *C. rouxii*, *C. belfantii*, and *C. silvaticum*. Infection is localized principally in the upper respiratory tract, and production of diphtheria toxin (encoded by the *tox* gene) can cause systemic complications. Cutaneous diphtheria and diphtheria endocarditis can also act as sources of respiratory infections (*1*–*4*). Diphtheria surveillance has traditionally focused on respiratory illness caused by toxigenic *C. diphtheriae* but has been expanded in some countries to include all *C. diphtheriae* species complex infections irrespective of species, infection site, or toxigenicity, enabling broader disease monitoring. *C. diphtheriae* spreads via human-to-human contact; *C. ulcerans* and *C. pseudotuberculosis* are transmitted to humans primarily through animal contact.

Diphtheria was once a major cause of infant death, but global incidence has declined over the past century, largely because of mass vaccination. Consequently, diphtheria is now often considered a forgotten disease (*5*). Nevertheless, diphtheria reemergence has been reported in high-income countries and is closely related to patient travel history. Diphtheria is considered endemic in Madagascar, Comoros, and Mayotte in the southwest Indian Ocean, but few cases have been reported on other islands, including Réunion Island, an overseas department of France, where cases emerged in 2015 (*6*,*7*). Vaccination coverage is poorer in Mayotte (45% for 7- to 11-year-old children) than in Réunion Island (96% for children 11 months of age). Recent improvements in laboratory diagnostic capabilities, such as mass spectrometry use, have increased reports of *C. diphtheriae* species complex infections (*8*). However, knowledge of prevalence and origin of those infections is limited in this region. The aims of this study were to review the clinical, epidemiologic, and microbiologic characteristics of *C. diphtheriae* species complex infections on

Author affiliations: Félix Guyon University Hospital Center, Saint-Denis, Réunion Island, France (T. Garrigos, A. Grimal, N. Traversier, M.-C. Jaffar-Bandjee, G. Miltgen, O. Belmonte); Processus Infectieux en Milieu Insulaire Tropical, University of La Réunion, Inserm, CNRS, IRD, Saint-Denis, Réunion Island, France (T. Garrigos, G. Miltgen); Institut Pasteur University of Paris Cité, Paris, France (E. Badell, J. Toubiana, S. Brisse); Institut Pasteur National Reference Center for Corynebacteria of the Diphtheriae Complex, Paris (E. Badell, J. Toubiana, S. Brisse); University Hospital of La Réunion, Saint Pierre, Réunion Island, France (S. Picot); Hospital Center West Réunion, Saint Paul, Réunion Island, France (A. Lignereux); Cerballiance Laboratory, Le Port, Réunion Island, France (M. Ramiandrisoa); Inovie RéuniLAB Laboratory, Sainte-Clotilde (C. Ben Cimon); University Hospital Center and University of Bourgogne Franche-Comté, Besançon, France (H. Gbaguidi-Haore); Necker-Enfants malades Hospital, Paris (J. Toubiana).

DOI: https://doi.org/10.3201/eid2908.230106

[1]These first authors contributed equally to this article.

[2]These authors contributed equally to this article.

Réunion Island during 2015–2020 and identify possible links with cases on other islands in the region.

The Study

We included all cases of *C. diphtheriae* species complex infections reported to the regional health agency and recorded at Réunion Island University Hospital during 2015–2020. We analyzed medical records and extracted age, sex, country of residence, recent travel, contact with animals, socioeconomic status, and diphtheria vaccination status for each case. We performed antimicrobial susceptibility testing; identified co-infecting strains; and determined *tox* gene presence, diphtheria toxin production, and biovar and sequence type (ST). We sent each isolate to the National Reference Center for Corynebacteria of the *diphtheriae* Complex (Institut Pasteur, Paris, France) to confirm species identity through multiplex PCR and biotyping as previously described (*8*–*10*). We detected the *tox* gene by using conventional PCR or, since 2019, by using multiplex real-time PCR (*10*). We assessed toxin production by using a modified Elek test (*11*). We determined antimicrobial drug susceptibility by using disk diffusion or by determining MICs (E-test; bioMérieux, https://www.biomerieux.com), in accordance with CASFM/EUCAST2021 (https://www.sfm-microbiologie.org/2021/04/23/casfm-avril-2021-v1-0) recommendations for benzylpenicillin, amoxicillin, cefotaxime, clindamycin, rifampin, and ciprofloxacin. We genotyped each isolate by using multilocus sequence typing (MLST) (*12*).

A total of 26 cases of *C. diphtheriae* species complex infections were recorded, from which 27 *C. diphtheriae* and 2 *C. ulcerans* isolates were cultured. Most (88.5%) infected patients were male; median age was 60 (interquartile range 32.5–67) years. Fourteen (50%) patients lived on Réunion Island, 3 (11.5%) in Mayotte, 4 (19.2%) in mainland France, 3 (11.5%) in Comoros, and 2 (7.8%) in Madagascar. Most (84.6%) patients had skin manifestations, and 16 patients were vaccinated (Table 1, https://wwwnc.cdc.gov/EID/article/29/8/23-0106-T1.htm; Appendix Figure, https://wwwnc.cdc.gov/EID/article/29/8/23-0106.pdf). Of 24 *C. diphtheriae* infections, 8 occurred in patients who had recently traveled to or originated from Madagascar, 4 who traveled to or originated from Mayotte, and 3 who traveled to or originated from Comoros. Since 2018, a total of 9 cases on Réunion Island have been considered locally acquired; all of those patients lived in poor socioeconomic conditions. *C. ulcerans* infections occurred in 2 patients living on Réunion Island who had not traveled recently but had contact with animals (Table 1; Figure). We performed a Spearman rank correlation to compare locally acquired strains isolated during 2015–2018 and 2019–2020; a 75% increase in locally acquired *C. diphtheriae* infections occurred in 2019–2020 (ρ = 0.8452; p = 0.0341).

Isolates were obtained from cutaneous lesion (n = 24), bone (n = 4), and respiratory (n = 1) samples. Eight of 27 *C. diphtheriae* isolates were toxigenic, yielding positive Elek test results. The 2 *C. ulcerans* isolates were nontoxigenic. *C. diphtheriae* isolates were characterized as biovars Mitis (n = 20) and Gravis (n = 7).

Patient isolates were co-infected most frequently with *Staphylococcus aureus* (n = 17) and *Streptococcus pyogenes* (n = 18). Benzylpenicillin resistance was observed in 80% of isolates according to CASFM/EUCAST2021 recommendations, but isolates were categorized as susceptible increased exposure according to EUCAST version 13.0 proposed breakpoints (https://www.eucast.org/clinical_breakpoints) (Appendix Table). One (3.5%) *C. diphtheriae* isolate was resistant to amoxicillin (CD8/FRC0402; MIC 1.5 mg/L),

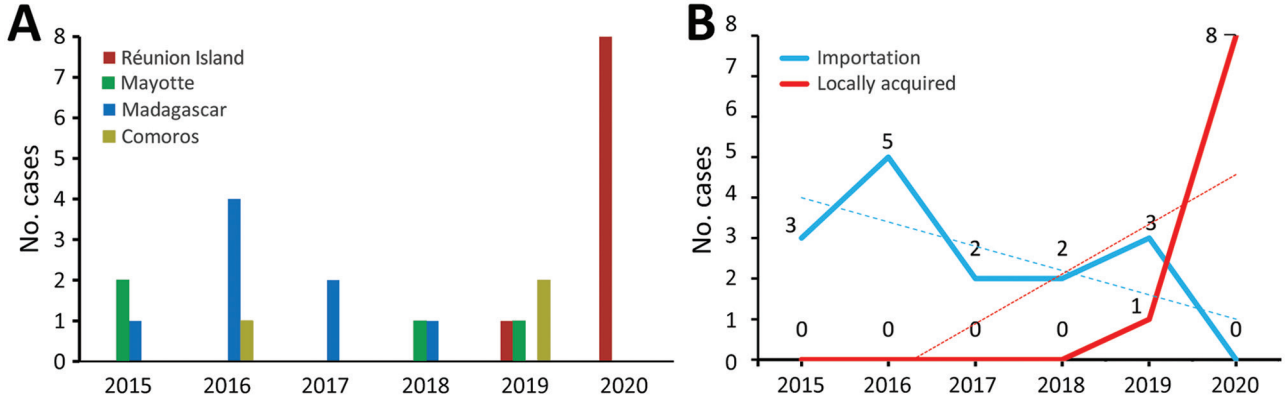

Figure. Number of cases diagnosed per year in study of emerging *Corynebacterium diphtheriae* species complex infections, Réunion Island, France, 2015–2020. Number of cases were classified according to geographic origin (A) or travel history of patients (B). Dotted lines indicate linear trends.

and 1 was resistant to rifampin. Both *C. ulcerans* isolates were resistant to clindamycin (100%, natural low susceptibility), whereas clindamycin resistance was observed for only 1 *C. diphtheriae* isolate.

We identified 21 STs by MLST analysis, including ST88 for *C. diphtheriae* isolates from 4 patients and ST339 for both *C. ulcerans* isolates (Table 2). All *C. diphtheriae* STs had 2–5 mismatches, except ST87 and ST237, which had 1 mismatch between them. ST339 (*C. ulcerans*) had 7 mismatches with all *C. diphtheriae* STs.

Conclusions

We report increased prevalence of cutaneous *C. diphtheriae* species complex infections on Réunion Island during 2015–2020. Introduction of mass spectrometry analysis in hospital laboratories and increased clinician awareness might have led to increased case reporting. Our study confirms that *C. diphtheriae* species complex members are circulating and are likely underestimated in the southwest Indian Ocean (*7*,*13*). Moreover, we observed emergence of locally acquired cutaneous *C. diphtheriae* infections on Réunion Island since 2019. The number of imported cases in 2020 was probably limited because of the COVID-19 pandemic, which reduced travel. Indeed, all *C. diphtheriae* cases identified during 2015–2018 occurred in patients who had traveled from other islands in the Indian Ocean. In addition, cutaneous diphtheria appeared to be associated with poor socioeconomic living conditions, in which alcoholism, drug dependence, and homelessness are factors that increase risk for human-to-human transmission and virulence (*14*).

A total of 8 (30%) *C. diphtheriae* isolates were toxigenic and caused cutaneous infections. Nontoxigenic *C. diphtheriae* isolates (70%, n = 19) were obtained from cutaneous lesions, respiratory samples, and bone samples. Clinicians should be aware that nontoxigenic *C. diphtheriae* can potentially cause severe disease (*1*,*14*,*15*). Moreover, all isolates were co-infected with pyogenic bacteria, suggesting diphtheria infection should be considered under polymicrobial conditions.

MLST analysis identified 21 different STs; most were unrelated (≥2 mistmatches) reflecting marked

Table 2. Characteristics of isolates from 26 patients in study of emerging *Corynebacterium diphtheriae* species complex infections, Réunion Island, France, 2015–2020*

Patient no.	Isolate	Year	Isolation site	Species	Biovar	*tox* gene	Elek test	ST†	Co-infections‡
1	CD1/FRC0304	2015	Cutaneous	*C. diphtheriae*	Gravis	Negative	NA	102	*S. pyogenes, S. aureus, A. haemolyticum*
	CD2/FRC0316	2015	Respiratory	*C. diphtheriae*	Mitis	Negative	NA	95	*S. aureus*
2	CD3/FRC0314	2015	Cutaneous	*C. diphtheriae*	Mitis	Positive	Positive	421	*S. aureus*
3	CD4/FRC0376	2015	Cutaneous	*C. diphtheriae*	Gravis	Positive	Positive	388	*S. pyogenes*
4	CD5/FRC0383	2016	Cutaneous	*C. diphtheriae*	Mitis	Negative	NA	423	*S. pyogenes, S. aureus*
	CD6/FRC0393	2016	Cutaneous	*C. diphtheriae*	Mitis	Negative	NA	423	*S. pyogenes, S. aureus*
5	CD7/FRC0385	2016	Cutaneous	*C. diphtheriae*	Mitis	Positive	Positive	91	*S. pyogenes*
6	CU1/FRC0391	2016	Cutaneous	*C. ulcerans*	NA	Negative	NA	**339**	*S. dysgalactiae*
7	CD8/FRC0402	2016	Cutaneous	*C. diphtheriae*	Mitis	Negative	NA	410	*S. dysgalactiae*
8	CD9/FRC0410	2016	Cutaneous	*C. diphtheriae*	Mitis	Negative	NA	415	*S. pyogenes*
9	CD10/FRC0423	2016	Cutaneous	*C. diphtheriae*	Gravis	Negative	NA	101	*S. aureus*
10	CD11/FRC0477	2017	Cutaneous	*C. diphtheriae*	Gravis	Negative	NA	481	*S. pyogenes, S. aureus, A. haemolyticum*
11	CD12/FRC0501	2017	Cutaneous	*C. diphtheriae*	Gravis	Positive	Positive	521	*S. pyogenes*
12	CD13/FRC0624	2018	Bone	*C. diphtheriae*	Mitis	Negative	NA	237	*S. aureus*
13	CD14/FRC0630	2018	Cutaneous	*C. diphtheriae*	Gravis	Negative	NA	606	*S. pyogenes, S. aureus*
14	CD15/FRC0733	2019	Cutaneous	*C. diphtheriae*	Mitis	Negative	NA	351	*S. pyogenes*
15	CD16/FRC0782	2019	Cutaneous	*C. diphtheriae*	Mitis	Positive	Positive	688	*S. pyogenes, S. aureus*
	CD17/FRC0809	2019	Cutaneous	*C. diphtheriae*	Mitis	Positive	Positive	688	*S. aureus*
16	CD18/FRC0819	2019	Cutaneous	*C. diphtheriae*	Gravis	Positive	Positive	87	*S. pyogenes, A. haemolyticum*
17	CU2/FRC0820	2019	Bone	*C. ulcerans*	NA	Negative	NA	**339**	*S. aureus*
18	CD19/FRC0849	2019	Cutaneous	*C. diphtheriae*	Mitis	Positive	Positive	426	*S. pyogenes, S. aureus*
19	CD20/FRC0865	2020	Cutaneous	*C. diphtheriae*	Mitis	Negative	NA	102	*S. pyogenes, S. aureus*
20	CD21/FRC0875	2020	Cutaneous	*C. diphtheriae*	Mitis	Negative	NA	707	*S. pyogenes*
21	CD22/FRC0893	2020	Cutaneous	*C. diphtheriae*	Mitis	Negative	NA	708	*S. pyogenes*
22	CD23/FRC0928	2020	Cutaneous	*C. diphtheriae*	Mitis	Negative	NA	**88**	*S. pyogenes*
23	CD24/FRC0970	2020	Cutaneous	*C. diphtheriae*	Mitis	Negative	NA	**88**	*S. pyogenes, S. aureus, A. haemolyticum*
24	CD25/FRC0975	2020	Cutaneous	*C. diphtheriae*	Mitis	Negative	NA	**88**	*S. aureus*
25	CD26/FRC1050	2020	Bone	*C. diphtheriae*	Mitis	Negative	NA	771	*A. haemolyticum*
26	CD27/FRC1065	2020	Bone	*C. diphtheriae*	Mitis	Negative	NA	**88**	*S. aureus*

*CD, *Corynebacterium diphtheriae*; CU, C. *ulcerans*; NA, not applicable; ST, sequence type.
†Numbers in bold indicate a common ST shared among strains from different patients.
‡Co-infections with *Arcanobacterium haemolyticum*, *Staphylococcus aureus*, *Streptococcus dysgalactiae*, or *Streptococcus pyogenes*.

genetic diversity of isolates. ST88 was found in 4 patients living on Réunion Island who had not traveled recently, indicating probable local acquisition. ST88 had previously been reported only in patients from Mayotte. Therefore, our results show that multiple *C. diphtheriae* species complex clones are circulating in the southwest Indian Ocean (*8*). Both *C. ulcerans* strains belonged to ST339. The National Reference Center reported that ST339 is the predominant *C. ulcerans* ST found in animals in France. Although considerable ST diversity was revealed, whole-genome sequencing will be required to further evaluate circulating *C. diphtheriae* clones in this region.

In conclusion, we describe emergence of locally acquired *C. diphtheriae* species complex infections on Réunion Island during 2019–2020. Local clinicians and microbiologists should remain aware of this neglected infection; improvements should be made in diagnostic methods and management of infected patients, such as maintaining availability of diphtheria antitoxin.

The National Reference Center for Corynebacteria of the *diphtheriae* Complex is supported financially by Santé publique France (Saint-Maurice, France).

About the Author

Dr. Garrigos is a research scientist in the microbiology department of Félix Guyon University Hospital of Réunion Island, France. His research interests focus on bacterial diseases, antimicrobial resistance, cystic fibrosis patients, and emerging infectious diseases.

References

1. Patey O, Bimet F, Riegel P, Halioua B, Emond JP, Estrangin E, et al.; Coryne Study Group. Clinical and molecular study of *Corynebacterium diphtheriae* systemic infections in France. J Clin Microbiol. 1997;35:441–5. https://doi.org/10.1128/jcm.35.2.441-445.1997
2. Hadfield TL, McEvoy P, Polotsky Y, Tzinserling VA, Yakovlev AA. The pathology of diphtheria. J Infect Dis. 2000;181:S116–20. https://doi.org/10.1086/315551
3. Levi LI, Barbut F, Chopin D, Rondeau P, Lalande V, Jolivet S, et al. Cutaneous diphtheria: three case reports to discuss determinants of re-emergence in resource-rich settings. Emerg Microbes Infect. 2021;10:2300–2. https://doi.org/10.1080/22221751.2021.2008774
4. Sangal V, Hoskisson PA. Evolution, epidemiology and diversity of *Corynebacterium diphtheriae*: new perspectives on an old foe. Infect Genet Evol. 2016;43:364–70. https://doi.org/10.1016/j.meegid.2016.06.024
5. Sharma NC, Efstratiou A, Mokrousov I, Mutreja A, Das B, Ramamurthy T. Diphtheria. Nat Rev Dis Primers. 2019;5:81. https://doi.org/10.1038/s41572-019-0131-y
6. Scheifer C, Rolland-Debord C, Badell E, Reibel F, Aubry A, Perignon A, et al. Re-emergence of *Corynebacterium diphtheriae*. Med Mal Infect. 2019;49:463–6. https://doi.org/10.1016/j.medmal.2018.12.001
7. Belchior E, Henry S, Badell E, Collet L, Benoit-Cattin T, de Montera AM, et al. Diphtheria in Mayotte, 2007–2015. Emerg Infect Dis. 2017;23:1218–20. https://doi.org/10.3201/eid2307.170262
8. Hennart M, Panunzi LG, Rodrigues C, Gaday Q, Baines SL, Barros-Pinkelnig M, et al. Population genomics and antimicrobial resistance in *Corynebacterium diphtheriae*. Genome Med. 2020;12:107. https://doi.org/10.1186/s13073-020-00805-7
9. Dazas M, Badell E, Carmi-Leroy A, Criscuolo A, Brisse S. Taxonomic status of *Corynebacterium diphtheriae* biovar Belfanti and proposal of *Corynebacterium belfantii* sp. nov. Int J Syst Evol Microbiol. 2018;68:3826–31. https://doi.org/10.1099/ijsem.0.003069
10. Badell E, Guillot S, Tulliez M, Pascal M, Panunzi LG, Rose S, et al. Improved quadruplex real-time PCR assay for the diagnosis of diphtheria. J Med Microbiol. 2019;68:1455–65. https://doi.org/10.1099/jmm.0.001070
11. Engler KH, Glushkevich T, Mazurova IK, George RC, Efstratiou A. A modified Elek test for detection of toxigenic corynebacteria in the diagnostic laboratory. J Clin Microbiol. 1997;35:495–8. https://doi.org/10.1128/jcm.35.2.495-498.1997
12. Bolt F, Cassiday P, Tondella ML, Dezoysa A, Efstratiou A, Sing A, et al. Multilocus sequence typing identifies evidence for recombination and two distinct lineages of *Corynebacterium diphtheriae*. J Clin Microbiol. 2010;48:4177–85. https://doi.org/10.1128/JCM.00274-10
13. Rakotomalala RS, Andrianirina ZZ, Ratsima E, Randrianandraina P, Randrianirina F, Edosoa GT, et al. *Corynebacterium diphtheriae* infection in Mahajanga, Madagascar: first case report. J Trop Pediatr. 2021;67:fmaa064. https://doi.org.10.1093/tropej/fmaa064
14. Badenschier F, Berger A, Dangel A, Sprenger A, Hobmaier B, Sievers C, et al. Outbreak of imported diphtheria with *Corynebacterium diphtheriae* among migrants arriving in Germany, 2022. Euro Surveill. 2022;27:2200849. https://doi.org/10.2807/1560-7917.ES.2022.27.46.2200849
15. Farfour E, Badell E, Zasada A, Hotzel H, Tomaso H, Guillot S, et al. Characterization and comparison of invasive *Corynebacterium diphtheriae* isolates from France and Poland. J Clin Microbiol. 2012;50:173–5. https://doi.org/10.1128/JCM.05811-11

Address for correspondence: Thomas Garrigos, Laboratoire de Microbiologie, Hôpital Universitaire Félix Guyon, Allée des Topazes, 97400 Saint-Denis, La Réunion, France; email: thomas.garrigos@chu-reunion.fr

Chromosome-Borne CTX-M-65 Extended-Spectrum β-Lactamase–Producing *Salmonella enterica* Serovar Infantis, Taiwan

Ying-Shu Liao, Hsiao-Lun Wei, Hung-Chih Kuo, Bo-Han Chen, You-Wun Wang, Ru-Hsiou Teng, Yu-Ping Hong, Jui-Hsien Chang, Shiu-Yun Liang, Chi-Sen Tsao, Chien-Shun Chiou

A CTX-M-65–producing *Salmonella enterica* serovar Infantis clone, probably originating in Latin America and initially reported in the United States, has emerged in Taiwan. Chicken meat is the most likely primary carrier. Four of the 9 drug resistance genes have integrated into the chromosome: $bla_{CTX\text{-}M\text{-}65}$, *tet(A)*, *sul1*, and *aadA1*.

Salmonella enterica serovar Infantis is one of the most common *Salmonella* serotypes (*1*); it is frequently isolated from humans and animals, particularly from poultry (*2*). An increasing incidence of *Salmonella* Infantis infections has been reported in the United States (*3*), accompanied by emergence and spread of an extended-spectrum β-lactamase CTX-M-65–producing *Salmonella* Infantis clone in humans, food animals, and retail chicken (*4*,*5*). The clone probably originated in South America because it was initially discovered in persons who had traveled back from Peru, Bolivia, Ecuador, and Chile since 2012 (*5*). Domestically acquired infections were not identified in the United States until 2014 (*5*).

This clone is characterized by having a D87Y mutation in the *gyrA* gene and carrying multiple resistance genes, including *aph(4)-Ia*, *aac(3)-IVa*, *aph(3')-Ic*, $bla_{CTX\text{-}M\text{-}65}$, *fosA3*, *floR*, *dfrA14*, *sul1*, *tet(A)*, and *aadA1*, located in 2 distinct regions of a pESI-like megaplasmid (*4*). The CTX-M-65–producing clone has been reported mostly in South America, North America, and some countries in Europe (*4*–*12*).

In Taiwan, *Salmonella* Infantis is not a common cause of human salmonellosis, accounting for only 0.61% (246/40,599) of all *Salmonella* isolates collected during 2004–2022. *Salmonella* Infantis isolates collected during 2004–2019 showed a low level of antimicrobial drug resistance (Appendix Table 1, https://wwwnc.cdc.gov/EID/article/29/8/23-0472-App1.pdf). However, in 2021, we identified that 7 of 14 *Salmonella* Infantis isolates from patients who had salmonellosis were multidrug-resistant (MDR), and in 2022, MDR strains accounted for 55% (21/38) of the *Salmonella* Infantis isolates recovered that year.

The 28 patients who contracted MDR *Salmonella* Infantis were from diverse age groups and geographic locations, and none of them had a history of international travel. During 2021 and 2022, the COVID-19 pandemic restricted travel abroad. We report a CTX-M-65–producing *Salmonella* Infantis clone in Taiwan.

The Study

We performed clustering analysis on pulsed-field gel electrophoresis (PFGE) patterns of *Salmonella* Infantis isolates, which showed that the MDR isolates recovered in 2021 and 2022 clustered closely together in a distinct group (Appendix Figure). Antimicrobial drug susceptibility testing showed that the MDR isolates had resistance to ampicillin, cefotaxime, ceftazidime, nalidixic acid, ciprofloxacin (intermediate susceptibility), gentamicin, chloramphenicol, sulfamethoxazole, trimethoprim, and tetracycline (Appendix Figure). The resistance profile closely resembled that of the widespread CTX-M-65–producing *Salmonella* Infantis clone (*5*).

We isolated *Salmonella* bacteria from retail raw chicken meat sold in 12 supermarket stores in Taichung City in 2022 to investigate the source of MDR *Salmonella* Infantis. All chicken meat samples were sourced from domestic farms. *Salmonella* bacteria were isolated from 191 (65.6%) of 291 chicken meat samples. A total of 379 *Salmonella* isolates were recovered from the 191 samples (1–2 isolates from each *Salmonella*-positive sample).

Author affiliations: Centers for Disease Control, Taichung, Taiwan (Y.-S. Liao, H.-L. Wei, B.-H. Chen, Y.-W. Wang, R.-H. Teng, Y.-P. Hong, J.-H. Chang, S.-Y. Liang, C.-S. Tsao, C.-S. Chiou); National Chiayi University, Chiayi, Taiwan (H.-C. Kuo)

DOI: https://doi.org/10.3201/eid2908.230472

Of the 379 isolates, 68.1% (258) were identified to be *Salmonella* Infantis, followed by *Salmonella* Kentucky (17.2%), *Salmonella* Brancaster (2.6%), *Salmonella* Goldcoast (2.6%), *Salmonella* Agona (2.4%), *Salmonella* Enteritidis (2.1%), and 6 other serovars (5.0%). Of the 191 samples, 11% were found to be contaminated with

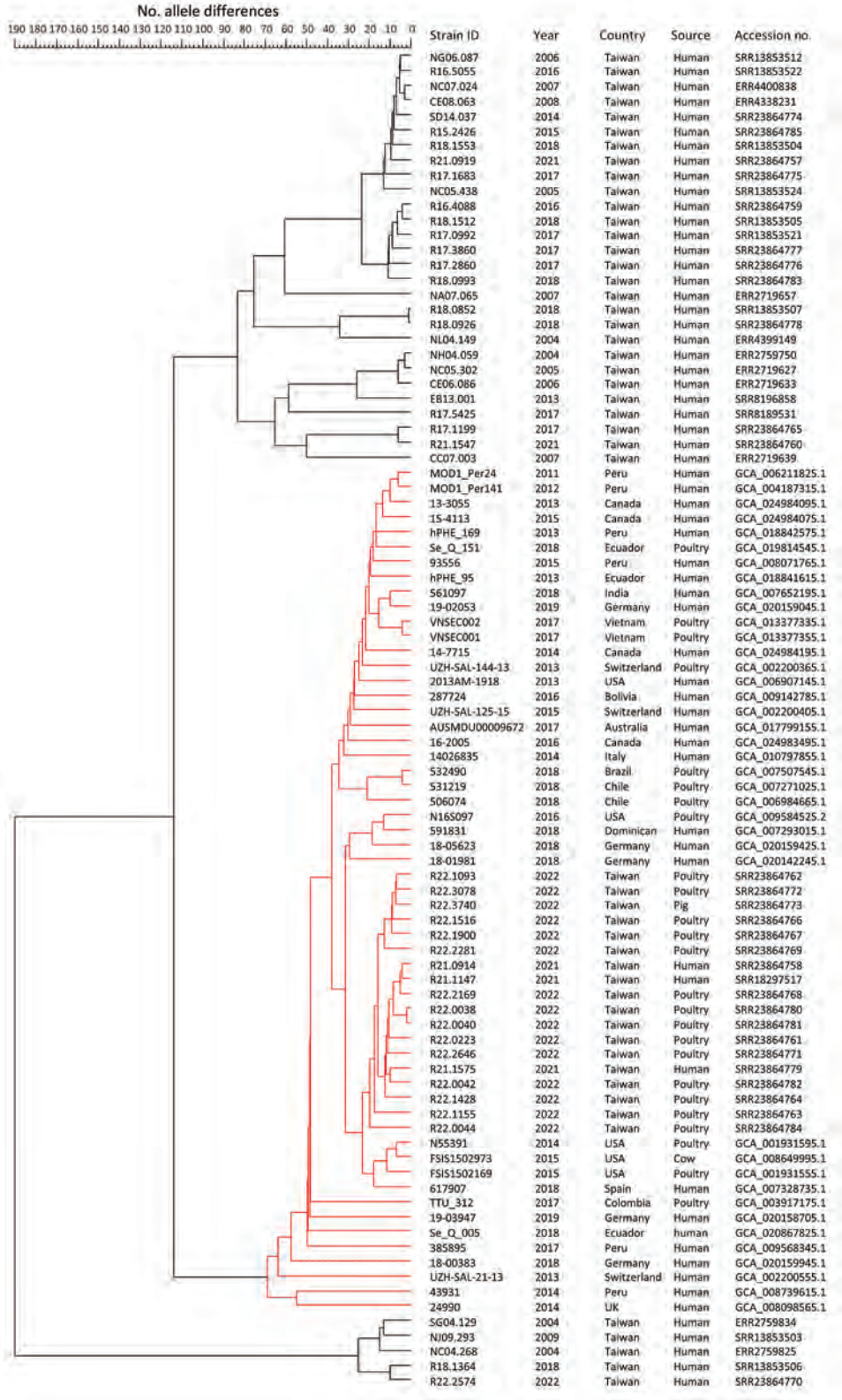

Figure 1. Core genome multilocus sequence typing tree and relevant information for investigation of chromosome-borne CTX-M-65 extended-spectrum β-lactamase–producing *Salmonella enterica* serovar Infantis, Taiwan. The cluster highlighted in red consists of $bla_{\text{CTX-M-65}}$–carrying strains. GenBank accession numbers are shown. ID, identification.

a mixture of *Salmonella* serovars. The 258 *Salmonella* Infantis isolates had 28 PFGE patterns, among which the 6 most common patterns were also observed in the MDR isolates from humans (Appendix Table 2). We performed a clustering analysis of PFGE profiles, which showed that the 258 *Salmonella* Infantis isolates from chicken meat, 28 MDR isolates from humans, and 1 isolate from a diseased pig recovered in 2022, were grouped in a common cluster (data not shown).

We conducted whole-genome sequencing of 51 *Salmonella* Infantis isolates from humans, chickens, and a pig by using the Illumina sequencing platform (https://www.illumina.com) to investigate drug resistance genetic determinants, plasmid incompatibility types, and their genetic relationships. Our analysis showed that all 51 *Salmonella* Infantis isolates belonged to sequence type 32, and 18 MDR *Salmonella* Infantis isolates recovered from humans, chickens, and a pig in 2021 and 2022 had a D87Y mutation in *gyrA*, along with an IncFIB plasmid and 4 common resistance genes: *aadA1*, $bla_{CTX-M-65}$, *sul1*, and *tet(A)* (Appendix Table 3). In addition, 15 of the 18 $bla_{CTX-M-65}$–carrying isolates had 5 other drug resistance genes: *aac(3)-IVa*, *aph(3')-Ia*, *aph(4)-Ia*, *dfrA14*, and *floR*. Two of the isolates had 4 of the 5 drug resistance genes, and 1 did not have any of the 5 genes.

We conducted clustering analysis of core genome multilocus sequence typing profiles, which showed that the $bla_{CTX-M-65}$–carrying isolates from Taiwan, when compared with non–$bla_{CTX-M-65}$–carrying strains, showed a closer genetic relationship with $bla_{CTX-M-65}$–carrying strains reported in North and South America, Europe, Australia, India, and Vietnam (Figure 1).

To investigate the location of drug resistance genes, we performed additional sequencing of 6 $bla_{CTX-M-65}$–carrying isolates and 1 pan-susceptible isolate by using the Oxford nanopore sequencing platform (https://nanoporetech.com). This approach provided long sequence reads, enabling us to assemble complete genome sequences. Our analysis showed that all 6 $bla_{CTX-M-65}$–carrying isolates from humans, chickens, and a pig had 5 drug resistance genes, *aac(3)-IVa*, *aph(3')-Ia*, *aph(4)-Ia*, *dfrA14*, and *floR*, within an ≈195-kb IncFIB plasmid. In contrast, *aadA1*, $bla_{CTX-M-65}$, *sul1*, and *tet(A)* were found in an ≈126-kb DNA segment inserted within an ABC-F family ATPase gene in the chromosomes (Appendix Tables 4, 5).

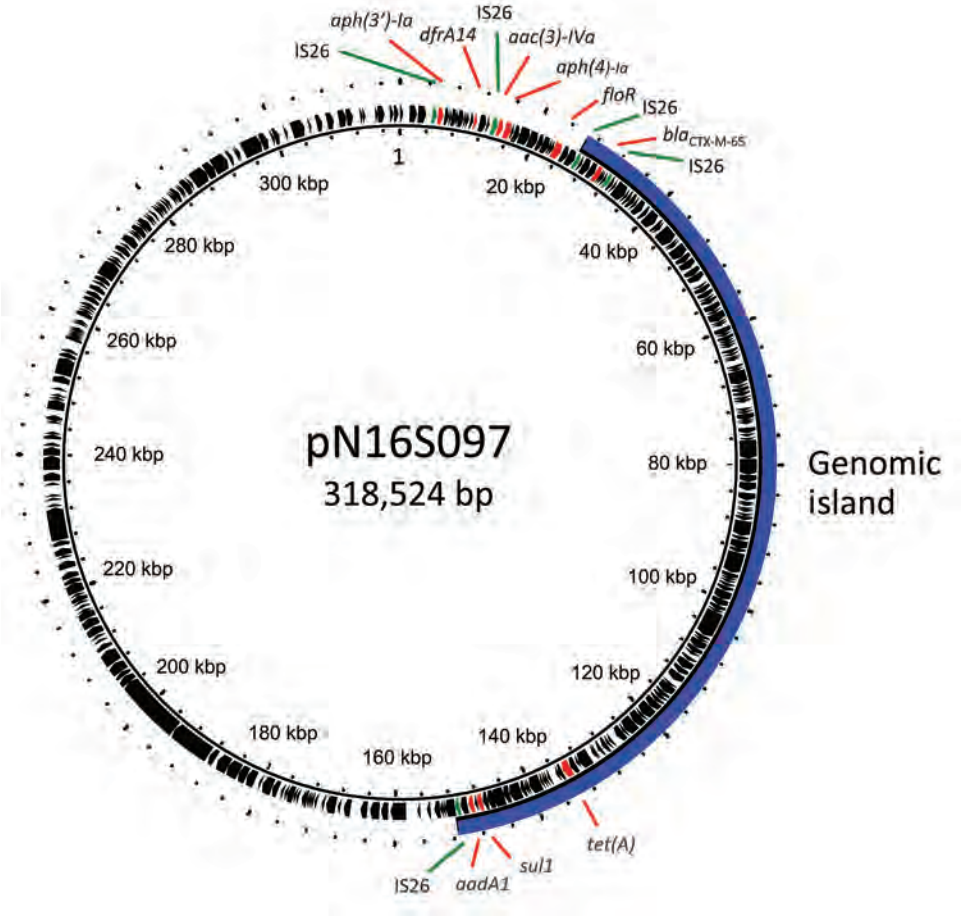

Figure 2. Genetic map of plasmid pN16S097 from investigation of chromosome-borne CTX-M-65 extended-spectrum β-lactamase–producing *Salmonella enterica* serovar Infantis, Taiwan. The locations of antimicrobial drug resistance genes and insertion sequence IS26 are indicated. A 125-kb segment, depicted by a blue solid arc, is translocated into the chromosomes of $bla_{CTX-M-65}$–carrying *Salmonella* Infantis strains emerging in Taiwan.

Our investigation suggested that the 195-kb IncFIB plasmids and the 126-kb genomic islands found in the chromosome probably originated from a plasmid similar to pN16S097. This megaplasmid, which has a length of 318,524 bp, was initially detected in a *Salmonella* Infantis strain and has 9 of the mentioned drug resistance genes in 2 distinct regions (*8*).

We hypothesize that the 126-kb segment carrying *aadA1*, $bla_{\text{CTX-M-65}}$, *sul1*, and *tet(A)* might have translocated from a pN16S097-like plasmid into a chromosome through IS26-mediated transposition, resulting in formation of an 8-bp (CCGGAAAG) tandem repeat at the insertion site. This process led to the loss of the megaplasmid, leaving a plasmid of ≈195 kb (Figure 2). Upon analyzing 5,253 genomes of $bla_{\text{CTX-M-65}}$–carrying *Salmonella* Infantis strains available in GenBank, we did not observe a large DNA segment or a $bla_{\text{CTX-M-65}}$–carrying segment inserted within an ABC-F family ATPase gene in the chromosomes.

Conclusions

The $bla_{\text{CTX-M-65}}$–carrying *Salmonella* Infantis clone, previously identified in South and North America and some countries in Europe, has been detected in Taiwan. Chickens are suspected to be the primary source of $bla_{\text{CTX-M-65}}$–carrying strains. Many PFGE genotypes have been found among the isolates from retail chicken meat, indicating that the $bla_{\text{CTX-M-65}}$–carrying *Salmonella* Infantis strains have probably evolved and proliferated on chicken farms, rather than being contaminants from chicken processing plants. Integration of $bla_{\text{CTX-M-65}}$ into the chromosome suggests that this drug resistance gene might be more resiliently maintained within the strains.

This study was supported by the Ministry of Health and Welfare, Taiwan (grant no. MOHW111-CDC-C-315-124306).

About the Author

Ms. Liao is a senior technical specialist at the Centers for Disease Control, Ministry of Health and Welfare, Taichung, Taiwan. Her primary research interests are molecular epidemiology and antimicrobial drug resistance of foodborne bacterial pathogens.

References

1. Hendriksen RS, Vieira AR, Karlsmose S, Lo Fo Wong DM, Jensen AB, Wegener HC, et al. Global monitoring of *Salmonella* serovar distribution from the World Health Organization Global Foodborne Infections Network Country Data Bank: results of quality assured laboratories from 2001 to 2007. Foodborne Pathog Dis. 2011;8:887–900. https://doi.org/10.1089/fpd.2010.0787
2. European Food Safety A, European Centre for Disease P, Control. The European Union One Health 2021 Zoonoses Report. EFSA J. 2022;20:e07666. https://doi.org/10.2903/j.efsa.2022.7666
3. Collins JP, Shah HJ, Weller DL, Ray LC, Smith K, McGuire S, et al. Preliminary incidence and trends of infections caused by pathogens transmitted commonly through food—Foodborne Diseases Active Surveillance Network, 10 U.S. Sites, 2016–2021. MMWR Morb Mortal Wkly Rep. 2022;71:1260–4. https://doi.org/10.15585/mmwr.mm7140a2
4. Tate H, Folster JP, Hsu CH, Chen J, Hoffmann M, Li C, et al. Comparative analysis of extended-spectrum-β-lactamase CTX-M-65-producing *Salmonella enterica* serovar Infantis isolates from humans, food animals, and retail chickens in the United States. Antimicrob Agents Chemother. 2017;61:e00488–17. https://doi.org/10.1128/AAC.00488-17
5. Brown AC, Chen JC, Watkins LK, Campbell D, Folster JP, Tate H, et al. CTX-M-65 extended-spectrum β-lactamase-producing *Salmonella enterica* serotype Infantis, United States. Emerg Infect Dis. 2018;24:2284–91. https://doi.org/10.3201/eid2412.180500
6. Franco A, Leekitcharoenphon P, Feltrin F, Alba P, Cordaro G, Iurescia M, et al. Emergence of a clonal lineage of multidrug-resistant ESBL-producing *Salmonella* Infantis transmitted from broilers and broiler meat to humans in Italy between 2011 and 2014. PLoS One. 2015;10:e0144802. https://doi.org/10.1371/journal.pone.0144802
7. Hindermann D, Gopinath G, Chase H, Negrete F, Althaus D, Zurfluh K, et al. *Salmonella enterica* serovar Infantis from food and human infections, Switzerland, 2010–2015: poultry-related multidrug resistant clones and an emerging ESBL producing clonal lineage. Front Microbiol. 2017;8:1322. https://doi.org/10.3389/fmicb.2017.01322
8. Tyson GH, Li C, Harrison LB, Martin G, Hsu CH, Tate H, et al. A multidrug-resistant *Salmonella* Infantis clone is spreading and recombining in the United States. Microb Drug Resist. 2021;27:792–9. https://doi.org/10.1089/mdr.2020.0389
9. Bharat A, Mataseje L, Parmley EJ, Avery BP, Cox G, Carson CA, et al. One health genomic analysis of extended-spectrum β-lactamase–producing *Salmonella enterica*, Canada, 2012–2016. Emerg Infect Dis. 2022;28:1410–20. https://doi.org/10.3201/eid2807.211528
10. Lee WW, Mattock J, Greig DR, Langridge GC, Baker D, Bloomfield S, et al. Characterization of a pESI-like plasmid and analysis of multidrug-resistant *Salmonella enterica* Infantis isolates in England and Wales. Microb Genom. 2021;7:000658. https://doi.org/10.1099/mgen.0.000658
11. Pietsch M, Simon S, Meinen A, Trost E, Banerji S, Pfeifer Y, et al. Third generation cephalosporin resistance in clinical non-typhoidal *Salmonella enterica* in Germany and emergence of $bla_{\text{CTX-M}}$-harbouring pESI plasmids. Microb Genom. 2021;7:000698. https://doi.org/10.1099/mgen.0.000698
12. Mejía L, Medina JL, Bayas R, Salazar CS, Villavicencio F, Zapata S, et al. Genomic epidemiology of *Salmonella* Infantis in Ecuador: from poultry farms to human infections. Front Vet Sci. 2020;7:547891. https://doi.org/10.3389/fvets.2020.547891

Address for correspondence: Chien-Shun Chiou, Central Region Laboratory, Center for Diagnostics and Vaccine Development, Centers for Disease Control, Taichung 40855, Taiwan; email: nipmcsc@cdc.gov.tw

Increase of Severe Pulmonary Infections in Adults Caused by $M1_{UK}$ *Streptococcus pyogenes*, Central Scotland, UK

Peter J.B. Davies, Clark D. Russell, Anna-Rose Morgan, Surabhi K. Taori, Diane Lindsay, Roisin Ure, Derek Brown, Andrew Smith

We characterized the epidemiology, host–pathogen characteristics, and outcomes of severe adult pulmonary *Streptococcus pyogenes* infections that coincided with a high community caseload in central Scotland, UK. The pulmonary infections had high illness and death rates and were associated with socioeconomic deprivation, influenza A co-infection, and the $M1_{UK}$ lineage of *S. pyogenes*.

The association between respiratory viruses and secondary invasive pulmonary bacterial disease is recognized, but the proportion of pulmonary invasive group A *Streptococcus* (PiGAS) infections after seasonal influenza is low compared with those for other bacterial pathogens (e.g., *Streptococcus pneumoniae*, *Haemophilus influenzae*, and *Staphylococcus aureus*) (*1*,*2*). However, PiGAS has been shown to complicate epidemics of measles and, notably, the 1918–1919 influenza pandemic (*3*).

Winter 2022–23 saw a marked increase in influenza and associated group A *Streptococcus* (GAS) infections in the United Kingdom as well as globally (https://www.gov.uk/government/publications/group-a-streptococcal-infections-activity-during-the-2022-to-2023-season/group-a-streptococcal-infections-second-update-on-seasonal-activity-in-england-2022-to-2023). In autumn 2022, an unusually high number of pediatric GAS pleural empyema cases associated with human metapneumovirus co-infection was described in Scotland (*4*). After similar cases were observed in adults, we aimed to characterize the burden of PiGAS in adults and contrast it to published and local historical data.

Author affiliations: Glasgow Royal Infirmary, Glasgow, Scotland, UK (P.J.B. Davies, D. Lindsay, R. Ure, D. Brown A. Smith); University of Edinburgh, Edinburgh, Scotland, UK (C.D. Russell); Royal Infirmary of Edinburgh, Edinburgh (C.D. Russell, S.B. Taori); Queen Elizabeth University Hospital, Glasgow (A,-R. Morgan); University of Glasgow, Glasgow (A. Smith)

DOI: https://doi.org/10.3201/eid2908.230569

The Study

We identified patients with pulmonary samples or blood cultures found positive for *S. pyogenes* by the National Health Service (NHS) of Greater Glasgow and Clyde (GGC), which serves a population of 1.4 million, during December 1, 2017–November 31, 2022, through the Laboratory Information Management System. We identified the same specimens from NHS Lothian (population 850,000) and GGC during December 1, 2022–February 28, 2023 (https://www.nrscotland.gov.uk/statistics-and-data/statistics/statistics-by-theme/population/population-estimates/mid-year-population-estimates/mid-2021).

Samples assessed were sputum (inpatient), pleural fluid, endotracheal aspirate, bronchoalveolar lavage pulmonary tissue (postmortem), and blood cultures. We also identified *S. pyogenes* by molecular techniques (i.e., specific GAS PCR testing and 16s PCR). We defined cases as definite or probable PiGAS. A definite case required microbiologic criteria (e.g., *S. pyogenes* identified in blood or deep respiratory or pleural sample) and radiologic criteria (e.g., multifocal consolidation or pleural effusion or empyema or parenchymal necrosis) to be present. Probable cases were those with sputum samples in the microbiologic criteria and unifocal consolidation in the radiologic criteria, capturing patients meeting both criteria but not those of a definite case.

We extracted demographic, clinical, and laboratory data from electronic patient records. We derived Scottish Index of Multiple Deprivation (SIMD) scores by using postcodes. We also calculated Charlson comorbidity index scores. We referred *S. pyogenes*

isolates to the Scottish Microbiology Reference Laboratory for M-typing and Illumina short read sequencing (*5*). We used an annotated whole genome–core genome multilocus sequence typing approach to compare isolate sequence data with a publicly available core genome multilocus sequence typing scheme implemented in Ridom SeqSphere+ version 8.5.1 (http://www.ridom.de/seqsphere), enabling assignment to the M1 lineages described in the European Nucleotide Archive (*5*,*6*). Currently, >200 recorded M-types are used to identify outbreaks and determine cluster management; M1 is most commonly associated with invasive disease (*7*).

NHS GGC and Lothian provides public healthcare for ≈39% of Scotland's population of 5.49 million (https://www.nrscotland.gov.uk/statistics-and-data/statistics/statistics-by-theme/population/population-estimates/mid-year-population-estimates/mid-2021). Like other countries, the United Kingdom is undergoing a resurgence of *S. pyogenes* infections that began in September 2022 (https://www.who.int/emergencies/disease-outbreak-news/item/2022-DON429). We identified 38 patients with PiGAS (30 definite, 8 probable) in the 3-month study period (22 in GGC, 16 in Lothian). In the previous 5-year period in GGC, we identified 15 cases (12 definite, 3 probable, 1 metastatic) (Figure 1).

We observed no significant difference in the median age between the 2022–23 cohort and historical records (45 [interquartile range (IQR) 26] years) vs. 57 [IQR 23.5] years). Both groups were healthy at baseline, having a median Charlson comorbidity index score of 0. We noted no significant difference in chronic respiratory underlying conditions. The 2022–23 cohort was associated with a more deprived SIMD postcode (median SIMD score of 3 vs. 5 for historical records). Other demographic, biochemical, and hematologic characteristics were comparable (Table). The PiGAS syndrome exhibits substantial leukopenia (median 0.53 [IQR 0.3–1] × 10^9 cells/L) with a normal median white cell count (9.5 [IQR 4–18.7] × 10^9 cells/L). Although respiratory symptoms predominated, diarrhea was reported in 18.4% (7/38) of cases in the 2022–23 outbreak. Microbiologically confirmed empyema was common, and a greater number of 2022–23 patients received an intercostal drain and exhibited radiologic evidence of empyema or pleural effusion (Table). Those characteristics, along with multifocal consolidation, were the radiologic hallmarks of PiGAS; cavitation also was common. A lower proportion of patients in the historical cohort had chest computed tomography results, precluding greater sensitivity (47% vs. 76%).

During 2017–2022, co-infecting respiratory viruses were varied, but in 2022–23, most patients tested positive for influenza A (Table; Figure 2). Only half of patients underwent an extended respiratory viral screen. Of typed *S. pyogenes* isolates from the current outbreak, 24/25 belonged to the $M1_{UK}$ lineage, contrasting with the historical cohort that involved a mixture of M types (M1, M12, M3.93, M44, and M5.23).

Conclusions

Europe is experiencing an increased incidence of invasive GAS disease (*4*). We report an unusually high incidence of severe PiGAS in adults from central Scotland. We also note an additional strong association with influenza A co-infection and the near-complete dominance of $M1_{UK}$, contrasting with local and published precedent. M1 comprised 38% of adult and 58% of pediatric invasive GAS referrals in England during 2022–23, in contrast to the 96% we report (https://www.gov.uk/government/publications/group-a-streptococcal-infections-activity-during-the-2022-to-2023-season/group-a-streptococcal-infections-second-update-on-seasonal-activity-

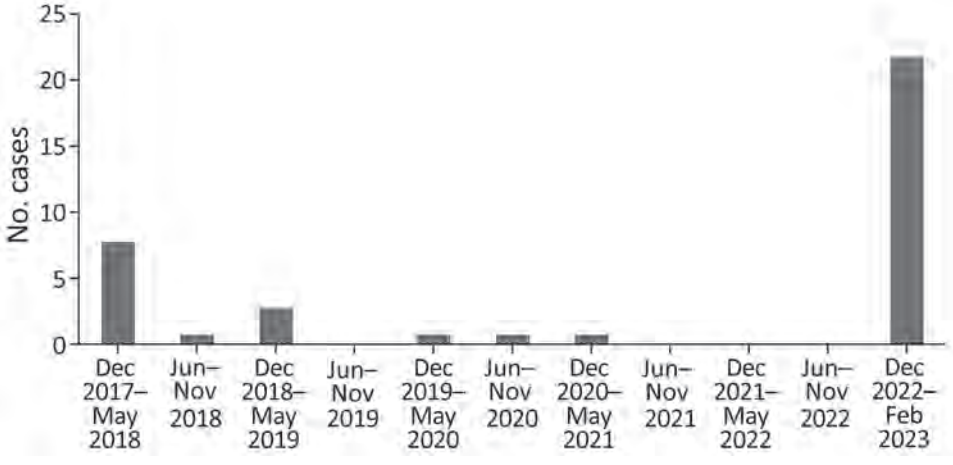

Figure 1. Monthly incidence of pulmonary invasive group A *Streptococcus* infections in adults ≥18 years of age, National Health Service Greater Glasgow and Clyde region, central Scotland, UK, December 2017–February 2023.

Table. Characteristics associated with a historical cohort (2017–2022) and a recent epidemic of severe pulmonary infections in adults (2022–23) caused by *Streptococcus pyogenes*, central Scotland, UK*

Characteristic	2017–2022, GGC only	2022–2023, GGC and Lothian
Demographic		
Total no. PiGAS cases	15	38
Median age, y (IQR)	57 (42.5–66)	45 (37–63)
Sex, no (%)		
M	13 (87)	20 (53)
F	2 (6)	18 (47)
Median SIMD score (IQR)	5 (3.5)	3 (1–5)
Blood parameters at admission		
Median C-reactive protein, mg/L (IQR)†	293 (198–360)	328 (172–410)
Median leukocyte count, $\times 10^9$ cells/L (IQR)‡	9.5 (3.1–13.7)	9.45 (4.1–22.1)
Median lymphocyte count, $\times 10^9$ cells/L (IQR)§	0.5 (0.3–0.7)	0.54 (0.31–1.35)
Radiographic, no. (%)		
Pleural effusion	8 (53)	23 (61)
Focal consolidation	3 (20)	9 (24)
Multifocal consolidation	11 (73)	28 (74)
Cavitation or necrosis	2 (13)	7 (18)
Background		
Chronic respiratory disease, no (%)	7 (47)	9 (24)
Smoker, no (%)	2 (13)	10 (26)
No past medical history, no (%)	4 (26.7)	17 (44.7)
Median CCI score (IQR)	0 (0–3)	0 (0–3)
Viral co-infection		
No. tested	12	33
Influenza A	1	19
Influenza B	3	0
Parainfluenza 1	1	0
Metapneumovirus	2	4
RSV	0	1
Adenovirus	0	1
None detected	5	8
Outcomes		
ICU admission, no (%)	8 (53)	21 (55)
Median ICU length of stay, d (IQR)	5 (2–9.8)	15 (3.5–27)
Vasopressors, no. (%)	4 (26)	15 (39)
Invasive mechanical ventilation, no. (%)	7 (46)	16 (42)
Death, no (%)	3 (20)	6 (16)
Median days from admission to death (IQR)	1 (1–2)	1 (0–2)
M type		
No. typed	8	25
1.0	3	24
12.0	1	1
3.93	1	0
44.0	1	0
5.23	2	0

*Historical cohort comprises cases identified among the population served by NHS Greater Glasgow and Clyde; cases from the recent epidemic are those identified among populations served by NHS Greater Glasgow and Clyde and NHS Lothian. CCI, Charlson comorbidity index; ICU, intensive care unit; IQR, interquartile range; NHS, National Health Service; PiGAS, pulmonary invasive group A *Streptococcus*; RSV, respiratory syncytial virus; SIMD, Scottish Index of Multiple Deprivation.
†Reference range ≤5 mg/L.
‡Reference range 4–10 $\times 10^9$ cells/L.
§Reference range 1.1–5.0 $\times 10^9$ cells/L.

in-england-2022-to-2023). The clinical phenotype of severe, often rapidly fatal PiGAS disease in young healthy adults parallels outbreaks described around World War I and in institutional facilities (*3*,*8*). The $M1_{UK}$ lineage is emerging as a dominant lineage within M1 worldwide and often associated with invasive GAS (*9*–*12*).

The pathophysiology of PiGAS after a respiratory viral infection (influenza A in our cohort) is incompletely understood. In vitro and in vivo studies suggest prior influenza A infection increases both GAS adherence and internalization by binding to viral hyaluronic acid on the infected host cell surface, which is followed by increases in the abundance of, and access to, bacterial receptors and the GAS ligands fibrinogen and fibronectin (*13*). Influenza B is also implicated, both in the literature and locally during 2017–2018 (*14*).

M1 has an established association with severe disease (*7*). In particular, the $M1_{UK}$ strain appears to have an enhanced capability for transmission and virulence and is now the predominant strain in the

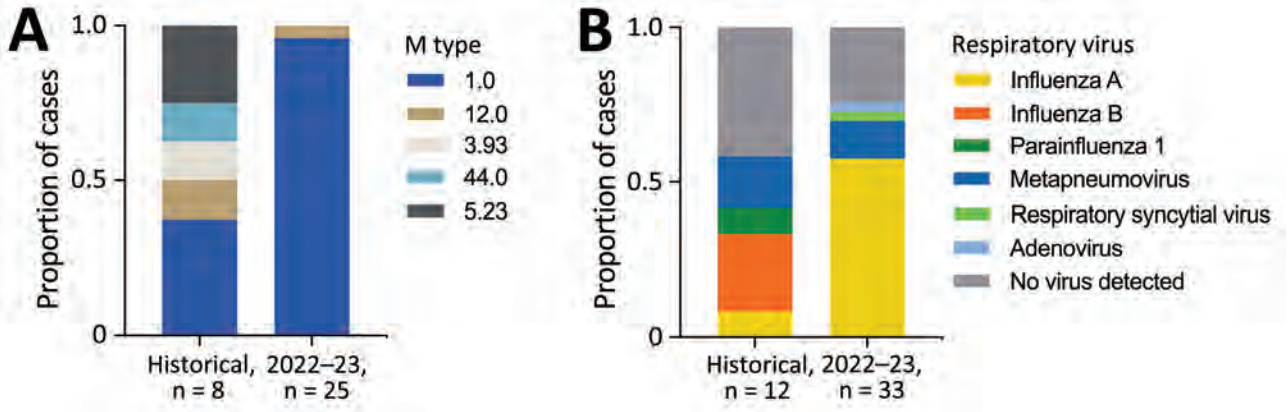

Figure 2. Microbiologic features of pulmonary invasive group A *Streptococcus* infections, central Scotland, UK, December 2017–February 2023. A) *Streptococcus pyogenes* isolate M type results, where available, comparing historical data (December 2017–November 2022) with 2022–23 cohort (December 2022–February 2023). B) Results of respiratory virus testing, where available, comparing historical data with 2022–23 cohort.

United Kingdom (*6*). This strain exhibits a hypervirulent phenotype because of greater expression of streptococcal pyrogenic exotoxin A than global M1 strains. Case reports of severe rapidly fatal M1 PiGAS in young healthy patients echo outcomes seen in our cohort (*15*).

Modern molecular techniques have revolutionized our ability to investigate patterns of disease (e.g., widespread availability of rapid point-of-care tests for COVID-19 and influenza). We are experiencing a major outbreak of *S. pyogenes* infections with an unusual predilection for severe pulmonary disease in addition to the usual manifestations of disease by this pathogen, including distinctive viral and M-type associations in the winter and spring of 2022–23. The PiGAS phenotype we describe is similar to those from more sporadic reports identified from a review of published case series of severe pulmonary infections from *S. pyogenes* (Appendix, https://wwwnc.cdc.gov/EID/article/29/8/23-0569-App1.pdf). Historical outbreaks probably underreported coexistent viral infections because of a lack of accessible point-of-care tests. Similarly, only half of patients had an extended viral respiratory screen, and we therefore risk underreporting metapneumovirus cases, an agent notable locally in GAS empyema in children immediately before December 2022 (*4*). Although our cohort is small, it is comparatively large compared with the few described in the literature and notable for the short timeframe of cases captured.

Our study highlights a new aggressive pattern of *S. pyogenes* infections linked to the dominant circulating M1$_{UK}$ strain, manifesting as severe pulmonary disease and having a strong association with influenza A co-infection. Clinicians and public health officials need to be vigilant of such clinical manifestations while rates of iGAS remain high.

Acknowledgments

We thank Pota Kalima for searching our Laboratory Information Management System to identify *S. pyogenes* specimens. We also thank Jörg Rothgänger for his assistance in preparing the core genome multilocus sequence typing scheme for use in SeqSphere+.

About the Author

Dr. Davies is an infectious diseases and microbiology specialist trainee at the National Health Service Greater Glasgow and Clyde in Scotland. His primary research interests are GAS disease and microbiology diagnostic pathways.

References

1. Chertow DS, Memoli MJ. Bacterial coinfection in influenza: a grand rounds review. JAMA. 2013;309:275–82. https://doi.org/10.1001/jama.2012.194139
2. Morris DE, Cleary DW, Clarke SC. Secondary bacterial infections associated with influenza pandemics. Front Microbiol. 2017;8:1041. https://doi.org/10.3389/fmicb.2017.01041
3. Morens DM, Taubenberger JK. A forgotten epidemic that changed medicine: measles in the US Army, 1917–18. Lancet Infect Dis. 2015;15:852–61. https://doi.org/10.1016/S1473-3099(15)00109-7
4. Holdstock V, Twynam-Perkins J, Bradnock T, Dickson EM, Harvey-Wood K, Kalima P, et al. National case series of group A streptococcus pleural empyema in children: clinical and microbiological features. Lancet Infect Dis. 2023;23:154–6. https://doi.org/10.1016/S1473-3099(23)00008-7
5. Friães A, Mamede R, Ferreira M, Melo-Cristino J, Ramirez M. Annotated whole-genome multilocus sequence typing schema for scalable high-resolution typing

of *Streptococcus pyogenes*. J Clin Microbiol. 2022;60:e0031522. https://doi.org/10.1128/jcm.00315-22
6. Zhi X, Li HK, Li H, Loboda Z, Charles S, Vieira A, et al. Emerging invasive group A *Streptococcus* $M1_{UK}$ lineage detected by allele-specific PCR, England, 2020. Emerg Infect Dis. 2023;29:1007–10. https://doi.org/10.3201/eid2905.221887
7. Lindsay DSJ, Brown AW, Scott KJ, Denham B, Thom L, Rundell G, et al. Circulating *emm* types of *Streptococcus pyogenes* in Scotland: 2011–2015. J Med Microbiol. 2016;65:1229–31. https://doi.org/10.1099/jmm.0.000335
8. Crum NF, Russell KL, Kaplan EL, Wallace MR, Wu J, Ashtari P, et al. Pneumonia outbreak associated with group A *Streptococcus* species at a military training facility. Clin Infect Dis. 2005;40:511–8. https://doi.org/10.1086/427502
9. Rümke LW, de Gier B, Vestjens SMT, van der Ende A, van Sorge NM, Vlaminckx BJM, et al. Dominance of $M1_{UK}$ clade among Dutch M1 *Streptococcus pyogenes*. Lancet Infect Dis. 2020;20:539–40. https://doi.org/10.1016/S1473-3099(20)30278-4
10. Davies MR, Keller N, Brouwer S, Jespersen MG, Cork AJ, Hayes AJ, et al. Detection of *Streptococcus pyogenes* $M1_{UK}$ in Australia and characterization of the mutation driving enhanced expression of superantigen SpeA. Nat Commun. 2023;14:1051. https://doi.org/10.1038/s41467-023-36717-4
11. Li Y, Nanduri SA, Van Beneden CA, Beall BW. $M1_{UK}$ lineage in invasive group A streptococcus isolates from the USA. Lancet Infect Dis. 2020;20:538–9. https://doi.org/10.1016/S1473-3099(20)30279-6
12. Demczuk W, Martin I, Domingo FR, MacDonald D, Mulvey MR. Identification of *Streptococcus pyogenes* $M1_{UK}$ clone in Canada. Lancet Infect Dis. 2019;19:1284–5. https://doi.org/10.1016/S1473-3099(19)30622-X
13. Herrera AL, Huber VC, Chaussee MS. The association between invasive group A streptococcal diseases and viral respiratory tract infections. Front Microbiol. 2016;7:342. https://doi.org/10.3389/fmicb.2016.00342
14. Aebi T, Weisser M, Bucher E, Hirsch HH, Marsch S, Siegemund M. Co-infection of influenza B and streptococci causing severe pneumonia and septic shock in healthy women. BMC Infect Dis. 2010;10:308. https://doi.org/10.1186/1471-2334-10-308
15. Santagati M, Spanu T, Scillato M, Santangelo R, Cavallaro F, Arena V, et al. Rapidly fatal hemorrhagic pneumonia and group A *Streptococcus* serotype M1. Emerg Infect Dis. 2014;20:98–101. https://doi.org/10.3201/eid2001.130233

Address for correspondence: Peter Davies, Infectious Diseases Department, Queen Elizabeth University Hospital, 1345 Govan Rd, Glasgow, Scotland G51 4TF, UK; email: peter.davies2@nhs.scot

Dengue Outbreak Response during COVID-19 Pandemic, Key Largo, Florida, USA, 2020

Devin Rowe, Catherine McDermott, Ysla Veliz, Alison Kerr, Mark Whiteside, Mikki Coss, Chad Huff, Andrea Leal, Edgar Kopp, Alexis LaCrue, Lea A. Heberlein, Laura E. Adams, Gilberto A. Santiago, Jorge L. Munoz-Jordan, Gabriela Paz-Bailey, Andrea M. Morrison; Florida Department of Health Dengue Investigation Team[1]

We report a dengue outbreak in Key Largo, Florida, USA, from February through August 2020, during the COVID-19 pandemic. Successful community engagement resulted in 61% of case-patients self-reporting. We also describe COVID-19 pandemic effects on the dengue outbreak investigation and the need to increase clinician awareness of dengue testing recommendations.

Dengue, an arboviral disease caused by dengue viruses 1–4 (DENV-1–4), is transmitted by *Aedes aegypti* mosquitoes (*1*). Before 1935, dengue was endemic in Florida, USA (*2*); however, no locally acquired cases were reported until an outbreak in Key West during 2009–2010 (*3*). Since then, at least 1 locally transmitted DENV infection has been reported annually in Florida except for 2017 and 2021 (*2*). Because Florida is vulnerable to establishment of *Ae. aegypti*–vectored viruses such as dengue, chikungunya, and Zika (*4*,*5*), surveillance is crucial to detect pathogen introduction.

During the COVID-19 pandemic, detecting the cause for other febrile illnesses was challenging (*6*) and reluctance to seek medical care during the pandemic was reported (*7*). We report the response to a dengue outbreak in Florida during the COVID-19 pandemic in 2020.

Author affiliations: Florida Department of Health, Tallahassee, Florida, USA (D. Rowe, C. McDermott, Y. Veliz, A. Kerr, M. Whiteside, E. Kopp, A. LaCrue, L.A. Heberlein, A.M. Morrison); Florida Keys Mosquito Control District, Marathon, Florida, USA (M. Coss, C. Huff, A. Leal); Centers for Disease Control and Prevention, San Juan, Puerto Rico, USA (L.E. Adams, G.A. Santiago, J.L. Munoz-Jordan, G. Paz-Bailey)

DOI: https://doi.org/10.3201/eid2908.221856

The Study

On February 28, 2020, the Florida Department of Health (FDOH) was notified of a possible locally acquired dengue case in a non-Florida resident who was visiting Key Largo; the case-patient had symptom onset on February 18. After confirming DENV-1 infection, FDOH issued a countywide public health mosquitoborne illness advisory for Monroe County on March 9 (Figure 1). During that same month, the governor of Florida issued a statewide public health emergency declaration for the COVID-19 pandemic (*8*). By the end of March, public access to nonessential businesses and facilities was further restricted in Monroe County because of increased COVID-19 case numbers (*9*). Additional locally acquired dengue cases were not identified until June 16, when several concerned Key Largo residents called FDOH reporting suspected dengue illness. A mosquitoborne illness alert was subsequently issued for the county after 8 local dengue cases were confirmed.

FDOH notified the Florida Keys Mosquito Control District (FKMCD) of possible mosquito exposure locations for suspected cases during the 2-week incubation period through the potential 1-week viremic period after symptom onset. FKMCD enhanced aerial and truck spraying and canvassed neighborhoods to conduct vector surveillance, remove or treat mosquito larval habitats, and provide mosquito control education.

While also responding to COVID-19, FDOH fielded hotline calls for residents reporting dengue-like illness, interviewed suspected case-patients, conducted site visits, provided frequent healthcare

[1]Members of the team are listed at the end of this article.

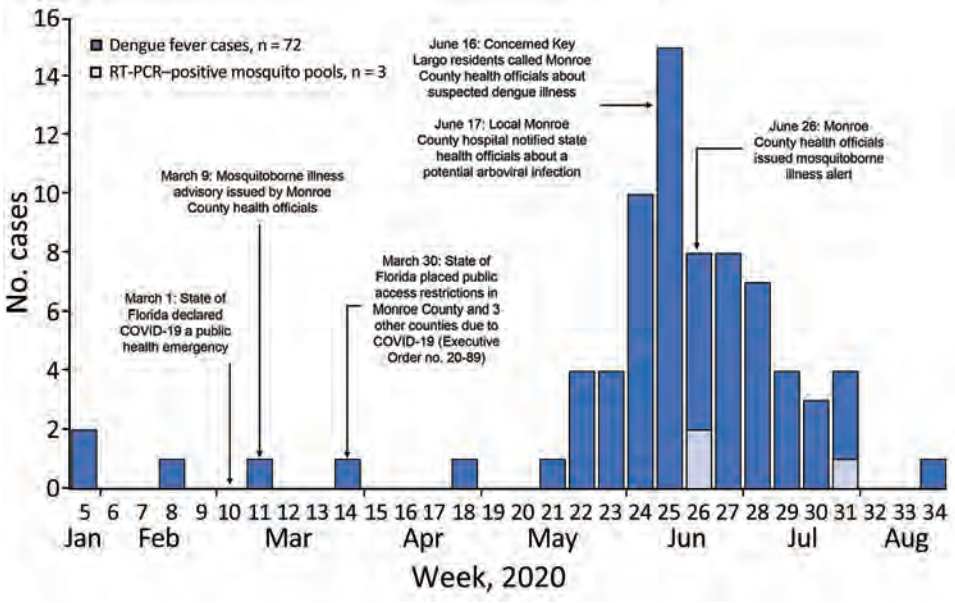

Figure 1. Timeline of dengue outbreak response during COVID-19 pandemic, Key Largo, Florida, USA, 2020. Timeline shows number of dengue cases, dengue virus RT-PCR–positive mosquito pools, and events per week during January 26–August 20, 2020. RT-PCR, reverse transcription PCR.

provider and community outreach, collected serum samples for DENV testing, and promptly provided updates to FKMCD and local media. Persons with suspected dengue were asked to provide contact information for other persons who shared mosquito exposure risks, such as persons from the same household, workplace, or outdoor events. FDOH reached out to contacts and offered DENV testing if they reported a recent unexplained febrile illness. Ethics approval was not required because the activities conducted were part of standard public health outbreak surveillance and response.

Table. Characteristics of case-patients in a dengue outbreak during the COVID-19 pandemic, Key Largo, Florida, USA, 2020*

Characteristics	No. (%) cases, n = 72
Sex	
F	37 (51)
M	35 (49)
Ethnicity	
Non-Hispanic	60 (83)
Hispanic	10 (14)
Unknown	2 (3)
Age group, y	
0–20	8 (11)
21–40	9 (13)
41–60	38 (53)
>60	17 (24)
Hospitalization status	
Hospitalized	8 (11)
Not hospitalized	62 (86)
Unknown	2 (3)
Laboratory test results†	
Positive RT-PCR	31 (43)
Positive IgM only	41 (57)
Tests ordered for acute dengue cases, n = 43‡	
COVID-19 tests; no known DENV tests	25 (58)
DENV and COVID-19 tests	13 (30)
DENV only; no COVID-19 tests	3 (7)
No DENV or COVID-19 tests	2 (5)

*DENV, dengue virus; RT-PCR, reverse transcription PCR.
†Samples for PCR collected 1–12 days after symptom onset; samples for IgM collected 5–213 days after symptom onset.
‡Acute cases were tested within 7 days after symptom onset. Data include only persons medically evaluated by a healthcare provider in the United States. Information on care-seeking behavior was determined through case interview and laboratory records. Negative COVID-19 results were required to be reported to Florida Department of Health, but negative dengue laboratory results are not, which might have resulted in underreporting of commercial dengue testing among persons who sought care.

FDOH also conducted syndromic surveillance for chief complaint and discharge diagnosis records from local hospitals. FDOH reviewed all syndromic surveillance records in the primary hospital serving the outbreak area and countywide, prioritizing chief complaints and discharge diagnoses mentioning dengue or fever and any combination of thrombocytopenia, rash, or arthralgia. FDOH requested medical records for patient visits with no alternative diagnosis. If only dengue serology had been ordered, FDOH requested that specimens be forwarded to the state laboratory for reverse transcription PCR (RT-PCR) testing. If no alternative diagnosis had been made and no DENV testing previously ordered, FDOH offered testing for persons with suspected cases.

Consistent with Centers for Disease Control and Prevention (CDC) guidelines, FDOH tested acute specimens collected within 7 days after symptom onset by using DENV RT-PCR and IgM tests. We only routinely performed antibody testing on convalescent samples collected >7 days after symptom onset. Specimens with positive or equivocal DENV test results at commercial laboratories were forwarded to FDOH and similarly retested. CDC assisted with serologic confirmation, serotyping RT-PCR–positive samples,

Figure 2. Phylogenetic reconstruction of dengue virus 1 from a dengue outbreak response during COVID-19 pandemic, Key Largo, Florida, USA, 2020. A) Central American lineage, 1986–2014; B) Caribbean lineage, 2008–2020. Maximum-likelihood tree of genotype V was inferred by using envelope gene sequences representing the Central American and Caribbean lineages. Red text indicates sequences obtained in this study. Sequence FL-Miami_human_2020 was obtained from a Miami-Dade County resident with recent travel history to Cuba. We obtained 2 sequences (GenBank accession nos. OM909246 and OM909247) from the National Reference Laboratory for Arboviruses, French Armed Forces Biomedical Research Institute, Bretigny-sur-Orge, France. Scale bar indicates nucleotide substitutions per site.

and provided RT-PCR testing for mosquito pools collected by FKMCD.

We identified 72 locally acquired dengue cases associated with Key Largo. Cases were primarily among female (51%) and non-Hispanic (83%) persons (Table). Self-reporting, including via contact outreach, drove initial case identification (61%), followed by commercial laboratory reporting (22%), and syndromic surveillance (7%); only 1 case was first identified through direct healthcare provider reporting. No case-patients had traveled outside the continental United States during the incubation period.

Overall, 31 cases were RT-PCR–positive and 41 were IgM-positive (Table). All RT-PCR–positive cases were DENV-1. Retrospective case finding and testing identified IgM-positive cases with reported symptom onset as early as January (Figure 1). Some persons identified through retrospective case finding reported a febrile illness several months prior. We presumed those febrile illnesses were dengue, but asymptomatic infections are common, and IgM is generally detectable for 3 months, making definitive confirmation of the timing of DENV infection difficult.

Among 96 *Ae. aegypti* mosquito pools collected during June 18–September 21, three tested positive for DENV-1 (Figure 1). We sequenced 15 positive samples, 12 from dengue cases and 3 from mosquito pools. Phylogenetic analysis showed grouping within the Caribbean lineage of DENV-1 genotype V (Figure 2). Sequences from mosquito pools and humans were almost identical. We published sequence data in GenBank (accession nos. OM831209–18, OM833055–59, and OM909246–47). Sequencing definitively differentiated this outbreak of Caribbean lineage DENV from the 2009–2010 Key West outbreak of Central American lineage.

Among case-patients, 43 (60%) visited a healthcare provider during the acute illness, within 1 week after symptom onset (Table). Providers considered COVID-19 as a potential diagnosis, which is evidenced by COVID-19 test orders for 38 (88%) of the acute dengue cases. Dengue was considered a potential diagnosis in only 16 acute cases, 13 of which had testing for both dengue and COVID-19. Providers primarily (75%) ordered dengue antibody testing when evaluating acute cases, which is inconsistent with CDC recommendations to use RT-PCR or DENV nonstructural protein 1 (NS1) test (*10*), an alternative to RT-PCR, in addition to IgM testing during the acute phase. No acute samples were tested using the DENV NS1 test. Among acute samples, 26 had comprehensive testing (both RT-PCR and IgM) performed at a reference laboratory at FDOH or CDC. Eight were positive for both assays, 14 were only DENV RT-PCR–positive, and 4 were only DENV IgM-positive. Ultimately, 54% of acute cases tested with only an IgM assay would have been missed if not for additional RT-PCR testing performed at a reference laboratory, compared with just 15% missed by using RT-PCR testing alone.

Conclusions

This investigation confirmed an ongoing dengue outbreak in the Key Largo area of Florida, USA, during January–August 2020. During that same timeframe, 1,692 COVID-19 cases were reported in Monroe County. We suspect the COVID-19 pandemic negatively affected dengue surveillance because of reluctance to seek medical care, competing demands on healthcare providers during a rapidly evolving pandemic, and similar clinical presentations between COVID-19 and dengue. The focus on COVID-19 was further evidenced by providers primarily ordering COVID-19 tests among patients with acute dengue seeking medical care. The use of multiple case-finding methods, including aggressive community engagement, helped mitigate some of those effects, as did pandemic-related travel restrictions in the county.

In conclusion, CDC recommends using either commercial DENV RT-PCR or NS1 tests in combination with serologic testing for samples collected during the acute phase of dengue illness (*10*). This outbreak highlights that those tests were underused. Improving clinician awareness of CDC recommendations could improve case detection in the future, especially for nonendemic areas at increased risk for DENV introduction.

Members of the Florida Department of Health Dengue Investigation Team: Angela Giaquinto, Brandie Peretz, Robert B. Eadie, Ian Stryker, Joseph Yglesias, Megan Ostl, Jazra Gibson, Jasmine Reiyce Boykin, and Danielle Stanek.

Acknowledgments

We are grateful to the residents of Key Largo and Monroe County, Florida, for their cooperation during this outbreak investigation. We also thank Janeen Laven, Kelly Fitzpatrick, Amanda Panella, and Jason Velez for their assistance with serologic testing for cross-reactive flaviviruses and Gilda Gard and Guillaume André Durand for their assistance with sequencing samples from 2 international travelers linked to the outbreak.

About the Author

Mr. Rowe was previously a vectorborne disease epidemiologist with the Florida Department of Health in Tallahassee, Florida, USA. He is currently continuing his interests in medical entomology as a PhD student at the University of Maine, researching browntail moth monitoring and control.

References

1. Gubler DJ. Dengue and dengue hemorrhagic fever. Clin Microbiol Rev. 1998;11:480–96. https://doi.org/10.1128/CMR.11.3.480
2. Florida Department of Health. Mosquito-borne disease surveillance [cited 2021 Dec 31]. https://www.floridahealth.gov/diseases-and-conditions/mosquito-borne-diseases/surveillance.html
3. Trout A, Baracco G, Rodriguez M, Barber J, Leal A, Radke E, et al.; Centers for Disease Control and Prevention (CDC). Locally acquired dengue—Key West, Florida, 2009–2010. MMWR Morb Mortal Wkly Rep. 2010;59:577–81.
4. Kendrick K, Stanek D, Blackmore C; Centers for Disease Control and Prevention (CDC). Notes from the field: transmission of chikungunya virus in the continental United States—Florida, 2014. MMWR Morb Mortal Wkly Rep. 2014;63:1137.
5. Likos A, Griffin I, Bingham AM, Stanek D, Fischer M, White S, et al. Local mosquito-borne transmission of Zika virus—Miami-Dade and Broward Counties, Florida, June–August 2016. MMWR Morb Mortal Wkly Rep. 2016;65:1032–8. https://doi.org/10.15585/mmwr.mm6538e1
6. Centers for Disease Control and Prevention. Is it dengue or is it COVID-19? [cited 2020 Dec 11]. https://www.cdc.gov/dengue/healthcare-providers/dengue-or-covid.html
7. Czeisler MÉ, Marynak K, Clarke KEN, Salah Z, Shakya I, Thierry JM, et al. Delay or avoidance of medical care because of COVID-19–related concerns—United States, June 2020. MMWR Morb Mortal Wkly Rep. 2020;69:1250–7. https://doi.org/10.15585/mmwr.mm6936a4
8. State of Florida. Executive order number 20-51. Establishes COVID-19 response protocol and directs public health emergency [cited 2021 Dec 31]. https://www.flgov.com/wp-content/uploads/orders/2020/EO_20-51.pdf
9. State of Florida Exec. Executive order number 20-89. Emergency management—COVID-19—Miami-Dade County, Broward County, Palm Beach County, Monroe County public access restrictions [cited 2021 Dec 31]. https://www.flgov.com/wp-content/uploads/orders/2020/EO_20-89.pdf
10. US Centers for Disease Control and Prevention. Dengue testing guidance for healthcare providers [cited 2020 Dec 11]. https://www.cdc.gov/dengue/healthcare-providers/testing/testing-guidance.html

Address for correspondence: Andrea Morrison, Florida Department of Health Bureau of Epidemiology, 4052 Bald Cypress Way, Bin A-12, Tallahassee, FL 32399, USA; email: Andrea.Morrison@flhealth.gov

etymologia revisited

Plague

[plāg]

Plague (from the Latin *plaga*, "stroke" or "wound") infections are believed to have been common since at least 3000 bce. Plague is caused by the ancestor of current *Yersinia* (named for Swiss bacteriologist Alexandre Yersin, who first isolated the bacterium) *pestis* strains. However, this ancestral *Y. pestis* lacked the critical *Yersinia* murine toxin (*ymt*) gene that enables vector-borne transmission. After acquiring this gene (sometime during 1600–950 bce), which encodes a phospholipase D that protects the bacterium inside the flea gut, *Y. pestis* evolved the ability to cause pandemics of bubonic plague. The first recoded of these, the Justinian Plague, began in 541 ace and eventually killed more than 25 million persons.

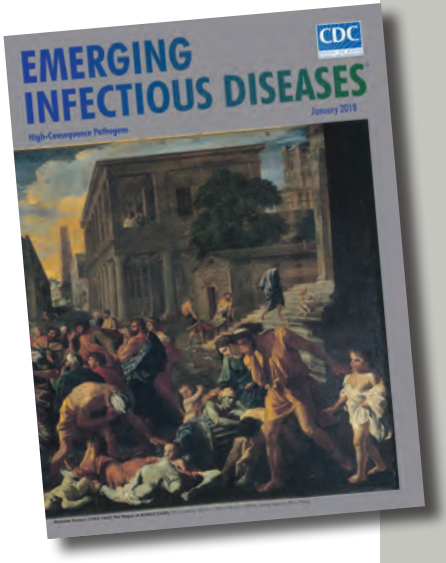

Originally published in January 2018

References:

1. Alexandre Yersin BW. Etymologia: yersinia. Emerg Infect Dis. 2010;16:496.
2. Centers for Disease Control and Prevention. History of plague [cited 2017 Oct 19]. https://www.cdc.gov/plague/history/index.html.
3. Rasmussen S, Allentoft ME, Nielsen K, Orlando L, Sikora M, Sjögren K-G, et al. Early divergent strains of Yersinia pestis in Eurasia 5,000 years ago. Cell. 2015;163:571–82.

https://wwwnc.cdc.gov/eid/article/24/1/et-2401_article

SARS-CoV-2 Variants and Age-Dependent Infection Rates among Household and Nonhousehold Contacts

Reiko Miyahara, Kosuke Tamura, Tomoko Kato, Mineko Nakazaki, Kanako Otani, Yura K. Ko, Taro Kamigaki, Yuzo Arima, Hideki Tani, Kazunori Oishi, Motoi Suzuki

To determine the effects of age and variants of concern on transmission of SARS-CoV-2, we analyzed infection rates among close contacts over 4 periods in Toyama Prefecture, Japan. Among household contacts, odds of infection were 6.2 times higher during the period of the Omicron variant than during previous periods, particularly among children and adolescents.

SARS-CoV-2 has been spreading globally since 2019; new variants of concern (VOCs) caused several epidemic waves during 2020–2022. According to a meta-analysis, the overall household secondary attack rates were higher for the Omicron variant (42.7%) than for the Alpha (36.4%) and Delta (29.7%) variants (*1*). The transmissibility and age-dependent susceptibility for Omicron and Delta exhibited significant heterogeneity among studies (*1*,*2*), and children were identified as being more vulnerable than adults to new variants (*2*). Infection rates among close contacts, determined by SARS-CoV-2 diagnostic tests, can vary according to study design, site settings, nonpharmacological control measures, and contact patterns (*3*). Thus, assessing infection rates among household and nonhousehold contacts within the same geographic area and population by using consistent methods over time could provide more reliable and valid information about changes in the effects of age and VOCs on transmission risk. With this study, we aimed to analyze the effects of age and VOCs on SARS-CoV-2 transmission by using contact tracing data of index case-patients and household and nonhousehold contacts in a city in Toyama Prefecture, Japan.

Author affiliations: National Institute of Infectious Diseases, Tokyo, Japan (R. Miyahara, K. Otani, T. Kamigaki, Y. Arima, M. Suzuki); Toyama Institute of Health, Toyama, Japan (K. Tamura, M. Nakazaki, H. Tani, K. Oishi); Takaoka Health and Welfare Center, Toyama (T. Kato); Tohoku University Graduate School of Medicine, Miyagi, Japan (Y.K. Ko)

DOI: https://doi.org/10.3201/eid2908.221582

The Study

We analyzed COVID-19 cases recorded in a city in Toyama Prefecture, Japan, over 4 periods, dominated by each of the 4 main virus variants: July 1–October 31, 2020 (pre-VOC period), April 1–30, 2021 (Alpha period), July 3–August 15, 2021 (Delta period), and January 3–23, 2022 (Omicron period) (Appendix Figure 1, https://wwwnc.cdc.gov/EID/article/29/8/22-1582-App1.pdf). Health center staff conducted telephone interviews with all COVID-19 case-patients, including those who were asymptomatic, to collect clinical information and recent activity history. According to the contact tracing guidelines of the National Institute of Infectious Diseases (Japan Ministry of Health, Labour and Welfare), we defined a close contact as someone who had contact with a COVID-19 case-patient during the period from 2 days before symptom onset until diagnosis (*4*). Close contacts were divided into household contacts (those who resided in the same household) and nonhousehold contacts (others who had contact with a confirmed COVID-19 case-patient for ≥15 minutes within a 1-meter distance without wearing any personal protective equipment). All contacts received SARS-CoV-2 PCR testing regardless of symptom status. If the PCR result for the first test was negative, contacts received PCR testing again if COVID-19–associated symptoms developed. We excluded from analysis close contacts with no PCR results.

All data management and analyses were conducted as part of the public health response in Toyama Prefecture and the National Institute of Infectious Diseases, and we used registered data collected according to the Infectious Diseases Law of Japan. Ethics approval was not required for this study.

First, we determined the baseline characteristics of the index case-patients and close contacts for each of the 4 periods. Second, we calculated infection rates stratified by the characteristics of index case-patients (age, sex, history of contact with COVID-19 case-patients before diagnosis, and symptom status) and close contacts (age, sex, and interval between diagnosis of index case-patients and PCR results of contacts). To adjust for clustering effects, we calculated infection rates as the total number of positive contacts divided by the total number of close contacts (with 95% CIs) by using the svyset command in Stata (StataCorp LLC, https://www.stata.com). To account for clustering among contacts exposed to the same index case-patients, we analyzed odds ratios of the infection rates (with 95% CIs) by using GEE (generalized estimating equations) logistic regression models with exchangeable correlations. We adjusted the models for the characteristics of both the index case-patients and their close contacts. Third, we described the contact matrix for the average number of contacts and infection rates based on the age of the index case-patients and contacts. We used Stata version 16.0 and R version 4.2.1 (The R Project for Statistical Computing, https://www.r-project.org) software to perform statistical analyses.

We enrolled 1,057 patients and 3,820 contacts: 123 index case-patients and 530 close contacts, in the pre-VOC period; 246 index case-patients and 988 close contacts in the Alpha period; 304 index case-patients and 984 close contacts in the Delta period; and 384 index case-patients and 1,318 close contacts in the Omicron period (Appendix Table 1). We excluded close contacts without PCR results: 45 (8.5%) persons from the pre-VOC period, 29 (2.9%) from the Alpha period, 111 (11.3%) from the Delta period, and 173 (13.1%) from the Omicron period. Infection rates during the Omicron period were 35.0% (95% CI 28.3–42.2) for household contacts and 15.1% (95% CI 10.0–22.5) for nonhousehold contacts. After adjustment for age, symptoms, sex, contact history, interval from diagnosis of index case-patient to PCR test, and household size, the odds ratios for infection were 6.22 times higher among household contacts and 3.55 times higher among nonhousehold contacts during the Omicron period than during the pre-VOC period (Table; Appendix Table 2). The risk for infection among household contacts 0–19 years of age increased significantly, from 3% in the pre-VOC period to 38% during the Omicron period (Appendix Figure 2). In contrast, during the study period, infection rates for nonhousehold contacts in this age group were

Table. Infection rates of SARS-CoV-2 infection among household and nonhousehold contacts in study of SARS-CoV-2 variants and age-dependent infection rates

	Household contacts				Nonhousehold contacts			
Variable	Total no.	No. PCR positive	Infection rate, %	Adjusted odds ratio (95% CI)*	Total no.	No. PCR positive	Infection rate, %	Adjusted odds ratio (95% CI)*
Total	1,144	294	25.7		2,318	302	13.0	
Period								
Pre-VOC	155	20	12.9	Referent	330	36	10.9	Referent
Alpha	251	48	19.1	1.91 (0.94–3.90)	708	71	10.0	1.47 (0.86–2.50)
Delta	329	83	25.2	3.75 (1.84–7.61)	544	84	15.4	2.34 (1.37–3.98)
Omicron	409	143	35.0	6.22 (3.04–12.70)	736	111	15.1	3.55 (2.09–6.06)
Index case-patient age, y								
0–19	214	54	25.2	0.42 (0.20–0.86)	852	34	4.0	0.16 (0.08–0.34)
20–39	493	111	22.5	0.36 (0.20–0.66)	973	182	18.7	0.42 (0.25–0.73)
40–59	309	84	27.2	0.45 (0.24–0.83)	317	48	15.1	0.40 (0.22–0.72)
≥60	129	45	35.2	Referent	176	38	21.6	Referent
Close contact age, y								
0–19	295	80	27.1	1.06 (0.70–1.62)	831	45	5.4	0.67 (0.39–1.17)
20–39	259	79	30.5	1.33 (0.89–2.00)	721	162	22.5	1.09 (0.70–1.71)
40–59	359	84	23.4	1.14 (0.78–1.68)	353	38	10.8	0.52 (0.31–0.85)
≥60	227	51	22.5	Referent	257	51	19.8	Referent
Unknown	4	0	0	NA	156	6	3.8	0.22 (0.07–0.66)

* Odds ratios were adjusted for age, sex, symptoms of index case-patients at the time of diagnosis, contact history, interval from diagnosis of index case-patient to PCR tests, and number of persons in the same household. NA, not applicable; VOC, variant of concern.

lower, despite a higher number of contacts compared with nonhousehold contacts in other age groups (Appendix Figure 3). Infection rates among household contacts ≥60 years of age decreased during the Delta period (12%) but increased again during the Omicron period (29%). Regarding infectivity throughout all time periods, the risk for infection from index case-patients ≥60 years of age was higher than that from index case-patients of other ages (Appendix Figure 2).

Conclusions

Our study showed that odds of infection were 6.2 times higher for household contacts during the Omicron period than during the pre-VOC period and that children and adolescents were particularly vulnerable (*2*). Despite increased nonhousehold contact among persons 0–19 years of age, nonphysical contact (*5*) and nonpharmacological control measures (*6*) in school and daycare centers may have led to lower infection rates and fewer large outbreaks in schools.

In addition, infection rates for contacts ≥60 years of age decreased during the Delta period but increased again during the Omicron period, potentially because of waning immunity associated with SARS-CoV-2 vaccination and the attenuated effect on the Omicron variant (*7*), even with high vaccination rates (93%) among persons >65 years of age during the Omicron period (Appendix Figure 1). In addition, the infectivity of elderly persons tended to be higher than that of persons in other age groups even after vaccine introduction (*8*), possibly because of close contact, such as caregiving and nursing care. The value of protecting those who care for elderly case-patients should thus be emphasized.

A limitation of this study was the varied timing and frequency of PCR testing. As the number of days from symptom onset to diagnosis decreased over time, infection rates were associated with the timing of testing and symptoms at the time of testing. We might have missed asymptomatic infections and potentially overcounted infected case-patients among contacts who might have been exposed to other places or infected persons.

Our finding of increased odds of infection among household contacts during the period of the Omicron variant, particularly among children and adolescents, highlights the need for periodic surveys to investigate comparative infectivity by epidemic strain as well as susceptibility and trends by age group over time in the same area and population. Such studies would account for variations in local conditions such as control regulation, contract tracing strategy, population age structure, and vaccination coverage.

Acknowledgments

We thank the public health centers and prefectural offices in Toyama Prefecture for data access.

This work was supported by grants from the National Center for Global Health and Medicine (20A2002D).

About the Author

Dr. Miyahara is a researcher at the Center for Surveillance, Immunization, and Epidemiologic Research, National Institute of Infectious Diseases, Tokyo, Japan. Her primary research interests are the clinical and genetic epidemiology of infectious diseases, including tuberculosis and COVID-19.

References

1. Madewell ZJ, Yang Y, Longini IM Jr, Halloran ME, Dean NE. Household secondary attack rates of SARS-CoV-2 by variant and vaccination status: an updated systematic review and meta-analysis. JAMA Netw Open. 2022;5:e229317. https://doi.org/10.1001/jamanetworkopen.2022.9317
2. Chen F, Tian Y, Zhang L, Shi Y. The role of children in household transmission of COVID-19: a systematic review and meta-analysis. Int J Infect Dis. 2022;122:266–75. https://doi.org/10.1016/j.ijid.2022.05.016
3. Madewell ZJ, Yang Y, Longini IM Jr, Halloran ME, Dean NE. Factors associated with household transmission of SARS-CoV-2: an updated systematic review and meta-analysis. JAMA Netw Open. 2021;4:e2122240. https://doi.org/10.1001/jamanetworkopen.2021.22240
4. National Institute of Infectious Diseases. Guidelines for active epidemiological investigation in patients with novel coronavirus infection [in Japanese] [cited 2022 Oct 8]. https://www.niid.go.jp/niid/ja/diseases/ka/corona-virus/2019-ncov/2484-idsc/9357-2019-ncov-02.html
5. Munasinghe L, Asai Y, Nishiura H. Quantifying heterogeneous contact patterns in Japan: a social contact survey. Theor Biol Med Model. 2019;16:6. https://doi.org/10.1186/s12976-019-0102-8
6. Budzyn SE, Panaggio MJ, Parks SE, Papazian M, Magid J, Eng M, et al. Pediatric COVID-19 cases in counties with and without school mask requirements — United States, July 1–September 4, 2021. MMWR Morb Mortal Wkly Rep. 2021;70:1377–8. https://doi.org/10.15585/mmwr.mm7039e3
7 Jalali N, Brustad HK, Frigessi A, MacDonald EA, Meijerink H, Feruglio SL, et al. Increased household transmission and immune escape of the SARS-CoV-2 Omicron compared to Delta variants. Nat Commun. 2022;13:5706. https://doi.org/10.1038/s41467-022-33233-9
8. Lyngse FP, Mortensen LH, Denwood MJ, Christiansen LE, Møller CH, Skov RL, et al. Household transmission of the SARS-CoV-2 Omicron variant in Denmark. Nat Commun. 2022;13:5573. https://doi.org/10.1038/s41467-022-33328-3

Address for correspondence: Reiko Miyahara, Center for Surveillance, Immunization, and Epidemiologic Research, National Institute of Infectious Diseases, 1-23-1 Toyama, Shinjuku-ku, Tokyo 162-8640, Japan; email: rmiyahara@niid.go.jp

Uniting for Ukraine Tuberculosis Screening Experience, San Francisco, California, USA

Janice K. Louie, Rocio Agraz-Lara, Laura Romo, Cristy Dieterich, Cathleen Xing, Susannah Graves

Ukraine surveillance data suggest high tuberculosis (TB) incidence, including multidrug resistance. Of 299 newcomers from Ukraine screened in San Francisco, California, USA, by using an interferon-γ-release-assay (IGRA) and chest radiograph, 7.4% were IGRA positive and 1 had laboratory-confirmed pansusceptible TB. Screening with IGRA and chest radiograph can help characterize TB risk.

World Health Organization surveillance data estimate that Ukraine has the fourth highest tuberculosis (TB) incidence in the European Region, at 71 cases/100,000 population in 2021 (*1*–*3*). Ukraine is believed to have a high burden of rifampin- and multidrug-resistant TB, accounting for ≈31% of culture-confirmed cases in 2021 (*2*,*3*). In addition, 22% of persons from Ukraine who have TB are infected with HIV; TB is the leading cause of death in this population (*2*,*3*).

In April 2022, the US Department of Homeland Security announced the Uniting for Ukraine (U4U) program to provide a pathway for citizens from Ukraine to enter the United States under humanitarian parole (*4*). U4U requires that parolees ≥2 years of age submit an attestation to the US Citizenship and Immigration Services confirming that TB screening with symptom review and an interferon-γ-release assay (IGRA) are performed within 90 days of US entry (*5*). In response, the San Francisco Department of Public Health TB Clinic partnered with the SFDPH Newcomers Health Program, a county Refugee Health Assessment Program, to reach out to community, professional, and faith-based groups to encourage expedited, no-cost TB screening to promptly identify and treat any U4U parolees who had latent or active TB (*6*,*7*).

Author affiliations: University of California, San Francisco, California, USA (J.K. Louie); San Francisco Department of Public Health, San Francisco (J.K. Louie, R. Agraz-Lara, L. Romo, C. Xing, S. Graves); San Francisco Department of Public Health Community Health Equity and Promotion Branch's Refugee Health Assessment Program, San Francisco (C. Dieterich)

DOI: https://doi.org/10.3201/eid2908.230347

The Study

To meet attestation requirements, U4U parolees who had a San Francisco address were screened for TB symptoms (fever, cough, night sweats, weight loss, fatigue, or hemoptysis) and tested by using the IGRA QuantiFERONTB Gold In-Tube Test (https://www.quantiferon.com). HIV testing was offered to all persons ≥2 years of age, and a chest radiograph was offered to persons ≥15 years of age to aid early identification of pulmonary TB. Parolees who had a positive IGRA result but unremarkable chest radiograph were offered latent TB infection (LTBI) treatment according to US Centers for Disease Control and Prevention recommendations (*8*).

Patients who had chest radiograph abnormalities suggestive of TB, regardless of IGRA result, underwent further evaluation by collection of 3 sputum samples for acid-fast bacilli (AFB) smear and culture and 1 sputum sample for nucleic acid amplification testing (NAAT) with the GeneXpert MTB/RIF assay (Cepheid, https://www.cepheid.com), which tests for TB and rifampin resistance. If sputum cultures were negative, LTBI treatment was recommended (*8*). Patients who had positive results for TB by NAAT or AFB culture were given treatment for active TB according to national recommendations (*9*).

During May 10, 2022–April 14, 2023, a total of 299 U4U parolees underwent TB screening (Table). Median age was 33 years (range 8 months–84 years); 116 (38.8%) were male. All patients denied previous active or latent TB. Of 298 patients ≥2 years of age, 274 (91.9%) agreed to HIV testing; all showed negative results. None of the 299 patients screened reported alcohol or substance use or previous incarceration. Three (1.0%) patients reported having a medical TB risk factor; all 3 had diabetes. All patients denied TB symptoms except for 1 (described later in this report).

Table. Characteristics of 299 parolees from Ukraine screened for tuberculosis, San Francisco, California, USA, May 2022–April 2023*

Characteristic	Value
Sex	
F	183 (61.2)
M	116 (38.8)
Median age, y (range)	33 (0.75–84)
TB medical risk factor per patient report	
Diabetes mellitus	3/299 (1.0)
HIV infection	0/299 (0.0)
Alcohol or substance use	0/299 (0.0)
Other†	0/299 (0.0)
Positive HIV test result‡	0/274 (0.0)
Positive IGRA result	22/299 (7.4)
Median age, y (range) with positive IGRA result	51.5 (17–81)
Chest radiograph performed§	240/245 (98.0)
Abnormalities on chest radiograph, all	7/240 (2.9)
Median age, y (range) with abnormal chest radiograph	43 (36–63)
Abnormalities on chest radiograph, IGRA negative	4/240 (1.7)
Diagnosis of active TB	1/299 (0.33)
LTBI treatment recommended	
Received treatment for LTBI/IGRA positive result	14/22 (63.6)
Not treated for LTBI/IGRA positive result	8/22 (36.4)
Refused treatment	5/22 (22.7)
Pending start of LTBI treatment	3/22 (13.6)

*Values are no. (%) or no. positive/no. tested (%) except as indicated. IGRA, interferon-γ-release assay; LTBI, latent TB infection; TB, tuberculosis.
†Other medical TB risk factors: severe kidney disease, silicosis, low bodyweight, organ transplant, head and neck cancer, and treatment with immunosuppressive agents (*10*).
‡All 298 parolees ≥2 years of age were offered HIV testing; 274 (91.9%) agreed.
§All 245 parolees ≥15 y of age were offered chest radiograph screening; 240 (98.0%) agreed.

Of the 299 patients, 22 (7.4%) had positive IGRA results; median age was 51.5 (range 17–81) years. Of 245 patients ≥15 years of age, 240 (98.0%) received a chest radiograph. Seven (2.9%) patients had abnormal chest radiograph results, consistent with possible TB, including 4 patients who had negative IGRA results; median age was 43 (range 36–63) years.

One parolee had laboratory confirmation of active TB. The patient reported productive cough and rhinorrhea for 10 days but no other TB symptoms. The patient had no epidemiologic or medical risk factors; HIV test result was negative, IGRA test result was positive, and chest radiograph identified upper lobe nodules. Sputum samples tested showed few AFB smear-positive, NAAT-positive results without rifampin resistance and grew *Mycobacterium tuberculosis* that was pansusceptible to isoniazid, rifampin, ethambutol, and pyrazinamide. The patient received TB therapy; all household contacts, including a child <5 years of age, tested negative by IGRA at baseline and 8–10 weeks later.

Conclusions

Despite surveillance data reporting high TB incidence (including drug-resistant TB) in Ukraine, only 7.4% of parolees in this investigation received diagnoses of LTBI, and only 1 had laboratory-confirmed, pansusceptible, active pulmonary disease (*1*–*3*). Most parolees were female, possibly reflecting that many men have remained in Ukraine during wartime. All parolees with LTBI were ≥18 years of age, consistent with reports that TB is uncommon in children from Ukraine (*1*–*3*). Most parolees reported no concurrent medical condition, and none tested were HIV positive. The percentages of U4U parolees testing positive by IGRA was low compared with other San Francisco immigrant populations; in the past 5 years, of clients undergoing screening for homeless shelter housing, 20.2% who originated from Mexico and 27.5% from Central America (including Belize, El Salvador, Guatemala, Honduras, and Nicaragua) have tested IGRA positive (San Francisco Department of Public Health, unpub. data).

U4U parolees might not be representative of populations from Ukraine most likely to be given a diagnosis of TB. For example, data for Ukraine for 2021 suggest that HIV, alcohol use, malnutrition, and diabetes are major TB risk factors; those factors were uncommon or absent in the San Francisco U4U population (*1*–*3*). Our numbers are reflective of the San Francisco U4U program only and might not be generalizable to other jurisdictions. Nevertheless, vigilance in the U4U population remains warranted because armed conflict and mass displacements have historically been associated with increases in TB incidence, drug-resistant TB, and TB deaths, possibly caused by disruptions in healthcare services, malnutrition, and need for temporary housing with associated crowding and poor hygiene (*11*).

The Centers for Disease Control and Prevention Division of Global Migration and Quarantine has established requirements for overseas screening

of new refugees before entry into the United States, which include medical history, physical examination, and TB screening (*12*). For persons originating from countries that have a TB incidence of ≥20 cases/100,000 persons, the overseas screening requirement for persons ≥15 years of age includes a chest radiograph (IGRA optional); for those 2–14 years of age, only IGRA is necessary (*12*). Within 90 days of US arrival, a domestic screening, including history, physical examination, and review of overseas screening results, is recommended; depending on the person, refugees might undergo further evaluation for LTBI (if overseas IGRA was not performed or the result is >6 months old) or active TB (if new symptoms or physical examination abnormalities have developed since overseas screening) (*13*).

In humanitarian situations through which newcomers enter the United States emergently from high-incidence countries without previous overseas evaluation, domestic TB screening with IGRA and chest radiograph (in persons ≥15 years of age) might be merited to match existing overseas refugee screening recommendations. Because IGRA can show false-negative results for >20% of persons who have active TB, addition of a chest radiograph can help enable rapid and sensitive detection of pulmonary TB, ensure prompt treatment, and prevent local transmission (*14*). Our inclusion of chest radiographs also provides reassuring data suggesting that infectious pulmonary TB is not being missed in U4U parolees entering San Francisco, despite the high incidence reported in surveillance data for Ukraine.

In late 2022 and early 2023, the Department of Homeland Security implemented programs similar to U4U for new parolees from Venezuela, Nicaragua, Cuba, and Haiti (*15*). Those parolees have not been screened overseas, have the same TB attestation requirements as U4U, and might have entered the United States under circumstances that convey higher TB risk (e.g., extreme poverty, expolitical prisoners, or long and crowded land journeys) (*15*). The establishment of U4U screening has enabled SFDPH to assess those populations similarly. To date, of 38 parolees from Venezuela and Nicaragua screened, LTBI has been identified in 3 from Nicaragua; an additional asymptomatic parolee from Nicaragua with a negative IGRA result was given a diagnosis of smear-positive active pulmonary TB. Parolee screening by both IGRA and chest radiograph has provided SFDPH with timely and informative data (including positive and negative results) about TB risk in the diverse parolee populations from high-incidence countries.

Acknowledgments

We thank Gloria Perez and Sammi Truong for generously working with the U4U population and the SFDPH TB clinic staff for providing dedicated care to our TB patients.

About the Author

Dr. Louie is medical director of the San Francisco Department of Public Health Tuberculosis Prevention and Control Program, San Francisco, CA. Her primary research interest is characterization of the epidemiology, clinical management, and treatment of tuberculosis in older and other vulnerable populations.

References

1. Dahl V, Migliori GB, Lange C, Wejse C. War in Ukraine: an immense threat to the fight against tuberculosis. Eur Respir J. 2022;59:2200493. https://doi.org/10.1183/13993003.00493-2022
2. European Centre for Disease Prevention and Control (ECDC)/World Health Organization Regional Office for Europe (WHO Europe). Tuberculosis surveillance and monitoring in Europe, 2022–2020 data. Copenhagen: WHO Regional Office for Europe and Stockholm/ECDC; 2022 [cited 2023 Jun 14]. https://www.ecdc.europa.eu/sites/default/files/documents/Tuberculosis-surveillance-monitoring-europe-2022_0.pdf
3. World Health Organization. Global tuberculosis report 2022. 2022 [cited 2024 Jun 14]. https://www.who.int/publications/i/item/9789240061729
4. Centers for Disease Control and Prevention. Dear colleague letters: Uniting for Ukraine program, June 21, 2022 [cited 2023 Jun 14]. https://www.cdc.gov/tb/publications/letters/2022/unitingforukraine-DCL.html
5. US Citizenship and Immigration Services. Uniting for Ukraine vaccine attestation [cited 2023 Jun 14]. https://www.uscis.gov/humanitarian/uniting-for-ukraine/uniting-for-ukraine-vaccine-attestation
6. California Department of Public Health Office of Refugee Health. Program overview [cited 2023 Jun 14]. https://www.cdph.ca.gov/Programs/CID/ORH/Pages/Program%20Overview.aspx
7. San Francisco Department of Public Health Newcomers Health Program. Our programs [cited 2023 Jun 14]. https://zuckerbergsanfranciscogeneral.org/patient-visitor-resources/refugee-services
8. Sterling TR, Njie G, Zenner D, Cohn DL, Reves R, Ahmed A, et al. Guidelines for the treatment of latent tuberculosis infection: recommendations from the National Tuberculosis Controllers Association and CDC, 2020. MMWR Recomm Rep. 2020;69(no. RR-1):1–11. https://doi.org/10.15585/mmwr.rr6901a1
9. Nahid P, Mase SR, Migliori GB, Sotgiu G, Bothamley GH, Brozek JL, et al. Treatment of drug-resistant tuberculosis. An official ATS/CDC/ERS/IDSA clinical practice guideline. Am J Respir Crit Care Med. 2019;200:e93–142. https://doi.org/10.1164/rccm.201909-1874ST
10. Centers for Disease Control and Prevention. TB risk factors. 2016 [cited 2023 Jun 14]. https://www.cdc.gov/tb/topic/basics/risk.html
11. Dahl VN, Tiberi S, Goletti D, Wejse C. Armed conflict and human displacement may lead to an increase in the burden

of tuberculosis in Europe. Int J Infect Dis. 2022;124(Suppl 1):S104–6. https://doi.org/10.1016/j.ijid.2022.03.040
12. Centers for Disease Control and Prevention. Tuberculosis technical instructions for panel physicians [cited 2023 Jun 14]. https://www.cdc.gov/immigrantrefugeehealth/panel-physicians/tuberculosis.html
13. Centers for Disease Control and Prevention. Immigrant, refugee, and migrant health. Guidance for screening for tuberculosis infection and disease during the domestic medical examination for newly arrived refugees [cited 2023 Jun 14]. https://www.cdc.gov/immigrantrefugeehealth/guidelines/domestic/tuberculosis-guidelines.html
14. Yamasue M, Komiya K, Usagawa Y, Umeki K, Nureki SI, Ando M, et al. Factors associated with false negative interferon-γ release assay results in patients with tuberculosis: a systematic review with meta-analysis. Sci Rep. 2020;10:1607. https://doi.org/10.1038/s41598-020-58459-9
15. US Citizenship and Immigration Services. Processes for Cubans, Haitians, Nicaraguans and Venezuelans [cited 2023 Jun14]. https://www.uscis.gov/sites/default/files/document/flyers/Process-for-Cubans-Haitians-Nicaraguans-and-Venezuelans-Flyer.pdf

Address for correspondence: Janice K. Louie, Tuberculosis Prevention and Control Program, San Francisco Department of Public Health, 2460 22nd St, Bldg 90, 4th Fl, San Francisco, CA 94110, USA; email: janice.louie@sfdph.org

Mycobacterium abscessus Meningitis Associated with Stem Cell Treatment During Medical Tourism

Andrew B. Wolf, Kelli M. Money, Arun Chandnani, Charles L. Daley, David E. Griffith, Lakshmi Chauhan, Nathan Coffman, Amanda L. Piquet, Kenneth L. Tyler, Shanta M. Zimmer, Brian T. Montague, Sarah Mann, Daniel M. Pastula

Mycobacterium abscessus infections have been reported as adverse events related to medical tourism. We report *M. abscessus* meningitis in a patient who traveled from Colorado, USA, to Mexico to receive intrathecal stem cell injections as treatment for multiple sclerosis. We also review the management of this challenging central nervous system infection.

Mycobacterium abscessus is a rapidly growing nontuberculous mycobacterium (NTM) commonly found in soil and water (*1*). Pulmonary, skin, and soft tissue infections are common nosocomial infections that are often associated with inadequate sterilization of water and reagents (*2*). Rarely, *M. abscessus* can infect the central nervous system (CNS), causing chronic meningitis or abscess, often in the setting of trauma, surgery, or dissemination in immunocompromised hosts (*3*). CNS infections typically manifest as subacute headache, fever, meningismus, or some combination, along with focal neurologic signs if there is an abscess (*3*). *M. abscessus* infection has been reported as a complication of medical tourism (i.e., when patients travel abroad for medical treatment or cosmetic surgeries) (*4*,*5*). *M. abscessus* infections are challenging to treat, requiring prolonged multidrug regimens or surgical intervention (*6*). We present a patient with *M. abscessus* meningitis associated with intrathecal stem cell injections during medical tourism.

Author affiliations: University of Colorado School of Medicine, Aurora, Colorado, USA (A.B. Wolf, K.M. Money, A. Chandani, L. Chauhan, N. Coffman, A.L. Piquet, K.L. Tyler, S.M. Zimmer, B.T. Montague, S. Mann, D.M. Pastula); National Jewish Health, Denver, Colorado, USA (C.L. Daley, D.E. Griffith); Colorado School of Public Health, Aurora (D.M. Pastula)

DOI: http://doi.org/10.3201/eid2908.230317

The Case

This report centers on an immunocompetent woman in her 30s who had been diagnosed with multiple sclerosis (MS) and met 2017 McDonald criteria 3 years before our initial encounter. Her initial MS symptoms were episodic left arm and left leg numbness, and she had multifocal brain, cervical, and thoracic spine demyelinating lesions identified by magnetic resonance imaging. She had never received disease-modifying therapies or other immunosuppressive medications. Results of her baseline neurologic examination was unremarkable.

In October 2022, the patient traveled to a commercial clinic in Baja California, Mexico. During a 4-day visit, she underwent 2 lumbar punctures for intrathecal injection of donor umbilical cord stem cells programmed to treat MS. She pursued treatment at this clinic after reviewing its associated website as part of her research on stem cell treatments for MS.

The day after the second intrathecal injection, she visited an emergency department in the United States for positional headache and received an epidural blood patch for presumed postlumbar puncture cerebrospinal fluid (CSF) leak. She reported nocturnal fevers, but vital signs, neurologic examination, complete blood counts, and computed tomography of the head were unremarkable. She was discharged after her headache improved but subsequently received 2 blood patches in the outpatient setting for recurrent headaches.

Because of persistent fevers, the patient was admitted to an outside hospital 5 days after receiving the third blood patch. At admission, she was febrile (101.3°F), but vital signs and complete blood counts were otherwise within reference ranges and HIV serology results were negative. Neurologic examination

Table 1. *Mycobacterium abscessus* antibiotic susceptibilities for case-patient who underwent intrathecal stem cell injections as treatment for multiple sclerosis at a clinic in Mexico*

Antimicrobial	MIC, μg/mL	Interpretation
Amikacin	64	Resistant
Cefoxitin	32	Intermediate
Ciprofloxacin	≥8	Resistant
Clarithromycin	1	Susceptible
Doxycycline	≥16	Resistant
Imipenem	16	Intermediate
Linezolid	8	Susceptible
Moxifloxacin	≥8	Resistant
Tigecycline	≥8	Resistant
Trimethoprim/sulfamethoxazole	≥8/152	Resistant

*Determined by using Clinical and Laboratory Standards Institute cutpoints for resistance (*7*). There is no recommended cutpoint for tigecycline.

remained unremarkable. Sampling of her CSF revealed 74 nucleated cells/μL (76% neutrophils, 20% lymphocytes, 2% monocytes), 64 red blood cells/μL, 84 mg/dL of protein, and 29 mg/dL of glucose (serum glucose 96 mg/dL). Results of herpes simplex virus PCR and enterovirus real-time reverse transcription PCR tests were negative. There was no growth on aerobic or anaerobic bacterial cultures. She received vancomycin and 1 dose of cefepime before changing over to meropenem because rash developed during cefepime infusion. She transitioned to imipenem for a 10-day total course; fever resolved, and headache improved.

Days after completing antibiotics, the patient experienced worsening headache and recurrence of fevers, prompting her admission to our institution. We resampled her CSF and found it contained 104 nucleated cells/μL (50% neutrophils, 42% lymphocytes, 8% monocytes), 3 red blood cells/μL, 47 mg/dL of protein, and 31 mg/dL of glucose (serum glucose 85 mg/dL). We identified 13 CSF-specific oligoclonal bands (reference <2) and noted her IgG index was 1.21 (reference <0.6); those values were consistent with MS but also a potential indicator of CNS infection). We obtained magnetic resonance images of the patient's brain and cervical, thoracic, and lumbar spine, with and without gadolinium, and found no evidence of active demyelination or infection. We prescribed a course of vancomycin and ceftriaxone as empiric meningitis coverage, and the patient noted improvement of fever and headaches. The patient's CSF culture became positive for a rapidly growing NTM after 7 days of incubation.

Table 2. Final treatment regimen for *Mycobacterium abscessus* meningitis for case patient who underwent intrathecal stem cell injections as treatment for multiple sclerosis at a clinic in Mexico

Drug	Dose
Azithromycin	500 mg IV 1×/d
Ceftaroline	600 mg IV 3×/d
Eravacycline	80 mg IV 1×/d
Imipenem	500 mg IV 4×/d
Tedizolid	200 mg orally 1×/d

*IV, intravenously.

We prescribed the patient a treatment course that included azithromycin (500 mg intravenously [IV] 1×/d), imipenem (500 mg IV 4×/d), and trimethoprim/sulfamethoxazole (5 mg/kg IV 3×/d), tedizolid (200 mg orally 1×/d), and ciprofloxacin (400 mg orally 3×/d), some of which led to intolerable gastrointestinal symptoms. After identifying the NTM as *M. abscessus*, we adjusted the patient's treatment course on the basis of drug susceptibilities using Clinical and Laboratory Standards Institute cutpoints for resistance (Table 1) (*7*). We stopped trimethoprim/sulfamethoxazole and ciprofloxacin and instituted eravacycline (80 mg IV 1×/d) due to favorable CNS penetration. We initiated ceftaroline (600 mg IV 3×/d) due to synergistic activity with imipenem (*8*). The final treatment regimen (Table 2) brought improvement in headaches and resolution of fevers. In total, it took 8 weeks of evaluations after her initial visit to the outside emergency department to identify and treat *M. abscessus*. Repeat CSF culture after 3 weeks of treatment revealed no growth. The patient has now completed >3 months of treatment without recurrent symptoms.

Conclusions

This patient's case highlights a serious complication associated with medical tourism. Promising preclinical studies of stem cell treatments has led to stem cell tourism (*9*). A purported ability of stem cell treatments to repair disabling CNS damage has encouraged patients to frequently pursue such treatments, despite the lack of demonstrated efficacy. Without regulatory approval, stem cell treatments are frequently marketed online, with scientific messaging and patient testimonials to project an aura of legitimacy. Such treatments have been linked to serious complications, leading to warnings from the US Centers for Disease Control and Prevention and the US Food and Drug Administration (*10*–*12*).

Peripheral stem cell treatments have been associated with a range of adverse events, including

infections and neoplasms (*10*). There is little to ensure the integrity of the manufacturing or administration for such unregulated treatments, and there is no postmarketing surveillance. Inadequate use of sterile technique or use of contaminated water during manufacture or administration of stem cell products may lead to infections. The largest reported incident involved 20 culture-confirmed bacterial infections secondary to donor umbilical cord blood products proposed as treatment for orthopedic conditions (*13*). In addition to infections, neoplastic and inflammatory lesions have been associated with intrathecal stem cell treatments (*9*,*10*).

Diagnosis of *M. abscessus* infection requires isolation of NTM and use of molecular techniques to identify species and subspecies (*1*). *M. abscessus* is difficult to treat becasue of its in vitro antimicrobial resistance and biofilm formation (*1*). The species is generally resistant to typical antituberculous drugs, and those used for prolonged multidrug regimens are often poorly tolerated (*14*,*15*). Drug efficacy is dramatically reduced by the presence in *M. abscessus* of an erythromycin ribosome methylase gene, *erm(41)*, which induces macrolide resistance, or mutational resistance via the 23S ribosomal RNA gene. As such, macrolide companion drugs must be carefully selected (*6*). Regimens to treat CNS *M. abscessus* infection are based on limited evidence because of the rarity of cases and unknown CSF penetrance of many drugs (*3*,*15*). Surgical debridement of abscesses may be necessary.

The literature describes cases of *M. abscessus* infection involving contributory immunosuppression, trauma, or neurosurgery, making our patient's case rather unique. She has completed >3 months of treatment without recurrent symptoms. In addition to the direct injury from *M. abscessus* meningitis, patients like the one we report face an increased risk of neurologic disability because chronic CNS infection precludes use of immunosuppressive therapies for MS. Therefore, counseling MS patients on the risks of stem cell tourism is fundamental. There is no proven benefit to intrathecal stem cell treatments, and such treatments should be offered only through registered clinical trials. Clinicians should be aware of potential harms of stem cell tourism and report adverse events to public health agencies.

Acknowledgments

We thank the patient discussed in this case report, those involved in her clinical care, and the Colorado Department of Public Health and Environment. The patient verbally consented to her deidentified case being reported and signed our institution's standard consent form.

About the Author

Dr. Wolf is a fellow at the Rocky Mountain Multiple Sclerosis Center at the University of Colorado School of Medicine. His primary research interests include optimizing the selection, sequencing, and safety of disease-modifying therapies for multiple sclerosis.

References

1. Johansen MD, Herrmann JL, Kremer L. Non-tuberculous mycobacteria and the rise of *Mycobacterium abscessus*. Nat Rev Microbiol. 2020;18:392–407. https://doi.org/10.1038/s41579-020-0331-1
2. Phillips MS, von Reyn CF. Nosocomial infections due to nontuberculous mycobacteria. Clin Infect Dis. 2001;33:1363–74. https://doi.org/10.1086/323126
3. Wu EL, Al-Heeti O, Hoff BM, et al. Role of therapeutic drug monitoring in the treatment of persistent *Mycobacterium abscessus* central nervous system infection: a case report and review of the literature. Open Forum Infect Dis. 2022;9:ofac392. PMID: 35983263. https://doi.org/10.1093/ofid/ofac392
4. Gaines J, Poy J, Musser KA, Benowitz I, Leung V, Carothers B, et al. Notes from the field: nontuberculous mycobacteria infections in US medical tourists associated with plastic surgery—Dominican Republic, 2017. MMWR Morb Mortal Wkly Rep. 2018;67:369–70. https://doi.org/10.15585/mmwr.mm6712a5
5. Schnabel D, Esposito DH, Gaines J, Ridpath A, Barry MA, Feldman KA, et al.; RGM Outbreak Investigation Team. Multistate US outbreak of rapidly growing mycobacterial infections associated with medical tourism to the Dominican Republic, 2013–20141. Emerg Infect Dis. 2016;22:1340–7. https://doi.org/10.3201/eid2208.151938
6. Griffith DE, Daley CL. Treatment of *Mycobacterium abscessus* pulmonary disease. Chest. 2022;161:64–75. https://doi.org/10.1016/j.chest.2021.07.035
7. Clinical and Laboratory Standards Institute. Performance standards for susceptibility testing of mycobacteria, *Nocardia* spp., and other aerobic Actinomycetes, 2nd edition. CLSI standard document M24. Wayne (PA): The Institute; 2023.
8. Nguyen DC, Dousa KM, Kurz SG, Brown ST, Drusano G, Holland SM, et al. "One-Two Punch": Synergistic ß-lactam combinations for *Mycobacterium abscessus* and target redundancy in the inhibition of peptidoglycan synthesis enzymes. Clin Infect Dis. 2021;73:1532–6. https://doi.org/10.1093/cid/ciab535
9. Julian K, Yuhasz N, Rai W, Salerno JA, Imitola J. Complications from "stem cell tourism" in neurology. Ann Neurol. 2020;88:661–8. https://doi.org/10.1002/ana.25842
10. Bauer G, Elsallab M, Abou-El-Enein M. Concise review: a comprehensive analysis of reported adverse events in patients receiving unproven stem cell-based interventions. Stem Cells Transl Med. 2018;7:676–85. https://doi.org/10.1002/sctm.17-0282
11. US Centers for Disease Control and Prevention. Outbreak and patient notification: Stem cell and exosome products. 2019 Dec 19 [cited 2022 Dec 18]. https://www.cdc.gov/hai/outbreaks/stem-cell-products.html
12. US Food and Drug Administration. Consumer update: FDA warns about stem cell therapies. 2020 Sep 9 [cited 2022 Dec 18]. https://www.fda.gov/consumers/consumer-updates/fda-warns-about-stem-cell-therapies

13. Hartnett KP, Powell KM, Rankin D, Gable P, Kim JJ, Spoto S, et al. Investigation of bacterial infections among patients treated with umbilical cord blood–derived products marketed as stem cell therapies. JAMA Netw Open. 2021;4:e2128615. https://doi.org/10.1001/jamanetworkopen.2021.28615
14. Lee MR, Cheng A, Lee YC, Yang CY, Lai CC, Huang YT, et al. CNS infections caused by *Mycobacterium abscessus* complex: clinical features and antimicrobial susceptibilities of isolates. J Antimicrob Chemother. 2012;67:222–5. https://doi.org/10.1093/jac/dkr420
15. Novosad SA, Beekmann SE, Polgreen PM, Mackey K, Winthrop KL; M. abscessus Study Team. Treatment of *Mycobacterium abscessus* infection. Emerg Infect Dis. 2016;22:511–4. https://doi.org/10.3201/eid2203.150828

Address for correspondence: Daniel Pastula, Departments of Neurology, Medicine (Infectious Diseases), and Epidemiology, University of Colorado School of Medicine and Colorado School of Public Health, 12700 E 19th Ave, Aurora, CO 80045, USA; email: daniel.pastula@cuanschutz.edu

Candidatus Neoehrlichia mikurensis Infection in Patient with Antecedent Hematologic Neoplasm, Spain[1]

Paola González-Carmona,[2,3] Aránzazu Portillo,[2]
Cristina Cervera-Acedo, Daniel González-Fernández, José A. Oteo

We report a confirmed case of *Candidatus* Neoehrlichia mikurensis infection in a woman in Spain who had a previous hematologic malignancy. *Candidatus* N. mikurensis infections should be especially suspected in immunocompromised patients who exhibit persistent fever and venous thrombosis, particularly if they live in environments where ticks are prevalent.

Candidatus Neoehrlichia mikurensis is an α1-proteobacterium (family Anaplasmataceae) transmitted by *Ixodes* spp. ticks. Although previously described in ticks and mammals in Europe and Asia, the species name was derived from a report in 2004 from Mikura Island, Japan, where the bacterium was found in endothelial cells from rat (*Rattus norvegicus*) spleens and in *Ixodes ovatus* ticks (*1*). In 2010, *Candidatus* N. mikurensis was identified as a human pathogen in Sweden (*2*). Since then, several case series and individual cases of patients with *Candidatus* N. mikurensis infections have been described, mainly in persons who were immunosuppressed because of hematologic neoplasms, splenectomies, or immunosuppressive drug treatment (*3*–*9*). However, *Candidatus* N. mikurensis can cause disease (neoehrlichiosis) in immunocompetent persons or cause asymptomatic infections (*10*,*11*). In 2019, *Candidatus* N. mikurensis was cultured in tick cell lines and infection was transferred to human endothelial cells derived from skin microvasculature and pulmonary arteries, demonstrating endothelial cell tropism. Tropism partly explains the clinical spectrum caused by the bacterium, usually consisting of persistent and recurrent fever and thrombosis and vasculitis with or without erysipelas-like skin lesions (*12*). In Spain, *Candidatus* N. mikurensis was found in *Ixodes ricinus* ticks removed from cows in 2013, but the bacterium was not detected in humans (*13*). We describe a case of *Candidatus* N. mikurensis infection in an immunocompromised patient from Asturias in northern Spain.

The Study

In September 2020, stage IV-B germinal center diffuse large B-cell lymphoma was diagnosed in a splenectomy specimen from a 68-year-old woman. She completed first-line treatment with rituximab plus cyclophosphamide, doxorubicin, vincristine, and prednisone and achieved complete remission. On June 21, 2021 (≈5 months after lymphoma treatment had ended), she experienced arthromyalgia, anorexia, night sweats, and vespertine fever. Her family physician began treatment with metamizole and cefuroxime at usual doses because of urine sediment alterations. Several days later, deep vein thrombosis developed in her right leg. Because of her previous malignancy and treatment, she was attended at her hospital's hematology service. She was slightly anemic (hemoglobin 11.7 g/dL, reference range 12–16 g/dL) and had leukopenia (2.28×10^3 leukocytes/μL, reference range 4–14 × 10^3 leukocytes/μL) and a low neutrophil count (0.4×10^3 neutrophils/μL, reference range 1.8–8.5 × 10^3 neutrophils/μL). C-reactive protein level was elevated (62 mg/L, reference range <10 mg/L), hyponatremia was

Author affiliations: Hospital de Jarrio, Asturias, Spain (P. González-Carmona, D. González-Fernández); Hospital Universitario San Pedro-CIBIR, La Rioja, Spain (A. Portillo, C. Cervera-Acedo, J.A. Oteo)

DOI: https://doi.org/10.3201/eid2908.230428

[1]Data from this study were presented at the joint LXIV National Conference of the Spanish Society of Hematology and Hemotherapy, XXXVIII National Conference of the Spanish Society of Thrombosis and Hemostasis, and 38th World Congress of the International Society of Hematology; October 6–8, 2022; Barcelona, Spain; and International Intracellular Bacteria Meeting; August 23–26, 2022; Lausanne, Switzerland.

[2]These first authors contributed equally to this article.

[3]Current affiliation: Hospital Universitario San Agustín, Asturias, Spain.

Table 1. PCR primer pairs and conditions used in study of *Candidatus* Neoehrlichia mikurensis infection in patient with antecedent hematologic neoplasm, Spain*

Organisms	Target gene	Primer name	Primer sequence, 5′ → 3′	Amplicon size	Tm, °C
Bacteria	16S rRNA	fD1	AGAGTTTGATCCTGGCTCAG	1,500 bp	60
		rP2	ACGGCTACCTTGTTACGACTT		
Anaplasmataceae†	16S rRNA-EHR	EHR16SD	GGTACCYACAGAAGAAGTCC	345 bp	55
		EHR16SR	TAGCACTCATCGTTTACAGC		
Anaplasma phagocytophilum	*msp2*	msp2–3F	CCAGCGTTTAGCAAGATAAGAG	334 bp	56
		msp2–3R	GCCCAGTAACAACATCATAAGC		
Candidatus N. mikurensis	*groEL*, 1st run	Ne-groEL-F	GAAGTATAGTTTAGTATTTTTGTC	1,275 bp	49
		Ne-groEL-R	TTAACTTCTACTTCGCTTG		
	groEL, 2nd run	Ne-groEL-F	GAAGTATAGTTTAGTATTTTTGTC	510 bp	49
		Ne-groEL_ne-1	ACATCACGTTTCATAGAA		
	groEL, 2nd run	Ne-groEL_ne-2	AAAGGAATTAGTATTAGAATCTTT	569 bp	49
		Ne-groEL_ne-4	CTTCCATTTTAACTGCTAA		
	groEL, 2nd run	Ne-groEL_ne-3	AATATAGCAAGATCAGGTAGAC	461 bp	49
		Ne-groEL-R	TTAACTTCTACTTCGCTTG		

*Tm, melting temperature.
†Includes *Anaplasma*, *Ehrlichia*, and *Candidatus* Neoehrlichia spp. 16S rRNA-EHR refers to the 16S rRNA sequence from the Anaplasmataceae family members, whereas 16S rRNA refers to the panbacterial 16S rRNA sequence.

present (133 mmol Na/L, reference range 135–145 mmol Na/L), and high levels of ferritin (536 μg /L, reference range 20–200 μg/L) and β2 microglobulin (8.50 mg/L, reference range 0.8–2.4 mg/L) were observed. Other measured hematologic and biochemical parameters, including procalcitonin, were within reference ranges. Other analyses, such as antinuclear antibody testing, blood and urine cultures, and serologic assays against *Coxiella burnetii*, herpes virus, cytomegalovirus, and Epstein-Barr virus, did not indicate acute infection. A chest radiograph and computed tomography scan and an abdominal ultrasound did not reveal pertinent abnormalities. Recurrence of lymphoma was suspected, and a positron emission tomography/computed tomography scan showed diffuse and homogeneous bone marrow hypermetabolism without evidence of neoplastic activity at other levels.

Empirical treatment was begun with piperacillin/tazobactam and granulocyte colony stimulating factor at conventional doses; 1 week later, the patient had recovered from leukopenia, but fever persisted. A bone marrow biopsy, which did not show neoplastic infiltration or alterations in hematopoietic cells, was performed and processed for different microbiologic tests. A possible tick-related infection was suspected because the patient lived in an area endemic for Lyme disease and other tickborne diseases. The patient recalled having suffered a tick bite 20 days before onset of symptoms. A bone marrow DNA extract and serum sample collected during the acute infection phase (August 2021) were sent to the Special Pathogens Laboratory, Center for Rickettsioses and Arthropod-Borne Diseases, at San Pedro University Hospital–Center for Biomedical Research of La Rioja in Logroño, Spain, to screen for *Candidatus* N. mikurensis by using PCR and *Anaplasma phagocytophilum* by using PCR and immunofluorescence assays.

We performed PCR targeting the panbacterial 16S rRNA gene, fragments of 16S rRNA gene from Anaplasmataceae (designated as 16S rRNA-EHR), *groEL* from *Candidatus* N. mikurensis, and *msp2* from *A. phagocytophilum* (Table 1). We detected PCR amplicons of the expected sizes for *groEL* and panbacteria and family-specific 16S rRNA in bone marrow and acute phase serum samples; nucleotide sequences corresponded to *Candidatus* N. mikurensis. The *groEL* amplicon (1,232 bp) showed the highest (99.3%) sequence similarity with that of *Candidatus* N. mikurensis from a wild rodent (*Microtus agrestis*) from Siberia in Russia (GenBank accession no. MN701626) but differed from other highly conserved sequences from Siberia and the Far East; the sequence was 98.8% identical to *Candidatus* N. mikurensis found in *Ixodes ricinus* ticks from Spain (*13*) (Table 2). We constructed a phylogenetic tree for *groEL* sequences by using the maximum likelihood method (Figure). We found no differences for the 16S rRNA-EHR sequence (306 bp). The panbacteria 16S rRNA sequence (available upon request from the authors) showed 3–27 mismatches with the 16S rRNA from *Candidatus* N. mikurensis. We did not detect *A. phagocytophilum* by PCR in the acute samples. We deposited nucleotide sequences of *groEL* and 16S rRNA genes generated in this study in GenBank under accession nos. OQ579033 (*groEL*) and OQ581737 (16S rRNA).

On the basis of PCR results, the patient was treated with doxycycline (100 mg 2×/d for 3 wk), and fever disappeared after 72 hours. Neutropenia was attributed to the intake of metamizole for symptom control. However, another case of doxycycline-treated *Candidatus* N. mikurensis infection associated with neutropenia has been reported (*8*). EDTA-anticoagulated blood and serum specimens were collected 4

Table 2. Sequence analyses of targeted genes after PCR of DNA from different clinical samples in study of *Candidatus* Neoehrlichia mikurensis infection in patient with antecedent hematologic neoplasm, Spain*

Disease stage	Clinical sample	PCR target genes		
		Panbacteria 16S rRNA	16S rRNA-EHR†	*groEL*‡
Acute	Bone marrow	98% (13,35/1,362) to 99.8% (1,359/1,362),§ CP054597	100% (306/306), CP054597	99.3% (1,224/1,233), MN701626; 98.9% (1,218/1,232), CP054597
	Serum	95.4% (753/789),§ CP054597	ND	99.3% (1,224/1,233), MN701626; 98.9% (1,218/1,232), CP054597
Convalescent, 4th mo	EDTA blood	98% (1,305/1,332), CP054597	ND	ND
	Serum	ND	ND	ND
Convalescent, 6th mo	EDTA blood	ND	ND	ND
	Serum	ND	ND	ND

*Values are highest % identity (identical base pairs/total base pairs), followed by GenBank accession number. ND, not detected.
†16S rRNA-EHR refers to the 16S rRNA sequence from the Anaplasmataceae family, which is different from the PCR-amplified panbacteria 16S rRNA sequence.
‡ Percentage of identity with *groEL Candidatus* N. mikurensis gene from a reference patient in Sweden (GenBank accession no. CP054597) was lower than that of *groEL Candidatus* N. mikurensis isolate Omsk-41_Micagr from a small mammal in Siberia, Russia (GenBank accession no. MN701626).
§Sequence with degenerate bases or obtained from only 1 DNA strand (insufficient sample).

(December 2021) and 6 (February 2022) months after onset of the acute infection phase, and we screened for *Candidatus* N. mikurensis at the Center for Rickettsioses and Arthropod-Borne Diseases, as previously described. We detected *Candidatus* N. mikurensis DNA in blood collected at 4 months but not in serum. The patient was healthy and blood test results did not show abnormalities at that time. Follow-up PCR of specimens collected at 6 months yielded negative results (Table 2). We did not detect IgG against *A. phagocytophilum*.

Conclusions

We report a confirmed case of *Candidatus* N. mikurensis infection in Spain, detected in human bone marrow aspirate, serum, and EDTA-blood samples, that was no longer detected months after completing antimicrobial drug treatment. A broad clinical spectrum of tickborne

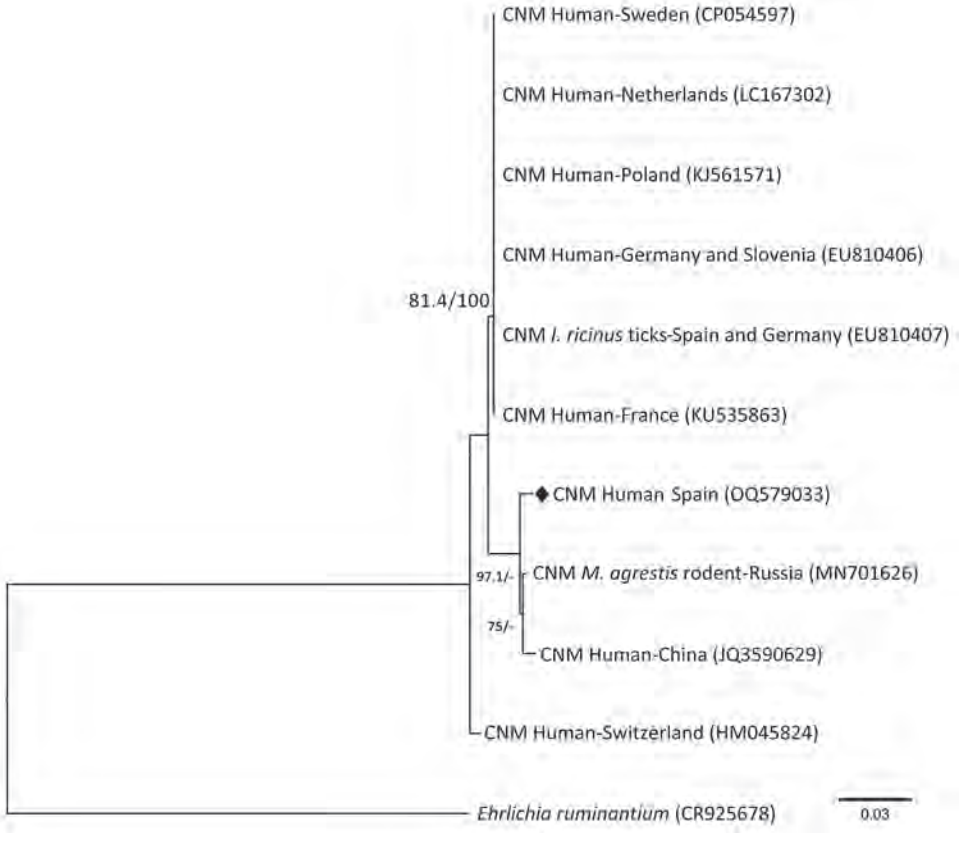

Figure. Phylogenetic analysis of *groEL* gene from *Candidatus* Neoehrlichia mikurensis infecting a patient with antecedent hematologic neoplasm, Spain. Phylogenetic tree was generated to compare 809 bp fragments of the 60-kDa heat shock protein gene *groEL* from *Candidatus* Neoehrlichia mikurensis by using IQ-tree software version 2.2.0 (http://www.iqtree.org), maximum-likelihood method, and substitution model consisting of 3-parameter model 2 plus empirical base frequencies with rate heterogeneity allowing for a proportion of invariable sites. Values are approximate likelihood ratio test/bootstrap percentages, indicating topologic branch support for maximum-likelihood analysis with 1,000 replicates; values >75% define high stability. Diamond indicates nucleotide sequence of *Candidatus* N. mikurensis *groEL* gene fragment obtained in this study. *Ehrlichia ruminantium* (Anaplasmataceae family) *groEL* sequence was used as the outgroup. GenBank accession numbers are in parentheses. CNM, *Candidatus* N. mikurensis; *I. ricunus*, *Ixodes ricunus*; *M. agrestis*, *Microtus agrestis*. Scale bar indicates nucleotide substitutions per site.

diseases is found in Spain. Human cases of Lyme borreliosis, Mediterranean spotted fever, and other tickborne rickettsioses have been described, including *Dermacentor* tick–borne necrosis erythema lymphadenopathy, *Rickettsia sibirica mongolitimonae* infection, *R. massiliae* infection, *R. aeschlimannii* infection, babesiosis, human anaplasmosis, tularemia, *Borrelia hispanica* relapsing fever, tick paralysis, Crimean-Congo hemorrhagic fever, and α-gal syndrome or other allergic reactions (*14*). Since we discovered *Candidatus* N. mikurensis in *I. ricinus* ticks in Spain (*13*), we have conducted surveillance of this bacterium. *Candidatus* N. mikurensis should be considered a potential cause of persistent fever and venous thrombosis in patients with hematologic malignancies who live in environments where ticks are prevalent. *Candidatus* N. mikurensis infections should be particularly suspected in patients who are immunosuppressed but also should be considered in patients with other vascular conditions who are not immunocompromised (*15*).

Acknowledgments

We thank Sonia Santibáñez, Ana M. Palomar, Ignacio Ruiz-Arrondo, and Paula Santibáñez for technical assistance.

This study was partially funded by Ministerio de Ciencia, Innovación y Universidades, Instituto de Salud Carlos III through the Spanish Network for Research in Infectious Diseases (RD16/0016/0013) (https://www.reipi.org) and co-funded by the European Regional Development Fund, A way to achieve Europe, ERDF.

About the Author

Dr. González-Carmona is a hematologist at Hospital de Jarrio in Asturias, Spain. Her research interests focus on opportunistic infections in cancer patients.

References

1. Kawahara M, Rikihisa Y, Isogai E, Takahashi M, Misumi H, Suto C, et al. Ultrastructure and phylogenetic analysis of '*Candidatus* Neoehrlichia mikurensis' in the family Anaplasmataceae, isolated from wild rats and found in *Ixodes ovatus* ticks. Int J Syst Evol Microbiol. 2004;54:1837–43. https://doi.org/10.1099/ijs.0.63260-0
2. Welinder-Olsson C, Kjellin E, Vaht K, Jacobsson S, Wennerås C. First case of human "*Candidatus* Neoehrlichia mikurensis" infection in a febrile patient with chronic lymphocytic leukemia. J Clin Microbiol. 2010;48:1956–9. https://doi.org/10.1128/JCM.02423-09
3. von Loewenich FD, Geissdörfer W, Disqué C, Matten J, Schett G, Sakka SG, et al. Detection of "*Candidatus* Neoehrlichia mikurensis" in two patients with severe febrile illnesses: evidence for a European sequence variant. J Clin Microbiol. 2010;48:2630–5. https://doi.org/10.1128/JCM.00588-10
4. Pekova S, Vydra J, Kabickova H, Frankova S, Haugvicova R, Mazal O, et al. *Candidatus* Neoehrlichia mikurensis infection identified in 2 hematooncologic patients: benefit of molecular techniques for rare pathogen detection. Diagn Microbiol Infect Dis. 2011;69:266–70. https://doi.org/10.1016/j.diagmicrobio.2010.10.004
5. Maurer FP, Keller PM, Beuret C, Joha C, Achermann Y, Gubler J, et al. Close geographic association of human neoehrlichiosis and tick populations carrying "*Candidatus* Neoehrlichia mikurensis" in eastern Switzerland. J Clin Microbiol. 2013;51:169–76. https://doi.org/10.1128/JCM.01955-12
6. Grankvist A, Andersson PO, Mattsson M, Sender M, Vaht K, Höper L, et al. Infections with the tick-borne bacterium "*Candidatus* Neoehrlichia mikurensis" mimic noninfectious conditions in patients with B cell malignancies or autoimmune diseases. Clin Infect Dis. 2014;58:1716–22. https://doi.org/10.1093/cid/ciu189
7. Andréasson K, Jönsson G, Lindell P, Gülfe A, Ingvarsson R, Lindqvist E, et al. Recurrent fever caused by *Candidatus* Neoehrlichia mikurensis in a rheumatoid arthritis patient treated with rituximab. Rheumatology (Oxford). 2015;54:369–71. https://doi.org/10.1093/rheumatology/keu441
8. Lenart M, Simoniti M, Strašek-Smrdel K, Špik VC, Selič-Kurinčič T, Avšič-Županc T. Case report: first symptomatic *Candidatus* Neoehrlichia mikurensis infection in Slovenia. BMC Infect Dis. 2021;21:579. https://doi.org/10.1186/s12879-021-06297-z
9. Boyer PH, Baldinger L, Degeilh B, Wirth X, Kamdem CM, Hansmann Y, et al. The emerging tick-borne pathogen *Neoehrlichia mikurensis*: first French case series and vector epidemiology. Emerg Microbes Infect. 2021;10:1731–8. https://doi.org/10.1080/22221751.2021.1973347
10. Li H, Jiang JF, Liu W, Zheng YC, Huo QB, Tang K, et al. Human infection with *Candidatus* Neoehrlichia mikurensis, China. Emerg Infect Dis. 2012;18:1636–9. https://doi.org/10.3201/eid1810.120594
11. Portillo A, Santibáñez P, Palomar AM, Santibáñez S, Oteo JA. '*Candidatus* Neoehrlichia mikurensis' in Europe. New Microbes New Infect. 2018;22:30–6. https://doi.org/10.1016/j.nmni.2017.12.011
12. Wass L, Grankvist A, Bell-Sakyi L, Bergström M, Ulfhammer E, Lingblom C, et al. Cultivation of the causative agent of human neoehrlichiosis from clinical isolates identifies vascular endothelium as a target of infection. Emerg Microbes Infect. 2019;8:413–25. https://doi.org/10.1080/22221751.2019.1584017
13. Palomar AM, García-Álvarez L, Santibáñez S, Portillo A, Oteo JA. Detection of tick-borne '*Candidatus* Neoehrlichia mikurensis' and *Anaplasma phagocytophilum* in Spain in 2013. Parasit Vectors. 2014;7:57. https://doi.org/10.1186/1756-3305-7-57
14. Portillo A, Ruiz-Arrondo I, Oteo JA. Arthropods as vectors of transmissible diseases in Spain. Med Clin (Engl Ed). 2018;151:450–9. https://doi.org/10.1016/j.medcle.2018.10.008
15. Höper L, Skoog E, Stenson M, Grankvist A, Wass L, Olsen B, et al. Vasculitis due to *Candidatus* Neoehrlichia mikurensis: a cohort study of 40 Swedish patients. Clin Infect Dis. 2021;73:e2372–8. https://doi.org/10.1093/cid/ciaa1217

Address for correspondence: José A. Oteo, Departamento de Enfermedades Infecciosas, Hospital Universitario San Pedro-CIBIR, Centro de Rickettsiosis y Enfermedades Transmitidas por Artrópodos Vectores, C/Piqueras 98, 26006 Logroño, La Rioja, Spain; email: jaoteo@riojasalud.es

Detection of Hantavirus during the COVID-19 Pandemic, Arizona, USA, 2020

Gavriella Hecht, Ariella P. Dale, Irene Ruberto, Guillermo Adame, Ryan Close, Sarah-Jean Snyder, Kathryn Pink, Nathanael Lemmon, Jessica Rudolfo, Michael Madsen, Andrea L. Wiens, Caitlin Cossaboom, Trevor Shoemaker, Mary J. Choi, Deborah Cannon, Inna Krapiunaya, Shannon Whitmer, Melissa Mobley, Emir Talundzic, John D. Klena, Heather Venkat

We identified 2 fatal cases of persons infected with hantavirus in Arizona, USA, 2020; 1 person was co-infected with SARS-CoV-2. Delayed identification of the cause of death led to a public health investigation that lasted ≈9 months after their deaths, which complicated the identification of a vector or exposure.

The COVID-19 pandemic has affected public health investigation and response activities for other illnesses; COVID-19 has particularly challenged the diagnosis of respiratory illnesses because of similar clinical manifestations. Hantavirus pulmonary syndrome is a rare disease transmitted predominantly by infected rodents shedding the virus through saliva, urine, and feces. Sin Nombre virus is the strain of hantavirus identified in 1993 in deer mice (*Peromyscus maniculatus*) in the Four Corners region of the southwestern United States; in total, 81 human cases of hantavirus have been documented throughout Arizona through 2019 (*1*–*3*).

In March 2020, deaths of a mother and son living both on and around the White Mountain Apache Reservation in Arizona, USA, just outside of the Four Corners region, were reported to the Arizona Department of Health Services (ADHS). On September 15, 2020, the Centers for Disease Control and Prevention (CDC) notified ADHS that the mother tested positive for hantavirus, and the son was confirmed to be co-infected with both hantavirus and SARS-CoV-2.

Author affiliations: Arizona Department of Health Services, Phoenix, Arizona, USA (G. Hecht, A.P. Dale, I. Ruberto, G. Adame, H. Venkat); Centers for Disease Control and Prevention, Atlanta, Georgia, USA (A.P. Dale, C. Cossaboom, T. Shoemaker, M.J. Choi, D. Cannon, I. Krapiunaya, S. Whitmer, M. Mobley, E. Talundzic, J.D. Klena, H. Venkat); Indian Health Service, Whiteriver, Arizona, USA (R. Close, K. Pink, N. Lemmon); Indian Health Service, Show Low, Arizona, USA (S.-J. Snyder); White Mountain Apache Tribe, Whiteriver (J. Rudolfo); Coconino County Health and Human Services, Flagstaff, Arizona, USA (M. Madsen); Maricopa County Office of the Medical Examiner, Phoenix (A.L. Wiens)

DOI: http://doi.org/10.3201/eid2908.221808

The Study

Patient 1 (P1) was a 25-year-old Native American woman with an unremarkable medical history who lived at her primary residence (residence A), a fourplex apartment on the White Mountain Apache Reservation, until her death in March 2020. She often visited her extended family at residence B, a single-family home 120 miles away, in eastern Arizona. P1 reported progressive shortness of breath beginning on March 12 (Figure 1). She stayed at a casino during March 13–17 and cleaned her apartment during March 17–18.

On March 18, P1 was transported to the hospital by emergency medical services (EMS) reporting shortness of breath, abdominal pain, and hemoptysis. In the emergency department (ED), she was febrile (temperature 101°F), tachypneic, and hypoxic; she was later intubated. Asphyxiation was initially suspected because of mixing cleaning chemicals. A chest radiograph showed diffuse bilateral infiltrates and an acute respiratory distress syndrome pattern. The ED physician documented that the radiograph looked suspicious for hantavirus, COVID-19, or diffuse bacterial pneumonia. ED physicians also diagnosed multiorgan system failure, metabolic acidosis, and metabolic encephalopathy. P1 was transferred to another hospital for a higher level of care; she was placed on extracorporeal membrane oxygenation. She died on

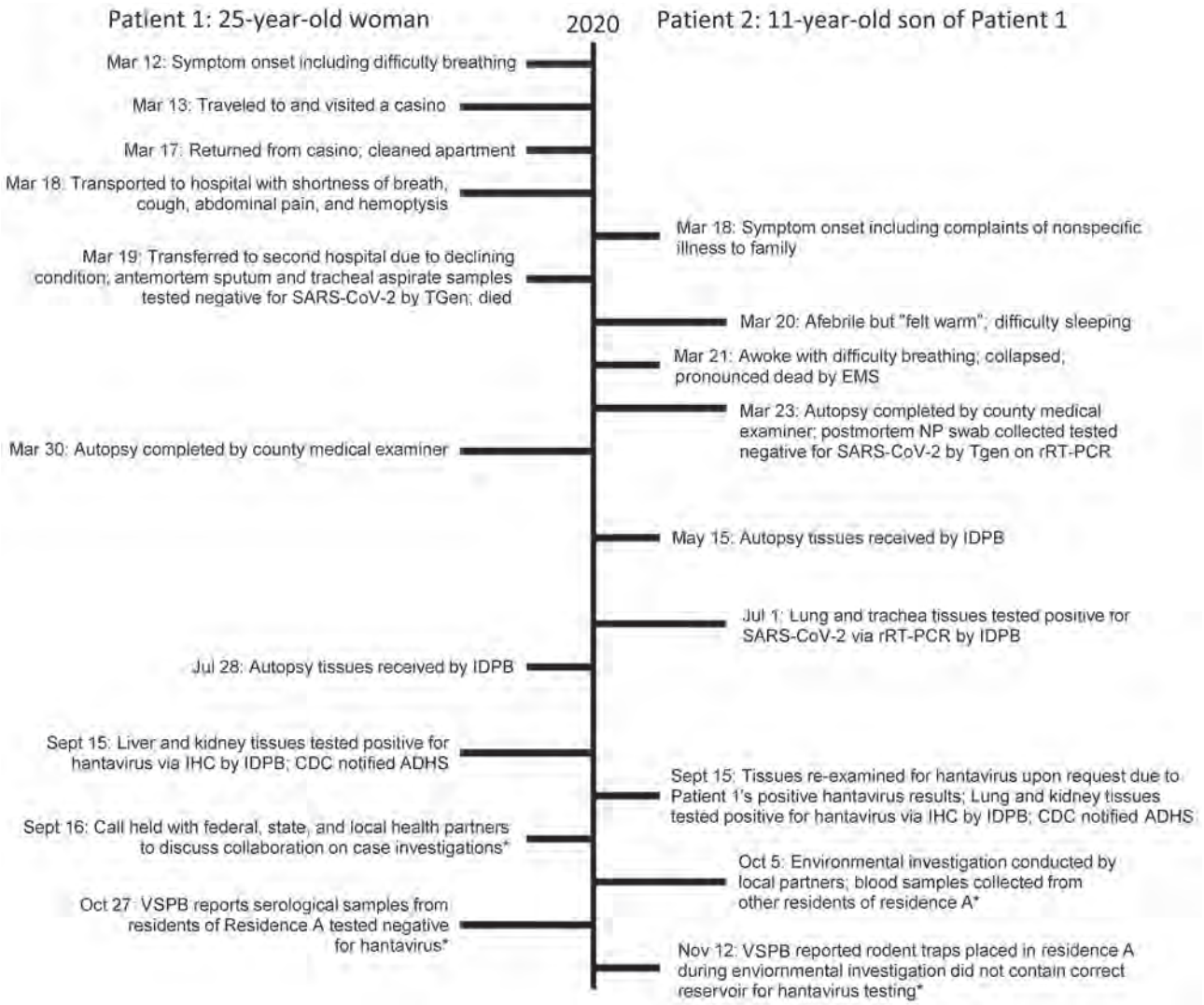

Figure 1. Timeline of illness course, laboratory testing, and public health investigations for 2 patients who died of hantavirus infection, Arizona, USA. Asterisk (*) indicates reported information that applies to both cases. IDPB, Infectious Diseases Pathology Branch, CDC (National Center for Emerging and Zoonotic Infectious Diseases, Division of High-Consequence Pathogens and Pathology); IHC, immunohistochemical testing; CDC, Centers for Disease Control and Prevention; NP, nasopharyngeal; rRT-PCR, real time reverse transcription PCR; TGen, Translational Genomics Research Institute; VSPB, Viral Special Pathogens Branch, CDC (National Center for Emerging and Zoonotic Infectious Diseases, Division of High-Consequence Pathogens and Pathology).

March 19. Antemortem nasopharyngeal swab real-time reverse transcription PCR (rRT-PCR) testing for SARS-CoV-2 and respiratory viral panel testing for influenza A/B were both negative (*4*).

Patient 2 (P2) was the 11-year-old Native American male child of P1 and had an unremarkable medical history. He split time between residence A (second half of February 2020) and residence B (March 2020); he visited residence A at least 1 time in March.

On the morning of March 20, P2 was reportedly feeling unwell for 2 days and was warm but afebrile, for which he was given aspirin (dose unknown). He vomited later that day and had difficulty sleeping that evening, for which he was given 2 diphenhydramine/acetaminophen tablets (dose unknown). He awoke during the night because of difficulty breathing and collapsed out of his bed. He became unresponsive. EMS subsequently transported him to the ED, where he was pronounced dead on March 21.

The county medical examiner performed an autopsy on P2 on March 23. Postmortem nasopharyngeal swab testing for SARS-CoV-2 was rRT-PCR negative. During the autopsy, the examiner suspected an underlying pulmonary process contributing to his cause of death. Multiple tissues were sent to CDC for analysis; samples were received on May 15. On July 1,

samples of P2's lung and trachea tissues tested positive for SARS-CoV-2 by rRT-PCR (*5*), despite negative immunohistochemical results.

Because of the epidemiologic link between the 2 cases and unknown etiology of death for P1, tissues from P1 were submitted to CDC and received on July 28. Pathologic findings for both cases were similar; however, P1 did not have evidence of SARS-CoV-2. The pathologist observed findings that resembled hantavirus infection, which were later confirmed by positive IHC assay on liver and kidney tissues on September 15 (*5*). Because of resemblance between tissues of the 2 case-patients, P2's tissues were reexamined, and hantavirus IHC results were positive on lung and kidney tissues. The county medical examiner later determined hantavirus to be the major

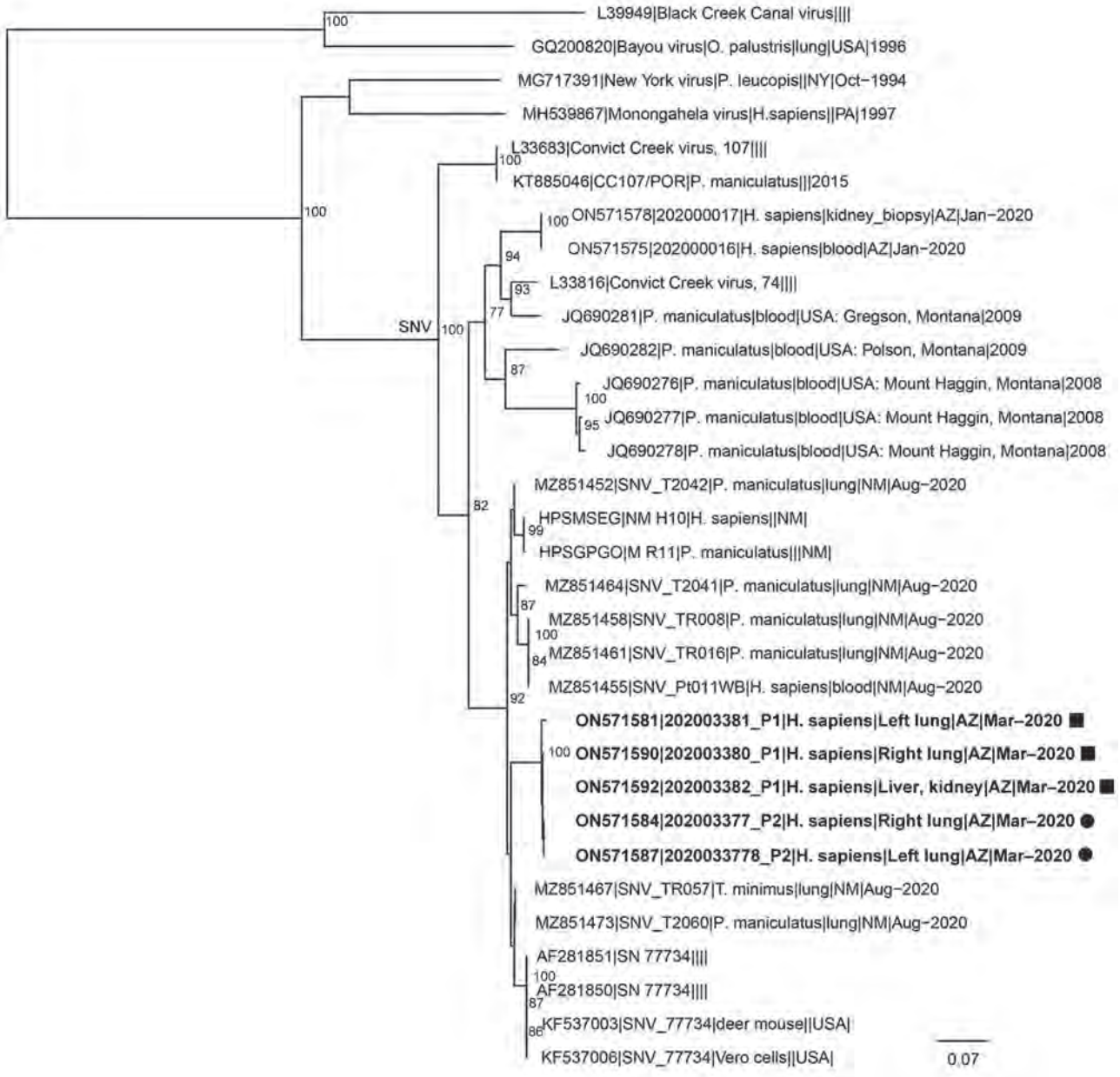

Figure 2. Phylogenetic tree for *Orthohantavirus* short (S) segment of samples from 2 patients who died of hantavirus infection, Arizona, USA. We inferred the phylogenetic history of full-length Sin Nombre virus S segment using maximum-likelihood estimation. Non–Sin Nombre virus species, Black Creek Canal virus, and Bayou virus are included as outgroups. Bold indicates isolates from this study; squares indicate those from patient 1 and circles those from patient 2. Numbers at nodes indicate bootstrap support >70% after 1,000 iterations. Phylogenetic trees were made using a nucleotide alignment of *Orthohantavirus* S segments. GenBank accession numbers are provided. Scale bar indicates nucleotide substitutions per site. Additional phylogenetic trees for *Orthohantavirus* medium and large segments of Sin Nombre virus are in the Appendix (https://wwwnc.cdc.gov/EID/article/29/8/22-1808-App1.pdf).

contributing factor to P1 and P2's deaths. Hantavirus genomes from P1 and P2 were closely related, indicating a common source of exposure (Figure 2). We submitted hantavirus sequences from the cases to GenBank (accession nos. ON571574–93).

On September 15, CDC alerted ADHS of the 2 positive hantavirus results. The next day, a call was held with federal, state, and local partners to coordinate a collaborative case investigation. On October 5, the Indian Health Service (IHS) conducted an environmental investigation of residence A and collected 16 human blood samples from 17 residents living in the fourplex, including household members of P1 and P2. Hantavirus serology assays for 16 human samples all tested negative for hantavirus IgM and IgG (*6*). IHS provided hantavirus prevention public service announcements to local health officials; the announcements were later disseminated to the community through newspaper and radio.

We conducted an environmental investigation because both residence A and residence B displayed potential for deer mice habitat. Trapping conducted in residence A confirmed the presence of rodents by identifying house mice (*Mus musculus*) in 4 of 6 snap traps; we did not test the mice because that species is not a known reservoir for hantavirus. Unfortunately, we were not able to conduct trapping at residence B. All partners involved mutually decided to end the investigation.

The time interval from symptom onset to diagnosis was ≈6 months. Despite the local ED physician suspecting hantavirus in P1, medical records showed no evidence of hantavirus testing ordered at either hospital. Local health and medical staff were focused on the response to initial cases of SARS-CoV-2 in the region. The time between postmortem tissue submission and subsequent sample testing contributed to the delay. Testing delays might have resulted from CDC requirement of confirmatory diagnostic testing on all confirmed or suspected COVID-19 deaths (*5*). Hantavirus was identified 6 weeks after P2's tissue examination; P1's lung tissue resembled that of P2 but tested negative for SARS-CoV-2. Delays in case identification caused the environmental investigation to be conducted 7 months after disease onset. The rodent population might have changed during that period, preventing identification of the vector and exposure.

Conclusions

In the cases we report, hantavirus infection was not promptly detected when patients sought medical care or during postmortem examination. To aid in the diagnosis of hantavirus, we recommend adoption of the 5-point hantavirus screening tool for areas outside the Four Corners region (*7*,*8*). The COVID-19 pandemic likely played a role in delayed detection of hantavirus for these cases because of its effects on aspects of healthcare and public health (*9*–*12*). Hantavirus education should continue to be a priority in healthcare facilities in disease-endemic regions, including on tribal lands. Community education can help to minimize the impact of hantavirus cases by offering tools to prevent exposure and encourage seeking prompt medical care.

During pandemic response, public health partners should continue to monitor and respond to other pathogens. Medical providers should consider both alternative and concurrent diagnoses in the presence of COVID-19–like illness, including rare pathogens such as hantavirus. Timely investigations of high-consequence illnesses will enable public health organizations to take prompt action.

Acknowledgments

We acknowledge the 2 patients, their families, and the White Mountain Apache Tribe. We also thank the many tribal health partners whose efforts were essential to this investigation. Last, we acknowledge the late Dr. Sherif Zaki and his team at the CDC Infectious Diseases Pathology Branch (National Center for Emerging and Zoonotic Infectious Diseases, Division of High-Consequence Pathogens and Pathology) for their collaborative efforts in this investigation.

This work was supported by the CDC Epidemiology and Laboratory Capacity for Infectious Diseases cooperative agreement. This report was supported in part by an appointment to the Applied Epidemiology Fellowship Program administered by the Council of State and Territorial Epidemiologists (CSTE) and funded by CDC cooperative agreement no. 1NU38OT000297-03-00.

About the Author

Ms. Hecht is a former CDC/CSTE Applied Epidemiology Fellow assigned to the Arizona Department of Health Services. At the time of publication, she is a first-year PhD student in medical geography at the University of Florida. Her primary research interests include disease ecology, spatial epidemiology, and understanding health at the human-animal-environment interface.

References

1. Sands L, Kioski C, Komatsu K. Hantavirus in the southwestern United States: epidemiology of an emerging pathogen. J Am Osteopath Assoc. 1993;93:1279–85.

2. Zaki SR, Greer PW, Coffield LM, Goldsmith CS, Nolte KB, Foucar K, et al. Hantavirus pulmonary syndrome. Pathogenesis of an emerging infectious disease. Am J Pathol. 1995;146:552–79.
3. Centers for Disease Control and Prevention. Reported cases of hantavirus disease. 2019 Feb 26 [cited 2021 Aug 4]. https://www.cdc.gov/hantavirus/surveillance/index.html
4. Emery SL, Erdman DD, Bowen MD, Newton BR, Winchell JM, Meyer RF, et al. Real-time reverse transcription-polymerase chain reaction assay for SARS-associated coronavirus. Emerg Infect Dis. 2004; 10:311–6. https://doi.org/10.3201/eid1002.030759
5. Bhatnagar J, Gary J, Reagan-Steiner S, Estetter LB, Tong S, Tao Y, et al. Evidence of severe acute respiratory syndrome coronavirus 2 replication and tropism in the lungs, airways, and vascular endothelium of patients with fatal coronavirus disease 2019: an autopsy case series. J Infect Dis. 2021;223:752–64. https://doi.org/10.1093/infdis/jiab039
6. MacNeil A, Comer JA, Ksiazek TG, Rollin PE. Sin Nombre virus-specific immunoglobulin M and G kinetics in hantavirus pulmonary syndrome and the role played by serologic responses in predicting disease outcome. J Infect Dis. 2010;202:242–6. https://doi.org/10.1086/653482
7. Koster F, Foucar K, Hjelle B, Scott A, Chong YY, Larson R, et al. Rapid presumptive diagnosis of hantavirus cardiopulmonary syndrome by peripheral blood smear review. Am J Clin Pathol. 2001;116:665–72. https://doi.org/10.1309/CNWF-DC72-QYMR-M8DA
8. Dvorscak L, Czuchlewski DR. Successful triage of suspected hantavirus cardiopulmonary syndrome by peripheral blood smear review: a decade of experience in an endemic region. Am J Clin Pathol. 2014;142:196–201. https://doi.org/10.1309/AJCPNFVWG46NUHED
9. Snapiri O, Rosenberg Danziger C, Krause I, Kravarusic D, Yulevich A, Balla U, et al. Delayed diagnosis of paediatric appendicitis during the COVID-19 pandemic. Acta Paediatr. 2020;109:1672–6. https://doi.org/10.1111/apa.15376
10. Harahsheh AS, Dahdah N, Newburger JW, Portman MA, Piram M, Tulloh R, et al. Missed or delayed diagnosis of Kawasaki disease during the 2019 novel coronavirus disease (COVID-19) pandemic. J Pediatr. 2020;222:261–2. https://doi.org/10.1016/j.jpeds.2020.04.052
11. Murri D, Botti C, Bassano E, Fornaciari M, Crocetta FM, Ghidini A. Reduction in healthcare services during the COVID-19 pandemic: patient screening based on symptoms is an effective strategy for avoiding delayed laryngeal cancer diagnosis. Am J Otolaryngol. 2021;42:103162. https://doi.org/10.1016/j.amjoto.2021.103162
12. Hassan H, Elazar A, Takabe K, Datta R, Takahashi H, Seitelman E. Scalp leiomyosarcoma: diagnosis and treatment during a global pandemic with COVID-19. World J Oncol. 2021;12:132–6. https://doi.org/10.14740/wjon1393

Address for correspondence: Gavriella Hecht, Arizona Department of Health Services, 150 N 18th Ave, Ste 140, Phoenix, AZ 85020, USA; email: gavriella.hecht@azdhs.gov

etymologia revisited

Originally published in March 2019

Streptomycin

strep'to-mi'sin

In the late 1930s, Selman Waksman, a soil microbiologist working at the New Jersey Agricultural Station of Rutgers University, began a large-scale program to screen soil bacteria for antimicrobial activity. By 1943, Albert Schatz, a PhD student working in Waksman's laboratory, had isolated streptomycin from *Streptomyces griseus* (from the Greek *strepto-* ["twisted"] + *mykēs* ["fungus"] and the Latin *griseus*, "gray").

In 1944, Willam H. Feldman and H. Corwin Hinshaw at the Mayo Clinic showed its efficacy against *Mycobacterium tuberculosis*. Waksman was awardeda Nobel Prize in 1952 for his discovery of streptomycin, although much of the credit for the discovery has since been ascribed to Schatz. Schatz later successfully sued to be legally recognized as a co-discoverer of streptomycin.

References:

1. Comroe JH Jr. Pay dirt: the story of streptomycin. Part I. From Waksman to Waksman. Am Rev Respir Dis. 1978;117:773–81.
2. Wainwright M. Streptomycin: discovery and resultant controversy. Hist Philos Life Sci. 1991;13:97–124.

https://wwwnc.cdc.gov/eid/article/25/3/et-2503_article

Multidrug-Resistant *Shigella sonnei* Bacteremia among Persons Experiencing Homelessness, Vancouver, British Columbia, Canada

A. Stefanovic, N. Matic, G. Ritchie, C.F. Lowe, V. Leung, M. Hull, M. Alam, M. Dawar, S. Champagne, M.G. Romney

Increased invasive bloodstream infections caused by multidrug resistant *Shigella sonnei* were noted in Vancouver, British Columbia, Canada, during 2021–2023. Whole-genome sequencing revealed clonal transmission of genotype 3.6.1.1.2 (CipR.MSM5) among persons experiencing homelessness. Improvements in identifying *Shigella* species, expanding treatment options for multidrug resistant infections, and developing public health partnerships are needed.

Shigellosis manifestations range from mild gastrointestinal infection to severe illness with dysentery and sepsis (*1*). In high-income countries, *Shigella sonnei* is the most common species, causing infections typically among men who have sex with men (MSM) and travelers (*1*,*2*). Transmission occurs through sexual contact in MSM or the fecal–oral route from contaminated water, food, or fomites (*3*). Although clinical manifestations range broadly, *S. sonnei* rarely causes invasive bloodstream infections. Only a few published case reports describe bacteremia (*4*–*6*), mostly among malnourished children, MSM, or adults with HIV, diabetes, cirrhosis, or immunosuppression (*4*,*6*,*7*). We describe the epidemiology, genotyping, and resistance determinants of clonal multidrug-resistant (MDR) *S. sonnei* bacteremia in Vancouver, British Columbia, Canada, and discuss challenges in diagnosing *Shigella* bacteremia in the microbiology laboratory. The University of British Columbia/Providence Health Care Research Ethics Board approved our study (H22–02183).

Author affiliations: St. Paul's Hospital, Vancouver, British Columbia, Canada (A. Stefanovic, N. Matic, G. Ritchie, C.F. Lowe, V. Leung, S. Champagne, M.G. Romney); University of British Columbia, Vancouver (A. Stefanovic, N. Matic, G. Ritchie, C.F. Lowe, V. Leung, M. Hull, M. Alam, S. Champagne, M.G. Romney); British Columbia Centre for Excellence in HIV/AIDS, Vancouver (M. Hull); Vancouver Coastal Health Authority, Vancouver (M. Dawar); University of British Columbia School of Population and Public Health, Vancouver (M. Dawar)

DOI: https://doi.org/10.3201/eid2908.230323

The Study

The microbiology laboratory at St. Paul's Hospital (Vancouver, BC, Canada) serves acute-care hospitals and the surrounding community in downtown Vancouver. We searched the laboratory database for *S. sonnei* found in feces and blood samples during January 2010–January 2023, separated into 2010–2020 (historical) and 2021–2023 (recent) periods. We reviewed medical records of patients with bacteremia and recorded demographics, symptoms, housing, sexual orientation, travel, substance use, coexisting conditions, hospitalization, antimicrobial susceptibility testing (AST), treatment, and mortality.

We processed positive blood cultures detected by BacT/AlertT system (bioMérieux, https://www.biomerieux.com) using VitekMS+ (bioMérieux) or FilmArray BCID (BioFire Diagnostics; https://www.biofiredx.com) with established microbiology protocols and identified pathogens. We identified *Shigella* in feces using benchtop biochemical methods, Vitek2 ID (bioMérieux) and Polyvalent Agglutination Sera (Remel, http://www.remel.com). If we suspected *Shigella* in blood samples, we used Vitek2 ID and polyvalent serology. No changes in laboratory testing protocols occurred during 2010–2023. We performed AST for ampicillin, trimethoprim/sulfamethoxazole, ciprofloxacin, ceftriaxone, and azithromycin according to Clinical and Laboratory Standards Institute M100 standards (https://clsi.org/

standards/products/microbiology/documents/m100). We performed whole-genome sequencing (WGS) on isolates incubated in Mueller-Hinton broth, extracted on MagNA Pure 24 (Roche; https://diagnostics.roche.com), and processed on GridION R10.4 flowcells (Nanopore, https://nanoporetech.com). We basecalled runs with Guppy version 6.3.9 (https://github.com/nanoporetech/rerio) and uploaded to BugSeq (https://bugseq.com) for automated analysis.

We identified 11 cases of *S. sonnei* bacteremia that occurred within the historical (n = 2) or recent (n = 9) periods during 2010–2023. We also observed a recent increase in fecal isolates with *S. sonnei* (Figure). Differences in the proportion of bacteremic among all shigellosis cases occurring during the recent compared with the historical period were not statistically significant (7.7% vs. 2.9%; p = 0.21 by Fisher exact test). Among recent cases, 89% (8/9) of patients were male (median 45 years of age, interquartile range 35–54 years) (Table). All but 1 were underhoused or experiencing homelessness and had polysubstance use disorder. Most (89%) inhabited Vancouver's downtown eastside, the neighborhood with the highest density of Vancouver's urban poor population. Unlike the historical case-patients, none were MSM or had travel histories. Most (89%) were not severely immunocompromised. Case-patient A had multiple myeloma but stable housing. Five (55%) patients presented with sepsis and 6 (67%) were hospitalized; the remaining patients declined recommended hospital admission.

Among the 2021–2023 cases, AST profiles were identical except in case A. The isolates were resistant to ampicillin, trimethoprim/sulfamethoxazole, ciprofloxacin, and azithromycin and susceptible to ceftriaxone. An isolate from case-patient A displayed ceftriaxone resistance and azithromycin susceptibility. *Shigella* was initially misidentified as *E. coli* in all 9 cases (8 by VitekMS+, 1 by FilmArray BCID). All isolates were indole negative, non–lactose fermenting (NLF) colonies, subsequently identified correctly as *S. sonnei* by Vitek2 ID and confirmed by polyvalent serology.

We performed WGS on all 2021–2023 *S. sonnei* isolates from blood samples. Using a new genotypic framework (*8*), we identified 8 of the 2021–2023 isolates as 3.6.1.1.2 (CipR.MSM5); the isolate from case-patient A genotyped as 3.6.3 (Central Asia III). The strain from the 2016 case genotyped as 3.7.18 (Global III); the 2013 strain did not undergo WGS. We identified mutations *gyrA* S83L, *gyrA* D87G, and *parC* S80I encoding ciprofloxacin resistance and plasmid AA336-borne *mphA* and *ermB* encoding azithromycin resistance in all isolates from persons experiencing homelessness (PEH). The 3.6.3 strain carried *qnrS1*, *gyrA* D87Y, *gyrA* S83L and *parC* S80I, which confers ciprofloxacin resistance, and $bla_{\text{CTX-M-15}}$, which confers ceftriaxone resistance.

Conclusions

The recent increase in *S. sonnei* bacteremia might reflect the overall increase in shigellosis, including *S. sonnei* isolated from feces. The increased proportion of bacteremia cases in the past 2 years compared with the 11-year historical period was not statistically significant. However, the 7.7% prevalence of bacteremia is still very high compared with a range of rates, 0.4%–7.3%, reported in the literature (*9*). Historically, shigellosis has occurred in British Columbia predominantly as a sexually transmitted enteric infection among MSM (*10*). In our study, invasive shigellosis among PEH was probably transmitted

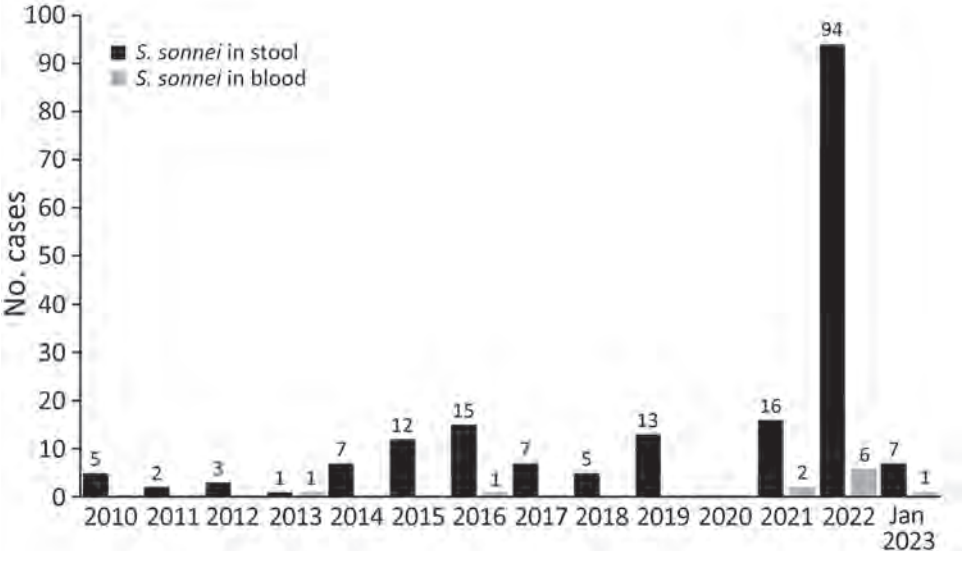

Figure. Epidemic curve of *Shigella sonnei* cases from feces and blood Vancouver, British Columbia, Canada, 2010–January 2023

Table. Characteristics and outcomes of cases of *Shigella sonnei* bacteremia during recent and historical time periods, Vancouver, British Columbia, Canada*

Characteristic	Cases of *Shigella sonnei* bacteremia	
	Recent, 2021–Jan 2023, n = 9	Historical, 2010–2020, n = 2
Age, y	Median 45, range 27–69	Median 62, range 56–68
Sex	8 (89%) male	2 (100%) male
Housing		
Private residence	1 (11)	2 (100)
Single room occupancy hotel/shelter	5 (56)	0
No fixed address	2 (22)	0
Rehabilitation center	1 (11)	0
Men who have sex with men	0	2 (100)
Travel history	0	1 (50)
Substance use	8 (89)	0
Coexisting conditions		
HIV	1 (11)	1 (50)
Immunocompromising conditions†	1 (11)	1 (50)
Liver disease	2 (22)	0
Pulmonary disease	1 (11)	0
Cardiac disease	1 (11)	0
Chronic renal disease	0	1 (50)
Recurrence	1 (11)	0
Hospitalization		
Admitted to hospital ward	6 (67)	2 (100)
Declined hospital admission	3 (33)	0
Antimicrobial test results		
Ampicillin resistant	9 (100)	2 (100)
Trimethoprim/sulfamethoxazole resistant	9 (100)	2 (100)
Ciprofloxacin resistant	9 (100)	0
Azithromycin resistant	8 (89)	Not tested
Ceftriaxone resistant	1 (11)	0
Treatment		
7–14 d of effective oral antimicrobial agent	0	1 (50)
7–14 d of effective IV antimicrobial agent	6 (67)	1 (50)
Incomplete	3 (33)	0
30-d all-cause mortality	0	0

*Values are no. (%) except as indicated. IV, intravenous.
†Organ transplantation, malignancy receiving chemotherapy, asplenia, uncontrolled HIV (CD4 count <200 cells/μL), and immunosuppressive medications.

fecal-orally through contaminated environment and hands. An outbreak among PEH in Oregon was similarly believed to have resulted from inadequate access to hygiene and sanitation (*11*). WHO warns of outbreak risk from *S. sonnei* being introduced into areas with suboptimal water, sanitation, and hygiene standards (*12*). Because patient immunosuppression fails to explain increased bacteremia, other factors, such as drug use, malnutrition, and high inoculum dose, should be considered.

A study in Seattle, Washington, USA described a contemporary increase in MDR *S. sonnei* cases among PEH (*13*). Although the report did not comment on bacteremia, it highlighted the circulation of extensively-drug resistant *S. sonnei* carrying the extended-spectrum β-lactamase CTX-M-27. Although extensively-drug resistant *S. sonnei* was rare in our review, increased hospitalization and the need for parenteral therapy because of MDR *S. sonnei* bacteremia still substantially affected the healthcare system. One third of our patients did not complete treatment, potentially leading to ongoing transmission and illness. In addition to finding and treating cases, essential community control measures include working with housing providers to promote handwashing and sanitation practices, providing advice on recognizing and controlling infectious diarrhea, and developing pathways to reengage those who refuse hospitalization to complete parenteral antimicrobial treatment as outpatients.

Isolates from 8/9 PEH were genotype 3.6.1.1.2 (CipR.MSM5/BAPS3), epidemiologically distinct from the single isolate typed as 3.6.3 (Central Asia III). The isolate from the 2016 case had a different genotype, 3.7.18, matching that from an outbreak reported in California, USA (*14*). Despite its geographic proximity to Vancouver, the recent *S. sonnei* outbreak among PEH in Seattle involved yet another different genotype, 3.7.29.1.4.1 (global III VN2.KH1.Aus) (*14*). The 3.6.1.1.2 strain predominant in our study has previously been described in Australia, England, and the United States (*8*).

Our study included analysis of data only from patients seeking treatment at a hospital where blood

cultures were collected, possibly representing the sickest cohort of patients, leading to underestimation of actual infections. Not all cases with *S. sonnei* isolated from feces have yet been analyzed to determine wider epidemiologic and antimicrobial resistance trends. Further studies are needed to elucidate whether the high rate of bacteremia reflects increased virulence of this strain, higher inoculum size, or host determinants.

Because current laboratory methods can misidentify *Shigella* as *E. coli* in bloodstream infections, laboratories must scrutinize diagnoses of *E. coli* bacteremia in high-risk patients with infectious diarrhea and sepsis. Clinicians and public health officials should be made aware of MDR *S. sonnei* bacteremia as a cause of increased illness among PEH and the need for parenteral therapy in the event of resistance to first- and second-line antimicrobial agents.

About the Author

Dr. Stefanovic is a medical microbiologist at St. Paul's Hospital and a clinical associate professor at the University of British Columbia in Vancouver, British Columbia, Canada.

References

1. Kotloff KL, Riddle MS, Platts-Mills JA, Pavlinac P, Zaidi AKM. Shigellosis. Lancet. 2018;391:801–12. https://doi.org/10.1016/S0140-6736(17)33296-8
2. Ram PK, Crump JA, Gupta SK, Miller MA, Mintz ED. Part II. Analysis of data gaps pertaining to *Shigella* infections in low and medium human development index countries, 1984–2005. Epidemiol Infect. 2008;136:577–603. https://doi.org/10.1017/S0950268807009351
3. Shiferaw B, Shallow S, Marcus R, Segler S, Soderlund D, Hardnett FP, et al.; Emerging Infections Program FoodNet Working Group. Trends in population-based active surveillance for shigellosis and demographic variability in FoodNet sites, 1996–1999. Clin Infect Dis. 2004;38(Suppl 3):S175–80. https://doi.org/10.1086/381584
4. Tobin-D'Angelo M, Oosmanally N, Wilson SN, Anderson EJ, Segler S, Poventud L. *Shigella* bacteremia, Georgia, USA, 2002–2012. Emerg Infect Dis. 2020;26:122–4. https://doi.org/10.3201/eid2601.181698
5. Hawkins C, Taiwo B, Bolon M, Julka K, Adewole A, Stosor V. *Shigella sonnei* bacteremia: two adult cases and review of the literature. Scand J Infect Dis. 2007;39:170–3. https://doi.org/10.1080/00365540600786580
6. Morduchowicz G, Huminer D, Siegman-Igra Y, Drucker M, Block CS, Pitlik SD. *Shigella* bacteremia in adults. A report of five cases and review of the literature. Arch Intern Med. 1987;147:2034–7. https://doi.org/10.1001/archinte.1987.00370110162025
7. Struelens MJ, Patte D, Kabir I, Salam A, Nath SK, Butler T. *Shigella* septicemia: prevalence, presentation, risk factors, and outcome. J Infect Dis. 1985;152:784–90. https://doi.org/10.1093/infdis/152.4.784
8. Hawkey J, Paranagama K, Baker KS, Bengtsson RJ, Weill FX, Thomson NR, et al. Global population structure and genotyping framework for genomic surveillance of the major dysentery pathogen, *Shigella sonnei*. Nat Commun. 2021;12:2684. https://doi.org/10.1038/s41467-021-22700-4
9. Struelens MJ, Patte D, Kabir I, Salam A, Nath SK, Butler T. *Shigella* septicemia: prevalence, presentation, risk factors, and outcome. J Infect Dis. 1985;152:784–90. https://doi.org/10.1093/infdis/152.4.784
10. Narayan S, Galanis E; BC STEI Group. Are enteric infections sexually transmitted in British Columbia? Can Commun Dis Rep. 2016;42:24–9. https://doi.org/10.14745/ccdr.v42i02a01
11. Harris CL. Notes from the field. Historian. 2020;81:393–7. https://doi.org/10.1111/hisn.13197
12. World Health Organization. Disease outbreak news: extensively drug-resistant *Shigella sonnei* infections—Europe—European region (EURO) [cited 2023 Feb 20]. https://www.who.int/emergencies/disease-outbreak-news/item/extensively-drug-resistant-shigella-sonnei-infections---europe
13. Tansarli GS, Long DR, Waalkes A, Bourassa LA, Libby SJ, Penewit K, et al. Genomic reconstruction and directed interventions in a multidrug-resistant shigellosis outbreak in Seattle, WA, USA: a genomic surveillance study. Lancet Infect Dis. 2023;23:740–50. https://doi.org/10.1016/S1473-3099(22)00879-9
14. Kozyreva VK, Jospin G, Greninger AL, Watt JP, Eisen JA, Chaturvedi V. Recent outbreaks of shigellosis in California caused by two distinct populations of *Shigella sonnei* with either increased virulence or fluoroquinolone resistance. MSphere. 2016;1:e00344–16. https://doi.org/10.1128/mSphere.00344-16

Address for correspondence: Aleksandra Stefanovic, St. Paul's Hospital, Providence Health Care, 1081 Burrard St, Vancouver, BC V6Z 1Y6, Canada; email: astefanovic@providencehealth.bc.ca

Pediatric SARS-CoV-2 Seroprevalence, Oregon, USA, November 1, 2020–June 30, 2022

Rebecca A. Falender, Paul G. Mitchell, Judith A. Guzman-Cottrill, Paul R. Cieslak, Melissa Sutton

We estimated SARS-CoV-2 seroprevalence in children in Oregon, USA, at 6 time points. Seroprevalence increased linearly during November 2020–December 2021 and peaked in February 2022 at 38.8% (95% CI 32.8%–46.5%). We observed no increase in the seroprevalence trend after widespread school reopening. Seroprevalence estimates complement case-based cumulative incidence.

Through June 30, 2022, a total of 140,820 pediatric cases of COVID-19 had been reported in Oregon, USA, representing ≈17.3% of all reported COVID-19 cases in the state. However, understanding the true burden of pediatric COVID-19 infection poses a challenge. Children are more likely to have asymptomatic or mild disease, and pediatric infections are, therefore, less likely to be reported to public health authorities (*1*,*2*). Clarifying pediatric SARS-CoV-2 prevalence is important because it is well established that children can transmit SARS-CoV-2 to other children and adults (*3*,*4*). In addition, children are at risk for severe complications, including postinfectious multisystem inflammatory syndrome in children (MIS-C) (*5*). Seroprevalence provides additional insight into the true cumulative incidence of COVID-19 in children.

The Study

To estimate the seroprevalence of COVID-19 infection in children in Oregon, blood was collected in 6 phases during November 1, 2020–June 30, 2022, from a cross-sectional convenience sample and tested for SARS-CoV-2 nucleocapsid IgG, in alignment with the World Health Organization seroepidemiologic investigation protocol (*6*). We recruited Oregon healthcare facilities with ≥6 inpatient pediatric hospital beds to participate in this study and asked them to provide ≤100 specimens per phase; 5 facilities agreed to participate. We asked facilities to submit random samples of deidentified residual serum samples from patients ≤17 years of age visiting any ambulatory, emergency, or inpatient healthcare setting and to include specimen collection date and patient's date of birth. The initial round of sampling was November 1–December 31, 2020. We extended the project timeline and collected additional samples bimonthly during October 1, 2021–June 30, 2022.

Specimens were stored according to instructions provided by the test manufacturer and transported to the Oregon State Public Health Laboratory (Hillsboro, Oregon, USA). We tested the specimens with a SARS-CoV-2 IgG assay (Abbott Laboratories, https://www.abbott.com), which detects antibodies to the nucleocapsid protein of SARS-CoV-2. Nucleocapsid IgG immunoassays detect antibodies produced after infection and do not detect antibodies produced after vaccination with vaccines licensed for use in the United States. The manufacturer reports test sensitivity (Sn) of 100% (95% CI 95.9%–100%) at ≥14 days past symptom onset and specificity (Sp) of 99.6% (95% CI 99.1%–99.9%). We calculated unadjusted seroprevalence estimates for each collection period as the percentage of all specimens that tested positive. We adjusted seroprevalence estimates for test performance as observed prevalence + (specificity – 1) divided by sensitivity + (specificity – 1) (*7*).

We obtained adjusted 95% CI with parametric bootstrapping (*8*). Because SARS-CoV-2 antibody detection is dependent on test timing and assay, we also performed sensitivity analysis with seroprevalence estimates adjusted for declining assay sensitivity over 130 days of convalescence (*9*,*10*) (Appendix, https://wwwnc.cdc.gov/EID/article/29/8/23-0471-App1.pdf) We used R version 4.1.2 (The R Foundation for

Author affiliations: Oregon Health Authority, Portland, Oregon, USA (R.A. Falender, P.R. Cieslak, M. Sutton); Oregon Health and Science University School of Medicine, Portland (P.G. Mitchell, J.A. Guzman-Cottrill)

DOI: http://doi.org/10.3201/eid2908.230471

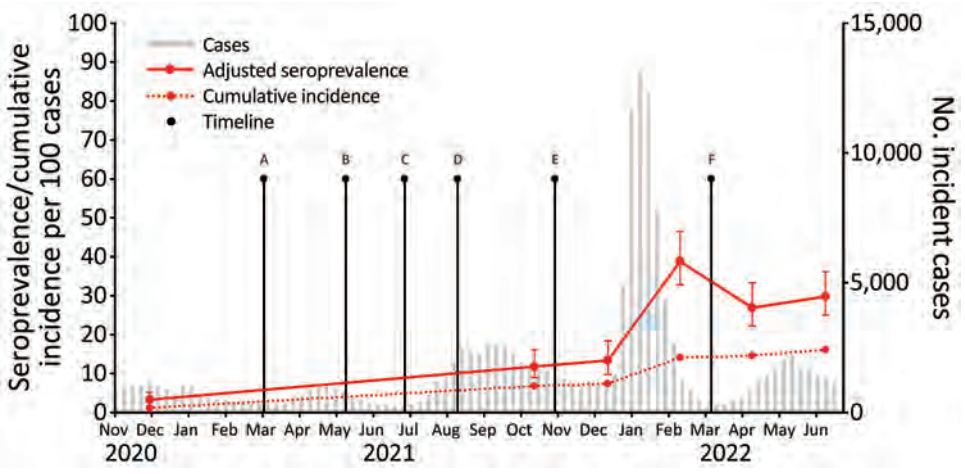

Figure. Adjusted SARS-CoV-2 nucleocapsid seroprevalence, incident cases, and cumulative incidence in children, Oregon, USA, November 1, 2020–June 30, 2022. We calculated cumulative incidence estimates at the midpoint of each collection period and plotted adjusted seroprevalence estimates with 95% CIs (error bars). Incident cases and cumulative incidence are plotted by epidemiologic week. Points A through F denote key timepoints: A, all public schools required to offer in-person instruction for grades K–5 by March 29, 2021, and grades 6–12 by April 19, 2021; B, COVID-19 vaccine available for children 12–15 years of age on May 12, 2021; C, statewide mask mandates lifted on June 30, 2021; D, statewide mask mandates reinstated on Aug 13, 2021; E, COVID-19 vaccine available for children 5–11 years of age on November 2, 2021; F, statewide mask mandates were lifted on March 12, 2022. Incident cases and case-based cumulative incidence estimates were calculated at the midpoint of each collection period and are obtained from pediatric COVID-19 cases reported to Oregon Health Authority since the beginning of the pandemic.

Statistical Computing, https://www.r-project.org) for all analyses.

We collected 1,869 specimens from 5 facilities during 6 phases. The mean number of specimens collected during each phase was 312 (range 215–438). Overall, we observed a strong linear trend (p = 0.001) for adjusted seroprevalence estimates during November 1, 2020—December 31, 2021; seroprevalence increased by ≈0.7% per 4-week period during that period (Figure). After the Omicron surge, adjusted seroprevalence increased sharply from 13.4% (95% CI 9.8%–18.4%) in December 2021 to 38.8% (95% CI 32.8%–46.5%) in February 2022. Adjusted seroprevalence estimates then decreased but did not return to pre–February 2022 levels (Table). Adjusting for declining assay sensitivity over time led to estimates that were larger and less stable over convalescence (Appendix).

Conclusions

Our repeated cross-sectional study estimated pediatric seroprevalence in Oregon at 6 points across 20 months of pandemic response. During that period, K–12 public schools reopened statewide, vaccines were rolled out in 2 phases to children 12–15 and 5–11 years of age, and universal indoor masking mandates remained in place during the school year until March 12, 2022 (Figure). After widespread school reopening in early 2021, with a masking mandate in place, pediatric seroprevalence in October 2021 was 11.8%, and no increase in trend was observed. The only sudden increase in pediatric seroprevalence followed the Omicron surge in early 2022. Seroprevalence began to decline after its February 2022 peak but did not return to pre-Omicron levels.

Seroprevalence can provide more accurate estimates of the true cumulative incidence of SARS-CoV-2 infection than case reporting to public health entities does, because seroprevalence data capture evidence of previous infection in persons who are not tested through the traditional healthcare system because of asymptomatic or mild disease, lack of testing access, refusal to test, or self-testing at home (*11*). We estimated 1.7–2.8 times the number of infections in children from seroprevalence than the reported cumulative incidence in Oregon (Figure). This total is a lower degree of underascertainment than had been

Table. Seroprevalence of SARS-CoV-2 nucleocapsid antibodies in children, Oregon, USA, November 1, 2020–June 30, 2022*

Collection dates	Sample size	Unadjusted seroprevalence (95% CI)	Adjusted seroprevalence (95% CI)
2020 Nov 1—Dec 31	438	0.032 (0.015–0.048)	0.033 (0.002–0.052)
2021 Oct 1—Oct 3	370	0.122 (0.090–0.159)	0.118 (0.090–0.161)
2021 Dec 1—Dec 31	278	0.137 (0.099–0.183)	0.134 (0.098–0.184)
2022 Feb 1—Feb 28	215	0.391 (0.325–0.459)	0.388 (0.328–0.465)
2022 Apr 1—Apr 30	279	0.272 (0.221–0.329)	0.269 (0.222–0.333)
2022 Jun 1—Jun 30	289	0.301 (0.249–0.358)	0.298 (0.250–0.362)

*We calculated adjusted prevalence as observed prevalence + (specificity – 1) divided by sensitivity + (specificity – 1). Adjusted 95% CI obtained with parametric bootstrapping.

reported in seroprevalence studies of children during May–July 2021 in the United States (*1*).

Because seroprevalence studies measure circulating antibodies at the time of testing and SARS-CoV-2 antibodies wane over time, seroprevalence is limited in its ability to estimate cumulative incidence as the pandemic progresses (*12*). In addition, time to seroreversion is dependent on the target antigen and the assay used (*9*,*10*,*13*). One study found a mean time of seroreversion of 19 weeks with use of the Abbott IgG immunoassay, compared with 91 weeks using the Roche pan-Ig immunoassay (*13*). In our study, waning immunity was apparent as estimated seroprevalence decreased following its Omicron-related peak in February 2022. A sensitivity analysis, adjusting for declining sensitivity of the Abbott immunoassay, partially accounted for this decline; more complex models have been published to correct seroprevalence estimates for assay performance (*13*). However, now that essentially all persons in the United States have been infected with SARS-CoV-2, the use of an assay with waning sensitivity to remote infections may permit continued examination of more granular temporal changes in seroprevalence in the context of changing policy and variant predominance.

The Centers for Disease Control and Prevention began collecting pediatric seroprevalence data for the Multistate Assessment of SARS-CoV-2 Seroprevalence in Commercial Labs (MASS-C) in July 2020 (*14*). MASS-C estimates of pediatric seroprevalence in Oregon are consistently higher than our estimates (*15*). Although MASS-C similarly derives its estimates from a convenience sample of serum specimens, testing is performed with the Roche antinucleocapsid total antibody assay (*14*). In addition, MASS-C estimates are weighted for age and sex, and the demographics of that pediatric population may demographically differ from our study population.

We obtained our convenience sample from children who received care from large pediatric healthcare facilities throughout the state; findings are not necessarily generalizable to the entire state pediatric population. Limitations of seroprevalence testing include lack of antibody development by some infected persons (including immunocompromised persons) and, in others, waning of antibodies to undetectable levels, such that seroprevalence becomes a less reliable proxy for cumulative incidence as the duration of the pandemic increases (*12*).

Traditional public health case-based reporting substantially underestimates the burden of COVID-19. In this study, seroprevalence estimates made using an assay with waning sensitivity to remote infections provided evidence that the widespread reopening of schools with a masking mandate in place did not increase the rate of pediatric SARS-CoV-2 infections. Case-based cumulative incidence estimates failed to capture the magnitude of the Omicron variant's effect on Oregon's pediatric population. Serosurveillance of SARS-CoV-2 antibodies in Oregon's pediatric population complements case-based surveillance and can inform future public health interventions and policy decisions.

This study and report were supported in part by an appointment to the Applied Epidemiology Fellowship Program administered by the Council of State and Territorial Epidemiologists and funded by the Centers for Disease Control and Prevention (cooperative agreement no. 1NU38OT000297-03-00).

About the Author

Dr. Falender is a Council of State and Territorial Epidemiologists applied epidemiology fellow at Oregon Health Authority, working in acute and communicable disease prevention. Her research interests include emerging infectious diseases and One Health.

References

1. O'Brien SC, Cole LD, Albanese BA, Mahon A, Knight V, Williams N, et al. SARS-CoV-2 seroprevalence compared with confirmed COVID-19 cases among children, Colorado, USA, May–July 2021. Emerg Infect Dis. 2023;29:929–36. https://doi.org/10.3201/eid2905.221541
2. Ludvigsson JF. Systematic review of COVID-19 in children shows milder cases and a better prognosis than adults. Acta Paediatr. 2020;109:1088–95. https://doi.org/10.1111/apa.15270
3. Laxminarayan R, Wahl B, Dudala SR, Gopal K, Mohan B C, Neelima S, et al. Epidemiology and transmission dynamics of COVID-19 in two Indian states. Science. 2020;370:691–7. https://doi.org/10.1126/science.abd7672
4. Szablewski CM, Chang KT, Brown MM, Chu VT, Yousaf AR, Anyalechi N, et al. SARS-CoV-2 transmission and infection among attendees of an overnight camp—Georgia, June 2020. MMWR Morb Mortal Wkly Rep. 2020;69:1023–5. https://doi.org/10.15585/mmwr.mm6931e1
5. Godfred-Cato S, Bryant B, Leung J, Oster ME, Conklin L, Abrams J, et al.; California MIS-C Response Team. COVID-19–associated multisystem inflammatory syndrome in children—United States, March–July 2020. MMWR Morb Mortal Wkly Rep. 2020;69:1074–80. https://doi.org/10.15585/mmwr.mm6932e2
6. World Health Organization. Population-based age-stratified seroepidemiological investigation protocol for COVID-19 virus infection, 17 March 2020. Geneva: The Organization; 2020.
7. Reiczigel J, Földi J, Ozsvári L. Exact confidence limits for prevalence of a disease with an imperfect diagnostic test. Epidemiol Infect. 2010;138:1674–8. https://doi.org/10.1017/S0950268810000385
8. Henrion MY. bootComb—an R package to derive confidence intervals for combinations of independent parameter

estimates. Oxford: Oxford University Press; 2021.
9. Peluso MJ, Takahashi S, Hakim J, Kelly JD, Torres L, Iyer NS, et al. SARS-CoV-2 antibody magnitude and detectability are driven by disease severity, timing, and assay. Sci Adv. 2021;7:eabh3409. https://doi.org/10.1126/sciadv.abh3409
10. Stone M, Grebe E, Sulaeman H, Di Germanio C, Dave H, Kelly K, et al. Evaluation of commercially available high-throughput SARS-CoV-2 serologic assays for serosurveillance and related applications. Emerg Infect Dis. 2022;28:672–83. https://doi.org/10.3201/eid2803.211885
11. Sutton M, Cieslak P, Linder M. Notes from the field: seroprevalence estimates of SARS-CoV-2 infection in convenience sample—Oregon, May 11–June 15, 2020. MMWR Morb Mortal Wkly Rep. 2020;69:1100–1. https://doi.org/10.15585/mmwr.mm6932a4
12. Post N, Eddy D, Huntley C, van Schalkwyk MCI, Shrotri M, Leeman D, et al. Antibody response to SARS-CoV-2 infection in humans: a systematic review. PLoS One. 2020;15:e0244126. https://doi.org/10.1371/journal.pone.0244126
13. García-Carreras B, Hitchings MDT, Johansson MA, Biggerstaff M, Slayton RB, Healy JM, et al. Accounting for assay performance when estimating the temporal dynamics in SARS-CoV-2 seroprevalence in the U.S. Nat Commun. 2023;14:2235. https://doi.org/10.1038/s41467-023-37944-5
14. Bajema KL, Wiegand RE, Cuffe K, Patel SV, Iachan R, Lim T, et al. Estimated SARS-CoV-2 seroprevalence in the US as of September 2020. JAMA Intern Med. 2021;181:450–60. https://doi.org/10.1001/jamainternmed.2020.7976
15. US Centers for Disease Control and Prevention. COVID data tracker: national commercial lab pediatric antibody seroprevalence. February 2, 2023 [cited 2023 Feb 6]. https://covid.cdc.gov/covid-data-tracker/#pediatric-seroprevalence

Address for correspondence: Melissa Sutton, Public Health Division, Oregon Health Authority, 800 NE Oregon St, Ste 772, Portland OR 97232, USA; email: Melissa.Sutton@oha.oregon.gov

Detection of *Orientia* spp. Bacteria in Field-Collected Free-Living *Eutrombicula* Chigger Mites, United States

Kaiying Chen, Nicholas V. Travanty, Reuben Garshong, Dac Crossley, Gideon Wasserberg, Charles S. Apperson, R. Michael Roe, Loganathan Ponnusamy

Scrub typhus, a rickettsial disease caused by *Orientia* spp., is transmitted by infected larval trombiculid mites (chiggers). We report the molecular detection of *Orientia* species in free-living *Eutrombicula* chiggers collected in an area in North Carolina, USA, to which spotted fever group rickettsiae infections are endemic.

Rickettsioses are distributed worldwide, caused by bacteria in the family Rickettsiaceae, genera *Orientia* and *Rickettsia* (*1*). The pathogens are transmitted by host-feeding arthropods, including ticks, mites, fleas, and lice (*2*). Among those arthropods are trombiculid mites, which have a widespread global distribution and high species diversity. Among the different stages of the lifecycle of trombiculid mites, only the larvae are ectoparasites, commonly known as chiggers (*3*). Some species are vectors of intracellular bacterial pathogens in the genus *Orientia* that causes a potentially lethal human febrile disease, scrub typhus (*4*,*5*). Scrub typhus results in considerable illness and death; it causes >1 million cases of illness each year (*5*). A recent review (*6*) concluded that trombiculid mites might be widespread vectors of other zoonotic agents not yet recognized. Spotted fever group rickettsiosis diseases, including Rocky Mountain spotted fever, have many of the same symptoms as scrub typhus. A recent review of the literature from 1997–2017 estimated >60% of the rickettsial diseases outside the United States were misdiagnosed (*7*).

Author affiliations: North Carolina State University, Raleigh, North Carolina, USA (K. Chen, N.V. Travanty, C.S. Apperson, R.M. Roe, L. Ponnusamy); University of North Carolina at Greensboro, Greensboro, North Carolina, USA (R. Garshong, G. Wasserberg); Georgia Museum of Natural History, Athens, Georgia, USA (D. Crossley)

DOI: http://doi.org/10.3201/eid2908.230528

Until recently, scrub typhus was exclusively reported from the so-called tsutsugamushi triangle, stretching from Pakistan in the west to far-eastern Russia in the east to northern Australia in the south. However, scrub typhus was reported recently in the Middle East, southern Chile, and Africa (*5*,*8*). The occurrence of scrub typhus pathogens in chiggers in the United States was not investigated. We report the identification of *Orientia* species in free-living chiggers collected at recreational parks in North Carolina, USA.

The Study

In 2022, we collected free-living chiggers using the tile method (*9*) in different locations in North Carolina: we placed tiles on the ground and then visually inspected for the presence of chiggers after ≈1 minute. When chiggers were present, we collected them with forceps or a small paintbrush and transferred them into vials with 95% ethanol. We identified subsamples from each collection location based on morphological characteristics using published taxonomic keys (*10*). We identified chiggers as *Eutrombicula* on the basis of their morphology. In addition, we obtained chigger images of *Eutrombicula* using scanning electron microscopy at the Analytical Instrumentation Facility at North Carolina State University (Raleigh, North Carolina, USA) (Appendix Figure 1, https://wwwnc.cdc.gov/EID/article/29/8/23-0528-App1.pdf).

We surface-sterilized individual free-living chiggers and extracted total nucleic acids using the DNeasy Blood & Tissue Kit (QIAGEN, https://www.qiagen.com) (*11*). In total, 95 chiggers from 10 different locations (10 chiggers/location; 1 location had 5 chiggers) were subjected to microbiome analyses (Figure 1). We randomly selected 8 chiggers for molecular identification using previously described 18S ribosomal RNA gene primers and PCR (*12*). Amplicons were Sanger

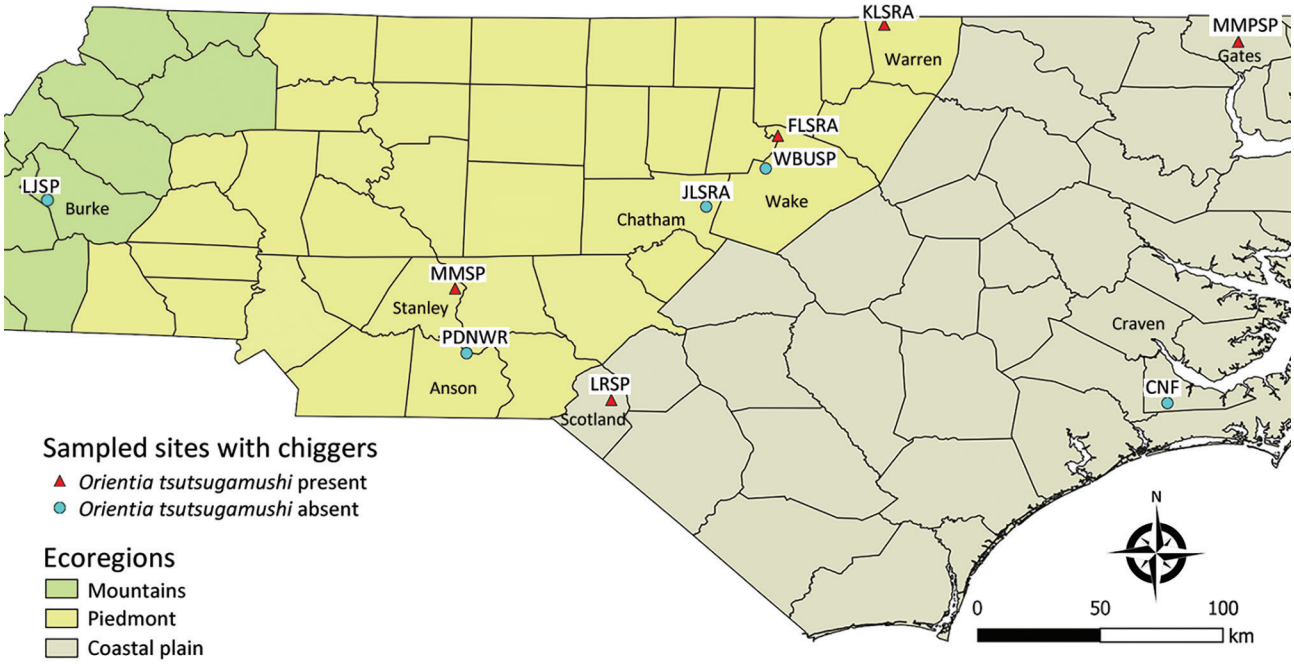

Figure 1. Study area for investigation of *Orientia* spp. bacteria in field-collected free-living *Eutrombicula* chigger mites, North Carolina, USA. Free-living chiggers were collected from 10 sites in 8 counties. CNF, Croatan National Forest; FLSRA, Falls Lake State Recreation Area; JLSRA, Jordan Lake State Recreation Area; KLSRA, Kerr Lake State Recreation Area; LJSP, Lake James State Park; LRSP, Lumber River State Park; MMPSP, Merchant Millpond State Park; MMSP, Morrow Mountain State Park; PDNWR, Pee Dee National Wildlife Refuge; WBUSP, William B. Umstead State Park.

sequenced at Eton Bioscience, Inc. (https://www.etonbio.com). The sequences (GenBank accession nos. OQ789321–5) were submitted for BLASTn (https://blast.ncbi.nlm.nih.gov/Blast.cgi) analysis and showed 99–100% identity with homologous sequences of *Eutrombicula* spp. (accession no. KY922159).

To determine the total bacteria present in the chiggers, we constructed a 16S rRNA sequence library of individual chiggers using the Illumina 16S rRNA (V3-V4 region) metagenomics sequencing library preparation protocol (Illumina, https://www.illumina.com) (*13*). Sequencing was performed at the University of North Carolina Microbiome Core Facility (Chapel Hill, North Carolina, USA). The Illumina FASTQ files were processed using Quantitative Insights into Microbial Ecology 2 (*14*) (Appendix). An analysis of amplicon sequence variants (ASVs) revealed that chigger mites contained reads of a bacterial sequence classified as *O. tsutsugamushi*. *O. tsutsugamushi*–positive chigger sequence reads were found in 5/10 sampling sites as follows: 3 sites in the Piedmont region (Falls Lake State Recreation Area [1 positive/10 chiggers], Kerr Lake State Recreation Area [8 positive/10 chiggers], and Morrow Mountain State Park [1 positive/10 chiggers]); and 2 sites in the Coastal Plains region (Lumber River State Park [9 positive/10 chiggers] and Merchant Millpond State Park [1 positive/5 chiggers]) (Figure 1). By using the Greengenes 16S rRNA database, we found 13 ASVs to *O. tsutsugamushi*. To further confirm those results, we extracted representative sequences from the sequencing data and conducted BLASTn searches against the National Center for Biotechnology Information (NCBI) databases. We found 12 ASVs showed a high nucleotide identity (99.5%–100%) to the *O. tsutsugamushi* strain Kato (D38624), isolated from a human scrub typhus case in Kurosawa village, Japan (https://u.osu.edu/scrubtyphus/the-kato-strain). One ASV exhibited 89.46% homology to an *O. tsutsugamushi* sequence that was excluded from the phylogenetic analysis. We then examined the approximate phylogenetic relationships for 12 of the *O. tsutsugamushi* sequence variants from our study sites with other *O. tsutsugamushi* sequences obtained from the NCBI database using BLASTn (accessed January 18, 2023). We performed multiple alignments with the ClustalW program and maximum-likelihood method tree with the Kimura 2-parameter method from the MEGA X (https://www.megasoftware.net) software package. The phylogenetic analysis revealed that all 12 of the *O. tsutsugamushi* ASVs clustered closely to *O. tsutsugamushi* strains from Asia (Figure 2).

To further verify the identity of *O. tsutsugamushi* detected in our free-living chigger samples, we amplified a 47-kDa *htrA* (high-temperature requirement A) gene in the 20 chigger samples that were positive for the *O. tsutsugamushi* 16S rRNA gene. The primers for the first round of PCR were *Ot*-145F and *Ot*-1780R, and for the second round, *Ot*-263F and *Ot*-1133R (*15*) (Appendix). The 47-kDa gene amplification products were Sanger sequenced at Eton Bioscience. Four samples (FC28, 36, 38, 109) were 92.6%–97.29% identical to the *O. tsutsugamushi* HN82 strain (GenBank accession no. LC431268) and 92%–97% identical to the *O. tsutsugamushi* Kato strain (accession no. LS398550) after trimming low-quality sequences. Sixteen samples yielded ambiguous sequences, suggesting the presence of multiple *Orientia* species or primer binding sites caused by high variation in the 47 kDa gene among *Orientia* species in our samples. Jiang et al. (*15*) studied the genetic variation of

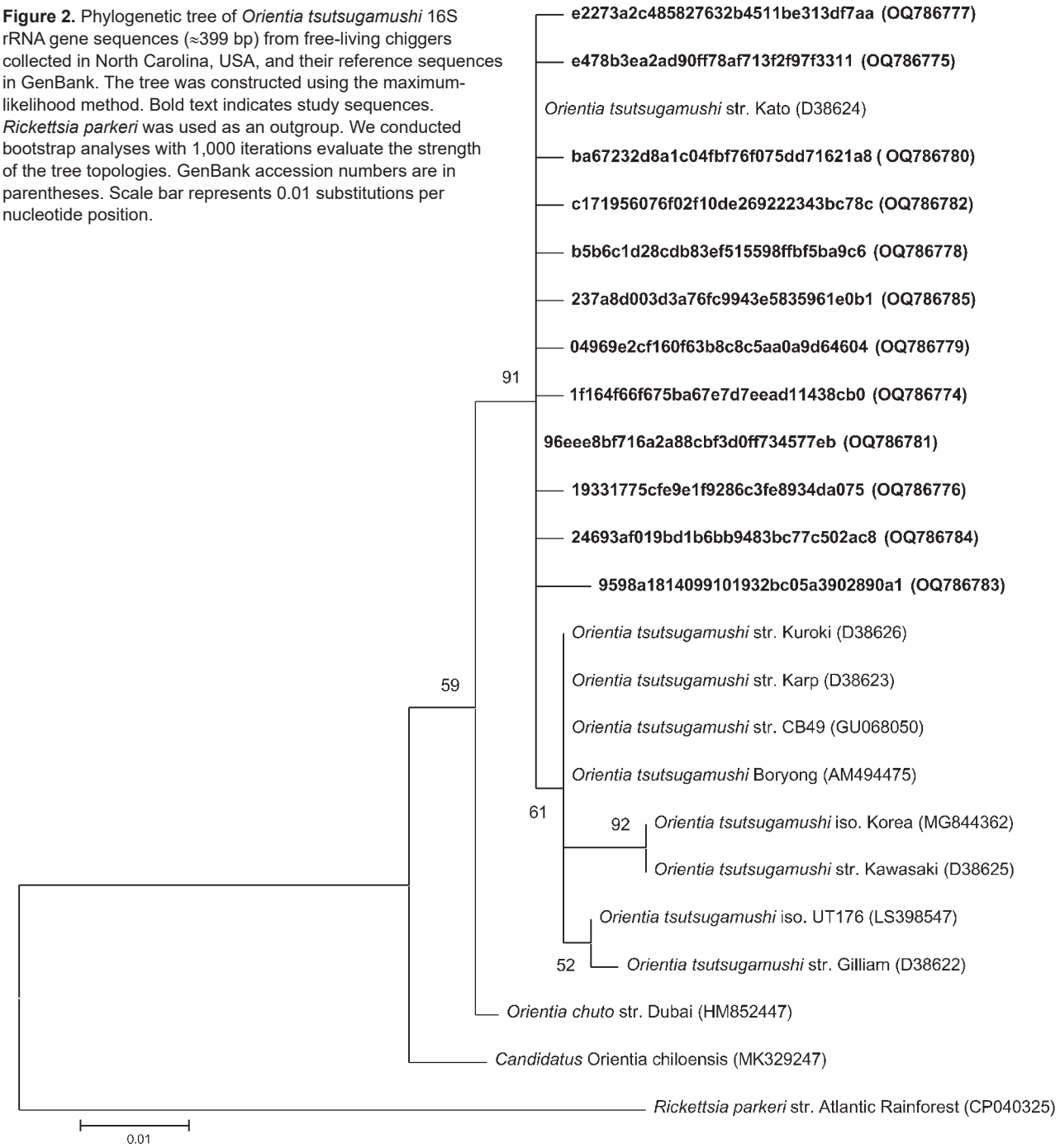

Figure 2. Phylogenetic tree of *Orientia tsutsugamushi* 16S rRNA gene sequences (≈399 bp) from free-living chiggers collected in North Carolina, USA, and their reference sequences in GenBank. The tree was constructed using the maximum-likelihood method. Bold text indicates study sequences. *Rickettsia parkeri* was used as an outgroup. We conducted bootstrap analyses with 1,000 iterations evaluate the strength of the tree topologies. GenBank accession numbers are in parentheses. Scale bar represents 0.01 substitutions per nucleotide position.

Orientia in this region of the genome and reported percent identity of 17 isolates of *Orientia* as 82.2%–83.3% (*15*). Among our 4 *Orientia* 47 kDa sequences from North Carolina chiggers, identity was 93.97%–98%. Phylogenetic analysis revealed that all 4 of those *O. tsutsugamushi* sequences clustered to *O. tsutsugamushi* strains from Asia (Appendix Figure 2).

Conclusions

This study identified *Orientia* species within the United States in free-living *Eutrombicula* chiggers that were collected in North Carolina. This result is epidemiologically significant because it indicates vertical circulation of *Orientia* species in chiggers collected within the continental United States. The presence of *Orientia* species in free-living larvae suggests that the bacteria are maintained through transovarial transmission. Further studies are needed to complete sequencing of the 47-kDa *htrA* gene (htrA) in our samples, determine how widely distributed *Orientia* spp.–infected free-living and host-attached chiggers are in the United States, and ascertain whether wild animals that serve as hosts for chiggers become infected and infectious and develop symptoms of illness. Clinicians in this region should be alert for possible human cases of illness resulting from *Orientia* spp. infection.

This research was supported by a grant from the National Institutes of Health, National Institute of Allergy and Infectious Diseases (grant no. 1R03AI166406-01). L.P. was supported by a grant from Southeast Center for Agricultural Health and Injury Prevention. This research was also supported by a grant from the Department of the Army, US Army Contracting Command, Aberdeen Proving Ground, Natick Contracting Division, Fort Detrick, Maryland, under a Deployed Warfighter Protection (DWFP) program grant (no. W911QY1910003 awarded to R.M.R.).

About the Author

Dr. Chen is a postdoctoral research scholar in the Department of Entomology and Plant Pathology at North Carolina State University. Her research interests include vector-borne diseases, microbiomes, and vector control.

References

1. Abdad MY, Abou Abdallah R, Fournier P-E, Stenos J, Vasoo S. A concise review of the epidemiology and diagnostics of rickettsioses: *Rickettsia* and *Orientia* spp. J Clin Microbiol. 2018;56:e01728-17. https://doi.org/10.1128/JCM.01728-17
2. Blanton LS. The rickettsioses: a practical update. Infect Dis Clin North Am. 2019;33:213–29. https://doi.org/10.1016/j.idc.2018.10.010
3. Chen K, Roe RM, Ponnusamy L. Biology, systematics, microbiome, pathogen transmission and control of chiggers (Acari: Trombiculidae, Leeuwenhoekiidae) with emphasis on the United States. Int J Environ Res Public Health. 2022;19:15147. https://doi.org/10.3390/ijerph192215147
4. Abarca K, Martínez-Valdebenito C, Angulo J, Jiang J, Farris CM, Richards AL, et al. Molecular description of a novel *Orientia* species causing scrub typhus in Chile. Emerg Infect Dis. 2020;26:2148–56.
5. Xu G, Walker DH, Jupiter D, Melby PC, Arcari CM. A review of the global epidemiology of scrub typhus. PLoS Negl Trop Dis. 2017;11:e0006062. https://doi.org/10.1371/journal.pntd.0006062
6. Weitzel T, Makepeace BL, Elliott I, Chaisiri K, Richards AL, Newton PN. Marginalized mites: neglected vectors of neglected diseases. PLoS Negl Trop Dis. 2020;14:e0008297. https://doi.org/10.1371/journal.pntd.0008297
7. van Eekeren LE, de Vries SG, Wagenaar JFP, Spijker R, Grobusch MP, Goorhuis A. Under-diagnosis of rickettsial disease in clinical practice: a systematic review. Travel Med Infect Dis. 2018;26:7–15. https://doi.org/10.1016/j.tmaid.2018.02.006
8. Acosta-Jamett G, Martínez-Valdebenito C, Beltrami E, Silva-de La Fuente MC, Jiang J, Richards AL, et al. Identification of trombiculid mites (Acari: Trombiculidae) on rodents from Chiloé Island and molecular evidence of infection with *Orientia* species. PLoS Negl Trop Dis. 2020;14:e0007619. https://doi.org/10.1371/journal.pntd.0007619
9. Upham RW Jr, Hubert AA, Phang OW, Mat YB, Rapmund G. Distribution of *Leptotrombidium* (*Leptotrombidium*) *arenicola* (Acarina: Trombiculidae) on the ground in West Malaysia. J Med Entomol. 1971;8:401–6. https://doi.org/10.1093/jmedent/8.4.401
10. Wharton GW, Fuller HS. A manual of the chiggers: the biology, classification, distribution and importance to man of the larvae of the family Trombiculidae (Acarina). Mem Entomol Soc Wash. 1952;4:1–185.
11. Ponnusamy L, Willcox AC, Roe RM, Davidson SA, Linsuwanon P, Schuster AL, et al. Bacterial microbiome of the chigger mite *Leptotrombidium imphalum* varies by life stage and infection with the scrub typhus pathogen *Orientia tsutsugamushi*. PLoS One. 2018;13:e0208327. https://doi.org/10.1371/journal.pone.0208327
12. Otto JC, Wilson K. Assessment of the usefulness of ribosomal 18S and mitochondrial COI sequences in *Prostigmata* phylogeny. In: Acarology: Proceedings of the 10th International Congress, 2001. Melbourne: CSIRO Publishing Melbourne; 2001.
13. Illumina. 16S Metagenomic sequencing library preparation. 2013 [cited 2023 Jun 26]. https://support.illumina.com/downloads/16s_metagenomic_sequencing_library_preparation.html
14. Bolyen E, Rideout JR, Dillon MR, Bokulich NA, Abnet CC, Al-Ghalith GA, et al. Reproducible, interactive, scalable and extensible microbiome data science using QIIME 2. Nat Biotechnol. 2019;37:852–7. https://doi.org/10.1038/s41587-019-0209-9
15. Jiang J, Paris DH, Blacksell SD, Aukkanit N, Newton PN, Phetsouvanh R, et al. Diversity of the 47-kD HtrA nucleic acid and translated amino acid sequences from 17 recent human isolates of *Orientia*. Vector Borne Zoonotic Dis. 2013;13:367–75. https://doi.org/10.1089/vbz.2012.1112

Address for correspondence: Loganathan Ponnusamy, Department of Entomology and Plant Pathology, North Carolina State University at Raleigh, 3230 Ligon St, Raleigh, NC 27595, USA; email: lponnus@ncsu.edu

Aneurysm Infection Caused by *Desulfovibrio desulfuricans*

Tatsuya Fujihara, Keigo Kimura, Hiroo Matsuo, Ryuichi Minoda Sada, Shigeto Hamaguchi, Go Yamamoto, Takuya Yamakura, Satoshi Kutsuna

Author affiliations: Osaka University Hospital, Osaka, Japan (T. Fujihara, K. Kimura, H. Matsuo); Osaka University Graduate School of Medicine, Osaka (R. Minoda Sada, S. Hamaguchi, G. Yamamoto, T. Yamakura, S. Kutsuna)

DOI: https://doi.org/10.3201/eid2908.230403

An 84-year-old man in Japan who had undergone endovascular aortic repair 9 years earlier had an infected aneurysm develop. We detected *Desulfovibrio desulfuricans* MB at the site. The patient recovered after surgical debridement, artificial vessel replacement, and appropriate antimicrobial therapy. Clinicians should suspect *Desulfovibrio* spp. infection in similar cases.

Desulfovibrio species are gram-negative, sulfate-reducing, nonfermenting, anaerobic bacteria found in the environment, including in soil, water, and sewage, as well as in the digestive tracts of humans and animals (*1*). They rarely cause human infections, and their clinical prevalence and features are unclear (*2*,*3*). We describe a case of an infected aneurysm caused by *Desulfovibrio desulfuricans* MB that was treated successfully with artificial vessel replacement and antimicrobial therapy after identification of the causative pathogen.

An 84-year-old man who had undergone endovascular aortic repair (EVAR) 9 years earlier was referred for suspected mycotic thoracoabdominal aortic aneurysm. His medical history included hypertension, type 2 diabetes mellitus, and chronic kidney disease. Six weeks before referral, he had eaten grilled fish; 2 weeks later, he had experienced fever with transient chills, followed by persistent abdominal pain for 2 weeks. Computed tomography revealed a fishbone lodged in the ileocecal tract, with a hyper-absorptive zone in the arterial wall; the post-EVAR abdominal aortic aneurysm was larger than it had been 4 months before. He had received antimicrobial therapy 5 days before referral. Blood cultures after treatment were negative.

At admission, the patient did not appear distressed. Blood pressure was 112/80 mm Hg, pulse rate 60 beats/min, body temperature 36.4°C, respiratory rate 18 breaths/min, and Glasgow coma scale score 15. On physical examination, chest and cardiovascular findings were unremarkable; abdominal tenderness was noted on palpation. Laboratory tests indicated that leukocyte count was 11.05 × 10^3 cells/L, C-reactive protein 12.12 mg/dL, serum creatinine 1.39 mg/dL, and hemoglobin A1c level 9.9. Results of additional blood culture performed under treatment with ampicillin/sulbactam (3 g/6 h) was also negative.

On day 5 of admission, surgical debridement was performed, followed by partial removal of the EVAR graft and in situ Y-graft placement with revascularization, including the bilateral renal and superior mesenteric arteries. Intraoperative findings showed partial abscess formation in the abdominal artery wall. Gram stain of the abscess pus showed gram-negative rods (Figure, panel A), and subsequent anaerobic intraoperative pus cultures were observed (Figure, panel B). Matrix-assisted laser desorption/ionization time-of-flight (MALDI-TOF) mass spectrometry using MALDI Biotyper library version 9 (Bruker Daltonics, https://www.bruker.com) did not reliably identify the pathogens (Appendix, https://wwwnc.cdc.gov/EID/article/29/8/23-0403-App1.pdf). We therefore conducted 16S ribosomal RNA

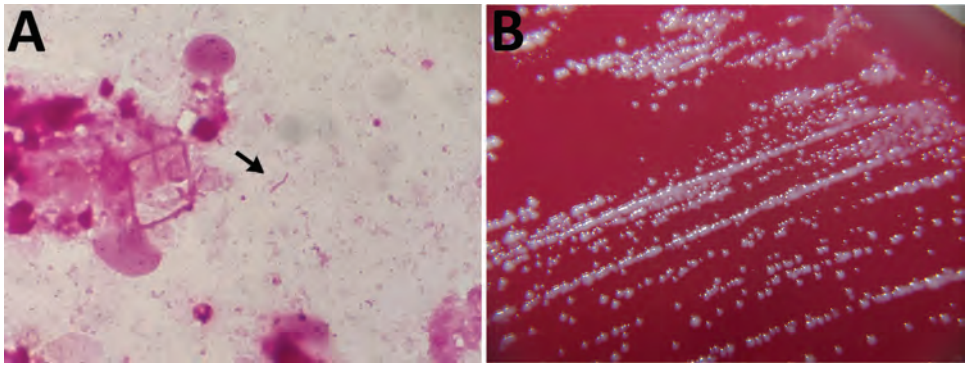

Figure. Detection and colonization of *Desulfovibrio desulfuricans* in an 84-year-old man in Japan who had undergone endovascular aortic repair 9 years earlier. A) Gram stain of pus. *D. desulfuricans* MB has a gram-negative spiral rod appearance (arrow). Original magnification ×1,000. B) Colonies of *D. desulfuricans* MB on ABHK agar. Biochemical properties showed positive results for catalase and negative for indole and urease. In vitro susceptibility testing revealed that it had the following MICs: meropenem, ≤2 μg/mL; cefotaxime, ≤2 μg/mL; ampicillin/sulbactam, ≤4 μg/mL; piperacillin/tazobactam, ≤16 μg/mL; and clindamycin, >8 μg/mL.

(16S rRNA) sequencing of the isolates by using the BLAST sequence homology search program (EzBioCloud, https://www.ezbiocloud.net) for analysis. Sequencing showed 99.86% homology with *D. desulfuricans* MB ATCC27774 (GenBank accession no. CP001358.1) and 1,470/1,472 bp nucleotide matches. The desulfoviridin test was positive, and the biochemical properties of the isolates were consistent with those of *D. desulfuricans* MB. On day 6, we performed thoracic endovascular aortic repair, coil embolization of the celiac and inferior mesenteric artery, and colonoscopic fishbone resection.

The postsurgical course and antibiotic treatment were uneventful. The patient received 4 weeks of ampicillin/sulbactam (3 g/6 h) treatment after surgical debridement. He was discharged with continued oral administration of amoxicillin/clavulanate. Because the infected EVAR graft was retained, ongoing antibiotic treatment was recommended.

D. desulfuricans, which has 2 genotypes (Essex and MB), is the most pathogenic among *Desulfovibrio* spp., and bacteremia occurs when there is bacterial translocation from the intestinal tract (*3*–*5*). *Desulfovibrio* spp. can also cause appendicitis, abdominal abscesses, and septic arthritis; however, an infected aneurysm is extremely rare, and only 2 cases, including 1 suspected case, have been previously reported (*3*,*6*). One of the reasons for the rarity is that *Desulfovibrio* spp. require a long incubation period (3–7 days) for detection in blood culture, and they cannot be identified by using biochemical reaction tests (*3*,*7*). Except in 2 instances, previous cases have also required identification using 16S rRNA. *Desulfovibrio* spp. were not included in many system databases until recently, possibly contributing to the inability to identify them using MALDI-TOF mass spectrometry (*2*). However, even though *Desulfovibrio* spp. are included in the MALDI-TOF mass spectrometry library we used, we were unable to identify the pathogen. Factors such as the absolute number of strains registered in the *Desulfovibrio* spp. library may make identification difficult, and the accuracy of identification may still be problematic. Difficulty in identification may therefore result in underdiagnosis.

In our patient, the fishbone perforated the ileocecal region, enabling hematogenous bacteremia to enter and cause the infection. Uncontrolled type 2 diabetes may also have played a role. No pathogens were detected in the blood cultures, possibly because of previous administration of antimicrobial therapy. However, after consultation with the infectious disease specialist and microbiologist, we performed 16S rRNA sequencing, which led to detection of *D. desulfuricans* MB and appropriate antimicrobial administration. When gram-negative bacilli are detected in anaerobic cultures of infected aneurysms, *Desulfovibrio* spp. infection should be suspected, especially when gastrointestinal disease is present.

In general, *Desulfovibrio* spp. are susceptible to chloramphenicol and metronidazole; most are susceptible to imipenem and clindamycin, but the optimal treatment for *Desulfovibrio* spp. infection has not been established (*3*,*7*). Our report suggests that ampicillin/sulbactam and amoxicillin/clavulanate may also be effective therapeutic options for *Desulfovibrio* spp. infections.

References

1. Gibson GR, Macfarlane GT, Cummings JH. Occurrence of sulphate-reducing bacteria in human faeces and the relationship of dissimilatory sulphate reduction to methanogenesis in the large gut. J Appl Bacteriol. 1988;65:103–11. https://doi.org/10.1111/j.1365-2672.1988.tb01498.x
2. Marquis TJ, Williams VJ, Banach DB. Septic arthritis caused by *Desulfovibrio desulfuricans*: a case report and review of the literature. Anaerobe. 2021;70:102407. https://doi.org/10.1016/j.anaerobe.2021.102407
3. Hagiya H, Kimura K, Nishi I, Yamamoto N, Yoshida H, Akeda Y, et al. *Desulfovibrio desulfuricans* bacteremia: a case report and literature review. Anaerobe. 2018;49:112–5. https://doi.org/10.1016/j.anaerobe.2017.12.013
4. Nakao K, Tanaka K, Ichiishi S, Mikamo H, Shibata T, Watanabe K. Susceptibilities of 23 *Desulfovibrio* isolates from humans. Antimicrob Agents Chemother. 2009;53:5308–11. https://doi.org/10.1128/AAC.00630-09
5. Vasoo S, Mason EL, Gustafson DR, Cunningham SA, Cole NC, Vetter EA, et al. *Desulfovibrio legallii* prosthetic shoulder joint infection and review of antimicrobial susceptibility and clinical characteristics of *Desulfovibrio* infections. J Clin Microbiol. 2014;52:3105–10. https://doi.org/10.1128/JCM.00083-14
6. Goldstein EJ, Citron DM, Peraino VA, Cross SA. *Desulfovibrio desulfuricans* bacteremia and review of human *Desulfovibrio* infections. J Clin Microbiol. 2003;41:2752–4. https://doi.org/10.1128/JCM.41.6.2752-2754.2003
7. Warren YA, Citron DM, Merriam CV, Goldstein EJ. Biochemical differentiation and comparison of *Desulfovibrio* species and other phenotypically similar genera. J Clin Microbiol. 2005;43:4041–5. https://doi.org/10.1128/JCM.43.8.4041-4045.2005

Address for correspondence: Tatsuya Fujihara, Osaka University Hospital, 2-15, Yamadaoka, Suita City, Osaka 566-0871, Japan; email: tatsuyahujihara898@gmail.com

Rapid Serologic Test for Diagnosis of Yaws in Patients with Suspicious Skin Ulcers

Clara Suñer, Lucy N. John, Wendy Houinei, Maria Ubals, Dan Ouchi, Andrea Alemany, Cristina Galván-Casas, Michael Marks, Oriol Mitjà, Martí Vall-Mayans, Camila G. Beiras

Author affiliations: Fight Infections Foundation, Badalona, Spain (C. Suñer, L.N. John, M. Ubals, D. Ouchi, A. Alemany, C. Galván-Casas, O. Mitjà, M. Vall-Mayans, C.G. Beiras); University Hospital Germans Trias i Pujol, Badalona (C. Suñer, M. Ubals, A. Alemany, O. Mitjà, M. Vall-Mayans, C.G. Beiras); National Department of Health, Port Moresby, Papua New Guinea (L.N. John, W. Houinei); University of Papua New Guinea, Port Moresby (L.N. John, O. Mitjà); Hospital Universitario de Móstoles, Madrid, Spain (C. Galván-Casas); London School of Hygiene & Tropical Medicine, London, UK (M. Marks); Hospital for Tropical Diseases, London (M. Marks); University College London, London (M. Marks)

DOI: https://doi.org/10.3201/eid2908.230608

The Chembio DPP (Dual Path Platform) Syphilis Screen & Confirm kit (https://chembio.com) is a rapid serologic test that can be used to diagnose yaws. We evaluated its capacity to detect patients with ulcers that tested PCR positive for *Treponema pallidum* subsp. *pertenue*. DPP detected 84% of ulcers that were positive by PCR.

Yaws is a neglected tropical disease caused by *Treponema pallidum* subsp. *pertenue* (TPE) that causes cutaneous ulcers. It predominantly affects children living in remote communities. The World Health Organization designated 2020 as the year that yaws would be eradicated. That year, 87,877 clinically suspected cases were reported, but only 346 (from 7 countries, primarily western Pacific countries) were confirmed as yaws (*1*). Thus, confirming a yaws diagnosis on the basis of ulcerative lesions remains challenging for yaws eradication (*2*). Standard tests for yaws diagnosis require sample processing in a laboratory, which is often unavailable in rural health centers where yaws is endemic (*3*). A mainstay for achieving yaws eradication is integration of point-of-care tests into surveillance strategies.

The Chembio DPP (Dual Path Platform) Syphilis Screen & Confirm kit (https://chembio.com) has been proposed as a point-of-care test for confirming yaws as the cause of tropical ulcers. This lateral-flow immune-chromatographic rapid test simultaneously detects antibodies against *T. pallidum* (T line) and non–*T. pallidum* (NT line) antigens in blood (*4*,*5*). Aside from the qualitative result, which is readable with the naked eye, a quantitative measurement that uses optical density microreaders has been developed. According to previous reports, the qualitative reading of the DPP NT line has 80% sensitivity and 96% specificity for TPE compared with the rapid plasma reagin serologic test (*6*). However, the ability of the DPP test to identify active TPE in skin ulcers with a positive PCR result has not been established.

We assessed the ability of qualitative and quantitative measurements of DPP to identify active TPE in tropical ulcers. We used data from a community trial of patients with skin ulcers suggestive of yaws, conducted in Namatanai, Papua New Guinea, during 2018–2019 (*7*). We compared ulcer PCR results for TPE with serologic results of the DPP test T line, NT line, or both, read by the naked eye or by using the quantitative reader. The study protocol was approved by the Medical Research Advisory Committee of the Papua New Guinea National Department of Health. Participants provided written informed consent for collection of biological samples.

We tested samples from 995 suspicious skin ulcers by using DPP and PCR. The mean age of participants was 15.9 (SD ±14.1) years, and 454 (46.5%) were female. Median ulcer duration was 4 (interquartile range 2–8) weeks; median size was 2.0 (interquartile range 1.5–2.5) cm. For 745 (78.1%) case-patients, the ulcer was a first episode, and 662 (72.4%) had only 1 ulcer at the time of examination. Overall, 287 (28.8%) had a positive TPE PCR result. Ulcers positive by PCR were more frequently found in younger persons with only 1 ulcer, which was long-lasting and a first episode (Appendix Table 1, https://wwwnc.cdc.gov/EID/article/29/8/23-0608-App1.pdf). DPP reader results were available for 828 (83.2%) of the ulcers, of which PCR results were positive for 247 (29.8%).

Sensitivity of DPP detection of TPE PCR-positive cases with the naked eye was highest when we used the NT line, and specificity was highest when we used a combination of T and NT lines (Table). Using the values from the reader, we evaluated the optimal combination of cutoff values for the DPP T and NT lines, which maximized the sum of sensitivity and specificity to distinguish lesions that were positive and negative for TPE by PCR (Figure). That combination (T ≥1 and NT ≥28) provided sensitivity of 75.7% and specificity of 77.6% (Table). The subanalysis of DPP performance according to participants' characteristics showed higher specificity for children <7

Table. Performance of DPP Syphilis Screen & Confirm kit in study of rapid serologic test for diagnosis of yaws in patients with suspicious skin ulcers

Detection technique	PCR negative			PCR positive					
	Detected, no.	Not detected, no.	Specificity, % (95% CI)	Detected, no.	Not detected, no.	Sensitivity, % (95% CI)	Sensitivity + specificity, %	PPV, % (95% CI)	NPV, % (95% CI)
Naked eye									
T line	357	351	49.6 (45.8–53.3)	227	60	79.1 (73.9–83.7)	128.7	38.9 (34.9–43.0)	85.4 (81.6–88.7)
NT line	278	430	60.7 (57.0–64.4)	241	46	84.0 (79.2–88.0)	144.7	46.4 (42.1–50.8)	90.3 (87.3–92.8)
T and NT line	222	486	68.6 (65.1–72.1)	214	73	74.6 (69.1–79.5)	143.2	49.1 (44.3–53.9)	86.9 (83.9–89.6)
Reader									
T ≥1 and NT reader ≥28†	130	451	77.6 (74.0–81.0)	187	60	75.7 (69.9–80.9)	153.3	59.0 (53.4–64.5)	88.3 (85.2–90.9)

*DPP (Dual Path Platform) Syphilis Screen & Confirm kit, Chembio (https://chembio.com). NPV, negative predictive value; NT line, antibodies against non–*Treponema pallidum* antigen; PPV, positive predictive value; T line, antibodies against *T. pallidum* antigen.
†Values used as cutoff with the DPP reader were calculated to maximize the sum of sensitivity and specificity (Figure).

years of age and for adults (>18 years of age) (Appendix Tables 2, 3).

The proportion of cutaneous ulcers in yaws-endemic regions that were TPE positive declined from 44% to 8% after 1 round of azithromycin mass drug administration (delivery to all consenting members of target community, regardless of diagnosis) (*7*,*8*). In that context, the combined T and NT lines, recommended for surveillance, would be sufficient to partially detect ongoing yaws transmission, but PCR confirmation would be required to discern TPE ulcers from latent cases or false-positive results (Appendix Table 4).

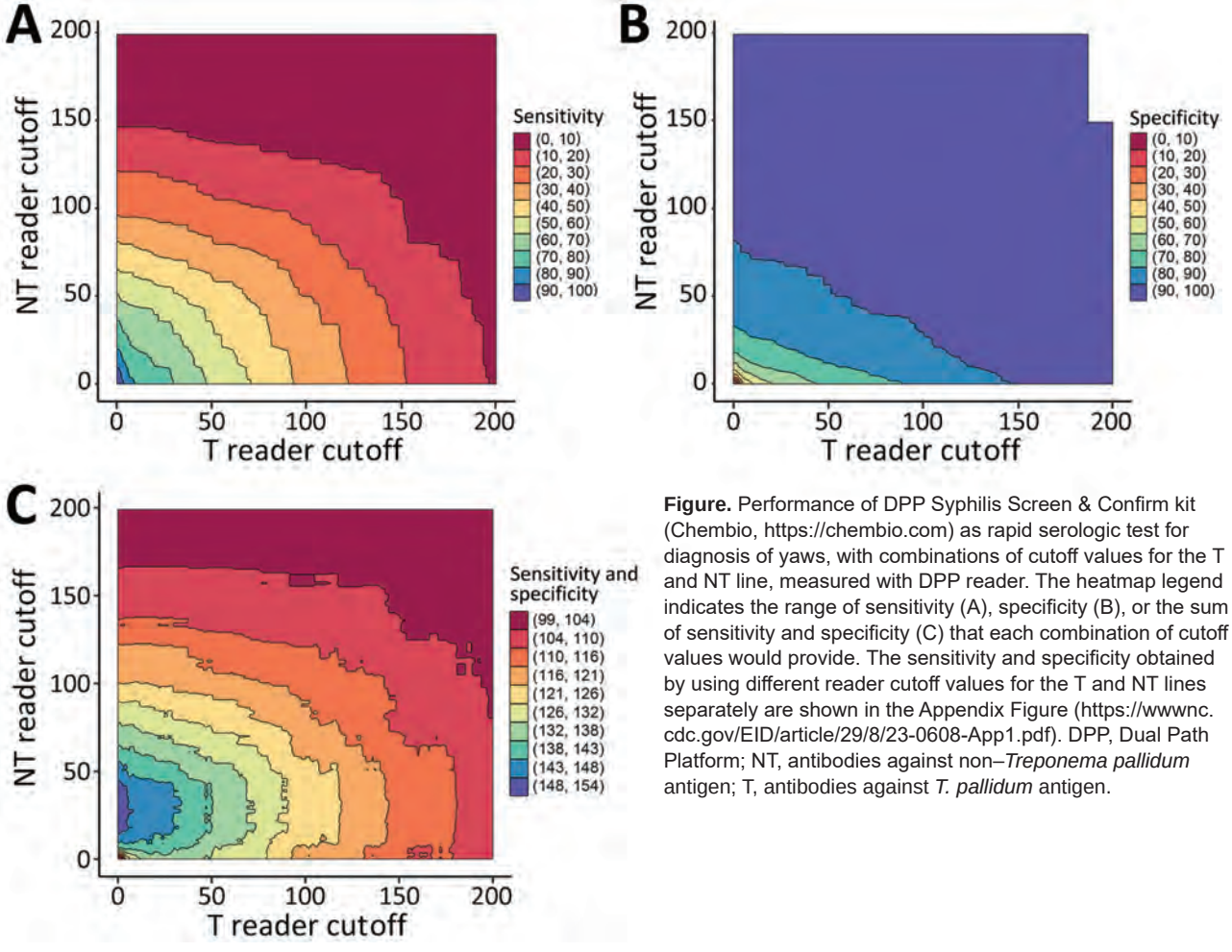

Figure. Performance of DPP Syphilis Screen & Confirm kit (Chembio, https://chembio.com) as rapid serologic test for diagnosis of yaws, with combinations of cutoff values for the T and NT line, measured with DPP reader. The heatmap legend indicates the range of sensitivity (A), specificity (B), or the sum of sensitivity and specificity (C) that each combination of cutoff values would provide. The sensitivity and specificity obtained by using different reader cutoff values for the T and NT lines separately are shown in the Appendix Figure (https://wwwnc.cdc.gov/EID/article/29/8/23-0608-App1.pdf). DPP, Dual Path Platform; NT, antibodies against non–*Treponema pallidum* antigen; T, antibodies against *T. pallidum* antigen.

The DPP test can provide up to 84% sensitivity for detecting TPE PCR-positive ulcers with the naked eye when using the NT line, although the specificity of this strategy is low (61%). The automatic reader did not increase sensitivity. Our results should be interpreted by bearing in mind that the reference and index tests provide information regarding different features or manifestations of yaws: skin ulcers with TPE DNA and serologic activity of the host. Therefore, different disease phases such as incubation period or latency, or other confounders such as syphilis infections, may contribute to conflicting PCR and DPP results.

Overall, the DPP test showed a reasonably high capacity to identify yaws in persons with TPE PCR-confirmed ulcers. That level of performance is suitable for qualitatively identifying ongoing transmission of yaws in the community during the late phases of eradication. However, for individual diagnoses, PCR confirmation of suspicious ulcers remains necessary; new point-of-care tests with higher sensitivity and specificity would be valuable.

Acknowledgments

We thank Gerard Carot-Sans for providing medical writing support during the preparation of an earlier version of the manuscript; the staff of New Ireland Provincial Health Authority, Namatanai District Health Facility, and Lihir Medical Centre for their support in executing the trial where these data were obtained; the community volunteers who helped in their respective villages; and Laia Bertran and Sergi Gavilan for the operational and financial management of the project.

O.M. is supported by the European Research Council under grant agreement 850450 (European Union's Horizon 2020 Research and Innovation Program, ERC-2019-STG funding scheme).

About the Author

Dr. Suñer is a senior scientist in infectious diseases at the Fight Infections Foundation in Barcelona. Her research interests include infectious disease transmission, diagnosis, and public health strategies.

References

1. World Health Organization. Yaws: key facts [cited 2022 Dec 30]. https://www.who.int/news-room/fact-sheets/detail/yaws
2. Marks M, Chi KH, Vahi V, Pillay A, Sokana O, Pavluck A, et al. *Haemophilus ducreyi* associated with skin ulcers among children, Solomon Islands. Emerg Infect Dis. 2014;20:1705–7. https://doi.org/10.3201/eid2010.140573
3. Janier M, Unemo M, Dupin N, Tiplica GS, Potočnik M, Patel R. 2020 European guideline on the management of syphilis. J Eur Acad Dermatol Venereol. 2021;35:574–88. https://doi.org/10.1111/jdv.16946
4. Yin YP, Chen XS, Wei WH, Gong KL, Cao WL, Yong G, et al. A dual point-of-care test shows good performance in simultaneously detecting nontreponemal and treponemal antibodies in patients with syphilis: a multisite evaluation study in China. Clin Infect Dis. 2013;56:659–65. https://doi.org/10.1093/cid/cis928
5. Castro AR, Esfandiari J, Kumar S, Ashton M, Kikkert SE, Park MM, et al. Novel point-of-care test for simultaneous detection of nontreponemal and treponemal antibodies in patients with syphilis. J Clin Microbiol. 2010;48:4615–9. https://doi.org/10.1128/JCM.00624-10
6. Marks M, Yin YP, Chen XS, Castro A, Causer L, Guy R, et al. Metaanalysis of the performance of a combined treponemal and nontreponemal rapid diagnostic test for syphilis and yaws. Clin Infect Dis. 2016;63:627–33. https://doi.org/10.1093/cid/ciw348
7. John LN, Beiras CG, Houinei W, Sabok M, Kolmau R, Jonathan E, et al. A trial of three rounds of mass drug administration with azithromycin for yaws. N Engl J Med. 2022;386:47–56.
8. World Health Organization. Eradication of yaws—the Morges Strategy. 2016 [cited 2022 Dec 30]. https://apps.who.int/iris/rest/bitstreams/959090/retrieve

Address for correspondence: Clara Suñer, University Hospital Germans Trias i Pujol Carretera de Canyet, s/n, 08916 Badalona, Barcelona, Spain; email: csuner@lluita.org

Soft Tissue Infection of Immunocompetent Man with Cat-Derived *Globicatella* Species

Nick K. Jones, Juliana Coelho, Julie M.J. Logan, Karen Broughton, Katie L. Hopkins, Bruno Pichon, Isabelle Potterill, Yu Wan, Alex W.N. Reid, Theodore Gouliouris

Author affiliations: Cambridge University Hospitals, Cambridge, UK (N.K. Jones, A.W.N. Reid, T. Gouliouris); University of Cambridge, Cambridge (N.K. Jones, T. Gouliouris); United Kingdom Health Security Agency Antimicrobial Resistance and Healthcare Associated Infections Reference Unit, Colindale, UK (J. Coelho, J.M.J. Logan, K. Broughton, K.L. Hopkins, B. Pichon, I. Potterill, Y. Wan); Imperial College London, London, UK (K.L. Hopkins, B. Pichon, Y. Wan)

DOI: https://doi.org/10.3201/eid2908.221770

We report a novel *Globicatella* species causing extensive soft tissue infection in a man bitten by a stray domestic cat in the United Kingdom. We identified this bacterium by 16S rRNA gene sequencing, whole-genome sequencing, and biochemical profiling and determined antimicrobial drug susceptibility.

Cats are major reservoirs of zoonotic infections. Their long, sharp teeth predispose to deep-tissue bite injuries, and direct inoculation of feline saliva gives high risk for secondary infection. Infecting pathogens usually reflect colonizing oral microbiota; *Pasteurella* and *Streptococcus* species are the most common (*1*). Bacteria of the genus *Globicatella* are small, gram-positive cocci that resemble viridans-group streptococci. *Globicatella sanguinis* is the only known species to cause human infection, having been implicated in small numbers of bloodstream, heart, central nervous system and urinary tract infections (*2*). *G. sulfidifaciens* is the only other known *Globicatella* species, but human infection has not been described (*3*). We report a novel *Globicatella* species causing extensive soft tissue infection and tenosynovitis in an immunocompetent man after cat bite injuries.

A 48-year-old obese man came to the emergency department in 2020 because of painful bilateral hand swelling, 8 hours after sustaining several bites from a single feral cat. He had multiple puncture wounds and abrasions, without evidence of surrounding cellulitis. His wounds were bathed in povidone–iodine solution and dressed, and a booster dose of tetanus vaccine was administered. He was discharged and given oral doxycycline, ciprofloxacin, and metronidazole treatment because of history of penicillin allergy. He returned to the emergency department 24 hours later because of evolving flexor sheath infection in his left little and right middle fingers and cellulitis of both forearms (Figure). He was given intravenous vancomycin, ciprofloxacin, and metronidazole, then underwent debridement and washout. He was given 5 days of oral doxycycline and metronidazole postoperatively and made a full recovery. The patient provided fully informed, written consent for this case to be published, with accompanying clinical photographs.

We obtained tissue samples from debridement sites and a swab specimen from the right middle finger for microbiological analysis with Gram stain and bacterial culture on blood, chocolate, cystine-lactose-electrolyte–deficient, and fastidious anaerobe agars. No organisms were seen on Gram stain. A scant growth of *Staphylococcus epidermidis* was isolated from the right middle finger tissue sample, as well as a *Streptococcus*-like organism that grew best on chocolate agar. Culture yield may have been affected by previous antimicrobial drug treatment.

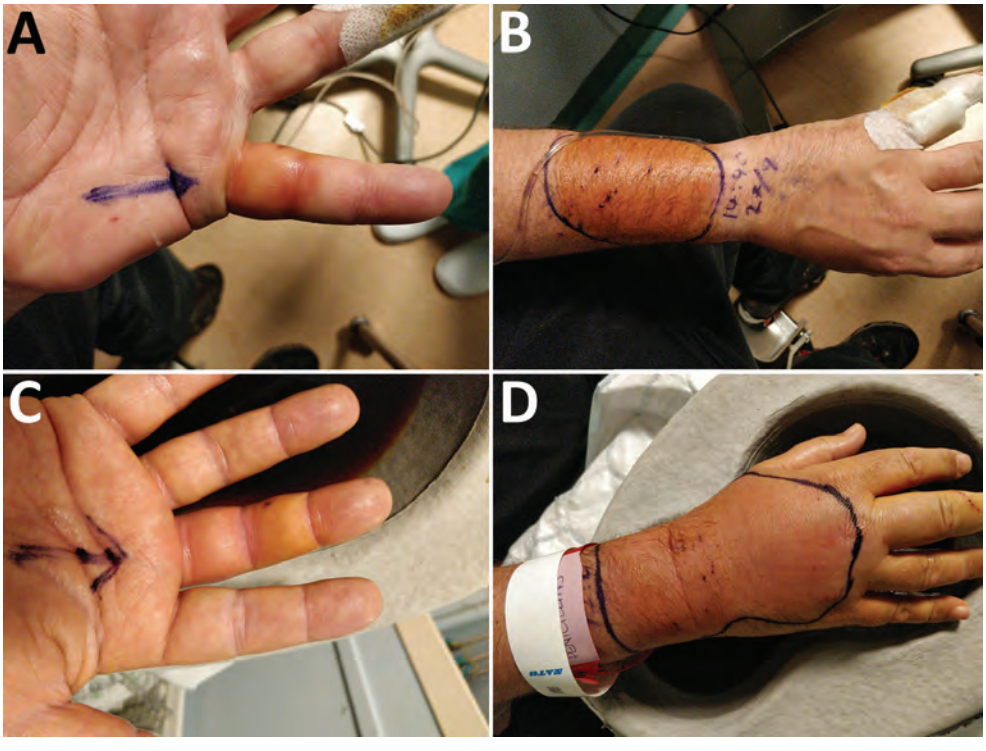

Figure. Clinically apparent areas of infection with *Globicatella* species in patient with soft tissue ianfection after cat bite, United Kingdom: A) left little finger, B) right forearm, C) right middle finger, and D) right hand.

Matrix-assisted laser desorption/ionization time-of-flight mass spectrometry (Bruker, https://www.bruker.com) of the *Streptococcus*-like organism gave no reliable identification (score 1.31). We referred this isolate (designated G1610988) to the UK Health Security Agency Reference Laboratory for further characterization.

We obtained partial 16S rRNA gene sequence data after block-based PCR as described (*4*). Those data did not match any named species in the GenBank database. The closest sequence database match was to *Globicatella* sp. feline oral taxon 122 (99%–100% identity) (*5*).

API Rapid ID 32 Strep analysis (bioMérieux, https://www.biomerieux.com) gave an organism identification of *Erysipelothrix rhusiopathiae* (98.7%). The isolate was negative for pyrrolidonyl aminopeptidase and leucine aminopeptidase and positive for bile aesculin (Diatabs; Rosco Diagnostica, https://www.rosco.dk) diagnostic tablets for bacterial identification. Repeat matrix-assisted laser desorption/ionization time-of-flight mass spectrometry at the reference laboratory gave no reliable identification (score 1.41). Comparison with biochemical profiling of *G. sanguinis* and *G. sulfidifaciens* type strains showed notable differences (Appendix, https://wwwnc.cdc.gov/EID/article/29/8/22-1770-App1.pdf). The conditions required for culture were not different between *Globicatella* species.

We conducted antimicrobial drug susceptibility testing by using MIC gradient strips (Liofilchem, https://www.liofilchem.com) and PK/PD and non–species-related breakpoints (*6*). Gentamicin was identified as an unsuitable treatment option, MIC 1.0 mg/L (breakpoint 0.5 mg/L). Treatments suitable for use with caution were ampicillin, MIC ≤0.016 mg/L (2.0 mg/L); cefotaxime, MIC 0.004 mg/L (1.0 mg/L); penicillin, MIC ≤0.016 mg/L (0.25 mg/L); linezolid, MIC 1.0 mg/L (2.0 mg/L); ciprofloxacin, MIC 0.032 mg/L (0.25 mg/L); and moxifloxacin, MIC 0.016 mg/L (0.25 mg/L). No PK/PD non–species-related breakpoints were available for teicoplanin, MIC 0.032 mg/L; vancomycin, MIC 0.25 mg/L; clindamycin, MIC 1.0 mg/L; erythromycin. MIC 0.032 mg/L; tetracycline, MIC 0.064 mg/L; chloramphenicol, MIC 2.0 mg/L; or rifampin, MIC 0.004 mg/L.

To corroborate the 16S rRNA gene sequence results, we conducted whole-genome sequencing on a HiSeq 2500 platform (Illumina, https://www.illumina.com) at the UK Health Security Agency Central Sequencing Laboratory by using its standard paired-end 101-bp sequencing protocol. We extracted genomic DNA from lysate by using the QIAsymphony DSP DNA Mini Kit and automated QIAsymphony SP/AS Instruments (QIAGEN, https://www.qiagen.com). We trimmed and filtered sequencing reads by using Trimmomatic (*7*) for quality control, then assembled by using SPAdes version 3.15 (*8*). Comparison with published *Globicatella* genomes by using FastANI (*9*) showed an average nucleotide divergence of 20.29% to its most closely related cluster (*G. sulfidifaciens*), suggesting a distinct and previously undescribed species (Appendix Figure).

Genomic sequences of isolate G1610988 have been deposited in the European Nucleotide Archive (Biosample accession no. SAMEA110751862). Partial sequence of the 16S rRNA gene has been deposited in GenBank (accession no. MW242777).

In conclusion, cat bites are common sources of zoonotic infection. This report highlights the role of cats as reservoirs of as yet undiscovered bacterial species that have human pathogenic potential. Currently recommended antimicrobial drug regimens for treating cat bites can be expected to include the *Globicatella* species described.

This study was conducted as part of our routine clinical and laboratory work. N.K.J. is a Cambridge Clinical Research Fellow, funded by Addenbrooke's Charitable Trust (Company no. 10469089, Charity no. 1170103, Grant no. G112768A) and the National Institute for Health and Care Research Cambridge Biomedical Research Centre training scheme. Y.W. is an Institutional Strategic Support Fund Springboard Fellow, funded by the Wellcome Trust and Imperial College London. K.L.H., B.P., and Y.W. are affiliated with the National Institute for Health Research Health Protection Unit in Healthcare Associated Infections and Antimicrobial Resistance at Imperial College London in partnership with the UK Health Security Agency (previously Public Health England), in collaboration with Imperial Healthcare Partners, the University of Cambridge, and the University of Warwick.

About the Author

Dr. Jones is a specialty registrar in medical microbiology and infectious diseases at Cambridge University Hospitals National Health Service Foundation Trust, Cambridge, UK, and a clinical research fellow at the University of Cambridge. His primary research interests are antimicrobial drug resistance and antimicrobial stewardship.

References

1. Abrahamian FM, Goldstein EJ. Microbiology of animal bite wound infections. Clin Microbiol Rev. 2011;24:231–46. https://doi.org/10.1128/CMR.00041-10
2. Miller AO, Buckwalter SP, Henry MW, Wu F, Maloney KF, Abraham BK, et al. *Globicatella sanguinis* osteomyelitis and bacteremia: review of an emerging human pathogen with an expanding spectrum of disease. Open Forum Infect Dis. 2017;4:ofw277. https://doi.org/10.1093/ofid/ofw277
3. Vandamme P, Hommez J, Snauwaert C, Hoste B, Cleenwerck I, Lefebvre K, et al. *Globicatella sulfidifaciens* sp. nov., isolated from purulent infections in domestic animals. Int J Syst Evol Microbiol. 2001;51:1745–9. https://doi.org/10.1099/00207713-51-5-1745
4. Edwards KJ, Logan JMJ, Langham S, Swift C, Gharbia SE. Utility of real-time amplification of selected 16S rRNA gene sequences as a tool for detection and identification of microbial signatures directly from clinical samples. J Med Microbiol. 2012;61:645–52. https://doi.org/10.1099/jmm.0.041764-0
5. Dewhirst FE, Klein EA, Bennett ML, Croft JM, Harris SJ, Marshall-Jones ZV. The feline oral microbiome: a provisional 16S rRNA gene based taxonomy with full-length reference sequences. Vet Microbiol. 2015;175:294–303. https://doi.org/10.1016/j.vetmic.2014.11.019
6. European Committee on Antimicrobial Susceptibility Testing (EUCAST). Antimicrobial susceptibility tests on groups of organisms or agents for which there are no EUCAST breakpoints. December 2021 [cited 2023 May 16]. https://www.eucast.org/clinical_breakpoints_and_dosing/when_there_are_no_breakpoints
7. Bolger AM, Lohse M, Usadel B. Trimmomatic: a flexible trimmer for Illumina sequence data. Bioinformatics. 2014;30:2114–20. https://doi.org/10.1093/bioinformatics/btu170
8. Bankevich A, Nurk S, Antipov D, Gurevich AA, Dvorkin M, Kulikov AS, et al. SPAdes: a new genome assembly algorithm and its applications to single-cell sequencing. J Comput Biol. 2012;19:455–77. https://doi.org/10.1089/cmb.2012.0021
9. Jain C, Rodriguez-R LM, Phillippy AM, Konstantinidis KT, Aluru S. High throughput ANI analysis of 90K prokaryotic genomes reveals clear species boundaries. Nat Commun. 2018;9:5114. https://doi.org/10.1038/s41467-018-07641-9

Address for correspondence: Nick K. Jones, Clinical Microbiology and Public Health Laboratory, Addenbrooke's Hospital, Hills Rd, Cambridge, CB2 0QQ, UK; email: nicholas.jones20@nhs.net

Imported Cholera Cases, South Africa, 2023

Anthony M. Smith, Phuti Sekwadi, Linda K. Erasmus, Christine C. Lee, Steven G. Stroika, Sinenhlanhla Ndzabandzaba, Vinitha Alex, Jeremy Nel, Elisabeth Njamkepo, Juno Thomas, François-Xavier Weill

Author affiliations: University of Pretoria, Pretoria, South Africa (A.M. Smith); National Institute for Communicable Diseases, Johannesburg, South Africa (A.M. Smith, P. Sekwadi, L.K. Erasmus, J. Thomas); US Centers for Disease Control and Prevention, Atlanta, Georgia, USA (C.C. Lee, S.G. Stroika); National Heath Laboratory Service, Johannesburg (S. Ndzabandzaba, V. Alex); University of the Witwatersrand, Johannesburg (S. Ndzabandzaba, V. Alex, J. Nel); Institut Pasteur, Université Paris Cité, Paris, France (E. Njamkepo, F.-X. Weill)

DOI: https://doi.org/10.3201/eid2908.230750

Since February 2022, Malawi has experienced a cholera outbreak of >54,000 cases. We investigated 6 cases in South Africa and found that isolates linked to the outbreak were *Vibrio cholerae* O1 serotype Ogawa from seventh pandemic El Tor sublineage AFR15, indicating a new introduction of cholera into Africa from south Asia.

The seventh cholera pandemic arrived in Africa during 1970, and the related cholera strain, *Vibrio cholerae* O1 biotype El Tor (7PET), has since become endemic in many countries in Africa (*1*–*3*). As of March 20, 2023, at least 24 countries globally reported ongoing cholera cases. Several countries in southeastern Africa, in particular Malawi and Mozambique, were experiencing outbreaks. In addition, outbreaks were spreading regionally, including to Tanzania, Zambia, Zimbabwe, and South Africa. The largest active cholera outbreak on the continent was in Malawi: 54,841 cases and 1,684 deaths reported during February 28, 2022–March 20, 2023 (*4*).

South Africa is not considered endemic for cholera; previous outbreaks have typically been associated with importation events. However, cholera remains under active surveillance in South Africa. The National Institute for Communicable Diseases is notified of all suspected cases. All *V. cholerae* isolates are submitted to the Centre for Enteric Diseases, which provides further laboratory investigation, including phenotypic and genotypic characterization (Appendix 1, https://wwwnc.cdc.gov/EID/article/29/8/23-0750-App1.pdf) (*5*). Ethics approval was obtained from the Human Research Ethics Committee, University of the Witwatersrand, Johannesburg, South Africa (protocol reference no. M210752).

Table. Characteristics of cholera cases and classification of *Vibrio cholerae* O1 serotype Ogawa sequence type 69 isolates from patient fecal samples, Gauteng Province, South Africa, 2023

Case	Date sample collected	Cholera case classification	Comment on case classification	Patient age, y/sex	Clinical manifestations
1	2023 Feb 1	Imported case	Infected in Malawi	37/F	Acute diarrhea and dehydration
2	2023 Feb 2	Imported case	Infected in Malawi	44/F	Mild diarrhea
3	2023 Feb 5	Related to imported case	Close household contact of case-patient 1 (direct link to imported case)	41/M	Acute diarrhea and dehydration
4	2023 Feb 16	Locally acquired indigenous case	No travel history; no evidence of direct link to an imported case	27/M	Acute diarrhea and dehydration
5	2023 Feb 12	Locally acquired indigenous case	No travel history; no evidence of direct link to an imported case	23/M	Mild diarrhea
6	2023 Feb 23	Locally acquired indigenous case	No travel history; no evidence of direct link to an imported case	19/F	Mild diarrhea

As of February 28, 2023, a total of 6 cholera cases in South Africa had been laboratory confirmed by the Centre for Enteric Diseases; fecal samples were collected from patients February 1–23, 2023. All cases occurred in Gauteng Province (Table); 3 case-patients were female (19–44 years of age) and 3 male (23–41 years of age). Cases 1–3 were imported or import-related cases. Case-patients 1 and 2 (sisters) left Johan-

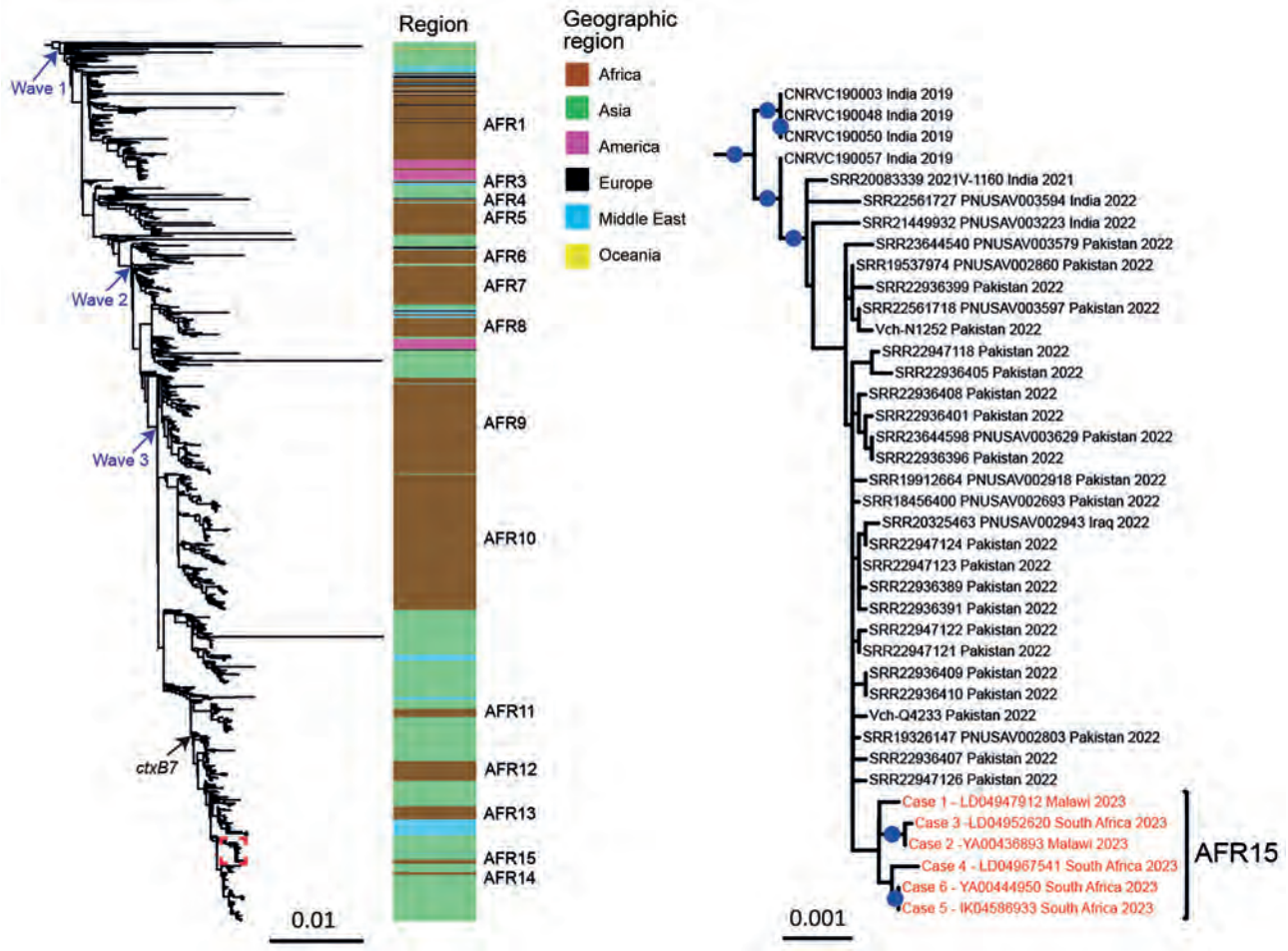

Figure. Maximum-likelihood phylogeny of *Vibrio cholerae* O1 El Tor isolates collected in South Africa, 2023, compared with 1,443 reference seventh pandemic *V. cholerae* El Tor (7PET) genomic sequences. A6 was used as the outgroup. The genomic waves and acquisition of the *ctxB7* allele are indicated. Color coding indicates the geographic origins of the isolates; sublineages previously introduced into Africa (AFR1, AFR3–AFR14) are shown at right. A magnification of the clade containing the 6 isolates from South Africa (red text) is shown at right. For each genome, name (or accession number), country where contamination occurred, and year of sample collection are shown at the tips of the tree. The 6 isolates collected in South Africa belong to a new 7PET wave 3 sublineage called AFR15. Blue dots indicate bootstrap values ≥90%. Scale bars indicate number of nucleotide substitutions per variable site.

nesburg on January 15, 2023, and traveled together to Chinsapo, Lilongwe, Malawi, in one of the districts reporting active outbreaks, where they stayed until their departure on January 29, 2023. Both women reported onset of symptoms within 12 hours of departure during the bus trip back to Johannesburg. Case-patient 3 was a close household contact of case-patient 1. Case-patients 4–6 acquired infection locally and were classified as indigenous cases; none had travelled or had any link to the imported or import-related cases or to one another. We identified isolates associated with all 6 cases as *V. cholerae* O1 serotype Ogawa and all were PCR-positive for the cholera toxin–producing gene.

We used whole-genome sequencing, comparative genomics, and phylogenetic analysis to further characterize the isolates (Appendix 2 Tables 1, 2, https://wwwnc.cdc.gov/EID/article/29/8/23-0750-App1.xlsx). The 6 *V. cholerae* O1 isolates had similar genomic features, including the toxin-coregulated pilus gene subunit A gene variant, *tcpA*^{CIRS101}, a deletion (ΔVC_0495-VC_0512) within the vibrio seventh pandemic island II (VSP-II), and an SXT/R391 integrating conjugating element called ICE*Vch*Ind5, encoding resistance to streptomycin (*strAB*), sulfonamides (*sul2*), trimethoprim (*dfrA1*), and trimethoprim/sulfamethoxazole (*dfrA1* and *sul2*) and resistance or intermediate resistance to chloramphenicol (*floR*). The isolates also had mutations of *VC_0715* (resulting in the R169C substitution) and *VC_A0637* (resulting in the premature stop codon Q5Stop) conferring nitrofuran resistance, and of the DNA gyrase, *gyrA* (S83I), and topoisomerase IV, *parC* (S85L) genes, conferring resistance to nalidixic acid and decreased susceptibility to ciprofloxacin (*3*,*6*). The isolates also had a specific nonsynonymous single-nucleotide variant (SNV) in the *vprA* gene (*VC_1320*) (resulting in the D89N substitution), conferring susceptibility to polymyxins (*6*).

To place these 6 isolates into a global phylogenetic context, we constructed a maximum-likelihood phylogeny of 1,443 genomes (Appendix 2 Table 3) with 10,679 SNVs evenly distributed over the nonrepetitive, nonrecombinant core genome. All isolates from South Africa clustered together (median pairwise distance of 4 [range 0–8] core-genome SNVs) in the 7PET lineage wave 3 clade, containing isolates carrying the *ctxB7* allele (Figure) (*6*). However, those isolates did not belong to any of the sublineages previously found in Africa (AFR1 and AFR3–AFR 14) (Figure) (*3*,*6*,*7*); instead, they tightly grouped with genomes of south Asia variants, suggesting that the 2022–2023 cholera outbreak in Malawi and cases in South Africa in our study were associated with a newly imported 7PET strain, sublineage AFR15, from south Asia. All but 1 of the closest genomes were either collected locally and identified in Pakistan during June–December 2022 or detected within the framework of cholera surveillance in the United States or Australia (*8*).

In conclusion, we show that isolates from cases in South Africa, which have been linked to the 2022–2023 cholera outbreak in Malawi, belong to the seventh pandemic El Tor sublineage AFR15. Those cases did not result from resurgence of a strain previously circulating in any region of Africa but were caused by a cholera agent newly introduced into Africa from south Asia. This finding offers valuable information to all public health authorities in Africa. Genomic microbial surveillance and cross-border collaborations have a key role to play in identifying new cholera introductions, areas prone to cholera importation, and the main routes of cholera circulation. All of these elements are key to better understanding cholera epidemiology in Africa.

Acknowledgement

We thank the Gauteng Department of Health for their contributions.

This study was made possible by support from the SEQAFRICA project, which is funded by the UK Department of Health and Social Care's Fleming Fund using UK aid.

About the Author

Dr. Smith is employed as a principal medical scientist at the Centre for Enteric Diseases, National Institute for Communicable Diseases, South Africa. He also holds the appointment of extraordinary professor with the University of Pretoria, South Africa. His interests include surveillance and epidemiology of enteric bacterial pathogens in South Africa.

References

1. Mintz ED, Tauxe RV. Cholera in Africa: a closer look and a time for action. J Infect Dis. 2013;208(Suppl 1):S4–7. https://doi.org/10.1093/infdis/jit205
2. Mutreja A, Kim DW, Thomson NR, Connor TR, Lee JH, Kariuki S, et al. Evidence for several waves of global transmission in the seventh cholera pandemic. Nature. 2011;477:462–5. https://doi.org/10.1038/nature10392
3. Weill FX, Domman D, Njamkepo E, Tarr C, Rauzier J, Fawal N, et al. Genomic history of the seventh pandemic of cholera in Africa. Science. 2017;358:785–9. https://doi.org/10.1126/science.aad5901
4. World Health Organization (WHO). 2023. Multi-country outbreak of cholera, external situation report #1—28 March 2023 [cited 2023 Apr 17]. https://www.who.int/publications/m/item/multi-country-outbreak-of-cholera--external-situation-report--1---28-march-2023
5. Smith AM, Weill FX, Njamkepo E, Ngomane HM, Ramalwa N, Sekwadi P, et al. Emergence of *Vibrio cholerae*

O1 sequence type 75, South Africa, 2018–2020. Emerg Infect Dis. 2021;27:2927–31. https://doi.org/10.3201/eid2711.211144
6. Weill FX, Domman D, Njamkepo E, Almesbahi AA, Naji M, Nasher SS, et al. Genomic insights into the 2016–2017 cholera epidemic in Yemen. Nature. 2019;565:230–3. https://doi.org/10.1038/s41586-018-0818-3
7. Benamrouche N, Belkader C, Njamkepo E, Zemam SS, Sadat S, Saighi K, et al. Outbreak of imported seventh pandemic *Vibrio cholerae* O1 El Tor, Algeria, 2018. Emerg Infect Dis. 2022;28:1241–5. https://doi.org/10.3201/eid2806.212451
8. Sim EM, Martinez E, Blackwell GA, Pham D, Millan G, Graham RMA, et al. Genomes of *Vibrio cholerae* O1 serotype Ogawa associated with current cholera activity in Pakistan. Microbiol Resour Announc. 2023;12:e0088722. https://doi.org/10.1128/mra.00887-22

Address for correspondence: Anthony Smith, Centre for Enteric Diseases, National Institute for Communicable Diseases, Private Bag X4, Sandringham, 2131, Johannesburg, South Africa; email: anthonys@nicd.ac.za

Asymptomatic Healthcare Worker PCR Screening during SARS-CoV-2 Omicron Surge, Germany, 2022

Ralph Bertram, Wolfgang Hitzl, Eike Steinmann, Joerg Steinmann

Author affiliations: Paracelsus Medical University, Nuremberg, Germany (R. Bertram, J. Steinmann); Paracelsus Medical University, Salzburg, Austria (W. Hitzl); Ruhr University Bochum, Bochum, Germany (E. Steinmann)

DOI: https://doi.org/10.3201/eid2908.230156

During 2022, a total of 9,515 asymptomatic healthcare workers of a large hospital in Germany underwent SARS-CoV-2 PCR screening twice weekly. Of 398,784 saliva samples, 3,555 (0.89%) were PCR positive (median cycle threshold value 30). Early identification of infected healthcare workers can help reduce SARS-CoV-2 transmission in the hospital environment.

COVID-19, caused by the SARS-CoV-2 virus, results in acute pulmonary and extrapulmonary manifestations and frequently causes long-term sequalae (*1*). In Germany, ≈38.5 million SARS-CoV-2 infections and ≈174,000 COVID-19 deaths had been reported through May 2023 (*2*). Among those, ≈30.2 million infections and ≈47,000 deaths occurred during 2022, when SARS-CoV-2 Omicron variant dominance was accompanied by a mean hospitalization incidence of 5.87 (*2*). SARS-CoV-2 infection rates among hospitalized patients were reported to be ≈10%–15% (*3*). Healthcare workers (HCWs) also were exposed to an elevated risk of acquiring and shedding SARS-CoV-2 infections (*4*). Regular SARS-CoV-2 testing of asymptomatic HCWs has been found to reduced viral transmission to patients and coworkers (*5*). We report data from a systematic SARS-CoV-2 PCR screening program comprising >9,500 HCWs in a large hospital in Germany during 2022.

Table. Characteristics and key indicators for a surveillance study among asymptomatic healthcare workers during SARS-CoV-2 Omicron surge, Germany, 2022*

Characteristic	Value
Total no. PCR tests	398,784
Median no. tests/wk (IQR)	7,559 (6,834–8,139)
Total no. PCR-positive tests	3,555
Median positivity rate, % (IQR)	0.9 (0.45–1.17)
Minimum, January 3–9	0.25
Maximum, March 14–20	1.89
Total no. HCWs tested	9,515
No. (%) infected	2,782 (29.2)
No. (%) HCWs with ≥2 infections	463 (4.87)
Sex, no. (%)	
M	705 (25.3)
F	2,077 (74.7)
Median age, y (IQR)	42 (30–53)
Median Ct value (IQR)	30 (27–32)
No. (%) completing immunization regimen†	8,926 (93.8)

*Ct, cycle threshold; HCW, healthcare worker.
†As of March 2022 (Appendix Table 2, https://wwwnc.cdc.gov/EID/article/29/8/23-0156-App1.pdf).

Klinikum Nürnberg is a tertiary care hospital with 2,233 beds at 2 sites in Nuremberg, Germany, and cares for ≈100,000 inpatients and ≈170,000 outpatients per year. During January–November 2022, all 9,515 hospital staff were instructed to participate in a government-mandated regular SARS-CoV-2 PCR screening program. According to federal law in Germany, participation was mandatory irrespective of the level of working exposure risk or vaccination status (Table; Appendix Table 1, https://wwwnc.cdc.gov/EID/article/29/8/23-0156-App1.pdf).

Asymptomatic HCWs collected saliva samples twice weekly via self-sampling using a reliable gargling method (*6*); part-time workers collected samples less frequently. Samples were subjected to PCR testing by an external provider, and turnaround time between sampling and electronic reporting was ≈24–38 h. However, staff with acute COVID-19 symptoms were immediately PCR tested in house. Persons with PCR-verified

infection were quarantined for 5–7 days and excluded from the testing program for the next 10 weeks. In November 2022, hospital staff who had no direct patient contact discontinued the screening program.

A total of 398,784 PCR tests were performed, among which 3,555 (0.89%) were positive; 2,782 persons tested positive ≥1. The cumulative infection rate of all tested asymptomatic HCWs was 29.2%. We observed a minimum positivity rate (0.25%) during January 2022 and the highest numbers of positive tests in March (1.89%) and October (1.69%) 2022 (Figure, panel A). The median cycle threshold (Ct) value of all positive PCR tests was 30 (interquartile range [IQR] 27–32), suggesting that SARS-CoV-2–positive staff were detected at an early phase of infection. Asymptomatic HCWs who tested SARS-CoV-2–positive frequently had symptoms develop a few days after detection, accompanied by lower Ct values (data not shown).

We categorized hospital staff into 5 groups: physicians, nurses, facility services, administration, and miscellaneous. Physicians constituted 13.4% of hospital staff and showed an infection rate of 13.6%. According to contingency table analysis, that rate results in a relative risk (RR) for infection of 1.02 (95% CI 0.91–1.14; p = 0.77 by Fisher exact test). Nurses accounted for 37.2% of hospital staff and exhibited an infection rate of 37.4% resulting in an RR for infection of 1.01 (95% CI 0.95–1.07; p = 0.81 by Fisher exact test). Thus, despite having the most intense contact with patients, neither of the 2 groups was significantly overrepresented in infection events (Figure, panel B; Appendix Table 1).

This 12-month SARS-CoV-2 PCR screening surveillance program of asymptomatic HCWs resulted in an average positivity rate of 0.89%. A meta-analysis of data from January–August 2020 collected by hospitals worldwide reported an average of 1.9% of asymptomatic HCWs tested PCR-positive for SARS-CoV-2 (*7*). We detected 3,555 COVID-19 cases among 2,782 (29.2%) HCWs infected ≥1 time. That number corresponds to results from another 12-month study in South Africa encompassing medical laboratory staff that had an overall cumulative infection rate of 25.7% (*8*). Comparisons warrant caution because of

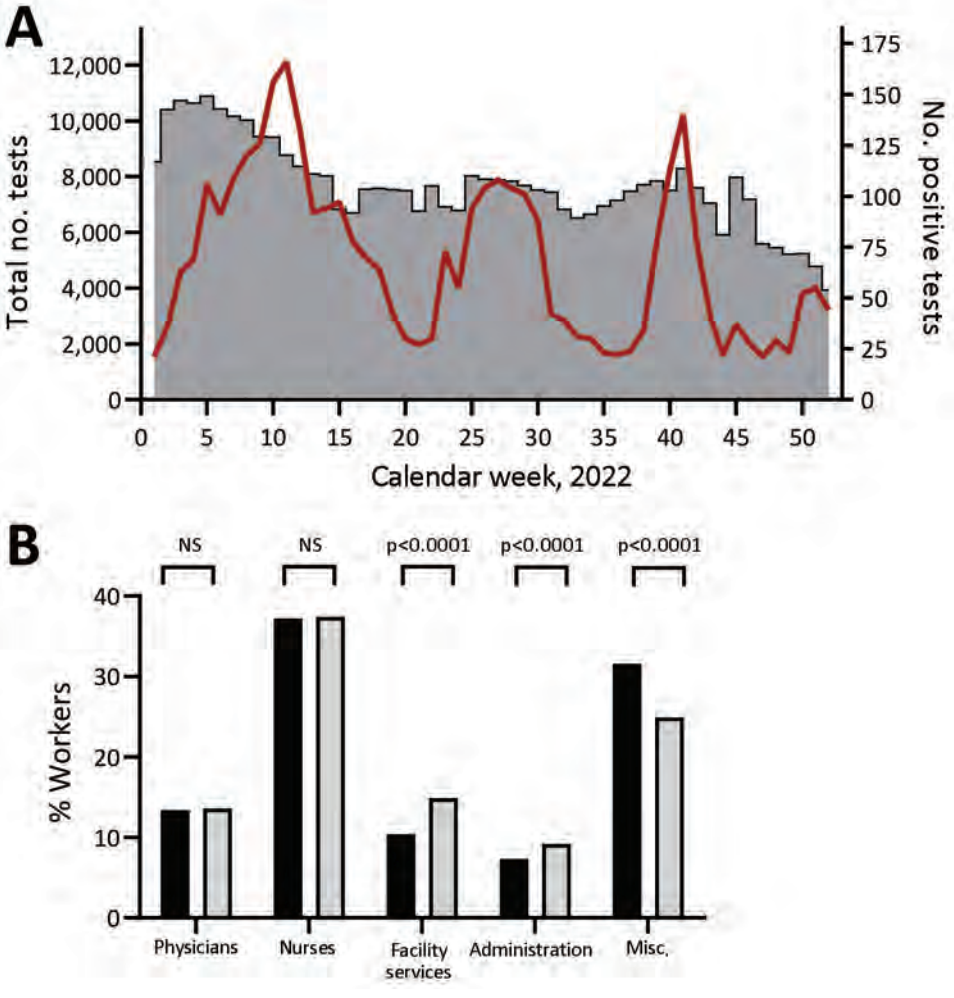

Figure. Number of tests performed and positivity rates for healthcare worker screening during SARS-CoV-2 Omicron surge, Germany, 2022. A) Total number of tests (gray bars) and number of positive tests (red line) per calendar week in 2022. B) Percentage positivity of each healthcare worker group in relation to total staff. Black bars indicate all staff; gray bars indicate the HCW groups. Misc., miscellaneous; NS, not statistically significant.

different spatiotemporal dominance of SARS-CoV-2 variants; vaccination status of HCWs, considering lower efficacy of vaccines against Omicron (*9*); and different infection control measures applied among hospitals (*10*). Furthermore, the surveillance study we report was not a randomized controlled trial, does not provide data on asymptomatic courses or rates of false positive PCR results, nor does it provide detailed information regarding seroprevalence or symptoms that developed.

The finding that physicians and nurses who were at the frontline of the COVID-19 outbreak response at Klinikum Nürnberg were not overrepresented in infection numbers speaks in favor of an efficient hygiene regimen. Besides measures such as compulsory patient screening, high-quality protective equipment, or regular ventilation, we believe that effective identification of asymptomatic HCWs in a preinfectious status might be one cornerstone of SARS-CoV-2 infection prevention in hospitals.

Acknowledgments

We thank Johanna Zeller and Florian Engelhardt for their support with data acquisition, Sabine Davison for proofreading and editing English, and the Paracelsus Medical University for their support.

About the Author

Dr. Ralph Bertram is a microbiologist and a researcher and lecturer in the Institute of Clinical Hygiene, Medical Microbiology and Infectiology, Klinikum Nürnberg, Paracelsus Medical University, Nuremberg, Germany. His research interests focus on infectious diseases, drug insensitivity of nosocomial pathogens and gene regulation.

References

1. Nalbandian A, Sehgal K, Gupta A, Madhavan MV, McGroder C, Stevens JS, et al. Post-acute COVID-19 syndrome. Nat Med. 2021;27:601–15. https://doi.org/10.1038/s41591-021-01283-z
2. Robert Koch-Institut. COVID-19: case numbers in Germany and worldwide [in German]. 2022 [cited 2023 May 29]. https://www.rki.de/DE/Content/InfAZ/N/Neuartiges_Coronavirus/nCoV.html
3. Barranco R, Vallega Bernucci Du Tremoul L, Ventura F. Hospital-acquired SARS-Cov-2 infections in patients: inevitable conditions or medical malpractice? Int J Environ Res Public Health. 2021;18:489. https://doi.org/10.3390/ijerph18020489
4. World Health Organization. Health workers exposure risk assessment and management in the context of COVID-19 virus: interim guidance, 4 March 2020 [cited 2023 Jan 30]. https://apps.who.int/iris/handle/10665/331340
5. Viswanathan M, Kahwati L, Jahn B, Giger K, Dobrescu AI, Hill C, et al. Universal screening for SARS-CoV-2 infection: a rapid review. Cochrane Database Syst Rev. 2020;9:CD013718.
6. Butler-Laporte G, Lawandi A, Schiller I, Yao M, Dendukuri N, McDonald EG, et al. Comparison of saliva and nasopharyngeal swab nucleic acid amplification testing for detection of SARS-CoV-2: a systematic review and meta-analysis. JAMA Intern Med. 2021;181:353–60. https://doi.org/10.1001/jamainternmed.2020.8876
7. Jabs JM, Schwabe A, Wollkopf AD, Gebel B, Stadelmaier J, Erdmann S, et al. The role of routine SARS-CoV-2 screening of healthcare-workers in acute care hospitals in 2020: a systematic review and meta-analysis. BMC Infect Dis. 2022;22:587. https://doi.org/10.1186/s12879-022-07554-5
8. Wilson KS, Ntlebi V, Made F, Sanabria N, Vetten M, Joseph J, et al. COVID-19 cases among medical laboratory services staff in South Africa, 2020–2021: a cohort study. PLoS One. 2022;17:e0268998. https://doi.org/10.1371/journal.pone.0268998
9. Ren SY, Wang WB, Gao RD, Zhou AM. Omicron variant (B.1.1.529) of SARS-CoV-2: mutation, infectivity, transmission, and vaccine resistance. World J Clin Cases. 2022;10:1–11. https://doi.org/10.12998/wjcc.v10.i1.1
10. Jin H, Chen Y, Fu Q, Qu Q. Occupational risk factors of contracting COVID-19 among health workers: a systematic review. Work. 2021;69:721–34. https://doi.org/10.3233/WOR-210477

Address for correspondence: Joerg Steinmann, Paracelsus Medical University, Prof.-Ernst-Nathan-Str. 1, Nuremberg 90419, Germany; email: joerg.steinmann@klinikum-nuernberg.de

Six Extensively Drug-Resistant Bacteria in an Injured Soldier, Ukraine

Patrick T. Mc Gann, Francois Lebreton, Brendan T. Jones, Henry D. Dao, Melissa J. Martin, Messiah J. Nelson, Ting Luo, Andrew C. Wyatt, Jason R. Smedberg, Joanna M. Kettlewell, Brain M. Cohee, Joshua S. Hawley-Molloy, Jason W. Bennett

Author affiliations: Multidrug-Resistant Organism Repository and Surveillance Network, Walter Reed Army Institute of Research, Silver Spring, Maryland, USA (P.T. Mc Gann, F. LeBreton, B.T. Jones, H.D. Dao, M.J. Martin, M.J. Nelson, T. Luo, J.W. Bennett); Landstuhl Regional Medical Center, Landstuhl, Germany (A.C. Wyatt, J.R. Smedberg, J.M. Kettlewell, J.S. Hawley-Malloy); 512th Field Hospital, Rhine Ordinance Barracks, Germany (B.M. Cohee)

DOI: http://doi.org/10.3201/eid2908.230567

Blood and surveillance cultures from an injured service member from Ukraine grew *Acinetobacter baumannii*, *Klebsiella pneumoniae*, *Enterococcus faecium*, and 3 distinct *Pseudomonas aeruginosa* strains. Isolates were nonsusceptible to most antibiotics and carried an array of antibiotic resistant genes, including carbapenemases (bla_{IMP-1}, bla_{NDM-1}, bla_{OXA-23}, bla_{OXA-48}, bla_{OXA-72}) and 16S methyltransferases (*armA* and *rmtB4*).

The ongiong conflict in Ukraine has placed extraordinary pressure on medical infrastructure and health delivery services in the region (*1*). Previous reports from Eastern Ukraine have noted the emergence of multidrug-resistant (MDR) *Acinetobacter baumanii*, *Pseudomonas aeruginosa*, and Enterobacterales infections during hospitalization (*2*). Those strains encompassed a variety of clonal lineages, with many carrying carbapenemases, extended-spectrum β-lactamases (ESBLs), and 16S methyltransferases (*2*,*3*). We describe the isolation of 6 extensively drug-resistant (XDR) organisms from a single soldier from Ukraine.

A man in his mid-50s suffered multiple traumatic injuries after a vehicle fire, including full-thickness burns covering 60% of his total body surface. He was initially treated in a medical facility near Dnipro, Ukraine, before being transferred to a hospital in Kyiv, Ukraine, where healthcare practitioners performed burn wound debridement and escharotomies. Thereafter, the patient was transported to a US military hospital in Germany, where doctors obtained blood, urine, respiratory, and peri-rectal surveillance cultures. Surveillance cultures grew *A. baumannii*, *Enterococcus faecium*, *Klebsiella pneumoniae,* and 2 distinct morphologies of *P. aeruginosa*. Blood cultures grew a third *P. aeruginosa* (Table). By using the Vitek 2 automated system (bioMérieux, https://www.biomerieux.com), the gram-negative organisms were found to be nonsusceptible to almost every antibiotic tested (Appendix Table 1, https://wwwwnc.cdc.gov/EID/article/29/8/23-0567-App1.pdf), with the exception of *A. baumannii*, which was susceptible to tetracycline (MIC 2 μg/mL). The *E. faecium* was nonsusceptible to vancomycin. Researchers used a customized Sensititer panel (Thermo Scientific, https://www.thermofisher.com) to test the gram-negative organisms against colistin, eravacycline, imipenem/relebactam, meropenem/vaborbactam, omadacycline, and plazomicin; they used disk diffusion (Hardy Diagnostics, https://hardydiagnostics.com) to test against cefiderocol (Appendix Table 1). Researchers performed whole-genome sequencing of all isolates by using an Illumina Miseq and the MiSeq Reagent Kit version 3 (600 cycles, 2 × 300 bp) (Illumina, https://www.illumina.com).

The *K. pneumoniae* isolate, designated MRSN 110821, was nonsusceptible to every antibiotic tested (Appendix Table 1). Testing identified 24 antimicrobial resistance genes, including the carbapenemases bla_{NDM-1} and bla_{OXA-48}, the RMTase *armA*, and the ESBL $bla_{CTX-M-15}$ (Table). Five plasmid replicons were identified (Appendix Table 2), but long-read sequencing is underway to better understand the plasmid structure (data not shown). Colistin resistance likely resulted from a previously characterized E82K mutation in the 2-component transcriptional regulator PhoP (*4*). Cefiderocol resistance could be linked to mutations in the outer membrane protein OmpK36 combined with NDM (*5*). The isolate also carried several hypervirulence genetic markers, including *ybt*16 (yersiniabactin siderophore), *iuc*1 (aerobactin), and *rmpADC*/*rmpA2* (mucoviscosity and capsule).

The isolate belonged to clade B1 of the clonal lineage sequence type (ST) 395 (*6*) and was K-antigen capsular biosynthesis loci, K39, and O-antigen

Table. Characteristics of 6 isolates cultured from an injured service member from Ukraine*

MRSN ID	Species	ST†	Antimicrobial resistance genes‡
110819	*Acinetobacter baumannii*	78	*aph(3')-Via*, *aac(6')-Ian*, ***armA***, *aadA5*, *ant(3'')-IIa*, ***bla*$_{OXA-23}$**, ***bla*$_{OXA-72}$**, bla_{OXA-90}, $bla_{ADC-152}$, ***bla*$_{CTX-M-115}$**, $bla_{CARB-16}$, *catA1*, *mph(E)*, *msr(E)*, *sul1*, *sul2*
110818	*Pseudomonas aeruginosa*	357	*aac(6')-II*, *aph(3')-IIb*, *aadA1*, bla_{OXA-10}, $bla_{OXA-846}$, bla_{PDC-11}, ***bla*$_{VEB-9}$**, *catB7*, *sul1*, *tet(A)*, *dfrB2*
110817	*P. aeruginosa*	773	*aph(3')-IIb*, *aadA11*, ***bla*$_{NDM-1}$**, bla_{PDC-16}, $bla_{OXA-395}$, *catB7*, *qnrVC1*, ***rmtB4***, *sul1*, *tet(G)*
110606§	*P. aeruginosa*	1047	*aac(6')-Ib3*, *aph(3')-IIb*, *aph(3'')-Ib*, *aph(6)-Id*, ***bla*$_{IMP-1}$**, bla_{OXA-10}, $bla_{OXA-488}$, bla_{PDC-12}, *catB7*, *sul1*
110821	*Klebsiella pneumoniae*	395	*aac(6')-Ib-cr5*, *aph(3')-VI*, *ant(2'')-Ia*, *aadA1*, ***armA***, ***bla*$_{NDM-1}$**, ***bla*$_{OXA-48}$**, ***bla*$_{CTX-M-15}$**, bla_{OXA-1}, bla_{SHV-11}, bla_{TEM-1}, *catA1*, *dfrA1*, *dfrA5*, *fosA*, *mph(A)*, *mph(E)*, *msr(E)*, *oqxA*, *oqxB*, *qnrS1*, *sul1*, *sul2*, *tet(A)*
110820	*Enterococcus faecium*	117	*aac(6')-Ie*, *aacA-ENT1*, *aph(2'')-Ia*, *catA7*, *dfrG*, *erm(B)*, *msr(C)*, ***vanA*** (operon)

*Bold indicates high-impact genes. MRSN, The Multidrug-Resistant Organism Repository and Surveillance Network; ID, identification; ST, sequence type.
† **In silico**–derived multilocus STs.
‡**In silico**–derived antimicrobial resistance gene content generated using MIGHT, a customized script wrapping ARIBA (https://github.com/sanger-pathogens/ariba) and AMRfinder (https://github.com/ncbi/amr).
§Blood culture isolate.

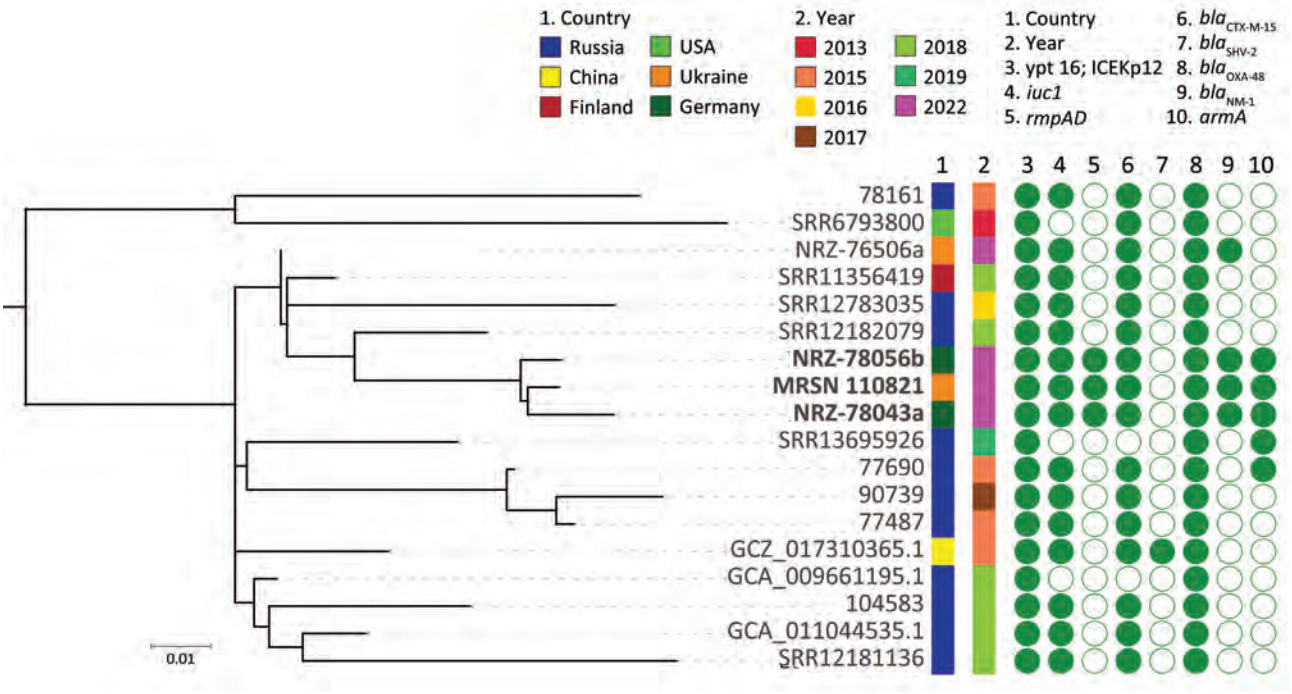

Figure. Core genome, SNP-based phylogenetic tree for *Klebsiella pneumoniae* from an injured service member from Ukraine (MRSN 110821) and 17 closely related sequence type 395 *K. pneumoniae*. In addition to MRSN 110821, the dataset included 14 subclade B2 isolates and 3 NDM-1/OXA-48–producing isolates available in public databases. Country of origin, year of collection, and presence (closed circle) or absence (open circle) of selected virulence and antimicrobial resistance genes are indicated. The midpoint was used as a root for the phylogenetic tree. *K. pneumoniae* MRSN 110821 from this study and the 2 highly related strains from Germany are highlighted in boldface. Scale bar indicates the ratio of substitutions per site for a 1,665 bp alignment of variable sites in the core genomes of the 18 strains.

type O2 variant 1 (O2v1). ST395 was first described in France in 2010, and carbapenemase-producing strains are increasingly being reported across Europe (*6*). We downloaded all clade B1 ST395 isolates from Pathogenwatch (https://pathogen.watch) and constructed a phylogenetic tree (Figure). We included 3 ST395 genomes identified by Sandfort et al, which they cultured from patients from Ukraine who were hospitalized in Germany (*7*). Of note, MRSN 110821 was separated by just 20 single nucleotide polymorphisms from NRZ-78043a from the Sandfort study and by just 19 from NRZ-78056b from that same study (Figure). Those 3 isolates clustered more broadly with isolates from Russia and Finland (Figure), but have since acquired *armA*, $bla_{\text{NDM-1}}$, and the mucoviscosity and capsule loci *rmpADC*, further increasing their antibiotic resistance profile and virulence potential.

We found *A. baumannii* MRSN 110819 to be resistant to all antibiotics except cefiderocol, colistin, eravacycline, and omadacycline (Appendix Table 1). The isolate carried 18 AMR genes, including the RMTase *armA*, the ESBL $bla_{\text{CTX-M-115}}$, and 2 carbapenemases, $bla_{\text{OXA-23}}$ and $bla_{\text{OXA-72}}$ (Table). The isolate was assigned to ST78, a clonal group known as the Italian clone because it emerged in Italy in the mid-2000s (*8*). This clonal group has also been identified in war wounds of service members from Ukraine during the earlier conflict in Eastern Ukraine (*2*).

The 3 *P. aeruginosa* isolates belonged to 3 distinct strains (Table). All 3 isolates had high MICs to 20 of the 23 antibiotics tested (Appendix Table 1). Only colistin and cefiderocol appeared effective in vitro, although MRSN 110818 was susceptible to imipenem/relebactam using US Food and Drug Administration breakpoints (MIC 2 mg/L). All 3 carried carbapenemases, ESBLs, and 16S methyltransferases (Table). MRSN 110818 and 110817 belonged to well-known (ST357) and emerging (ST773) epidemic, high-risk clones that are increasingly associated with horizontally acquired β-lactamases (*9*). The single blood isolate was assigned to ST1047.

E. faecium MRSN 110820 carried 8 AMR genes, including the *vanA* operon (Table). The strain was assigned to ST117, a member of clonal complex 78.

Gaps in such services as infection control, caused by limited resources and personnel, are

exacerbating the transmission of MDR organisms in Ukraine. As a result, healthcare networks in Europe now consider prior hospitalization in Ukraine to be a critical risk factor for colonization of MDR organisms (*7*,*10*). Healthcare practitioners treating citizens of Ukraine need to be cognizant of the increased risk for MDR organism transmission and infection imposed by the conflict in Ukraine and implement appropriate infection control measures to mitigate their spread.

Isolates for this study were collected under the auspices of routine public health surveillance. Sequences have been deposited into GenBank (BioProject nos. PRJNA950448, PRJNA950449, PRJNA950450, and PRJNA950451). The Multidrug-Resistant Organism Repository and Surveillance Network (MRSN) is a department within Walter Reed Army Institute of Research's Bacterial Diseases Branch, a unique entity that serves as the primary surveillance organization for antibiotic-resistant bacteria across the Army, Navy, and Air Force.

Funding for this study was provided by the US Department of the Army, Operation and Maintenance, Army. Material has been reviewed by the Walter Reed Army Institute of Research. There is no objection to its presentation and/or publication. The opinions or assertions contained herein do not necessarily reflect the opinions of the Department of the Army or the Department of Defense.

About the Author

Dr. Mc Gann is a microbiologist and deputy director of the Multidrug-Resistant Organism Repository and Surveillance Network in Silver Spring, Maryland, USA. His primary research interests are the emergence and spread of antibiotic resistance and using whole-genome sequencing techniques to unravel bacterial epidemiology.

References

1. Kazmirchuk A, Yarmoliuk Y, Lurin I, Gybalo R, Burianov O, Derkach S, et al. Ukraine's experience with management of combat casualties using NATO's four-tier "Changing as Needed" healthcare system. World J Surg. 2022;46:2858–62. https://doi.org/10.1007/s00268-022-06718-3
2. Kondratiuk V, Jones BT, Kovalchuk V, Kovalenko I, Ganiuk V, Kondratiuk O, et al. Phenotypic and genotypic characterization of antibiotic resistance in military hospital-associated bacteria from war injuries in the Eastern Ukraine conflict between 2014 and 2020. J Hosp Infect. 2021;112:69–76. https://doi.org/10.1016/j.jhin.2021.03.020
3. Higgins PG, Hagen RM, Podbielski A, Frickmann H, Warnke P. Molecular epidemiology of carbapenem-resistant *Acinetobacter baumannii* isolated from war-injured patients from the eastern Ukraine. Antibiotics (Basel). 2020;9:579. https://doi.org/10.3390/antibiotics9090579
4. Wand ME, Bock LJ, Bonney LC, Sutton JM. Mechanisms of increased resistance to chlorhexidine and cross-resistance to colistin following exposure of *Klebsiella pneumoniae* clinical isolates to chlorhexidine. Antimicrob Agents Chemother. 2016;61:e01162-16. https://doi.org/10.1128/AAC.01162-16
5. Simner PJ, Beisken S, Bergman Y, Ante M, Posch AE, Tamma PD. Defining baseline mechanisms of cefiderocol resistance in the Enterobacterales. Microb Drug Resist. 2022;28:161–70. https://doi.org/10.1089/mdr.2021.0095
6. Shaidullina ER, Schwabe M, Rohde T, Shapovalova VV, Dyachkova MS, Matsvay AD, et al. Genomic analysis of the international high-risk clonal lineage *Klebsiella pneumoniae* sequence type 395. Genome Med. 2023;15:9. https://doi.org/10.1186/s13073-023-01159-6
7. Sandfort M, Hans JB, Fischer MA, Reichert F, Cremanns M, Eisfeld J, et al. Increase in NDM-1 and NDM-1/OXA-48-producing *Klebsiella pneumoniae* in Germany associated with the war in Ukraine, 2022. Euro Surveill. 2022;27:2200926. https://doi.org/10.2807/1560-7917.ES.2022.27.50.2200926
8. Giannouli M, Cuccurullo S, Crivaro V, Di Popolo A, Bernardo M, Tomasone F, et al. Molecular epidemiology of multidrug-resistant *Acinetobacter baumannii* in a tertiary care hospital in Naples, Italy, shows the emergence of a novel epidemic clone. J Clin Microbiol. 2010;48:1223–30. https://doi.org/10.1128/JCM.02263-09
9. Del Barrio-Tofiño E, López-Causapé C, Oliver A. *Pseudomonas aeruginosa* epidemic high-risk clones and their association with horizontally-acquired β-lactamases: 2020 update. Int J Antimicrob Agents. 2020;56:106196. https://doi.org/10.1016/j.ijantimicag.2020.106196
10. Zwittink RD, Notermans DW, Verkaik NJ, Schoffelen AF, Witteveen S, Ganesh VA, et al, on behalf of the Dutch CPE and MRSA Surveillance Study Groups. Multidrug-resistant organisms in patients from Ukraine in the Netherlands, March to August 2022. Eurosurveillance. 2022;27(50):2200896. https://doi.org/10.2807/1560-7917.ES.2022.27.50.2200896

Address for correspondence: Patrick Mc GannWalter Reed Army Institute of Research, 503 Robert Grant Ave, 2A36, Silver Spring, MD 20910, USA; email: patrick.t.mcgann4.civ@health.mil

Highly Pathogenic Avian Influenza A(H5N1) Clade 2.3.4.4b Virus in Domestic Cat, France, 2022

François-Xavier Briand, Florent Souchaud, Isabelle Pierre, Véronique Beven, Edouard Hirchaud, Fabrice Hérault, René Planel, Angélina Rigaudeau, Sibylle Bernard-Stoecklin, Sylvie Van der Werf, Bruno Lina, Guillaume Gerbier, Nicolas Eterradossi, Audrey Schmitz, Eric Niqueux, Béatrice Grasland

Author affiliations: ANSES, Ploufragan, France (F.-X. Briand, F. Souchaud, I. Pierre, V. Beven, E. Hirchaud, N. Eterradossi, A. Schmitz, E. Niqueux, B. Grasland); Clinique Vétérinaire des Deux Rivières, Mauléon, France (F. Hérault); Clinique Vétérinaire Filiavet, Bressuire, France (R. Planel); Resalab Ouest site de Labovet Analyse, Les Herbiers, France (A. Rigaudeau); Santé publique France, Saint-Maurice, France (S. Bernard-Stoecklin); Université Paris Cité Institut Pasteur National Reference Center, Paris, France (S. Van der Werf); National Reference Center for Respiratory Viruses, Lyon, France (B. Lina); Université de Lyon, Lyon (B. Lina); French Ministry of Food and Agriculture, Paris (G. Gerbier)

DOI: https://doi.org/10.3201/eid2908.230188

We detected highly pathogenic avian influenza A(H5N1) clade 2.3.4.4b virus in a domestic cat that lived near a duck farm infected by a closely related virus in France during December 2022. Enhanced surveillance of symptomatic domestic carnivores in contact with infected birds is recommended to prevent further spread to mammals and humans.

On December 27, 2022, the avian influenza National Reference Laboratory of the Agency for Food, Environmental and Occupational Health & Safety in France confirmed a case of highly pathogenic avian influenza (HPAI) A(H5N1) clade 2.3.4.4b virus in a domestic cat. The cat lived with a human family next to a breeding duck farm, which had notified the animal health services of possible HPAI on December 9, 2022, after observing a 20% drop in egg production. After HPAI H5N1 clade 2.3.4.4b virus was confirmed at the farm, 8,375 ducks were culled on December 14. On December 20, the cat displayed disturbances in general condition, including apathy and mild hyperthermia, and was seen by a veterinary surgeon. The cat's condition worsened; pronounced neurologic and respiratory (dyspnea) symptoms appeared, resulting in compassionate euthanasia on December 24. Veterinarians collected sinonasal, tracheal, and anal swab samples after death, and a screening laboratory performed real-time reverse transcription PCR (RT-PCR) targeting the matrix protein and hemagglutinin (H5) genes. The laboratory sent H5-positive tracheal and sinonasal swab samples to the National Reference Laboratory, which confirmed HPAI H5N1 virus by using specific real-time RT-PCR for H5 clade 2.3.4.4b and neuraminidase (N1) genes (Table).

We compared the complete sequence of the HPAI H5N1 virus found in the cat (A/cat/France/22P026544/2022) with other HPAI H5N1 virus sequences circulating in France in the same area, including the virus found in the neighboring duck farm (A/duck/France/22P025647/2022). Phylogenetic analyses of HPAI H5N1 genomes indicated that the virus from the cat belonged to the A/duck/Saratov/29-02/2021–like genotype, which has been the predominant virus genotype circulating in France and Europe since September 2022. The cat virus sequence was directly related to virus sequences identified in the same area in December 2022 (Figure). Furthermore, the virus isolated from the neighboring duck farm (Figure) had only 2 nt differences (out of 13,507 total nts) compared with the cat virus, resulting in an E627K mutation in polymerase basic protein 2 and E26G mutation in nonstructural protein 2 in the cat virus. The E627K mutation has been described as a major marker of influenza virus adaptation to mammalian hosts (*1*). The E26G mutation has a possible role in virus adaptation to temperature changes (*2*). Since September 2021, a total of 90 sequences of HPAI H5N1 clade 2.3.4.4b viruses detected in mammals have been available in the GISAID EpiFlu database (https://www.gisaid.org), 20 of which have the E627K mutation, most probably indicating a rapid selection of this mutation in mammalian hosts (*3*). This virulence marker is in addition to those already observed in circulating HPAI H5N1 viruses detected in birds in Europe, such as the PB1-F2 N66S mutation (*4*).

Since winter 2021–22, the number of reported cases of HPAI H5N1 clade 2.3.4.4b infections in mammals has increased (*5*,*6*), likely caused by several factors. First, a higher prevalence of HPAI H5 viruses in wild and domestic birds might increase the probability of interactions between infected birds and mammals (scavenging, shared habitat). Second, increased surveillance of avian influenza in wildlife might lead to more detection in mammals. Third, currently circulating viruses might infect mammalian hosts more easily. HPAI H5N1 virus detection in mammals is often linked to clinical signs, such as neurologic symp-

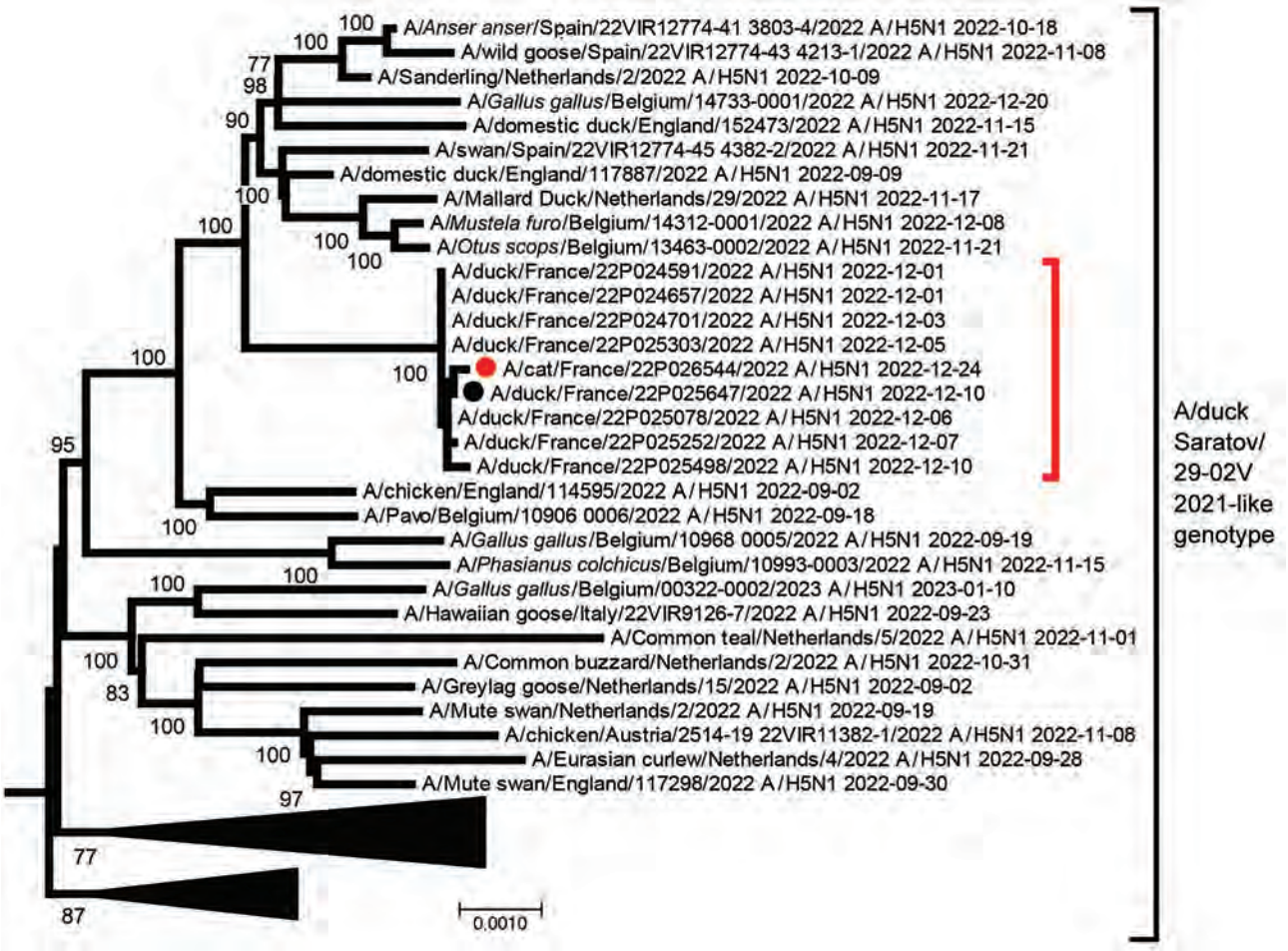

Figure. Phylogenetic analysis of highly pathogenic avian influenza A(H5N1) clade 2.3.4.4b virus detected in domestic cat, France, 2022. Tree was created by using MEGA 7 software (https://megasoftware.net) and the neighbor-joining method with 1,000 bootstrap replicates for complete concatenated HPAI H5N1 virus segments. All sequences belong to the A/duck/Saratov/29-02V/2021–like genotype. Red solid circle indicates virus sequence from cat; black solid circle indicates sequence from a nearby duck farm. Both sequences are available in the GISAID database (https://www.gisaid.org) under accession nos. EPI_ISL_16395206 (cat) and EPI_ISL_16740903 (duck). Red bracket indicates closely related sequences detected during the same period and area in France from domestic bird farms. Scale bar indicates nucleotide substitutions per site.

toms, or death of the animal (*3*,*7*). Few indications of intermammal HPAI H5N1 clade 2.3.4.4b contamination exist with the exception of massive infections in seal colonies in the United States (*6*) and a mink farm in Spain in 2022 (*6*,*7*). In our case report, negative results from serologic and real-time RT-PCR analyses of samples from the dog and other cat in the same household indicate a lack of intermammal transmission.

In conclusion, we show that HPAI H5N1 clade 2.3.4.4b can infect cats; HPAI H5N1 clade 1 and clade 2.2 have been sporadically detected in cats since 2004 (*8*). The close interactions and proximity of domestic cats and humans and rapid selection of mutations (after 1 passage from bird to mammal) could result in a virus with potential for interhuman transmission, indicating a considerable public health threat. Given that HPAI H5N1 circulates at high levels in wild and domestic birds, and virus was detected in a domestic cat,

Table. Real-time reverse transcription PCR results for different clinical samples in study of highly pathogenic avian influenza A(H5N1) clade 2.3.4.4b virus in domestic cat, France, 2022*

	PCR target gene			
Sample	Matrix protein	H5 hemagglutinin	H5 hemagglutinin 2.3.4.4b	N1 neuraminidase
Tracheal swab	25.5	25.5	26	29.4
Sinonasal swab	33.3	31.5	32.9	36.7
Anal swab	ND	ND	NA	NA

*Values are PCR cycle thresholds. NA, not applicable; ND, not detected.

we recommend enhanced surveillance of symptomatic domestic carnivores in contact with infected birds to rapidly identify potential transmission events to other domestic animals and prevent further spread to humans. Our report also indicates that adequate protective equipment and barrier measures should be provided to avoid direct transmission of HPAI to persons exposed to infected birds (*6*,*9*).

Acknowledgments

We thank all originating laboratories, where specimens were first obtained, and submitting laboratories, where sequence data used for the phylogenetic analyses were generated and submitted to the GISAID EpiFlu database (Appendix, https://wwwnc.cdc.gov/EID/article/29/8/23-0188-App1.xlsx); and Benjamin Houillé, Pascale Massin, Martine Cherbonnel-Pansart, Claire Martenot, Rachel Busson, Angelina Orosco, Katell Louboutin, Carole Guillemoto, Yannick Blanchard, Alice Herteau, Anne Bernadou, Christine Castor, Laurent Filleul, and Karim Tararbit for aiding in the avian influenza diagnostic analyses and further investigations.

About the Author

Mr. Briand is a scientist at the National Reference Laboratory for avian influenza and Newcastle disease in France. His research interests focus on phylogeny, virology, and molecular epidemiology, especially for avian influenza and Newcastle disease viruses.

References

1. Gabriel G, Czudai-Matwich V, Klenk HD. Adaptive mutations in the H5N1 polymerase complex. Virus Res. 2013;178:53–62. https://doi.org/10.1016/j.virusres.2013.05.010
2. Hussain S, Turnbull ML, Pinto RM, McCauley JW, Engelhardt OG, Digard P. Segment 2 from influenza A(H1N1) 2009 pandemic viruses confers temperature-sensitive haemagglutinin yield on candidate vaccine virus growth in eggs that can be epistatically complemented by PB2 701D. J Gen Virol. 2019;100:1079–92. https://doi.org/10.1099/jgv.0.001279
3. Bordes L, Vreman S, Heutink R, Roose M, Venema S, Pritz-Verschuren SBE, et al. Highly pathogenic avian influenza H5N1 virus infections in wild red foxes (*Vulpes vulpes*) show neurotropism and adaptive virus mutations. Microbiol Spectr. 2023;11:e0286722. https://doi.org/10.1128/spectrum.02867-22
4. Conenello GM, Tisoncik JR, Rosenzweig E, Varga ZT, Palese P, Katze MG. A single N66S mutation in the PB1-F2 protein of influenza A virus increases virulence by inhibiting the early interferon response in vivo. J Virol. 2011;85:652–62. https://doi.org/10.1128/JVI.01987-10
5. US Department of Agriculture Animal and Plant Health Inspection Service. 2022–2023 detections of highly pathogenic avian influenza in mammals [cited 2023 Jan 4]. https://www.aphis.usda.gov/aphis/ourfocus/animalhealth/animal-disease-information/avian/avian-influenza/hpai-2022/2022-hpai-mammals
6. Adlhoch C, Fusaro A, Gonzales JL, Kuiken T, Marangon S, Niqueux É, et al.; European Food Safety Authoriy, European Centre for Disease Prevention and Control, European Union Reference Laboratory for Avian Influenza. Avian influenza overview September–December 2022. EFSA J. 2023;21:e07786. PubMed https://doi.org/10.2903/j.efsa.2023.7786
7. Agüero M, Monne I, Sánchez A, Zecchin B, Fusaro A, Ruano MJ, et al. Highly pathogenic avian influenza A(H5N1) virus infection in farmed minks, Spain, October 2022. Euro Surveill. 2023;28:2300001. https://doi.org/10.2807/1560-7917.ES.2023.28.3.2300001
8. Frymus T, Belák S, Egberink H, Hofmann-Lehmann R, Marsilio F, Addie DD, et al. Influenza virus infections in cats. Viruses. 2021;13:1435. https://doi.org/10.3390/v13081435
9. Haut Conseil de la Santé Publique. Avis relatif à la prévention de la transmission à l'homme des virus influenza porcins et aviaires. 2021 [cited 2023 Jan 4]. https://www.hcsp.fr/Explore.cgi/avisrapportsdomaine?clefr=1142

Address for correspondence: François-Xavier Briand, Anses, Laboratoire de Ploufragan-Plouzané-Niort, Zoopôle-Les Croix, BP 53, 22440 Ploufragan, France; email: francois-xavier.briand@anses.fr

Case Report of Leprosy in Central Florida, USA, 2022

Aashni Bhukhan, Charles Dunn, Rajiv Nathoo

Author affiliation: Kansas City University–Graduate Medical Education/Advanced Dermatology and Cosmetic Surgery Consortium, Orlando, Florida, USA

DOI: http://doi.org/10.3201/eid2908.220367

Florida, USA, has witnessed an increased incidence of leprosy cases lacking traditional risk factors. Those trends, in addition to decreasing diagnoses in foreign-born persons, contribute to rising evidence that leprosy has become endemic in the southeastern United States. Travel to Florida should be considered when conducting leprosy contact tracing in any state.

Leprosy, or Hansen disease, is a chronic infectious disease caused by the acid-fast rod *Mycobacterium leprae*. Leprosy primarily affects the skin and peripheral nervous system, and disease course is largely dependent on individual susceptibility to *M. leprae* (*1*). Leprosy has been historically uncommon in the United States; incidence peaked around 1983, and a drastic

reduction in the annual number of documented cases occurred from the 1980s through 2000 (*2*). However, since then, reports demonstrate a gradual increase in the incidence of leprosy in the United States. The number of reported cases has more than doubled in the southeastern states over the last decade (*2*). According to the National Hansen's Disease Program, 159 new cases were reported in the United States in 2020; Florida was among the top reporting states (*2*).

Central Florida, in particular, accounted for 81% of cases reported in Florida and almost one fifth of nationally reported cases (*3*). Whereas leprosy in the United States previously affected persons who had immigrated from leprosy-endemic areas, ≈34% of new case-patients during 2015–2020 appeared to have locally acquired the disease (*4*). Several cases in central Florida demonstrate no clear evidence of zoonotic exposure or traditionally known risk factors. We report a case of lepromatous leprosy in central Florida in a man without risk factors for known transmission routes. We also review the mounting epidemiologic evidence supporting leprosy as an endemic process in the southeastern United States.

A 54-year-old man sought treatment at a dermatology clinic for a painful and progressive erythematous rash (Figure). The lesions began on his distal extensor extremities and progressed to involve his trunk and face. He denied any domestic or foreign travel, exposure to armadillos, prolonged contact with immigrants from leprosy-endemic countries, or connections with someone known to have leprosy. He has resided in central Florida his entire life, works in landscaping, and spends long periods of time outdoors. Biopsies of multiple sites demonstrated a diffuse dermal infiltrate composed of disorganized aggregates of foamy histiocytes and lymphocytes. Fite stains revealed acid-fast bacilli within histiocytes and cutaneous nerve twigs, a pathognomonic finding of leprosy. He was referred to an infectious disease specialist who, under the direction of the National Hansen's Disease Program, prescribed triple therapy with dapsone, rifampin, and clofazimine.

Transmission of leprosy has not been fully elucidated. Prolonged person-to-person contact through respiratory droplets is the most widely recognized route of transmission (*1*). A high percentage of unrelated leprosy cases in the southern United States were found to carry the same unique strain of *M. leprae* as nine-banded armadillos in the region, suggesting a

Figure. Lepromatous leprosy in a 54-year-old man in central Florida, USA, 2022. A, B) Leonine facies with waxy yellow papules. C) Violaceous nonblanching macules coalescing into patches along dorsum of feet bilaterally. D, E) Erythematous papules coalescing into plaques along extensor aspects of upper and lower extremities bilaterally. Plaques notably demonstrated a moderate degree of dysesthesia.

strong likelihood of zoonotic transmission (*4*). A recent systematic review analyzing studies conducted during 1945–2019 supports an increasing role of anthroponotic and zoonotic transmission of leprosy (*5*). However, Rendini et al. demonstrated that many cases reported in eastern United States, including Georgia and central Florida, lacked zoonotic exposure or recent residence outside of the United States (*6*).

Given those reports, there is some support for the theory that international migration of persons with leprosy is a potential source of autochthonous transmission. Reports from Spain linked an increase in migration from other countries to an increase in autochthonous leprosy (*7*). The number of international migrants in North America increased from 27.6 million persons in 1990 to 58.7 million in 2020 (*8*), so a link to migration may account for the increase in incidence of leprosy in historically nonendemic areas. Further, reports from the Centers for Disease Control and Prevention show that, although the incidence of leprosy has been increasing, the rates of new diagnoses in persons born outside of the United States has been declining since 2002 (Appendix Figure, https://wwwnc.cdc.gov/EID/article/29/8/22-0367-App1.pdf) (*9*). This information suggests that leprosy has become an endemic disease process in Florida, warranting further research into other methods of autochthonous transmission.

Leprosy is a reportable condition in the state of Florida and is monitored primarily through passive surveillance. According to the Florida Department of Health, practitioners are required to report leprosy in Florida by the next business day (*10*). Contact tracing is critical to identifying sources and reducing transmission. In our case, contact tracing was done by the National Hansen's Disease Program and revealed no associated risk factors, including travel, zoonotic exposure, occupational association, or personal contacts. The absence of traditional risk factors in many recent cases of leprosy in Florida, coupled with the high proportion of residents, like our patient, who spend a great deal of time outdoors, supports the investigation into environmental reservoirs as a potential source of transmission.

In summary, our case adds to the growing body of literature suggesting that central Florida represents an endemic location for leprosy. Travel to this area, even in the absence of other risk factors, should prompt consideration of leprosy in the appropriate clinical context. By increasing local physician efforts to report incidence and supporting further research to assess routes of transmission, a congruent effort can be made to identify and reduce spread of the disease.

The patient described in the case report reviewed the text and photographs in the report and gave written consent to publish them. A copy of the consent form is on file with the authors. This report was deemed exempt from Institutional Review Board approval by Kansas City University.

About the Author

Dr. Bhukhan is an upcoming transitional year resident at the University of Central Florida/HCA Osceola Hospital and upon completion will join the Kansas City University–Graduate Medical Education/Advanced Dermatology and Cosmetic Surgery Dermatology Residency program in Orlando. Her primary research interests include dermatology, infectious disease, and global health.

References

1. Fischer M. Leprosy—an overview of clinical features, diagnosis, and treatment. J Dtsch Dermatol Ges. 2017;15:801–27. https://doi.org/10.1111/ddg.13301
2. US Department of Health and Human Services Health Resources & Services Administration. National Hansen's Disease (Leprosy) Program [cited 2022 May 19]. https://www.hrsa.gov/hansens-disease
3. Florida Department of Health. Hansen's disease (leprosy). FLHealth CHARTS. 2019 [cited 2022 May 19]. https://www.flhealthcharts.gov/ChartsDashboards/rdPage.aspx?rdReport=NonVitalIndNoGrpCounts.Dataviewer&cid=174
4. Truman RW, Singh P, Sharma R, Busso P, Rougemont J, Paniz-Mondolfi A, et al. Probable zoonotic leprosy in the southern United States. N Engl J Med. 2011;364:1626–33. https://doi.org/10.1056/NEJMoa1010536
5. Ploemacher T, Faber WR, Menke H, Rutten V, Pieters T. Reservoirs and transmission routes of leprosy; A systematic review. PLoS Negl Trop Dis. 2020;14:e0008276. https://doi.org/10.1371/journal.pntd.0008276
6. Rendini T, Levis W. Autochthonous leprosy without armadillo exposure, Eastern United States. Emerg Infect Dis. 2017;23:1928. https://doi.org/10.3201/eid2311.171145
7. Ramos JM, Romero D, Belinchón I. Epidemiology of leprosy in Spain: the role of the international migration. PLoS Negl Trop Dis. 2016;10:e0004321. https://doi.org/10.1371/journal.pntd.0004321
8. International Organization for Migration. World Migration Report 2020 [cited 2022 May 19]. https://publications.iom.int/system/files/pdf/wmr_2020.pdf
9. Nolen L, Haberling D, Scollard D, Truman R, Rodriguez-Lainz A, Blum L, et al.; Centers for Disease Control and Prevention (CDC). Incidence of Hansen's disease—United States, 1994-2011. MMWR Morb Mortal Wkly Rep. 2014;63:969–72.
10. Florida Department of Health. Reportable disease/conditions in Florida. 2021 [cited 2022 May 19]. https://www.floridahealth.gov/diseases-and-conditions/disease-reporting-and-management/_documents/reportable-diseases-list-practitioners.pdf

Address for correspondence: Charles Dunn, Kansas City University-GME/ADCS Consortium, 151 Southhall Ln, Ste 300, Maitland, FL 32751, USA; email: charles.luck.dunn@gmail.com

Advanced Age and Increased Risk for Severe Outcomes of Dengue Infection, Taiwan, 2014–2015

Nicole Huang, Yi Jung Shen, Yiing Jenq Chou, Theodore F. Tsai, Chia En Lien[1]

Author affiliations: National Yang Ming Chiao Tung University, Taipei, Taiwan (N. Huang, Y.J. Chou); Boston University, Boston, Massachusetts, USA (Y.J. Shen); Office of the Deputy Superintendent, National Yang Ming Chiao Tung University Hospital, Yilan County, Taiwan (Y.J. Chou); Takeda Vaccines, Cambridge, Massachusetts, USA (T.F. Tsai, C. En Lien)

DOI: http://doi.org/10.3201/eid2908.230014

Dengue, a mosquitoborne flavivirus infection, is increasingly a disease of older adults who are more likely to have chronic diseases that confer risk for severe outcomes of dengue infection. In a population-based study in Taiwan, adjusted risks for dengue-related hospitalization, intensive care unit admission, and death increased progressively with age.

Dengue is an *Aedes aegypti* mosquito–borne flavivirus infection; a secular trend for dengue is a shift in the age of case-patients and deaths from children to adults and older adults (*1*,*2*). We report a population-based study of age-specific dengue risks for hospitalization, intensive care unit (ICU) admission, and death in Taiwan.

Dengue is not endemic in Taiwan but is introduced frequently; population immunity is low. In 2014–2015, large outbreaks led to 51,344 cases confirmed by the Taiwan Centers for Disease Control (Taiwan CDC) (*3*). In those years, suspected cases were tested at the Taiwan CDC by reverse transcription PCR, IgM/IgG, and paired IgM/IgG for seroconversion to confirm dengue infection; point-of-care NS1 antigen detection assays were introduced in September 2015. The database of reported cases was linked to the national administrative health database to report patient outcomes and to establish age-specific rates. Because reporting is required for reimbursement, the National Health Insurance Research Database provides near-complete ascertainment of all medical encounters for >99% of the island's population. We adjusted for sex, socioeconomic status, and presence of underlying conditions (*2*). We did not review individual patients' medical records in this linked-database analysis.

Age-specific attack rates during the outbreak were similar across age groups (Appendix Figure, https://wwwnc.cdc.gov/EID/article/29/8/23-0014-App1.pdf), consistent with low population immunity rates. Lower attack rates in children <10 years of age, in whom infections are more likely to be asymptomatic or mildly symptomatic, likely reflected a lower frequency of medical consultation and laboratory confirmation. We examined records of 51,344 case-patients, 15,847 of whom were hospitalized, in an analysis of healthcare utilization and deaths. Adjusted rates for hospitalization, ICU admission, and death within 30 days of confirmation of dengue illness increased sharply with advancing age, compared with rates among young adults (Figure). In contrast, case rates by age group were relatively flat.

The epidemiologic shift of dengue to adults and older adults has increased recognition that advanced age is a risk factor for severe and fatal outcome after dengue infection (*2*,*3*), adding dengue to the list of other flavivirus infections for which advanced age is well established to be a cardinal risk factor for severe disease. Age-specific curves by age for clinically severe dengue, seasonal influenza, and COVID-19 are similar; however, mortality rates and case-fatality ratios for dengue are considerably lower (*4*,*5*). Case-fatality ratios for dengue in Pan American Health Organization countries are <0.05%; in southern Brazil, mortality rates for dengue are 10-fold to 100-fold lower than for seasonal influenza (*4*–*6*).

Adults and older adults comprise an increasing proportion of dengue cases in many countries, even as those populations reach ages where the prevalence of chronic diseases increases (*7*). Because chronic diseases contribute to more severe dengue outcomes, the overall effects of dengue attributed to those underlying conditions are increasing in turn. In adults, underlying diseases, specifically diabetes, chronic renal disease, and heart disease, are associated with higher relative odds for progression to severe disease than secondary infection (*8*). However, in administrative database studies in Mexico, Brazil, and Colombia, comorbidities were shown to confer a higher risk for death in hospitalized patients across the age spectrum (*8*,*9*). Our understanding of pathophysiological mechanisms associated with increased dengue severity in patients with comorbidities and advanced age is limited, as it is for patients with influenza and COVID-19.

[1]Current affiliate: Medigen Vaccines Biologics Corporation, Taipei, Taiwan.

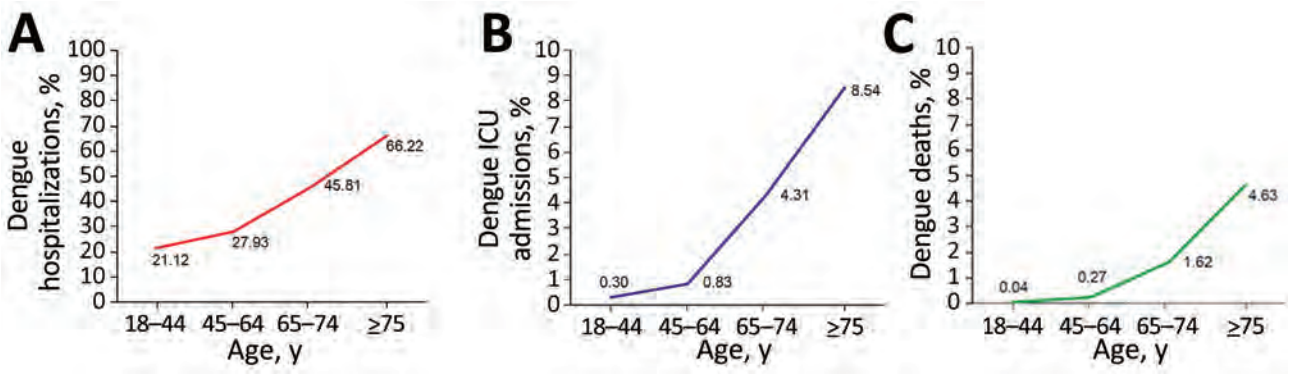

Figure. Dengue outcome event rates by age group in Taiwan. A) Hospitalizations; B) ICU admissions; C) deaths. ICU, intensive care unit.

Since 1990, dengue cases and deaths have increased disproportionately among adults >50 years of age compared with children <15 years of age, in whom the number and proportion of cases and, especially, deaths, have declined (*1*). As of May 2023, Asia accounts for most global dengue cases; it is also the fastest-aging region, containing more than half of the world's population ≥65 years of age. Projections suggest that 10% of the total global population by 2060 will be persons ≥65 years of age living in Asia (*10*). Ongoing demographic trends and the 2 risk factors, advanced age and chronic disease, for developing severe to fatal dengue underscore the need to improve protection from dengue for older adults and persons with chronic diseases in all regions in which dengue is endemic, particularly in Asia.

Takeda Vaccines provided funding as a collaborative research project with National Yang Ming Chiao Tung University. Medical writing support was provided by Envision Pharma Group.

About the Author

Dr. Huang is a professor at the Institute of Hospital and Health Care Administration of the College of Medicine at National Yang Ming Chiao Tung University, Taipei. Dr. Huang's primary research interest has been assessing how individual, provider, and system characteristics may influence provision and quality of care for communicable and noncommunicable diseases.

References

1. Yang XR, Quam MBM, Zhang T, Sang S. Global burden for dengue and the evolving pattern in the past 30 years. J Travel Medicine. 2021;28:taab146. https://doi.org/10.1093/jtm/taab146
2. Huang AT, Takahashi S, Salje H, Wang L, Garcia-Carreras B, Anderson K, et al. Assessing the role of multiple mechanisms increasing the age of dengue cases in Thailand. Proc Natl Acad Sci U S A. 2022;119:e2115790119. https://doi.org/10.1073/pnas.2115790119
3. Lien CE, Chou YJ, Shen YJ, Tsai T, Huang N. A population-based cohort study on chronic comorbidity risk factors for adverse dengue outcomes. Am J Trop Med Hyg. 2021;105:1544–51. https://doi.org/10.4269/ajtmh.21-0716
4. Santana LMR, Santos-Baquero O, Yurika-Maeda A, Silva-Nogueira J. Chiaravalloti-Neto F. Spatio-temporal dynamics of dengue-related deaths and associated factors. Rev Inst Med Trop S Paulo. 2022;64:e30. http://doi.org/10.1590/S1678-9946202264030
5. Freitas ARR, Donalisio MR. Excess of mortality in adults and elderly and circulation of subtypes of influenza virus in southern Brazil. Front Immunol. 2018;8:1903. https://doi.org/10.3389/fimmu.2017.01903
6. Pan American Health Organization. Dengue case fatality rate percentage for subregions of the Americas. 2023 [cited May 12, 2023]. https://www3.paho.org/data/index.php/en/mnu-topics/indicadores-dengue-en/dengue-regional-en/317-reg-dengue-lethality-en.html
7. Bennett JE, Stevens GA, Mathers CD, Bonita R, Rehm J, Kruk ME, et al. NCD Countdown 2030: worldwide trends in non-communicable disease mortality and progress towards Sustainable Development Goal target 3.4. Lancet. 2018;392:1072–88. https://doi.org/10.1016/S0140-6736(18)31992-5
8. Sangkaew S, Ming D, Boonyasiri A, Honeyford K, Kalayanarooj S, Yacoub S, et al. Risk predictors of progression to severe disease during the febrile phase of dengue: a systematic review and meta-analysis. Lancet Infect Dis. 2021;21:1014–26. https://doi.org/10.1016/S1473-3099(20)30601-0
9. Macias AE, Werneck GL, Castro R, Mascareñas C, Coudeville L, Morley D, et al. Mortality among hospitalized dengue patients with comorbidities in Mexico, Brazil, and Colombia. Am J Trop Med Hyg. 2021;105:102–9. https://doi.org/10.4269/ajtmh.20-1163
10. He W, Goodkind D, Kowal P, Almasarweh IS, Giang TL, Islan MM, et al. U.S. Census Bureau, International Population Reports, P95/22–1. Asia aging: demographic, economic, and health transitions. Washington (DC): US Government Publishing Office; June 2022.

Address for correspondence; Theodore F. Tsai, Takeda Vaccines, 40 Landsdowne St, Cambridge, MA 02139 USA; email: Ted.tsai@takeda.com

Fatal Meningitis from Shiga Toxin–Producing *Escherichia coli* in 2 Full-Term Neonates, France

Guillaume Geslain, Aurélie Cointe, Philippe Bidet, Céline Courroux, Soumeth Abasse, Patricia Mariani, Stéphane Bonacorsi

Author affiliations: Robert Debré University Hospital Assistance Publique-Hôpitaux de Paris, Paris, France (G. Geslain, A. Cointe, P. Bidet, C. Courroux, P. Mariani, S. Bonacorsi); Université Paris Cité INSERM, Paris (G. Geslain, A. Cointe, P. Bidet, S. Bonacorsi); Mayotte Hospital, Mamoudzou, Mayotte Island, France (S. Abasse)

DOI: https://doi.org/10.3201/eid2908.230169

We report fatal meningitis in 2 neonates in France caused by Shiga toxin 1–producing *Escherichia coli*. Virulence factors capsular K1 antigen and salmochelin were present in both strains, potentially representing a new hybrid pathotype. Clinicians should remain aware of emerging pathotypes and design therapeutic strategies for neonatal *E. coli* infections.

Escherichia coli can acquire virulence factors associated with increased pathogenicity, causing intestinal or extraintestinal infections. Shiga toxin (Stx)–producing *E. coli* (STEC) cause intestinal infections and hemolytic uremic syndrome (HUS). *E. coli* virulence factors K1 antigen and salmochelin are associated with neonatal *E. coli* meningitis (*1*). Hybrid pathotypes have been described, such as Stx-producing O80:H2, which causes HUS and bacteremia because of extraintestinal virulence–associated plasmid pS88 (*2*). We report 2 cases of full-term neonates who died of meningitis caused by STEC serotypes O117:H7 and O156:H7.

Patient 1, an 8-day-old full-term boy born in the Paris, France, area, was seen at the emergency department because of a 48-hour history of abdominal pain and rectorrhagia without fever and drowsiness since that morning. Septic shock with colitis developed rapidly, requiring admission to the pediatric intensive care unit (PICU). Hemolysis was not observed, and initial acute kidney failure resolved promptly. Blood culture results were positive for *E. coli* K1, urine culture results were negative, and 3 stool cultures yielded STEC. Cerebral magnetic resonance imaging on PICU day 7 showed severe diffuse lesions indicating meningoencephalitis and subdural empyema. Cerebrospinal fluid (CSF) obtained by lumbar puncture 2 days later contained 2,270 leukocytes/mm^3, showed negative Gram stain and culture, and was PCR-positive for K1 and β-glucuronidase genes, indicating *E. coli* meningitis. Prompted by clinical and laboratory features potentially associated with HUS, PCR on blood and CSF DNA were performed and identified *stx1*. The patient died on day 28.

Table. Genes encoding confirmed or putative virulence factors found in Shiga toxin–producing *Escherichia coli* ST504 strains that caused fatal meningitis in 2 full-term neonates, France*

Gene	Gene function	*E. coli* O117:H7	*E. coli* O156:H7
iucC	Aerobactin biosynthesis	Positive	Negative
iutA	Aerobactin receptor	Positive	Negative
fyuA	Yersiniabactin receptor	Positive	Positive
irp2	Yersiniabactin biosynthesis	Positive	Positive
iroN	Salmochelin receptor	Positive	Positive
iroD	Salmochelin biosynthesis	Positive	Positive
chuA	Hemin uptake	Negative	Positive
cvaA	Colicin V	Negative	Positive
iss	Increased serum survival protein	Positive	Negative
sitA	Iron transport protein	Positive	Positive
ibeA	Invasin	Negative	Positive
vat	Vacuolating autotransporter toxin	Negative	Positive
ihA-like	Putative Iha-like adhesin	Positive	Positive
mchB	Microcin	Positive	Positive
mchC	Microcin	Negative	Positive
mchF	Microcin	Negative	Positive
mcmA	Microcin	Negative	Positive
gad	Glutamate decarboxylase	Positive	Positive
iha	Adherence protein	Positive	Positive
capU	Hexosyltransferase homologue protein	Positive	Positive
sigA	Serine protease autotransporter	Positive	Positive
stx1A-a	Shiga toxin 1 variant a subunit A	Positive	Positive
stx1B-a	Shiga toxin 1 variant a subunit B	Positive	Positive
kpsF	Polysialic acid group 2 capsule expression protein	Positive	Positive
kpsD	Translocation of capsule of groups 2 and 3	Positive	Positive
neuC	K1 capsular antigen	Positive	Positive

**E. coli* serotypes were O117:H7 (case 1, 8-day-old boy) and O156:H7 (case 2, 4-day-old boy). ST, sequence type.

Patient 2, a full-term boy born in an overseas department of France, was transferred to a PICU at 4 days of age because of fever, drowsiness, and failure to feed. Septic shock without colitis developed rapidly, without hemolysis or initial thrombocytopenia. On PICU day 4, blood culture results were positive and urine culture results negative for *E. coli*; CSF contained 900 leukocytes/mm^3 and showed *E. coli* growth in culture; Stx was not initially evaluated. The patient died on PICU day 9.

Whole-genome sequencing of blood and stool isolates (patient 1) and CSF isolate (patient 2) indicated the *E. coli* strains belonged to sequence type (ST)504 and phylogroup B2; serotypes were O117:H7 for patient 1 and O156:H7 for patient 2. Both strains harbored the gene encoding Stx1a protein but not *eae* (intimin) or *ehxA* (enterohemolysin) genes (*3*,*4*). Genetic determinants for extraintestinal virulence factors K1 capsular antigen, yersiniabactin, and salmochelin were present in both strains and the aerobactin operon in the O117:H7 strain. Screening for confirmed or putative virulence factors as previously described (*5*) (Table) showed neither strain harbored an pS88-like plasmid (*6*).

Both strains differed substantially from *E. coli* K1 strains usually reported as causes of meningitis. K1 strains mainly belong to the ST95 complex (*7*) and most common serogroups are O18, O1, O7, O83, and O45 S88 (*6*,*8*). STEC O117:H7 ST504 strains were described in 2005 in 20 adults with persistent traveler's diarrhea (*3*). Those strains and STEC strains described in another study of traveler's diarrhea were atypical because they did not express lysine decarboxylase, β-galactosidase, intimin, or enterohemolysin (*4*). No invasive infections were reported before the 2 cases we describe, although some strains expressed extraintestinal virulence factors. However, because PCR for Stx is not routinely performed on neonatal invasive *E. coli* strains, STEC O117:H7 might be underestimated. Whole-genome sequencing of neonatal *E. coli* meningitis strains would help determine the role of STEC in fatal neonatal meningitis. In our patients, simultaneous presence of K1 antigen and salmochelin might explain isolate invasiveness (*1*). Moreover, STEC O156:H7 harbored the invasin IbeA, which promotes blood–brain barrier translocation.

When we analyzed the EnteroBase database (*9*) in late 2022, we identified only 4 O156:H7 and 39 O117:H7 strains distributed among 4 STs (ST504, n = 17; ST5292, n = 18; ST6880, n = 3; and ST9996, n = 1), all belonging to the ST504 complex. BLAST (https://blast.ncbi.nlm.nih.gov) analysis of STEC O117:H7 ST504 complex sequences from Enterobase consistently identified extraintestinal virulence factors yersinibactin and aerobactin (*5*); salmochelin (12 of 39 sequences) and K1 antigen (20 of 39 sequences) were inconsistently present. Since routine STEC sequencing began in 2017 in France, 3 other STEC O117:H7 ST504 complex strains have been identified (2 from patients with nonhemorrhagic diarrhea and 1 from an asymptomatic carrier).

Neither neonate described in this report had typical HUS, possibly because the *E. coli* strains lacked genes encoding Stx2, intimin, and enterohemolysin. However, Stx might have promoted intestinal translocation of the bacteria. Furthermore, antimicrobial drug therapy might have induced intracerebral Stx production, thereby contributing to fatal outcomes (*10*).

ST504 complex STEC strains exhibit only moderate intestinal virulence. However, we show that those strains can translocate into blood and CSF in neonates, especially if they produce K1 antigen and salmochelin. ST504-complex STEC expressing K1 antigen and salmochelin might be new hybrid pathotypes in neonates, even for those born at full term, with both extraintestinal pathogenic and neonatal meningitis virulence factors. Clinicians should remain aware of emerging pathotypes and new preventive and therapeutic strategies for *E. coli* infections in neonates.

About the Author

Dr. Geslain is a pediatrician in the pediatric intensive care unit at Robert Debré University Hospital in Paris and a PhD student in the infection, antimicrobials, modelling, evolution laboratory at the Université Paris Cité INSERM. His research interests focus on infectious diseases.

References

1. Leying H, Suerbaum S, Kroll HP, Stahl D, Opferkuch W. The capsular polysaccharide is a major determinant of serum resistance in K-1–positive blood culture isolates of *Escherichia coli*. Infect Immun. 1990;58:222–7. https://doi.org/10.1128/iai.58.1.222-227.1990
2. Mariani-Kurkdjian P, Lemaître C, Bidet P, Perez D, Boggini L, Kwon T, et al. Haemolytic-uraemic syndrome with bacteraemia caused by a new hybrid *Escherichia coli* pathotype. New Microbes New Infect. 2014;2:127–31. https://doi.org/10.1002/nmi2.49
3. Olesen B, Jensen C, Olsen K, Fussing V, Gerner-Smidt P, Scheutz F. VTEC O117:K1:H7. A new clonal group of *E. coli* associated with persistent diarrhoea in Danish travellers. Scand J Infect Dis. 2005;37:288–94. https://doi.org/10.1080/00365540410021090
4. Dallman T, Cross L, Bishop C, Perry N, Olesen B, Grant KA, et al. Whole-genome sequencing of an unusual serotype of Shiga toxin–producing *Escherichia coli*. Emerg Infect Dis. 2013;19:1302–4. https://doi.org/10.3201/eid1908.130016
5. Bidet P, Birgy A, Ouldali N, Béchet S, Levy C, Madhi F, et al. Comparative genomic analysis of ESBL-producing

Escherichia coli from faecal carriage and febrile urinary tract infection in children: a prospective multicentre study. JAC Antimicrob Resist. 2022;4:dlac056. https://doi.org/10.1093/jacamr/dlac056
6. Peigne C, Bidet P, Mahjoub-Messai F, Plainvert C, Barbe V, Médigue C, et al. The plasmid of *Escherichia coli* strain S88 (O45:K1:H7) that causes neonatal meningitis is closely related to avian pathogenic *E. coli* plasmids and is associated with high-level bacteremia in a neonatal rat meningitis model. Infect Immun. 2009;77:2272–84. https://doi.org/10.1128/IAI.01333-08
7. Basmaci R, Bonacorsi S, Bidet P, Biran V, Aujard Y, Bingen E, et al. *Escherichia coli* meningitis features in 325 children from 2001 to 2013 in France. Clin Infect Dis. 2015;61:779–86. https://doi.org/10.1093/cid/civ367
8. Bonacorsi S, Clermont O, Houdouin V, Cordevant C, Brahimi N, Marecat A, et al. Molecular analysis and experimental virulence of French and North American *Escherichia coli* neonatal meningitis isolates: identification of a new virulent clone. J Infect Dis. 2003;187:1895–906. https://doi.org/10.1086/375347
9. Zhou Z, Alikhan NF, Mohamed K, Fan Y, Achtman M; Agama Study Group. The EnteroBase user's guide, with case studies on *Salmonella* transmissions, *Yersinia pestis* phylogeny, and *Escherichia* core genomic diversity. Genome Res. 2020;30:138–52. https://doi.org/10.1101/gr.251678.119
10. Cointe A, Birgy A, Bridier-Nahmias A, Mariani-Kurkdjian P, Walewski V, Lévy C, et al. *Escherichia coli* O80 hybrid pathotype strains producing Shiga toxin and ESBL: molecular characterization and potential therapeutic options. J Antimicrob Chemother. 2020;75:537–42. https://doi.org/10.1093/jac/dkz484

Address for correspondence: Guillaume Geslain, Pediatric Intensive Care Unit, Robert Debré Hospital, AP-HP, 48 Boulevard Sérurier, 75019 Paris, France; email: guillaume.geslain@aphp.fr

Rio Negro Virus Infection, Bolivia, 2021

Roxana Loayza Mafayle,[1] Maria E. Morales-Betoulle,[1] Shannon Whitmer,[1] Caitlin Cossaboom,[1] Jimmy Revollo, Nelly Mendoza Loayza, Hilary Aguilera Méndez, Joel Alejandro Chuquimia Valdez, Freddy Armijo Subieta, Maya Xochitl Espinoza Morales, María Valeria Canedo Sánchez, Miriam Eugenia Romero Romero, Aaron C. Brault, Holly R. Hugues, Jairo Mendez-Rico, Jason H. Malenfant, Trevor Shoemaker, John D. Klena, Joel M. Montgomery,[2] Jhonatan David Marquina Salas[2]

Author affiliations: Centro Nacional de Enfermedades Tropicales, Santa Cruz de la Sierra, Bolivia (R. Loayza Mafayle, J. Revollo, N. Mendoza Loayza, H. Aguilera Méndez, J.A. Chuquimia Valdez, J.D. Marquina Salas); Centers for Disease Control and Prevention, Atlanta, Georgia, USA (M.E. Morales-Betoulle, S. Whitmer, C. Cossaboom, J.H. Malenfant, T. Shoemaker, J.D. Klena, J.M. Montgomery); Unidad de Epidemiología, Ministerio de Salud, La Paz, Bolivia (F. Armijo Subieta); Unidad de Gestión de Riesgos en Salud Ambiental, Emergencias y Desastres Ministerio de Salud, La Paz (M.X. Espinoza Morales); Bolivia Ministerio de Salud Programa Salud Familiar Comunitaria Intercultural, Padcaya, Bolivia (M.V. Canedo Sánchez, M.E. Romero Romero); Centers for Disease Control and Prevention, Fort Collins, Colorado, USA (A.C. Brault, H.R. Hugues); Pan-American Health Organization, Washington, DC, USA (J. Mendez-Rico)

DOI: https://doi.org/10.3201/eid2908.221885

In May 2021, an agricultural worker originally from Trementinal, Argentina, sought treatment for febrile illness in Tarija, Bolivia, where he resided at the time of illness onset. The patient tested negative for hantavirus RNA, but next-generation sequencing of a serum sample yielded a complete genome for Rio Negro virus.

Rio Negro virus (RNV; family Togaviridae, genus *Alphavirus*), a Venezuelan equine encephalitis virus (VEEV) antigenic subtype VI virus, was first reported in 1987 after being isolated from mosquitoes collected in Chaco, Argentina (*1*). The virus has since been isolated or molecularly detected in mosquitoes and rodents in Argentina and bats in Uruguay (*2*–*6*). Although RNV was serologically associated with an outbreak of undifferentiated febrile illness in Argentina, molecular evidence of RNV infection in humans is lacking (*4*,*7*,*8*). High RNV seroprevalence among horses in Uruguay suggests the virus likely circulates throughout the region (*9*). Dengue viruses 1–4 are leading causes of acute febrile illnesses in Latin America, but confirmatory testing is often not performed. Surveillance is also not routinely performed for other viral etiologies of acute febrile illnesses (e.g., arenaviruses, hantaviruses, other arboviruses). In regions of Bolivia where hantaviruses are known to circulate, a national surveillance program collects blood samples, along with clinical and epidemiologic information, including risk factors associated with hantavirus infection (e.g., agricultural work) from patients manifesting nonspecific signs and symptoms (e.g., fever, headache, nausea, myalgia, ar-

[1]These authors contributed equally to this article.

[2]These senior authors contributed equally to this article.

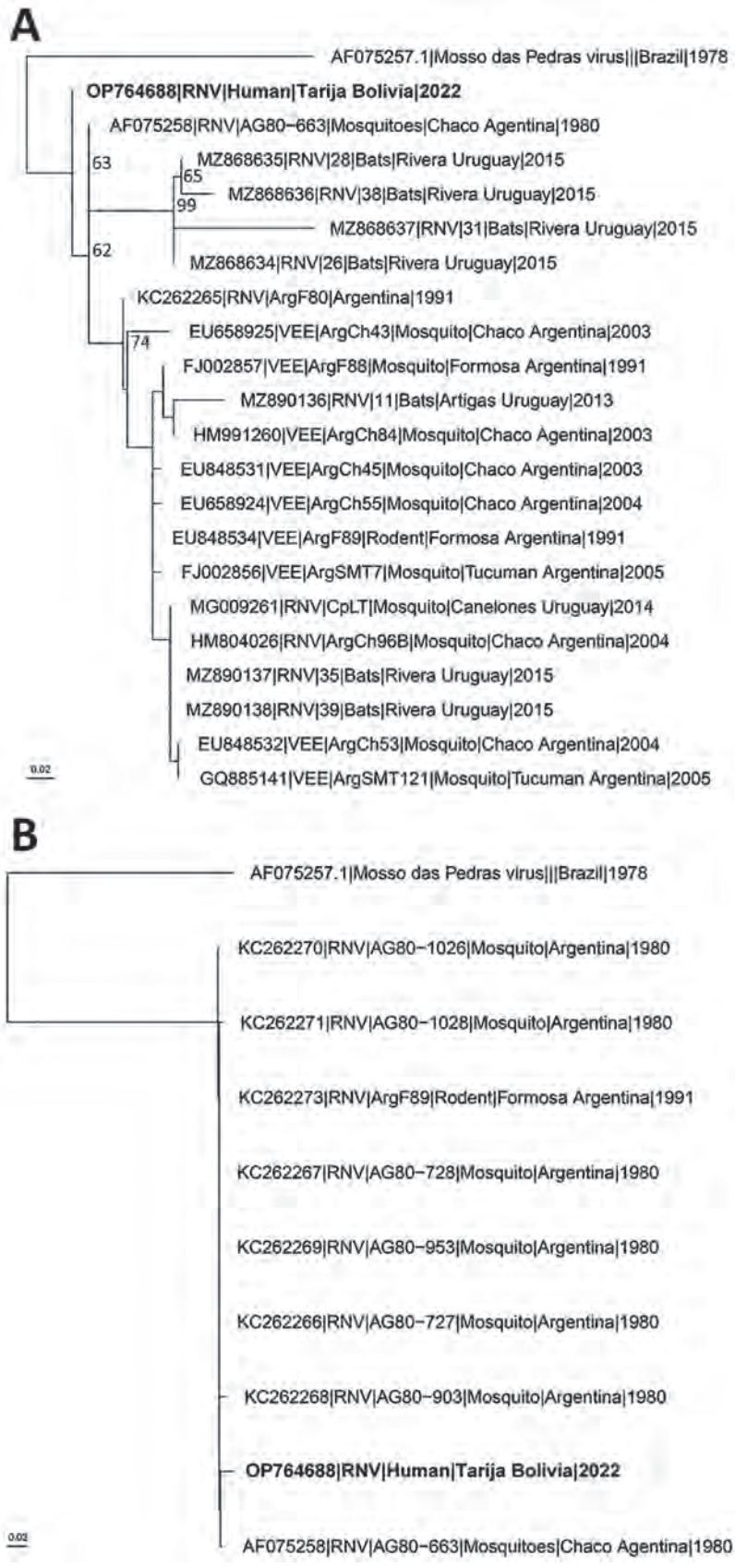

Figure. Inferred phylogenetic relationships of Rio Negro viruses collected from mosquitoes, bats, and rodents in South America and the human-derived RNV sequence described in this report from Tarija, Bolivia (bold text). A) Phylogenetic tree made with an alignment of partial nsP4 sequences of Rio Negro viruses. Mossa das Pedras virus is included as an outgroup. B) Phylogenetic tree made with an alignment of partial E3/GP2 sequences of Rio Negro viruses. Mossa das Pedras virus is included as an outgroup. GenBank accession numbers are provided. Scale bars indicate substitutions per site.

thralgia, shortness of breath) for hantavirus testing at the Centro Nacional de Enfermedades Tropicales (CENETROP) in Santa Cruz de la Sierra, Bolivia. After hantavirus testing, a subset of RNA specimens was sent to the US Centers for Disease Control and Prevention (CDC) for further characterization using next-generation sequencing (NGS). We report molecular evidence of human infection with RNV, characterized by NGS and genomic analysis.

A 21-year-old man, a migrant agricultural worker originally from Trementinal, Argentina, with no related medical history, sought treatment on May 31, 2021, in Padcaya Municipality, Tarija Department, Bolivia, where he resided at the time of illness onset (Appendix Figure, https://wwwnc.cdc.gov/EID/article/29/8/22-1885-App1.pdf). On arrival, he reported a 1-day history of fever, chills, headache, nausea, arthralgia, myalgia, thoracic pain, back pain, and hyperemia; his temperature at the time, 37.6°C, was the maximum during his hospitalization. Physical examination revealed bibasilar crackles but observations were otherwise unremarkable. He was admitted to hospital with suspected SARS-CoV-2 or hantavirus infection, but other infectious etiologies, such as dengue or a bacterial urinary tract infection, were also considered. The antimicrobial levofloxacin and corticosteroids dexamethasone and betamethasone were empirically prescribed. Initial clinical testing included complete blood count, basic metabolic panel, and urinalysis; all results were unremarkable. Results of a SARS-CoV-2 rapid test was negative. A blood sample was sent to CENETROP for hantavirus testing. The patient ultimately made a full recovery and was discharged after 5 days on June 5, 2021.

In December 2021, archived samples collected for hantavirus surveillance were inactivated in CENETROP's Biosafety Level 3 laboratory and tested for hantavirus antibodies and RNA using CDC ELISA and real-time reverse transcription PCR (RT-PCR) (Appendix). RNA from RT-PCR–positive and –negative samples was sent to CDC for NGS. The specimen collected from the patient was negative for hantavirus RNA. A near-complete genome (excluding 40 of >11K nt) was obtained using NGS and identified by genomic analysis as RNV (Figure 1), a result supported by alphavirus RT-PCR followed by sequencing. The RT-PCR amplicon had highest identity, 97.8% (441/451 nt), to GenBank RNV reference strain NC_038674, suggesting the amplicon was not a product of laboratory contamination. RNV was not identified in a subset of hantavirus RNA–positive (n = 7) and –negative (n = 4) specimens collected from the same area or in negative controls.

VEEV is a substantial human and animal pathogen considered a persistent zoonosis in Latin America; RNV is a VEEV subtype VI arbovirus, closely related to subtype I viruses, which have resulted in large-scale human outbreaks of >100,000 cases (*10*). RNV has been isolated from *Culex* spp. mosquitoes and rodents in Argentina (*2*–*5*). Evidence of RNV infection in humans has been limited to serologic studies (*4*,*7*,*8*). We report molecular evidence of human infection with RNV in a patient who sought treatment with signs and symptoms of a nonspecific febrile illness. No serum specimen from the patient was available for serologic testing for RNV. No other complete or nearly complete pathogen genomes (>50% coverage) were generated by de novo analysis in this patient sample, and RNV RNA was not detected in other tested specimens or the negative sequencing control.

Because the patient sought treatment in a rural area of Bolivia, follow-up has been challenging, and limited information is available on the patient's epidemiologic history. Additional information is lacking on the patient's travel history and potential exposures to mosquitoes, rodents, bats, and horses that could further characterize the potential distribution and risk factors for RNV infection in the region. The true burden of RNV as a cause of human disease in Bolivia and the region is unknown; however, because initial manifestation consists of nonspecific signs and symptoms, RNV infections could be overlooked or misdiagnosed. To bolster surveillance and diagnostic capacity for RNV and other emerging viruses, it is critical for healthcare sectors in Latin America to look beyond dengue and other common causes of acute febrile illnesses.

Acknowledgments

The authors thank Carson Telford of CDC's Viral Special Pathogens Branch (National Center for Emerging and Zoonotic Infectious Diseases, Division of High-Consequence Pathogens and Pathology) for supporting development of the Appendix Figure and Paulina Rosso Caisiri and Danitza Ordoñez, members of the patient's clinical care team, for providing clinical details on this case. We also thank Yersina Alba Flores Velasquez and Franz Rafael Zenteno Jurado for their support of this work.

This work was largely financed by the Bolivia Ministry of Health, Centro Nacional de Enfermedades Tropicales, and emerging infections funding from the US Centers for Disease Control and Prevention. The work was also supported in-kind by the Pan American Health Organization.

Conceptualization: R.L.M., M.M.B., S.M.W., C.M.C., J.R., N.M., J.M.R., T.S., J.D.K., J.M.M., J.M.S. Formal analysis: R.L.M., M.M.B., S.M.W., C.M.C., J.R., H.A.M., J.A.C.V., J. M. H.H., A.B. Investigation: R.L.M., M.M.B., S.M.W., C.M.C., J.R., N.M., J.M.R., J.M., N.F.A.S, M.X.E.M., T.S., J.D.K., J.M.M., J.D.M.S. Methodology: R.L.M., M.M.B., S.M.W., C.M.C, J.R., H.H., A.B. Patient care and clinical data collection: M.V.C.S., M.E.R.R. Visualization: S.M.W., C.M.C. Funding acquisition: J.D.M.S, N.M., N.F.A.S, M.X.E.M., J.M.R., T.S., J.D.K., J.M.M. Project administration: R.L.M., M.M.B., S.M.W., C.M.C., J.M.R., T.S., J.D.K., J.M.M., J.D.M.S. Supervision: N.M., J.M.R., T.S., J.D.K., J.M.M., J.D.M.S. Writing, original draft: M.M.B., S.M.W., C.M.C. Writing, review, and editing: R.L.M., S.M.W., M.M.B., C.M.C., J.R., J.M., A.B., H.H., T. S., J.D.K., J.M.M.

About the Author

Ms. Loayza Mafayle, a pharmaceutical biochemist and MSc in clinical microbiology, is head of the molecular biology laboratory at Centro Nacional de Enfermedades Tropicales in Santa Cruz de La Sierra, Bolivia. Her areas of expertise include laboratory surveillance of a variety of viruses affecting the health of Bolivian citizens, including arboviruses, hantavirus, New World arenavirus, influenza, SARS-CoV-2, and mpox.

References

1. Mitchell CJ, Monath TP, Sabattini MS, Cropp CB, Daffner JF, Calisher CH, et al. Arbovirus investigations in Argentina, 1977–1980. II. Arthropod collections and virus isolations from Argentine mosquitoes. Am J Trop Med Hyg. 1985;34:945–55. https://doi.org/10.4269/ajtmh.1985.34.945
2. Mitchell CJ, Monath TP, Sabattini MS, Daffner JF, Cropp CB, Calisher CH, et al. Arbovirus isolations from mosquitoes collected during and after the 1982–1983 epizootic of western equine encephalitis in Argentina. Am J Trop Med Hyg. 1987;36:107–13. https://doi.org/10.4269/ajtmh.1987.36.107
3. Pisano MB, Ré VE, Díaz LA, Farías A, Stein M, Sanchez-Seco MP, et al. Enzootic activity of pixuna and Rio Negro viruses (Venezuelan equine encephalitis complex) in a neotropical region of Argentina. Vector Borne Zoonotic Dis. 2010;10:199–201. https://doi.org/10.1089/vbz.2008.0156
4. Pisano MB, Spinsanti LI, Díaz LA, Farías AA, Almirón WR, Ré VE, et al. First detection of Rio Negro virus (Venezuelan equine encephalitis complex subtype VI) in Córdoba, Argentina. Mem Inst Oswaldo Cruz. 2012;107:125–8. https://doi.org/10.1590/S0074-02762012000100017
5. Contigiani MSCA, Spinsanti L, Díaz G. Biochemical and biological characterization of strains of the Venezuelan equine encephalitis complex virus (family Togaviridae) [in Spanish]. Anales de la Fundación Alberto Roemmers. 1999;12:119–23.
6. Moreira Marrero L, Botto Nuñez G, Frabasile S, Delfraro A. Alphavirus identification in neotropical bats. Viruses. 2022;14:269. https://doi.org/10.3390/v14020269
7. Contigiani MS BM, Cámara A et al. Presence of antibodies against subtype VI Venezuelan equine encephalitis virus in patients with acute febrile illness [in Spanish]. Rev Argent Microbiol. 1993;25:212–20.
8. Cámara A, Díaz G, Vega V, Basualdo M, Contigiani M. Seroprevalence of antibodies to Venezuelan equine encephalitis complex (subtypes IAB and VI) in humans from General Belgrano island, Formosa, Argentina. Rev Inst Med Trop São Paulo. 2003;45:201–4. https://doi.org/10.1590/S0036-46652003000400005
9. Burgueño A, Frabasile S, Díaz LA, Cabrera A, Pisano MB, Rivarola ME, et al. Genomic characterization and seroprevalence studies on alphaviruses in Uruguay. Am J Trop Med Hyg. 2018;98:1811–8. https://doi.org/10.4269/ajtmh.17-0980
10. Guzmán-Terán C, Calderón-Rangel A, Rodriguez-Morales A, Mattar S. Venezuelan equine encephalitis virus: the problem is not over for tropical America. Ann Clin Microbiol Antimicrob. 2020;19:19. https://doi.org/10.1186/s12941-020-00360-4

Address for correspondence: Maria E. Morales-Betoulle, Centers for Disease Control and Prevention, 1600 Clifton Rd, Mailstop H18-SSB, Atlanta, Georgia 30329-4027, USA; email: fof7@cdc.gov

Case of Extensively Drug-Resistant *Shigella sonnei* Infection, United States

Hosoon Choi, Dhammika H. Navarathna, Brennon L. Harston, Munok Hwang, Brandon Corona, Ma Rowena San Juan, Chetan Jinadatha

Author affiliations: Central Texas Veterans Health Care System, Temple, Texas, USA (H. Choi, D.H. Navarathna, B.L. Harston, M. Hwang, B. Coronaa, M.R. San Juan, C. Jinadatha); Texas A&M University, Bryan, Texas, USA (C. Jinadatha)

DOI: https://doi.org/10.3201/eid2908.230411

We report extensively drug-resistant (XDR) *Shigella sonnei* infection in an immunocompromised patient in Texas, USA. Matrix-assisted laser desorption/ionization time-of-flight mass spectrometry failed to identify XDR *Shigella*, but whole-genome sequencing accurately characterized the strain. First-line antimicrobials are not effective against emerging XDR *Shigella*. Fosfomycin, carbapenems, and tigecycline are potential alternatives.

Shigella, the causative agent of shigellosis, can invade human gut mucosa and cause acute bacterial diarrhea. In the United States, antimicrobial resistant *Shigella* infections are frequently associated with men who have sex with men, persons experiencing homelessness, international travelers, immunocompromised persons, and persons living with HIV (*1*). The Infectious Diseases Society of America (https://www.idsociety.org) recommends ciprofloxacin, azithromycin, and ceftriaxone as first-line antimicrobials for shigellosis and trimethoprim/sulfamethoxazole and ampicillin as alternatives. Recently, extensively drug-resistant (XDR) *Shigella* species resistant to all 5 of those recommended agents have rapidly increased. XDR *Shigella* now accounts for 5% of all *Shigella* isolates in the United States (*1*). We describe possible challenges associated with accurately diagnosing a new, emerging strain, XDR *S. sonnei*, because traditional microbiologic tools may fail to identify this pathogen.

In January 2023, a man, 33 years of age, sought treatment at an emergency department (ED) for acute onset of loose stools and abdominal pain. The patient reported previous history of recurrent small bowel obstructions because of adhesions from an appendectomy. He first tested positive for HIV in January 2022 and was taking bictegravir/emtricitabine/tenofovir alafenamide. His HIV viral load was undetectable, and CD4 count was 828 cells/μL at the time of admission.

In the ED, we initially treated the patient with 1 dose each of intravenous ciprofloxacin (400 mg) and oral metronidazole (500 mg), along with fluid resuscitation. Upon patient admission, we started him on piperacillin/tazobactam (4.5 mg IV every 6 h [5 doses total]) and oral vancomycin (125 mg 4×/d [4 doses total]). After PCR was negative for *Clostridioides difficile* (Cepheid Xpert C. difficile; https://www.cepheid.com), we discontinued oral vancomycin. Enteric bacterial molecular panel (BD_MAX Extended Enteric Bacterial Panel; Fisher Scientific, https://www.fishersci.com) was positive for *Shigella* spp. On day 2 of his hospital stay, the patient voluntarily discharged against medical advice with 7-day prescriptions for oral doxycycline and oral ciprofloxacin. Antimicrobial and biochemical susceptibility identification results (VITEK Solutions; bioMérieux; https://www.biomerieux.com) were available 1 day after discharge. During follow-up with his primary care physician 2 weeks after being hospitalized, the patient reported that all symptoms of abdominal pain and diarrhea had resolved despite ineffective antimicrobial therapy.

We isolated a non–lactose fermenter colony forming unit from the cultured fecal sample. Although MALDI-TOF (matrix-assisted laser desorption/ionization-time of flight) mass spectrometry using VITEK MS (bioMérieux) misidentified the isolate as *Escherichia coli*, a VITEK biochemical panel correctly identified the isolate as *S. sonnei*. Using bioMérieux API50 CH strips, we biochemically characterized the isolate, which we classified as *S. sonnei* biotype g (ONPG +, rhamnose –, xylose –) (*2*). Phenotypic antimicrobial susceptibility testing showed the strain was resistant to all 5 antimicrobial drugs recommended for *Shigella* infection (Table). The isolate was resistant to ampicillin/sulbactam, 1st generation cephalosporins, cefuroxime, cefuroxime/axetil, cefpodoxime, ceftazidime, and cefepime, as well as all quinolones and tetracycline. However, that strain of XDR *Shigella* is susceptible to fosfomycin, carbapenems, and tigecycline, which can be used as therapeutic alternatives (Table). In spite of in vitro susceptibilities of the strain to some other antimicrobial drugs—cephalosporins, aminoglycosides, and nitrofurans—they do not penetrate the intestinal mucosa well and so are not recommended for treatment (*1*).

Whole-genome sequencing average nucleotide identity analysis determined the isolate was *S. sonnei* (98.56% identity) (*3*). Other closely related species had lower average nucleotide identity values: *S. flexneri* (98.37%), *S. dysenteriae* (97.94%), and *E. coli* NC_011601.1 (96.86%). The closest bacterial genome identified using KmerFinder was *S. sonnei* NZ_CP053751.1 (*4*). The isolate was MLST sequence type 152, the predominant *S. sonnei* isolate (*5*,*6*); cgMLST type was 194163 (*7*).

ResFinder identified putative antimicrobial resistance genes from the genome (Table) (*8*). Extended-spectrum β-lactamase $bla_{\text{CTX-M-27}}$ was the putative resistance gene against penicillin and cephalosporins. Chromosomal mutation *gyrA* (*p.S83L*) and plasmid-encoded *qnrB19* were the ciprofloxacin-resistant genes of the isolate. *Mph*(*A*) was responsible for azithromycin resistance. *Sul1*, *sul2*, *dfrA1*, and

dfrA17 were the putative resistance genes potentially responsible for trimethoprim/sulfamethoxazole resistance. We found virulence genes using VirulenceFinder (http://cge.cbs.dtu.dk/services/VirulenceFinder) (*9*). *SigA* in the SHI-1 pathogenicity island and *iucC*, *iutA*, *shiA*, and *shiB* in the SHI-2 pathogenicity island were present in the genome (*5*). Other virulence genes in the genome were *anr*, *cia*, *colE7*, *csgA*, *hlyE*, *lpfA*, *nlpI*, *senB*, *sitA*, *terC*, *traT*, *yehA*, *yehB*, *yehC*, and *yehD*. Whole-genome shotgun sequencing and antibiogram results and other information on this isolate are available from the National Center for Biotechnology Information BioSample database (no. SAMN34030354).

In our study, we found *Shigella sonnei* causing abdominal pain and diarrhea in a patient; MALDI-TOF mass spectrometry initially misidentified the pathogen as *E. coli*, but biochemical testing, confirmed by whole-genome sequencing, correctly identified *S. sonnei*. Clinicians and laboratories should be vigilant for this emerging XDR strain predominantly circulating among HIV-infected MSM (*10*) and aware of its resistance to all commonly recommended empiric and alternative antimicrobial drugs.

Table. Antimicrobial MICs and putative resistance genes of *Shigella sonnei* strain MB23166 from a case of XDR *S. sonnei* infection, United States*

Antimicrobial	MIC	Interpretation	Putative resistance genes
First-line antimicrobial treatment†			
Ciprofloxacin	≥4	R	qnrB19, *gyrA* (p.S83L)
Ceftriaxone	≥64	R	$bla_{CTX-M-27}$
Azithromycin	≥256	R	*mph(A)*
Alternative antimicrobial treatment†			
Ampicillin	≥32	R	$bla_{CTX-M-27}$
Trimethoprim/sulfamethoxazole	≥320	R	*sul1*, *sul2*, *dfrA1*, *dfrA17*
Other antimicrobials used for the patient before identification of XDR *Shigella*			
Metronidazole	≥256	R	NA
Piperacillin/tazobactam	64	I	NA
Doxycycline	24	R	*tet(A)*
Potential antimicrobials for XDR *Shigella*			
Fosfomycin	1.5	S	NA
Ertapenem	≤0.5	S	NA
Imipenem	≤0.25	S	NA
Meropenem	≤0.25	S	NA
Tigecycline	≤0.5	S	NA
Mecillinam (pivmecillinam)	0.032	S	NA
Other antimicrobials			
Amoxicillin/clavulanic acid	4	S	NA
Cefotetan	≤4	S‡	NA
Cefoxitin	≤4	S‡	NA
Ceftizoxime	≤1	S‡	NA
Amikacin	4	S‡	NA
Gentamicin	≤1	S‡	NA
Tobramycin	2	S‡	NA
Nitrofurantoin	≤16	S	NA
Aztreonam	4	S	$bla_{CTX-M-27}$
Ampicillin/sulbactam	≥32	R	NA
Ticarcillin	≥128	R	$bla_{CTX-M-27}$
Piperacillin	≥128	R	$bla_{CTX-M-27}$
Cephalothin	≥64	R	NA
Cefazolin	≥64	R	NA
Cefuroxime	≥64	R	NA
Cefuroxime/axetil	≥64	R	NA
Cefpodoxime	≥8	R	NA
Cefotaxime	16	I	$bla_{CTX-M-27}$
Ceftazidime	≥64	R	$bla_{CTX-M-27}$
Cefepime	≥64	R	$bla_{CTX-M-27}$
Nalidixic acid	≥32	R	*gyrA* (p.D87G), *gyrA* (p.S83L)
Levofloxacin	≥8	R	NA
Moxifloxacin	≥8	R	NA
Norfloxacin	≥16	R	NA
Tetracycline	≥16	R	*tet(A)*
Chloramphenicol	16	I	NA

*I, intermediate; NA, not applicable; R, resistant; S, susceptible; XDR, extensively drug-resistant.
†According to 2017 Infectious Diseases Society of America guidelines (https://www.idsociety.org).
‡Although susceptible in vitro, not effective clinically for *Shigella* species according to Clinical and Laboratory Standards Institute Performance Standards for Antimicrobial Susceptibility Testing, 32nd edition(https://clsi.org).

This work was supported by a grant from the US Department of Veterans Affairs/Office of Research and Development as part of funding for VASeqCURE, which in turn received funding from the American Rescue Plan Act funds, with additional support from Central Texas Veterans Health Care System, Temple, Texas, USA.

About the Author

Dr. Choi is a research scientist at the Central Texas Veterans Health Care System, Temple, Texas, USA. His primary research interests focus on infectious disease and whole-genome sequencing.

References

1. Centers for Disease Control and Prevention. Epidemiology, testing, and management of extensively drug-resistant shigellosis [cited 2023 March 22]. https://emergency.cdc.gov/coca/calls/2023/callinfo_022823.asp
2. Ud-Din AI, Wahid SU, Latif HA, Shahnaij M, Akter M, Azmi IJ, et al. Changing trends in the prevalence of *Shigella* species: emergence of multi-drug resistant *Shigella sonnei* biotype g in Bangladesh. PLoS One. 2013;8:e82601. https://doi.org/10.1371/journal.pone.0082601
3. Lee I, Ouk Kim Y, Park SC, Chun J. OrthoANI: An improved algorithm and software for calculating average nucleotide identity. Int J Syst Evol Microbiol. 2016;66:1100–3. https://doi.org/10.1099/ijsem.0.000760
4. Larsen MV, Cosentino S, Lukjancenko O, Saputra D, Rasmussen S, Hasman H, et al. Benchmarking of methods for genomic taxonomy. J Clin Microbiol. 2014;52:1529–39. https://doi.org/10.1128/JCM.02981-13
5. van den Beld MJC, Reubsaet FAG, Pijnacker R, Harpal A, Kuiling S, Heerkens EM, et al. A multifactorial approach for surveillance of *Shigella* spp. and entero-invasive *Escherichia coli* is important for detecting (inter)national clusters. Front Microbiol. 2020;11:564103. https://doi.org/10.3389/fmicb.2020.564103
6. Larsen MV, Cosentino S, Rasmussen S, Friis C, Hasman H, Marvig RL, et al. Multilocus sequence typing of total-genome-sequenced bacteria. J Clin Microbiol. 2012;50:1355–61. https://doi.org/10.1128/JCM.06094-11
7. Clausen PTLC, Aarestrup FM, Lund O. Rapid and precise alignment of raw reads against redundant databases with KMA. BMC Bioinformatics. 2018;19:307. https://doi.org/10.1186/s12859-018-2336-6
8. Bortolaia V, Kaas RS, Ruppe E, Roberts MC, Schwarz S, Cattoir V, et al. ResFinder 4.0 for predictions of phenotypes from genotypes. J Antimicrob Chemother. 2020;75:3491–500. https://doi.org/10.1093/jac/dkaa345
9. Malberg Tetzschner AM, Johnson JR, Johnston BD, Lund O, Scheutz F. In silico genotyping of *Escherichia coli* isolates for extraintestinal virulence genes by use of whole-genome sequencing data. J Clin Microbiol. 2020;58:e01269-20. https://doi.org/10.1128/JCM.01269-20
10. Thorley K, Charles H, Greig DR, Prochazka M, Mason LCE, Baker KS, et.al. Emergence of extensively drug-resistant and multidrug-resistant *Shigella flexneri* serotype 2a associated with sexual transmission among gay, bisexual, and other men who have sex with men, in England: a descriptive epidemiological study. Lancet Infect Dis. 2023:S1473–3099:00807–6. https://doi.org/10.1016/S1473-3099(22)00807-6

Address for correspondence: Chetan Jinadatha, Central Texas Veterans Health Care System, 1901 S Veterans Dr, Temple, TX 76504, USA; email: Chetan.Jinadatha@va.gov

Longitudinal Association of COVID-19 Hospitalization and Death with Online Search for Loss of Smell or Taste

Derek Toomre, Sasikiran Kandula, Jeffrey Shaman

Author affiliations: Yale University School of Medicine, New Haven, Connecticut, USA (D. Toomre); Columbia University Mailman School of Public Health, New York, New York, USA (S. Kandula, J. Shaman); Columbia University School of Climate, New York (J. Shaman)

DOI: https://doi.org/10.3201/eid2908.230071

Surveillance of COVID-19 is challenging but critical for mitigating disease, particularly if predictive of future disease burden. We report a robust multiyear lead-lag association between internet search activity for loss of smell or taste and COVID-19–associated hospitalization and deaths. These search data could help predict COVID-19 surges.

A challenge throughout the COVID-19 pandemic has been forecasting surges in hospitalizations and deaths so that health officials can plan and mitigate accordingly. However, effective COVID-19 surveillance and forecasting has been complicated by numerous factors: reported new cases variably underestimate true incidence; wastewater surveillance of SARS-CoV-2 is limited; variants have different virulence levels (*1*); and the risk for severe outcomes depends on previous immunizations, infections, and duration of the immune response, which is increasingly heterogeneous and variant-dependent. Ideally, independent proxies could help surveil the risk for increases in levels of severe COVID-19 disease; however, such proxies should be predictive and include a sufficient lead-lag relationship to enable public health mitigation. We investigated a possible lead-lag relationship between Google searches for "loss of smell" and "loss of taste" and COVID-19 hospitalizations and deaths.

Online search activity has previously been shown to have some predictive power for other diseases (*2*). Multiple symptoms are associated with COVID-19, but "new loss of smell or taste" is highly specific (odds ratio ≈10) (*3*). Loss of taste is confounded because flavor occurs partly through retronasal olfaction, and most persons do not differentiate between changes in taste versus flavor. In psychophysical smell and taste tests of persons with acute COVID-19, 72% had an olfactory defect and 19% had a gustatory defect (*4*). Early studies in the pandemic noted a correlation between Google Trends searches for loss of smell and taste and COVID-19 cases (*5*,*6*). This correlation occurred even before anosmia was publicly recognized as a COVID-19 symptom (*6*), underscoring the possibility that olfactory and gustatory symptoms are useful indicators for COVID-19 surveillance.

SARS-CoV-2–induced olfactory dysfunction has been studied at the cellular level and in human trials (*7*). Nasal sustentacular epithelial cells adjacent to olfactory neurons have high angiotensin-converting enzyme 2 receptor levels and are a key site of virus replication. SARS-CoV-2 enters cells either by fusing at the cell surface or in endosomes (*7*). Those 2 pathways vary between cell and tissue types; respiratory and olfactory epithelial cells use endosomal and cell surface pathways, and cell surface pathways require activation by cell surface proteases (e.g., TMPRSS2) (*7*). Mutations associated with Omicron caused it to be TMPRSS2-resistant (*8*) and display enhanced replication in the upper respiratory tract, consistent with less severe lung disease, lower mortality rates (*9*), and less frequent self-reported olfactory dysfunction (*10*). A hypothetical correlate is that olfactory dysfunction might be a proxy for general risk for infection of lung cells at the population level. Given this potential link, we examined whether Internet searches for "loss of smell" and "loss of taste" correlate with waves of COVID-19 deaths with a lead-lag relationship, and if so, whether that correlation is maintained across different waves of COVID-19 variants.

To robustly test for a potential association, we analyzed Google Trends searches for "loss of smell" and "loss of taste" across 5 different English-speaking countries and 3 different years (2020, 2021, and 2022) and examined the correlation to reported COVID-19 hospitalizations and deaths (Figure). We retrieved weekly query frequencies for "loss of smell" (or "anosmia") and "loss of taste" (or "ageusia") from the Google Extended Trends API for Australia, Canada, South Africa, the United Kingdom, and the United States. Using public sources, we computed weekly COVID-19–associated mortality and hospitalization

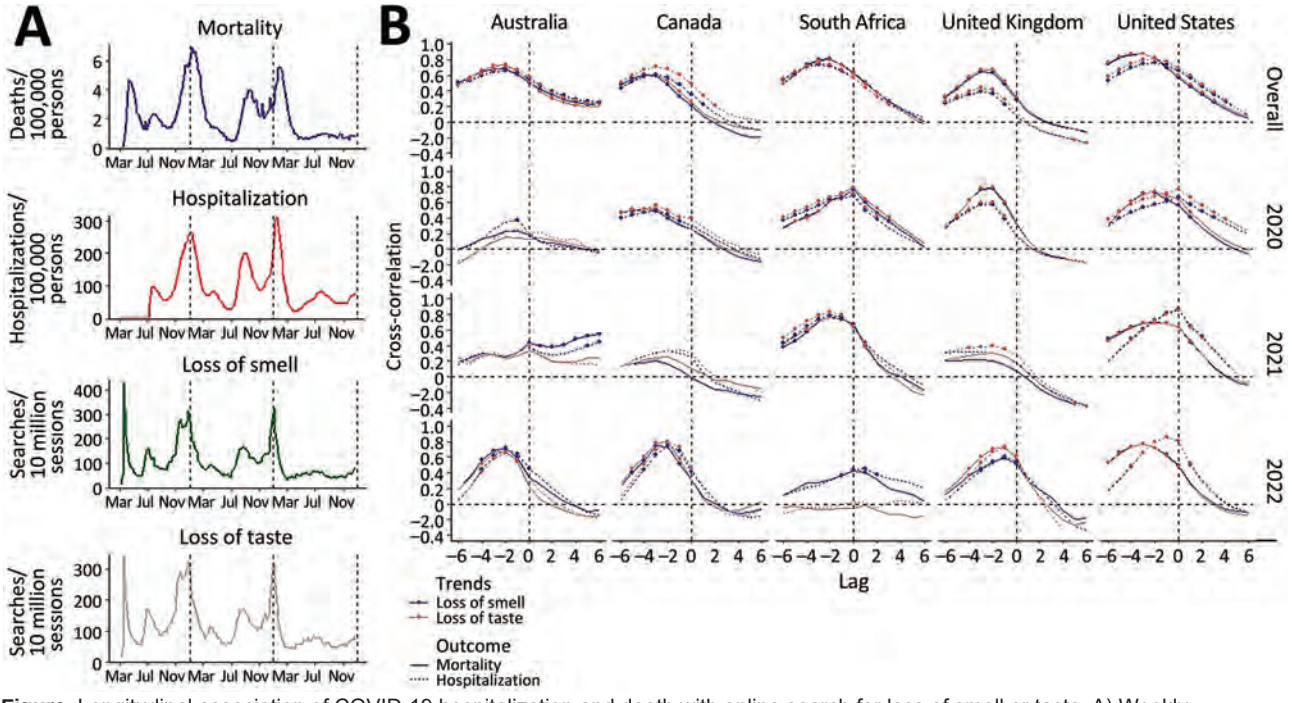

Figure. Longitudinal association of COVID-19 hospitalization and death with online search for loss of smell or taste. A) Weekly COVID-19–associated deaths (per 100,000 population), hospitalizations (per 100,000 population), and Google search trends for 'loss of smell' and 'loss of taste' (per 10 million search sessions) in the United States during March 2020–September 2022. Vertical broken lines delimit calendar years. B) Cross-correlation between Google trends of the 2 search queries, and the 2 outcomes in 5 countries (columns) over the entire COVID-19 pandemic period of March 2020–September 2022 (top row) and disaggregated by calendar year. Statistically significant correlations ($p<0.01$) are indicated by a data point. Lag between paired search trend and outcome is shown in weeks.

rates for February 2020–August 2022. For each country, we computed cross-correlation between paired search trend and outcome for each week between −6 (lead) and 6 (lag) for the study period and each calendar year (Appendix, https://wwwnc.cdc.gov/EID/article/29/8/23-0071-App1.pdf).

We observed a strong correlation in the United States between deaths, hospitalization, and searches for loss of smell or taste with surprisingly similar amplitudes for all major waves (Figure, panel A), including those associated with Omicron in December 2021. Cross-correlation was high (0.68–0.85) and significant ($p<0.01$) across all 5 countries; the peak trend for loss of smell or taste preceded hospitalization and deaths by 2–3 weeks (Figure, panel B). This correlation was seen across all years combined and was evident for most country–year combinations. The association appeared weak in years when outcome rates were low (e.g., Australia in 2020). The analysis indicates the correlation is robust over 3 years and multiple variant waves and that loss of smell or taste might give officials a useful lead indicator of the risk for COVID-19–associated hospitalizations and deaths. However, if this finding is to be used predictively, the persistence of this association would need to be closely tracked and monitored.

Strengths of this investigation are the long-duration longitudinal analysis across multiple countries, the use of simple search criteria and variable search terms, and analysis of the temporal lead-lag relationship. Limitations include potential for bias on the basis of media news cycles, the population scale of the analysis, and socioeconomic selection bias related to internet access. Future correlations will need to be monitored. Search activity might be a more useful indicator of infection levels than COVID-19–associated deaths. Despite these caveats, this accessible metric should be considered as a public health predictor.

This work was supported by Centers for Disease Control and Prevention contract no. 75D30122C14289.

D.T. declares competing interests as a founder of olfactory test company (u-Smell-it LLC) and for European Union patent (DM/212486) and pending US patents (29,743,100 and 29,750,313). J.S. and Columbia University disclose partial ownership of SK Analytics. J.S. discloses consulting for BNI.

About the Author

Dr. Toomre is a professor in the department of cell biology at Yale University School of Medicine. His research focus is the quantitative studies of exocytic traffic in living cells, including primary cilia, which are specialized cellular antennae that play roles in vision and smell.

References

1. Yang W, Shaman JL. COVID-19 pandemic dynamics in South Africa and epidemiological characteristics of three variants of concern (Beta, Delta, and Omicron). eLife. 2022;11:e78933. https://doi.org/10.7554/eLife.78933
2. Yang S, Santillana M, Kou SC. Accurate estimation of influenza epidemics using Google search data via ARGO. Proc Natl Acad Sci U S A. 2015;112:14473–8. https://doi.org/10.1073/pnas.1515373112
3. Payne DC, Smith-Jeffcoat SE, Nowak G, Chukwuma U, Geibe JR, Hawkins RJ, et al.; CDC COVID-19 Surge Laboratory Group. SARS-CoV-2 infections and serologic responses from a sample of U.S. Navy Service Members—USS Theodore Roosevelt, April 2020. MMWR Morb Mortal Wkly Rep. 2020;69:714–21. https://doi.org/10.15585/mmwr.mm6923e4
4. Prem B, Liu DT, Besser G, Sharma G, Dultinger LE, Hofer SV, et al. Long-lasting olfactory dysfunction in COVID-19 patients. Eur Arch Otorhinolaryngol. 2022;279:3485–92. https://doi.org/10.1007/s00405-021-07153-1
5. Pierron D, Pereda-Loth V, Mantel M, Moranges M, Bignon E, Alva O, et al. Smell and taste changes are early indicators of the COVID-19 pandemic and political decision effectiveness. Nat Commun. 2020;11:5152. https://doi.org/10.1038/s41467-020-18963-y
6. Walker A, Hopkins C, Surda P. Use of Google Trends to investigate loss-of-smell-related searches during the COVID-19 outbreak. Int Forum Allergy Rhinol. 2020;10:839–47. https://doi.org/10.1002/alr.22580
7. Jackson CB, Farzan M, Chen B, Choe H. Mechanisms of SARS-CoV-2 entry into cells. Nat Rev Mol Cell Biol. 2022;23:3–20. https://doi.org/10.1038/s41580-021-00418-x
8. Meng B, Abdullahi A, Ferreira IATM, Goonawardane N, Saito A, Kimura I, et al.; CITIID-NIHR BioResource COVID-19 Collaboration; Genotype to Phenotype Japan (G2P-Japan) Consortium; Ecuador-COVID19 Consortium. Altered TMPRSS2 usage by SARS-CoV-2 Omicron impacts infectivity and fusogenicity. Nature. 2022;603:706–14. https://doi.org/10.1038/s41586-022-04474-x
9. Nyberg T, Ferguson NM, Nash SG, Webster HH, Flaxman S, Andrews N, et al.; COVID-19 Genomics UK (COG-UK) consortium. Comparative analysis of the risks of hospitalisation and death associated with SARS-CoV-2 omicron (B.1.1.529) and delta (B.1.617.2) variants in England: a cohort study. Lancet. 2022;399:1303–12. https://doi.org/10.1016/S0140-6736(22)00462-7
10. Cardoso CC, Rossi ÁD, Galliez RM, Faffe DS, Tanuri A, Castiñeiras TMPP. Olfactory dysfunction in patients with mild COVID-19 during Gamma, Delta, and Omicron waves in Rio de Janeiro, Brazil. JAMA. 2022;328:582–3. https://doi.org/10.1001/jama.2022.11006

Address for correspondence: Derek Toomre, Yale University School of Medicine, Department of Cell Biology, SHM-C227, 333 Cedar St, PO Box 208002, New Haven, CT 06520-8002, USA; email: derek.toomre@yale.edu; Jeffrey Shaman, Columbia University Mailman School of Public Health, Department of Environmental Health Sciences, 722 W 168th St, New York, NY 10032, USA; email: jls106@cumc.columbia.edu

Alexis Rockman (1962–), *Ark*, 2014. Oil and alkyd on wood, 44 in x 56 in/112 cm x 142 cm. © 2023 Alexis Rockman/Artists Rights Society (ARS), New York, New York, USA.

Unexpected Hazards, Unanticipated Risks

Byron Breedlove

Contemporary American artist Alexis Rockman was born and raised in New York City and studied animation at the Rhode Island School of Design and fine arts at the School of Visual Arts in Manhattan. His meticulously detailed paintings, which often depict ecosystems transformed by climate change, invasive species, and human activity, are found in public and private collections around the world. The Princeton University Art Museum states: "The artist's vivid series of large canvases and intimate watercolors points to how an increasingly interconnected world has generated profound ecological change. Rockman is among the most accomplished contemporary eco-artists, having for several decades examined issues at the nexus of natural history, climate change, and biodiversity."

Author affiliation: Centers for Disease Control and Prevention, Atlanta, Georgia, USA

DOI: https://doi.org/10.3201/eid2908.AC2908

Those same issues mirror in large degree the central thesis of One Health, which stresses interconnections among the health of humans, animals, plants, and their shared environment. One Health issues include emerging and reemerging zoonotic diseases, neglected tropical diseases, vectorborne diseases, antimicrobial resistance, and environmental contamination. According to a 2022 analysis published in *Nature Climate Change* by Camilo Mora and other environmental scientists, humans are now more likely to come in contact with a broader range of infectious agents than ever before. Sometimes infectious diseases are spread by new or unexpected routes, including environmental sources, medical tourism, contaminated food and water from sources thought to be safe, or expansion of disease vectors into new areas.

Rockman's painting *Ark*, featured on this month's cover, shows the aftermath following the capsizing of a cargo vessel laden with animals and provides a visual touchstone for contemplating the jarring im-pact of unexpected calamity. This disaster may have been triggered by instability from the ship's being overloaded, collision with underwater wreckage, or rough waters spawned by a cyclone. The unnatu-ral reddish glare of the sky contrasts with the lurid green polluted water teeming with mutated crea-tures, and together with a glimpse of land crusted with plastic and other debris reveal a ravished envi-ronment. Many of the animals being ferried to safer havens have been thrown into the water. Perhaps the elephant will make it to land, but others such as the moose and camels bobbing on the surface will likely drown or fall prey to the aquatic predators. Still cling-ing to the ship are a rhinoceros, leopard, panda, polar bear, and various other animals, alive but trapped.

Ark serves as a potent reminder of best laid plans gone awry and countermeasures thwarted. Its inher-ent metaphor is perhaps analogous to the realm of infectious diseases. Despite having improved diag-nostics and treatments, effective and safe vaccines, and interventions to mitigate health threats, it is not smooth sailing for public health professionals challenged by known issues such as an underfunded infrastructure and by an unexpected rise in the spread and acceptance of misinformation as fact. Continued support for laboratory and epidemiology resources needed for ongoing surveillance of emerging and reemerging infectious disease threats of the future remain crucial to maintain strong, stable public health systems.

Note: EID has previously featured artwork by Alexis Rockman on its April 2006 and May 2009 covers.

Bibliography

1. Centers for Disease Control and Prevention. One Health basics [cited 2023 Jul 2]. https://www.cdc.gov/onehealth/basics/index.html
2. Centers from Disease Control and Prevention Health Alert Network. Locally acquired malaria cases identified in the United States [cited 2023 Jun 26]. https://emergency.cdc.gov/han/2023/han00494.asp?ACSTrackingID=USCDC_511-DM108019&ACSTrackingLabel=HAN%20494%20-%20General%20Public&deliveryName=USCDC_511-DM108019
3. Kracalik I, Ham DC, McAllister G, Smith AR, Vowles M, Kauber K, et al.; Verona Integron-Encoded Metallo-β-Lactamase–Producing Carbapenem-Resistant Pseudomonas aeruginosa Medical Tourism Investigation Team. Extensively drug-resistant carbapenemase-producing *Pseudomonas aeruginosa* and medical tourism from the United States to Mexico, 2018–2019. Emerg Infect Dis. 2022;28:51–61. https://doi.org/10.3201/eid2801.211880
4. Mora C, McKenzie T, Gaw IM, Dean JM, von Hammerstein H, Knudson TA, et al. Over half of known human pathogenic diseases can be aggravated by climate change. Nat Clim Chang. 2022;12:869–75. https://doi.org/10.1038/s41558-022-01426-1
5. Potter P. Manifesting ecologic and microbial connections. Emerg Infect Dis. 2006;12:715–6. https://doi.org/10.3201/eid1204.AC1204
6. Princeton University Art Museum. Art@Bainbridge | Alexis Rockman: shipwrecks [cited 2023 Jun 23]. https://artmuseum.princeton.edu/art/exhibitions/3752
7. Smithsonian American Art Museum. Alexis Rockman: a fable for tomorrow [cited 2023 Jun 23]. https://americanart.si.edu/exhibitions/rockman

Address for correspondence: Byron Breedlove, EID Journal, Centers for Disease Control and Prevention, 1600 Clifton Rd NE, Mailstop H16-2, Atlanta, GA 30329-4027, USA; email: wbb1@cdc.gov

EMERGING INFECTIOUS DISEASES®

Upcoming Issue • Viruses

- Foodborne Botulism, Canada, 2006–2021
- Characteristics of Hard Tick Relapsing Fever Caused by *Borrelia miyamotoi*, United States, 2013–2019
- Participatory Mathematical Modeling Approach for Policymaking during the First Year of the COVID-19 Crisis, Jordan
- Compliance Trajectory and Patterns of COVID-19 Preventive Measures, Japan, 2020–2022
- Interspecies Transmission of Swine Influenza A Viruses and Human Seasonal Vaccine-Mediated Protection Investigated in Ferret Model
- Genomic Characteristics of Emerging Intraerythrocytic Anaplasma capra and High Prevalence in Goats, China
- COVID-19 Epidemiology in Delta Variant Dominance Period in 45 High-Income Countries, 2020–2021
- Pharyngeal Co-Infections with Monkeypox Virus and Group A *Streptococcus*, United States, 2022
- Highly Pathogenic Avian Influenza H5N1 Clade 2.3.4.4b Virus in Wild Birds, Chile
- Rat Hepatitis E Virus in Norway Rats, Ontario, Canada, 2018–2021
- Emergence of GII.4 Sydney[P16]-like Norovirus-Associated Gastroenteritis, China, 2020–2022
- Laboratory Diagnosis of Mpox, Central African Republic, 2016–2022
- Population-Based Serological Survey of *Vibrio cholerae* Antibody Titers before Cholera Outbreak, Haiti, 2022
- Fatal Necrotizing Enterocolitis in Neonate Caused by *Cronobacter sakazakii* Sequence Type 64 Strain of CRISPR Sublineage b
- Lymphocytic Choriomeningitis Virus in a Person Living with HIV, Connecticut, USA, 2021
- *Anaplasma bovis*–Like Infections in Humans, United States, 2015–2017
- Reoccurring *Escherichia coli* O157:H7 Strain Linked to Leafy Greens–Associated Outbreaks, 2016–2019
- Patients Characteristics During Early Transmission of SARS-CoV-2, Palau, January 13–February 24, 2022

Complete list of articles in the September issue at https://wwwnc.cdc.gov/eid/#issue-302

Earning CME Credit

To obtain credit, you should first read the journal article. After reading the article, you should be able to answer the following, related, multiple-choice questions. To complete the questions (with a minimum 75% passing score) and earn continuing medical education (CME) credit, please go to http://www.medscape.org/journal/eid. Credit cannot be obtained for tests completed on paper, although you may use the worksheet below to keep a record of your answers.

You must be a registered user on http://www.medscape.org. If you are not registered on http://www.medscape.org, please click on the "Register" link on the right hand side of the website.

Only one answer is correct for each question. Once you successfully answer all post-test questions, you will be able to view and/or print your certificate. For questions regarding this activity, contact the accredited provider, CME@medscape.net. For technical assistance, contact CME@medscape.net. American Medical Association's Physician's Recognition Award (AMA PRA) credits are accepted in the US as evidence of participation in CME activities. For further information on this award, please go to https://www.ama-assn.org. The AMA has determined that physicians not licensed in the US who participate in this CME activity are eligible for *AMA PRA Category 1 Credits*™. Through agreements that the AMA has made with agencies in some countries, AMA PRA credit may be acceptable as evidence of participation in CME activities. If you are not licensed in the US, please complete the questions online, print the AMA PRA CME credit certificate, and present it to your national medical association for review.

Article Title

Clinical Characteristics of *Corynebacterium ulcerans* Infection, Japan

CME Questions

1. Your patient is a 64-year-old man with clinical symptoms of diphtheria. On the basis of the case series of 34 patients in Japan from 2001 to 2020 by Yamamoto and colleagues, which one of the following statements about the demographic and clinical characteristics of patients with *Corynebacterium ulcerans* infection is correct?

A. Incidence rate remained stable during the study period
B. Mortality rate was 2%
C. About two-thirds of *C. ulcerans* disease was respiratory and one-third nonrespiratory
D. Nonrespiratory cases were primarily bloodstream infections

2. On the basis of the case series of 34 patients in Japan from 2001 to 2020 by Yamamoto and colleagues, which one of the following statements about clinical characteristics compared between patients with respiratory vs nonrespiratory symptoms of *C. ulcerans* infection, and among the 3 severity subgroups of patients with respiratory symptoms, is correct?

A. Patients in the respiratory symptom group were significantly younger than those in the nonrespiratory group
B. Cases in the respiratory symptom group were less severe than those in the nonrespiratory group
C. The 3 respiratory subgroups did not differ significantly in C-reactive protein (CRP) levels
D. 4 of 10 severe cases, but no mild (n=5) or moderate (n=6) respiratory cases, received diphtheria antitoxin

3. According to the case series of 34 patients in Japan from 2001 to 2020 by Yamamoto and colleagues, which one of the following statements about clinical and treatment implications of clinical characteristics, treatment-related factors, and outcomes of *C. ulcerans* infection is correct?

A. To prevent spread of *C. ulcerans* and *Corynebacterium diphtheriae*, adults should be vaccinated with diphtheria toxoid vaccine
B. All patients with moderate or severe *C. ulcerans* infection should receive diphtheria antitoxin
C. *C. ulcerans* infection in the UK, Belgium, and Japan is primarily transmitted via livestock farming
D. *C. ulcerans* infections do not need to be reported to public health agencies

Earning CME Credit

To obtain credit, you should first read the journal article. After reading the article, you should be able to answer the following, related, multiple-choice questions. To complete the questions (with a minimum 75% passing score) and earn continuing medical education (CME) credit, please go to http://www.medscape.org/journal/eid. Credit cannot be obtained for tests completed on paper, although you may use the worksheet below to keep a record of your answers.

You must be a registered user on http://www.medscape.org. If you are not registered on http://www.medscape.org, please click on the "Register" link on the right hand side of the website.

Only one answer is correct for each question. Once you successfully answer all post-test questions, you will be able to view and/or print your certificate. For questions regarding this activity, contact the accredited provider, CME@medscape.net. For technical assistance, contact CME@medscape.net. American Medical Association's Physician's Recognition Award (AMA PRA) credits are accepted in the US as evidence of participation in CME activities. For further information on this award, please go to https://www.ama-assn.org. The AMA has determined that physicians not licensed in the US who participate in this CME activity are eligible for *AMA PRA Category 1 Credits*™. Through agreements that the AMA has made with agencies in some countries, AMA PRA credit may be acceptable as evidence of participation in CME activities. If you are not licensed in the US, please complete the questions online, print the AMA PRA CME credit certificate, and present it to your national medical association for review.

Article Title

Healthcare-Associated Infections Caused by *Mycolicibacterium neoaurum*

CME Questions

1. You are advising a large health maintenance organization about health care-related *Mycolicibacterium neoaurum* infection. On the basis of the new case report and case series of 36 previously reported episodes of *M. neoaurum* infection by Shapiro and colleagues, which one of the following statements about demographic and clinical characteristics of *M. neoaurum* infection is correct?

A. Infections were most common in children
B. 36 of 37 patients had serious chronic comorbidities
C. One quarter of infections involved medical devices such as central venous catheters (CVCs)
D. The most common infection was pneumonia

2. On the basis of the new case report and case series of 36 previously reported episodes of *M. neoaurum* infection by Shapiro and colleagues, which one of the following statements about diagnosis and management of *M. neoaurum* infection is correct?

A. Most *M. neoaurum* infections were identified promptly
B. *M. neoaurum* strains were resistant to multiple antimicrobial drugs
C. One quarter of patients died
D. 16 of 19 patients with CVC-related bacteremia had the CVC removed, with relative risk for relapse 0.083

3. According to the new case report and case series of 36 previously reported episodes of *M. neoaurum* infection by Shapiro and colleagues, which one of the following statements about clinical implications of demographic and clinical characteristics, diagnosis, and management of *M. neoaurum* infection is correct?

A. *M. neoaurum* infections primarily affect immunocompromised persons
B. Compared with most other RGM, *M. neoaurum* is more virulent
C. As the population of persons with chronic medical morbidities increases, it is likely that more *M. neoaurum* infections will be recognized
D. The study proved that *M. neoaurum* infections should be treated with combination antimicrobial therapy